U.S. DEPARTMENT OF COMMERCE
National Technical Information Service

PB-257 956

Compilation and Critique of Information Pertaining to Potential Severe Accidents at a Large LMFBR

Science Applications, Inc, Palo Alto, Calif

Prepared for

Office of Radiation Programs, Washington, D C

Jun 75

273092

SAI/SR-101-PA

PB 257 956

OFFICE OF RADIATION PROGRAMS
ENVIRONMENTAL PROTECTION AGENCY
CONTRACT NO. 68-01-2937

COMPILATION AND CRITIQUE OF INFORMATION PERTAINING TO POTENTIAL SEVERE ACCIDENTS AT A LARGE LMFBR

Final Report

R.R. Fullwood
Principal Investigator

June 1975

REPRODUCED BY
NATIONAL TECHNICAL
INFORMATION SERVICE
U. S. DEPARTMENT OF COMMERCE
SPRINGFIELD, VA. 22161

714

BIBLIOGRAPHIC DATA SHEET	1. Report No. SAI/SR-101-PA	2.	3. Recipient's Accession No. PB-257 956

4. Title and Subtitle
Compilation and Critique of Information Pertaining to Potential Severe Accidents at a Large LMFBR

5. Report Date
Jun 75

6.

7. Author(s)
R. R. Fullwood

8. Performing Organization Rept. No.

9. Performing Organization Name and Address
Science Applications, Inc.
Palo Alto, California

10. Project/Task/Work Unit No.

11. Contract/Grant No.
EPA-68-01-2937

12. Sponsoring Organization Name and Address
Office of Radiation Programs
Washington, D.C.

13. Type of Report & Period Covered

14.

15. Supplementary Notes

16. Abstracts

The Office of Radiation Programs (ORP) has undertaken an assessment of the status of knowledge relating to the safe operation of a large liquid Metal Fast Breeder Reactor (LMFBR) powered electric generating station. This compilation and critique was performed to assist ORP in that assessment by evaluating the accident potential of a large LMFBR and consequent environmental effects. Topics discussed in the report include the following: Accident descriptions, Experimental research, Accident analysis codes.

17. Key Words and Document Analysis. 17a. Descriptors

*Breeder reactors,
*Nuclear reactor accidents,
*Nuclear power plants,
*Environmental surveys,

Nuclear reactor safety,
Reactor cores,
Critical assemblies,
Nuclear fuel assemblies,
Failure,
Computation.

17b. Identifiers/Open-Ended Terms

*Liquid metal fast breeder reactors,
Scram,
Loss of coolant.

17c. COSATI Field/Group 18 I

18. Availability Statement
National Technical Information Service
Springfield, Virginia 22161

19. Security Class (This Report)
UNCLASSIFIED

20. Security Class (This Page
UNCLASSIFIED

21. No. of Pages
714p

22. Price
18.75/3.00

SAI/SR-101-PA

OFFICE OF RADIATION PROGRAMS
ENVIRONMENTAL PROTECTION AGENCY
CONTRACT NO. 68-01-2937

COMPILATION AND CRITIQUE OF INFORMATION PERTAINING TO POTENTIAL SEVERE ACCIDENTS AT A LARGE LMFBR

Final Report

R.R. Fullwood
Principal Investigator

June 1975

SCIENCE APPLICATIONS, INC., 2680 Hanover Street, P.O. Box 10268
Palo Alto, California 94303, (415) 493-4761

FOREWORD

This report was written by R.C. Erdmann, R.R. Fullwood, N.J. McCormick and E.T. Rumble. We appreciate the consultation provided by David Okrent of the University of California at Los Angeles and Paul Bleiweis of the University of Illinois. The compilation of information is from the open literature. The critiques that summarize each section and the general critiques in sections 1.5 and 1.6 represent the consensus opinion of the authors.

OUTLINE FOR EPA CONTRACT WA 74-R302

Compilation and Critique of Information Pertaining
to Potential Severe Accidents at a Large LMFBR

FOREWORD

1.0 INTRODUCTION AND CRITIQUE 1

1.1 Relevance to EPA/ORP Programs 1

1.2 Liquid Metal Fast Breeder Reactor 1

1.3 LMFBR Licensing Philosophy 6

1.4 Critique and Summary 17

1.5 Status Matrix 24

1.6 Report Organization 27

2.0 ACCIDENT DESCRIPTIONS 28

2.1 Accident Initiation 33

2.1.1 Loss of Coolant Without Scram 33

2.1.2 Reactivity Transient Without Scram . . . 65

2.1.3 Core Clamp Initiated Accidents 118

2.1.4 Decay Heat Caused Fuel Failure and Core Meltdown 119

2.1.5 Fuel Handling Accidents 133

2.1.6 Steam Generator Failure 138

2.1.7 Loss of Heat Sink 153

2.1.8 Sodium Fires and Aerosols 157

2.2 Accident Propagators 170

Outline (con't)

2.2.1 Doppler Effect on Accidents 170

2.2.2 Sodium Superheat and Rapid Heat Transfer to the Coolant 178

2.2.3 Autocatalysis and Strong Fuel Motion . . 219

2.2.4 Fuel Element Failure Propagation 225

2.3 Post Accident Phenomena 254

2.3.1 Post Accident Heat Removal 254

2.3.2 Reassembly after Core Meltdown 273

2.4 Summary. 295

3.0 EXPERIMENTAL RESEARCH 297

3.1 TREAT Data and Related Experiments 297

3.2 ANL Fuel-Coolant Experiments 375

3.3 SRI Scaled Vessel Accident Rupture Experiments 401

3.4 EBR Operational History 421

3.5 HEDL Fuel Studies 451

3.6 ANL Critical Facilities 467

4.0 ACCIDENT ANALYSIS CODES 489

4.1 Introduction 489

4.2 Steady State Codes. 512

4.3 Accident Initiation Codes 552

4.4 Disassembly Codes 623

4.5 Damage Evaluation 648

4.6 Summary. 690

1.0 INTRODUCTION

1.1 Report Relevance to EPA/ORP Program

ORP has undertaken an assessment of the status of knowledge relating to the safe operation of a large Liquid Metal Fast Breeder Reactor (LMFBR) powered electric generating station. This compilation and critique was performed to assist ORP in that assessment by evaluating the accident potential of a large LMFBR and consequent environmental effects.

This review was carried out by a group of specialists in the field of LMFBR safety. The evaluation of accident potentials was performed in an unbiased manner.

1.2 Liquid Metal Fast Breeder Reactor

The two basic reactor configurations, pool and loop types indicated in Table I are shown schematically in Figure 1. Table I also shows that the U.S.S.R., France and the United Kingdom have operational reactors that are at about the power level of the U.S. demonstration plant, the Clinch River Breeder Reactor (CRBR), shown conceptually in Figure 2.

Table I. Comparison of Reactor and Plant Characteristics.

Characteristics	BN-350	Phenix	PFR	SNR	MONJU	U.S. Demo Plant	Commercial Plant
	USSR	FRANCE	U.K.	W.GER.	JAPAN	U.S.	U.S.
Full power operation, year	1973	1973	1973	1978	—	1979	
Reactor size, MWe	300	250	250	280	300	350	1,000-1,500
Core:							
Fuel type	Mixed oxide	Mixed oxide	Mixed oxide	Mixed oxide	Mixed oxide	Mixed oxide	Mixed oxide, carbide or nitride
Expected peak burnup, MWD/MT	46,000	50,000	69,000	100,000	80,000 Avg.	124,000	—
Peak power limit, kW/foot	13	14	14	14	—	15	17-25
Breeding ratio	—	—	—	—	1.2	1.2	1.2-1.4
Reactor outlet temperature, °F	930	1,040	1,050	1,010	1,000	1,000	1,100-1,150
Core Δ T, °F	360	285	290	300	268	280	300-340
Configuration	Loop, cold leg pump	Pool	Pool	Loop, hot leg pump	Loop, cold leg pump	Loop	?
Refueling	Open cell	Under head, single rotating plug	Under head, single rotating plug	Under head	Under head, single rotating plug	—	?
Number of coolant loops	5	3	3	3	3	3	3-4
Steam generator type	Bayonet recirculating	Once-through serpentine modular	Recirculating U-tube	Once-through, helical coil or straight tube	Once-through, helical coil or straight tube	Recirculating	Once-through
Steam cycle							
Reheat (sodium or steam)	—	Yes (sodium)	Yes (sodium)	Yes (steam)	Yes (sodium)	No	Yes
Steam pressure, psig	730	2,340	2,360	2,500	1,810	1,450-1,800	2,400-3,500
Steam temperature, °F	810	950	1,000	930	900	900	950-1,000
Net plant efficiency, %	35	~40	~40	38	38	37	40-43

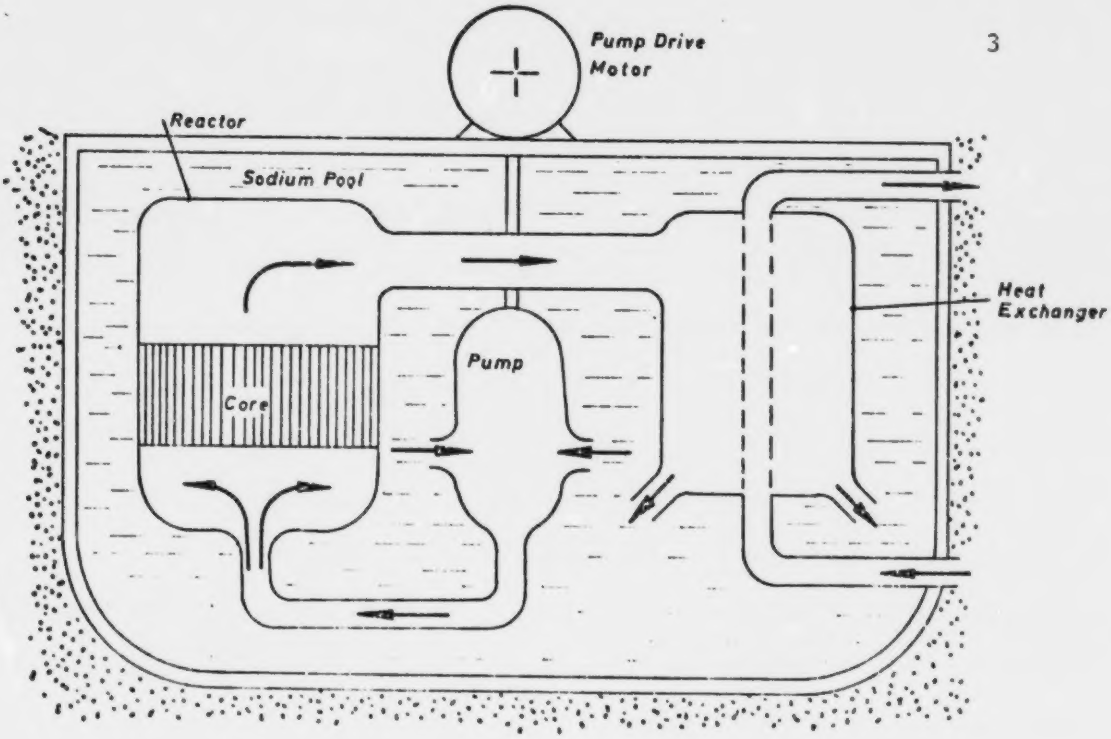
Pump Drive
Motor
Reactor
Sodium Pool
Heat
Exchanger
Pump
Core

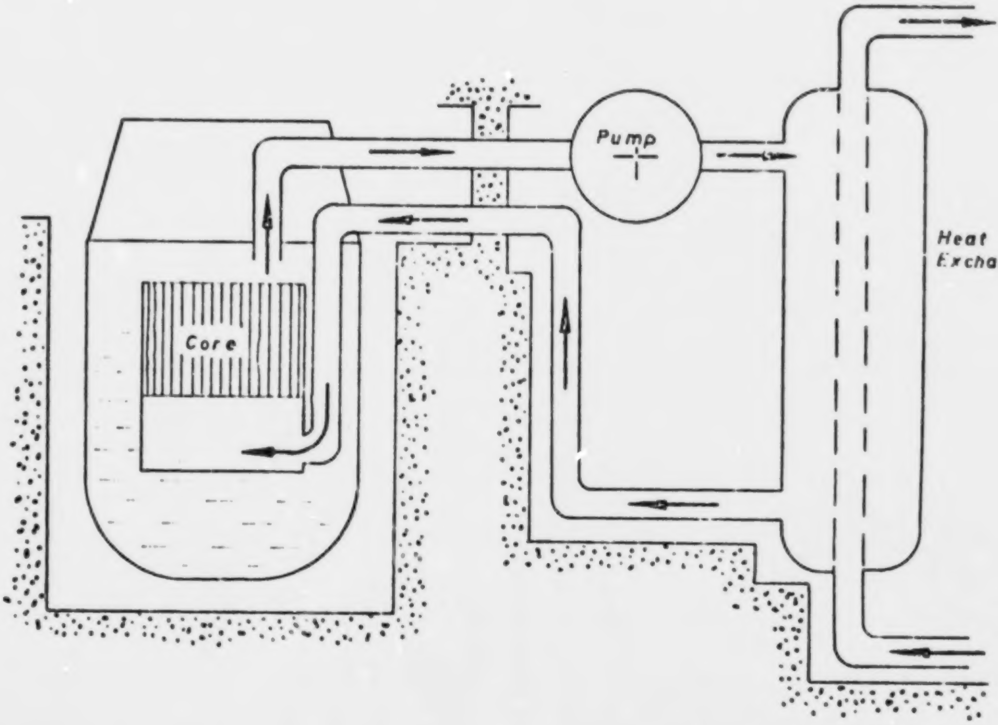
Pump
Heat
Exchanger
Core

Fig. 1. Schematic View of Pool (above) and Loop (below). Design of the Primary Cooling System.

In the case of a general LMFBR, the fuel may be mixed oxide with possibly carbides or nitrides being employed in the future. The fuel is clad in stainless steel and may be vented or sealed. The coolant is sodium at atmospheric pressure if a cold leg pump is used or at several atmospheres of cover gas if a hot leg pump is used. The configuration is either pool type or loop type and has an outlet temperature of about 1000°F with multiple cooling loops connecting with steam generators producing steam at about 1000°F and 2000 psig. The primary and secondary sodium coolant is contained with double walled stainless steel piping in vessels contained within guard vessels to provide redundant boundaries. Such a reactor will probably have a redundant scram system using two different shutdown mechanisms and uses a remote refueling cell. Another characteristic difference from the LWR is the radioactivity from activation of the sodium.

In many other respects, there are similarities with the LWR. Both plants must have adequate shielding, safety and protection from natural phenomena such as earthquakes. Attention must be given to quality control for both types of plants, consistent with the derived level of safety.

Specific items of difference are the use of relatively thin-wall stainless piping for the high-temperature sodium systems;

rigorous attention to cleanliness in the construction of the sodium piping systems; the use of a large inert cell with low-leakage characteristics for the radioactive sodium systems; the added electrical requirements because of the trace heating systems; the added requirements on insulation and heating and ventiliating systems to account for the higher temperature coolant utilized; and the structural design of liners or drip pans required to accommodate large sodium spills without degrading the integrity of containment barriers. The maximum hypothetical accident, taken by tradition to be a reactivity addition without scram, imposes large loads on the reactor vessel supports and associated structures. Finally, in the case of the pool type concept, exemplified by EBR-2, PFR, and Phenix, the construction sequencing and the fabrication techniques for the large field-fabricated tanks and associated structures pose additional problems.

1.3 LMFBR Licensing Philosophy

1.3.1 Introduction

To adequately assess the state of knowledge of LMFBR behavior it should be kept in mind that some if not most of this behavior will be designed into these plants in response to operational requirements and to licensing and safety requirements. In this section we attempt to link future plant design variations to alternative licensing and safety considerations, and in this section we strike a parallel with LWR safety design where possible.

As out knowledge of the behavior of the LMFBR increases, the development of safe reliable plants will also improve. There will be feedback effects in this system as there were in LWR design and some of the success attributed to the LWR will cause some channeling of safety design in the LMFBR.

For example, core catchers were not made a part of LWR design because it was argued and subsequently made a requirement that the plants be designed such that the situations requiring use of a core catcher be so remote as to be of no concern. It has only been very recently, with the publication of WASH-1400, that the probability of LWR core meltdown and its consequences were considered in detail. The preliminary results from this work confirm the remoteness of this event, based in part on past design requirements. However, the potential impact of core meltdown is receiving further consideration (e.g., floating nuclear plants, also in the Draft of WASH-1400).

Safety design and LMFBR plant licensing will therefore mutually reenforce each other and cause certain plant equipment concepts to prevail. It is important, therefore, that we recognize at the outset the routes that are being taken in the licensing approach to LMFBR siting. This may help prevent major future reassessments of LMFBR safety adequacy and redesign of plants.

In principle one can envision several licensing approaches to the LMFBR, there being some overlap among them. They are:

Safety design to either preclude the possibility of HCDAs or to make their likelihood exceedingly remote.

Mechanistic accident analysis of identified key HCDAs and design for their control and safe shutdown without excessive public impact.

Insure against lack of knowledge of major accident paths in the new system by designing protective barriers which would provide accident mitigation through very conservative containment, heat removal, and radioactive removal features.

Conduct a risk assessment for the LMFBR, possibly by using a set of Farmer limit lines, to identify the major identifiable contributors to loss of plant safety.

A discussion of each of these approaches and their attributes is given next.

1.3.2 Discussion

One could in principle, with sufficient system knowledge and engineering talent, *Safety Design* a LMFBR from melting down (with an acceptably low probability). Severe accidents would be terminated before excessive energy was generated, should they be initiated. Heat removal in that case would be needed only for decay heat and for initially hot fuel and primary coolant. The core would remain intact. Moreover, disruptive pressure effects would be nonexistent. Hence, vessels and support structures could be constructed with less margin for explosive disassembly and less expense in this regard, although other considerations of reliability could raise costs. This view corresponds to that in LWR *licensing* where rapid neutronic shutdown precludes concern for reactivity accidents with core motion. Pressure effects in the LWR are due to initial primary system pressures or anticipated transients without scram, and have no parallel in the LMFBR.

Safe and rapid shutdown of an LMFBR to prevent core degradation would require rapid and accurate indication of evolving situations which could lead, if left alone, to an HCDA. There appear to be three types of incidents that lead to potential large accident situations. These are:

lack of sufficient coolant

transient events

externally caused events

Many accident sequences would fall into more than one of these categories. The intent of this list is not to define accidents and categorize them. Rather it is to indicate that, as one vital factor in the reliability approach, a great deal of diverse signal processing would have to be integrated so that the shut-down system will be told to function when it is needed. It remains to be ascertained that the instruments used will provide sufficient information to be comprehensive in identifying accident preconditions. For example, certain core voiding patterns may not register neutronically but they may lead to fuel coolant interactions and possibly to a core disruptive accident.

The shutdown system would have to be mechanically and electrically reliable (c.f. WASH-1270) and this may require diversity of machinery or mode of shutdown. It also has to be quickly responsive to a valid action signal. This "hair trigger" mode of operation will, of necessity, lead to more shutdowns than might be required for safe operation.

Just how strongly one moves in this Safety Design direction will be reflected in control and heat removal system development. However, an overall "reliability" approach would encompass further detailed review of many other aspects of plant design, e.g., seismic design conservatism and testability, etc.

If large accidents are precluded, then containment and post accident heat and radiological control are somewhat less serious problems than they are in current LWR designs. The potential savings here could be rechannelled into safe shutdown system design and other factors required to assure the needed reliability.

In the Mechanistic Accident Analysis approach a select number of possibly "bounding and agreed upon" accident sequences are examined in detail and their consequences mitigated so that they are acceptable to the public. The LOCA sequences for the LWR designs are examples of these, as are the Flow Coastdown and Transient Overpower Sequences for FFTF. This route might lead to a situation like the current LOCA/ECCS, with the constant requirement for more and better experiments and computer codes. Moreover, for the LMFBR it might be more difficult to pursue than for the LWR/LOCA.

When one chooses a select few HCDA sequences, safety design is then focused on their prevention and mitigation. The safety systems are designed to function to prevent these accidents from becoming excessive. Barriers are located and sized from these accidents, containments are built to withstand pressures generated in these accidents, and the time phasing of the safety systems are set to optimize the reduction in severity of these accidents.

Thus the mechanistic approach focuses on engineering design. It is often argued, seldom proved, and usually taken for granted that by designing for these severe (and thought to be bounding) accidents one has the capacity to protect the plant from all manner of lesser accidents, however variable their sequences. Any accident not considered, or found to be outside the scope of the safety equipment for its mitigation, is proved, usually heuristically, to be unlikely, or negligible, or both. WASH-1400 provides some indication of shortcomings to this approach. However, one cannot argue with the so far unblemished record of commercial LWRs which were designed partially from the mechanistic viewpoint.

The major concerns to this approach must be:

1. the possibility of missing, through inexperience, some key accident sequences or HCDAs, and
2. the possibility that by designing for specific accidents we are not designing to maximize our response to the actual spectrum of accidents.

Protection Barrier licensing has really two, somewhat different philosophic approaches. One is to set primary containment system (and other appropriate) capabilities very conservatively indeed, at values far beyond those energy release requirements calculated by the more conservative accident analyses. In this approach, research and development might well be directed more at providing such capabilities by new design approaches which are still compatible with normal operation of the plant. The intent, in part, would be to remove detailed, mechanistic accident calculations as a vital input to the decision-making process.

A second approach to protection barrier licensing can be thought of as an intermediate stage caused by lack of complete system behavioral knowledge but rooted in mechanistic thinking. One takes the point of view that disruptive accidents can happen, and that it is difficult to conceive of and analyze properly all accident circumstances. Therefore accident analyses would be performed to provide a basis for engineering design assessment but this analysis would not be entirely mechanistic.

Rather the variety of end results from HCDAs would be examined and possible barriers to accident propagation would be constructed on a semi-arbitrary design basis. Where possible accident likelihood would be reduced (in a comparative manner) through the use of redundancy, diversity, and human response, conservatively designed containment to protect against fire, overpressure, and internally generated missiles would be developed as would the passive core catcher. It is expected that atmospheric release would have more immediate impact than meltthrough of containment (c.f. WASH-1400) so the removal of radioactivity from the building atmosphere would be studied. Recriticality would also have to be considered here.

In essence then this approach would, while attempting to mitigate accident likelihood, attempt to define general containment design concepts which could handle the end results of many accident sequences, some of which are not currently defined.

LMFBR licensing from a Risk Assessment viewpoint is not currently used in the U.S., nor has it even been used in the past in this country for LWR licensing. It would attempt to quantify the accident consequences and likelihoods for a reactor (in this case an LMFBR) and by so doing to define, as realistically and as accurately as current knowledge permits, the level of safety or the impact from a reactor. One form of this methodology was used recently in the analysis carried out in WASH-1400. Alternate risk methodologies can be used depending upon the state of knowledge of the plant to be licensed.

The basis for the method lies in the construction of a consequence-probability plot for a given reactor. An example is shown in Figure 3 for organic iodine and such a plot can be drawn for each class of isotopes thought important. To these plots one adds meteorology and demography to assess accident impacts on the public. To generate these plots one needs all of the knowledge discussed in the three previous approaches. The probabilistic and the consequence analysis are both important as can be seen in the figure. This plot then is an assemblage of all the information required in the previous licensing approaches. Moreover one can superpose on this plot an acceptable limit line. One such line is drawn in the figure. Then any points falling above this line would indicate unacceptable consequences and would require design changes to lower the points. Such an indication is given in the figure for several points.

For an LMFBR key isotope groupings would be made and acceptable limit lines drawn. Then accident sequencing would be analyzed. Whenever a new accident was postulated it would

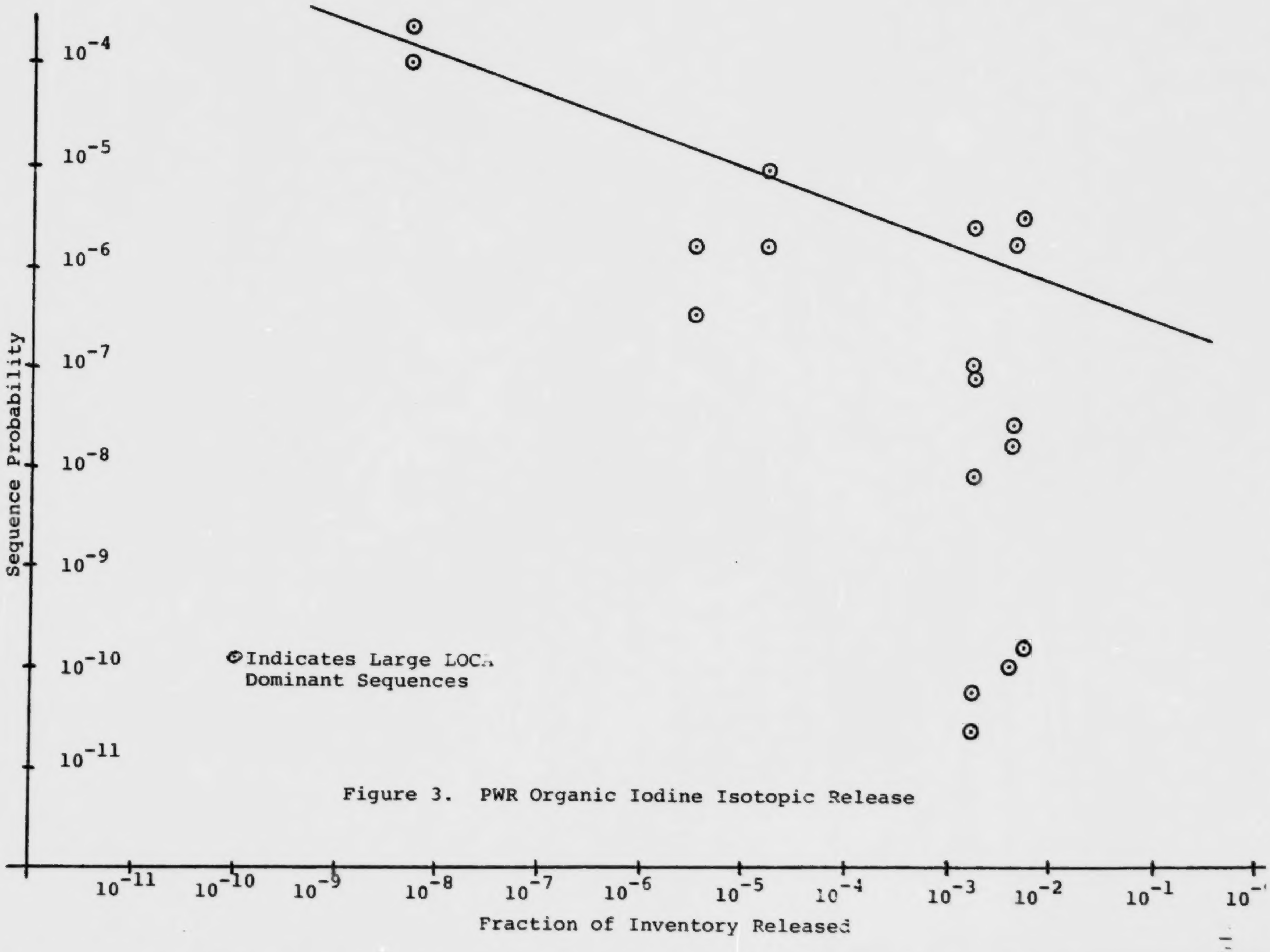

Figure 3. PWR Organic Iodine Isotopic Release

be compared to the limit lines and system effectiveness quantified. Moreover general design effectiveness, of barriers and core catchers for example, could be quantified from a risk viewpoint, viea these plots.

1.3.3 Summary of Licensing Philosophy

The choices of approach to safety in licensing have a truly major impact on the proper distribution of resources for safety research and development and on the depth of knowledge required experimentally and analytically, with regard to the multiple, complex accident sequences currently under scrutiny. The analogy arises directly in the LWR where, if ECCS systems were clearly capable of overwhelming any LOCA, independent of the intricacies involved in predicting blowdown heat transfer core re-flooding rates, cooling by core sprays, etc., far less effort would be required on elaborate calculations (which are still lacking in ability to determine the true difference among many design options) and many aspects of the experimental program. Of course, a sufficient understanding of the fundamental phenomena involved would still be required that one could be sure no unsuspected "Achilles' heel" existed.

1.4 Critique and Summary

In section 1.3 a discussion of the impact of the LMFBR licensing philosophy on safety design was presented. What is apparently happening in the United States is that the mechanistic approach to accident analysis described in that section, is being carried out. Two dominant hypothetical core disruptive accidents (HCDAs) are extensively studied and these are, of course, the flow coast down accident, and the transient overpower or ramp accident. Very detailed analysis of the sequences associated with these two initiating events are carried out. System response to these accidents are quantified using categories of codes as described in section 4.0 of this report.

Many phenomena are included in these codes, some of which (and can be) only estimated. Certainly the potential variations of extensive fuel motion in accidents and the resultant core variability, geometry, and thermodynamics may preclude any well-defined sequence of events as being highly likely. All one can anticipate is a rather large ensemble of accident phenomenology occurring based on the two initiating events given above.

In the light of this thinking, four suggestions are in order. 1) A continuing reassessment must be made of fast reactor core dynamics to make sure that these two accidents do indeed dominate the consequences of hypothetical core disruptive accidents for an LMFBR. Based on LWR technology, externally-caused events or anticipated transients may occur which could alter the concern for these two HCDAs as being the more likely maximum accidents possible.

2) The industry should begin a probabilistic analysis of the accident spectrum for a liquid-metal fast breeder reactor. It is only through the combination of probability and consequence that one can indded minimize public risks from these devices. We may find, through this combined (probability/consequence) that certain preconceived notions about the importance of given accident sequences may become more important when one considers the two viewpoints rather than merely the large consequence viewpoint. One might argue that it is premature to consider probabilistic analysis when the system is ill-defined. However, we feel this not to be the case.

3) Increased contacts and cooperation in fast reactor development with the Common Market countries and especially Great Britaink France, and Germany already under partial implementation by ERDA should be amplified. This is important for two reasons. One is the obvious fact that LMFBR research programs are necessarily very expensive, so avoiding duplication of efforts should be beneficial to all countries. Secondly, each country has some expertise to give, and also to gain. For example, the analytical

program in the United States has a lot to offer to the world, whereas the U.S. experimental program is somewhat behind that of the Common Market countries, due in part to a slightly different approach to program development.

4) The philosophy governing the selection of sites for LMFBRs should follow that for the early siting of LWRs. That is, wherever possible the LMFBR site should be remote, and possibly at locations like the Nuclear Reactor Testing Station in Idaho or Hanford in Washington. At the same time, a vigorous effort should be made to study the environmental impact of the LMFBR as if it had been placed in another site. In this way the impact of an accident could be minimized while gaining sufficient operating experience necessary to more fully justify other istes, as done with probabilistic safety studies. This initial remote siting could aid in covering accident uncertainties while not overburdening the early LMFBRs with certain costly safety features.

In reviewing the accident analysis carried out thus far in the industry, it is apparent that most of the concern is focused on core behavior. Core clamp accidents, extensive fuel motion accidents and the flow coastdown and transient overpower accidents all focus on core response and subsequent possible meltdown of the core. Lesser effort, although by no means less sophisticated, is applied to steam generator failures, anticipated transients from the balance of plant equipment operation, and externally caused events. These accident scenarios should be brought into balance so that possible coupling between accident initiators and safety systems can be correctly taken into account. Perhaps at an early stage, safety can impact design so that a possibly unforeseen spectrum of accidents can also be protected against. This is also hinted at in section 1.3.

No matter what the extent of core meltdown, it appears that a core-catcher, probably of an ex-vessel variety, will be necessary in fast reactor design. This system has not been prevalent in light-water reactors and probably will not be in the future. As such it is almost unique to LMFBR plants. ERDA is carrying out development programs in core-catcher design. This program should be followed carefully as it becomes a last barrier to foundation penetration by a molten core. It is our feeling that a passive approach to core-catcher design is almost essential to guarantee reliability of operation. It should be possible within reasonable cost to design such a core-catcher using high melting point materials which are structurally sound and can withstand the accident conditions.

We suggest that strong consideration be given to blast barriers in the upward direction from an LMFBR core. The contain ment building should be designed to almost what it is for a light-water reactor. Since atmospheric releases are much more significant than foundation penetration releases, we suggest that EPA make certain that the likelihood of atmospheric release be kept to a minimum through strong containment having adequate cooling and pressure reducing systems provided within it. Sodium degradation of the containment must also be accounted for.

Experimentally facilities and their applicability to the LMFBR safety program are treated in section 3.0. In addition to those systems discussed, the fast-flux test facility is under construction in Washington State. EPA should examine carefully the design philosophy used in the construction of FFTF. Operation of this facility will provide data for future LMFBRs and as such should be constantly monitored for releases and unforeseen situations that might possibly lead to uncontrolled releases of radioactivity. The reasoning behind the lack of a core-catcher in FFTF should be examined by EPA. The scram system behavior of FFTF would also be worth noting.

The LMFBR community has been discussing the possibility of constructing a safety test facility. Several of the national laboratories and a variety of consultants are reviewing and discussing plans for such a site, possibly funded by the RSR part of NRC. We suggest that EPA provide input to this facility evaluation so that possible design and experiments could be suggested that might eliminate some of the uncertainties in environmental impact from accidents involving large liquid metal fast breeder reactors. For example, plutonium behavior during an accident would be worth examining as would sodium plate-out. Moreover, core-catcher behavior could be examined through the use of this facility.

We recommend that EPA consider external plant behavior to make sure that weather dynamics are not substantially different for an LMFBR accident as they would be for a light-water reactor accident. Certainly the nature of the release in both radioactivity and chemical form is an important part of the knowledge needed to mitigate the consequences of any large accident. We suggest that a reexamination of 10 CFR 100 be carried out to make certain that the exclusion radius doses are within acceptable limits from EPA's viewpoint.

Specific comments about certain accidents discussed in this report are given next.

The analysis of accident phenomena becomes increasingly scenario-dependent (and, hence, imprecise) under a major core disruption. More emphasis should be placed on terminating an accident condition before such an uncertain situation arises. Along this line redundant shutdown systems must be designed, tested and proven such that they are inherently not subject to common mode failure. Similarly cooling channel blockage is a possible initiator of a serious core melt accident. It is important that such blockage be quickly identified such as from failed fuel detection of from acoustic methods and corrective action taken. The loss of off-site power is not an unusual event. Presently reactors cannot operate to supply their own cooling under such circumstances and standby power sources of a single type must be relied upon. An independent and alternative means of cooling (both power source and sodium supply) would increase the level of safety.

Molten fuel-coolant interactions present the possibility of explosive reactions. The consequences could be the most severe of any possible accidents as was the case found in WASH-1400. It is important that this accident be understood and the necessary conditions be so improbable that this accident risk is consistent with and comparable to that of other accidents.

On the plus side, sodium fires are understood and engineering designs are available for their containment and extinguishment but care must be exercised to see that proper procedures are implemented in plant design and maintained in plant operation. Also the problem of the Doppler coefficient has been quite well resolved and computation methods are at hand for its prediction.

In summary we feel that a great deal of effort and time has been spent on safety design and safety analysis of the liquid-metal fast breeder reactor. Progress is being made on many fronts and understanding of the key phenomena involved in possible accidents is being furthered. Test facilities and codes are being developed so that key accident sequences are quantified accurately.

1.5 Status Matrix

Table 2 presents a highly simplified and subjective matrix of the present status of the LMFBR accident related subjects discussed in this report. The table, by its nature, is an over simplification of the material treated in section 2.0 through 4.0 of this report. The rankings 1 through 4 represent consensus opinions among four of the authors of this report.

Table 2. Status Matrix of LMFBR Accident Related Subjects

Blank - not appropriate
1 - Low
2 - Medium
3 - High
4 - Very High

	Quality of Past & Present Work	Estimated Risk Significance	Experimental Support Needed	Theoretical Support Needed	Engineering Needed
Loss of Coolant With Scram	3	4	1	3	4
Reactivity Transient Without Scram	3	3	1	3	4
Core Clamp Initiated Accidents	2	2	2	1	3
Loss of Heat Sink	2	2	1	1	3
Fuel Handling Accident	3	2	1	1	3
Steam Generator Failure	3	3	4	2	3
Doppler Effect on Accidents	4	3	1	1	3
Decay Heat Caused Fuel Failure	4	3	1	1	2
Post Accident Heat Removal	2	3	4	4	4
Reassembly after Core Meltdown	2	2	3	3	3
Sodium Superheat and Rapid Heat Transfer to the Coolant	3	2	3	2	2
Autocatalysis and Strong Fuel Motion	2	3	2	2	2
Fuel Element Failure Propagation	2	2	2	2	2

Table 2 (con't). Status Matrix of LMFBR Accident Related Subjects

Blank - not appropriate
1 - Low
2 - Medium
3 - High
4 - Very High

	Quality of Past & Present Work	Estimated Risk Significance	Experimental Support Needed	Theoretical Support Needed	Engineering Needed
Sodium Fires and Aerosols	3	2	2	2	3
Treat Data and Related Experiments	4	3	3	3	
ANL Fuel Coolant Experiments	4	3		4	4
Scaled Vessel Accident Rupture Experiments	3	3	3	3	2
EBR Operational History	3	2	2	2	
HEDL Fuel Studies	4	3	3	3	
ANL Critical Facilities	3	2	2	2	
Initial Condition Codes	3	3	3	1	
Steady State Codes	3	2	3	1	
Accident Initiation Codes	3	3	4	3	
Disassembly Codes	3	3	4	4	
Damage Evaluation Codes	3	3	3	3	

1.6 Report Organization

With this introduction in mind, this report is organized into a compilation consisting of sections 2, 3, and 4. Section 2 presents accident descriptions and is organized into Accident Initiators (2.1), Accident Propagators (2.2), and Event Likelihoods (2.3). Section 3 summarizes safety research related to the LMFBR and Section 4 summarizes the Accident Analysis Codes subdivided into Initial Condition Codes (4.1), Steady State Codes (4.2), Accident Initiation Codes (4.3), Dissassembly Codes (4.4) and Accident Evaluation Codes (4.5).

2.0 ACCIDENT DESCRIPTIONS

Potential accidents in a LMFBR can be roughly broken down into three phases, as shown in Fig. 1. The accident initiators, propagators, and post accident phenomena obviously form only an important, but small, part of the entire approach to LMFBR safety. These phases are related to the initiation of phenomena coincident with the failure of the appropriate accident safeguards systems designed to prevent or mitigate against such occurrences.

Even with the occurrence of any of the accident initiators, early termination would occur, as represented by the dashed lines in Fig. 1. The complete analysis of the probability for such early termination requires the use of fault trees and event trees and would require complete and detailed plant specifications, as well as operating experience from similar plants. Such a study was done for light water reactors in WASH-1400, the Reactor Safety Study. As discussed in section 2.4 on event likelihoods, however, an elaborate analysis of this type is somewhat premature at this time, and so the present emphasis has been directed at the initiation and follow-on stages of accidents.

In Fig. 2 is shown the breakdown of accident initiators into in-core and out-of-core malfunctions. Each of the accident sources

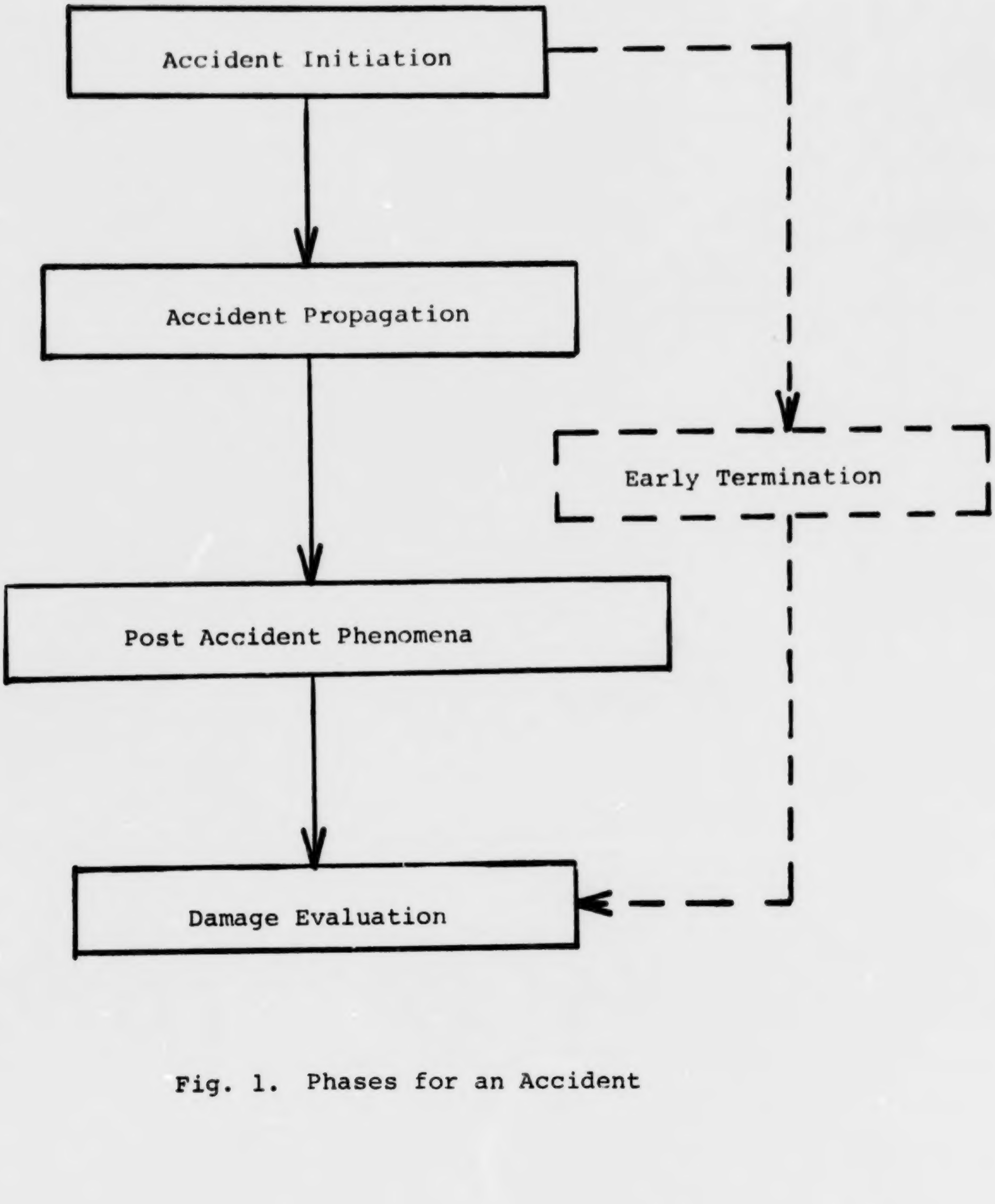
Accident Initiation
Accident Propagation
Early Termination
Post Accident Phenomena
Damage Evaluation

Fig. 1. Phases for an Accident

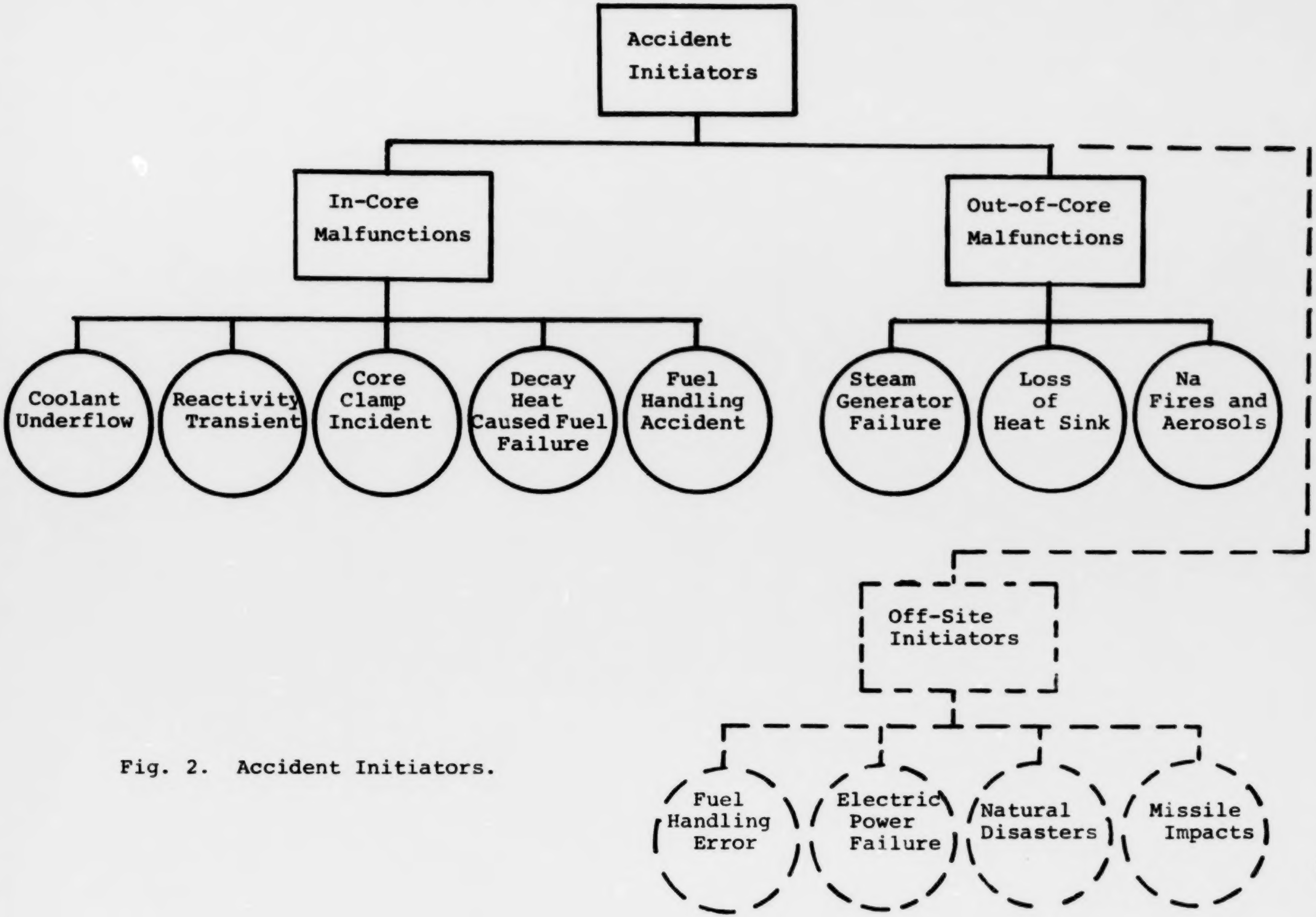
Accident Initiators
In-Core Malfunctions
Out-of-Core Malfunctions
Coolant Underflow
Reactivity Transient
Core Clamp Incident
Decay Heat Caused Fuel Failure
Fuel Handling Accident
Steam Generator Failure
Loss of Heat Sink
Na Fires and Aerosols
Off-Site Initiators
Fuel Handling Error
Electric Power Failure
Natural Disasters
Missile Impacts

Fig. 2. Accident Initiators.

shown with solid lines is discussed in section 2.1. Again it is observed that some sources of accidents, as shown with dashed lines, are not being considered here. These other accident initiators are best studies within the framework of a probabilistic safety study, as in WASH-1400. That is, inherent, internally generated LMFBR accidents have been considered here, but not the externally-initiated accidents.

The propagation of accidents which have already been initiated by some other mechanism is discussed in section 2.2. As shown in Table I, again all accidents are related to the nuclear reactor core, rather than elsewhere. The same holds for the post accident phenomena of Table I, considered in section 2.3.

TABLE I. Accident Propagators and Post Accident Phenomena Considered.

Accident Propagators

- Lack of sufficient Doppler effect
- Sodium superheat and rapid heat transfer to the coolant
- Autocatalysis and strong fuel motion
- Fuel element failure propagation

Post Accident Phenomena

- Insufficient post accident heat removal
- Reassembly after core meltdown

2.1 Accident Initiation

2.1.1 Loss of Coolant Flow Without Scram

2.1.1.1 Introduction

Gas or liquid metals may be used as coolants in fast reactors. The effectiveness of gas is entirely dependent on maintaining a high pressure and forced circulation, even for the removal of fission product decay heating. Liquid metal coolants can be operated, however, at atmospheric pressure, they are capable of removing decay heating by natural convection, they provide a large heat sink of high effective thermal diffusivity, and because of their low Prandtl number give heat transfer characteristics which are relatively insensitive to coolant velocity. To retain the advantages of liquid metal such as sodium it must be kept below the boiling point, if not, there is the danger of flow instability and vapor blanketing on local surfaces. In addition, marked changes in coolant density also produce reactivity changes. The effect and magnitude of these changes varies between design, however, local decreases in density can produce positive reactivity changes in at least a portion of the core.

The specific thermal and physical characteristics of liquid sodium provide a large margin of inherent safety to deal with loss of coolant flow with scram accidents. Most of the effort in analyzing the whole core loss of coolant flow accident has considered the additional malfunction the failure to scram. This accident initiation event was formulated initially to analyze energetic excursions.

Early studies of fast reactor accidents emphasized the analysis of energetic excursions (Ref.1,2,3). Fuel compaction has long been recognized as a potential source of positive reactivity, and therefore has been used extensively as a mechanism to initiate excursions. Somewhat arbitrary, but hopefully conservative, fuel compaction modes were postulated in most early studies. For example, the EBR-II Hazards Summary (Ref.1) considered a mode in which the upper half of the core fell coherently toward the somewhat densified lower half of the core. This mode was partially motivated by the notion that some of the fuel near the core center could potentially melt, run down into the cooler portion of the core, and freeze. The upper portion of the core could then fall down through the region vacated by the melted fuel and induce a prompt critical burst. The very coherent and idealized manner in which these events were treated resulted in a reactivity insertion rate of several hundred dollars per second.

The role that such hypothetical core disruptive accidents (HCDAs) should play in the overall safety evaluation of fast reactors has not always been well defined nor universally agreed upon. They have become a traditional consideration in LMFBR safety, however.

The current philosophy in the United States (Ref.4) embraces three levels of safety consideration in fast reactor design. The first level emphasizes proper design and construction in order to produce an inherently safe and reliable reactor. The second level provides protection systems to ensure that any off-normal conditions can be safely arrested or accommodated. The third level considers special features that provide an additional margin of public protection in case extremely unlikely or unforeseen circumstances should arise. HCDAs are usually considered as part of this third-level evaluation.

The extent to which core disruptive accidents should be considered in reactor design is a matter of continuing debate. There is the usual trade-off between safety and economics that exists in almost any other engineered product. Providing a design that would accommodate the consequences of an overly conservative and unrealistic HCDA could impose undesirable economic penalties. On the other hand, the need for adequate public protection is obvious.

2.1.1.2 Accident Description

The study of the loss of coolant flow accident without scram (LOF) has been conducted in somewhat reverse fashion. Initially, the accident was suggested as a means by which the core could meltdown and the analytical efforts focused on potential excursions from the meltdown configuration. Further efforts then involved a mechanistic analysis approach to the initiation phase. This phase of the accident involves a calculation of the core neutronics and thermal behavior up to the point of loss-of-subassembly geometry. Since most LMFBR designs have used rigid subassembly ducts, then intact subassemblies are only coupled through inlet and outlet thermal-hydraulic conditions and reactor power. Subassemblies with similar power, flow and irradiation conditions are generally lumped together into groups for the purpose of analysis. All the subassemblies within a given group, or "channel," are assumed to behave identically. Phenomena such as transient thermal-hydraulics, sodium boiling, fuel-pin mechanics and failure, cladding and fuel motion, and fuel-coolant interactions are treated with one-dimensional models. Multichannel codes of this type which were developed under USAEC sponsorship are the FREADM, (Ref.5), MELT,(Ref.6), and SAS, (Ref.7) systems. The original purpose of these codes was to give a reasonable and conservative accounting of the reactivity effects in order to provide initial conditions for the core meltdown excursion codes (Ref.8-14). Recently, however, the phenomenological modeling has become increasingly more detailed.

Most recently, safety analysts have thought to focus more attention towards the design quantification of shutdown systems. With a clear understanding of diverse shutdown systems and their reliability quantified to an acceptable level, it is argued that the HCDA accidents then could become insignificant in their potential risk effect.

Table 1 and the following approach by J. Graham indicates a recommended approach towards the incorporation of standard margins for safety in generic LMFBR's (Ref.15). In this present example, a loop type plant is considered, but the same approach can also be applied to pool type plants.

2.1.1.3 Accident Sequences

2.1.1.2.1 Accident Initiation

The sequence of events during a LOF is sensitive to the particular reactor design and specific conditions at the onset. Differences in thermohydraulic data, rod power, time dependent mass flow rates, material properties and behavior, etc. will influence the course of events.

In the SNR-300, it has been calculated that the boiling temperature is reached after about 5 seconds at full power. In the FFTF design, however, the boiling temperature is not reached until about 19 seconds (Ref. 20). The time until boiling temperature is reached influences the axial and radial fuel and coolant temperature profiles at the onset of boiling and has corresponding effects on the evaporation and condensation events. Ultimately this will effect the flow regime. In addition, the hydraulic conditions are different. The SNR subassembly has grid-type spacers and the FFTF subassembly helical wire spacers, the latter producing lower pressure losses. The net effect of these factors is to produce boiling much earlier in SNR characterized as transient boiling dominated by liquid slugs and a few bubbles. The FFTF situation would likely tend to be characterized by much latter boiling inception and the possibility of stable short-term boiling. The Phenix reactor has again different characteristics. Due to the rather large negative fuel bowing reactivity coefficient, the reactor power decreases considerably during pump coast down so that the boiling temperature is obtained only after a longer period of time at reduced power. This favors a temporary boiling process which has been designated as quasi-stable boiling.

In summary the various phenomena and their sequence of occurrence vary greatly between reactor designs. Even in the present day smaller LMFBR's such as Phenix, FFTF, and SNR-300 a great deal of difference exists. The various experiments and modeling efforts used thus far have been concerned with smaller mixed oxide cores. It is not presently possible to evaluate the validity of these studies in connection with large LMFBR's. Further research is needed to evaluate large reactor phenomena. In fairly general terms, but not necessarily being inclusive or complete the sequence of events may proceed as outlined.

The LOF is assumed to begin at full power and is induced by either whole core total blockage or pump failure. The scram systems are assumed to be inoperable. As the flow slows down the sodium coolant begins to heatup. Since the current designs of LMFBR's maintain at least 200°C to 300°C of subcooling during normal operation, considerable thermodynamic changes must occur to the fluid before has reached an enthalpy state near the saturation point.

The process of sodium boiling will be determined by (Ref. 21): the thermophysical properties of the liquid metal such as good thermal conductivity, high density ratio of liquid to vapor, and the tendency of the liquid to nucleate; the geometrical conditions in the subassemblies, small hydraulic diameter together with a great length of the cooling channel; and a high heat flux with a small pressure drop at the fuel element inlet section.

A basic understanding of nucleation and superheating of liquid sodium is needed to develop an analytic, predictive capability of these processes (refer to section 2.2.5). The potential sources of nucleation include the following (Ref. 22): homogeneous nucleation due to the spontaneous formation of critical-size nuclei containing no foreign matter and disallowing the possibility of nucleation at the container walls; vapor free heterogeneous nucleation due to wetted suspended microscopic particles or wetted surfaces; heterogeneous nucleation within the liquid due to suspended microscopic particles that contain permanent gas pockets or, more particularly, due to suspended small bubbles of inert gas; and heating at the walls with surface crevices or cavities containing gas and/or vapor. The bubble growth in any case is accomplished against the liquid pressure and the surface tension forces by an elevation of the pressure of the vapor. Since the vapor and liquid across the bubble surface must be in thermal equilibrium, the temperature must be higher than the saturation temperature of the liquid. The liquid superheat is defined as $T_{wall} - T_{saturation}$ at the initiation of nucleation.

Theoretically, under identical surface conditions superheats for sodium systems are about an order of magnitude greater than for nonmetallic systems. (Ref.21). The higher sodium superheat for sodium is primarily due to the higher boiling point, higher surface tension, and lower vapor density of sodium in the low-pressure region. However, the governing mechanisms for sodium vs. water boiling require careful consideration of the effective size of the active wall cavity and/or bubble size in the liquid. In addition, the consequences of boiling initiation at a given degree of superheat in sodium are considerably different than for nonmetallic systems. As a result of the low conductivity of water, near the wall a very steep temperature profile characteristic of high-Prandtl-number (≈ 0.7) fluids is observed. Hence only a small portion of the nonmetallic fluid near the wall is superheated, whereas the rest remains subcooled. For liquid metals, with Prandtl number 0.004 to 0.005, the temperature profile is much less steep at the wall so that a much larger fraction of the liquid can generally be superheated. The more shallow temperature profile and the small film temperature drop for sodium allow the superheat energy that can be stored in a sodium system to exceed that of a water system.

The events following nucleation in the two systems (flow regime and void growth) can, therefore, be expected to be quite different. In the case of sodium, the first bubble that nucleates will contain vapor at a higher pressure than the static pressure in the surrounding liquid because of the superheat, high thermal conductivity, and shallow temperature gradient. This pressure increase will tend to deactivate any other potential nucleation sites in the neighborhood of the first bubble and therefore gives rise to a single large bubble rather than very many small bubbles obtained in reactor water systems.

Likely locations for bubble nucleation in an LMFBR would include locations high in the active core where hot spots occur. Wire wrappers or fuel pin spacers contacting pins near the center of a subassembly may provide the environment for initial bubble formation. The first subassembly to start boiling would likely be the one with the highest operating power to flow ratio, normally the central subassemblies.

The radial temperature gradient across a subassembly is quite significant during normal operation and is enhanced as the flow is reduced. The subchannels near the subassembly walls are cooler and thus boiling in the outer regions of the subassembly will be delayed. This radial incoherency in the subassemblies which is not presently included in analytic models will have a significant effect on the boiling behavior and void growth rate in the subassemblies (Ref. 22).

The actual void growth patterns in subassemblies will consist of large bubbles. These bubbles expand from nucleation as determined by the liquid columns above and below them and evaporation of the liquid film on the fuel pin clad in contact with the bubbles. Expansion of the bubble causes a deceleration of the upstream liquid. The residual liquid flow transports the bubble into the blanket region where it condenses completely or in part. The resulting pressure drop causes sufficient superheat to allow additional bubbles to form. The repeated formation of bubbles followed by flow delay and flow reversal of the upstream liquid causes the boiling zone to extend towards the core center.

In addition to the bubbles, a liquid film will exist on the clad and subassembly surfaces in contact with them. This liquid film will be controlled by condensation and vaporization with the vapor, gravity and the shear forces caused by the vapor velocity (Ref. 23,24). In addition, it is very possible that some liquid will be entrained in the vapor.

After sufficient bubble growth, the flow regime may tend from slug flow to annular flow. The vapor flow in the annular regime is caused by evaporation of the liquid film at the hot surfaces and condensation of the vapor at colder surfaces out of the core region. This alternating evaporation and condensation will cause pressure fluctuations which may lead to chugging of the liquid at the fuel inlet and outlet. The reduction in inlet flow to subassesmblies which are undergoing boiling will cause added flow to outer cooler subassemblies.

After the liquid coolant phase is first ejected from the channel, evaporation of the residual film will hinder reentry of the lower liquid slug. This can then proceed to a condition of complete liquid film dryout and loss of the cladding heat sink.

At this stage of the accident, the time at which the clad may begin to melt relative to the progression of fuel heatup and melting is determined by the thermal and hydraulic considerations of each specific subassembly and pin. Since loss of clad implies loss of heat sink for the fuel, the fuel will assume a greatly increased heatup rate after clad melting and thus begin melting no later than a short time after clad melt.

2.1.1.3.2 Fuel Pin Clad Failure

Clad melting results in the possibility of clad relocation under the influence of gravity and the shear forces from the sodium vapor (Ref. 25). It has been suggested that upward sodium velocities could be high enough to cause wave formation, and the resulting high friction drag would lead to upward cladding motion, similar to the sodium-film stripping effect (Ref. 25). This could then cause initial cladding plug formation above the fuel region, followed by draining of later cladding to melt and plugging below the fuel region.

In addition to the mechanical effect on sodium boiling and fuel dispersal, cladding relocation has an important reactivity effect which would likely be positive since the clad will move out of the core region. Neutron streaming effects, however, may reduce this positive reactivity effect. (Ref. 26).

In addition to clad motion, the fuel will also be subjected to forces tending to relocate it. The potential sources that could be available to move the fuel include gravity, fission gas pressure, stainless-steel vapor pressure, sodium vapor pressure and fuel vapor pressure (Ref. 27). The timing and relative magnitude of these effects is not well known and depends to a large extent on the specific local situation. Effects that may occur include the following, (Ref.26): 1) the melting fuel releases the retained fission gases and/or fuel jets may be driven out of the pin, 2) fuel moves down the central pin cavity and fills it up. This may lead to a decrease in reactivity at the beginning of the downward motion. Later an increase of reactivity can follow, when the central pin cavity has been sufficiently filled, 3) in irradiated pins the fission gas pressure inside may burst the pins relatively early, while in fresh fuel, melting can be the dominant mode, 4) after the loss of mechanical pin stability the upper, no longer supported parts of the fuel may move towards the midplane of the core, thus increasing the reactivity.

At present, there is no firm understanding of the manner in which the pins will lose their structural integrity. The question of whether the fuel will fall towards the bottom of the core or if driving forces such as steel vapor, fuel vapor or fission gas could cause eructation is important as this will effect the reactivity. In addition the radial incoherency of these fuel and clad relocation effects in a subassembly are also important in assessing the overall reactivity effects. Incoherences could result in a reduction in the reactivity insertion from fuel motion.

2.1.1.3.3 Core Disruption

The question of the further behavior of the core after voiding in some subassemblies and loss of their integrity depends on their reactivity effects. Further power operation of the reactor could lead to additional destruction of the core structure and the development of a large region of mixed steel and fuel. This transition phase of the accident can include the situation when only a few subassemblies are molten, or the whole core is contained in the pool.

In most cases, the material will be boiling due to fission or decay heating. The steel will be boiling from the mixture because it has a much lower boiling point than the fuel. However, new steel will be entering the pool due to the melting attack on the surrounding structure. The characteristics of the pool's behavior will depend upon a number of phenomena. These include: (Ref.28), the rate of the melting attack on the surrounding structures in all directions including neighboring subassemblies, control rod assemblies, and core blockages; the ability of the pool to remain boiled up keeping the fuel dispersed and the rate of reactivity addition if it collapses; how rapidly the pool region will pressurize if it becomes sealed up and the rate of material ejection either through boil out or melt out or blow out.

2.1.1.3.4 Primary System Failure

If the boiling pool did collapse inducing a prompt-burst heat condition, a hydrodynamic situation would occur. Depending on the severity of the excursion, the pressures could cause a disruption of the surrounding structure and rapidly disperse the core. For less severe incidents, only small dispersion could result allowing for the possibilities of fuel recompaction and further criticalities.

The possibility of fuel dispersion can induce a reentry situation in which the dispersed fuel is driven back or falls back into a critical configuration causing a criticality event. Reentry from above appears to be a likely source of recriticality although it could occur from any direction.

In order for molten material to be ejected up through and out of the subassembly area, it generally must pass through a substantial distance of rather tightly packed and relatively cold structures. In addition, blockages are expected to form near the top and bottom of the active core region in some situations due to molten cladding being relocated and freezing. The fuel could cluster in two components after meltdown of subassemblies. A large portion of the fuel would remain in the molten pool held up by the lower blockages. Another portion of the fuel may be driven upward into the upper blockages. This mass of fuel high in the core then has the potential of downward motion into the pool formed in the lower portion of the core.

Motion of the fuel will be determined by gravity and other pressure sources which can act on it. If sodium were present, the potential for motion could be increased through rapid vaporization of the sodium. The amount of fuel, the rate at which it moves back into the pool and the shape of the pool will influence the magnitude of the excursion.

The likelihood of this kind of an event given core meltdown appears quite small because of the influence of noncoherency factors. Some of the phenomena that may lead to noncoherence are the following (Ref. 29):

1) The molten fuel is ejected from the core region by spatially varying pressure sources. Thus, the molten fuel enters the above core structure at different times and with different velocities, temperatures and molten steel content.
2) In most cases, the molten materials would be expected to penetrate and subsequently reenter intact, or partially intact from above the core duct structure. Therefore, the fuel within each subassembly would be nearly thermally and mechanically independent.
3) Pressures which remain in the core region may cause reentering fuel to behave in an unstable fashion, and to run down assembly walls.
4) Some fuel may remain frozen and lodged in the upper structure, causing the fuel which melts to fall down in a rain-like fashion.

2.1.1.3.5 Containment Failure

Once an accident has progressed into a gross disruption of the core, a sizable fraction of the fuel must be permanently dispersed from the core region to ensure long-term subcriticality. This can occur through melt-out, boil-out or mechanical disassembly phenomena as outlined above. The core debris will eventually come to rest on horizontal surfaces in the system. Decay heating of the debris will continue to be an important factor in the ability of the primary system and core catcher to contain the debris. The potential for the core debris to melt out through the primary system and containment exists and is being investigated today (Ref. 30-37). Other possible containment failure modes include reactions with structural material such as concrete. At high temperatures the concrete may release water vapor. Sodium water reactions and the resultant generation of hydrogen could be significant.

2.1.1.4 Evaluation of Information

The large body of information available in the literature shows a wide spectrum in the level of understanding concerning the phenomena which could occur in a loss of flow accident without scram. In general, as one proceeds from the initiating events into the possible accident sequences, given that an accident has occurred, the degree of uncertainty analysis becomes greater. This is true for a number of reasons.

1) Given a LOF has occurred, the initial conditions can be defined.
2) In the early stages of the accident, the geometry is well known.
3) Phenomena occurring in the early stages can be identified and assessed in experiments.
4) The number of possible interacting events and mechanisms increases rapidly as materials are stressed beyond their design levels.
5) Because of inter-reactions and complexities of the likely sequence of events and phenomena it becomes increasingly more difficult to make conservative assumptions and perform conservative analysis.

The conceptual designs for shutdown systems are being formulated and a major effort is being extended to build in the largest possible amount of reliability (Ref. 38-41). Since the various systems are presently in the design or formulation stage, it is not realistic to presently assess their reliability characteristic except to estimate that they should be at least as good from a failure standpoint as other systems under the same stress conditions, etc. One problem occurs, however, in that the resultant design must carefully consider inspectability and avoid to the greatest extent possible common-mode failure sources. The shutdown systems should be diverse to the extent that they function using different fundamental principles.

Assuming a LOF accident has been initiated, the consideration of possible shutdown system operation after initiation is not included in the analysis. Since the time from initiation to incipient boiling will be on the order of seconds and film dryout will not occur until further time delay, there is some increased chance that the scram system will be operated.

Considering then that a LOF did occur, the sequence of events which may follow are determined to a large extent by the design of the specific reactor. The phenomena which may occur and lead up to perforation of the first barrier, the fuel pin cladding are listed below.

Phenomena Leading to Fuel Pin Cladding Failure

Coolant heatup and nucleation

Coolant boiling

Coolant dryout

Fission Plenum Rupture and Fission Gas Ejection Clad Melting

Fuel melting and fission gas effects in lower power pins

These phenomena are in general understood to the point that reasonably accurate predictions can be made in the case of mixed oxide fueled small LMFBR's. Once the first barrier is penetrated and fuel melting begins to occur, the problems of analyzing the events become much more complex. The onset of material motion has a marked effect on the reactivity and thus the power of the core. The power in the core will determine further clad failures in conjunction with incoherency and other effects.

The phenomena which can effect the amount of core disruption include the following:

1) Sodium voiding patterns
2) Sodium voiding reactivity effects
3) Flow and power incoherency between pins of the same subassembly and between subassemblies
4) Fuel and clad motion in the earliest failed pins
5) Fuel and clad motion reactivity effect
6) Diverted liquid sodium flow rates to subassemblies not initially boiling
7) Effect of the disrupted core section on the remaining intact core with respect to melt through, structural damage and ability for natural circulation

Effects such as fuel and clad motion are complex in nature and extremely difficult to analyze. In the case of fuel and clad motion, the geometry is not well defined, the materials involved are out of their designed state and there are many possible combinations of possible interacting forces.

Further assessment of the penetration of the primary system barrier and the containment barrier becomes even more difficult. The present state-of-the-art appears to be at level of obtaining a qualitative understanding of the possible phenomena which could take place. Penetration of the primary system barrier may occur in this type of an accident sequence through either blow out or melt through. Thus, the thermal and mechanical stresses which could be placed on the system are approximated from the events occurring during the core disruption phase. Some of major phenomenological sources effecting primary system failure are listed below.

Major Phenomena Effecting Primary System Failure

1. Core compaction events leading to prompt bursts and blow-outs.
2. Fuel reentry events leading to prompt-bursts and blow-outs.
3. Fuel melt through.

These phenomena quite necessarily become more broad and general as they depend on the state of the core during the disruption phase of the accident.

The factors which may cause the final barrier, the outer containment, to be penetrated include those which cause primary system failure as well as those possible interactions with systems, components and materials external to the primary system. The major categories of these factors are listed below.

Major Phenomena Effecting Outer Containment Failure

1. Fuel Melt through
2. Missile impacts
3. Sodium-Water Reactions and Hydrogen Generation
4. Blow-Out

Some of the various factors leading to releases from a LOF have been stated. The effort involved to determine probability of occurrence versus consequences for these class of accidents would require an extreme effort. On the other hand, it is relevant to compare LWR's with LMFBR's and their ability to maintain safety during this accident. Some features make the LMFBR more attractive on grounds of safety and some act to make it more hazardous. These points of difference are rarely solely beneficial or harmful and require thorough analysis to understand. In regards to the LOF accident the fast reactor has the following characteristics (Ref. 42).

a) a small prompt neutron lifetime

b) a coolant at low pressure and well below its boiling point

c) a coolant which is very reactive chemically

d) a fuel with high plutonium content

e) a core which is not in the most reactive configuration

The small neutron lifetime is not an important factor for reactivity additions in which delayed neutron effects predominate. For fast reactivity additions exceeding the delayed neutron fraction, the neutron lifetime is not an important factor as the rate of increase of power is limited by Doppler feed-back. Current designs for large LMFBR's include the maintenance of an adequate value of the Doppler coefficient. The sodium void coefficient is positive over sections of the core but the total whole core magnitude in many current designs is near zero or even negative. Voiding which develops simultaneously in many subassemblies could lead to significant reactivity insertion and could become more of a problem as the large cores are designed.

The use of low pressure liquid sodium as a coolant generally adds to safe operation. The good heat transfer properties and high chemical reactivity of sodium are important factors to be considered. The heat transfer characteristics and low operating pressure allow for a large reduction in the potential consequences of loss of coolant incidents and provide a large thermal margin. The ability of sodium to provide a barrier against the escape of fission products because of its low operating pressure and chemical reactivity could be very important. This depends on: the behavior of fission products in the sodium, e.g., possible chemical reactions with sodium, solubilities; the volatility of the fission products from sodium and the extent they would be released on vaporization of the sodium; and the extent to which the fission products would be released in a sodium fire or other interaction with the environment.

The inventory of plutonium in a LMFBR is only about two to three times greater than the plutonium which accumulates in a thermal reactor (Ref.42). This does not represent a significantly greater quantity in terms of possible hazard.

The question of core reconfiguration or compaction during a disruption accident is one of the key issues to be analyzed apart from thermal systems. There are many factors which influence the severity of the resultant excursions and at present there does not appear to be a firm knowledge of the magnitude of these events, even for the smaller LMFBR's. Nicholson stated at the April, 1974, Fast Reactor Safety Meeting (Ref.17):

> "To demonstrate safe meltdown is a formidable task and the demonstration is very much dependent on the details of a particular design. Some of the analysts are arguing that their calculations combined with certain experiments show that meltdown will not lead to prompt critical reactivity and a severe power excursion. In my opinion such calcula-

tions are not yet reliable enough to accept for licensing purposes. Even if the calculations done now seem to show safe meltdown we must nevertheless still assume otherwise. Gradually we understand the problem better and increase our confidence, but we are still far from our goal. We will not likely reach it until better experimental facilities are provided to verify the analytical modeling of the phenomena. It is important that new facilities be built and that the meltdown accident studies be pursued vigorously in support of our breeder program."

REFERENCES

1. L. J. Koch *et al.*,"Hazard Summary Report--Experimental Breeder Reactor II (EBR-II)," ANL-5719 (1957).

2. W.J. McCarthy, Jr. *et al.*, "Studies of Nuclear Accidents in Fast Power Reactors, *Proceedings of the Second UN International Conference on the Peaceful Uses of Atomic Energy*, Geneva, Switzerland, *12* (1958).

3. J.D. Geier (editor), "Fast Reactor Test Facility (FARET), Volume II--Summary of Preliminary Safety Analysis," ANL-7168 (1966).

4. E.E. Kintner, "Engineering of U.S. Fast Breeder Reactors for Safe and Reliable Operation," *Proc. Conf. on Engineering of Fast Reactors for Safe and Reliable Operation*, Vol. 1, pp. 9, Karlsruhe, Germany (Ocotber, 1972).

5. D.D. Freeman, "FREADM Code Development--A Status Report," GEAP-13936 (1973).

6. A.E. Waltar, A. Padilla, Jr., and R.J. Shield, "Melt-II, A Two-dimensional Neutronics-Heat Transfer Code for Fast Reactor Safety Analysis," HEDL-TME 72-43 (1972).

7. M.G. Stevenson *et al.*, "Current Status and Experimental Basis of the SAS LMFBR Accident Analysis Code System," *Proc. of the Fast Reactor Safety Meeting*, USAEC CONF-740401, (1974).

8. H.A. Bethe and J. H. Tait, "An Estimate of the Order of Magnitude of the Explosion When the Core of a Fast Reactor Collapses," UKAEA-RHM(56)/113 (1956).

9. R.B. Nicholson, "Methods for Determining the Energy Release in Hypothetical Fast Reactor Meltdown Accidents," Nuc. Sci. Engr. *18*, pp. 207 (1964).

10. D. Okrent *et al.*, "AX-1, A Computing Program for Coupled Neutronics-Hydrodynamics Calculations on the IBM-704," ANL-5977 (1959).

11. W.R. Stratton, L.B. Engle, and D.M. Peterson, "Reactor Power Excursion Studies," Proc. Conf. on Eng. of Fast Reactors for Safe and Reliable Operation, Vol. 3, pp. 1331, Karlsruhe, Germay (1972).

12. N. Hirakawa, "MARS--A Two-dimensional Excursion Code," APDA-198 (1967).

13. W.T. Sha and T.H. Hughes, "VENUS: A Two-dimensional Coupled Neutronics-Hydrodynamics Computer Program for Fast-reactor Power Excursions," ANL-7701 (October, 1970).

14. J.F. Jackson and R.B. Nicholson, "VENUS-II: An LMFBR Disassembly Program," ANL-7951 (1972).

15. J.Graham, "Selection of Safety Design Bases for Fast Power Reactors," Proc. of the Fast Reactor Safety Meeting, USAEC CONF-740401,(1974).

16. B.Wolfe, A.P. Bray, and J.S. Moore in ANS Special Session, "Design Basis Accidents for Power Reactors," ANS Transactions, 16, 203-205, 1973 Annual Meeting, Chicago, Illinois, June, 1973.

17. R. Nicholson, "The Role of Hypothetical Accident Analysis in Fast Breeder Design and Licensing," Proc. of the Fast Reactor Safety Meeting, USAEC CONF-740401, 1974.

18. Reactor Safety Study WASH-1400 USA.

19. E.B. Ash, "Unique Features of a Sodium-Cooled Fast-Breeder Reactor," Frontiers of Power Technology Conference, Oklahoma State University, Oklahoma, 1968.

20. K. Gast, W.Peppler and D. Smidt, "Sodium Boiling Experiments and their Importance for the Reactor Safety," Proc. of the Fast Reactor Safety Meeting, USAEC CONF-740401, 1974.

21. H. Fauske, "Nucleation of Liquid Sodium in Fast Reactors," Reactor Technology, Vol. 15, No. 4, Winter 1972-1973.

22. T.C. Chawla and H. K. Fauske, "On the Incoherency in Subassembly Voiding in FTR and its Possible Effect on the Loss-of-Flow Accident Sequence," Trans. Am. Nucl. Soc., 16 (2), p. 285 (Nov. 1973).

23. M.A. Grolmes and H.K. Fauske,"Liquid Film Thickness and Mechanism for Dryout During LMFBR Loos-of-Flow Accidents," Trans. Am. Nucl. Soc., 14 (2) 743 (1971).

24. G. Hoppner and F.E. Dunn, "Sodium Film Model in SAS2A Voiding," Trans Am. Nucl. Soc., 16 (2) (Nov. 1973).

25. W.R. Bohl and T. J. Heames, "A Clad Motion Model for LMFBR Loss-of-Flow Accident Analysis," Trans. Am. Nucl. Soc., 16, 358 (1973).

26. G. Angerer, E. Eisemann, E.A. Fischer, H. Jacobs, H. Kirsters, L. Mayer, P. Schmuck and D. Thiem, "Critical Discussions of Some Important Topics in Fast Reactor Safety Analysis," Proc. of the Fast Reactor Safety Meeting, USAEC CONF-740401, 1974.

27. M.G. Stevenson, W.R. Bohl, F.E. Dunn, T.J. Heames, G.Hoppner, and L.L. Smith, "Current Status and Experimental Basis of the SAS LMFBR Accident Analysis Code System," Proc. of the Fast Reactor Safety Meeting, USAEC CONF-740401, 1974.

28. J.F. Jackson, M.G. Stevenson, J.F. Marchaterre, R.H. Levy, R.Avery, and K. Ott, "Trends in LMFBR - Hypothetical-Accident Analysis," Proc. of the Fast Reactor Safety Meeting, USAEC CONF-740401, 1974.

29. J.E. Boudreau and J.F. Jackson, "Recriticality Considerations in LMFBR Accidents," Proc. of the Fast Reactor Safety Meeting, USAEC CONF-740401, 1974.

30. T.R. Johnson, L. Baker, Jr., and J.R. Pavlik, "Large-scale Molten Fuel-Sodium Interaction Experiments," Proc. ANS Fast Reactor Safety Meeting. (1974).

31. D.R. Armstrong, F.J. Testa, and D. Raudon, "Interaction of Sodium with Molten VO$_2$ and Stainless Steel Using a Dropping Mode of Contact," ANL-7890 (December, 1971).

32. D.L. Swift and L. Baker, Jr., "Experimental Studies of the High-temperature Interaction of Fuel and Cladding Materials with Liquid Sodium," Proc. Conf. Safety, Fuels, and Core Design in Large Power Reactors, ANL-7120, Argonne National Laboratory.

33. F.A. Kulacki and R.J. Goldstein, J. Fluid Mech., Vol 55, (2), 271, 1972.

34. J.D. Gabor, E.S.Sowa, L. Baker, Jr., and J.C. Cassulo, "Studies and Experiments on Heat Removal from Fuel Debris in Sodium," Proc. ANS Fast Reactor Safety Meeting, (1974).

35. R.P. Stein, J.C. Hesson, and W.H. Gunther, "Studies of Heat Removal from Heat Generating Boiling Pools," Proc. ANS Fast Reactor Safety Meeting, 1974.

36. I.Catton and R.X. Erdmann, "Post-Accident Core Retention for LMFBR's," UCLA-ENG.-7343, July, 1973.

37. S.M. Zivi, "A Passive Safety Device Against a Melt-Through Accident," Nuclear Applications 5. p. 53, August, 1968.

38. F.H. Morgenstern, H. Buchholz, H. Kruger, H. Rohrs, "Diverse Shutdown Systems for the KNK-1, KNK-2 and SNR-300," Proc. of the Fast Reactor Safety Meeting, USAEC CONF-740401, 1974.

39. M.M.P. Clauzon, P. Marmonier, A. Meyer Heine, J. Lodet, "Considerations Relative to a Backup System," Proc. of the Fast Reactor Safety Meeting, USAEC CONF-740401, 1974.

40. R.C. Noyes and J.C.Gilbertson, "LMFBR Alternate Shutdown Systems - Test Experience and General Design Criteria," Proc. of the Fast Reactor Safety Meeting, USAEC CONF-740401, 1974.

41. E.R. McKeehan, B.M. Shawver, "The Alternate Shutdown System Development Program," Proc. of the Fast Reactor Safety Meeting, USAEC CONF-740401, 1974.

42. An Appreciation of Fast Reactor Safety, Safeguards Division, A.H.S.B., UKAEA.

2.1.2 Reactivity Transient Without Scram

2.1.2.1 General

Hypothetical Core Disruptive Accidents were first analyzed by initially specifying a fuel compaction mode (Ref. 1, 2). This approach assumed partial melting of the core followed by fuel motion driven by gravity to a more dense configuration. The reactivity insertion rate was determined from a series of static calculations of increasingly more dense core configurations. This was used to obtain the energy released as the core materials expanded (due to pressure gradients from rapid heatup and thermal expansion). This approach was thought to give an upper bound to the accident's severity. The amount of energy released during the postulated accident (e.g., the equivalent of 160 kilograms of TNT in Ref. 1) was then used to assess the reactor containment system to demonstrate the type of limiting conditions for which it protects the public.

Further studies of HCDAs led to improved and more sophisticated treatment (Refs. 3, 4, 5) of the approach first used by Bethe and Tait (Ref. 1). The most recent of these is the VENUS-II (Refs. 6, 7) code developed at Argonne. In addition, a large effort was initiated to mechanistically follow the sequence of events from accident initiation so that more precise initial conditions for disassembly computer codes such as MARS (Ref. 4) and VENUS would be provided.

Two different whole core accident chains have been specified for studying HCDAs: the overpower excursion accident and the loss-of-flow accident. The first accident assumes a fixed reactivity insertion rate with failure to scram while the second assumes the coolant pumps lose power and coast-down with failure to scram. A third type of accident which has also received attention considers propagation of local faults. Although numerous accident chains can be envisioned, these three types of accidents are frequently assumed to envelope all the possible consequences of core disruptive accidents. This assumption may warrant further scrutiny as specific designs evolve and if fuel type changes.

Since the geometry and technique of analysis needed for the various portions of the accident chains are different, the mechanistic approach of accident analysis has been organized into four phases. These include: the accident initiation phase which lasts until the initial core geometry is sufficiently altered: the disassembly phase in which the energy released from the new, prompt critical configuration is calculated; the damage evaluation phase in which the response of the reactor containment system is determined; and the post accident heat removal phase to assess long term heat removal from the fuel debris following the accident.

Most recently, investigators (Ref. 8, 9) have described the need and have begun development of models which treat the transition between the initiation phase and the disassembly phase. These models describe situations in which a portion of the core has been transformed into a pool of various mixtures of steel, coolant and fuel. Further heatup allows melting of previously solid core materials and their addition to the pool.

In addition to modeling efforts, an extensive experimental program has been developed to study fuel pin behavior in simulated accident environments. The Transient Reactor Test Facility (TREAT) (Refs. 10, 11, 12) is a thermal, pulsed testing reactor designed and built by Argonne National Laboratory to meet the needs of fast reactor safety research (refer to section 3.1). A large number of out-of-pile experiments are also conducted to study a variety of phenomena and are described in the proceedings of various conferences. Further information concerning experiments will be discussed in the next section.

2.1.2.2 Background

This section deals with the initiation phase of the overpower excursion accident in which the protective scram system is considered inoperative. Early studies (Ref. 13, 14) of the initiation phase concentrated on obtaining upper bound information which was then used as initial conditions for core disassembly calculations. At this time the major effort was placed in coupling disassembly codes such as MARS (Ref. 5) and VENUS (Ref. 6) with initiation phase codes such as MELT (Ref. 14) and SAS (Ref. 15).

In addition, during this period, development of several computer codes (Ref. 16, 17, 18) began under USAEC sponsorship to mechanistically follow the initiation phase of HCDAs in greater detail. These models assume that the rigid subassembly ducts maintain their integrity and are coupled only through thermal-hydraulic boundary conditions and reactor power. Groups of subassemblies with similar power, coolant flow and fuel characteristics are then lumped together and assumed to behave identically to a representative subassembly. Normally an average fuel pin of the subassembly with its associated coolant is used to model the representative subassembly or channel. A number of channels (or representative subassemblies) coupled by the reactor power are used to describe the entire core.

Other investigators who have studied the initiation phase of the overpower transient have found possible mitigating mechanisms. The FISFAX (Ref. 19) model described a situation in which ejected fuel from failed fuel pins might be dispersed by sodium drag forces and act to reduce the induced ramp rate for sodium voiding. Other studies (Ref. 20, 21), also indicated that the phenomenon of fuel motion in the coolant channel after pin failure is an important consideration and may reduce the severity of the accident. This phenomenon is complicated, difficult to analyze experimentally and sensitive to the failure locations of the fuel pins. References 22 and 23 are early attempts to characterize the various mechanisms which may cause clad failure during an overpower accident and to qualitatively assess the location of fuel pin failures.

Development of the integrated models of the initiation phase of HCDA's has continued to include increased physical quantities and sophistication of a large variety of phenomena such as fuel motion. Usually these models include descriptions of both loss-of-flow and overpower excursion phenomena. Probably the most advanced model, the SAS computer code (refer to section 4.4), is described in Ref. 9. Briefly, this integrated computer code treats transient thermal-hydraulics, sodium boiling, cladding and fuel motion, fuel pin mechanics and failure, fission gas plenum rupture, and the thermal interactions occurring when ejected fuel contacts the sodium coolant (fuel-coolant interactions). Two specific areas, fuel pin mechanics and fuel motion, are of paramount importance to the nature of the overpower excursion accident and will be discussed further.

2.1.2.3 Fuel Pin Mechanics

Fuel pin mechanics models and modules (Ref. 24, 25) of integrated initiation phase codes have concentrated on differential fuelclad thermal expansion as a source of clad deformation. As discussed by Culley (Ref. 23), Dias (Ref. 26, 27) and further emphasized by Stevenson (Ref. 9), there are a variety of possible modes which can induce clad deformation and failure. In addition to differential fuel-clad thermal expansion, fresh fuel pins (pins without any fission product gas) are susceptible to clad melt through and/or internal pressurization from fill gas and fuel vapor. The specific failure mode depends on the density of the fuel, and severity of the ramp rate, the thermal-hydraulic conditions of the surrounding coolant and the fuel pin design.

Irradiated fuel pins present failure mode possibilities connected with fission products. During the transient, fission gas bubbles (mainly from Xe and Kr) that have nucleated previously or which then nucleate, may grow. This intragranular fission gas bubble growth, caused either by collection of fission gas bubble coalescence, results in total intragranular bubble volume inducing fuel swelling. This mode of fuel expansion can add to the thermal expansion of the fuel. In addition, fission gas on the grain boundaries, and gas released to a free space (such as fuel cracks, the central cavity and the fuel-clad gap) undergo thermal expansion which stresses the fuel. Thus a variety of stress inducing modes are available to deform fuel pin cladding during the overpower transient. Presently, the extent to which each mode contributes to clad failure for various accident conditions is not well known.

The FRAS (Ref. 9) and GRASS (Ref. 28) computer codes were developed specifically to analyze fission gas behavior. These codes model the nucleation of gas atoms to form bubbles, radiation-induced re-solution of the bubbles, bubble motion and bubble coalescence. Fuel swelling is calculated from the resultant bubble distributions and the amount of fission gas released to the center void is found in GRASS. These codes do not treat molten fuel nor do they model grain boundary breakup caused by the intergranular fission gas. Nevertheless, models such as these coupled with present or improved mechanics codes which include the effects of fuel cracking, grain boundary fragmentation and the effects of the steady state irradiation will be needed to properly analyze clad failures.

2.1.2.4 Fuel Motion Phenomena

Physical phenomena which may occur in an overpower transient after fuel pin clad failure include ejection of solid and molten fuel and fission gas, fragmentation of the fuel and thermal interaction between the hot fuel and sodium coolant. Ejection of fuel from irradiated fuel pins is driven by the released fission gas. Fuel vapor or the hydraulic pressure of the molten fuel are possible driving sources for fresh fuel ejection. Two competing effects occur in the coolant: heatup of the fuel by the coolant causing increased pressures, and expansion of the coolant against the surrounding constraints which reduces the pressure. Cronenberg (Ref. 29) gives an excellent review of early fragmentation and fuel-coolant interaction studies.

The fuel ejection and fuel-coolant interaction module presently incorporated in SAS is well described in Ref. 30. Ejection of fuel and fission gas from the failed fuel pin is modeled using a time dependent Bernoulli equation. Ejected fuel is homogeneously removed from the fuel pin molten zone. In the coolant channel, a one-dimensional model is used which assumes a single interaction zone based on the Cho, Ivins and Wright model (Ref. 31). The interaction zone may include solid fuel, molten fuel, fission gas, sodium liquid and sodium vapor. When the fuel-fission gas mixture is ejected from a predefined clad rupture area, the fuel is assumed to be homogeneously distributed in the interaction zone.

The heat transfer rate from the fuel to the coolant is controlled by a representative particle size, the sodium void fraction and the conductivity of the fuel. Fragmentation of ejected fuel, which

2.1.2.6 Accident Sequence

The object of this subsection is to discuss the overheating, melting and following sequence of events which occur during a hypothetical whole-core reactivity insertion accident. This accident assumes initial normal sodium coolant flow and inactive safety shutdown mechanisms. Emphasis is usually placed on reactivity addition rates between 10 cents and 10 dollars per second.

The sequence of physical events occurring during this transient are dependent on the core fuel loading. Fresh and irradiated fuel pins will behave quite differently. Fig. 1 shows the important variables and their relative importance. The logic and reasons for the variable selection and location in Fig. 1 will be discussed during the description of the transient. The initial phase of transient is defined as that portion in which the subassembly wrappers maintain their integrity (Ref. 48, 49). The behavior of a representative fuel pin in one subassembly is usually analysed to describe an entire subassembly. A number of these subassemblies are then combined to represent the entire core. Further studies are needed to determine the incoherencies associated with these assumptions.

1. A threshold temperature exists. Without any mechanical disturbance, fragmentation will not occur if the water is above a bulk temperature of 70°C. Near saturation (95°C for atmospheric conditions) fragmentation does not occur even with mechanical disturbance.

2. The "dwell time", or the time between when the tin first enters the water and the initiation of the interaction, increases with increasing tin temperature.

3. The percentage of the tin which fragments increases with increasing tin temperatures, and then drops off.

4. High speed photographs show the phenomenon involves a multiple set of interactions with increasing intensity characterized by the growth and collapse of vapor bubbles.

The explanation given in Ref. 47 for the existence of a threshold temperature involves stable film boiling. If the molten metal's surface temperature is high enough, or equivalently if the bulk temperature of the water is high enough, a stable vapor film will be generated, preventing liquid-liquid contact. Other experiments (Ref. 44, 45), performed with different materials follow these general characteristics, although specific evidence has not been obtained for the case of sodium and molten uranium dioxide which establishes a cut-off state.

The effect of the fragmentation process on fuel motion in the coolant channel is significant since the rate of energy transfer from the fuel to the coolant is strongly dependent on the particle sizes. Since the energy of the ejected fuel which is transferred to the coolant ultimately causes fuel motion deviations from the steady coolant flow case, the amount of and the time in which fragmentation occurs is important.

model of fuel-fission gas mixture ejection from a clad failure is being added. Models to describe transient, irradiated fuel melting and fuel motion after clad failure are presently being developed for CAPRI.

2.1.2.5 Experiments

Experimental support of the overpower transient accident using TREAT (refer to section 3.1) is reviewed in Ref. 37 through 39. Some examples of efforts to model TREAT experiments are given in Ref. 25, 29 and 39 through 42. In general, the experiments show qualitative agreement with the different phenomena being developed analytically. Difficulties arise since the TREAT experiments in some respects are not prototypical and the analytic models must therefore be modified when used to evaluate the experiments.

A large number of investigators (Ref. 43-46) have conducted studies to learn about fragmentation and fuel-coolant interaction phenomena. Molten metal/water experiments (Ref. 43) have been valuable since they can be visually observed.

The procedure used in these molten metal/water experiments involves dropping or placing the molten metal in a pool of water. In Ref. 43, a set of experiments are described in which the water temperature ranged from 10°C to near saturation and metal temperatures from 250°C to 900°C. The main results of these experiments were:

Wider (Ref. 33, 34) has developed an improved model at Argonne to describe ejection of fuel and fission gas from the fuel pin and the fuel-coolant interaction phenomena. In this new model, PLUTO, the fuel-fission gas flow in the failed fuel pin is treated as homogeneous, compressible, and one-dimensional with a nonuniform flow cross section.

In the coolant channel, axial flow of the fission gas, liquid and vaporized coolant (if two phase coolant conditions exist) is treated as homogeneous and compressible using one-dimensional Lagrangian hydrodynamics. Each Lagrangian mesh cell containing fuel particles is treated as a single interaction zone containing fuel, coolant and fission gas. Drag forces and pressure gradients causing fuel motion are then found by solving the momentum equation which is applied to representative particles. This treatment removes the limitations of a single fuel-coolant interaction zone and thus gives the axially dependent location and state of the coolant and the fuel. In the future, PLUTO will be added to the integrated computer code, SAS (Ref. 9).

Two additional integrated computer codes for modeling the initiation phase of HCDA's are MELT III (Ref. 35) and CAPRI (Ref. 36. MELT III contains models for describing fuel motion as well as many other phenomena. Presently, a one-dimensional compressible flow in reality would cause a time dependent heat transfer area for the fuel particles, is presently not based on a firm theoretical understanding or even well correlated experimental information (Ref. 32). In SAS, an exponential factor with an input time constant is used to describe the fuel's heat transfer area during initial fragmentation and mixing phenomena. Three equations are then used to describe the resultant interaction: an energy equation which models the energy transferred in or out of the interaction from the fuel and surrounding surfaces; an equation of state which gives the single and two phase sodium pressure, volume and temperature relations; and an equation of constraint which describes the inertial constraints on the interaction zone. Solution of these three equations gives the state of the sodium interaction zone and thus the motion of the upper and lower interaction zone interfaces. An additional energy balance for the fuel particles gives the time dependent fuel temperatures. Cronenberg (Ref. 29) was the first to include energy transfer with all surfaces of the expanding interaction zone and to check such a model with an experiment.

Once the vertical motion of the interaction zone interfaces is known, an assumption about the sodium velocity within the zone must be made. Normally, as in SAS, it is assumed that the sodium velocity varies linearly between the upper and lower zone interfaces. The forces on representative fuel particles due to sodium drag, gravity and buoyancy are then found and the resultant motion of the fuel in the channel is determined.

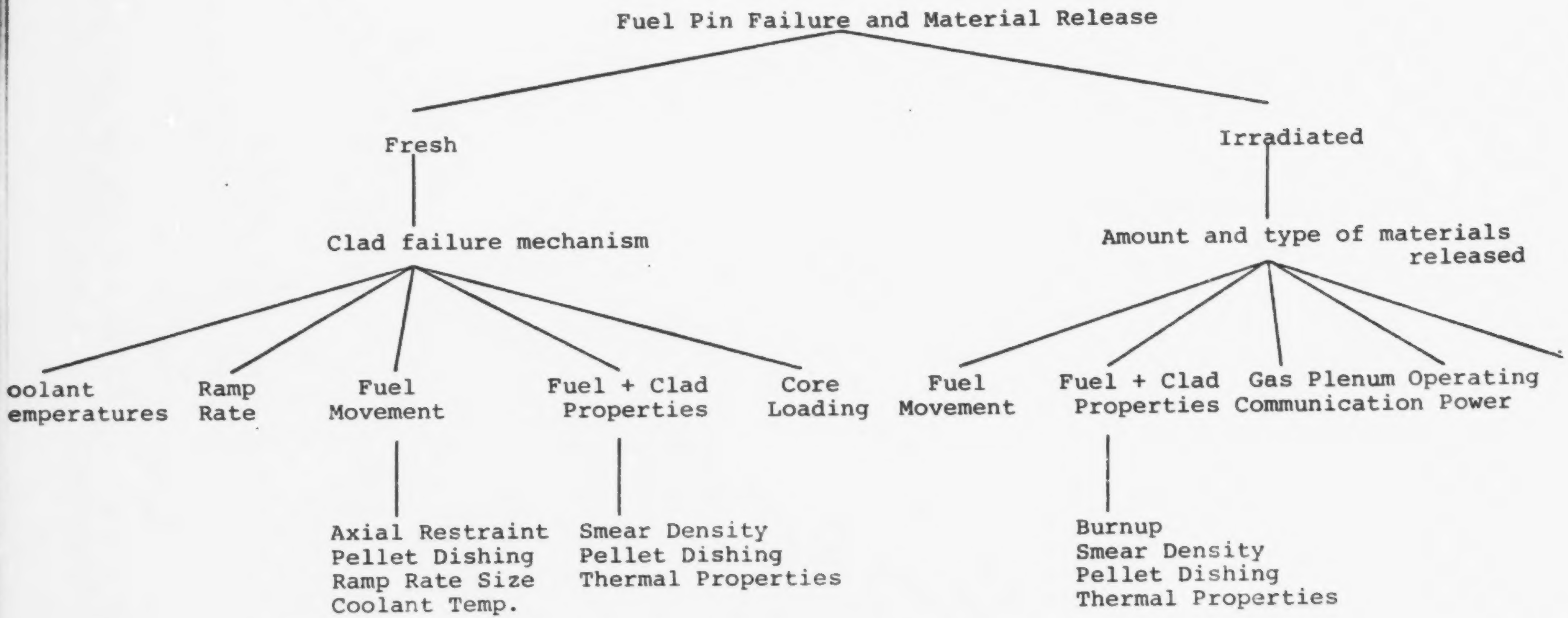
Fuel Pin Failure and Material Release
Fresh
Irradiated
Clad failure mechanism
Amount and type of materials released
oolant emperatures
Ramp Rate
Fuel Movement
Fuel + Clad Properties
Core Loading
Fuel Movement
Fuel + Clad Properties
Gas Plenum Communication
Operating Power
Axial Restraint
Pellet Dishing
Ramp Rate Size
Coolant Temp.
Smear Density
Pellet Dishing
Thermal Properties
Burnup
Smear Density
Pellet Dishing
Thermal Properties

Fig. 1. Factors Effecting the Nature of Fuel Pin Failure during the Transient.

TABLE I FUEL DESCRIPTION AND EFFECTS

TYPE	FUEL/CLAD DESCRIPTION	CONDITIONS EFFECTING FUEL MOVEMENT	FUEL MOVEMENT IN PIN	CLAD STRAIN MECHANISMS	CLAD FAILURE MECHANISMS	CLAD FAILURE DESCRIPTION
FRESH UP TO ~3000 MWd/Mt	Fresh pellets Maximum clad-fuel gap No fission gas Sorbed gas and fill gas only	Pellets separate Maximum fuel-clad gap Some amount of axial restraint of fuel pellets by pin design Cracks	Axial movement possible into blankets or radially outward between pellets and then along fuel-clad gap Movement in cracks also possible	Fuel-clad differential thermal expansion	Strain on Clad Melting of clad from outside caused by boiling and film dry out. Melting of clad from inside caused by contact with molten fuel	Gross failure near the top of the fuel. Pressure of the compressed liquid and possible vapor fuel drives fuel into channel Last pin type to fail
LOW POWER (<9KW/ft)	Some equiaxed grain growth Smaller clad-fuel gap Clad strength reduced Fission gas retained in fuel	Pellets possibly fused together Axial restraint can be increased by friction between clad and fuel Interconnected pore passageways and cracks	Movement possible as in fresh fuel core Interconnected pores could also allow movement in equiaxed grain area	Fuel-clad differential thermal expansion Intragranular fission gas induced fuel [illegible] Transient release of intergranular fission gas	Strain on clad, each strain source being additive Transient release of intergranular fission gas likely to be primary source	Localized failure at the top of the melt zone Failure possible before fuel melting Fission gas pressure drives fuel into channel
HIGH POWER (>12KW/ft)	Central void columnar grain and equiaxeds grain growth Clad strength and clad-fuel gap reduced Fission gas retained in equaxed and unre-	Pellets possibly fused together Central void Axial restraint by above 2 mechanisms Cracks and interconnected pore passageways	Axial movement possible in central void. Function of void diameter and fuel temperature axial variation Cracks and pores can provide passageway as in low power core	Some as low power case	Some as low power case	Localized failures at the top of the melt zone. Appreciable fuel melting before clad failure Fission gas pressure drives fuel into cha

Reproduced from best available copy.

2.1.2.6.1 Fresh Fuel Pins

Description

Fresh fuel pins are characterized by having an insignificant amount of fission gas. Only the fill gas and residual sorbed gases from the manufacturing process are present. The clad is at its maximum strength and the fuel-clad gap is at its maximum before the transient. These conditions exist up to approximately 3000 MWd/MT burnup (4). Table I provides a simple summary of fuel description.

Fuel Heatup and Movement Before Clad Failure

The transient proceeds with increased fuel temperatures and the solid fuel will begin to expand. The fuel-clad gap will acoommodate expansion in the radial direction. There will also be volumetric expansion when the fuel in the central portion of the pin begins to melt. Depending on the fuel initial density, the fuel pellets will contain some porosity to accommodate this phenomena. Expansion in the axial direction may be restrained by shear forces between the fuel and clad or some other device. Pellet dishing (Ref. 51, 52) can be employed to minimize axial solid fuel pellet expansion. By dishing the pellets, pellet contact occurs only at the outer radial edge where the fuel is the coldest. Thus, the solid fuel axial expansion is controlled only by the colder fuel and its effect minimized. When the solid fuel and clad are mechanically tight axial fuel expansion should be minimized to prevent resultant stress on the clad.

As the fuel temperature increases, more of the fuel will melt. Fig. 2 shows, as is easily predicted, that a solid fuel shell persists around the molten zone. When the fuel centerline temperature reaches 3600 K, a solid fuel shell almost 0.4 mm may still remain. Thus, before any appreciable molten fuel movement into the channel can take place, this boundary must be broken. The pressure in the molten zone due to the state of the fuel will exert force in all directions on the solid fuel. In the radial direction, the possibility exists that the molten fuel will push out between the fuel pellets to the fuel-clad gap and then move axially in the gap. Axial movement is also possible if there is a passageway into the blanket or the blanket pellets are able to move away from the core. References 53, 54, and 55 describe a fresh fuel pin for which post transient analysis indicated fuel motion of this type.

Clad Failure and Solid Fuel Shell Failure

Figures 3 and 4 describe the logic involved which leads either to a fresh molten fuel-coolant interaction or to the absence of this event during the transient. In Fig. 3, it is shown that there appears to be three possible clad failure mechanisms; boiling in the coolant channel followed by film dryout and resulting clad melt,

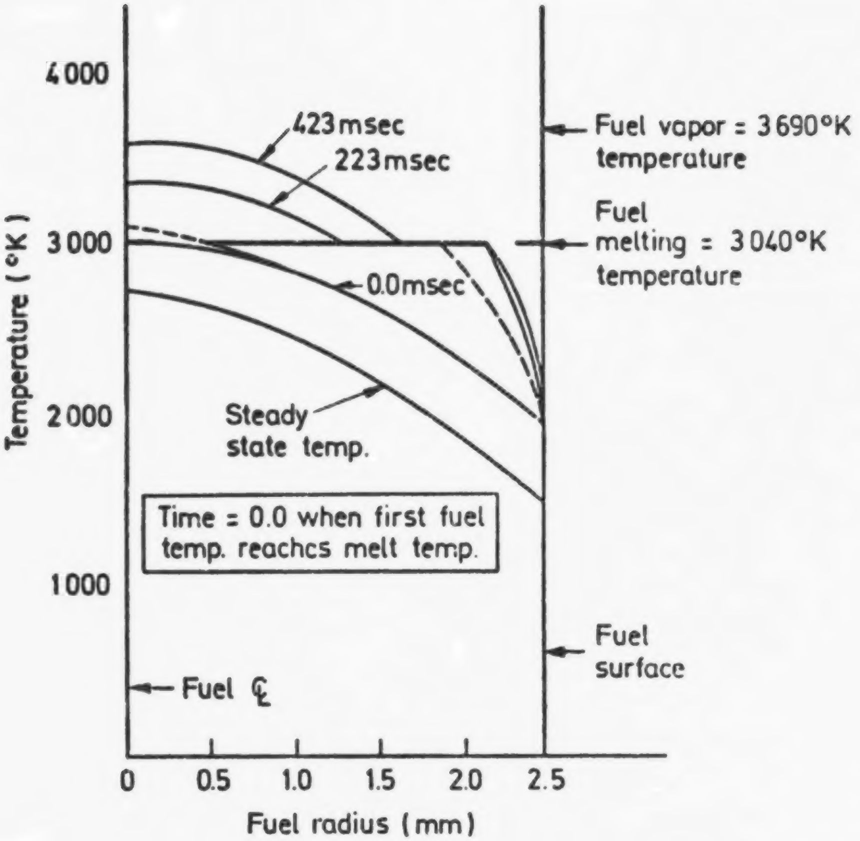

Fig. 2. Typical LMFBR Fuel Radial Temperature Profile.

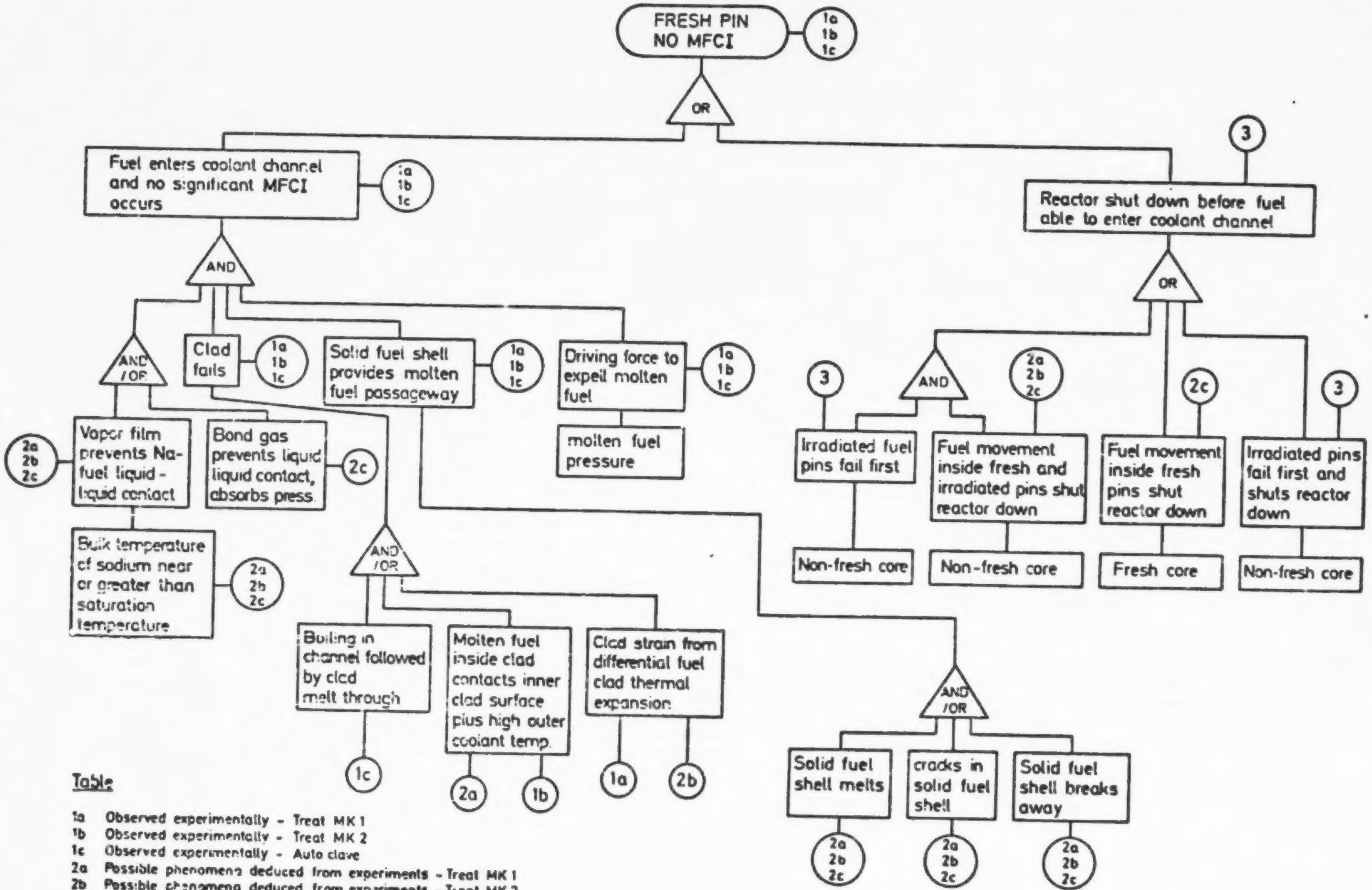
FRESH PIN NO MFCI
1a 1b 1c
OR
Fuel enters coolant channel and no significant MFCI occurs
1a 1b 1c
3
Reactor shut down before fuel able to enter coolant channel
AND
AND /OR
Clad fails
1a 1b 1c
Solid fuel shell provides molten fuel passageway
1a 1b 1c
Driving force to expell molten fuel
1a 1b 1c
molten fuel pressure
Vapor film prevents Na-fuel liquid - liquid contact
2a 2b 2c
Bond gas prevents liquid liquid contact, absorbs press.
2c
Bulk temperature of sodium near or greater than saturation temperature
2a 2b 2c
AND /OR
Boiling in channel followed by clad melt through
1c
Molten fuel inside clad contacts inner clad surface plus high outer coolant temp.
2a
1b
Clad strain from differential fuel clad thermal expansion
1a
2b
OR
AND
3
Irradiated fuel pins fail first
Non-fresh core
Fuel movement inside fresh and irradiated pins shut reactor down
2a 2b 2c
Non-fresh core
Fuel movement inside fresh pins shut reactor down
2c
Fresh core
Irradiated pins fail first and shuts reactor down
3
Non-fresh core
AND /OR
Solid fuel shell melts
2a 2b 2c
cracks in solid fuel shell
2a 2b 2c
Solid fuel shell breaks away
2a 2b 2c

Table

1a	Observed experimentally - Treat MK 1
1b	Observed experimentally - Treat MK 2
1c	Observed experimentally - Auto clave
2a	Possible phenomena deduced from experiments - Treat MK 1
2b	Possible phenomena deduced from experiments - Treat MK 2
2c	Possible phenomena deduced from experiments - Auto clave
3	Theoretical possibility, but not experimentally observed

Reproduced from best available copy.

Fig. 3. Fresh Fuel Pin, no Molten Fuel-Collant Interaction.

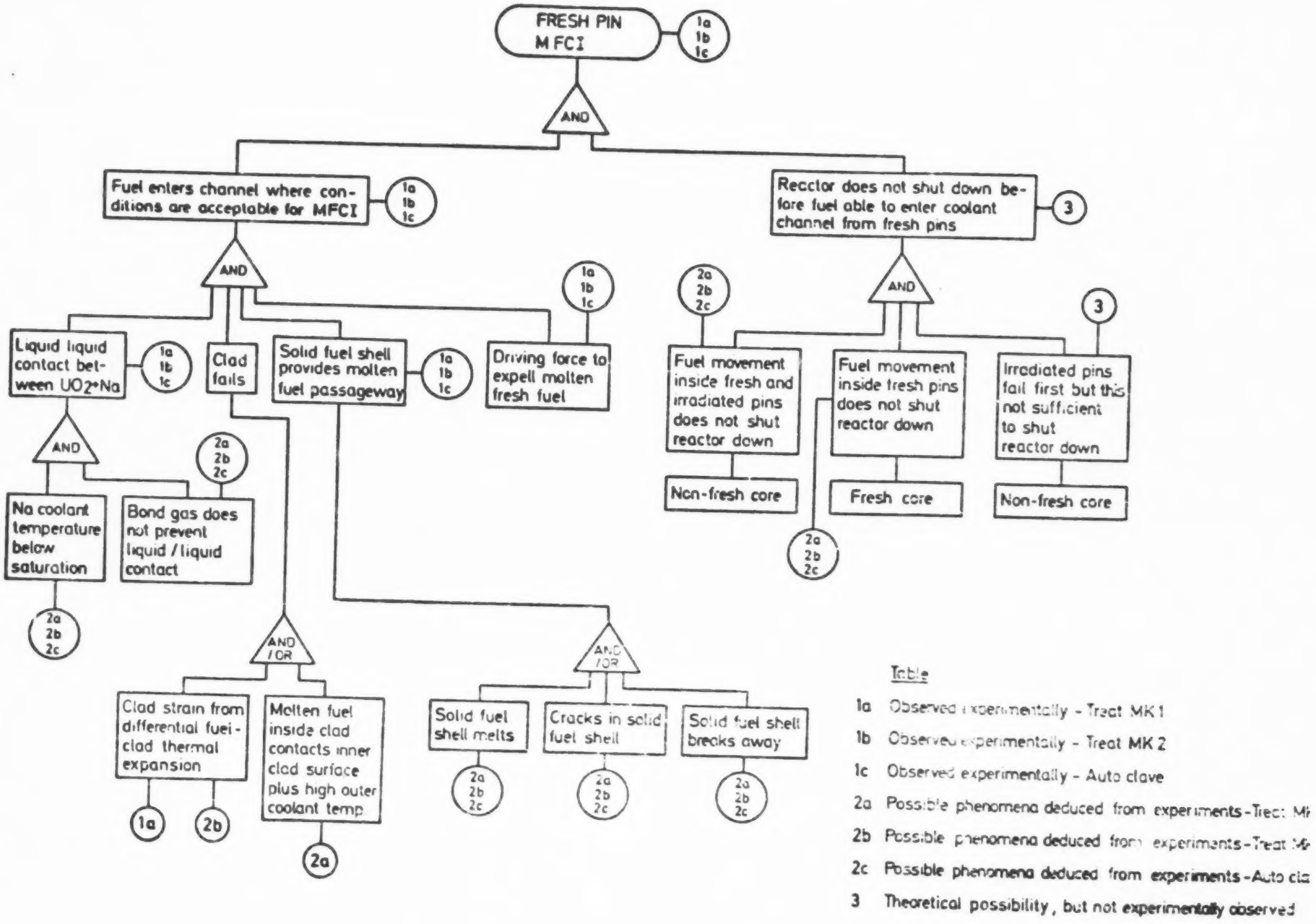
FRESH PIN MFCI
1a 1b 1c
AND
Fuel enters channel where conditions are acceptable for MFCI
1a 1b 1c
Reactor does not shut down before fuel able to enter coolant channel from fresh pins
3
AND
Liquid liquid contact between UO2+Na
1a 1b 1c
Clad fails
Solid fuel shell provides molten fuel passageway
1a 1b 1c
Driving force to expell molten fresh fuel
1a 1b 1c
AND
2a 2b 2c
Fuel movement inside fresh and irradiated pins does not shut reactor down
Non-fresh core
Fuel movement inside fresh pins does not shut reactor down
Fresh core
2a 2b 2c
3
Irradiated pins fail first but this not sufficient to shut reactor down
Non-fresh core
AND
2a 2b 2c
Na coolant temperature below saturation
2a 2b 2c
Bond gas does not prevent liquid / liquid contact
AND /OR
Clad strain from differential fuel-clad thermal expansion
1a
2b
Molten fuel inside clad contacts inner clad surface plus high outer coolant temp
2a
AND /OR
Solid fuel shell melts
2a 2b 2c
Cracks in solid fuel shell
2a 2b 2c
Solid fuel shell breaks away
2a 2b 2c
Table
1a Observed experimentally - Treat MK1
1b Observed experimentally - Treat MK 2
1c Observed experimentally - Auto clave
2a Possible phenomena deduced from experiments-Treat M
2b Possible phenomena deduced from experiments-Treat M
2c Possible phenomena deduced from experiments-Auto cla
3 Theoretical possibility, but not experimentally observed

Fig. 4. Fresh Fuel Pin, Molten Fuel-Coolant Interaction.

molten fuel inside the clad contacting and melting the clad, and clad strain from differential fuel clad thermal expansion (Ref. 50, 56-61).

Factors effecting the determination of the ultimate failure mechanism include those listed in Table II.

If the fuel pin fails because of fuel-clad differential thermal expansion, the location of the failure is a function of clad strain and temperature. At the time of failure, over 50% perhaps 80%, of the fuel in the pin will be molten. With a large molten zone, the stress on the clad should be fairly uniform since the large liquid volume will communicate fuel expansion tendencies. Thus, the clad may fail at or above the molten zone, where the clad is the hottest. The clad may also fail near the top of the core if the mechanism was due to clad melt from coolant boiling and film dryout. For clad melt from molten fuel, high clad temperatures are required (Ref. 58). In addition radial seepage is most likely between the upper blanket-core pellet interface or the next lower interface between core fuel pellets. This is true since the molten fuel axially pushes against a larger area on one of these two pellets depending on the upper core fuel pellet melt fraction. In addition this exerted force is applied at a time when coolant temperatures are high enough to support clad melt from molten fuel. This occurred in the C4A experiment (Ref. 55).

When the fresh fuel pin clad fails, the molten fuel must find a passageway from the molten zone through the solid fuel shell

Table II. Fresh Fuel Clad Failure Mechanism Determination Factors.

Factor	Failure mechanism likelihood		
	Clad melt from coolant boiling	Clad melt from molten fuel	Clad strain
Higher coolant temp.	more	more	more
Larger ramp rates	less	small	more
Larger smear density	less	less	more
Greater porosity	more	more	more
Greater enrichment	less	less	more
Greater axial restraint	less	less	more
Larger clad strain limit to failure	more	more	less
Presence of clad defects	less	less	more
Pin sodium logged	more	less	less

to escape out of the clad. Thus, as shown in Figs. 3 and 4, the fuel must move through cracks, break away the restricting solid fuel or move through a melted solid fuel shell. When this passageway is present, the fuel is free to move into the coolant channel.

Molten Fuel in the Coolant Channel

As is evident in Figs. 4 and 5, for the fresh fuel pin, there are two cases to consider:

1. (Fig. 3) Molten fuel enters the coolant channel and no significant molten fuel-coolant interaction (MFCI) takes place.
2. (Fig. 4) Molten fuel enters the coolant channel and a MFCI occurs.

The conditions leading to Case 1 are that a driving force exists to expell the fuel (experimentally observed) (Ref. 55, 56, 62) and one of the following:

1. Bulk temperature of the sodium coolant is very near the saturation temperature causing a vapor film to form between the sodium and the molten fuel. This prevents liquid-liquid contact and no MFCI will occur (Ref. 63, 64).
2. Fill gas escapes from the pin and prevents liquid-liquid contact provides a cushion for any pressure pulses produced and reduces the effect of the fragmentation mechanism (Ref. 64, 65).
3. Gross bulk boiling is present in the coolant channel with significant amounts of coolant vapor to provide the same effect as the fill gas in number 2 above.

For a MFCI to occur, as shown in Fig. 4, the fuel must form liquid-liquid contact with sodium. This is most likely in the case of clad failure by clad-fuel differential thermal expansion.

Once the fuel begins to move in the coolant channel, either dragged along by the sodium flow or expelled during the MFCI, it is not clear to what extent fuel clogs the channel and flow blockage will occur. This is true since movement will depend on fuel particle size distribution, presence of solid fuel in the channel, forces on the fuel particles and the mechanical details of the fuel pin subassembly structure (e.g., wire wrapping).

In any event, it is most probable that fresh fuel pin failure will result in substantial negative reactivity from the movement of the fuel. This is true since the fuel will move axially upward to the clad failure and then out into the channel where it is swept up by normal sodium flow or a MFCI occurs.

In the event of a MFCI, the resultant bubble expansion would be preferentially upward as the immediate restraining pressure from above is much less. This is true since in this direction, the bubble will loose heat in the immediate upper cooler region (Ref. 66, 67).

Summary

The following points concerning fresh fuel pins should be emphasized:

1. As shown in the right hand portion of Figs. 3 and 4, there are a number of possibilities which will prevent fresh pins from failing. In the case of a non-fresh core, internal fuel movement and the fact that irradiated pins will fail first (to be discussed) will in many cases prevent fresh fuel pin failure.
2. Three different mechanisms are possible to fail the fresh fuel pin cladding. All failures may be high in the core region and occur after significant coolant channel temperature increases.
3. A large possibility exists that the molten fuel will move into the channel, but no interaction will take place. The fuel would then be dragged by the normal sodium flow. This allows for the potential of delayed MFCI's if the vapor bubble collapses from condensation upon cold steel surfaces.
4. Interior and exterior molten fuel movement in fresh fuel pins can be expected to produce negative reactivity effects.
5. Experiments to determine the extent of fuel clogging and flow blockage as fuel attempts to move out of a subassembly are necessary.

In the following section, attention is directed to irradiated fuel pins.

Irradiated Fuel Pins

Description

Fuel pins other than fresh ones are divided here into two characteristic regions. Each irradiated fuel pin will have some combination or mixture of these depending on the axial and radial power shapes and the pin location. Table I is again useful for a simple summary of various fuel characteristics.

1. Low Power Region (< 9kw/ft) (Fuel at low operating temperature)

This portion is characterized by the presence of fission gas, unrestructured fuel and some equiaxed grain growth. The power level is insufficient to cause columnar grain growth and the associated central void. Fission gas is retained both in the radial center of the fuel pin (equiaxed grain region) and also in the unrestructured fuel. In addition clad strength has deteriorated and the fuel-clad gap is small.

Stress on the clad is caused by differential clad-fuel thermal expansion, intragranular (within the grains) fission gas induced fuel swelling and the transient release of intergranular (between the grains) fission gas (Ref. 50, 56). The intergranular fission gas is completely released upon fuel melting. In addition this intergranular fission gas may be released below melting depending on the temperature and available volume (Ref. 50, 61). The available volume in the solid fuel case consists of cracks, grain boundaries and interconnected pores, and in the molten case of the liquid zone. Because of the high temperature and limited volume for expansion, a very small amount of this gas can cause high local transient pressures.

2. High Power Region (>12kw/ft) (Fuel at high operating temperature)

In this region, fission gas is present, the fuel-clad gap is smaller and clad strength is reduced as before. The major change is that significant amounts of restructured fuel are present. There is a central void, columnar grain growth, equiaxed grain region and unrestructured fuel near its surface. The columnar and central void regions could account for 60% of the cross sectional area. Retained fission gas exists in significant amounts only in the outer equiaxed grain and unrestructured fuel regions.

Stress on the clad is produced by the same three mechanisms as in the low power case. In this portion, however, the amount of retained fission gas is much less.

Fuel Heatup and Movement Before Clad Failure

During irradiated fuel heatup and melt, axial fuel motion is possible. In a strictly low power fuel pin, with no central void, motion is possible in the same manner as described in the fresh fuel case and summarized in Table I. It is possible, however, that the fuel pellets may be fused together preventing radial seepage through the interfaces (Ref. 60, 61). Cracks and interconnected pores, however may be present to provide for radial movement (Ref. 60, 61, 68). In addition the fuel-clad gap will be smaller.

When the irradiated fuel does contain a central void, motion is possible in the void. Table III gives a summary of this motion. The important consideration here, is the available volume present in the central void for movement. If the axial temperature profile is quite flat, then fuel will tend to simultaneously melt along the entire central void thus preventing fuel movement.

When the equiaxed grain fuel melts, the retained entrapped fission gas is released and quickly expands. The resultant fuel-fission gas mixture is described in the literature as a froth or foam (Ref. 69-71). The froth which is much less dense than the liquid state will try to expand outwardly in the void (Ref. 67).

Clad Failure and Solid Fuel Shell Failure

The most likely cause of irradiated fuel pin failure is the transient release of intergranular fission gas (Ref. 50, 56) as summarized in Table I. This gas, which can be released before the melting temperature is reached (Ref. 50, 56, 59), expands against small cracks, interconnected pores or grain boundary walls. Resultant local pressures can, if properly located, work on the clad to produce its failure. Nearly all the remaining intergranular fission gas is released upon melting and is free to expand in the void volume. It must be emphasized also, that the other methods of producing clad strain as mentioned before and summarized in Table I will also contribute to clad failure (Ref. 61).

Clad failures from this mechanism should in general be local and not as large as fresh fuel pin failures. Failures will occur where there are large amounts of retained intergranular fission gas and high clad temperatures. For a fairly high power irradiated pin, the concentration of this retained gas will be higher towards the end of the fuel pin due to the axial power shape. Thus, clad failures will occur most probably between the center and top of the fuel pin core region. A logical sequence of events leading to an irradiated fuel pin MFCI is presented in Fig. 5.

TABLE III IRRADIATED FUEL PIN PRE-FAILURE FUEL MOVEMENT (CENTRAL VOID PRESENT)

	Central columnar grain fuel	Equiaxed grain fuel	Outer unrestructured fuel
Melt and movement description	Melts first, no fission gas is released. Molten liquid fuel formed. Gravity provides the force for possible movement.	Next radial section to melt. Fission gas is released and fuel froth formation is possible. Fission gas pressure will try to force froth away from the melting area.	Very likely that the fuel pin clad will fail before any significant amount of this fuel melts. If it does melt it will behave similar to the equiaxed fuel.
Effect of ramp size, axial temperature shape and central void size on fuel movement	A large axial temperature gradient, small ramp rate and large central void will increase amount of fuel movement.	Fuel movement will be effected in the same manner as in the columnar grain case.	Similar to equiaxed grain fuel.

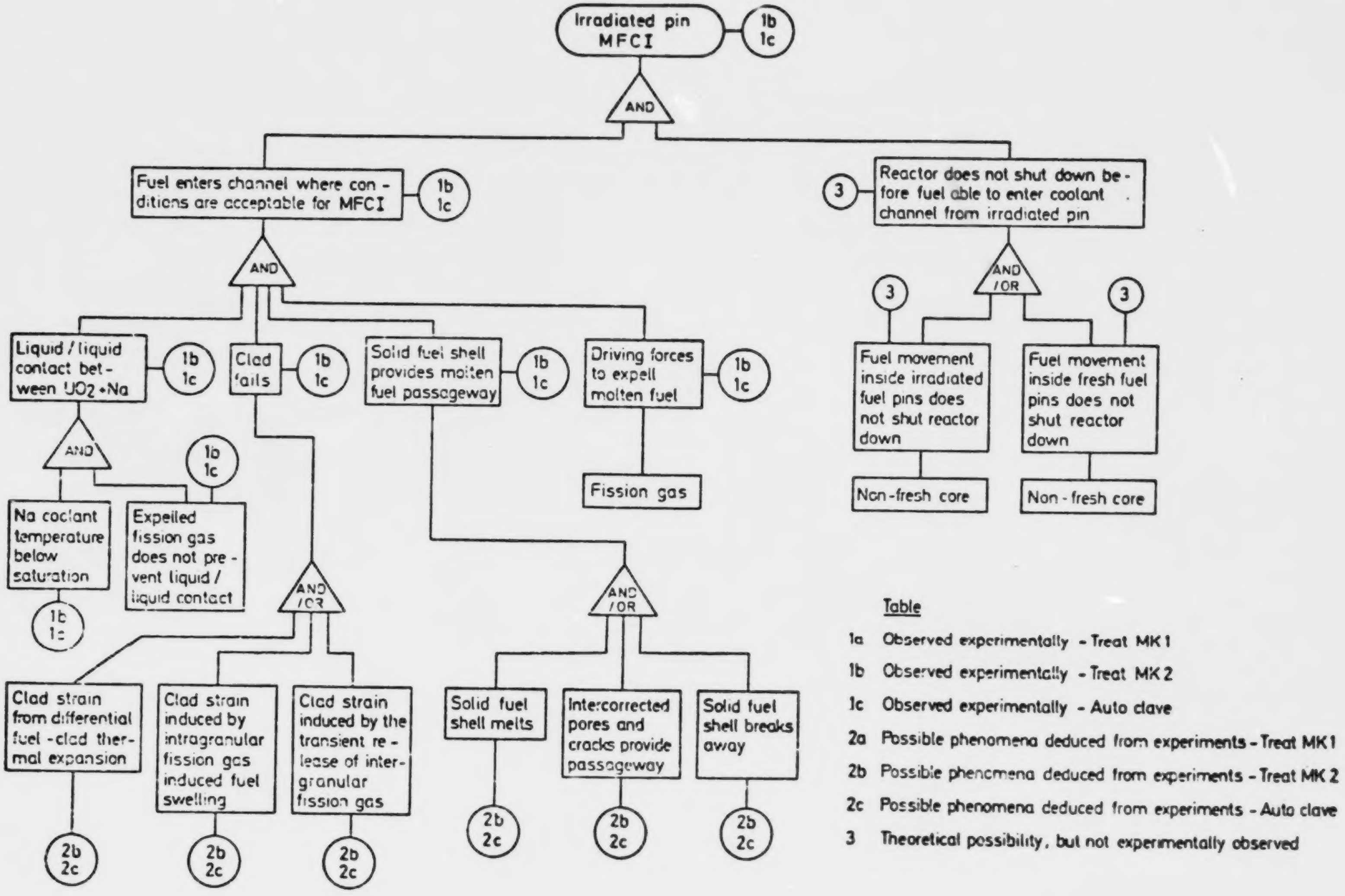
Irradiated pin MFCI
1b 1c
AND
Fuel enters channel where conditions are acceptable for MFCI
1b 1c
Reactor does not shut down before fuel able to enter coolant channel from irradiated pin
3
AND
AND /OR
3
3
Liquid / liquid contact between UO2 + Na
1b 1c
Clad fails
1b 1c
Solid fuel shell provides molten fuel passageway
1b 1c
Driving forces to expell molten fuel
1b 1c
Fuel movement inside irradiated fuel pins does not shut reactor down
Fuel movement inside fresh fuel pins does not shut reactor down
AND
1b 1c
Fission gas
Non-fresh core
Non - fresh core
Na coolant temperature below saturation
Expelled fission gas does not prevent liquid / liquid contact
1b 1c
AND /OR
AND /OR
Clad strain from differential fuel - clad thermal expansion
Clad strain induced by intragranular fission gas induced fuel swelling
Clad strain induced by the transient release of intergranular fission gas
Solid fuel shell melts
Intercorrected pores and cracks provide passageway
Solid fuel shell breaks away
2b 2c
2b 2c
2b 2c
2b 2c
2b 2c
2b 2c

Table

1a	Observed experimentally - Treat MK1
1b	Observed experimentally - Treat MK2
1c	Observed experimentally - Auto clave
2a	Possible phenomena deduced from experiments - Treat MK1
2b	Possible phenomena deduced from experiments - Treat MK2
2c	Possible phenomena deduced from experiments - Auto clave
3	Theoretical possibility, but not experimentally observed

Fig.5. Irradiated Fuel Pin, Molten Fuel-Coolant Interaction.

The fact that clad failure has occurred does not lead directly to molten fuel release. The fission gas which caused the failure will escape immediately into the coolant channel. References 55 and 68 show that this gas volume can possibly blanket a portion of the clad and cause clad melt. Calculations based upon observed phenomenon in test specimen C4J (Ref. 72) indicate that this occurred in a period of 200 msec after gas release. Thus, this mechanism is not considered important for these short transients (Ref. 72).

As indicated in Fig. 5, additional fission gas, from fuel will not escape from the pin until the solid fuel shell around the molten zone is penetrated. The solid fuel remaining may be composed of both restructured and unrestructured fuel which will have different passage properties. The inner restructured region will contain passageways. At low burnups, sufficient radial crack volume will exist to pass fission gas or a limited amount of fuel. Numerous cracks about 10 μ in width will be present. At burnups greater than .5 atom.% interconnected radial pores roughly 50 to 100 μ apart with .5 to 10 μ diameter will be present (Ref. 68). The outer unrestructured fuel region, which is of most importance here, will most likely have some radial crack volume depending on burnup power and transient effects. In addition, the fuel pellets will probably be fused together preventing seepage through the interface (Ref. 60, 61).

It is most likely that no appreciable passageway will exist to allow for significant fuel ejection. First, the solid fuel shell must be broken by additional stress, weakening through melting or a combination of these mechanism. Next, and only after a clear path for fuel escape exists, the effects of fuel in the coolant channel must be considered.

Molten Fuel In the Coolant Channel

It should be reemphasized that clad failure, especially in low irradiated fuel pins, can take place before any appreciable melting can occur. Thus it is quite possible that during the transient, more than one local failure could occur.

The state of a typical irradiated fuel pin at this point of the transient is characterized by one or more clad failures. In addition, a passageway is present for fuel and fission gas escape. A small volume of fission gas causing the clad failure should have already escaped.

A driving force from the high pressure fission gas is available to eject the fuel or froth. It is not clear exactly how large the fission gas volume will be since this depends on the communication of the gas plenum. Reference 73 discusses an experiment where fission gas release rates were determined from punctured irradiated pins 40,000 MWd/Mt. Results indicate that the rate was between .0002 %/msec* for the first 40 seconds depending on puncture location. Since the test was conducted at room temperature, there are two competing effects. First, the fission gas pressure would be 3 to 3 1/2 times higher at operating conditions. Second, the resistance to flow would most likely be greater at operating temperature since the clad-fuel gap is opened up and radial cracking occurred when the fuel pin were cooled down. It is considered here and elsewhere in the literature, that the gas plenum is effectively isolated during the short duration of the transient (Ref.50,61).

For a given failed irradiated fuel pin, the higher the operation power, the larger the amount of fuel that may initially flow in the channel. This characteristic is further developed in Table IV. In addition, it follows that smaller volumes of fission gas will be expelled initially, the higher the pin operating power. As the transient proceeds more fuel will melt, more froth will be produced and this mixture will move into the coolant channel when the pressure gradient is sufficient.

---

*Figures here give percent of fuel pin initial gas volume escaping per msec.

The molten fuel-coolant interaction (MFCI) will be limited by the following factors:

1. Existence of significant amounts of fission gas in the coolant channel both separate and mixed with the fuel in the fuel froth.
2. The limited amount of the fuel gas mixture discharged into the channel will limit the first interactions because of the sodium vapor present in the channel.
3. Since the failure is most likely high in the core, the upward expulsion slug will lose heat quickly as vapor condensation will occur to the sodium film on the blanket cladding, fuel pin top piece and other surrounding colder material (Ref.66,67).

Fission gas and sodium vapor reduces the effect of the MFCI for three reasons:

1. The amount of liquid-liquid contact is reduced by the interference of the gas.
2. The postulated mechanisms which fragment the molten fuel have less energy when gas is present.
3. The gas will provide cushioning action against any pressure pulses produced.

Again as in the case of fresh fuel pins, the possibility of delayed MFCI's exists. It is not clear to what extent fuel clogs the channel and coolant flow blockage will occur.

Summary

The following points concerning irradiated fuel pins should be emphasized:

1. In similar environments, an irradiated fuel pin will probably fail before a fresh fuel pin. In addition the low power irradiated fuel pin may likely experience one or more clad failures before appreciable fuel melting.
2. Internal fuel movement in irradiated fuel pins is possible but very hard to predict.
3. Clad failures may be likely to occur at or above the axial centerplane, although there is nothing to prevent failure at any axial height. The higher the fuel pin operating power, the higher the potential for clad failure location (Table IV) due to the stresses presently considered.
4. Fission gas, the limited amount of fuel ejection and the possible presence of sodium vapor will tend to reduce the effect of the molten fuel-coolant interaction.

TABLE IV IRRADIATED FUEL PIN RELEASE BEHAVIOR VERSUS OPERATING POWER

Behavior	**Higher** fuel pin operating power (Higher operating temperature)
Amount of retained fission gas	Less
Relative clad failure time	Nearly the same, perhaps a few milliseconds spread between high and low power pins in the same environment depending on the ramp rate
Relative clad failure locations	Higher in the core corresponding to retained fission gas concentration
Amount of molten fuel at failure time	more
Escaping material characteristics	Decreases amount of fission gas separately escaping and decreases amount of fission gas in fuel-fission gas mixture (froth)

2.1.2.7 Conclusions

The case of a total fresh core is much different from that when irradiated fuel pins are present. In the fresh core, main consideration is focused on the clad failure mechanism and coolant channel conditions at failure time. Thus, two discrete options evolve, either the channel conditions are acceptable for a molten fuel-coolant interaction or they are not. Logically proceeding then, either the sodium vapor resulting from an MFCI or the normal sodium flow will drag the molten fuel. Delayed MFCI's could also occur.

The non-fresh core composed of various quantities of irradiated and fresh fuel pins will exhibit, in contrast, a diverse behavior. The fresh fuel pins (depending somewhat on their location) will not likely fail because the irradiated pins will tend to fail earlier in the transient and insert large amounts of negative reactivity. Failure of irradiated fuel pins will result in a range of values for quantities such as melt fraction at time of clad failure, clad failure locations, amount of fuel entering the channel, and ratio of fuel-fission gas entering the channel. This occurs because the pins form a spectrum of mixtures of high and low power fuel characteristics. Thus, as a subassembly group of irradiated fuel pins fail, a range of resultant molten fuel-coolant interactions and reactivity effects will follow.

In a given enrichment zone, non-fresh fuel would likely fail from the radial center outward or high operating power pins first to low operating pins last. This is true since high operating power pins will experience a larger input energy rate. Thus it may be expected that a band of behavioral characteristics as shown in Figure 6 would occur. In addition, the source of fuel movement would vary from vapor drag (high operating power fuel pin) to drag motion from fission gas and normal sodium flow (low operating power fuel pin). It is difficult to assess the resultant reactivity effects as a function of the operating power of failed subassemblies. This is true since the reactivity caused by sodium expulsion, direction and speed of fuel movement and fuel worth must be considered.

The effect of input ramp rate, burnup and pin operating power upon clad failure location was assessed using simple models in the HOPE code (Refs.74,74,76). In addition, the effect of clad failure location upon the nature of the accident was studied using HOPE and some results are shown in TABLE IV. The results which depend on the models in the computer code and specific reactor design show that if the pins are forced to

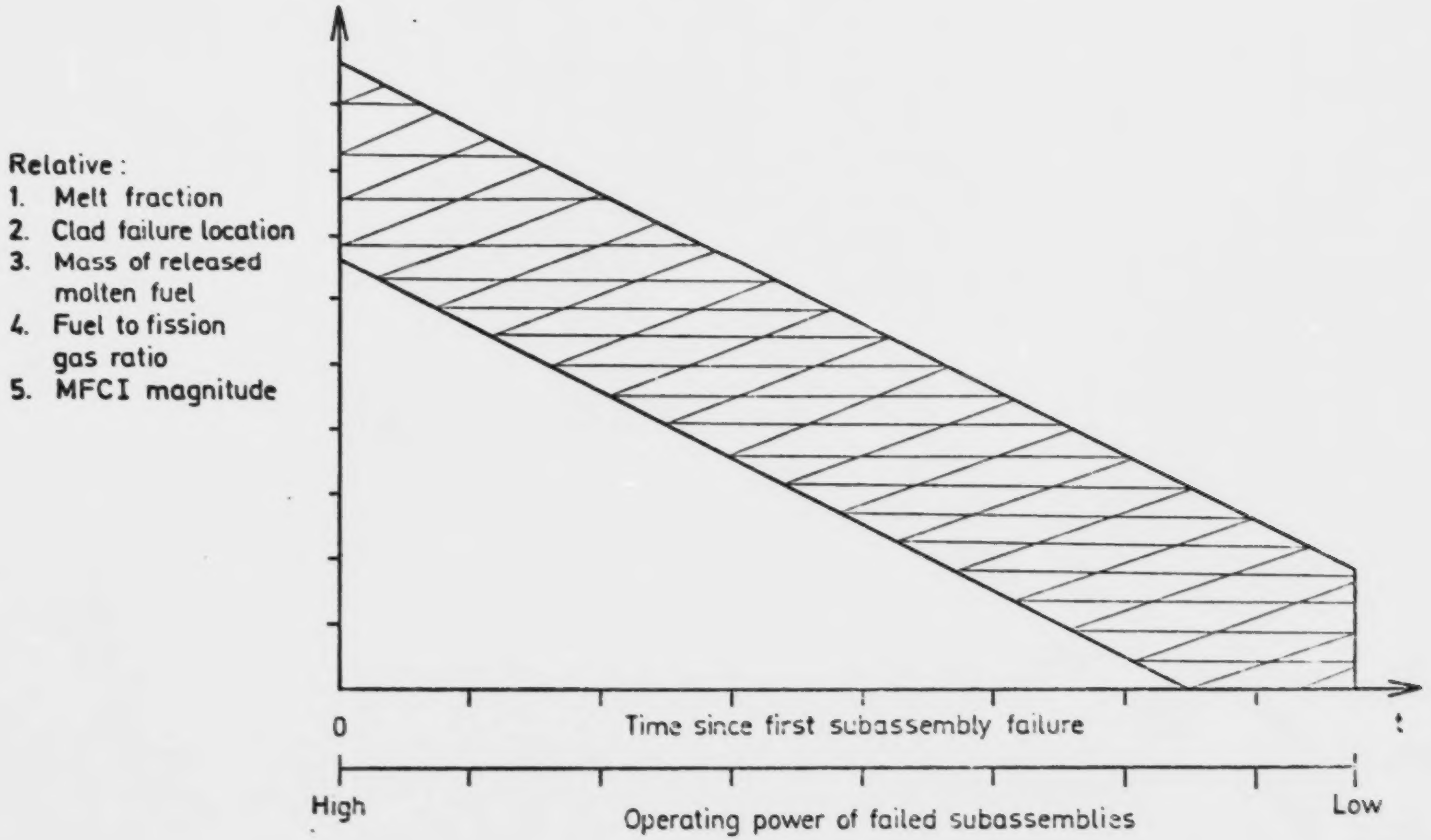

Fig. 6 Irradiated fuel pin failure behavior in one enrichment zone

fail at the midplane, the accident is severe and leads to loss of core structural integrity. This occurred in TABLE IV in all midplane or low failure cases except the \$.10/sec ramp rate case, Case 17. When the fuel pin failures occur above the midplane, the accidents are much less severe. For the \$.50/sec cases, Cases 7-10, the core shuts down and may maintain structural integrity for some time.

Future research and analysis dealing with the overpower excursion accident should emphasize fuel pin failure modes. This entails experimental and analytical studies of fuel and clad behavior during steady state and transient operations. Specific phenomena that need further investigation include the following (Ref. 74).

1. Refined steady state clad and fuel conditions at the time the excursion begins should be accounted for. Effects such as fuel and clad swelling, thermal expansion, clad creep, and loss of ductility should be considered when determining the initial state of the fuel and clad. Axially dependent variations, for example, might cause a specific axial portion of the clad to be stressed to the elastic limit or be especially brittle as the excursion commences thus influencing the clad failure location.

TABLE IV

WHOLE CORE STUDIES OF SNR - 300 Mark 1

Case	Input Ramp ($ SEC)	Pin Failure Loc.[1]	BU AT%	HOPE RESULTS[2]	#CH. Failed[3]	Time of First Pin Failure (SEC)	Max. Total ΔK/K ($)[4]
1	5.0	Midplane	0	C	9	.34	.34[4]
2	5.0	P	0	B	7	.34	.34[4]
3	5.0	P	2	C	9	.32	.33[4]
4	1.0	P	0	A	4	1.53	.80
5	1.0	P	2	B	9	1.46	1.65[4]
6	0.5	Midplane	0	C	8	2.78	2.78[4]
7	0.5	P	0	A	3	2.78	.67
8	0.5	P	2	A	4	2.67	.65
9[5]	0.5	P	2	A	5	2.82	.85
10	0.5	P	10	A	5	2.63	.70
11	0.5	Midplane	2	C	9	2.67	2.69
12	0.5	Low	2	C	9	2.67	2.69
13	0.2	Midplane	0	C	8	5.90	5.90[4]
14	0.2	Midplane	2	C	9	5.78	5.83[4]
15	0.2	Low	0	C	5	5.90	5.91[4]
16	0.2	Low	2	C	9	5.78	5.82[4]
17	0.1	Midplane	2	A	5	10.18	.88

NOTES:

1. P = Predicted by HOPE, Low = 26% Active Core Height
2. A = Core shutdown, structural integrity maintained, B = Core shutdown after reaching prompt criticality, structural integrity questionable, C = Core loses structural integrity, disassembly likely.
3. 10 Channel representation, Channel #10 = Radial blanket.
4. Prompt criticality reached, time (sec) when ΔK/K first equals 1.0 specified.
5. Case 9: Operating Power = 69% of Nominal.

2. Further studies concerning transient fuel swelling should be conducted. Both detailed evaluations of bubble behavior and integrated studies in which the influence of the fuel's hydrostatic stress is directly included are needed to further understand fuel swelling. In addition, the compressibility of gas bearing fuel should be determined for calculations of the fuel pin's internal pressure (especially at high pressures).

3. The extent and characteristics of fuel cracking (if it occurs) during the transient is necessary to analyze fuel pin failure modes. Fuel cracks provide free space for enhanced free fission gas movement and also reduce the strength of the fuel. Experimental information is difficult to obtain since post-transient cooldown may cause fuel cracking.

4. Further understanding of the mobility of gas bubbles caused by the connection of various free spaces in the fuel (e.g. fragmented grain boundaries, pores and cracks) is necessary. Released intergranular fission gas is another source of clad strain since it can. either directly or through the fuel, transmit stress to the clad. In addition, further knowledge of expected bubble sizes of fission gas released during the melting process is necessary to develop an improved Equation of State for molten fuel-fission gas mixtures.

5. The ability and extent of the gas plenum to communicate with the fuel pin cavity during the transient should be further investigated. Perhaps experiments using fuel pins with a small gas plenum could not only provide information about gas flow rates, but also help determine the extent of fuel cracking during overpower excursions.

6. Axial fuel motion within the fuel pin cavity before clad failure should be studied to determine if and when this may be a significant factor. Pin failure times and locations may be sensitive to this effect since outward axial motion of the solid pellets will cause pressure relief in the cavity.

7. Other additional factors should be considered in fuel pin failure studies. Clad manufacturing defects, hot spots,aggravated areas from fuel pellet interactions during operation and the effects of wirewraps or spacers may influence failure locations in significant quantities of fuel pins. In addition, fuel pins may experience multiple failures.

With a more comprehensive understanding of these effects, an integrated fuel pin mechanics model can be developed and checked with experiments. Until more knowledge concerning pin failures can be gained, failure location should be treated as an input parameter. The analysis should be carried out at a number of failure heights.

Additional areas for future research include further investigations of molten fuel-clad interactions and the effects of this phenomenon on fuel motion. Following this, studies of ejected fuel motion and deposition in the primary system should be analyzed for extended periods of time. In the future, detailed safety analyses must also be carried out for larger systems which contain advanced types of fuel.

REFERENCES

1. Bethe, H. A. and J. H. Tait. "An Estimate of the Order of Magnitude of the Explosion When the Core of a Fast Reactor Collapses," United Kingdom Atomic Energy Authority, Harwell, England, UKAEA-RHM(56)/113, April 1956.

2. Koch, L. J., et al. "Hazard Summary Report--Experimental Breeder Reactor II (EBR-II)," Argonne National Laboratory, Argonne, Illinois, ANL-5719, 1957.

3. Okrent, D., et al. "AX-1, A Computing Program for Coupled Neutronics-Hydrodynamics Calculations on the IBM-704," Argonne National Laboratory, Argonne, Illinois, ANL-5977, 1959.

4. Hirakawa, N. "MARS--A Two-dimensional Excursion Code," Atomic Power Development Associates, Detroit, Michigan, APDA-198, June 1967.

5. Sha, W. T. and T. H. Hughes. "VENUS: A Two-dimensional Coupled Neutronics-Hydrodynamics Computer Program for Fast-Reactor Power Excursions," Argonne National Laboratory, Argonne, Illinois, ANL-7701, October 1970.

6. Jackson, J. F. and R. B. Nicholson. "VENUS-II: An LMFBR Disassembly Program," Argonne National Laboratory, Argonne, Illinois, ANL-7951, 1972.

7. R.B. Nicholson and J.F. Jackson, "A Sensitivity Study for Fast-Reactor Disassembly Calculations", Argonne National Laboratory, Argonne, Illinois, ANL-7952, 1974.

8. Jackson, J. F., et al. "Trends in LMFBR Hypothetical-Accident Analysis," Proceedings of the Conference on Fast Reactor Safety, Beverly Hills, California, April 1974, American Nuclear Society, to be published [will be available from the U.S. National Technical Information Service, USAEC, CONF-740401].

9. Stevenson, M. G., et al. "Current Status and Experimental Basis of the SAS LMFBR Accident Analysis Code System," Proceedings of the Conference on Fast Reactor Safety, Beverly Hills, California, April 1974, American Nuclear Society, to be published [will be available from the U.S. National Technical Information Service, USAEC, CONF-740401].

10. Freund, G. A., et al. "Design Summary Report on the Transient Reactor Test Facility (TREAT)," Argonne National Laboratory, Argonne, Illinois, ANL-6034, 1960.

11. Agrawal, A. K., C. E. Dickerman and A. B. Rothman. "Analysis of Fuel Failure Experiments in Treat," Proceedings of the Conference on New Developments in Reactor Mathematics and Applications, Idaho Falls, Idaho, March 1971, American Nuclear Society, 1971, Vol. 1, pp. 97-101 [available from the National Technical Information Service, USAEC, CONF-710302(1)].

12. Dickerman, C. E., L. W. Deitrich, L. E. Robinson, A. B. Rothman, and J. C. Carter. "Fuel Dynamics Experiments on Fast Reactor Oxide Fuel Performance Under Transient Heating Conditions Using the TREAT Reactor," Proceedings of the Conference on Fast Reactor Fuel Element Technology, New Orleans, April 1971, American Nuclear Society, Hinsdale, Illinois, 1971, pp. 643-655.

13. MacFarlane, D. R., N. A. McNeal, T. J. Heames, W. T. Sha, and C. L. Youngdahl. "Reactivity Transients Leading to Disassembly in Oxide-Fueled Fast Reactors," Trans. Am. Nucl. Soc., 12:342-343, 1969 (paper presented at ANS Annual Meeting, Seattle, Washington, June 1969).

14. Sha, W. T. and A. E. Waltar. "An Integrated Model for Analyzing Disruptive Accidents in Fast Reactors," Nuclear Science and Engineering, 44:135-156, May 1971.

15. MacFarlane, D. R., ed. "SAS1A, A Computer Code for the Analysis of Fast Reactor Power and Flow Transients," Argonne National Laboratory, Argonne, Illinois, ANL-7607, October 1970.

16. Dunn, F. E., T. J. Heames, P. A. Pizzica, and G. Fischer. "The SAS2A LMFBR Accident Analysis Code," Proceedings of the Conference on New Developments in Reactor Mathematics amd Applications, Idaho Falls, Idaho, March 1971, American Nuclear Society, Vol. 1, pp. 120-127 [available from the National Technical Information Service, USAEC, CONF-710302].

17. Freeman, D. D. "FREADM Code Development--A Status Report," Breeder Reactor Development Operation, General Electric Co., Sunnyvale, California, GEAP-13936, 1973.

18. Waltar, A. E., A. Padilla Jr., and R. J. Shields. "MELT-II, A Two-Dimensional Neutronics-Heat Transfer Program for Fast Reactor Safety Analysis," Hanford Engineering Development Laboratory, Richland, Washington, HEDL-TME 72-43, April 1972.

19. Lorenzini, P. G. and G. F. Flanagan. "An Evaluation of Fuel-Coolant Interactions During Disassembly of an LMFBR," *Proceedings of the Conference on New Developments in Reactor Mathematics and Applications*, Idaho Falls, Idaho, March 1971, American Nuclear Society, Vol. 1, pp. 50-78 [available from the National Technical Information Service, USAEC, CONF-710302].

20. Mills, J. C. and W. E. Kastenberg. "An Axial Kinetics Model for Fast Reactor Disassembly Accidents," *Proceedings of the Conference on New Developments in Reactor Mathematics and Applications*, Idaho Falls, Idaho, March 1971, American Nuclear Society, Vol. 1, pp. 167-179 [available from the National Technical Information Service, USAEC, CONF-710302].

21. Kastenberg, W. E. and E. T. Rumble. "On the Analysis of the Pre-disassembly Phase of the Unprotected Overpower Transient Accident for LMFBR's," *Nuclear Engineering and Design*, 25:248-256, July 1973.

22. Okrent, D., K. P. Cohen, and W. B. Loewenstein. "Some Nuclear and Safety Considerations in the Design of Large Fast Power Reactors," *Proceedings of the Third International Conference on the Peaceful Uses of Atomic Energy*, Geneva, 1964, 6:137-148.

23. Culley, G. E., J. E. Hanson, W. L. Partain, J. H. Scott, and A. E. Waltar. "Fast Reactor Safety Implications of Recent Assessments of Fuel Pin Transient Behavior," *Proceedings of the Conference on Engineering of Fast Reactors for Safe and Reliable Operation*, Karlsruhe, October 1972, Gesellschaft für Kernforshung, Karlsruhe, Germany, 1973, Vol. II, pp. 626-642.

24. Watanabe, A. and A. M. Judd. "A Computer Code for Predicting the Behavior of Oxide Fuel in Accidents," *Trans. Am. Nucl. Soc.*, 14: 733-735, 1971 (paper presented at ANS Winter Meeting, Miami Beach, Florida, October 1971).

25. Royl, P., A. Watanabe, and A. K. Agrawal. "Transient Fuel-Cladding Deformation Analysis of the In-Pile H3 TREAT Test with the SAS2A/DEFORM-II Code," *Proceedings of the 2nd International Conference on Structural Mechanics in Reactor Technology*, Berlin, 1973, International Association for Structural Mechanics in Reactor Technology, to be published [will be available from North-Holland Publishing Company, EUR-4820].

26. Dias, J. W. and R. B. Poeppel. "Transient Swelling Studies with the GRASS Code," Argonne National Laboratory, Argonne, Illinois, ANL-7992, 1973.

27. Dias, J.W. Analysis of the Behavior of Fission Product Gas in Solid Fast Reactor Oxide Fuel Under Transient Heating Conditions, Ph.D. Dissertation in Engineering, University of California, Los Angeles, July 1973 and Erdmann, R.C. "Transient Analysis of LMFBR Oxide Fuel Elements During Accidents," UCLA-ENG.-7362, Aug. 1973.

28. Poeppel, R. B. "An Advanced Gas Release and Swelling Subroutine," Proceedings of the Conference on Fast Reactor Fuel Technology, New Orleans, April 1971, American Nuclear Society, Hinsdale, Illinois, 1971, pp. 311-326.

29. Cronenberg, A. W. "A Thermodynamic Model for Molten UO_2-Na Interaction, Pertaining to Fast-Reactor Fuel-Failure Accidents," Argonne National Laboratory, Argonne, Illinois, ANL-7947, June 1972.

30. Smith, L. L., J. R. Travis, M. G. Stevenson, F. E. Dunn, and G. J. Fischer. "SAS/FCI, A Fuel-Coolant Interaction Model for LMFBR Whole-Core Accident Analysis," Proceedings of the Topical Meeting on Mathematical Models and Computational Techniques for Analysis of Nuclear Systems, Ann Arbor, Michigan, April 1973, American Nuclear Society, 1973, Vol. 1, pp. 137-158 (available from the U.S. National Technical Information Service, USAEC, CONF-730414-P1].

31. Cho, D. H., R. O. Ivins, and R. W. Wright. "A Rate-Limited Model of Molten Fuel/Coolant Interactions: Model Development and Preliminary Calculations," Argonne National Laboratory, Argonne, Illinois, ANL-7919, March 1972.

32. Caldarola, L. "The State of the Art of the Molten Fuel/Sodium-Thermal Interaction after the CREST Second Specialist Meeting on Sodium Fuel Interaction in Fast Reactors, held in Ispra in November 1973," Gesellschaft für Kernforschung, Karlsruhe, Germany, KFK 1944, to be published.

33. Wider, H. "An Improved Analysis of Fuel Motion During an Overpower Excursion," Proceedings of the Conference on Fast Reactor Safety, Beverly Hills, California, April 1974, American Nuclear Society, to be published [will be available from the U.S. National Technical Information Service, USAEC, CONF-740401].

34. Wider, H. An Improved Analysis of Fuel Motion During an Overpower Excursion, Ph.D. Dissertation in Engineering, Northwestern University, Evanston, Illinois, November 1973.

35. Willenberg, H. J., W. L. Partain, and A. E. Waltar. "Dynamics of Molten Fuel Motion During a Fast Reactor Overpower Transient," Proceedings of the Conference on Fast Reactor Safety, Bevery Hills, California, April 1974, American Nuclear Society, to be published [will be available from the U.S. National Technical Information Service, USAEC, CONF-740401].

36. Angerer, G., E. A. Fischer, B. Kuczera, D. Struwe, and P. H. Wirtz. "CAPRI-A Computer Code for the Analysis of Hypothetical Core Disruptive Accidents in the Predisassembly Phase," Proceedings of the Conference on Fast Reactor Safety, Bevery Hills, California, April 1974, American Nuclear Society, to be published [will be available from the U.S. National Technical Information Service, USAEC, CONF-740401].

37. Rothman, A. B., C. E. Dickerman, R. C. Doerner, A. E. Wright, and L. W. Deitrich. "A Review of TREAT Experiments in Support of Transient Overpower (TOP) Analysis for Fast Reactor Safety," Proceedings of the Conference on Fast Reactor Safety, Beverly Hills, California, April 1974, American Nuclear Society, to be published [will be available from the U.S. National Technical Information Service, USAEC, CONF-740401].

38. Rumble, E. T. "Analysis of Experiments and Suggested Models for Examining a LMFBR Hypothetical Whole-Core Unprotected Overpower Transient," Gesellschaft für Kernforschung, Karlsruhe, Germany, Projekt Schneller Bruter Bericht Nr. 430/73, February 1973.

39. Epstein, M., and D. H. Cho. "Fuel Vaporization and Quenching by Cold Sodium; Interpretation of TREAT Test S-11," Proceedings of the Conference on Fast Reactor Safety, Beverly Hills, California, April 1974, American Nuclear Society, to be published [will be available from the U.S. National Technical Information Service, USAEC, CONF-740401].

40. Sonnichsen, J. C., W. L. Partain, R. J. Shields, and A. E. Waltar. "Analytic Modeling of MKII-A TREAT Loop for Fuel Motion and Sodium Experimental Studies," Proceedings of the Conference on Fast Reactor Safety, Beverly Hills, California, April 1974, American Nuclear Society, to be published [will be available from the U.S. National Technical Information Service, USAEC, CONF-740401].

41. Erdman, C. A., P. L. Garner, P. M. Haas, and A. B. Reynolds. "Improvements in Modeling Fuel-Coolant Interactions and Interpretation of the S-11 TREAT Test," Proceedings of the Conference on Fast Reactor Safety, Beverly Hills, California, April 1974, American Nuclear Society, to be published [will be available from the U.S. National Technical Information Service, USAEC, CONF-740401].

42. Watanabe, A., and M. G. Stevenson. "Preliminary Cladding Deformation Analysis of H5 TREAT Test by SAS2A/DEFORM-II," Trans. Am. Nucl. Soc., 17:363-364, 1973 (paper presented at ANS Winter Meeting, San Francisco, California, November 1973).

43. Board, S. J., and C. L. Farmer. "Fragmentation in Thermal Explosion," Berkeley Nuclear Laboratories, Central Electricity Generating Board, Berkeley, England, RD/B/N 2423, October 1972.

44. Armstrong, D. R., et al. "Interaction of Sodium with Molten UO_2 and Stainless Steel Using a Dropping Mode of Contact," Argonne National Laboratory, Argonne, Illinois, ANL-7890, December 1971.

45. Ivins, R. O. "Interactions of Fuel, Cladding and Coolant," Argonne National Laboratory, Argonne, Illinois, Reactor Development Progress Report, ANL-7399, December 1967.

46. Farahat, M. M. "Transient Boiling Heat Transfer from Spheres to Sodium," Argonne National Laboratory, Argonne, Illinois, ANL-7909, 1972.

47. Caldarola, L. and W. E. Kastenberg. "A Model and Conditions for Fragmentation During Molten Fuel/Sodium Interactions," *Proceedings of the 2nd International Conference on Structural Mechanics in Reactor Technology*, Berlin, 1973, International Association for Structural Mechanics in Reactor Technology, to be published [will be available from North-Holland Publishing Company, EUR-4820].

48. Aldeanueva, J.M., et al., "Damage to an LMFBR Fuel Assembly Duct Following Fuel Failure," Transactions of the American Nuclear Society, 141 (June 1971) 287.

49. Pedersen, D.R., et al. "Subassembly - to Subassembly Failure Propagation," *ANL-RDP 8*, (August, 1972) 9.1.

50. Culley, G.E. etal., "Fast Reactor Safety Implications of Recent Assessments of Fuel Pin Transient Behavior," *International Conference on Engineering of Fast Reactors for Safe and Reliable Operation*, Karlsruhe (1972).

51. Steinar, AAS., "Mechanical Interaction Between Fuel and Cladding," *Nuclear Engineering and Design*, 21 (1972) 237.

52. Burgess, C.A. and French, P.M. "Evolution: FTR Fuel Pin Design to Procurement," *American Nuclear Society Proc. of the New Orleans Conf. on Fast Reactor Fuel Element Technology*,

53. Thomas, G.R. and Field, J.H., "Response of Axially Restrained Pellet Fuel to Transient Overpower," *Trans. of the American Nuclear Society*, 11 2 (1968) 697.

54. Thomas, G.R. and Field, J.H. "Destructive Examination of an Axially Restrained Pelleted Mixed-Oxide Specimen That Failed During Transient Overpower Conditions," *Trans. of the American Nuclear Society*, 11 2 (1968) 697.

55. Thomas, G. and J. Field "Oxide Fuel Behavior During Transient Overpower Conditions," American Nucl. Soc. Proc. of the New Orleans Conf. on Fast Reactor Fuel Element Technology, (April, 1971) 679.

56. Culley, G.E., et al. "Transient Overpower Response of Mixed-Oxide Fuel Pins," Trans. of the Amer. Nucl. Soc., 15, (1972) 341.

57. Dickerman, C.E. et al. "Fuel Dynamics Experiments on Fast Reactor Oxide Fuel Performance Under Transient Heating Conditions Using the TREAT Reactor," Trans. of the Amer. Nucl. Soc., 14, 1 (April, 1971) 28 (Experiment E-2).

58. Agrawal, A.K. "Analysis of Pin Failure in a Closely Packed Seven-Pin Cluster Autoclave Experiment," Trans. of the Amer. Nucl. Soc., 14, 2 (Oct. 1971) 731 (Experiment S-6).

59. Hanson, J.E. and W.R. Roake "FTR Driver Fuel Development Program Status," Amer. Nuc. Soc., Proc. of the New Orleans Conf. on Fast Reactor Fuel Element Technology, (April, 1971) 497.

60. Lambert, J.D.G. et al. "Performance of Mixed-Oxide Fuel Elements - ANL Experience," Amer. Nuc. Soc. Proc. of the New Orleans Conf. on Fast Reactor Fuel Element Technology, (April 1971) 517.

61. Culley, G.E. et al. "Response of an EBR-II Irradiated Mixed-Oxide Fuel Pin to an Overpower Transient in TREAT," Amer. Nucl. Soc. Proc. of the New Orleans Conf. on Fast Reactor Fuel Element Technology, (April, 1971) 657.

62. Dickermann, C.E. et al., "Fuel Dynamics Experiments on Fast Reactor Oxide Fuel Performance Under Transient Heating Conditions Using the TREAT Reactor," Amer. Nuc. Soc. Proc. of the New Orleans Conf. on Fast Reactor Fuel Element Technology (April, 1971) 643.

63. Caldarola, L. and Kastenberg. W.E., "A Model for Fuel Fragmentation During Fuel/Coolant Thermal Interaction and Description of an Experiment to Prove the Validity of the Proposed Model," IASR-RSP-Notiz Nr. 47, Kernforschungszentrum Karlsruhe, 1973.

64. Caldarola, L. Personal Communication, 31, Jan 1973.

65. Cho, D.H., et al, "Effects of Gas/Vapor Blanketing on Pressure Pulses and Mechanical Work Produced by Molten Fuel/Coolant Interactions," *Trans. of the Amer. Nucl. Soc*., 15 (1972) 344.

66. Cronenberg, A.W. and H.K. Fauske, "Some Safety Aspects of Film Condensation During Fuel-Failure Accidents," *Trans. of the Amer. Nucl. Soc*.,14 2 (Oct. 1971) 739.

67. Tilbrock, R.W. "Effect of Condensation on Fuel-Sodium Interaction Voiding Transients," *Trans. of the Amer. Nucl. Soc*., 14 1 (June 1971) 241.

68. Carelli, M.D. and R.D. Cabfield, " Fission Gas Ejection Characteristics and their Effect on Adjacent Fuel Pins in an LMFBR," *American Nuclear Society Proc. of the New Orleans Conf. on Fast Reactor Fuel Technology* (April 1971) 617.

69. Wolfe, B. "Liquid Metal Fast Reactor Accidents," *Amer. Nucl. Soc. Material Topical Meeting on New Developments in Reactor Mathematics and Applications*, Idaho Falls, Idaho (March 1971) 1.

70. Stuart, R.G. and G.R. Thomas, "Effects of Fission Gas on Transient Overpower Fuel Rod Failure," *Trans. of the Amer. Nucl. Soc*. 13, 2 (1970) 654.

71. Fisher, G.J., et al., "Progress in Analysis of Severe Accidents," *Intl. Conf. on Eng. of Fast Reactors for Safe and Reliable Operation*, Karlsruhe (1972).

72. Thomas, G. R. and J.H. Field, "Transient Performance of Mixed Oxide Powder Fuel With up to 60% Melting," *Trans. of the Amer. Nucl. Soc.,* 12, (1969) 343 (Exp. C45).

73. Craig, C.N. et al., "Steady State Performance of PuO_2-UO_2 Fast Reactor Fuels," *Amer. Nuc. Soc. Proc. of the New Orleans Conf. on Fast Reactor Fuel Element Technology* (April 1971) 555.

74. Rumble, E.T. "A Hypothetical Overpower Excursion Model for Liquid Metal-Cooled Fast Breeder Reactors," PhD. Dissertation in Engineering, June 1974, University of California, L.A.

75. Rumble, E.T., W.E. Kastenberg, D. Okrent and J.O. Cermak "Fuel Movement Investigations During LMFBR Overpower Excursions Using a New Model," Proc. of the Fast Reactor Safety Meeting, Beverly Hills, Calif. April, 1974.

76. Rumble, E.T., W.F.Kastenberg, D. Okrent, "Sensitivity Analysis of an LMFBR to Whole Core Overpower Excursion," Trans. of the ANS, 1974 Winter Meeting, 1974.

2.1.3 Core Clamp Initiated Accidents

Because of stainless steel swelling it is necessary to restrain an LMFBR core from radiation induced growth in the radial direction. This requires the use of either fixed or adjustable vise-like clamps at several axial locations - usually the midplane and top. It is possible that the clamped geometry is not the most compact geometry. With further irradiation, in this clamp-restrained geometry, stresses will buildup and slippage or internal core readjustments may occur that result in reactivity changes. Some informal worst case analyses have predicted as much as 60ϕ reactivity change. In this compilation no documents have been found that present this information. There have been informed discussions which are the bases of the preceding discussion. It is important to assume in the design of an LMFBR that these sudden changes cannot occur or if it is not possible to design out this problem to assure that the reactivity changes are less thab $1.00 and the reactor is at all times controllable.

It would be appropriate to present these concerns in the open literature to determine whether or not a significant problem exists. Analysis should be performed to determine:

> Clamp failure or core readjustment can only lead to reactivity reductions.
>
> Magnitudes of internal adjustments that might occur spontaneously between core elements and relate this to a reactivity addition which must be tolerable via system design and response
>
> In connection with other transient events, make certain that core motions due to clamp related stress release do not aggravate excessively an already bad situation.

2.1.4 Decay Heat Caused Fuel Failure and Core Meltdown

2.1.4.1 Decay Heat Calculations

To calculate a reference decay heat curve for a fast reactor fuel, the appropriate nuclear data must be assembled. This is a non-negligible task since 770 isotopes (Ref. 1), or more, may be included. Yields, half-lives, and capture cross sections for these isotopes, appropriate to the reactor spectrum, must be obtained as well as beta and gamma decay energies. For example, the total beta energy release associated with the fission products of the FFTF for ^{239}Pu was 7.3 Mev/fission, for ^{238}U was 9.8 Mev/fission and for ^{235}U was 7.75 Mev/fission (Ref. 1). Likewise the gamma energy values were needed and were taken as 6.7 ± 0.7 Mev for ^{239}Pu, 9.0 ± 0.7 Mev for ^{238}U, and 7.1 ± 1.3 Mev for ^{235}U. Furthermore, such things as branching raios need to be specified.

With this nuclear data, a reference decay heat curve may be obtained with a code like RIBD (Ref. 2) or ORIGEN (Ref. 3). It has been concluded that both codes give essentially the same results (provided they start from the identical data base) even though the calculations use different numerical methods (Ref. 4). A flux level and an average exposure must be specified, and an assumption must be made for the conversion rate of ^{238}U to ^{239}Pu. Flux level affects the fission product inventory by transmuting one isotope into another through neutron absorption. As most of these absorptions in a reactor are (n,γ) in nature, the effect, on the average, is to move the isotope farther from stability and hence, to increase the decay heat. At longer decay times when statistical considerations are no longer applicable, one must consider the burnout and burnin of the individual isotopes to determine whether there is a net increase in the decay heat.

It was shown (Ref. 1) that this effect on decay heat is small, becoming appreciable only as the flux approaches 10^{16}. However, the effect on individual isotopic powers can be substantial. An extreme is represented by the so-called shielded isotopes, that is, those that have no direct fission yield and cannot be produced by beta decay due to the beta stability of the potential parent. Thus, they can be produced only by neutron capture. An example of this is ^{134}Cs (2.1 year half-life) which at 10^8 seconds decay produces about 5% of the total decay heat in FFTF. In large measure, this one isotope establishes the flux level effect at this decay time.

Similarly, the shielded isotopes ^{136}Cs and ^{148}Pm, with half-lives of 13 and 41 days, respectively, are significant contributors to the effect at 10^6 seconds decay.

Fuel exposure can be changed in two basic ways. One is to change the power level while maintaining the time (or operating history) constant. For this case, the decay power is proportional to the operating power level. Thus, the reference decay heat curve, as a percentage of the operating power, can be used for any exposure as long as the operating history is the same as the base case. The other way to change the exposure is to keep the power level constant and change the irradiation time. Then the decay heat at short times is not a function of irradiation time because the short-lived isotopes, which are the primary contributors at these times, are at equilibrium. At the long decay times, the longer-lived isotopes contribute significantly. They are not at equilibrium, and so the longer the exposure, the higher the decay heat.

An example of a reference decay heat curve is provided in Fig. 1 for the Fast Test Reactor (FTR) of the FFTF (Ref. 1). The calculations were done for a core power of 400 MWt, a flux level of 7.3 x 10^{15} n/cm^2-sec, a 75% operating efficiency, and

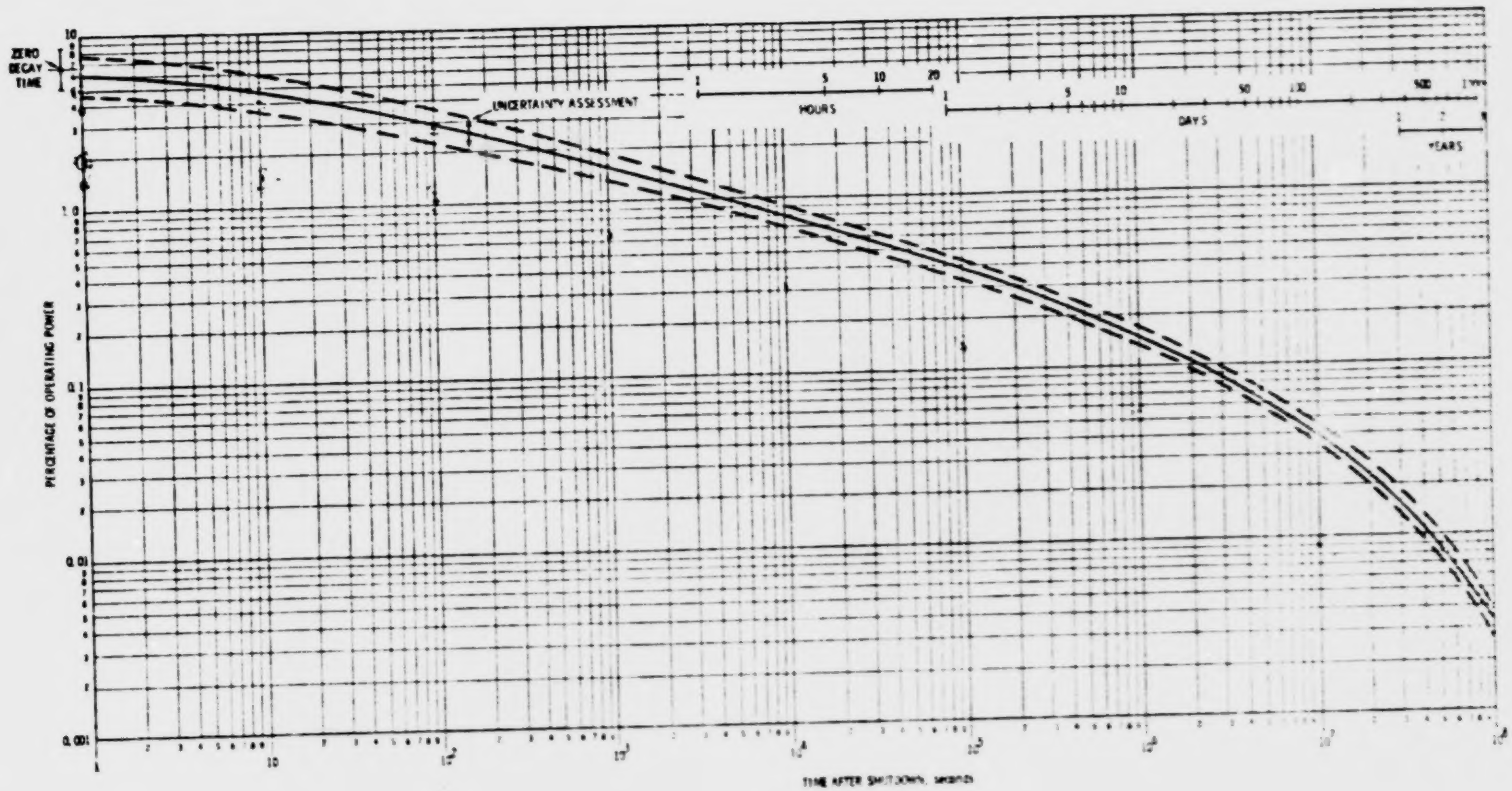

FIGURE 1. FTR Decay Heat at Goal Exposure

an average exposure of 45,000 MWd/tonne.

The curve was calculated with the RIBD code which combines the use of two calculational methods. The basic procedure is based upon the summation of individual fission product isotopes; such a procedure is adequate for the longer decay times typical of fuel handling provided the effects introduced by neutron-induced transmutation of fission products during irradiation are included. Such a procedure is inaccurate for the short decay times involved in emergency cooling, and so for times less than say 100 sec, either integration of burst experimental data may be used or a statistical assembly treatment may be matched to experimental data. For the study of the FFTF (Ref. 1) using the RIBD code (Ref. 2), the decay heat values at short times are normalized to experimental data by the inclusion of a statistical array of unknown isotopes whose half-lives and decay energies were established empirically. Thus the advantages of the summation method at long decay times have been combined with the advantages of a statistical assembly at short decay times. The technique yields good agreement over a wide range of decay times.

Were not more extensive efforts being planned to provide data for reference decay heat curve calculations for fast reactors in ENDF-B/V, a direct recommendation could be made that such work be done. As it is now, calculations of decay heat from fission products have been made using the summation method for fast and thermal reactor systems. In addition, uncertainty estimate calculations have been initiated using both exact and approximate summation method formulas. More recent calculations (Ref. 5) use ENDF/B-IV as the primary source of data, where fission yield, cross section and decay data (half lives, β and γ energies, branching, etc.) for 824 fission product isotopes are contained in the fission product and fissionable isotopes files. This extensive data set represents a recent two year effort by the Cross Section Evaluation Working Group Task Force on "Nuclear Data For Fission Product Decay Heat and Burnup Calculations." The initial emphasis of the Task Force's work was on accurate calculations for short cooling times ($t_C < 1000$ sec), where application to loss of flow analyses is appropriate. The data and methods, however, are also applicable to longer cooling times where many additional related problems exist.

The main uncertainties in the summation calculation stem from the input data rather than from any numerical procedure (Ref. 4). Thus, sensitivity studies and statistical methods have been applied to determine which parameters as well as which isotopes are most important for the decay heat problem (Ref. 5). These techniques have also been used to obtain decay heat uncertainty based on uncertainty in the initial data. Particular attention has been given to short cooling times, where experimental decay heat measurements are difficult. In order to facilitate the uncertainty analyses, approximate methods have been developed that are accurate to within 20% of the standard summation method for the short cooling time period. These approximate solutions have then been used to obtain analytic expressions in the uncertainty analyses (Ref. 5).

2.1.4.2 Other LMFBR Decay Heat Studies

In conjunction with study of postaccident heat removal in LMFBR's (Ref. 6), which contained specific numerical results based on the Fast Test Reactor (FTR), the RIBD code was also used. For a scram transient insertion of 0.02 k, the results of Figs. 2 and 3 were obtained.

Other ways of presenting the data are given in Table 1 (Ref. 6), where the decay heat is shown as a fraction f of reactor power versus time, as well as values of $f\Delta t$, $\Sigma f\Delta t$, $\sqrt{f}$, $\sqrt{f\Delta t}$, and $\Sigma\sqrt{f\Delta t}$, which are used in computations. Some values of $P\Sigma f\Delta t$ are also shown, where P is the reactor power of 400 MWt. These values include the total decay heat. Table 2 shows the decay heat versus time as a fraction f of reactor power as well as the fraction r of decay heat remaining with the fuel. In addition, values of $\sqrt{fr}$, $fr\Delta t$, $\Sigma fr\Delta t$, $\sqrt{fr\Delta t}$, and $\Sigma\sqrt{fr\Delta t}$, which are used in postaccident heat removal computations, are included. These values include only the estimated decay heat remaining with the fuel.

It is believed (Ref. 6) that the computed values, f, of decay heating as a fraction of reactor power are accurate to ±10%. Such an accuracy should be sufficient for most postacci-

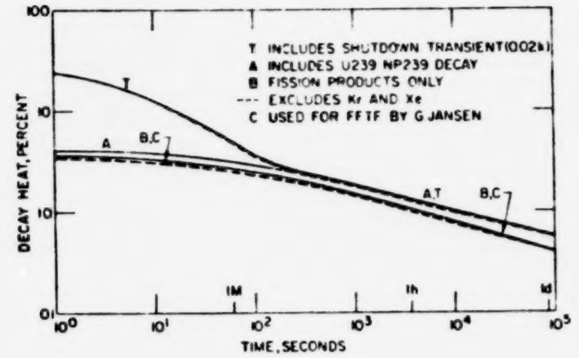

Fig. 2
FFTF Decay Heat (1 to 10^5 Sec after One-year Irradiation).
ANL Neg. No. 900-975.

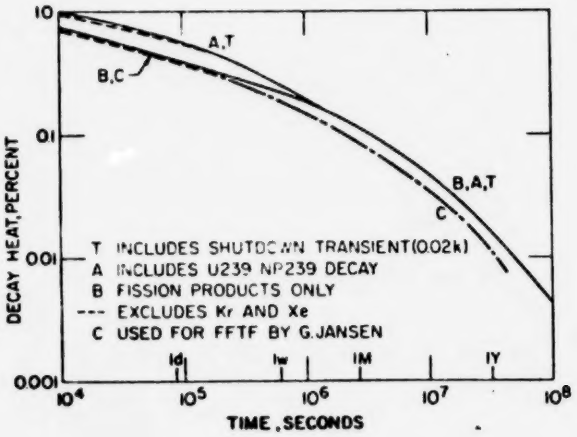

Fig. 3
FFTF Decay Heat (10^4 to 10^8 Sec after One-year Irradiation).
ANL Neg. No. 900-974.

TABLE I. FFTF Decay Heat

One-year Irradiation
80% Pu-20% U Fissions

Time	Time t, sec	Fraction of Decay Heat, f	$f\Delta t$	$\Sigma f\Delta t$	$\sqrt{f}$	$\sqrt{f}\Delta t$	$\Sigma\sqrt{f}\Delta t$	$P\Sigma f\Delta t$, 10^8 cal
	0	1.00	0	0	1.00	0	0	0
	1	0.24	0.62	0.62	0.490	0.74	0.74	0.59
	2	0.21	0.22	0.84	0.459	0.47	1.22	0.60
	5	0.165	0.56	1.40	0.406	1.29	2.51	1.33
	10	0.125	0.73	2.13	0.353	1.90	4.41	2.03
	20	0.09	1.07	3.20	0.300	3.27	7.68	3.06
	50	0.055	2.17	5.38	0.234	8.01	15.70	5.14
	100	0.037	2.30	7.68	0.192	10.67	26.37	7.34
	200	0.028	3.25	10.93	0.167	17.98	44.35	10.44
	500	0.022	7.50	18.43	0.148	47.34	91.70	17.61
	1000	0.0185	10.12	28.55	0.136	71.08	162.78	27.[illegible]
0.55 hr	2000	0.0152	16.85	45.40	0.123	129.65	292.43	43.39
1.38 hr	5000	0.012	40.80	86.20	0.109	349.24	641.68	82.39
	1×10^4	0.010	55.00	141.20	0.100	523.85	1165.54	
	2×10^4	0.0085	92.50	233.70	0.0921	960.97	2126.51	
13.88 hr	5×10^4	0.0067	228.00	461.70	0.0818	2610.72	4737.23	
1.15 d	1×10^5	0.0056	307.50	769.20	0.0746	3919.00	8654.30	
2.31 d	2×10^5	0.0044	500.00	1269.20	0.0663	7058.00	15712.00	
5.78 d	5×10^5	0.00285	1087.00	2356.00	0.0533	17957.00	33669.00	
11.57 d	1×10^6	0.00195	1200.00	3536.00	0.0441	24385.00	58055.00	
23.15 d	2×10^6	0.00133	1640.00	5196.00	0.0364	0313.00	98368.00	
57.87 d	5×10^6	0.00070	3045.00	8241.00	0.0264	94389.00	192757.00	
115.74 d	1×10^7	0.00048	2950.00	11191.00	0.0219	120910.00	313667.00	
231.48 d	2×10^7	0.00026	3700.00	14891.00	0.0161	190160.00	503827.00	
578.70 d	5×10^7	0.000097	8900.00	23791.00	0.0098	389580.00	893407.00	
1157.40 d	1×10^8	0.000042	6900.00	30691.00	0.0064	408200.00	1301607.00	

The FFTF reactor power is P = 400 MWt = 95.579×10^6 cal/sec, and the average specific power is $(95.579 \times 10^6)/(2.86 \times 10^6$ g) = 33.4 cal/sec-g fuel = 334 cal/sec-cm^3 fuel.

TABLE 11. FFTF Decay Heat

One-year Irradiation
80% Pu-20% U Fissions

Time	Time t, sec	Fraction of Decay Heat, f	Fraction in Fuel, r	$\sqrt{fr}$	$fr\Delta t$	$\Sigma fr\Delta t$	$\sqrt{fr}\Delta t$	$\Sigma\sqrt{fr}\Delta t$
	0	1.000	0.58	0.761	0.00	0.00	0.00	0.00
	1	0.24	0.59	0.376	0.36	0.36	0.56	0.56
	2	0.21	0.60	0.354	0.13	0.49	0.37	0.93
	5	0.165	0.61	0.317	0.34	0.83	1.01	1.94
	10	0.125	0.62	0.278	0.44	1.28	1.49	3.43
	20	0.09	0.625	0.237	0.67	1.95	2.58	6.01
	50	0.055	0.63	0.186	1.36	3.31	6.35	12.36
	100	0.037	0.64	0.153	1.46	4.77	8.50	20.86
	200	0.028	0.64	0.133	2.08	6.85	14.39	35.75
	500	0.022	0.645	0.119	4.82	11.67	37.95	73.20
	1000	0.0185	0.65	0.109	6.55	18.22	57.19	130.39
0.55 hr	2000	0.0152	0.67	0.101	11.10	29.32	105.29	235.68
1.38 hr	5000	0.012	0.69	0.091	27.70	57.02	287.86	523.54
	1×10^4	0.010	0.71	0.0843	38.45	95.47	438.14	961.67
	2×10^4	0.0085	0.73	0.0787	66.50	167.00	815.10	1776.80
13.88 hr	5×10^4	0.0067	0.75	0.0706	168.40	330.40	2244.80	4021.70
1.15 d	1×10^5	0.0056	0.78	0.0661	234.80	565.20	3424.40	7446.10
2.31 d	2×10^5	0.0044	0.80	0.0593	394.40	959.60	6270.90	13717.00
5.78 d	5×10^5	0.00285	0.82	0.0483	878.00	1838.00	16150.00	29867.00
11.57 d	1×10^6	0.00195	0.84	0.04047	993.00	2831.00	22203.00	52071.00

The FFTF reactor power is P = 400 MWt = 95.579×10^6 cal/sec and the average specific power is $(95.529 \times 10^6)/(2.86 \times 10^6\ g)$ = 33.4 cal/sec-g fuel = 334 cal/sec-cm^3 fuel.

dent heat removal calculations. In computations involving total heat removal the total decay heat is used. Other computations, involving meltthrough of fuel beds, use the results of both Tables 1 and 2 to show the differences due to volatilization of decay heat sources from the fuel (Ref. 6).

2.1.4.3 Experimental Verification of Decay Heat Removal in an LMFBR

The capacity of the PHENIX reactor for decay heat cooling has been tested (Ref. 7). After several preliminary tests, all sodium pumps were shut down when the reactor was operating at 4 MWt, and control rods were moved to simulate decay power at this level. Tests showed that there was sufficient natural convection in the primary loop, and later in the secondary loops, to maintain a stable operating level.

The temperature was then raised step by step to 510°C, which corresponded to operating conditions of 522°C in the primary hot sodium, a temperature difference across the core of 153°C, a thermal power of 160 MWt. The primary pump speed was 290 rpm and the secondary pump speed was 170 rpm.

Of course this test sequence was not entirely representative of actual conditions, particularly regarding initial distribution of temperatures, but it was one indication that natural convection can be relied upon to provide natural convection flow in the PHENIX reactor. However, this conclusion may not be valid for another LMFBR because 1) it may not be a pool type reactor, 2) the PHENIX experiment assumed structural integrity, which may not be present after an accident, and 3) in a loss-of-coolant accident, the coolant may not be present.

2.1.4.4 Summary

It is important to recognize that decay heat is always present and so "decay heat caused fuel failure and core meltdown" can arise only with an inadequate design of cooling systems to provide for removal of the heat, or with a failure of such systems, possibly in conjunction with reactor accidents. The analysis of the consequences of inadequate heat removal are handled under the area of postaccident heat removal, and so with regard to decay heating itself, only two questions need be answered.

The first question pertains to the calculational methods employed to obtain reference decay heat curves. The state-of-the-art may be considered adequate at the present time, and developments currently underway will provide improvements in the future. The second question involves the capability of reactor systems to dissipate decay heat after shutdown, and experience to date indicates that present reactors have been successfully designed.

REFERENCES

1. D.R. Marr and W.L. Bunch, "FTR Fission Product Decay Heat," Hanford Engineering Development Lab., HEDL-TME-71-27 (Feb. 1971).

2. R.O. Gumprecht, "Mathematical Basis of Computer Code RIBD," Douglas United Nuclear Report DUN-4136 (June, 1968).

3. M.J. Bell, "ORIGEN - The ORNL Isotope Generation and Depletion Code," Oak Ridge National Lab Report ORNL-4628 (May, 1973).

4. C.W. Kee, C.R. Weisbin, and R.E. Schenter, "Processing and Testing of ENDF/B-IV Fission Product and Transmutation Data," *Trans. Am. Nucl. Soc. 19,* 398 (1974).

5. R.E. Schenter and F. Schmittroth, "Radioactive Decay Heat Analyses," *Proc. Conf. on Nuclear Cross Sections and Technology (3-7 March 1975)*, to be published.

6. J.C. Hesson, R.H. Sevy, and T.J. Marciniak, "Postaccident Heat Removal in LMFBR's: In-Vessel Considerations," Argonne National Laboratory Report ANL-7859 (Sept., 1971).

7. R. Carle, J. Megy, B.Guillemard, E. Robert, T. LeMarechal, J.P.Crette, and P. Labot, "Phenix Startup," *Proc. Fast Reactor Safety Meeting*, CONF-740401-P2, 1009 (1974).

2.1.5 Fuel Handling Accidents

2.1.5.1 General

As a part of fuel handling accidents, the loading of improperly enriched fuel pellets into the pins in a subassembly is not considered here. This is typically considered as a problem associated with fuel failure and its propagation. Fuel handling accidents are classified as those involving the transfer and temporary storage of fuel.

The transparent nature of water makes refueling in BWRs and PWRs relatively straight-forward in concept, whereas the opacity of sodium and its chemical reactivity with air and water introduce some complexity to the LMFBR refueling process. One of the outcomes of design options usually employed is use of what are basically double containment barriers between fuel being handled and the outer containment atmosphere. A number of possible failures have been analyzed. These include:

1. complete loss of cooling of fuel transfer machines,
2. complete loss of cooling in interim fuel assembly examination (IEM) cells, and

Although these would be unlikely events, precautions must be taken to insure severe consequences are avoided if failure does occur.

2.1.5.2 Complete Loss of Cooling of Fuel Transfer Machines

The complete loss of gas cooling of fuel transfer machines for the FFTF reactor is mitigated against by redundant coolers, both of which are provided with a backup power supply. Furthermore, all fuel transfer activities will be performed in sodium-filled pots, which will greatly increase heat removal capability.

For the ex-vessel handling machine, the fuel pin clad temperatures with normal cooling would be held to less than 1000°F. Should normal power to the machine be lost, emergency power would be supplied to maintain normal cooling levels. In the event all normal cooling were lost, natural circulation of the air through the machine would be sufficient to keep fuel from melting (Ref.1). Even assuming the contents of the ex-vessel fuel handling machine, including an entire high-power fuel subassembly plus the pot of sodium, were spilled onto the reactor building floor, the resultant doses were calculated to be well below 10 CFR 100 guideline values (Ref.1).

For reactor plants larger than FFTF, the offsite dose for such an event would be expected to be no more than about a factor of 3 greater than that calculated for FFTF, and still well within the guideline values of 10 CFR 100. This example illustrates the capability of the reactor containment building to limit the release from even extremely unlikely fuel handling accidents.

The in-vessel handling machine (IVHM) of the FFTF involves "under-the-plug" refueling, which means that double containment is normally maintained at all times and therefore the potential for environmental release of radioactive material is extremely low.

2.1.5.3 Complete Loss of Cooling in IEM Cells

In the IEM cells, with the maximum decay heat from an FFTF subassembly, pin rupture would occur approximately 25 minutes after loss of gas cooling, with clad melting occurring about 20 minutes later (Ref.2).

A second problem with the IEM cells is that as the cell atmosphere heats up, the internal pressure of the IEM would cease to be negative, and the design leak rate of 0.01 cfm would provide a leakage of approximately 0.002 Ci/sec into the containment work area. Even for this situation, containment isolation would afford ample mitigation and control of the release. The IEM cell atmosphere is constantly circulated to the cell atmosphere processing system, in which case virtually no release of radioactivity would take place. While the inventories and specific process flow activities might vary significantly in a commercial LMFBR from those for the FFTF, it is concluded that design provisions related to fuel storage or transfer can be initiated to minimize the potential for serious accidents and, if such accidents should occur, to render any resultant releases relatively inconsequential.

2.1.5.4 Other Accidents

A conceivable accident involving fuel handling is that associated with positioning of a fuel subassembly in the core. Invariably this is precluded in the design of the reactor. For example, for the FFTF, the lower subassembly nozzles provide a mechanical key system to prevent placement of subassemblies into adverse unplanned core locations. The keying arrangement assures that the subassemblies will be located in positions of proper cooling; thus the location of a highly orificed subassembly in a higher power zone, and the location of a fuel assembly in a control rod location, is impossible.

Still another potential accident, which could be included under the fuel handling category is that of dropped heavy loads. This would be expected to occur only through operator error. In some LMFBR designs, however, failure of the crane itself could initiate a major accident.

In conclusion, reasonable precautions have been taken to prevent fuel handling accidents for the FFTF facility, and further design improvements are anticipated for subsequent LMFBR designs.

REFERENCES

1. "Fast Flux Test Facility - Preliminary Safety Analysis Report," Vol. 2, Appendix 2 (1972).

2. "Fast Flux Test Facility, Design Safety Assessment," HEDL - SRI - 1 (1973).

2.1.6 Steam Generator Failure

It is well known that, in the current state of technology, the steam generator is the weakest link in the heat transfer system. Water or steam leaks may occur in the water tubes because of manufacturing defects or of weakening induced by vibrations or metal fatigue. It is vital to assess the consequences of such leakage on other tubes in the bundle and on the tube itself.

The principal directions of investigation has been on leak growth (wastage), reaction strength and leak detection methods.

2.1.6.1 Leak Growth and Propagation

Experience with the Fermi reactor steam generators (Ref.1) in late 1962 and subsequent tests by the British (Ref. 2) indicated that very small water leaks into sodium could cause high metal loss rates from heat transfer tubes. This phenomenon was called wastage. Since that time, wastage has been investigated by many organizations throughout the world. Wastage is believed to occur in a reaction zone existing at an interface between sodium-water-metal tube. This zone is thin, temperature measurements indicate it is <0.030 in. thick. Within the reaction zone, temperatures are high (2200°F) compared to 600°F for the bulk sodium and 300°F measured inside the water jet.

Figure 1 shows conceptually how wastage can propagate failure in a steam generator. If the water jet has insufficient strength to penetrate across the tube-to-tube separation, there will be negligible wastage of the target tube (Fig. a). As the jet increases in strength, it will penetrate to the adjacent tube, first as a gentle wash of reaction products over a large part of the surface (Fig. b), until an optimum jet geometry is reached at which the jet impinges squarely onto the target tube with the reaction zone having a minimum area (Fig.c). Increasing the jet strength further causes the water to hit the target tube and sply outward, the reaction zone becoming a ring on the target tube (Fig. d). If the jet is sufficiently strong, the water may completely pass around the tube, leaving little wastage damage or splash onto adjacent tubes to give a complex pattern of wastage.

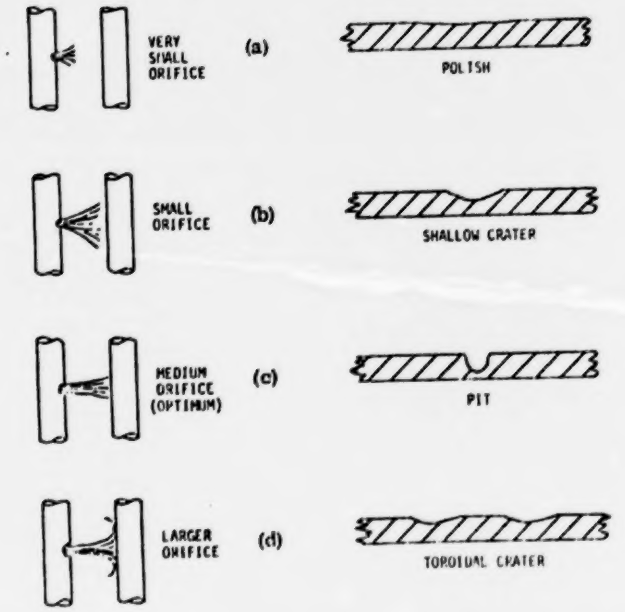
VERY SMALL ORIFICE
(a)
POLISH
SMALL ORIFICE
(b)
SHALLOW CRATER
MEDIUM ORIFICE (OPTIMUM)
(c)
PIT
LARGER ORIFICE
(d)
TOROIDAL CRATER

Fig. 1 Effect of orifice size on wastage (constant water pressure).

In a series of wastage tests by GE and APDA (Ref. 3) it was found that the wastage could be presented as:

$$\begin{bmatrix}\text{quantity of metal}\\ \text{removed (in.}^3\text{)}\end{bmatrix} = 0.014 \times \begin{bmatrix}\text{quantity of water}\\ \text{injected (lb)}\end{bmatrix}. \qquad (1)$$

These tests were performed for water pressure up to 1450 psia, sodium velocities 0 to 4 ft/sec, sodium temperature 950°F, tube material 2.25:1 Cr:Mo steel, tube spacing 0.75 in. or greater.

Wastage measurement specifically in support of MONJU have been performed (Ref. 4) using sodium velocity of 0.78 ft/sec, nozzle-to-target spacing of 0.69 in. for leak rates in the range 0.07 to 7 g/sec and a sodium range 270 to 540°C. Target materials were 2.25 $Cr\text{-}1M_O$ steel and stainless steel. Their results were least-squares fitted to the empirical relationship

$$W_L = 252e^{-[0.255(\ln \frac{G}{5.12})^2 + \frac{5460}{T}]} \tag{2}$$

for $Cr\text{-}M_O$ steel and

$$W_L = 526e^{-[0.287(\ln \frac{G}{5.12})^2 + \frac{7180}{T}]} \tag{3}$$

for stainless steel where W_L is the wastage rate (mm/sec), G is the water leak rate (g/sec) and T is the sodium temperature (°K). These results are presented for CrM_O in comparison with the measurements of Reference 3 in figure 2.

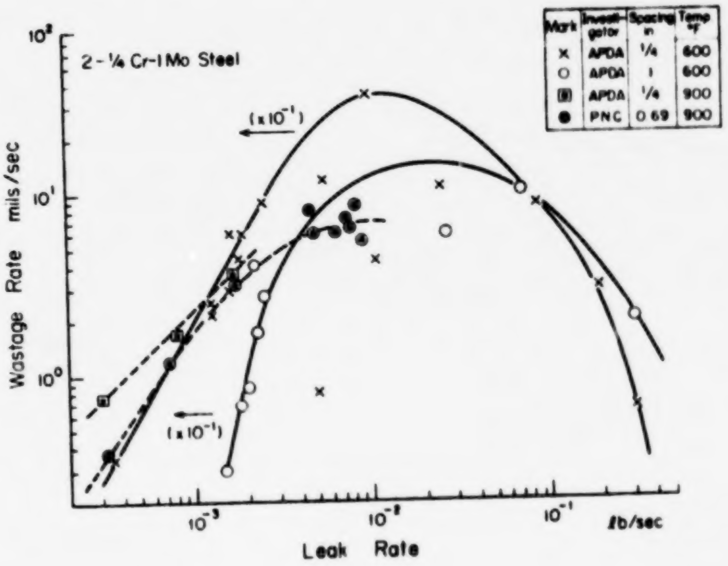

Figure 2. Comparison of Wastage Rates as Observed by APDA (Ref. 3) and PNC (Ref. 4). Curves are plots of the empirical relationship (equation 2).

One hundred and fifty tests of ferric and austensic steel wastage from water and steam leaks have been performed in support of PHENIX reactor (Ref. 5). They find that the wastage rate is inversely proportional to the sodium flow rate. As the sodium flow rate increases, it deviates and disperses the jet of water thereby reducing the mechanical energy on target.

An increase in sodium temperature increases the wastage rate. For leakage rates greater than 10 g/sec on 2.25 Cr-/M_O steel, raising the temperature from 350 to 450°C increased the wastage by 4 times. Similarly raising the water temperature from 350 to 500°C caused the wastage to triple.

The French tests also showed a shape factor L/D (ratio of injector-target distance to initial orifice diameter) effect on wastage. These observations were made for flow rates varying from 0.2 to 50 g/sec, values of L from 15 to 45 mm and D values of 0.1 to 0.8 mm. These results are shown in Figure 3.

FIGURE 3

WASTAGE RATE: INFLUENCE OF THE SHAPE FACTOR

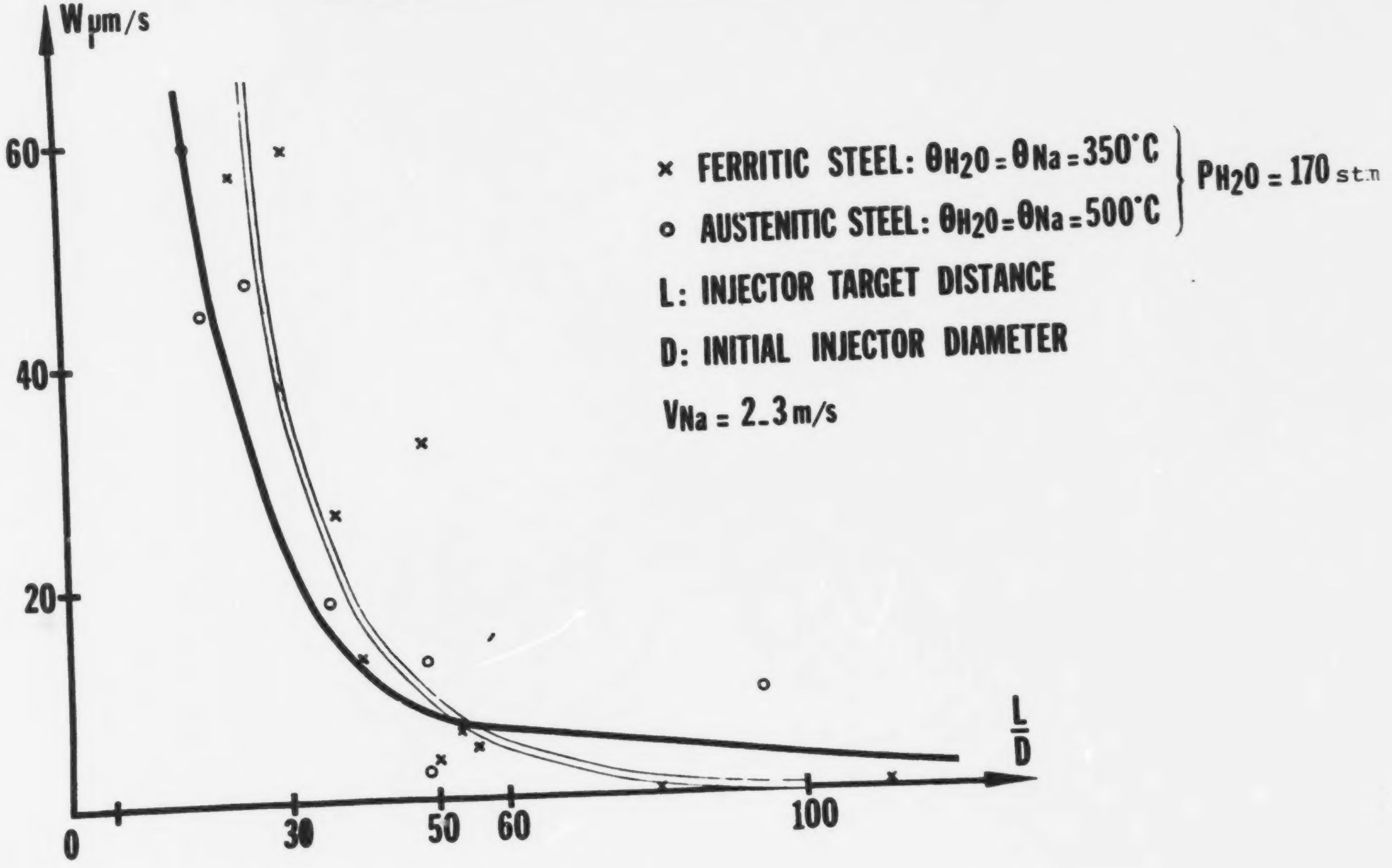

2.1.6.2 Accident Analysis

Should water or steam leak into the sodium loop, hydrogen will be produced and chemical energy released. The reactions are:

$$2Na + H_2O \rightarrow Na_2O + H_2$$

$$2Na + 2H_2O \rightarrow 2NaOH + H_2$$

In large scale tests, UK AEA reports (Ref. 6) that large scale sodium-water tests produced roughly equivalent amounts of NaOH as Na_2O and the hydrogen release was roughly 60% of the total release model. The quantity of hydrogen which enters the cover gas is less than 1% of the maximum quantity available from the water. The hydrogen reacts with the sodium vapor to form sodium hydride (Ref. 7).

$$4Na + H_2O \rightarrow Na_2O + 2NaH$$

Although anticipated steam generator failure rate is not expected to be large (one every 3 or 4 years for a 700 MWt plant, ref. 8), plant design calls for multiple steam generators so that any failed exchangers or generators can be valved out for repair. The Clinch River Breeder Reactor (CRBR) calls for 9 steam generators arranged in groups of 3 to each intermediate heat exchanger. Each sodium-water relief system consists of a small and a large leak relief system. The large leak relief system consists of twin 12 in. rupture disks that blow down through 18 in. pipes into a cyclone reaction products separation system.

There are various computer codes for analyzing the piping shock effects from a sodium water reaction such as SWEAR (Ref.9), TRANSWRAP (Ref. 10), SWAC (Ref. 11,12) and CEBUG (Ref. 13).

CEBUG has been used to analyze the steam generating system for a sodium-water reaction in the CRBR. The steam generator sodium hydraulic behavior is modeled by five subsystems. The tube region in which hydrogen bubble growth can occur is modeled by a two or three dimensional finite element system. All other sodium channels are represented in one-dimension. Up to ten channels may contain cover gas regions, each with its own rupture disc. The pressure relief system is modeled with compressible flow to follow sodium and cover gas expulsion after rupture disc burst.

The worst case (Ref. 14) appears to be the complete tube bottom tip guillotine rupture. The sodium can be accelerated upward toward the gas space. However, even in this case, the relief disc rupture relieves the overpressure and pressure relief takes place as designed.

2.1.6.3 Leak Detection

The major remaining question associated with the leak detection system is time of response. APDA data (Ref. 15) on wastage prove that wastage rates of at least 1 mil/sec can occur with an optimum water jet. Assuming 1/8 in. wall thickness, a hole could be cut in the target tube in <120 sec. The response time of cover gas hydrogen monitors is far above this value (i.e., gas chromatograph samples at 5-min. intervals).

Instruments for detecting small increases in the hydrogen content of sodium are being developed here (Ref. 16, 17, 18) and abroad (Ref. 19, 20, 21) for early detection of small leaks of steam or water into sodium in LMFBR steam generators.

One method (Ref. 22) consists of a nickel diffusion-membrane tube immersed in the sodium stream and continuously evacuated by an 11 litre/sec ion pump. The ion-pump current serves as a measure of the hydrogen content of the sodium. The response time of the hydrogen diffusion tube detector is of the order of 15 sec. The maximum sensitivity (Ref. 22) is about equivalent to a leak of $2\text{x}10^{-5}$ lb H_2O/sec in the CRBR plant.

Acoustic emission is another possible method for water leak detection. APDA measured the noise character and levels associated with a small water leak into sodium. No distinctive frequencies were clearly associated with the small sodium-water reaction, and no evidence of a strong high-frequency component was found. The noise levels associated with the leak were very low compared to the background levels measured in Fermi steam generators.

The Japanese (Ref. 23) have found for their test loop, a leak of water into sodium as small as 0.07 grams H_2O/sec can be detected using RMS averaging of the accoustic emission signal and subtracting the RMS background signal. It was also found that the RMS signal varies as the 1/3 power of the water leak rate but is affected by the sodium temperature.

2.1.6.4 Summary

Steam generator failures must be expected in LMFBR systems and included in the design. Investigations of wastage show that leaks can grow and propagate fairly rapidly so that in extreme cases leak detector response time is too slow for

for automatic shutdown. Codes for analyzing sodium-water reactions in steam generators are well developed and produce results that correlate well with experiments. Such codes predict that the reaction can be contained without component failure. Present codes may be overpredicting hydrogen formation by not allowing for NaH formation, however, this does not have safety implications.

REFERENCES

1. R.H. Anderson, J.A. Ford, and P.S. Lindsey, "Design, Fabrication, and Preliminary Operation of the Steam Generators for the ENRICO FERMI Atomic Power Plant," APDA-307 Atomic Power Development Associates, Inc., 1968.

2. J.A. Bray, "A Review of Some Sodium/Water Reaction Experiments," BNES J., p. 107, April 1971.

3. "Quarterly Technical Progress Report on AEC-Sponsored Activities. March to June, 1967," APDA-206, Atomic Power Development Associates,Inc., 1967.

4. H. Nei, K. Ujihara, I. Ohahima and M. Hori, "Wastage of Steam Generator Tubes during Small Leak of Steam into Sodium," Proc. of the fast Reactor Safety Meeting, Beverly Hills, Ca. April 2-4, 1974 CONF-740401-Pl.

5. N. Lyons, J. Biscarel, A. Lafon, C. Chedeville, and G. Ferretti, "Study of the Effects pf Small Leakage of Water into Sodium of a Steam Generator," Proc. of the Fast Reactor Safety Meeting, Beverly Hills, Ca. April 2-4, 1974 CONF-740401-Pl

6. E. Fielder et al., "Alkali Liquid Metals" (symposium report) paper, SM-85.14, 1966.

7. D.A. Greene, "The Leakage of Water into Sodium in Steam Generators and TEst Rigs," Nucl. Tech 18 pp. 267-276, June 1973.

8. J. Graham, "Fast Reactor Safety," Academic Press, NY, 1971, p. 133.

9. D.A. Greene, "Steam Generator Vessel Pressures Resulting from a Sodium-Water Reaction - A Computer Analysis with the SWEAR Code," Nucl. Technol., 18, 218,1972.

10. C.R.Bell, "TRANSWRAP - A Code for Analyzing the System Effects of Large-Leak Sodium-Water Reactions in LMFBR Steam Generators," Proc. of the Fast Reactor Safety Meeting, Beverly Hills, Ca., April 2-4, 1974 CONF-740401-Pl.

11. Y. Tanaka, K. Sakano and Y. Shindo, "Analysis of Pressure Wave Propagation Tests in Piping System," 1972 Fall Meeting on Reactor Physics and Engineering. C.33, 1972. Atomic Energy Society of Japan.

12. H. Ogasawara and T. Kawabe, "Analysis of Transient Pressures in the Secondary-Loop of LMFBR at the Accident of Sodium-Water Reactions. 1972 Annual Meeting of the Atomic Energy Society of Japan.

13. D.W. Stuteville and P. K. Doherty, "CEBUG 3A-A Code for Steam Generating Systems Sodium-Water Reactor Analysis," Combustion Engineering, Unpublished, June 1973.

14. D.W. Stuteville, "The Interaction of Steam Generator Modules During a Sodium-Water Reaction," Proc. of the Fast Reactor Safety Meeting, Beverly Hills, Ca., April 2-4, 1974 CONF-740401-P1.

15. H.V. Chamberlain, "Project Summary: Sodium-Water Reactions Related to LMFBR Steam Generators," APDA-257, Atomic Power Development Associates, Inc., 1970.

16. D.R. Vissers et al., "A Hydrogen Monitor for Detection of Leaks in LMFBR Steam Generators," Nucl. Tech. 12, 218, Ocotber 1971.

17. R.E. Witkowski et al., Trans. Amer. Nucl. Soc. 15(1), 234, 1972.

18. Prodyot Roy and Douglas N. Rodgers, "Characterization of a Diffusion Tube Hydrogen Detector in a Dynamic Sodium System," Nucl. Technol. 12, 388, December 1971.

19. R.A. Davies et al., "The Detection of Small Water Leaks in Sodium Cooled Heat Exchangers," Paper presented at British Nuclear Energy Society Conf. on Liquid Alkali Metals, Nottingham, England, April 4-5, 1973.

20. P. Lecocq et al., "Monitoring Sodium-Water Tightness in Sodium Heated Steam Generators by Hydrogen Measurement. Industrial Application for the 'C.G.V.S.'" Paper No. LAE/SM 168/E7 presented at IAEA Colloquium on the Operation and Instrumentation of Nuclear Power Stations, Prague, January 22-26, 1973.

21. F.A. Kozlov et al., "Methods of Indication, Operation of a Steam Generator and Secondary Circuit in the Case of a Slight Leakage of Water into Sodium." Paper presented at IAEA Specialists' Meeting on Sodium-Water Reactions, Melekess, USSR, May 18-21, 1971, paper number 71-7992. English Translation issued as U.S. AEC Document CONF-710548.

22. J.M. McKee and L.E. Pohl, "Use of In-Sodium Hydrogen, Detectors during Steam Generator Tests in the SCTI," Proc. of the Fast Reactor Safety Meeting, Beverly Hills, Ca. April 2-4, 1974. CONF-740401-P1.

23. Hiromichi Nei, Iwao Ohshima, Kozaburo Ujihara and Masao Hori, "Acoustic Detection for Small-Leak Sodium Water Reaction," Proc. of the Fast Reactor Safety Meeting, Beverly Hills, Ca., April 2-4, 1974. CONF-740401-P1.

2.1.7 Loss of Heat Sink

2.1.7.1 Loss of Ultimate Heat Sink

The loss of the ultimate heat sink--lack, river or bay--presents the same set of problems as for a light water reactor and is dependent on design and siting. The Reactor Safety Study (reference 1) did not consider the event probable enough to analyze.

Should such a loss occur, there would be ample time to shut the reactor down so that decay heat is the energy source and even though convective sodium cooling is adequate for removing the decay heat as is the case for PHENIX, without an ultimate heat sink, the core will melt. The AEC Regulatory position (Ref. 2) for LWR's on the ultimate heat sink (UHS) is that it should be capable of providing sufficient cooling for at least 30 days to permit simultaneous safe shut down of all units it serves and maintain them in safe shut down. The UHS should be capable of withstanding the most severe natural phenomenon associated with the site. The UHS should consist of at least two sources of water, including retaining structures, unless it can be demonstrated that there is an extremely small probability of losing a single source. There should be at least two conduits connecting the UHS with the intake structure. Technical specifications should include emergency procedures in case of loss or partial loss of UHS.

2.1.7.2 Loss of On-Site Power

A more probable occurrance in an LMFBR would be the loss of off-site power and the failure of all emergency power generators for a sustained time (est. <1 hour). If LMFBR designs follow LWR designs, the reactor will not be able to operate on as light a load as its own circulating pumps so there is no power source to operate its own pumps and the result is the same as the loss of the ultimate heat sink. Reference 1 gives this as a probability of 10^{-5}/plant-year.

2.1.7.3 Other Causes of Cooling Incapability

Other causes of the loss of heat sink could be the loss of all the circulating pumps in a loop. Since the designs are three or four loops, if the failures are random, this would be a low probability (10^{-5} to 10^{-8}/reactor-year) because even one loop would be sufficient to remove the decay heat. In some LMFBR designs, convective sodium cooling will remove the decay heat so it is only necessary to maintain water circulation. These considerations are all based on the premise that no common mode failure (such as the previous example of loss of all on-site power) could make all pumps fail.

Complete loss of sodium from the loop could also cause loss of heat sink. The loss of the primary or secondary loop would cause loss of heat sink and core melt down. In the secondary loops, they are independent and only a severe earthquake could cause such a common mode effect. In the case of the primary loop, the linings should retain the sodium but whether or not it can still cool the core depends on plant design and cannot be answered categorically.

2.1.7.4 Summary

The AEC Regulatory position on the ultimate heat sink for LWR is probably adequate for the LMFBR. Common-mode causes of loss of heat sink,in particular loss of on-site electrical power,affect the LMFBR as severely as the LWR. It would seem prudent to investigate backup pump drive such as sodium turbines (in analogy to the helium turbines on HTGR) on the pumps or operation on its own electrical power without an off-site load.

REFERENCES

1. USAEC, "An Assessment of Accident Risks in U.S. Commerical Nuclear Power Plants," WASH-1400, August 1974.

2. USAEC, "Safety Guide 27 - Ultimate Heat Sink," March 23, 1972.

2.1.8 Sodium Fires and Aerosols

2.1.8.1 General Description

Sodium reacts with oxygen according to the reactions (Ref.1)

$$2Na + 1/2O_2 \quad Na_2O \quad \delta H = -104 \text{ k cal/mole}$$

$$2Na + O_2 \quad Na_2O_2 \quad \delta H = -20 \text{ k cal/mole}$$

The interaction is characterized by low flames and dense white smoke. The harmful effects of the smoke are (1) it rapidly reduces visibility, making surveillance and fire fighting very difficult and possibly hampering personnel evacuation, (2) the smoke particles are an extreme irritant and if not controlled can create a hazard to operating personnel and the public, and (3) the smoke particles are also corrosive and can damage metal structures, switchgear and instrumentation. The beneficial effects of the smoke are: (1) the opacity of the smoke cloud acts as a radiative heat shield and protects nearby equipment from reaching high temperatures, and (2) the smoke can reduce radioactive release significantly by agglomerating or reacting with the released fission products (Ref.2).

Sodium fires are regarded as unlikely but serious problems and were used as the design basis accident (DBA) for the licensing of the Rapsodie and Phenix reactors.

The sequence of events usually postulated in defining the consequences of a sodium fire are the following: the reactor has been shut down for several days to permit decay of the ^{24}Na activity preparatory to opening a primary cell for maintenance operations the cell is opened and its inert atmosphere is replaced with normal air. Some failure such as operator error, is assumed to result in draining the loop sodium onto the cell floor and burning commences (Ref. 3).

Calculations based on such an event sequence predicts pressures of a few psig and temperatures of about 250°F (Ref. 4,5).

If the spill is postulated to occur in a closed cell with a small spray component the pressure may reach 10 psig, but if sprayed under pump pressure with splashing and fire dispersal the pressure could theoretically reach 30 psig and 1050 °F.

In terms of operating experience, the Dounreay fast reactor experienced a sodium leak in the primary sodium system after four years of full power and three years of low power testing. This leak resulted from a poor weld at the junction of a pipe with the tank wall. It was repaired by contact welding and the use of temporary radiation shields. It is noteworthy that this repair was made in a location that had carried highly radioactive sodium-potassium coolant for many years. The reactor was returned to service and has been working without further primary coolant difficulties.

2.1.8.2 Low Velocity Jets and Pool Fires

An important concern relating to sodium fires has been whether the temperature of the pool will exceed the sodium boiling temperature (880°C.) and lead to very rapid combustion if the pool is large enough. In the model used in the SOFIRE II code (Ref. 6,7), the rate of combustion is determined by the rate of diffusion of oxygen through the nitrogen boundary layer. Huber et al (Ref.8) use a more complete model that allows for the sodium diffusion across the nitrogen layer to an oxygen region where combustion can take place (Figure 2.2.8.1).

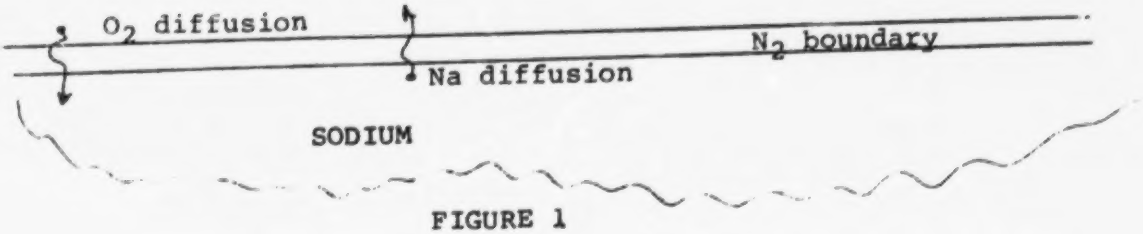

FIGURE 1

Model for Sodium-Air Burning

At temperatures below 650°C the sodium vapor transport through the layer of nitrogen is unimportant due to the low vapor pressure. With increasing temperature and vapor pressure, however, the reaction zone moves away from the sodium surface. That means that the reaction takes place in the vapor phase exclusively. This statement is supported additionally by the following consideration. Because of the excellent heat conductivity of sodium there is a negligible temperature drop at the surface of the sodium caused by the heat withdrawn by vaporization. That means the sodium vapor pressure corresponds to the sodium pool temperature. Now, if the vapor pressure immediately near the surface were to decrease to nearly zero by reaction with oxygen a very steep concentration gradient would arise for the sodium vapor transport. This, however, would lead to an increased vaporization rate and thereby to a reaction rate much higher than measured in the experiments. Therefore, the reaction cannot take place at the sodium surface proper.

These assumptions on the counter-current behavior lead to the prediction of steady state pool temperatures which has been confirmed experimentally. Huber et al (Ref.8) ran tests using a simulated sodium leak of 190 kg into a steel pan of 4.5 m^2. The sodium was sprayed at 645 °C after about 10 minutes a steady state temperature of about 730°C was reached. Because of the constant burning temperature it is expected that a constant burning rate would be seen. Such is observed at about 43 kg/m^2h. This is in contradiction with the estimated sodium reaction rate of 80 kg/m^2h observed in the Phenix experiments (Ref. 9,10). It is thought that this higher reaction rate could be due to sodium-concrete reactions. This test of the equilibrium burning temperature was further confirmed by Huber et al by heating sodium to 820°C in a closed stainless pan. When the cover was removed the sodium ignited and after about 10 minutes the temperature had dropped to 725-745°C.

2.1.8.3 Aerosol Formation

In case the sodium is released under some pressure, droplets of .03 in. dia. or less may be formed (Ref.11) accompanied by strong gas convection. Good mixing and large sodium surface areas lead to intense burning rates. This problem is modeled in the code SPRAY (Ref. 12-15). This code models the vessel walls as perfectly insulated cylinders and no attempt is made to model obstructions to convective flow such as piping, vessels etc. It is assumed that the spray is directed at the ceiling and the sodium droplets taken to be of uniform size rain downward. The droplet falls under the force of gravity which is opposed by the bouyancy and combined drag of droplet motion and gas circulation. The gas convection results from a balance of the force of gas bouyancy due to the thermal difference in the hot spray region and the cool outer annulus, the droplet drag forces and the flow friction forces. The droplet burning is modeled using the oxygen diffusion through the nitrogen layer. The heat transfer is modeled using a Nusselt number correlation for forced convection heat transfer and the mass transfer from the droplet surface is modeled using the Sherwood number. These procedures are contained within the code SPRAY which was tested against the Atomics Internation sodium jet experiments (Ref.16). Figures 2 and 3 show some of the poorer comparisons between model and experiment as presented in reference 15.

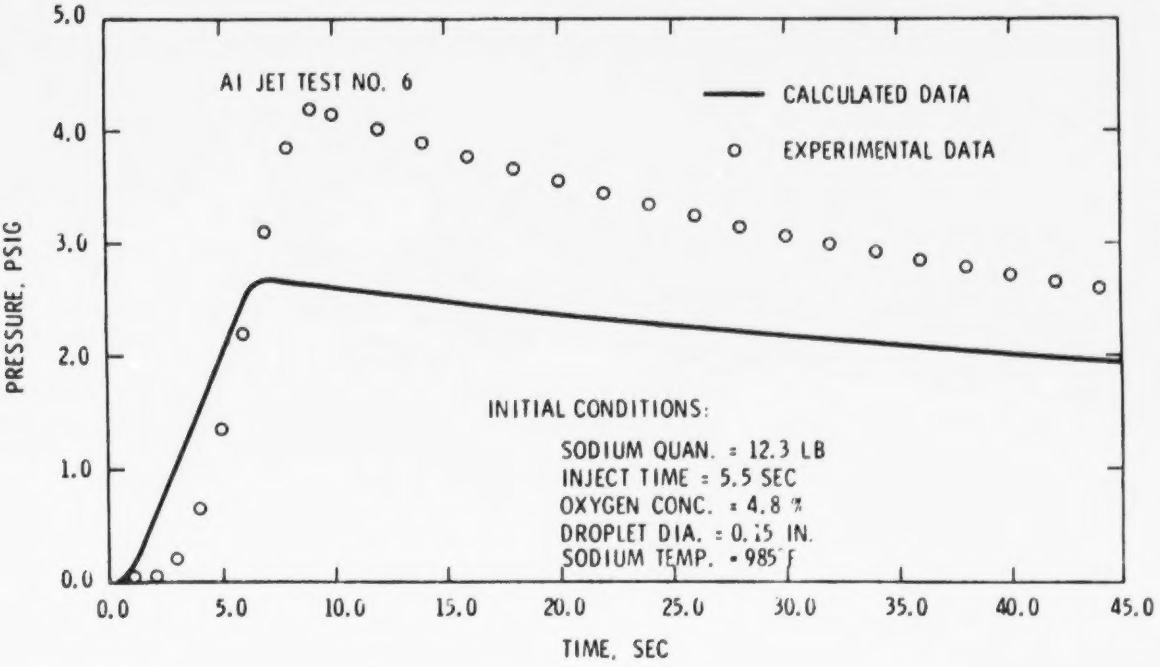

Figure 2 AI Jet Test No. 6 - Pressure vs Time During Sodium Spray Fire

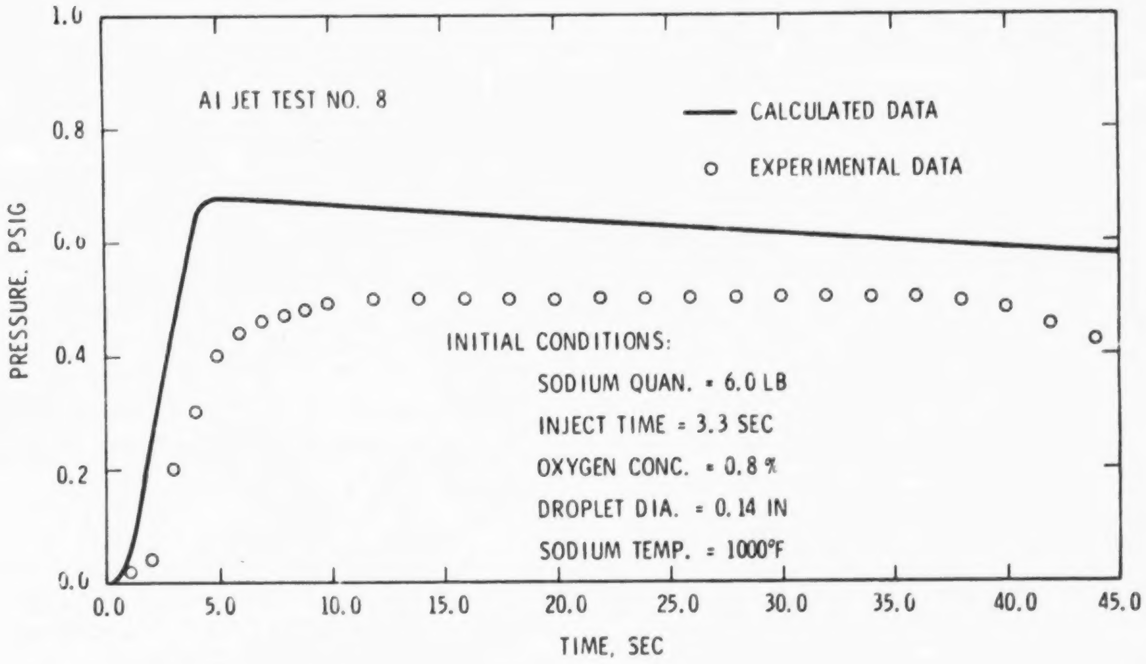

Figure 3 AI Jet Test No. 8 - Pressure vs Time During Sodium Spray Fire

2.1.8.4 Fire Extinguishing and Mitigation

The basic approach to preventing sodium fires is to confine the sodium in a double stainless steel barrier which is located in an inert gas filled cell. However, a very inert atmosphere is required to prevent reaction with oxygen. When there is less than 4% oxygen, burning will not occur in the case of exposed pool of sodium above its ignition temperature but there will be considerable incandescence and smoke (Ref.1). This situation prevails until the oxygen content of the atmosphere is reduced to 0.1% of oxygen. In the FFTF reactor, cells are used to isolate a sodium spill and after the detection of the smoke characteristic of a sodium fire, a nitrogen purge begins about 15 minutes after the spill. This purge is not immediately initiated to allow the sodium to burn up the oxygen in the cell. The nitrogen flooding at a rate of about 60 ft^3/min. further reduces the oxygen content and provides an overpressure to prevent oxygen from diffusing into the cell.

The British have proposed a similar nitrogen inerting arrangement but instead of gaseous nitrogen flooding this scheme would use liquid nitrogen and take advantage of the cooling effect as well as the inerting property of the nitrogen.

As for solid extinguishing agents, materials such as sodium chloride, sodium carbonate, graphite powder and dry sand are commonly used for small fires about reactors and test facilities but none have proved effective for large fires. One of the reasons for this lack of success may be the convection of the sodium pool preventing the cover powder from staying on the surface. Cleanup problems following the use of these powder extinguishants especially sodium chloride would be particularly difficult. It is well known that chloride ions in contact with stainless steel can result in chloride stress corrosion problems. Similarly, carburization of stainless steel by carbonate materials and nitriding by extinguishing gases are recongized as problems although no experimental evidence is presently available.

Sumps with perforated covers can be used to greatly reduce the rate of sodium burning and the temperature of combustion. Huber et al (Ref.8) found that a large catch pan with a corrogated perforated cover reduced the combustion rate to 5.2 kg/m^2 hr or nearly an order of magnitude less than an open pan.

This is carried a step further in the Phenix reactor; perforated-cover catch pans are used but with steel rods coursing through the sump for rapid heat transfer out thereby quenching the sodium below the combustion temperature. This is used in conjunction with a nitrogen-gas purge.

The United Kingdom Prototype Fast Reactor used a perforated plate covered catch basin which is covered over with vermiculite and further oxygen exclusion by argon flooding below the plate.

2.1.8.5 Summary

Although sodium combustion poses problems for LMFBR they are fairly well understood. The combustion of sodium in large pools has been shown to burn at a constant temperature about 140°C below the sodium boiling temperature thus assuring a fairly constant rate of combustion of about 43 kg/m^2 hr. The SOFIRE code should be tested against recent experiments and modified to include sodium diffusion. The more complex phenomena of spray fires can be predicted within a factor of 2 using a code such as SPRAY.

There are numerous ingenous designs for sodium fire extinguishing using inerting and cooling. Precautions should be taken that fire prevention methods do not result in material deterioration such as stress corrosion cracking of the stainless steel.

REFERENCES

1. J. Graham, "Fast Reactor Safety," Academic Press, N.Y. 1971.
2. R.K. Hilliard, "IAFA-IWGFR Meeting on Sodium Combustion and Its Extinguishment," Nuclear Safety 15, 2, pp.146-150, March-April 1974.
3. USAEC, "Liquid Metal Fast Breeder Reactor Program," WASH-1535 Vol. 2, March 1974.
4. "Task III Report, Conceptual Design Report Plant Safety Analyses," A3-AEC-12792 Vol. III 1968.
5. "Fast Flux Test Facility," Design Safety Assessment," Project No. 448, Directorate of Licensing, Oct.1972.
6. F.P. Beiriger et al, "SOFIRE II User Report" AI-AEC-13055, 1973.
7. Argonne Code Center "SOFIRE 2 1-and 2-Cell" Program Abstract 559, ANL 74-11.
8. F. Huber, P.Mengenhauer, W. Peppler, W. Till, "Behavior of Sodium Area Conflagrations and Suitable Protecting Systems," Proceeding of the Beverly Hills Fast Reactor Safety Meeting. CONF-740401-P1 April 2-4, 1974, pp.417-430.
9. IAEA-NPR: Meeting of Specialists on Sodium Combustion and its Extinguishment-Techniques and Technology, Summary Report Hanford Engineering Development Lab. Richland, Washington, USA, May 22-25, 1972.
10. Feux De Sodium Et Reacteurs Rapides, M. Falgayrettes, CEA-CEN/Cadarache, p. 1363 Proceedings of the Intl. Conference, Engineering of Fast Reactors for Safe and Reliable Operation, Kernforschungszentrum, Oct. 9-13, 1972.

11. T.S. Krolikowski, "Violently Sprayed Sodium-Air Reaction in an Enclosed Volume," ANL-7472 (September 1968).

12. P.R. Shire, "SPRAY Code User Manual," Westinghouse Hanford Co., in preparation.

13. P.R. Shire, "A Combustion Model for Hypothetical Sodium Spray Fire Within Containment of an LMFBR," M.S. Thesis, University of Washington, 1972.

14. P.R. Shire, et. al., "A Sodium Droplet Combustion Model For Reactor Accident Analysis," Trans. Am. Nucl. Soc., 15, 812, 1972.

15. P.R. Shire, "Reactor Sodium Coolant Hypothetical Spray Release for Containment Accident Analysis: Comparison of Theory with Experiment," Proc. of the Beverly Hills Fast Reactor Safety Meeting, CONF-740401-P1, April 2-4, 1974 pp. 474-487.

16. H.A. Morewitz, et. al., "Simulations of Sodium Jet Discharge," Quarterly Technical Progress Report LMFBR Safety Programs, January-March 1972, AI-AEC-13026, Atomics International, Canoga Park, Calif.

17. R.K. Hilliard, P.E. McPherson and J.M. Yatabe, "Sodium Fire Protection by Space Isolation with Inert Gas Flooding," Proc. of the Beverly Hills Fast Reactor Safety Meeting, CONF-740401-P1, April 2-4, 1974, pp.431-445.

2.2 Accident Propagators

2.2.1 Doppler Effect on Accidents

2.2.1.1 General

It is possible to design large fast reactors to have a substantially negative Doppler coefficient of reactivity. In Reference 1, D. Okrent states:

> "It is generally accepted that large fast power reactors can be designed to have a substantially negative Doppler coefficient of reactivity. The fertile U^{238} (or thorium) has been measured and calculated to provide significant negative reactivity effects upon heating (Ref.2-5). Furthermore, theory and experiment indicate that the reactivity contribution from the fissile isotopes should be quite small (Ref.5-8). Other things being equal, the reactor having a higher concentration of U^{238} or a higher proportion of low-energy neutron flux in the region from 500 to several thousand electron-volts will have a larger Doppler effect. Oxide fuel provides a somewhat softer neutron energy spectrum than does carbide. Small amounts of moderator can be added to either reactor type (or to a metal-fueled reactor) to augment the Doppler coefficient or to help maintain its value in the absence of sodium.

> However, softening the neutron energy spectrum also leads to an increase in parasitic capture in Pu^{239} and in fission products, and the breeding ratio drops somewhat."

If the Doppler effect is non-negative, an accident prognosis (Ref. 9) proceeds with a power excursion (say \$1/sec) rapidly passing prompt critical. The power continues to increase until the outward pressure results in core disassembly and shut-down. If there is a strong negative Doppler effect, the situation can be quite different (Ref.11). The excursion begins the same, continuing beyond prompt critical but the fuel heating can turn the reactivity around and can either shut it down or cause oscillations in power until disassembly occurs.

2.2.1.2 Dependence Upon Temperature

The Doppler coefficient, dK_D/dT_f varies approximately as the inverse of the absolute temperature over the temperature range of interest (Ref.5,11). A better approximation is the following form:

$$\frac{dK_D}{dT_f} = aT_f^{-1} + bT_f^{-3/2}$$

where a and b are constants and T_f is the fuel temperature (Ref.12). This allows for the fact that the coefficient will fall off more rapidly for high temperatures. The Doppler effect is also dependent upon the amount of sodium in the core. For full sodium conditions, the designers of FFTF have estimated the Doppler effect to be twice as large as for the sodium out conditions (Ref. 12).

2.2.1.3 Doppler Effect Upon Disassembly

A sensitivity study of the effect of the Doppler coefficient upon disassembly calculations was conducted by Nicholson and Jackson (Ref. 13). With a nominal Doppler coefficient, Tdk/dT = -0.0025, the following base case results were obtained using VENUS-II (Ref. 12).

Reactivity Insertions $/sec	Total Energy MW - sec	Peak Power 10^9 W	Time at Peak Power msec	Final Pressure at Core Center atm	Final Temp. at Core Center °K
20	1580	245	7.925	35.7	4884
100	2620	1206	1.50	399	6287

The sensitivity study using a factor-of-two variations of the nominal value Doppler coefficient resulted in the following.

Base Case	TdK/dt	Total Energy Released	Final Pressures at Core Center	Final Temp. at Core Center
\$20/sec	$0.5D_o$	$1.45E_o$[a]	$4.33P_o$[a]	$1.15T_o$[a]
	$2.0D_o$	$0.59E_o$	$0.14P_o$	$0.86T_o$
\$100/sec	$0.5D_o$	$1.32E_o$	$2.45P_o$	$1.13T_o$
	$2.0D_o$	$0.63E_o$	$0.20P_o$	$0.84T_o$

a - E_o, P_o and T_o refer to the base-case values for the energy, pressure, and temperature of the base core.

In Reference 13, Nicholson and Jackson made the following conclusions concerning the Doppler effect.

> " It is evident that the Doppler effect is an important parameter in these accidents. This would be expected, since Doppler feedback is almost entirely responsible for initially turning over the power burst. For the \$20/sec case, the total energy release is found to be inversely proportional to about the 0.75 power of the Doppler coefficient over the range studied. This sensitivity is somewhat less for the \$100/sec excursion, where the energy release is roughly inversely proportional to the square root of the coefficient. It does not appear that these scaling laws would hold over a much wider range.

The peak pressures attained are much more sensitive than the energy release. The final pressures vary from 5 to 155 atm in the mild excursion and from 80 to 980 atm in the more severe excursion. Due to the extremely nonlinear behavior of the pressure-energy relationship, there does not appear to be a simple scaling law to relate the pressure variations to changes in the Doppler coefficient.

Although the results are quite sensitive to variations in the Doppler coefficient, one expects to be able to calculate the Doppler effect with errors less than 30%, even for accident situations. Thus, the uncertainty in the Doppler coefficient should only introduce about a 15-20% uncertainty in the calculated energy release and an uncertainty by a factor of about two in the maximum pressure.

In some previous sensitivity studies (Ref. 14),the Doppler effect has been observed to produce one or more power-time oscillations before disassembly. As a result, the curve for energy release versus T dk/dT also displayed oscillations. These are not present in this study. They might possibly develop at higher values of T dk/dT, but that would be outside the range of physical interest for the FFTF reactor."

The Doppler effect can also add positive feedback in those instances when fuel is chilled by some colder material. This is a strong possibility, for example, when molten fuel contacts liquid sodium or stainless steel. The significance of this effect is directly proportional to the amount of fuel involved. A study of the transient overpower accident (Ref.15) showed this effect to be of second order importance. The fuel's low thermal conductivity, the presence of fission heating, the insulation effects of sodium vapor films that develop, and the large heat of fusion help to mitigate fuel chilling and reduce its impact with respect to Doppler reactivity.

2.2.1.4 Summary

In summary, it is expected that large LMFBR's with mixed oxide or carbide fuel will have a significant negative Doppler feedback. This feedback will have a significant impact on reducing the severity of power excursions. 15-20% uncertainty is due to this effect in the calculated energy release and an uncertainty by a factor of two in the maximum pressure.

REFERENCES

1. Okrent, D., "Design and Safety In Large Fast Power Reactors," Atomic Energy Review, International Atomic Energy Agency, Vienna, 1969.

2. Fischer, G. J., Meneley, D.A., Hwang, R.N., Groh, E.F. Till, C.E., "Doppler Effect Measurements in Plutonimum-Fueled Fast Power Breeder Reactor Spectra," Nucl. Sci. Eng., 1969.

3. Greebler, P., Pflasterer, G.R., "Doppler and Sodium Void Reactivity Effects in Fast Reactors," in Reactor Physics in the Resonance and Thermal Regions, II, Resonance Absorption, MIT Press, Cambridge, Massachusetts, 1966.

4. Till, C.E., Lewis, R.A., Hwang, R.N., "ZPR-3 Doppler Measurements and Comparisons with Theory," Proc. Int. Conf. Fast Critical Experiments and Their Analysis, October 10-13, 1966, USAEC Rep. ANL-7320, pp. 319-333.

5. Nicholson, R.B., Fischer, E.A., "The Doppler Effect in Fast Reactors," in Advances in Nuclear Science and Technology, Academic Press, New York, 1968.

6. Argonne National Laboratory, Proc. Conf. Fast Critical Experiments and Their Analysis, Oct. 10-13, 1966, USAEC Rep. ANL 7320.

7. Hummel, H.H. Okrent, D., Reactivity Coefficients in Large Fast Power Reactors, ANS Monograph, 1969.

8. Till, C.E., Fissile Doppler Effect Measurement and the Effects of Thermal Expansion, Reactor Physics Div. Ann. Ref. July 1, 1966-June 30, 1967, USAEC Rep. ANL 7310 (1968).

9. W.J. McCarthy, Jr. and D. Okrent, "Fast Reactor Kinetics," Technology of Nuclear Reactor Safety, MIT Press, Cambridge, Mass. 1964, p.530-607.

10. B. Wolfe, N. Friedman, and D. Riley, "Influence of the Doppler Effect on the Meltdown Accident," GEAP-4420 (1963).

11. Hwang, R.N. Ott, K., Comparison and Analysis of Theoretical Doppler Coefficient Results for Fast Reactors, Argonne Nat. Lab., USAEC Rep. ANL-7269 (1966).

12. J.F. Jackson and R.B. Nicholson, "Venus II: On LMFBR Disassembly Program, ANL-7951, Argonne National Lab., Argonne, Illinois, 1972.

13. R.B. Nicholson and J.F. Jackson, "A Sensitivity Study for Fast Reactor Disassembly Calculation," ANL-7952, Argonne National Lab., Argonne, Illinois, 1972.

14. P.A. Meyer, B. Wolfe, and N.F. Friedman, "A Parameter Study of Large Fast Reactor Meltdown Accidents," *Proc. Conf. on Safety, Fuels, and Core Design in Large Fast Power Reactors*, October 11-14, 1965, ANL-7120, pp. 671-685.

15. E.T. Rumble, "A Hypothetical Overpower Excursion Model for Liquid Metal-Cooled Fast Breeder Reactors," Ph.D. Dissertation in Engineering, University of California, Los Angeles, Cal., June, 1974.

2.2.2 Sodium Superheat and Rapid Heat Transfer to the Coolant

2.2.2.1 Introduction

In the current design of sodium-cooled fast breeder reactors, a coolant temperature at least 200 to 300°C below the saturation temperature is anticipated during normal operation. Despite this large safety margin and the fact that current and future designs of liquid metal-cooled fast breeder reactors (LMFBRs) will assure that loss-of-cooling incident is an event of small probability, reactor safety analysis must consider coolant- temperature excursions to the extent that boiling may occur. Two rather distinct boiling processes are of major interest in the analysis of abnormal reactor behavior. The first, termed channel voiding, concerns sodium boiling and motion within relatively intact reactor-coolant channels. The second, termed violent boiling, concerns vapor production and pressure generation as collapsing fuel elements or molten fuel-element material contact sodium. The primary interest in channel voiding results from the need to assess rates of sodium-voiding reactivity feedback. The primary interest in violent boiling results from the need to assess the magnitude of potentially destructive pressure pulses.

2.2.2.2 Sodium Boiling and Expulsion

Sodium boiling and expulsion is considered to be a primary cause for reactivity ramps (Ref. 1). Reasons for this uncontrolled heating are:

- Increase of neutron flux
- Flow reduction in a subassembly or in whole core
- Partial or total blockage of coolant flow

It has been observed that sodium shows a strong tendency for superheat. This superheat depends on the fact that no or few nuclei for bubble formation are present in sodium. The reasons for this lack of nuclei are:

1. the perfect wetting of metal surfaces by sodium
2. the strong chemical reactivity of sodium
3. the high solubility of gases in sodium

The degree of superheat appears to be a strong function of surface finish and sodium purity. Than many factors enter into the degree of superheat is illustrated in Figures 1 and 2 of data presented at the Aix Conference.

Some of the factors affecting the possible degree of superheat of liquid metals are: (a) Experimental heating method, (b) Flow Velocity, (f) Pressure and Pressure-temperature history (g) Instability, (h) Purity and Gas Content, (i) Radiation.

(a). Experimental Heating Method

Investigators who have used direct heating (Ref. 8,9) (joule heating in the liquid metal itself) report superheats considerably higher than do those who have used indirect heating methods (Ref. 10,11) (conduction heating through the coolant-channel wall). The latter are more representative of the type of heating that takes place in an actual reactor coolant channel. Considering the direct-heating studies of Ref. 9 and taking into account the resistivities and thermal capacities of steel and sodium, it appears that approximately two-thirds of the thermal energy supplied was dissipated in the sodium and that one-third was stored in the wall. Perhaps direct heating causes homogeneous nucleation (and, therefore, higher superheats) rather than the wall nucleation that occurs with indirect heating. [And perhaps not; reference 7 shows early Argonne National Laboratory (ANL) data obtained via direct heating where observed superheat values are relatively small.] It should also be noted that, quite possibly, variables other than the heating method may have caused the differing results, as will be seen later.

The importance of indirect heating is emphasized by the results of experiments in which subcooled nucleate boiling occurred (Ref. 6).

(b). Surface Condition

French superheat data (Ref. 9) spread from about 20 to 200°C. These values were considered compatible with the condition of the surface of the experimental tube used. One of the simplest models for the effects of surface imperfections on superheat is that of Hsu[12]. This model states that for a given cavity of radius r_c to produce vapor bubbles, a necessary condition is that the temperature in the fluid thermal layer at a distance r_c from the heater surface be greater than or equal to the temperature required by the equilibrium equation,

$$T = T_{sat} + \frac{2\sigma}{r} \frac{T_{sat}}{h_{fg} \rho_V}$$

This criterion clearly indicates the radius r, of tolerable wall imperfections and is well borne out for water superheat. For liquid metals, however, the high thermal conductivity tends to flatten the temperature profile and the excellent wetting properties tend to flood the cavities with the net effect that superheats much higher than Hsu criterion are observed.

Thorough studies of the relation between surfaces and incipient boiling have been published (Ref. 2,4,13) and they clearly show the effect of roughness. With as-received surfaces (commercially smooth), measured potassium superheats have ranged from 500°F (saturation temperature) down to 230°F at 1770°F, but, when eight 0.0006-in. dia holes were drilled 0.040 in. deep in the same surface, the superheat was reduced (Ref. 2) about 40 fold. In a more recent paper (Ref. 13), it appears that these data represent the behavior of the superheat existing in the stable boiling mode and that the incipient superheat is more closely related to the saturation temperature than to the cavity size or surface condition.

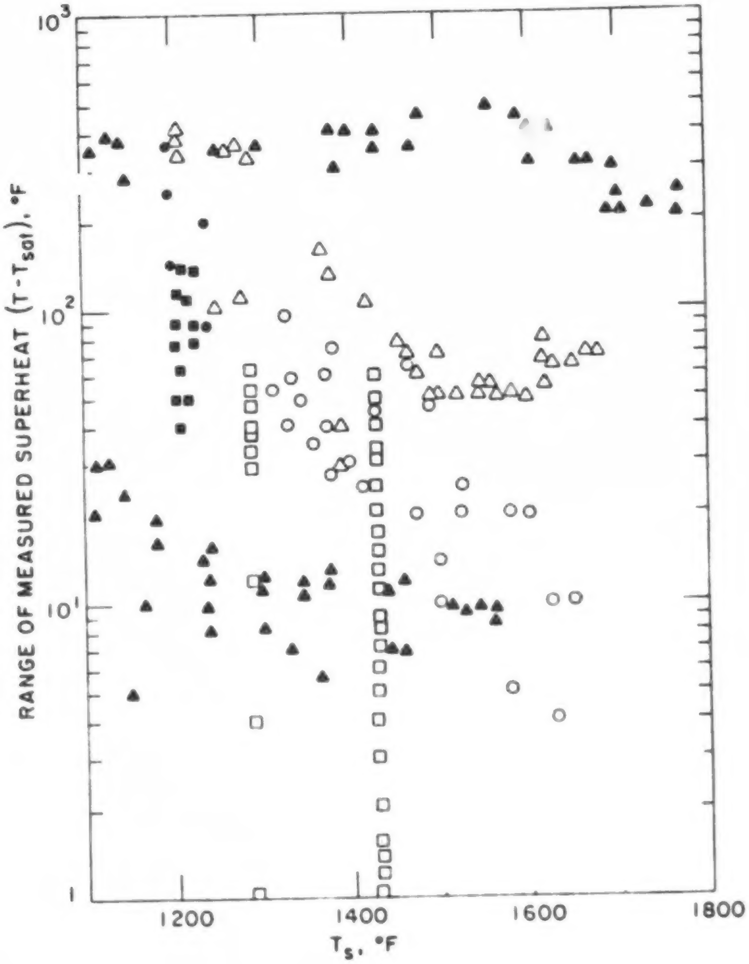

FIGURE 1
Liquid Metal Superheat Data Presented Prior to 1968.

K(Ref. 2), Na(Ref. 3), Na(Ref. 4 and 5)

Na(Ref. 2), Na(Ref. 6), Na(Ref. 7)

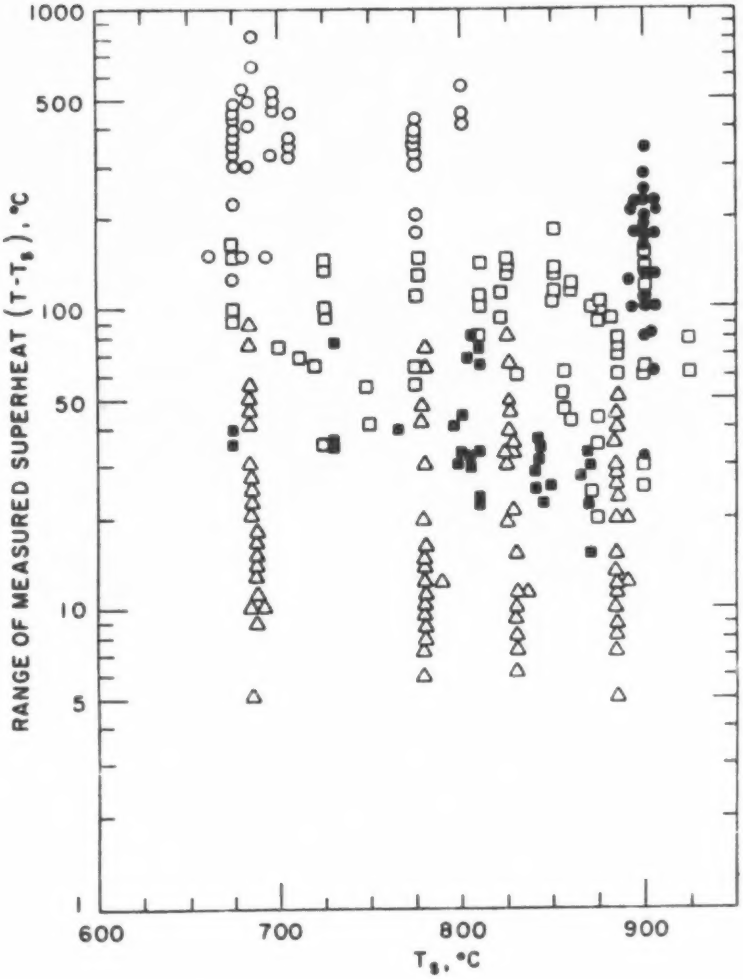

FIGURE 2
Liquid Metal Superheat Data Presented at the Aix Conference
(1968)

o K(Ref. 8), Na(Ref. 8), Na(Ref. 9)

Na(Ref. 10), Na(Ref. 11)

(c) Aging

In the recent French experiments (Ref. 9), the mean value of the superheats reached for a given pressure appears to increase slowly with time. This observation is in agreement with the Ispra data (Ref. 7) show the opposite trend; aging effects were not reported by the experimenters who used conduction heating techniques (Ref. 10,11).

The possible increase in superheat with time appears to be an important consideration in further studies on superheat. During the life of a fast reactor, the coolant could conceivably clean the heating surface to a large degree, leaving smaller and smaller cavities available for nucleation.

(d) Heat Flux

Differing results were reported at the Aix Conference concerning heat flux. Heating power sometimes appears to be an unimportant parameter (Ref. 8,9) but Refs. 10 and 11 indicated a definite heat-flux dependency. Reference 11 reports a decrease in superheat with increasing heat flux - Ref. 10 an increase. A Russian paper (Ref. 3) published in

1966 says, "The tendency of the nucleate boiling to change to natural convection can be noticed at low heat fluxes. In this case, the value of the liquid superheat sharply increases." In a more recent study (Ref. 2), there was no sizeable effect of heat flux upon incipient superheat.

e. Flow Velocity

In recent Ispra experiments, measured superheats were generally lower under forced or natural circulation than under stagnant conditions, for the same mockup and filling, (Ref.8), but no quantitative velocity dependency was reported. However, this velocity relation agrees with earlier data (Ref. 7) where relatively low superheat values were observed during forced circulation. More recent data (Ref. 6) show a definite velocity effect (Fig. 3). These data are for bulk superheats and could differ significantly from results with wall superheats.

f. Pressure and Pressure-temperature History

Both pressure and pressure-temperature history were shown by ANL to be important variables (Ref. 10)(Fig. 4).

This is also apparent in the French data (Ref. 9) and in earlier published data (Ref. 7, 15). A simplified analysis (Ref. 14) appears to predict the effects of pressure-temperature history reasonably well (Ref.10), and may explain part of the variation found in published data where this variable is not accounted for.

The pressure-temperature-history model has met with partial success in explaining experimental results. The model has continued to undergo evolution. In a recent modification, Holtz et al. (Ref. 16) attempted to allow for the diffusion of inert gas in and out of unwetted surface cavities and for the effect of the cover gas system on superheats. Modifications and refinements have been made on the pressure-temperature-history model by Chen (Ref.15), Dwyer (Ref.17), Collier and Kosky (Ref. 18) and Singer and Holtz (Ref. 19).

g. Instability

The characteristic instability of boiling sodium--intermittent bubbling--was noted only at low heat fluxes and pressures (Ref.10,11). Recent observations are in agreement with previous work (Ref. 3,20,21), where analyses have shown that stability increases with increasing heat flux and pressure.

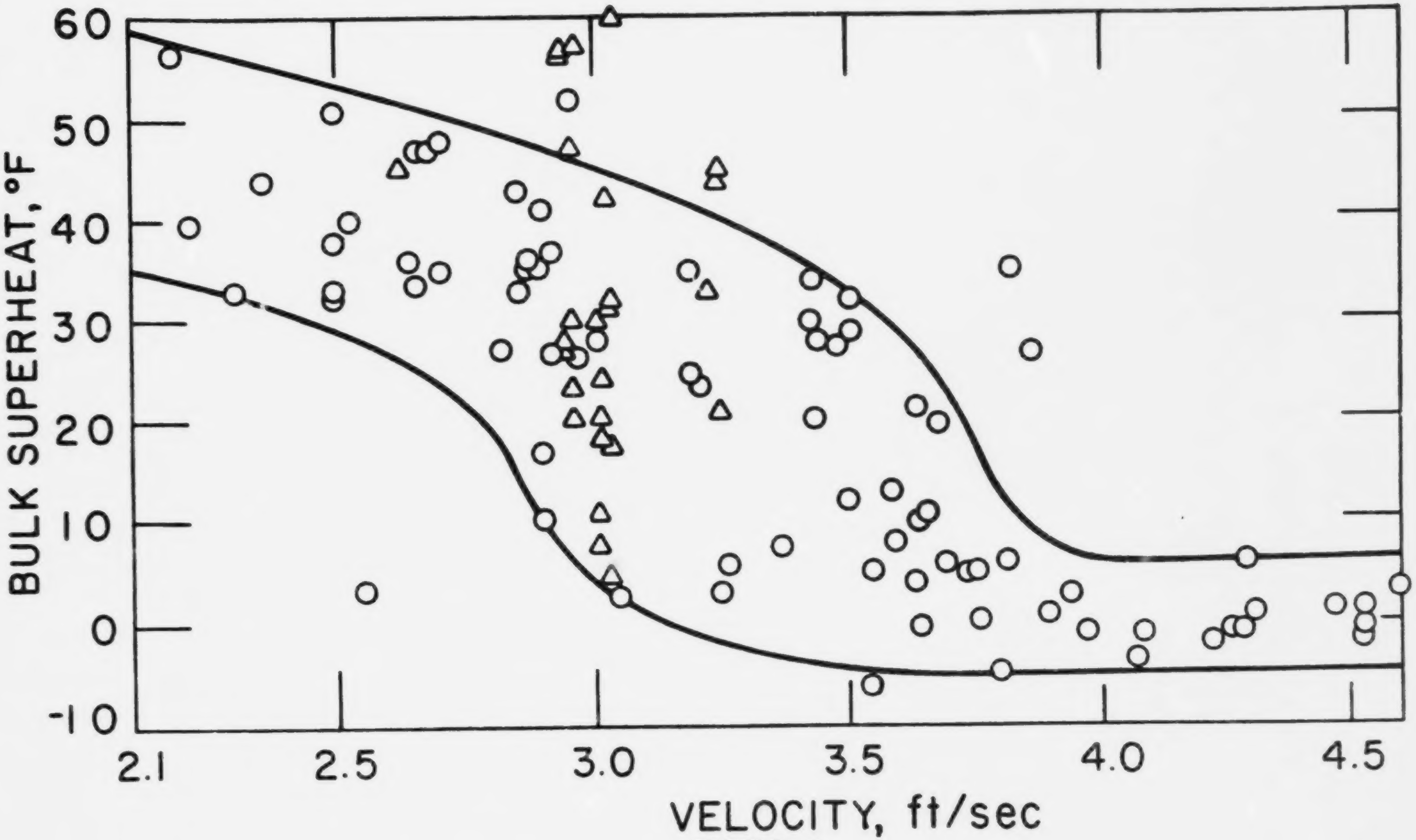

FIGURE 3

. A Velocity Effect is Apparent in These Data for Bulk Superheat in Sodium at 5 psia

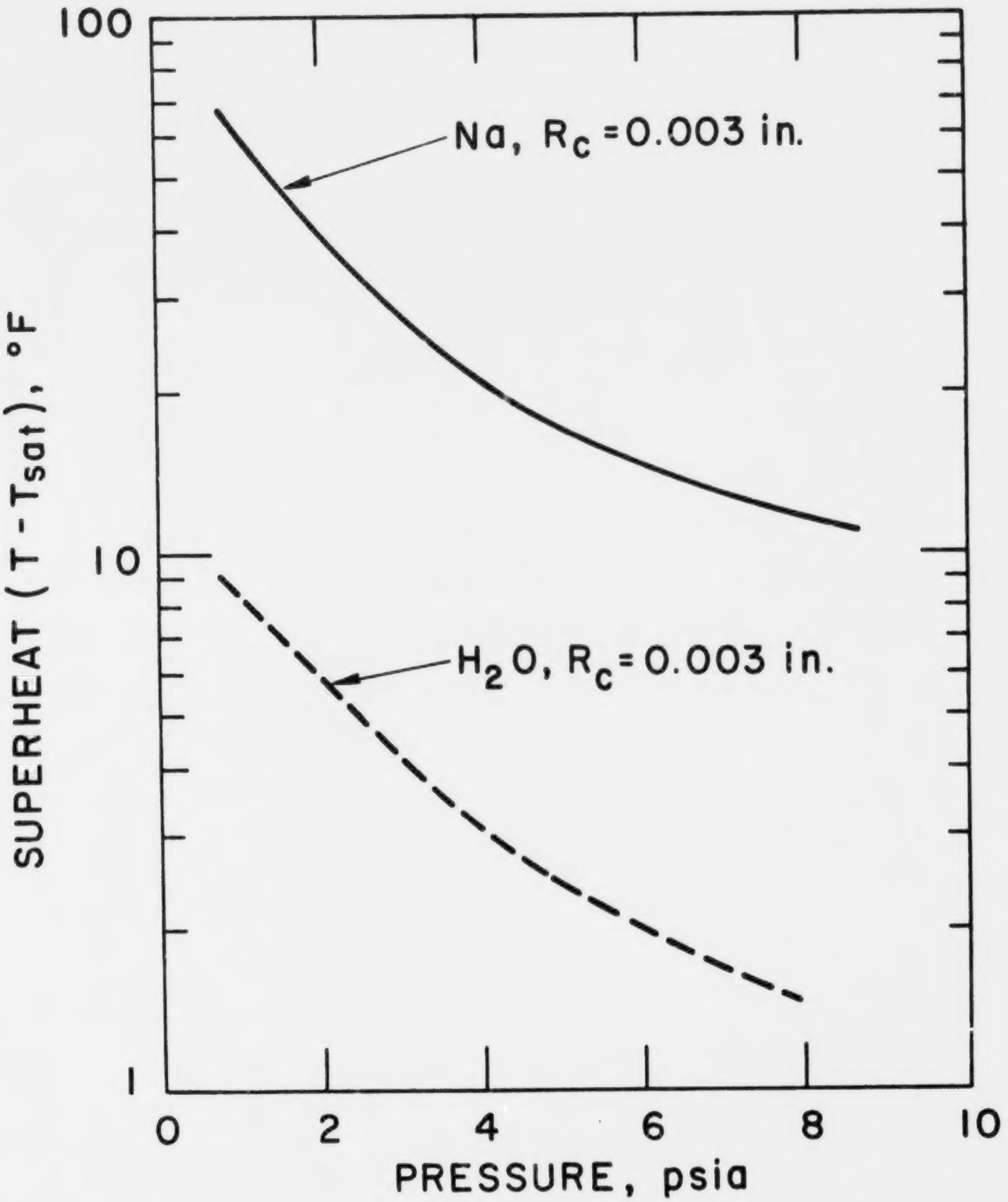

FIGURE 4
Superheat Values for Sodium and Water for a Given Cavity Size

Two new papers (Ref. 13,22) also discuss the instability of alkali-metal boiling. An instability map that indicates pressure levels and heat fluxes necessary to maintain stable boiling for a particular surface is given in Ref. 10.

h. Purity and Gas Content

"The extremely high values of superheat reported in the Ispra paper (Ref. 8) were attributed primarily to a more efficient purification of the liquid metals before testing. System cleanliness undoubtedly is very important. However, in most experiments reported, neither the actual purity of the liquid metal nor the dissolved gas content has been very well known. Better agreement among various laboratories will be achieved when the systems and the fluids in them are better defined.

i. Radiation

The effects of nuclear radiation on incipient boiling were discussed in a British paper at the Aix Conference (Ref.23). Several different types of radiation were considered: electrons, protons, alpha particles, photons, neutron, fission fragments, and alpha recoils. It was concluded to be highly unlikely that, at saturation pressures near 1 atm, any nuclear radiation encountered would induce nucleation of vapor bubbles in bulk sodium before boiling would occur at surface cavities. However, a number of assumptions were made in these theoretical calculations; experimental verification seems in order.

2.2.2.3 Rapid Heat Transfer to the Coolant (Explosive Interaction)

2.2.2.3.1 Significance of the Phenomenon

The previous discussion was concerned with water-solid interactions; this section is concerned with liquid-liquid interaction.

When molten metal comes into contact with a quenching fluid, a violent explosion can occur. This so-called "vapor or physical explosion" is a well-known, but little understood, phenomenon. A vapor explosion is usually characterized by an initiating event that leads to fragmentation and by the sudden conversion of thermal energy to mechanical energy due to very rapid heat transfer accompanied by a subsequent pressure wave. The violence, or magnitude, of such an explosion depends upon the quantity and rate of energy release. Numerous incidents have been reported in the literature (Ref. 24-35). Such explosions have occurred in the steel (Ref. 24-27), aluminum (Ref. 28,29), copper smelting (Ref. 28), paper (Ref. 30,31), and nuclear industries (Ref. 32,33).

The mechanism that triggers or initiates the explosion is not known; however, two basic facts have been established. First, the causative mechanism is not due to chemical reaction (Ref.36), and second, fragmentation of the sample material is usually involved. Both experimental results and analyses (Ref.37) have shown that the heat-transfer rates required to release the observed energy from a smooth metal sample are several orders of magnitude higher than the maximum rates that can be obtained in laboratory studies. Thus it has been concluded by numerous investigators that fragmentation of the metal to generate large surface areas is required to obtain the observed explosion violence.

Several review articles have considered the potential problem of steam explosions with reference to the safety of nuclear reactors (Ref. 35,38). The articles by Brauer, et al. (Ref.39), Ergen (Ref. 40), Witte, et al. (Ref.35), and Flory, et al. (Ref.41) describe the various factors thought to be involved in steam explosions, while Pearlman (Ref.42) reviewed chemical reactions which occur between water and certain metals at elevated temperature. Epstein summarized many of the early developments regarding both physical and chemical metal-water explosions (Ref.38). A variety of materials have been examined including molten aluminum in water (Ref. 28,29,43), copper in water (Refs. 44,45), iron in water (Ref.46.47), smelt in water (Ref.30,31) and, more recently molten UO_2 in water (Ref. 48,49) and UO_2 in sodium (Ref. 49,50,51,52). An intensive investigation into the fundamental causes of physical explosions is being pursued at the University of Houston (Ref. 34,53,54,55,56,57). The Reactor Safety Study of light water reactors credits the molten core steam explosion with being involved in all of the severest consequences to the public.

In 1965, Hicks and Menzies (Ref.59) reported the results of their analysis, which placed a practical upper limit on the work done by the energy in the fuel when sodium is brought into intimate contact with molten fuel in the core. They have shown that it is thermodynamically feasible for the conversion of fuel thermal energy into mechanical work to be as high as 30%. Energetic interaction of this magnitude could produce sizable structural damage and indeed would impose major safety problems. However, all TREAT experiments (Ref.60) (E-, H-, and S-series) to date involving transient meltdown of multi-pin arrays of clad fuel in sodium indicate the above analysis is extremely conservative since energy conversion ratios from these tests have been below the thermodynamic limit by at least two orders of magnitude.

2.2.2.3.2 Description of the Phenomenon

In the liquid-liquid system, three fundamental heat-transfer regimes exist: direct contact liquid-liquid convective heat transfer, spontaneous nucleation heat transfer, and film boiling heat transfer. These heat-transfer regimes may occur either by themselves (if a relatively small mass of either the volatile or the host fluid is involved) or all three regimes may exist simultaneously (if large masses of both the volatile and hose fluids are involved). The nucleate boiling regime (nucleation from preferred sites on the solid surface) generally observed with solid-liquid systems is absent in the liquid-liquid system because of lack of preexisting nucleation sites. The convective-heat-transfer regime can therefore exist in a liquid-liquid system despite the presence of very large superheating of the more volatile liquid. The spontaneous nucleation regime is of particular interest since the vapor generation rate associated with this regime is sufficiently fast to produce shock waves; i.e., in accordance with our definition, the occurrence of spontaneous nucleation can therefore be referred to at least as one form of explosive boiling. A knowledge of the film-boiling regime and its boundary is of equal importance since it determines whether direct liquid-liquid contact is possible in a given system.

a. Direct Contact Liquid-Liquid Heat Transfer

The well-known nucleate boiling regime observed with solid-liquid systems at relatively small liquid superheats is generally explained by nucleation from gas- and/or vapor-filled cavities located on the solid heater surface. Since a liquid represents essentially a perfectly smooth surface, this form of nucleation site is not present in the liquid-liquid system, hence the absence of the nucleate boiling regime. The direct contact between two fluids, in the case where the temperature of the host fluid exceeds the boiling point of the more volatile fluid by a substantial amount, is therefore possible since gas is not trapped at the interface. The only requirement is that the gas layer present prior to direct contact must be squeezed out, i.e., certain hydrodynamic conditions must be satisfied, including sufficient impact velocities and/or disturbances. Geometric shapes and quantities of the two liquids will largely determine whether liquid-liquid contact, film boiling, or both regimes participate in the heat-transfer process. Typical examples of direct-contact liquid-liquid heat transfer in the absence of the other heat-transfer regimes discussed above is exemplified in the paper of Fauske (Ref.52) for water droplets in Freon-11. Because of the complete entrainment in this case, the Freon droplets remain in a metastable state without evaporation. This form of entrainment, wetting, and superheating should also be possible when liquid sodium is injected into a bath of molten UO_2 or molten steel. Waldram (Ref.61) shows another example for a pentane-silicone oil system, where sustained liquid-liquid contact and simple surface evaporation is achieved despite the oil temperature being approximately 110°C above the normal boiling point of pentane. In this case, the impact velocity of the pentane droplet is sufficient to squeeze out completely the gas layer existing between the droplet and the oil, thereby resulting in wetting and spreading.

b. Spontaneous Nucleation Threshold

The magnitude of the spontaneous nucleation temperature is crucial in determining the violence of direct-contact explosive boiling. The spontaneous nucleation rate J due to statistical density fluctuations can be calculated and is dependent upon the excess temperature required above saturation temperature for liquid water and sodium to nucleate homogeneously, are shown in Fig. 7. At these temperatures, the number of bubbles formed per unit time changes from a very small number to a very large number.

After displacement of the gas layer, equilibration of the characteristic contact angle (or interfacial tension) following direct liquid-liquid contact requires a finite time. It therefore follows that the spontaneous nucleation temperature for a given liquid-liquid system varies with time. If the interfacial temperature (T_i) at the instant of contact

$$\frac{T_i - T_c}{T_H - T_c} = \left(\frac{K_H \rho_H C_H}{K_c \rho_c C_c}\right)^{1/2} \qquad (1)$$

(where subscripts H and c represent hot and cold liquid respectively, K is the thermal conductivity, ρ is the density, and C is the specific heat) is below the homogeneous nucleation temperature, than the spontaneous nucleation temperature threshold depends upon the heating rate. If the time constant for contact angle equilibration is less than the characteristic heating rate, then the threshold temperature is determined by the characteristic equilibrium contact angle of the system. If this value is near or equal to zero, homogeneous nucleation is possible, as illustrated by the solid curves in Fig. 8. An example of this type of behavior can again be illustrated by the pentane-silicone oil system (Ref.61). In this case, spontaneous nucleation takes place when the oil temperature exceeds the homogeneous nucleation temperature of pentane.

c. Film Boiling

The phenomenon of direct contact between a hot and cold liquid can be evaluated by examining the requirements for film boiling. Much improved correlations have recently become available to predict the Leidenfrost and minimum temperatures. Henry's (Ref.63) correlation is based upon hydrodynamic considerations as outlined by Berenson (Ref.64), while Baumeister's correlation (Ref.65) is largely based upon the "foam limit" as proposed by Spiegler et al. (Ref.66). The correlations are developed from data obtained with solid-liquid systems including liquid metals. However, since large differences in nucleation characteristics exist between solid-liquid and liquid-liquid systems (Ref.67), and since the nucleation and wetting phenomena are believed to play an important role in determining the appropriate boiling regime, direct extrapolation to a liquid-liquid system appears difficult (Ref.68). Thermodynamic considerations suggest an alternate method for evaluating the minimum temperature for film boiling in a liquid-liquid system. The approach includes the thermal properties of the more volatile liquid as well as the hot liquid following the method proposed by Henry (Ref.63) and the stability limit (T_S) is calculated based upon the well-known kinetic approach discussed briefly above rather than from Van der Waals equation as used by Spiegler (Ref.66). In this way, the possibility of spontaneous nucleation at the liquid-liquid or solid-liquid interface as compared to the bulk can be

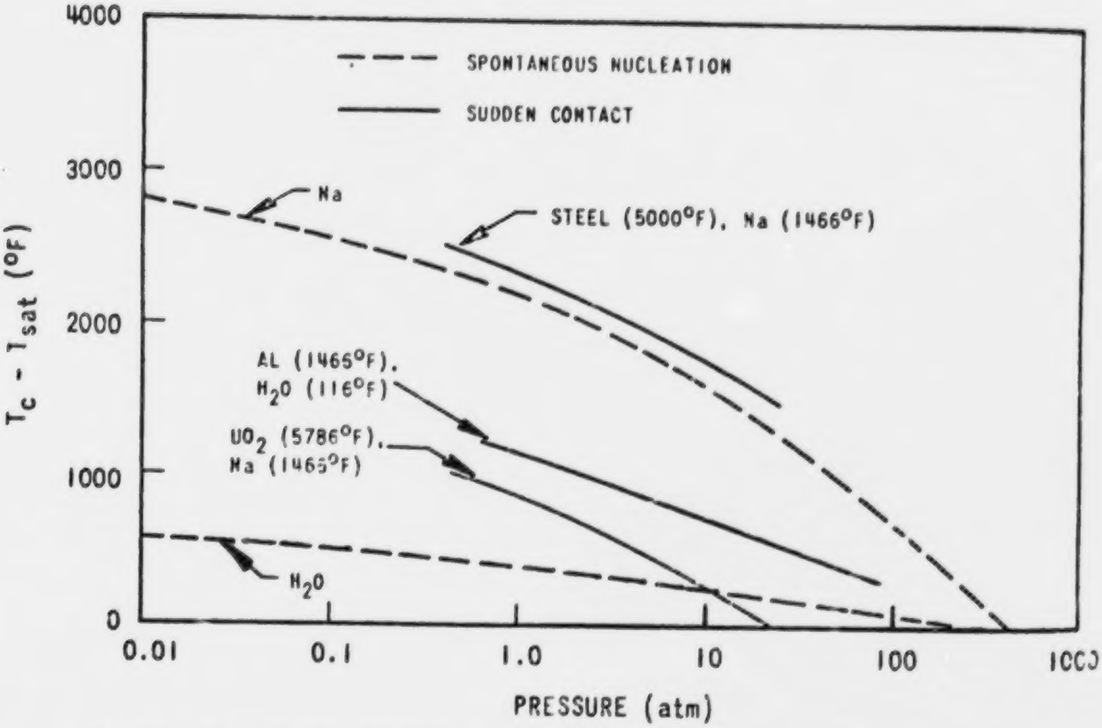

Fig. 7 Comparison between spontaneous nucleation temperatures and sudden contact temperatures for three different systems.

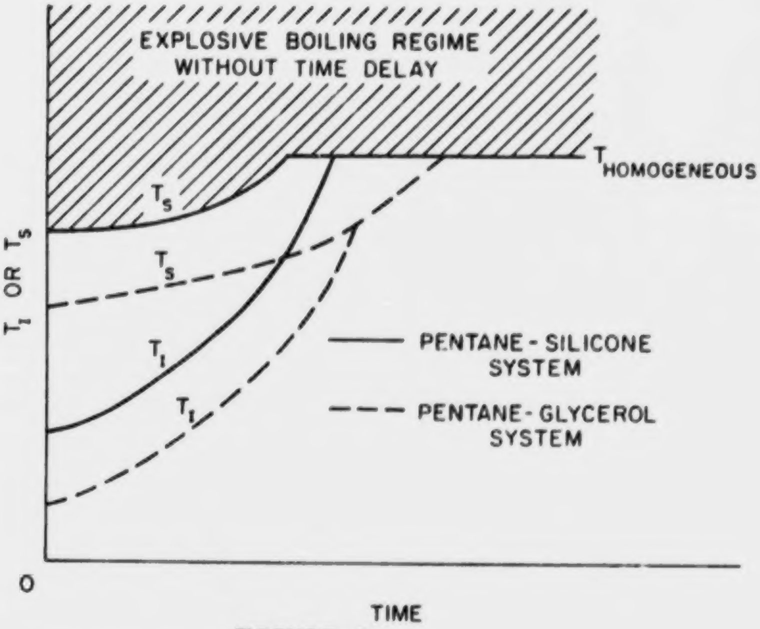

EXPLOSIVE BOILING REGIME WITHOUT TIME DELAY
T HOMOGENEOUS
T_s
T_s
T_I
T_I
T_I OR T_s
PENTANE - SILICONE SYSTEM
PENTANE - GLYCEROL SYSTEM
0
TIME

FIGURE 8
Qualitative illustration of spontaneous nucleation temperature and explosive boiling regime variation with time, including typical behavior of two systems with same volatile fluid but two different host fluids.

accounted for if the interfacial tension or the contact angle for the particular system in question is known. The method implies that film boiling must occur when the interface temperature (see Eq. 2) exceeds the spontaneous nucleation temperature (see Eq. 1), since sustained liquid-liquid contact is not possible for these conditions. This method may be misleading, however, since proper constraint may lead to continuous explosive boiling rather than film boiling.

To assess the true minimum temperature for film boiling in a given liquid-liquid system, hydrodynamic considerations, including impact velocities and/or disturbances in addition to geometric shapes of the two liquids, must be considered. The magnitude of the subcooling (resulting in collapse) of the volatile fluid and whether the host fluid is in a liquid state or flashing two-phase state are also important considerations.

2.2.2.3.3 Vapor Explosion Mechanism

To generate shock waves, the vapor must be produced at extremely high rates. This requirement is at least satisfied when the vapor generation is a result of exceeding the stability limit or the spontaneous nucleation temperature (T_s) of the more volatile liquid. As discussed above, spontaneous or explosive boiling can occur with and without a time delay following initial liquid-liquid contact. In the absence of nucleation sites or in the case of rapid heating, a small-mass explosion is, therefore, possible if the hot fluid temperature is above T_s. In the absence of mechanical (external forces) and/or hydrodynamic disturbances (subcooling), significant liquid-liquid contact in an unconstrained system would appear difficult when the contact temperature T_i exceeds the spontaneous nucleation limit T_s (i.e., film boiling is more likely). However, in a properly constrained system (the more volatile liquid is surrounded by the hot fluid or vice versa), repeated liquid-liquid contact can occur despite the fact that T_i exceeds T_s. This form of boiling in a liquid-liquid system has been referred to as "continuous explosive" boiling, and with proper geometric configuration and constraint can escalate into a large-mass vapor explosion, i.e., instantaneous explosive mixing and generation of surface area much like a chain reaction. The above discussion suggests the following requirements must be satisfied in order to cause a large-mass vapor explosion in a liquid-liquid system:

1. Direct liquid-liquid contact is required, implying a breakdown in the gas layer between the two fluids.

2. Explosive boiling immediately upon contact, implying that the interfacial temperatures must exceed the spontaneous nucleation temperature characteristic of the system upon initial contact. This process results in fragmentation and mixing of both the hot and cold fluid without time delay.

3. For the above processes to escalate on a time scale required for a large-mass explosion, proper initial constraint is also required.

The first requirement explains largely why vapor explosions cannot occur if the temperature difference is too large between the hot and cold fluid (example: fresh LNG and H_2O),(Ref.69), or that a large external force is required if the quantities involved are relatively small (example: impact-column experiment of Wright *et al.*(Ref.70). The second requirement is consistent with the sharp temperature-threshold effect noted for vapor explosions (Ref. 69,71).

The temperature-threshold effect is clearly demonstrated with experiments involving Freons and mineral oil as the host fluid (Ref.71). Within the uncertainties in physical properties, the noted temperature threshold corresponds to an interfacial temperature T_I approximately equal to the homogeneous nucleation temperature for Freon-22. This result is consistent with the fact that this system is known to exhibit excellent wetting (the two fluids are highly miscible), i.e., the contact angle immediately upon direct liquid-liquid contact is essentially at its equilibrium value. On the other hand, for Freons using water as the host fluid, the threshold is found to correspond to an interfacial temperature below the homogeneous nucleation limit (Ref.69,71). This is again consistent with the known wetting characteristics of these systems (Freons and water are almost immiscible), i.e., the contact angle upon initial contact is considerably above the characteristic equilibrium contact angle of the system. The spontaneous nucleation threshold for a given liquid-liquid system is generally not well known (i.e., the ability to sustain superheat upon initial contact), although for systems of interest, this threshold appears relatively close to the homogeneous nucleation limit.

The third requirement of proper constraint largely determines the intensity of the resultant explosion, and explains why in many systems efficient large-mass explosions occur on a somewhat random basis. This is illustrated particularly well in experiments with the salt-water system (Ref.72). These experiments also clearly demonstrate the important fact that a one-step heating and fragmentation process cannot supply enough energy to explain the experimental results, and that the major energy transfer takes place after the initiation of the explosion. In summary, the conditions that constitute the necessary constraint for a localized event to escalate into a large-scale vapor explosion are not well understood in ideal laboratory experiments and, therefore, even to a lesser degree in practical systems.

2.2.2.3.4 UO_2 - Sodium Experiments

Although many experiments (Ref. 49-52) have been performed on UO_2-sodium systems, those of Armstrong (Ref.73) and Johnson et al. (Ref.74) will be discussed. Experimental laboratory studies by Armstrong have shown that vapor explosions can occur with LMFBR materials. Six experiments were carried out where small amounts of liquid sodium were injected into a crucible containing molten UO_2. Table 1 shows the conditions for each of the runs. The first experiment in the series produced a vapor explosion; a total 2.3 cm^3 of sodium had been injected at the time of the event. Upon initial contact, sodium vapor and droplets spewed out the top of the crucible in a relatively mild manner. However, data recorded from pressure and force transducers and from the high-speed motion pictures both indicated that a vapor explosion was recorded by a blast microphone ~15 cm from the open top of the UO_2 crucible, which indicated a 0.5-atm shock pressure in the helium. Experiments 2 and 4 gave no indication of pressurization. Post-test examinations of the crucible showed that the velocity apparently was too low to penetrate the UO_2 surface in experiment 2, and that a crust of solid UO_2 had formed ~2 cm above the surface of molten UO_2 in experiment 4 and therefore blocked the sodium jet. Run 3 apparently yielded the largest

Conditions for Experiments in Which Sodium Was Injected into Molten UO_2

Run	Na Temp (°C)	Injection Velocity (m/sec)	Injection Height (cm)	UO_2 Load (g)	UO_2 Temp (°C)
1	400	5	1	29	3000
2	400	3.5	1	31	3000
3	400	7.5	2	51	3000
4	400	7.5	2	49	3000
5	400	7.5	2	49	3100
6	400	9.5	2	50	3100

TABLE I.

explosion of the series, but no quantitative information was obtained because of equipment failure. With run 5, two small reactions occurred. The first was 35 msec after the start of the injection, corresponding to ~0.3 g of sodium injected; the second occurred ~8 msec later. The last run of the test series produced a more violent interaction 9 msec after initiation of sodium injection. Again, a shock pressure in the helium of ~0.3 atm was recorded by a blast microphone ~20 cm from the open top of the crucible. At this time, ~0.15 g of sodium had been injected.

Prior to the above tests, a series of 12 experiments were carried out with molten UO_2 and stainless steel (Ref. 51), where the molten materials were injected into a pool of liquid sodium. With this mode of contact, no vapor explosions were observed, although extensive fragmentation of UO_2 and stainless steel took place. The observed rates of pressurization events shown on the films and the lack of detectable atmospheric overpressurization provide evidence of the relative slowness of the pressurizations.

The following conclusions from these experiments may be drawn:

1. True vapor explosions have only been observed when liquid sodium has been injected into a pool of molten UO_2.

2. When molten UO_2 and stainless steel have been injected into a pool of liquid sodium, no explosions have been observed. This method of contact is characteristic of existing TREAT experiments which indicate low thermal-to-mechanical energy conversion ratios.

3. Extensive fragmentation of the hot materials occurs when they are injected into liquid sodium. The occurrence of extensive fragmentation does not lead to vapor explosions but rather to just violent noisy boiling.

In the work of Johnson et al. (Ref. 74) large (~kg) quantities of UO_2 melted by a thermite type of reaction with MoO_3 powder were dropped into molten sodium. Table II from Johnson summarizes the three experiments. The results of these experiments showed that for larger quantities than used by Armstrong of molten uranium incident on molten sodium, no vapor explosions were found.

Large-scale UO_2-Sodium Interactions Experimental Conditions and Results

RUN #	M1	M2	M3
Conditions			
Quantity UO_2-Mo-Cr Released (lb)	1.4	6.8	3.0
Quantity Sodium (lb)	6.6	7.1	6.5
Temperature Sodium (°F)	550	570	1160
Vessel Pressure at Entry (psia)	50.	56	26.
Estimated Entry Velocity (ft/sec)	11(1)	60(2)	13(1)
Calculated Adiabatic Temperature(3) (°F)	1170	2160	1960
Results			
Final Sodium Temperature (maximum measured) (°F)	740(4)	1300(5)	1450(4)
Maximum Vessel Pressure (psia)	62	100(6)	(>40(7) < 100)
Sodium Ejected from Crucible (lb)	0.02	5.0	4.6
UO_2-Mo-Cr Ejected from Crucible (lb)	0.01	1.33	1.21
Average Particle Size UO_2-Mo-Cr			
- total material (μm)	510	220(8)	170
- material in crucible (μm)	510	300(8)	200
- ejected material (μm)	-	140	180

1. Velocity calculated from time of fall.
2. Velocity estimated from motion pictures.
3. Assumed no boiling of Na and thermite enthalpy = 670 Btu/lb.
4. Temperature from thermocouple under crucible.
5. Temperature from immersion thermocouple.
6. Vessel cover opened about 90 psia.
7. Vessel pressure at time of transducer failure.
8. Not including large porous pieces.

TABLE II

2.2.2.3.5 Conclusions

The subject of liquid-solid superheat is reasonably well understood and modeled. There is no evidence of explosive reactions that could serve as severe accident initiators but control and flow problems could be induced and must be considered in the reactor design.

The situation with liquid-liquid reactions is potentially more serious. There is ample evidence of vapor explosions in other industries and they have been created on a laboratory scale for sodium incident on uranium. If it can be demonstrated that a requirement for a vapor explosion is homogenous nucleation,then the problem is more assuring. In the UO_2-Na system, it is important to recognize that the initial contact temperature is substantially below the homogeneous nucleation limit (see Fig. 8). Furthermore, because of the apparent excellent wetting characteristics at elevated temperatures, it is reasonable to assume that the initial interface temperature is also well below the characteristic spontaneous nucleation temperature corresponding to initial liquid-liquid contact. This suggests that the UO_2-Na system provides for considerable time to allow the homogeneous nucleation limit to be approached. Since the interfacial temperature is also well below the spontaneous solidification temperature for UO_2 at the instant of contact (Ref. 75), vapor nucleation will most likely occur from a solid-liquid system, In the UO_2-Na system, it would appear difficult to achieve explosive boiling without a considerable time delay. In accordance with the proposed requirements for large-mass vapor explosions, the UO_2-Na system involving large masses would fall in the category of violent boiling.

Consistent with the above discussion, the thermodynamic approach to film boiling ($T_i \geq T_s$) suggests that sustained liquid-liquid contact is readily achieved for the UO_2-Na system for temperatures of interest. For saturated sodium, a bulk temperature of UO_2 in excess of 5000°C is required to remain in the film-boiling regime, assuming a contact angle equal to zero. Likewise, Henry's film-boiling correlation (which is based on hydrodynamic considerations and includes sodium data) predicts UO_2 bulk temperature of ~7000°C in order to maintain film boiling in Armstrong's laboratory experiments with the UO_2-Na system. The small-mass vapor explosions observed in these experiments have been explained by entrainment, wetting, and superheating similar to that demonstrated for the Freon-11-water system (Ref. 52). The lack of nucleation sites in the liquid-liquid like system results in overheating of the liquid sodium until spontaneous nucleation occurs.

REFERENCES

1. D. Okrent and H.K. Fauske, "Lecture Background Notes on Transient Sodium Boiling and Voiding in Fast Reactors," Argonne Center for Education Affairs, ANL/ACEA-101, January, 1972.

2. J.A. Edwards and H.W. Hoffman, "Superheat with Boiling Alkali Metals," in Proc. of the Conf. on Application of High-Temperature Instrumentation to Liquid-Metal Experiments, Sept. 28-29, 1965, USAEC Report ANL-7100, pp. 515-534, Argonne National Laboratory.

3. B.S Petukhov, S.A. Kovaler, and V.M. Zhukov, "Study of Sodium Boiling Heat Transfer," in Proc. of the Third Intl. Heat Transfer Conf., Chicago, Illinois, Vol. 5, p. 80, Aug. 1966.

4. P.J. Marto and W.M. Rohsenow, "Effects of Surface Conditions on Nucleate Pool Boiling of Sodium," J. Heat Transfer, 88(2) p. 196, 1966.

5. I. Shai, "The Mechanism of Nucleate Pool Boiling Heat Transfer to Sodium and the Criterion for Stable Boiling," USAEC Report TID-23790 (DSR-76303-45), M.I.T., Jan. 1967.

6. Atomics International, AEC Unclassified Programs Quarterly Technical Progress Report, January-March 1967, USAEC Report NAA-SR-12395, May 31, 1967.

7. J.B. Heinenman, "Forced-Convection Boiling Sodium Studies at Low Pressure," in Proc. of the Conf. on Application of High-Temperature Instrucmentation of Liquid-Metal Experiments, Sept. 28-29, 1965, USAEC Report ANL-7100, pp. 189-194, ANL.

8. G. Grass et al., "Measurements of the Superheating and Studies Abount Boiling Phenomena in Liquid Metals," Proc. of the Int. Conf. on the Safety of Fast Reactors, Aix-en-Provence, France, Sept. 19-22, 1967.

9. B. Le Gonidec et al., "Experimental Studies on Sodium Boiling," Proc. of the Int. Conf. on the Safety of Fast Reacors, Aix-en-Provence, France, Sept. 19-22, 1967.

10. R.E. Holtz and R.M. Singer, "On the Superheating of Sodium and the Gneration of Pressure Pulses," Proc. of the Int. Conf. on the Safety of Fast REactors, Aix-en-Provence, France, Sept. 19-22, 1967.

11. G.C. Pinchera et al., "Experimental Boiling Studies Related to Fast Reactor Safety," Proc. of the Int. Conf. on the Safety of Fast Reactors, Aix-en-Provence, France, Sept. 19-22, 1967.

12. Y.Y. Hsu, "On the Size Range of Active Nucleation Cavities on a Heating Surface," Trans. ASME, Journal of Heat Transfer, Vol. 84, p. 207, 1962.

13. J.A. Edwards and H.W. Hoffman, "Incipient and Stable Boiling Superheat for Potassium Boiling on a Surface Containing Reentrant Cavities," JSME Semi-Int. Symposium, Tokyo, Japan, Sept. 4-8, 1967, in preparation.

14. R.E. Holtz, "The Effect of the Pressure-Temperature History upon Incipient-Boiling Superheats, USAEC Report ANL-7184, Argonne National Laboratory, June 1966.

15. J.C. Chen, "Incipient Boiling Superheat in Liquid Metals," Journal of Heat Transfer, Series C, 90, No. 3, pp. 303-312, 1968.

16. R.E. Holtz, H.K. Fauske, and D.T. Eggen, "The Prediction of Incipient-Boiling Superheats in Liquid-Metal-Cooled Reactor System," Journal of Nuclear Eng. and Design, 16, 1971.

17. O.E. Dwyer, "On Incipient Boiling Wall Superheats in Liquid Metals," Int. Journal Heat and Mass Transfer, 12, p. 1403, Pergamon Press, 1969.

18. J.G. Collier and P.G. Kosky, "Natural Convective Boiling of the Alkali Metals - A Critical Review," AERE-R5436, 1967.

19. R.M. Singer and R.E. Holtz, "On the Role of Inert Gas in Incipient Boiling Liquid-Metal Experiments," Int. Journal Heat and Mass Transfer, 12, No.9, p. 1045, Pergamon Press, 1969.

20. P.J. Marto and W.M. Rohsenow, "Nucleate Boiling Instability of Alkali Metals," J. Heat Transfer, 88 (2) p. 183, 1966.

21. I. Shai, "The Mechanism of Nucleate Pool Boiling Heat Transfer to Sodium and the Criterion for Stable Boiling," USAEC Report TID-23790 (DSR-76303-45), M.I.T. Jan. 1967.

22. G.I. Bobrovich, B.P. Auksentyuk, and N.N. Mamontova, "On the Mechanism of Boiling of Liquid Metals, JSME Semi-Int. Symposium, Tokyo, Japan, Sept. 4-8, 1967, in preparation.

23. K.T. Claxton, "The Influence of Radiation on the Inception of Boiling in Liquid Sodium," Proc. of the Int. Conf. on the Safety of Fast Reactors, Aix-en-Provence, France, Sept. 19-22, 1967.

24. "A Method for Handling Steelmaking Slag," Iron & Steel Eng., 28 (10), 85-89, Oct. 1951.

25. Tetzner, Herman, "Slag Explosions in Open-Hearth Steelworks," Neue Hutte, 6 (4), 352-359, June, 1959.

26. "Water was Energy Source in Ladle Explosion," Steel Times, pp. 56-57, January, 1964.

27. Lipsett, S.B., "Explosions from Molten Material and Water," Fire Technology, 2 (2), 118-126, May, 1966.

28. Long, G., Stroup, P.T., and Ennor, W.T., "Explosions of Aluminum and Water," Report No. 2-50-33 (NP-5471), Process Metallurgy Div., Aluminum Research Lab., Aluminum Company of American (1950); Long, G., "Explosions of Aluminum and Water-Cause and Prevention," Metal Progr., pp. 107-112, May, 1957.

29. Rengstorff, G.W.P., Lemmon, A.W., Jr., and Hoffman, A.O., "Review of Knowledge on Explosions Between Molten Aluminum and Water to the Aluminum Assoc.," Battelle's Columbus Laboratories, p. 53, April, 1969.

30. Sallack, J.A., "An Investigation of Explosions in the Soda Smelt Dissolving Operation," Pulp and Paper Mag. (Canada), 56, (9), 114-118, 1955.

31. Nelson, W., and Kennedy, E.H., "What Causes Kraft Dissolving Tank Explosions - I. Lab. Experiments," Paper Trade J., 140 (7), 50-56, July, 1956.

32. Ivins, R.O., and Baker, L., "Chemical Eng. Div. Semiannual Report, January-June, 1964," ANL-6900, pp. 270-280 August, 1964.

33. Mally, C.T., et al., "Kinetic Studies of Heterogenous Water Reactors. Annual Summary Report, 1964," STL-372-12 Dec. 30, 1964.

34. Bouvier, J.E., Witte, L.C., and Cox, J.E., "The Vapor Explosion - Heat Transfer and Fragmentation. I. Introduction to Explosive Vapor Formation," Technical Report No. ORO-3936-1, Dept. of Mechanical Eng., Univ. of Houston, 21 pp., November, 1969.

35. Witte, L.C., Cox, J.E., and Bouvier, J.E. "The Vapor Explosion," J. of Metals, 22 (2) 39-44, February, 1970.

36. Epstein, L.F., "Analytical Formulation for the Reaction Rate," Metal Water Reactions, 6, 37-39, Sept. 1959.

37. Higgins, H.M., "The Reaction of Molten Uranium and Zirconium Alloys with Water," Aerojet General Report No. AGC-AE-7, p. 18, April, 1965.

38. Epstein, L.F., "Recent Development in the Study of Metal-Water Reactions," Progr. Nucl. Energy, Ser. IV, 4, 461-483, 1961.

39. Brauer, S.D., Green, N.W., and Masler, R.B., "Metal/Water Explosions," Nucl. Sci. Eng., 31 (3), 551-554, 1968.

40. Ergen, W.K., et al., "Emergency Core Cooling - Report of Advisory Task Force on Power Reactor Emergency Cooling," TID-24226, 1966

41. Flory, K., Paoli, R., and Mesler, R., "Molten Metal-Water Explosions," Chemical Eng. Progr., 65(12), 50-54, Dec., 1969.

42. Pearlman, H., "Chemical Reactions Between Water and Certain Metals at Elevated Temperatures," U.S. AEC, NAA-SR-Memo-858 p. 22, 1954.

43. Hess, P.D., and Brondyke, K.J., "Causes of Molten Aluminum-Water Explosions and Their Prevention," Metal Prog., (4), pp. 93-199, April, 1969. (Presented at the Metals Cong., Detroit, October, 1968.)

44. Azuma, Kiyoshi, Goto, Sakichi, Kametani, and Hiroshi, "The Explosion of Mat by Water. I. Nature of the Explosion," Nippon Kogyo Kaishi, 73, 295-300, 1957.

45. Azuma, Kiyoshi, Goto, Sakichi, Kametani, Hiroshi, "The Explosion of Mat by Water. II. Chemical Reaction Between the Molten Copper Mat and Steam," Nippon Kogyo Kaishi 73, 449-452, 1957.

46. Marty, G.V.L.N., Subba Rao, D., and Ramaswami, T.R., "Highly Water-Reactive Forms of Transitional Elements of the Iron Groups," Current Sci. (India) 25,197-188, 1956.

47. Gasik, M.I., and Kyitrik, S.I., "Interaction of Liquid Iron with a Steam-Hydrogen Mixture," Met. i Koksokhim., Mezhvedonstv. Resp. Nauchn.-Tekhn. Sb. 3,5-16, 1965.

48. Gilby, R.L., "Reaction of Molten UO_2 With Water," BNWL-362, 1967.

49. Amblard, M., Semeria, R., Vernier, P., Gouzy, A., and Najuc, M., "Contact Effect Between Molten UO2 and Sodium and Molten $UO_2$and Water," EURFNR-811, March 3, 1970.

50. Anderson, R.P., and Armstrong, D.R., "Laboratory Tests of Molten-Fuel-Coolant Interactions," Trans. Amer. Nucl. Soc., 15 (1), 313, June, 1972.

51. Armstrong, D.R., Testa, F.J., and Raridon, D., Jr., "Interaction of Sodium with Molten UO_2 and Stainless Steel Using a Dropping Mode of Contact," ANL-7890, Dec., 1971.

52. Fauske, Hans K., "On the Mechanism of UO2-Na Vapor Explosions," Nuclear Science Eng., 51, 95-101, 1973.

53. Stevens, J.W., Bullock, R.L., Witte, L.C., and Cox, J.E., "Transition Boiling from Spheres to Water," AEC Report ORO-3936-3, April, 1970.

54. Hsico, K.H., Cox, J.E., Hedgecox, P.G., and Witte, L.C., "Pressurization of a Solidifying Sphere," AEC Report ORO 3936-4, April, 1970.

55. Witte, L.C., et al., "Rapid Quenching of Molten Metal," AEC Report ORO 3936-6, August, 1971.

56. Bradley, R.H., et al., "Investigation of the Vapor Explosion Phenomenon Using a Molten-Metal Jet Injected into Distilled Water," AEC Report ORO-3936-7, October, 1971.

57. Witte, L.C., et al., "Transition Film and Transition Boiling from a Sphere," AEC Report ORO-3936-9, Sept., 1972.

58. Reactor Safety Study, "An Assessment of Accident Risks in U.S. Commercial Nuclear Power Plants," USAEC Report WASH-1400, August, 1974.

59. E.P. Hicks, and D.C. Menzies, "Theoretical Studies on the Fast Reactors in Maximum Accident," Proc. Conf. Safety, Fuels, and Core Design in Large Fast Power Reactors, p. 654, ANL-7120, Argonne National Laboratory, 1965.

60. J.F. Marchaterre, H.K. Fauske, L. Baker, C.E. Dickerman, and R.W. Wright, "Experimental Studies of Liquid Metal Fast Reactor Accident Conditions," Proc. Intern. Conf. Eng. of Fast Reactors for Safe and Reliable Operation,

61. K. Waldram, M. Sc. Thesis, Northwestern University, Evanston, Illinois, April, 1973.

62. H.K. Fauske, "Some Aspects of Liquid-Liquid Heat Transfer and Explosive Boiling," Proc. of the Fast Reactor Safety Meeting, Beverly Hills, Ca., April 2-4, 1974. CONF. 740401-P2, pp. 992-1005.

63. R.E. Henry, AIChE Preprint 14, Presented at the Fouteenth National Heat Transfer Conf., Atlanta, Ga., August 5-8, 1973.

64. P.J. Berenson, Trans. ASME, Jr. of Heat Transfer, 83, 351-358, 1961.

65. K.J. Baumeister and F.F. Simon, Trans. ASME, Jr. of Heat Transfer, 95, 2, pp. 166-173, 1973.

66. P. Spiegler et al., Int. J. Heat Mass Transfer, 6, pp. 987-989, 1963.

67. H. K. Fauske, J. Reactor Technol., 15, 4, pp. 278-302, 1972.

68. R.E. Henry, D.J. Quinn, and E.A. Spleha, "An Experimental Study of the Minimum Film Boiling Point for Liquid-Liquid Sysytems," Accepted for presentation at the Int. Heat Transfer Conf., Tokyo, Japan, 1974.

69. T.Enger and D.E. Hartman, "Explosive Boiling of Liquified Gases on Water," Paper presented at the National Research Council Conf. on LNG Importation and Terminal Safety, Boston, Massachusetts, June 13, 1972.

70. R.W. Writght et al., "Kinetics Studies of Heterogeneous Water Reactors, 1965 Annual Summary Report," STL 372-30, TWR Systems, 1965.

71. R.E. Henry, et al.,"Large Scale Vapor Explosions," Proc. of the Fast Reactor Safety Meeting, Beverly Hills, Ca., April 2-4, 1974. CONF.-740401-P2, pp. 922-934.

72. R.P. Anderson and D.R. Armstrong, AIChE Pre print 16, Presented at the Fourteenth National Heat Transfer Conf., Atlanta, Ga., August 5-8, 1973.

73. D.R. Armstrong, "Reactor Development Program Progress Report," ANL-RDP-2, p. 8.31, ANL, 1972.

74. T.R. Johnson, L. Baker Jr., and J.R. Pavlik, "Large-Scale Molten Fuel-Sodium Interaction Experiments," Proc. of the Fast Reactor Safety Meeting, Beverly Hills, Ca. April 2-4, 1974. CONF.-740401-P2 pp. 883-896.

75. A.W. Cronenberg and H. K. Fauske, "UO_2 Solidification Phenomena and Fragmentation during Quenching in Sodium Coolant," Trans. Am. Nucl. Soc. 18 (1), p.213, 1974.

2.2.3 Autocatalysis and Strong Fuel Motion

2.2.3.1 Introduction

In this section we discuss the behavior of an LMFBR during an accident in which a great deal of fuel motion takes place. The literature in this area is rather sparse and consists of two published papers and one proposal. In essence it can be said that extended fuel motion problems have until recently been overlooked. The true extent of their impact on HCDA analysis is currently unknown. Future work will be required in this area to scope this problem and the beginnings of such scoping calculations are currently being carried out at ANL and at LASL. In the next section we discuss the two papers and proposals in detail, and following that there is an assessment section on what work ought to be done in the future.

2.2.3.2 Discussion

In the paper by Boudreau and Erdmann (Ref.1) on autocatalysis during fast reactor disassembly, extensive fuel motion problems are analyzed in symmetrical, cylindrical geometry. VENUS and TWOTRAN were coupled together to carry out this numerical study. Fuel motions were based upon past accidents and were inferred from previous VENUS calculations done at Argonne National Laboratories. Little in the way of fuel coolant interactions were carried out in this paper. Reactor studies included the GE LMFBR design and the FFTF reactor design. It was concluded that VENUS underpredicted the reactor subcriticality significantly after an extensive fuel motion accident. Table I taken from this paper summarizes the results of the calculations in words. Possible reentry of the fuel into the initiallly voided core is also hinted at in this paper.

In the paper by Boudreau and Jackson (Ref. 2) a rather hueristic discussion is presented of the variety of phenomena that might occur in an extensive fuel motion type accident in an LMFBR. The accident emphasized in this paper is one in which initially fuel is driven accidently out of the reactor and then falls or is driven back into the reactor either by gravity or by sodium vapor pressure. This reentering fuel then provides a rather healthy ramp to the partially disabled core causing again additional disassembly. Fuel slumping to the bottom of the core is also considered as an alternate form of criticality phenomenon.

It is concluded that such incidents are possible. Little in the way of definitive analysis is contained in this second paper, but the following summarizes their results. Ramp rates may range from $1500 to $1700 per second depending upon the type of fuel reentry. In the case of small reactors, some form or incoherent reentry is likely, and reentry velocities may be limited at prompt criticality. It may be estimated that

TABLE 1

Summary of Factors Influencing Autocatalysis

An Increase in:	When core fuel displacement is characterized by:	Generally means that the tendency for autocatalysis will:
1. Core Height/ Diameter Ratio	Outward Radial Motion	decrease. For a tall reactor, neutron leakage is predominantly radial. Rearrangement causes an increase in this already strong leakage, along with a relatively weak density increase.
2. Core Height/ Diameter Ratio	Outward Axial Motion	increase. Moving fuel axially in a tall reactor has little effect on overall neutron leakage, and the density increase is stronger for the same fuel displacement than in the radial case.
3. Zonal Enrichment; flattening of radial flux shape in inner zone	Outward Radial Motion	increase. Because central flux is initially flat in the radial direction, moving the fuel radially weakly affects its influence on radial leakage, and the density increase dominates.
4. Zonal Enrichment	Outward Axial Motion	increase. Overall radial leakage is larger for a zoned core than for a single enrichment core of the same size. The effect, for axial motion, is similar to the effect when H/D is increased.
5. Size of Core (overall dimensions)	Outward Motion in Either Direction	increase. In a core with larger overall dimensions, assuming the material composition fixed except for fissile enrichment, the reactor is larger in neutron mean-free-paths. This means that fuel displacement (compaction) enhances multiplication more than it increases leakage. A second effect is a decrease in the magnitude of the reactivity effect from fuel motion (whether positive or negative) because the fissile enrichment is lower.
6. Absorption in Blankets (Σ_a)	Outward Motion in Either Direction	decrease. Assuming that the scattering cross section in the blanket is fixed, an increase in Σ_a means that moving fuel toward the blanket will cause a higher percentage of the neutrons which subsequently leak into the blanket to be lost in absorption.
7. Scattering in Blankets (Σ_{tr})	Outward Motion in Either Direction	increase. With Σ_a fixed, an increase in Σ_{tr} means that when material is moved toward the blankets, a higher percentage of the neutrons are reflected back into the core.

recriticality ramp rates may be of the order of $100 per second for smaller reactors. No estimates are provided for larger LMFBR ramp rates from this type of accident. Recriticality in the lower dome following a core disassembly is considered unlikely.

Work is currently being carried out at Los Alamos Scientific Laboratories to construct an extended fuel motion capability. This work will include the careful study of the phenomenology and material properties involved in such accidents, the preparation of a materials dynamics computer algorithm, two-dimensional time-dependent transport theory algorithm, and a coupling of the material dynamics and neutron kinetics algorithm into a single code. No results have appeared in the literature regarding the progress on this project.

2.2.3.3 Assessment

Because of the complexities involved in extensive type disassemblies and because of the minimal amount of work done on this problem so far, it is felt that conclusions regarding the importance of extensive fuel motion to LMFBR safety and environmental impact are premature. A great deal of additional work must be carried out in this area before one can determine which are the key mechanisms or mechanistic sequences involved in recriticality and what the outcome of such sequences might be. The symmetries and homogeneities in both space and time may cause this problem to diminish the magnitude of its consequences. However, because of the myriad possibilities of fuel motion we feel that well-defined sequential analysis is inappropriate in this accident. Rather, bounding calculations are needed.

REFERENCES

1. J.F. Boudreau and R.C. Erdmann, "On Autocatalysis During Fast Reactor Disassembly," Nucl. Sci. Eng. 51, 206 (1973).

2. J.E. Boudreau and J.F. Jackson, "Recriticality Considerations in LMFBR Accidents," Proc. Fast Reactor Safety Meeting, U.S. Atomic Energy Commission Report CONF-740401-P3, p. 1265 (1974).

2.2.4 FUEL ELEMENT FAILURE PROPAGATION

2.2.4.1 Introduction

The evaluation of the potential for failure propagation in fuel subassemblies of LMFBR's of current design (mixed U-Pu oxide pellets, stainless steel cladding) has been the subject of considerable research over a number of years in most countries involved in the development of the LMFBR. The study of fuel-failure propagation is concerned with the occurrence of initially small local faults in the core and the possibility of their growth into more widespread serious faults.

There are two broad categories in which to place fuel propagation problems: subassembly-to-subassembly propagation and pin-to-pin propagation within a subassembly. Of course the first presents a potentially more severe source accident than the second and has a lower probability of occurrence, but even the possibility of a single subassembly meltdown must be kept remote since such an accident could eventually lead to a whole-core incident.

The two subclasses of fuel failure propagation are distinguished by the detection methods used to identify the presence of the failed fuel propagation and by the time constants associated with the propagation. Generally, the subassembly-to-subassembly propagation is expected to require a longer time unless there is a common mode mechanism also contributing to the failure. No extensive experimental studies on this have been done, but times on the order of a few seconds to several minutes seem appropriate, depending upon the mechanism postulated for failure. This is to be contrasted to the times estimated for the pin-to-pin propagation, where propagation times as small as 0.25 sec. need be considered. (Ref.1).

Pin failures can be induced on a large scale by subjecting the fuel subassembly in question to a severe power-to-flow mismatch; for such conditions the concept of pin-to-pin failure propagation obviously does not apply since the fuel pins will fail irrespective of the failure of adjacent pins. Therefore it is appropriate to limit the attention here to operating conditions prior to the initiating event which are characterized by power-to-flow ratios smaller than, or close to, the nominal value. This includes also conditions during plant startup when the coolant flow may be low.

Because of the very large number of fuel pins ($\sim 10^5$ pins in a 1000 MWe LMFBR of current design), random cladding failure, followed by fission gas release and possibly washout of fuel particles, has a finite probability of occurrence over the life time of a reactor core. The probabilities associated with the formation of local blockages and the occurrence of fuel pin enrichment errors resulting in release of small amounts of molten fuel, are expected to be smaller. (Ref.1).

There are two areas of concern regarding problems arising from fuel failure propagation:

1. The events which could initiate such potential pin-to-pin failures.
2. Potential propagating mechanisms.

Also of interest is:

3. A general scenerio for failure propagation.
4. Detection of failure propagation.

2.2.4.2 Initiating Events

Several general types of initiating events are of concern in potential pin-to-pin propagation (Ref. 1-4):

a) random fuel pin cladding failure due to e.g., manufacturing defects,

b) subassembly inlet blockages,

c) fuel pin enrichment errors,

d) local coolant blockages inside fuel subassemblies due to inert foreign or fissile particulate matter in the coolant.

At present there does not seem to be any way to guarantee that random fuel pin failures will not occur. Hence, most of the current design techniques are devoted to confining such a failure to a single pin, and to detecting the failed subassembly with a fuel element detection and location (FEDAL) system.

Near complete subassembly inlet blockages are rendered nearly impossible, whenever the geometry of the subassembly remains intact, by the arrangement of the coolant inlet openings (Ref.5). Such a precaution is a natural outgrowth of the experience gained from the Enrico Fermi reactor incident in 1966.

Lack of quality control during the manufacturing process could possibly result in enrichment errors affecting a number of fuel pins, although careful quality assurance procedures should make the probability for their occurrence small. Large enrichment errors affecting an entire fuel subassembly are not relevant here, since they can be detected during start-up by means of subassembly outlet instrumentation prior to the occurrence of fuel damage.

Analyses have been reported on possible pin-to-pin damage propagation due to enrichment error (Ref. 6-8). Experimental tests to correlate the theory were performed in the TREAT reactor on a 7-pin assembly with the peripheral pins of 20%-enriched UO_2 fuel and with the central pin containing a 1.5 in. section at the midplane of fully enriched fuel between end regions of 26%-enriched fuel. The peak-to-average power density for the assembly was a factor of 2.1, which was sufficient to cause 50% melting in the oxide. During the 10 sec test, the cladding was not breached and there was no release of the fuel into the coolant, although considerable cracking of fuel pellets was observed. The conclusion from the test was that sufficient axial movement of the oxide occurred to prevent cladding strain. Based upon this test and analyses, and upon the expectation of adequate quality control standards to avoid such a mis-match of enrichments of fuel pellets, such a potential source accident is considered to be of minor importance.

Local coolant blockages would tend to be formed at random radial locations of the subassembly cross-sectional flow area, and also at random locations in the axial direction if wire-wrap spacers are used. With grid spacers, on the other hand, the subchannel flow obstructions would most likely occur at such axial locations. Of course, most LMFBR designs envisage the use of sieves, and this should eliminate particles above a certain size from circulating.

Propagation of a local coolant blockage could possibly occur by release of fuel particles from failed pins or by swelling of failed pins due to fuel-coolant chemical interaction. Once this would occur, and if localized sodium boiling occurred downstream of a blockage, than a rapid growth of the fault possibly could occur by either one or combined effects of: (Ref. 5,10)

1. Vapor blanketing, dryout and failure of fuel pins, possibly accompanied by the ejection of molten fuel.
2. Production of sufficiently large amounts of sodium vapor to interfere with the overall coolant flow through the subassembly, thereby leading to hydrodynamic instability and bulk sodium boiling.

Predictions have been made independently by Gast (Ref.5), Fauske (Ref.11), and others (Ref.12-14) that even if boiling were to occur over more than 50% of the cross-sectional flow area of a subassembly, local boiling would be very unlikely to cause overheating of the rod cladding or flow instability in the affected subassembly. Therefore, rapid fault propagation due to direct thermal-hydraulic effects of local boiling is not to be expected. It is not possible, however, to rule out delayed failure of the fuel rods, due mainly to cyclic thermal stresses in the cladding caused by the rapid growth and collapse of the bubbles in the sodium.

There is also some evidence (Ref.15) that in the wake of an impermeable blockage a recirculation zone is formed, resulting in an effective heat removal from the local regions behind the blockage. If confirmed experimentally for sodium coolant in an LMFBR reactor subassembly, this would provide further reason for belief that local boiling would not occur in the wake of a blockage large enough to be detectable by subassembly outlet instrumentation. Experiments and analyses on electrically heated bundles and sodium coolant have tended to confirm these conclusions. (Ref.16).

It is also comforting to know that blockages, if they are formed at all, are most likely not to be completely impermeable. For example, it has been calculated that a seepage flow of about 16% of the nominal flow is sufficient to avoid boiling in the wake region of a porous flow blockage. (Ref.5). Other studies (Ref.17) confirm that a significant amount of fuel per flow subchannel, exceeding 2 g, would be required to produce coolant boiling in the blockage.

In summary, the initiation of a potential fuel pin failure propagation is considered much less likely, and probably much less damaging, than was believed five years ago in the program to develop the LMFBR.

2.2.4.3 Potential Propagating Mechanisms

Associated with the initiating events are three types of potential propagation mechanisms, namely:

(1) release of fission gas,

(2) local coolant temperature increase and possibly local coolant boiling, and

(3) release of small amounts of molten fuel.

Of these three, only the first is of primary concern since the latter two have already been shown in the previous discussion to be of low probability as initiating events.

At the end of life, the fission gas (predominantly xenon) could amount to as much as 450 cc (STP), or a pressure of up to 1000 psia, depending upon the power history of the fuel and the gas-plenum size. Release of fission gas in an LMFBR subassembly, due to rupture of one or more fuel pins, could potentially result in fuel failure propagation through either:

(a) temperature transients in the cladding of adjacent fuel pins, which exceed the threshold temperature for failure at the operating conditions, and

(b) transitory mechanical loads on adjacent fuel pins due to pressure pulses which could potentially induce sufficient deflection to cause brittle rupture, especially near the end of fuel life.

A schematic representation of the different mechanisms is nicely illustrated in Fig. 1 from van Erp et al. (Ref. 1, 18). Here the slow mechanisms are classed as those with gas release occurring in time periods exceeding 0.25 sec, while the fast releases are expected to occur in less than 0.1 sec.

The potential of gas-jet impingement for causing fuel failure propagation has received the most attention and is not considered as a serious slow release mechanism because the

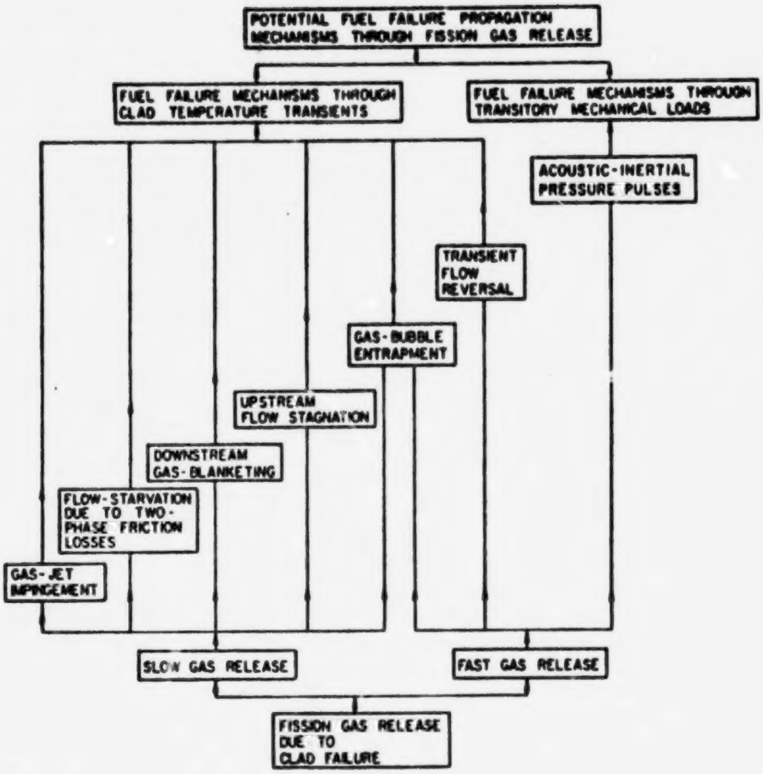
POTENTIAL FUEL FAILURE PROPAGATION MECHANISMS THROUGH FISSION GAS RELEASE
FUEL FAILURE MECHANISMS THROUGH CLAD TEMPERATURE TRANSIENTS
FUEL FAILURE MECHANISMS THROUGH TRANSITORY MECHANICAL LOADS
ACOUSTIC-INERTIAL PRESSURE PULSES
TRANSIENT FLOW REVERSAL
GAS-BUBBLE ENTRAPMENT
UPSTREAM FLOW STAGNATION
DOWNSTREAM GAS-BLANKETING
FLOW-STARVATION DUE TO TWO-PHASE FRICTION LOSSES
GAS-JET IMPINGEMENT
SLOW GAS RELEASE
FAST GAS RELEASE
FISSION GAS RELEASE DUE TO CLAD FAILURE

Fig. 1 Schematic representation of potential pin-to-pin fuel failure propagation mechanisms due to fission-gas release in LMFBR fuel subassemblies.

calculated maximum stresses in a pin, subjected to the appropriate non-uniform temperature distribution experimentally measured and corresponding to the worst-mode of gas-jet impingement, was well below allowable values, (Ref.19). Any such incident would probably tend to be self-limiting in any case (Refs. 1.3), because the jets would preferentially cause failure of adjacent pins in such a way that the gas coming from subsequently failed pins would be directly mainly toward the pins which have already failed (Refs. 1,3).

Release of fission gas into an LMFBR fuel subassembly may potentially cause flow starvation and downstream gas blanketing in a limited number of coolant subchannels, due to increased (two-phase) frictional pressure losses and due to dilution and displacement of the coolant. The main difference between these two phenomena is that for flow starvation the cladding temperature rise is caused by the coolant temperature rise, whereas in case of downstream gas blanketing the cooling of the fuel pins in the affected region is drastically reduced due to displacement of the liquid-phase coolant. The degree of flow starvation, and the probability for occurrence of downstream gas blanketing will, all other things being equal, be greater for small values than for large values of the radial dispersion rate of the gas inside the fuel subassembly. Due to the decrease of the coolant mass flow rate in the affected subchannels, the local coolant temperatures will increase, resulting in higher clad temperatures which potentially could exceed the failure threshold.

In order for the phenomenon of downstream gas blanketing to cause high cladding temperature rises, two principal conditions are required to be fulfilled, namely, (a) a considerable part of the circumferential area of a fuel pin has to be insulated by a gas layer from the bulk coolant flow, so as to minimize circumferential conductive heat removal, and (b) the gas velocity must be high enough to remove the liquid coolant film from the affected area. Neither of these conditions can exist, based upon the low gas release rates experimentally determined. (Ref.20,21). Furthermore, the type of nonuniform temperature distribution that could be induced by downstream gas blanketing is less severe and less localized than that encountered for worst-type gas-jet impingement, so that failure of the fuel pins due to thermal stresses will not occur.

Sufficient evidence therefore exists to conclude that flow starvation and downstream gas blanketing in LMFBR fuel subassemblies do not constitute viable mechanisms for pin-to-pin fuel failure propagation. (Ref.22-24). Likewise, van Erp et al. have concluded that upstream flow stagnation in LMFBR subassemblies due to fission gas release does not constitute a mechanism for fuel failure propagation. (Ref.1).

In the wakes of flow obstructions, there is a tendancy for gas bubbles to become entrapped. For a very low Reynolds number characterizing the flow (say Re $\leq$ 20,000), bubbles may remain entrapped for long periods of time after the gas release has stopped, whereas at higher Reynolds the bubbles tend to collect together and remain entrapped for shorter times. It is felt that this could be a potential problem for LMFBR fuel subassemblies with grid spacers unless the design of the grids is properly done, whereas no problem is expected for fuel subassemblies with wire-wrap spacers.

To eliminate rapid gas release, there are currently two views on the need to design a system to minimize the effects. For the German SNR facility, a fuel pin design is utilized which will enable the fission gas to be released only slowly; this is accomplished by partitioning the pin plenum into a series of smaller volumes interconnected by small holes. (Ref.5,25).

On the other hand, it has been concluded by van Erp et al. (Ref.1) that such precautions may not be necessary because of a study which indicates that times for rapid gas-blanketing of up to 30 FFTF-type pins ($\sim$0.1 sec) are less than the minimum required time of 0.25 sec for cladding failure to occur. (Ref.26). It should be noted, however, that the experimental studies and analytical model preserved the integrity of the geometry; if there were a coupling of difficulties due to fission gas impingement plus partial coolant channel blockage, the compartmentalized subassembly design might be very advantageous.

Another rapid gas release phenomenon which has been considered is the possibility that a pressure pulse could cause failure of pins having a low ductility because of high burnup. An analysis regarding the inertial and viscous effects of the transversal coolant flow due to an expanding gas bubble in a fuel assembly indicate, however, that the probability for propagation of pin failure by this mechanism is low. (Ref.27). Besides, the high fission-gas release rate is only possible if the cladding failure occurs in or near the gas plenum region of the fuel pin, where the ductility is higher than that in the core fuel region because the irradiation is less.

In summary, it is concluded that the occurrence of pin-to-pin failure propagation in LMFBR fuel subassemblies due to fission gas release is very unlikely unless the power-to-flow is significantly greater than the nominal value.

2.2.4.4 A General Scenerio for Pin-to-Pin Failure Propagation

There are four stages of development of a local incident (Ref.4):

1. Local (single phase) cooling disturbances and pin failures in the fuel rod bundle,
2. Local sodium boiling,
3. Bulk sodium boiling in the subassembly,
4. Gross melting of the fuel and clad, constituting a FCI.

Local disturbances may originate from changes in subchannel geometry, due to thermal bowing of rods, clad inflation, or local failure of spacer grids. Such changes can cause only a small termperature rise and hence are less important. Accumulation of particulate matter, another potential initiating source of local cooling problems, is minimized with the use of a screen in the subassembly inlet region. Thus, the ejection of fission gas or the escape of fuel are the primary concerns for cooling disturbances which could propagate to other assemblies.

Neither fission gas ejection nor "washing out" of solid fuel particles can cause rapid failure propagation, (Ref.4), which means that ejection of molten fuel, leading to a rapid growth of the blockage or the generation of pressure pulses due to a local FCI, is the primary mechanism for rapid pin-to-pin propagation. Molten fuel could be caused by:

1. an elevated coolant temperature in the disturbed region,
2. an increase in the thermal gap resistance caused by increased gap spacing,
3. chemical attack of fuel by sodium following a clad failure producing a reaction product of lower density and thermal conductivity,
4. higher enrichment of individual pellets, arising from a fuel handling incident.

If fuel becomes molten, there is some evidence that it will relocate axially within the pin (Ref.3). Insufficient in-pile experiments on failure mechanisms at elevated clad temperatures have been reported, however, particularly at considerable burnup, to exclude this as a possible source accident.

Once pin failure has propagated so that local boiling occurs, such boiling could either initiate a rather fast growth of the fault, by causing rapid pin failures due to dryout and melting, or degenerate to bulk boiling due to vapor production and hydrodynamic instability of flow. There is encouraging evidence that local boiling is unlikely to occur in the wake even if as much as 50% of the bundle cross section is completely blocked. (Ref.28). Unfortunately such blockages are not readily detected by straight-forward monitoring techniques involving the outlet temperature or flow.

Several conclusions have been reached regarding local boiling:

a. Local boiling will neither cause rapid pin failures due to dryout and melting nor hydrodynamic instability of flow.

b. Local boiling will cause bulk coolant flow pulsations of several 10% with ramps of the order 10/sec, which may be detected by a probe type flowmeter.

c. Local boiling does not cause a rapid growth of the fault even in case of large size blockages which can be detected by monitoring subassembly outlet temperature; in particular, transition to gross boiling due to hydrodynamic instability is not to be expected for such blockage sizes.

d. As in the first stage, the prevailing mechanism of the postulated progression of the fault is blockage growth by pin failure propagation;

this process - if at all existing - would be considerably retarded, however, because of the enhanced heat removal under local boiling conditions.

e. There appears to be a good chance in many incidents to detect local boiling by monitoring outlet flow.

If the subassembly coolant flow is reduced below about 35% of its nominal value either due to continued growth of a local blockage or to an inlet blockage, the incident enters into the bulk boiling phase. Under these circumstances, the characteristics of the fuel failure problem become the same as those analyzed for the loss-of-flow incident. Hence, the concern is then no longer with propagation of the fuel failure, but rather with the effects of a major accident.

2.2.4.5 Detection of a Failure Propagation

Possible detection methods for fuel failure propagation between pins are (Ref.29):

1. subassembly outlet temperature sensors,
2. subassembly outlet flow sensors,
3. failed element detection and location (FEDAL) systems, such as fission gas detection along with gas tagging,

4. pressure pulse (acoustic) sensors,
5. anomalous reactivity detectors, and
6. neutron noise analyzers.

The use of these sensing techniques in a reactor can be put into perspective with the diagram in Fig. 2.

Of these techniques, all have the potential of providing a signal to implement reactor shutdown before loss of hermeticity of a pin except that of the FEDAL scheme. The FEDAL scheme employs a sensor to detect gaseous fission products which, in the case of the heated thermocouple probe concept (Ref.5), may be capable of responding within a second to such a signal for purposes of actuating a scram mechanism. Such a burst-can detection system (BCD) is based on the separation and accumulation of fission gas bubbles at the subassembly outlet by means of a vortex generator; the electrically-heated thermocouple gives a fast and large signal if surrounded by gas instead of sodium. Such a system is not capable, however, of identifying either subassembly-to-subassembly or pin-to-pin failure propagation.

The location portion of the gas detection system is done with the principle of gas tagging. Gas tagging utilizes the release of specified amounts of various isotopes of noble

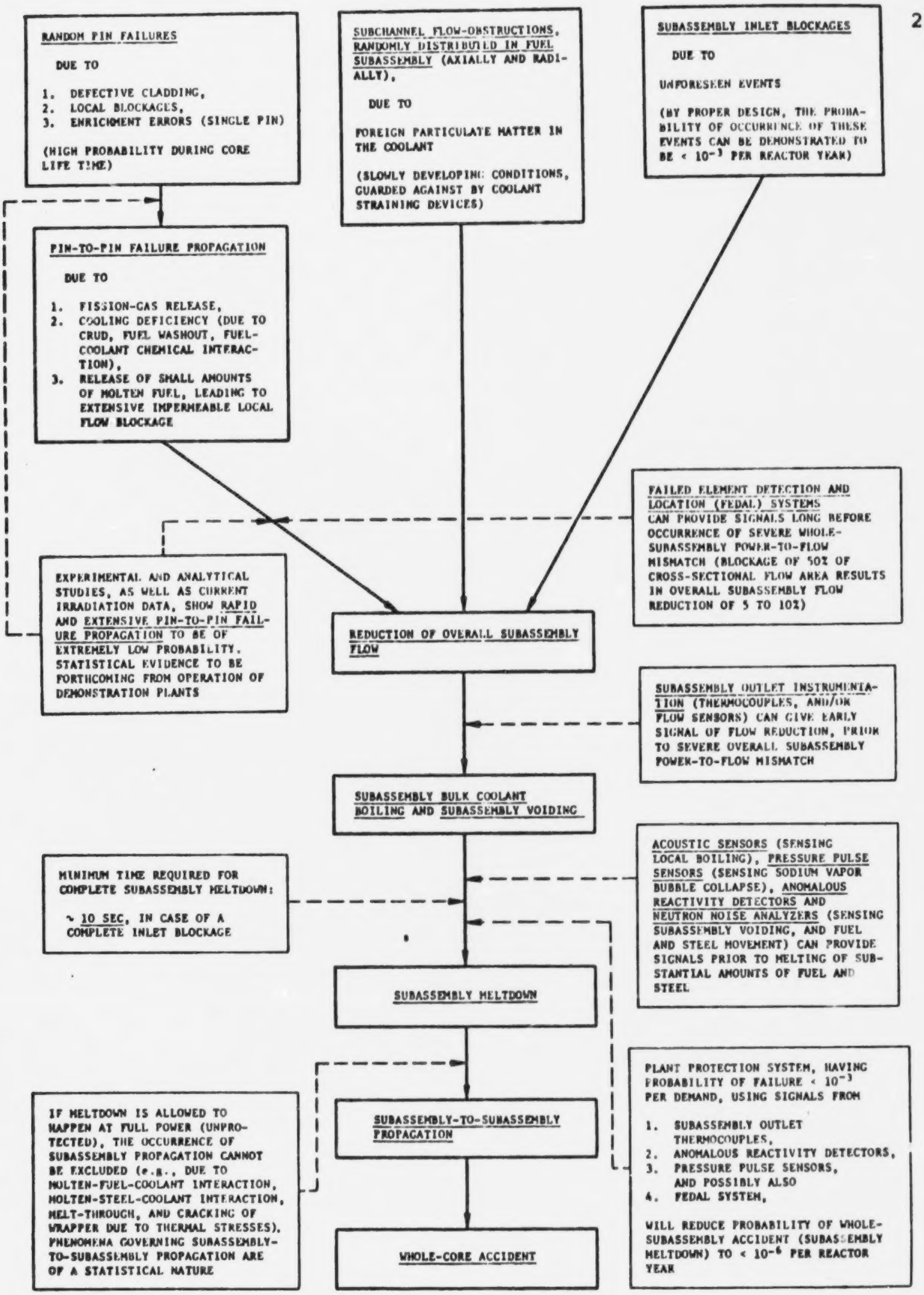
RANDOM PIN FAILURES DUE TO 1. DEFECTIVE CLADDING, 2. LOCAL BLOCKAGES, 3. ENRICHMENT ERRORS (SINGLE PIN) (HIGH PROBABILITY DURING CORE LIFE TIME)
SUBCHANNEL FLOW-OBSTRUCTIONS, RANDOMLY DISTRIBUTED IN FUEL SUBASSEMBLY (AXIALLY AND RADIALLY), DUE TO FOREIGN PARTICULATE MATTER IN THE COOLANT (SLOWLY DEVELOPING CONDITIONS, GUARDED AGAINST BY COOLANT STRAINING DEVICES)
SUBASSEMBLY INLET BLOCKAGES DUE TO UNFORESEEN EVENTS (BY PROPER DESIGN, THE PROBABILITY OF OCCURRENCE OF THESE EVENTS CAN BE DEMONSTRATED TO BE < 10⁻³ PER REACTOR YEAR)
PIN-TO-PIN FAILURE PROPAGATION DUE TO 1. FISSION-GAS RELEASE, 2. COOLING DEFICIENCY (DUE TO CRUD, FUEL WASHOUT, FUEL-COOLANT CHEMICAL INTERACTION), 3. RELEASE OF SMALL AMOUNTS OF MOLTEN FUEL, LEADING TO EXTENSIVE IMPERMEABLE LOCAL FLOW BLOCKAGE
FAILED ELEMENT DETECTION AND LOCATION (FEDAL) SYSTEMS CAN PROVIDE SIGNALS LONG BEFORE OCCURRENCE OF SEVERE WHOLE-SUBASSEMBLY POWER-TO-FLOW MISMATCH (BLOCKAGE OF 50% OF CROSS-SECTIONAL FLOW AREA RESULTS IN OVERALL SUBASSEMBLY FLOW REDUCTION OF 5 TO 10%)
EXPERIMENTAL AND ANALYTICAL STUDIES, AS WELL AS CURRENT IRRADIATION DATA, SHOW RAPID AND EXTENSIVE PIN-TO-PIN FAILURE PROPAGATION TO BE OF EXTREMELY LOW PROBABILITY. STATISTICAL EVIDENCE TO BE FORTHCOMING FROM OPERATION OF DEMONSTRATION PLANTS
REDUCTION OF OVERALL SUBASSEMBLY FLOW
SUBASSEMBLY OUTLET INSTRUMENTATION (THERMOCOUPLES, AND/OR FLOW SENSORS) CAN GIVE EARLY SIGNAL OF FLOW REDUCTION, PRIOR TO SEVERE OVERALL SUBASSEMBLY POWER-TO-FLOW MISMATCH
SUBASSEMBLY BULK COOLANT BOILING AND SUBASSEMBLY VOIDING
MINIMUM TIME REQUIRED FOR COMPLETE SUBASSEMBLY MELTDOWN: ~ 10 SEC, IN CASE OF A COMPLETE INLET BLOCKAGE
ACOUSTIC SENSORS (SENSING LOCAL BOILING), PRESSURE PULSE SENSORS (SENSING SODIUM VAPOR BUBBLE COLLAPSE), ANOMALOUS REACTIVITY DETECTORS AND NEUTRON NOISE ANALYZERS (SENSING SUBASSEMBLY VOIDING, AND FUEL AND STEEL MOVEMENT) CAN PROVIDE SIGNALS PRIOR TO MELTING OF SUBSTANTIAL AMOUNTS OF FUEL AND STEEL
SUBASSEMBLY MELTDOWN
PLANT PROTECTION SYSTEM, HAVING PROBABILITY OF FAILURE < 10⁻³ PER DEMAND, USING SIGNALS FROM 1. SUBASSEMBLY OUTLET THERMOCOUPLES, 2. ANOMALOUS REACTIVITY DETECTORS, 3. PRESSURE PULSE SENSORS, AND POSSIBLY ALSO 4. FEDAL SYSTEM, WILL REDUCE PROBABILITY OF WHOLE-SUBASSEMBLY ACCIDENT (SUBASSEMBLY MELTDOWN) TO < 10⁻⁶ PER REACTOR YEAR
IF MELTDOWN IS ALLOWED TO HAPPEN AT FULL POWER (UNPROTECTED), THE OCCURRENCE OF SUBASSEMBLY PROPAGATION CANNOT BE EXCLUDED (e.g., DUE TO MOLTEN-FUEL-COOLANT INTERACTION, MOLTEN-STEEL-COOLANT INTERACTION, MELT-THROUGH, AND CRACKING OF WRAPPER DUE TO THERMAL STRESSES). PHENOMENA GOVERNING SUBASSEMBLY-TO-SUBASSEMBLY PROPAGATION ARE OF A STATISTICAL NATURE
SUBASSEMBLY-TO-SUBASSEMBLY PROPAGATION
WHOLE-CORE ACCIDENT

Fig. 2 Schematic Representation of a Hypothetical Sequence of Events Leading, Via a Single-Subassembly Accident, to a Whole-Core Accident.

gases into the plenum of each fuel pin upon fabrication. (By a judicious selection of the concentrations of each isotope, a unique tag can be assigned to each subassembly in the reactor, with every pin in a subassembly having the same set of isotope ratios as all other pins in that assembly). Once the cladding has been breached, the fission gas in the plenum, as well as the tag gas, is released and detected in the cover gas of the reactor.

By matching the ratios of the measured isotopic concentrations of the tag gas in the cover gas to the known gas ratios enables the defective assembly to be identified. This matching, however, requires the collection of the tag gas on a charcoal trap, and subsequent analysis by a mass spectrometer. Hence the gas tagging approach, although undoubtedly the most reliable for identifying less severe single pin and multiple failures (Ref.30,31), is not useful as a prompt-acting indicator of a failure propagation; only the fission gas detection is capable of this task. The gas tagging method, as being developed for the Fast Flux Test Facility, should be capable of distinquishing most subassembly-to-subassembly failure propagation in an operating reactor, but is incapable of detecting pin-to-pin failure propagation. (Ref.32,33).

Acoustic sensors, anomalous reactivity detectors, and neutron noise analysis systems are all under development for the fast breeder program, and all show some promise of ultimately being desirable as a part in an integrated system for detection of failed fuel. At the present time the sensitivity has not been sufficiently established to allow determination of the usefulness of such schemes for the propagation of pin or subassembly failures. Thus, aside from the FEDAL instrumentation, the subassembly outlet temperature and flow rate sensors are the detectors potentially capable of indicating the propagation of failed fuel.

Because subassembly outlet thermocouples (and possibly also flow sensors) are required in reactor start-up procedures and for optimum plant operation, it is natural to desire to use the output signals to decrease the probability for the occurrence of accidents involving the propagation of a major fraction of the pins in a subassembly. To develop a prompt-acting mechanism, however, requires the use of sufficient computer software capability to simultaneously monitor the outputs. The computer system must also incorporate a logic system which can reduce the probability of emitting spurious shutdown signals while at the same time be capable of responding with sufficient sensitivity to the important signals.

Currently under development in Germany is a Multi Input Safety System which will be used for processing the large quantity of data from the subassembly instrumentation and for initiating scram signals (Ref.34). Such units typically consist of several multiplexer/analog-digital converter units and synchronized, separate process computers working in a 2 out of 3 logic. Similar developments are underway in the United States, but full-scale tests have not yet been performed to demonstrate the sensitivity and reliability of the sensor-computer software package.

The difficulty with the use of thermocouples and/or flowmeters for the detection of local failure propagation is that generally a substantial portion of the cross-sectional flow area of the subassembly need be reduced before failure can be identified (Ref.1). If this happens during a self-limiting or slow propagation of pin failure, even the FEDAL fission product detector will serve as a satisfactory annuciator. Thus, for purposes of studying the fuel failure propagation problem, the primary concern is for the rapid pin-to-pin propagation which is postulated to take place on a time scale too short (<1 min) to enable detecting the phenomena and shutting down the reactor prior to the involvement of the entire subassembly.

2.2.4.6 Conclusions

The occurrence of pin-to-pin propagation of failed fuel presently is envisioned to not be a major source of potential accidents. This general conclusion was reached earlier for the FFTF reactor (Ref.35), and it has been substantiated by the considerable number of experimental and analytical studies discussed in the foregoing. It is concluded that rapid and extensive pin-to-pin failure propagation in LMFBR fuel subassemblies at, or close to, nominal operation is highly improbable for the following reasons (Ref.1):

(1) The most probable effect of fission gas release is minor overheating of the cladding, with coolant temperatures remaining well below the boiling point, even if very conservative gas release rates are assumed.

(2) Local blockages of sufficient size to result in local boiling are extremely improbable; however, even if such a blockage is assumed, it is unlikely to result in excessive overheating, propagation of boiling and flow instability.

(3) Release of molten fuel within a subassembly is very improbable at, or close to, nominal operating conditions; however, even if such a release is assumed to occur, it is unlikely to result in

failure propagation due to pressure generation and void growth.

A second important conclusion that can be drawn (Ref.1) is that pin-to-pin failure propagation in LMFBR fuel subassemblies does not constitute, within the range of nominal operating conditions, a matter of immediate concern to the health and safety of the general public. There is ample time available to detect fuel failures provided an adequate Failed Element Detection and Location (FEDAL) instrumentation system has been installed. Fuel failure is thus primarily an operational problem, which may occasionally require only some remedial action as part of the normal plant-operational procedures.

REFERENCES

1. J. B. van Erp, T. C. Chawla, and H. K. Fauske, "An Evaluation of Pin-to-Pin Failure Propagation in LMFBR Fuel Assemblies," Proc. Fast Reactor Safety Meeting, CONF - 740401 - P2, p. 615 (1974).

2. C. E. Dickerman, "U.S. Studies on LMFBR Fuel Behavior Under Accident Conditions," Nuclear Safety 14, 452 (1973).

3. J. F. Marchaterre, H. K. Fauske, L. Baker, C. E. Dickermann, and R. W. Wright, "Experimental Studies of Liquid-Metal Fast-Reactor Accident Conditions," Int. Conf. on Engineering of Fast Reactors for Safe and Reliable Operation, Karlsruhe, Germany, CONF-721006, p. 763 (1972).

4. K. Gast and D. Smidt, "Single Subassembly Fault Detection System— Functional Requirements and Shut-off Criteria," Proc. Fast Reactor Safety Meeting, CONF-740401 - P3, p. 1415 (1974).

5. K. Gast, "Die Aus breitung örtlicher Störungen im Kern Schneller Natriumgekühlter Reaktoren und ihre Bedeutung fur die Reaktorsicherheit," Kernforschungszentrum Karlsruhe KFK-1380 (1971).

6. W. W. Marr and D. H. Thompson, "Prediction of Fuel Melting in an LMFBR Fuel Element," Trans. Am. Nucl. Soc.14, No. 2, p. 150 (1971).

7. D. H. Thompson and W.W. Marr, "Prediction of Maximum Temperature or Melting Fraction in an LMFBR Fuel Element," Nucl. Eng. Design 17, p. 361 (1971).

8. A. Padilla and R.M. Crawford, "Molten Fuel Relocation in an Overenriched Fuel Pin," Trans. Am. Nucl. Soc. 15, p. 342 (1972).

9. L.W. Dietrich et al., "TREAT Mark-II Loop Experiments on FFTF-Like Pins Having Local Overenrichment," Trans. Am. Nucl. Soc. 15, p. 816 (1972).

10. K. Gast and D. Smidt, "Cooling Disturbances in the Core of Sodium-Cooled Fast Reactors as Causes of Fast Failure Propagation," Nucl. Eng. Design 14, p.10 (1970).

11. H.K. Fauske, "Evaluation of Dryout and Flow Instability in the Wake Downstream of a Blockage in an LMFBR Subassembly," Trans. Am. Nucl. Soc. 15, No.1 p.351 (1972).

12. J.P.H. Blake, C.V. Gregory, R. Herbert, and D.C.G. Smith, "Theoretical Studies Related to Local Blockages in Fast Reactor Subassemblies," Int. Conf. on Engineering of Fast Reactors for Safe and Reliable Operation, Karlsruhe, Germany CONF-721006 (1972).

13. K. Gast and K. Schleisiek, "Local Boiling in a Partially Blocked LMFBR Subassembly," Int. Conf. on Engineering of Fast Reactors for Safe and Reliable Operation, Karlsruhe, Germany, CONF-721006, p.730 (1972).

14. J.P.H. Blake, C. V. Gregory, R. Herbert, and D.C.G. Smith, "Theoretical Studies Related to Local Blockages in Fast Reactor Subassemblies," Int. Conf. on Engineering of Fast Reactors for Safe and Reliable Operation, Karlsruhe, Germany, CONF-721006 p.713 (1972).

15. D. Kirsch, "The Temperature Distribution in the Recirculation Flow Downstream of Local Coolant Blockages in Rod Bundle Subassemblies," Int. Meeting on Reactor Heat Transfer, Karlsruhe, Germany (1973).

16. M.H.Fontana, P.A. Gnadt, T.S. Kress, R.E. MacPherson, L.F. Parsly, and J.L. Wantland, "Effect of Inlet Blockages in 19-rod Simulated LMFBR Fuel Subassemblies," Trans. Am. Nucl. Soc. 17, p. 345 (1973).

17. D. H. Thompson and W.W. Marr, "Prediction of Maximum Temperature or Melting Fraction in an LMFBR Fuel Element," Nucl. Eng. Design 17, p.361 (1971).

18. J.B. van Erp, T.C. Chawla, and R.E. Wilson, "Potential Fuel Failure Propagation Due to Fission-Gas Release in LMFBR Subassemblies," Am.Soc. Mech. Eng. Paper 72-WA/NE-14 (1972).

19. J.M. Kennedy, T.C. Chawla, and J.B. van Erp, "Stress Analysis for an LMFBR Fuel Pin with Temperature Distribution Pertaining to Fission-gas Jet Impingement," Trans. Am. Nucl. Soc. 17, p.343 (1973).

20. R.E. Murata, G.E. Hittle, K.E. Gregoire, and C.N. Craig, "Friction Factor for Gas Flow from Defected Fuel Rods," Trans. Am. Nucl. Soc. 16, p. 216 (1973).

21. J.F. Koenig and R.V. Strain, "Performance of a Mixed-Oxide Fuel Element Irradiated to End-of-Life Conditions in EBR-II: Seven-Element Test in Subassembly X106," Argonne National Laboratory Report ANL-7993 (1973).

22. J.B. van Erp, C.J.Roop, and P.L. Zaleski, "Simulation of Slow Fission Gas Release in an LMFBR Fuel Subassembly," *Trans. Am. Nucl. Soc. 14*, No.1, p.277 (1971).

23. H. Freslon, H.K. Fauske, and D.T. Eggen, "Local Flow Starvation in an LMFBR Subassembly due to Fission Gas Release," *Trans. Am. Nucl. Soc. 16*, p.197 (1973).

24. A.M. Judd, "Approximate Analysis of Rapid Fission Gas Release in a Sodium Cooled Fast Reactor Subassembly," *J. Brit. Nucl. Energy Soc. 12*, p. 43 (1973).

25. K.Gast, *Trans. Am. Nucl. Soc. 15*, p.838 (1972).

26. T.C. Chawla and B.M. Hoglund, *Nucl. Sci. Eng. 44*, p.320 (1971).

27. R. Krieg and R.M. Crawford, "Deformations in a 19-Pin Bundle due to Sudden Fluid Expansion," *Proc. Fast Reactor Safety Meeting*, CONF-740401-P2, p.748 (1974).

28. D. Kirsch, "The Temperature Distribution in the Recirculating Flow Downstream of Local Coolant Blockages in Rod Bundle Subassemblies," *Int. Meeting on Reactor Heat Transfer*, Karlsruhe, Germany (1973).

29. J.B. van Erp and H.K. Fauske, "Role and Development of LMFBR Protection Systems," *Proc. Fast Reactor Safety Meeting*, CONF-740401-P3, p.1430 (1974).

30. R.J. Cash, F.E. Holt, and Y.S. Tang, eds., "FFTF Fuel Failure Location System Recommendations and Rationale," Hanford Engineering Development Laboratory HEDL-TME-72-96 (to be published).

31. J.F. Koenig, E.R. Ebersole, C.C. Ford, R.M.Fryer, R.R. Smith, and R.V. Strain, "Performance in the EBR-II of a Mixed Oxide Fuel Element with an Intentional Cladding Defect," Argonne National Laboratory ANL-7912 (1972).

32. N.J. McCormick and R.E. Schenter, "Gas Tag Identification of Failed Fuel-I. Synergistic Use of Inert Gases," Nucl. Technol. 24, 149 (1974).

33. N.J. McCormick, "Gas Tag Identification of Failed Fuel-II, Resolution Between Single and Multiple Failures," Nucl. Technol. 24, 156 (1974).

34. S. Jacobi, H. Lenhardt, and R. Schneider, "Schutzsysteme für Schnelle Natriumgekühlte Reaktoren," Kernforschungszentrum Karlsruhe KFK-1735 (1973).

35. R. D. Coffield and P.L. Wattelet, "An Analytical Evaluation of Fuel Failure Propagation for the Fast Flux Test Facility," Westinghouse Report WARD-2171-11 (1970).

2.3 Post Accident Phenomena

2.3.1 Post Accident Heat Removal After a Core Disruptive Accident

2.3.1 Introduction

The EBR II, DFR, Enrico Fermi I, Rapsodie, SEFOR, PFR, Phoenix, FFTF, and SNR reactors, among others, have all been designed to cope with some kind of postulated core destructive accident, which as an aftermath leaves a partially or largely disrupted core geometry and a large mass of hot, molten or vaporized fuel. Following containment of the pressures associated with such a postulated energy release, there remains the task of assuring retention within the primary containment of the hot and molten fuel, allowing for fission product decay heat. Of course, it is also possible, in principle, to postulate accidents having little or no mechanical energy release associated with them, but which lead to a loss of original core geometry and potential decay heat removal problems; the EBR I meltdown is an example of such an actual event.

Treatment of post accident heat removal varies for the various reactors built in the past. To some extent, small reactor power levels or power densities eased the complexity of the problem. In some of these reactors special design features have been included, but complete test and analysis of their efficacy is either unavailable or was precluded by the lateness of specification of the design feature with regard to the construction program. In the most recent reactors the detailed approach remains to be fully specified.

Various possible design approaches have been proposed, including in-reactor-vessel, in-reactor-tank, sodium-cooled trays in the reactor cavity, cooled reactor-cavity liner, and sacrificial bed.

Early analyses have indicated that sodium has the potential to provide enough heat removal capability from the bottom of a tray-type concept (or equivalent) if enough spreading-out of the core fuel occurs, and if film-boiling of the sodium is avoided. However, in the actual design of a post-accident-heat removal system, many additional phenomena and conditions must be considered, including the original state and disposition of the fuel and other molten materials, the disposition of the fission products, the effect of fuel-coolant interactions, initially and on a continuing basis, the manner in which the hot fuel, etc., reaches the retention structure, the ability to hold the fuel within the structure, the nature of the heat transfer to the bulk coolant and through the retention structure, and various metallurgical and stress considerations.

A sacrificial concept involves some of the above phenomena and brings in several new ones, including the manner of interaction between fuel and sacrificial material and rates of solution and interdiffusion.

Considerable progress has been made in some of the areas important to the design and performance evaluation of post-accident heat removal systems for an LMFBR. However, much remains to be learned out-of-pile, and an in-pile experimental program is yet to be announced.

2.3.1.2 Previous Analyses

Most analysis on PAHR performed heretofore is of a preliminary nature. It is based on insufficient knowledge of heat transfer phenomena and whether or not conservative designs are achieved is unclear. Based on this lack of knowledge, in-vessel use of sacrificial materials may be warranted in light of the possibility of molten fuel streaming through small openings and impinging on surfaces with local damage. Selection of the sacrificial material must consider density effects. Ex-vessel systems have not been extensively studied and some under consideration use basalt as the sacrificial material. It is not clear that the mixing of molten basalt and molten UO_2 required for feasibility will take place.

Coolability of a crumpled core or debris bed is not fully established. Further work in this regard is necessary before passing judgment on the adequacy of a PAHR system based on a crumpled core or fuel debris bed. In the interim it is more conservative to assume that the core melts and agglomerates. The initial melt-through of the core support structure has not been treated adequately. It is thought that some streaming of the molten fuel (if it becomes molten) will occur with local high heat transfer where the stream impinges on structural material. If the streaming molten fuel interacts with sodium and results in a debris bed, the spreading of the debris is important because a mound of debris could again become molten due to dryout. When and if a molten layer forms, estimates of the heat transfer to the containing structure must be made. Only for the simple infinite layer can heat transfer be predicted and then only under limited circumstances. Various geometries need to be considered both for internally heated fluids and for natural convection caused by heated surfaces. In particular, heat transfer to the lateral confining boundaries is not known well. Superposed layer problems such as occur in ex-vessel schemes when the sacrificial material is basalt (which is less dense) have received no quantitative treatment. Even the use of ThO_2 is not without problems. The ThO_2 melting temperature is not well established. A further consideration is that molten UO_2 may transfer significant amounts of heat by thermal radiation. Little consideration has been given to this mode of heat transfer.

Most of the heat transfer phenomena mentioned in the previous paragraph assumes a quiescent layer. Even though much is unknown, a further complication must be considered. Sloshing due to falling debris or MFCI could remove the protective oxide coating that is assumed to exist adjacent to the structure and rapid melting could occur. A need exists to somehow quantify or bound this effect.

Properties of materials necessary for analysis of a hypothetical core meltdown are incomplete. The thermal conductivity of molten UO_2 is only an estimate and is needed over the range $2880^{\circ}C < T < 3411^{\circ}C$. The two available measurements of the boiling point of UO_2 are different by $453^{\circ}C$. This must be pinned down more closely to assess whether or not boiling will occur. The remaining properties, with the exception of optical properties, given in the table have an unknown accuracy in many cases but allow one to make estimates for PAHR that are within the accuracy of the predictive method used. The optical properties are not sufficient. The spectral absorption coefficient is needed for temperatures up to the boiling point of UO_2. Almost no data are available on the physical properties of molten steel, although some data have been found on density and viscosity for molten steels.

The fission products, or decay heat, will be redistributed during core meltdown accidents by two procedures; by gas phase transport of the more volatile fission products which vaporize from the fuel-fission product system, and by physical movement of the less volatile fission products between molten mixed fuel oxide and molten iron due to bubbling, gravity, convection forces, etc. To determine these behaviors properly, two sets of thermodynamic data are needed. The free energies of formation of the condensed oxides will be important to determine the oxidation states of the less volatile fission products, and the free energies of formation of the gaseous fission products are importnat to predict the vapor pressures of the more volatile fission products.

2.3.1.3 Experiments

In general, the experimental measurements for the free energies of formation of the fission product condensed oxides are limited to much lower temperatures than those of interest. Since the small uncertainties of the data at low temperature could cause unacceptable discrepancies when extrapolated to the higher temperatures, further experimental work should be carried out to establish reasonable data with sufficient accuracy.

Although the free energies of formation of the gaseous monatomic fission products are generally well established, some of the free energies of formation of the gaseous fission product oxides such as Cd and In need more experimental work due to the uncertainties in the standard heat of formation. Accurate vapor pressures of the uranium oxides and plutonium oxides are needed not only to determine the redistribution of uranium and plutonium by gaseous transport but also to calculate the oxygen potentials at higher temperatures in the mixed oxide fuel with respect to O/M ratio. Further experimental work is required to establish the actual reactions and miscibility relationships as well as to determine the thermodynamic data for the compounds which could be formed among the mixed fuel oxide, fission products, coolant, and cladding materials.

A number of heat transfer experiments are necessary to obtain an understanding of PAHR systems. Both particle bed dryout and leveling experiments should be extended to include boiling induced cellular motion (keeps bed from drying out) and the effects of large chunks of steel and UO_2. Some induction heating experiments are necessary to validate the ANL approach wherein bottom heating results are used to predict dryout of volume heated beds. The work of Kulacki and Goldstein should be extended to consider the effects of stabilizing temperature gradients and a liquid-liquid upper surface. Thermal radiation as has been pointed out, may be important in UO_2 fluid layers. Experiments with hot molten salts, with internal heat generation and radiative properties similar to those of molten UO_2, should be carried out with a Kulacki and Goldstein type apparatus to establish whether or not thermal radiation is a contributor. Of considerable importance is the heat transfer to lateral confining boundaries. A series of experiments are necessary to establish the magnitude of the horizontal heat transfer to such boundaries.

The transition of convection heat transfer to boiling heat transfer should be investigated for the fluid layers. It is not clear where the onset of boiling will occur as a function of the maximum temperature in the layer. The onset will probably be a function of the nucleation sites in the fluid. This should be a variable in the experiments. The transition from the beginning of boiling to fully developed boiling should be investigated. This transition experiment should be done with both a fixed and free upper boundary to see what effect the sizing of the bubbles may have on the transition and also fully developed boiling. The possibility of mass transfer by vapor condensation and mixing of two fluids should also be investigated. The fate of fission products will depend largely upon bubble condensation and mixing with upper layers. Container shape should also be investigated to see if large convection patterns will exist in the boiling layer. The onset and type of cellular patterns caused by bubbles rising in fluids is important in determining the types of boiling correlations to be used. Again, heat transfer to the lateral confining boundaries is important.

2.3.1.4 Passive Core Catchers

2.3.1.4.1 Introduction

The specification of initial and boundary conditions for the final stages of LMFBR meltdown accidents are largely unknown. The extent and characterization of the core's disruption leads to a wide spectrum of possible steel, sodium, fuel and fission product mixes of varying compositions and characteristics. The current unpredictability of flow and the melting attack of this material on the core support plate and structure, followed by the melting attack on the reactor and guard vessel, allows only a qualitative assessment of the amount and rate of debris collection in an ex-vessel core catcher.

Various ex-vessel core catcher design concepts have been suggested such as completely passive, passive with natural circulation and with forced circulation systems. The paramount

questions related to catcher adequacy concern the rate of melt progression downward, pool growth outward and the thermal effects upon surrounding structural material, such as concrete.
A concern with active components in these systems also includes their ability to function on demand for the necessary time.

The question of debris bed behavior is invariably addressed in post accident heat removal studies. Molten core materials in contact with any available liquid sodium are expected to fragment into small particulate matter having particle sizes in the range of several hundred microns for fuel (Ref.1,2). Contacting tests performed with molten stainless steel and sodium also demonstrate particulate formation with average sizes several times greater than that of fuel (Ref. 2,3). Therefore, one can reasonably expect that during the core disruption phase of an accident the large mass potentially available for deposition in the core catcher will be quite fragmentary. In addition, some of this material will come to rest on horizontal surfaces above the catcher. This does not preclude the possibility of guard vessel or reactor vessel sections dropping into the core catcher. In general, however, the analyst can proceed with core catcher studies using a physical model of a core catcher design filled with a specified mass of particulate fuel, steel, sodium and fission products. There are also many other conditions to consider, depending upon the amount of sodium available, for example.

Specifically, one may include in the analysis the effects of a volume of sodium above the debris bed, although there is no guarantee that a significant amount of sodium would be present.

After formation of a debris bed the decay heat generated by the fuel within must be removed or the bed temperature will increase. If the heat source is large enough, bed dryout results and then possibly leads to the formation of a molten pool. The sequence then continues by observing that the molten pool could grow, thus destroying the containability of the core catcher, its designed function.

2.3.1.4.2 Experience

There is little experience with molten pool behavior having internal heat generation in either natural or man-made applications. Molten lakes of lava have formed on the floor of Halemaumau, a deep pit in the floor of Kilauea's summit caldera. These lakes are characterized as having a high silica content, high viscosity, maximum temperatures of about 1000°C and no internal heat generation. They are contained from outward melt progression by spatter ramparts formed around the edge of the lake. Normally, thin crust sections form on the top of the lake, but strong currents (thermal convection induced, as well as from possible underlying fissure pressures) are set up causing their fragmentation. Crust fragments are dragged down into the liquid and as this occurs, gas bubbles previously contained in the crust are released during melting, causing further agitation and mixing. This cycle of crust formation and fragmentation is a continuing one. The bulk of the lava lake therefore does not thermally stratify to a large extent. Instead, the pools solidify inward from the cooler outer surfaces with considerable thermal convection induced mixing in spite of the relatively high viscosity of the lava.

Direct application of this natural phenomenon to reactor situations requires careful consideration of the differences in material properties, heat generation rates and size of the pool among other factors. The effect of no internal heat generation, for example, may tend to increase outer thermal convection effects, however, possible boiling convection forces in the reactor case may tend to counterbalance this thermal convection difference. Motion pictures of these lakes are available from the Hawaii Natural History Association and they provide excellent documentation for extracting basic large pool behavioral phenomena.

Experimental effort in post accident heat removal studies to date has, as indicated by available documentation, centered on qualitative assessment of debris-bed behavior and correlation of data to obtain outward heat transfer rates (Ref. 4-7). The experiments of Kulacki and Goldstein (Ref. 4) in which heat transfer was measured from the top and bottom of a horizontal layer with constant and equal boundary temperatures adds to the basic knowledge of possible molten pool states. Extrapolation of their data to more realizable reactor conditions is quite uncertain, however. The experiments (Ref. 6) conducted at Argonne using water in rectangular containers again adds information to help predict horizontal and vertical heat transfer rates. Correlations for determining boiling induced convection and thermal convection heat transfer regimes are important in the overall understanding of pool behavior. The transformation of this data to reactor materials and geometries again implies further uncertainties even after the qualitative behavior is known.

In the reactor situation, phenomena such as crust formation and breakup, formation and motion of liquid films upon the container surfaces, volatilization of fission products, behavior of intermixed steel and other impurities, and thermal interaction with the core catcher need to be accounted for before realistic analysis can be provided. This is true since these factors may cause qualitative changes in the energy transfer phenomena invalidating previously developed correlations and analytical models.

2.3.1.4.3 Analytical Studies

There may be some significance to studying the problem of the core catcher in reverse order of the sequence of events as they may occur. An effort to understand the amount of heat transfer necessary to cause unacceptable pool melt progression and growth rates is of value and may be worth pursuing. A major effort now seems to be focused on heat transfer rates from various molten pool and debris-bed formations. With further understanding of melt progression and pool growth phenomena, their sensitivity as a function of heat flux and other factors can be assessed. Conclusions concerning the accuracy needed in the heat transfer calculations will be made based on these data.

Zivi (Ref. 8) suggested a completely passive UO_2 barrier and analyzed the rate of penetration by the fuel mass. He determined that this rate would be very low for three main reasons: (1) the large heat of fusion of the sacrificial UO_2 would tend to make the melt process slow; (2) the molten fuel containing the heat-generating fission products would tend to rise above the other melted material because of its higher temperature and dissolved lighter elements; and (3) a layer of previously melted sacrificial material would limit energy transfer from the heat generating fuel to the solid material below.

Zivi's analysis utilized a semi-infinite slab and assumed that its thermal properties were not changed by melting to determine the vertical melt front penetration rate.

This analysis does not address sideways growth of the molten pool or account for thermal or possible boiling convection forces which could increase the heat transfer rate to the sacrificial material. In addition, the deposition and resulting thermal loading on surrounding core catcher support materials must also be considered. A major problem of the structure involves high concrete temperatures which could liberate water vapor, initiate sodium/water contact, and initiate other consequences.

Further analysis of melt penetration and growth phenomena would include accounting for pool mixing and lateral growth. For example, initial studies might consider a vertical semi-infinite slab in which sacrificial UO_2 is drained away as melting progresses. The model shown in Fig. 1 would constantly impose heat generating molten fuel in contact with the solid urania.

The energy and momentum transfer between materials should be accounted for. Refinements to include specific thermophysical and chemical properties of the fuel, fission products and sacrificial material should be included in these

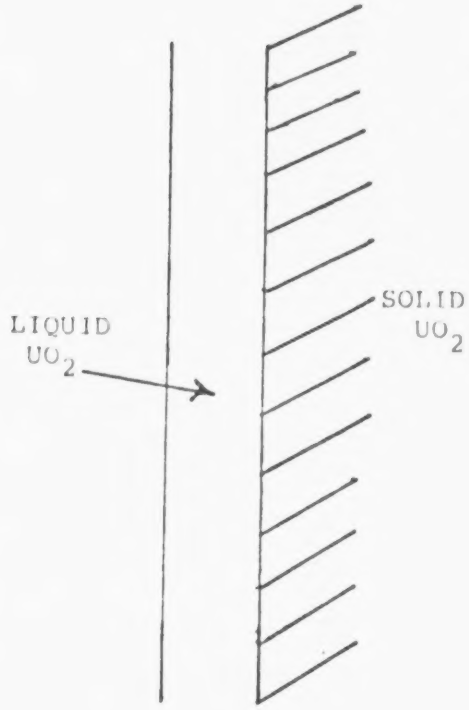
LIQUID
UO_2
SOLID
UO_2

Figure 1. Vertical Model

Further studies could then lead to more realistic geometries, such as indicated in Figure 2.

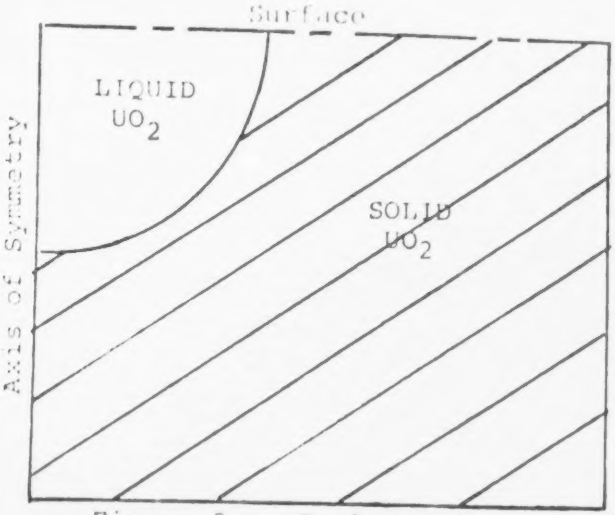
Surface
LIQUID
UO_2
SOLID
UO_2
Axis of Symmetry

Figure 2. Pool Model

initial scoping calculations in an attempt to realize the behavior of the phenomena involved.

After initial scoping calculations have been performed and the assessment of the sensitivity of various parameters has been made further analysis should include consideration of an integrated model to study specific core catcher designs. Additional considerations of the chemical interactions between the various components would serve to more accurately define the fission product source as a function of time.

The characteristics of an integrated model which would be helpful in studying melt progression and pool behavior would likely include the following:

1. Two dimensional geometrical effects.
2. Multi-component systems - fission products, molten fuel, molten sacrificial material, solid sacrificial material, and sodium.
3. Conduction and various convection heat transfer modes.
4. A model of the motion of the liquid components.
5. Material phase changes.

2.3.1.4.4 Summary

The phenomena that are now presently understood to be significant in the study of core catchers and their effects must be taken into account in an integrated model. The following is a preliminary list of some of these factors and their effects.

PHENOMENON	EFFECT
Crust formation and breakup	Heat transfer from surface, circulation in the pool
Thermal and boiling convection	Circulation in pool, heat transfer out of pool bottom and sides
Chemical deposition and mechanical separation of fission products	Determination of the magnitude and distribution of internal heat generation
Motion of molten sacrificial material	Heat transfer out of pool bottom and sides
Influence of steel	Heat transfer effects, circulation effects.

With an integrated model, the study of various core catcher designs could be facilitated through sensitivity studies as well.

REFERENCES

1. T. R. Johnson, L. Baker, Jr., and J. R. Pavlik, "Large-scale Molten Fuel-Sodium Interaction Experiments," Proc. ANS Fast Reactor Safety Meeting. (1974).

2. D. R. Armstrong, F. J. Testa, and D. Raudon, "Interaction of Sodium with Molten VO_2 and Stainless Steel Using a Dropping Mode of Contact," ANL-7890 (December, 1971).

3. D. L. Swift and L. Baker, Jr., "Experimental Studies of the High-temperature Interaction of Fuel and Cladding Materials with Liquid Sodium," Proc. Conf. Safety, Fuels, and Core Design in Large Power Reactors, ANL-7120, Argonne National Laboratory.

4. F. A. Kulacki and R. J. Goldstein, J. Fluid Mech., Vol. 55, (2), 271, 1972.

5. J. D. Gabor, E. S. Sowa, L. Baker, Jr., and J. C. Cassulo, "Studies and Experiments on Heat Removal from Fuel Debris in Sodium," Proc. ANS Fast Reactor Safety Meeting, (1974).

6. R.P. Stein, J. C. Hesson, and W. H. Gunther, "Studies of Heat Removal from Heat Generating Boiling Pools," Proc. ANS Fast Reactor Safety Meeting, (1974).

7. I. Catton and R. C. Erdmann, "Post-Accident Core Retention for LMFBR's," UCLA-ENG.-7343, July, 1973.

8. S.M. Zivi,"A Passive Safety Device Against a Melt-Through Accident," Nuclear Applications 5. p. 53, (August, 1968).

2.3.2 Reassembly after Core Meltdown

2.3.2.1 General

For the Overpower Transient and the Flow Coastdown the following discussion helps clarify the final disposition of fuel after the accident.

It is necessary to know the nature and amount of fuel that has moved from its original position in the core so that an accurate assessment of post accident heat removal requirements can be carried out. Fig. 1 contains a sketch (roughly to scale) of the primary vessel of the FFTF. Fig. 2 contains a sketch of the region immediately below the core. Any possible fuel motion following an uncontrolled excursion would have trajectories that would be strongly affected by the post-accident geometry in the reactor vessel.

Post-accident geometry can vary from being essentially the same as it was prior to the accident to being distorted in any number of ways depending upon the magnitude of the accident experienced. It is expected that most of the distortion experienced by the fuel will be in the high power generation region of the core. The damage can be extended to other fuel regions because of sodium pressure effects however.

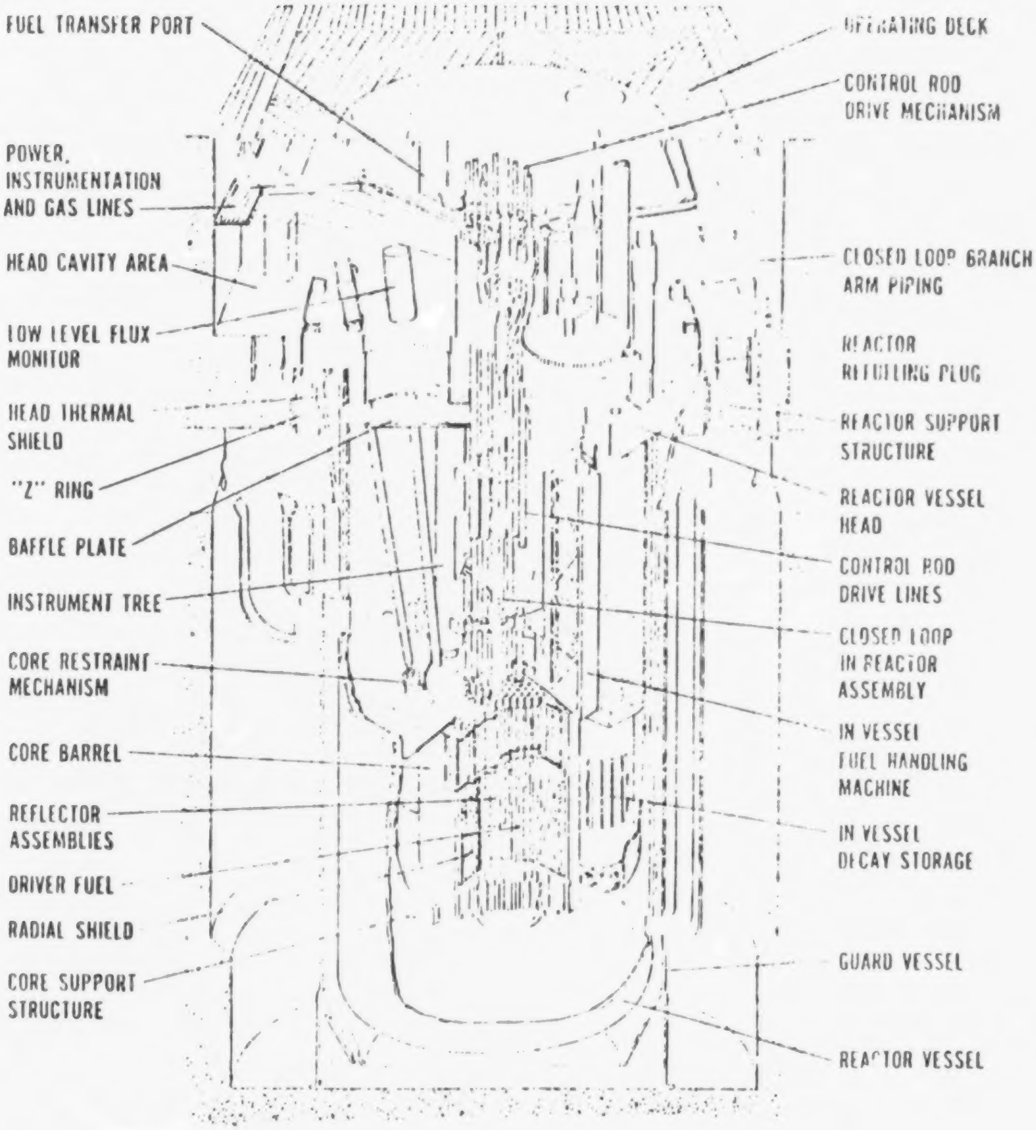
FUEL TRANSFER PORT
POWER, INSTRUMENTATION AND GAS LINES
HEAD CAVITY AREA
LOW LEVEL FLUX MONITOR
HEAD THERMAL SHIELD
"Z" RING
BAFFLE PLATE
INSTRUMENT TREE
CORE RESTRAINT MECHANISM
CORE BARREL
REFLECTOR ASSEMBLIES
DRIVER FUEL
RADIAL SHIELD
CORE SUPPORT STRUCTURE
OPERATING DECK
CONTROL ROD DRIVE MECHANISM
CLOSED LOOP BRANCH ARM PIPING
REACTOR REFUELING PLUG
REACTOR SUPPORT STRUCTURE
REACTOR VESSEL HEAD
CONTROL ROD DRIVE LINES
CLOSED LOOP IN REACTOR ASSEMBLY
IN VESSEL FUEL HANDLING MACHINE
IN VESSEL DECAY STORAGE
GUARD VESSEL
REACTOR VESSEL

Fig. 1. Primary Vessel of the FFTF.

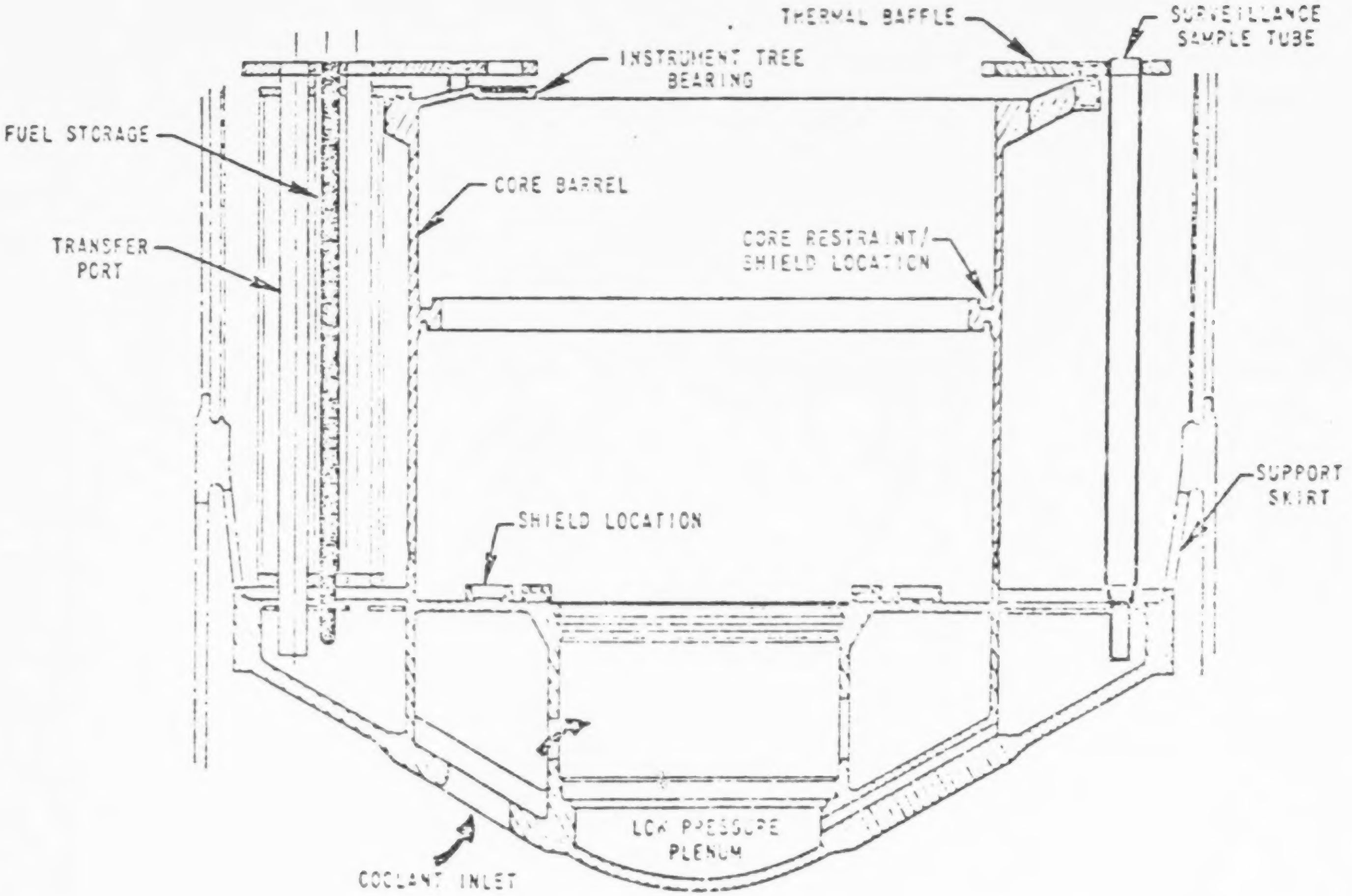
THERMAL BAFFLE
SURVEILLANCE SAMPLE TUBE
INSTRUMENT TREE BEARING
FUEL STORAGE
CORE BARREL
TRANSFER PORT
CORE RESTRAINT/ SHIELD LOCATION
SUPPORT SKIRT
SHIELD LOCATION
LOW PRESSURE PLENUM
COOLANT INLET

Fig. 2. FFTF Core Support Structure.

The spectrum of accidents in an LMFBR core may vary from modest overpower transients to large prompt critical reactivity transients or flow coastdown accidents. Core shutdown in a design basis accident results from fuel being rearranged in such a way as to become subcritical. Fuel motion can be hydraulic, whereby the fuel moves out of the core along with the sodium flow, or hydrodynamic, whereby the fuel or fuel/sodium interactions are so strong as to disrupt previously established flow patterns. In very severe accidents, gross distortion of the reflector assemblies and the core barrel itself appear unlikely during the accident.

Subsequent to the disruptive phase of a DBA there may be continued fuel displacements. Loss of sodium flow through certain channels, combined with decay heat generation can lead to significant melting of core materials and their related structural support members.

2.3.2.2 Reactivity Transient Fuel Deposition

The nature of a reactivity transient depends upon the sequence of events one chooses to follow out of the number of possible, although perhaps unlikely, alternate sequences. Fuel failure location has been postulated (refer to 2.1.2) in this accident to occur in upper core region with the explicit location being determined by local fuel power level. New fuel, it is suggested, fails by melt-through of the clad because there is little driving force within the fuel pin. Low or high power fuel fails by fission gas pressure causing excessive clad strain.

In the overpower transient the core is expected to be full of sodium. One would also expect that the fuel, when ejected from the fuel pin, would interact with the sodium, fragment and transfer some of its thermal energy to the sodium. The fuel is ceramic, and many TREAT experiments have indicated that the fragmentation can yield fuel particle sizes from that of chunks of fuel. It is unlikely in a sodium environment that the fuel will remain molten even if it is in that state within the pin prior to expulsion.

There may be an initial injection of fuel into the channel which might possibly void the immediate area of liquid sodium. Subsequent fuel injected into this region will not be cooled as efficiently and may remain molten for a longer period of time. If these mixing processes are carried on during a subprompt critical phase it is likely that the fuel will be either swept upward out of the active core, if the sodium velocity is high enough and the particles of debris are small enough, or some of it may lodge in the upper areas of the core-blanket region. In either case there will be sufficient sodium to freeze the molten fuel and possibly fragment it. Many of these motions will provide negative fuel reactivity inputs into the accident dynamics.

Such a sequence of fuel pin failure and fuel fragment sweeping out of the core is a continuing one since the original ramp input continually overrides the shutdown provided by the sweeping. As such there is no ultimate shutdown provided for this accident and one can conceive of many of the fuel pins having failed and their contents lifted out of the core. Of concern then is the disposition of this fuel after it leaves the core.

Rather small particles of fuel can be carried with the sodium throughout the primary system. The larger particles will settle out of the flow in a number of places. One place is a baffle plate placed horizontally at the top of the core barrel which contains a number of access ports; fuel particles can collect in layers on this plate. If the particles pass below this plate (through the many holes) they come to rest on the bottom of the reactor vessel. There may exist the possibility that the fuel residue will also settle near the in-vessel decay storage area. In fact it is not clear, from Fig. 1 for example, which area will be most likely to collect fuel debris swept out of the core.

Hence it is expected that particulate core debris will collect on horizontal surfaces throughout the reactor vessel away from those areas having large sodium flow. It will also tend to settle toward the bottom of the primary vessel out of the main sodium flow paths. The debris should be particulate in nature and be at roughly ambient temperature when it settles. The sodium fuel particles should be in intimate contact as the particles settle out.

It is not known what fraction of fuel will get hung up on its way out of the core. No quantitative data on such a process exists. One expects that the larger the fuel debris the more likely it would be to be ensnared by the wire wrap/clad pathway it must transverse. Fuel particles having dimension as large or larger than the average pin spacing will most likely get caught in the core channels. Fuel particles much smaller than the average pin spacing will, for the most part, pass through the core. If the average particle size is 200 μ and if the average spacing between pins is 0.050 inch one would expect very little fuel (in numbers of particles) to get caught in the core. If fragmentation does not produce small particles, then the fuel chunks will get caught.

2.3.2.3 Scenarios for Design Basis Accidents

If a super-prompt critical burst is experienced, the above concept of local fuel-coolant interaction with ejection of fuel debris out of the top of the core will have to be reconsidered. A major fraction of the core fuel may burst, nearly simultaneously, into the channels full of sodium. A rather violent reaction could then occur dismantling the rest of the core and expelling material both up and down. There is a large mass of material radially which would tend to damp any gross horizontal motion compared to that in the vertical direction.

After such a gross DBA the extent of core destruction is uncertain. There may be large areas of core which are essentially free of sodium and remain that way due to blockage, sodium vapor binding and other pressure effects. In these areas the decay heat added to the initially high heat content in the fuel may cause the remaining fuel to melt and slump under gravity to regions below the core. Although there will be local sodium "free" regions, the entire core will always be under a sea of sodium. Hence there is always the possibility that sodium will enter into these high temperature voided areas and be vaporized, causing sodium pressure forces to further disrupt the core, while at the same time cooling it.

In one scenario of this post DBA, the large chunks of fuel pins and fragments of frozen fuel will fall to the core bottom onto the core support structure where its decay heat will continue to add energy to the pool and to the fuel debris itself. Such a bed of core debris would then begin to heat up and interact with the surrounding sodium and with the support layer beneath it.

In a second scenario a molten volume of fuel would fall onto the core support structure where it would perhaps bore a hole through the support and permit the remaining fuel to pour onto the subsequent in-vessel barrier.

If the core is voided due to sodium blockage then perhaps the steel clad will melt and fall to the bottom of the core where it will form a barrier upon contact with sodium. This then could form a barrier through which core material would have to pass.

It is not clear which of these versions is the more likely or whether others still more likely exist. What is clear is the great variety of end results from a large overpower transient. If there is sodium in the core region then it is quite unlikely that a large amount of molten fuel will exist immediately after this DBA. Were sodium to be blocked (due to the accident) from entering certain channels, then a molten fuel volume falling under gravity is likely and it will interact with whatever lies below it whether it is steel, molten or solid, or a porous region of sodium and core debris. Hence a combination of steel and fuel, some of each molten and some of solid, is quite possibly the only description we can place on the post DBA condition of the fuel after an overpower transient that is hydrodynamic in nature.

2.3.2.4 Flow Coastdown Fuel Disposition

A flow coastdown accident is a result of the loss of adequate sodium flow while the reactor is operating at power. There is a tendency during this accident for some (and possibly most) of the core channels to be void of sodium except for any film that may remain after boiling. Shutdown is caused by core disruption which implies fuel motion into a less reactive configuration. This accident appears to be more energetic than the overpower transient, this conclusion being based upon a limited amount of industrial examination and little, if any, real data.

Any energetic disruption of an LMFBR core will cause severe distortion and possibly structural failure of many core support components. Because of the sodium voiding in this accident the disassembly mechanism may be fuel vapor pressure thereby implying a much higher fuel temperature in general, throughout the core. There will also be a large amount of molten fuel as well. Once the core materials get very hot, they will perhaps prevent sodium reentry and cooling by setting up a Na vapor film between the core regions and the sodium pool. Hence in this accident, the post DBA condition can be one of a large amount of molten fuel and steel tending to move onto the core support structure. This is in contrast to the particle fuel debris of the overpower transient DBA because there is less tendency for sodium to be in the core to cool down the fuel.

2.3.2.5 Criticality

Criticality after reassembly will depend upon geometry and material properties. There are conflicting calculations as to whether the reassembled core will be critical. At present that area is uncertain.

Whether critical or merely hot via radioactive decay the reassembled core debris will be geometrically unstable. It is expected that heat induced turbulence and phase charges will cause continued downward penetration by the heavy oxide core debris.

2.4 Event Likelihoods

2.4.1 General Comments

Because the LMFBR is such a new system practically no experience exists on subsystem operation and reliability. Moreover no information of any quantitative nature exists on the probability of the various accidents taking place. The accidents considered in the past in LMFBR safety analysis are usually taken to be upper limit accidents. These then would be expected to be quite unlikely. Lesser versions of these accidetns would, however, be more likely by inference.

2.4.2 Overall Plant Analysis

Godbout has performed a risk assessment of a hypothetical 1000 MWe LMFBR which can be considered suggestive of the possible event likelihoods and consequences. He used fault tree methods to analyze 6 major accident types:

1. Loss of primary coolant flow accident
2. Primary coolant pipe rupture accident
3. Loss of heat sink accident
4. Reactivity excursion accident
5. Sodium fire accident
6. Fuel handling accident

Tornado and earthquake caused accidents were also included in the study. The results of this study are summarized in Figures 1 and 2 which present mortality risk envelopes at 1000 and 100 meters from the plant. The report suffers from the weakness of the component failure rate data base. (The Liquid Metal Engineering Center only collected data for several years (Ref. 2)). It also suffers from the lack of inclusion of plant specific protection. For example, fault trees are constructed for the accident sequences but there are no fault trees for the full plant protection. McLaughlin (Ref. 3) has performed an overall conventional fault tree analysis of the FFTF and Fullwood and Erdmann (Ref.4) have applied the leak path method to the FFTF. The leak path method brings into the analysis complex system interrelationships that affect overall plant protection.

2.4.3 System Analysis

Cave (Ref. 5) has presented a comparative analysis of system reliability in a LMFBR and in a GCFR. He finds the frequency of primary faults as shown in Table

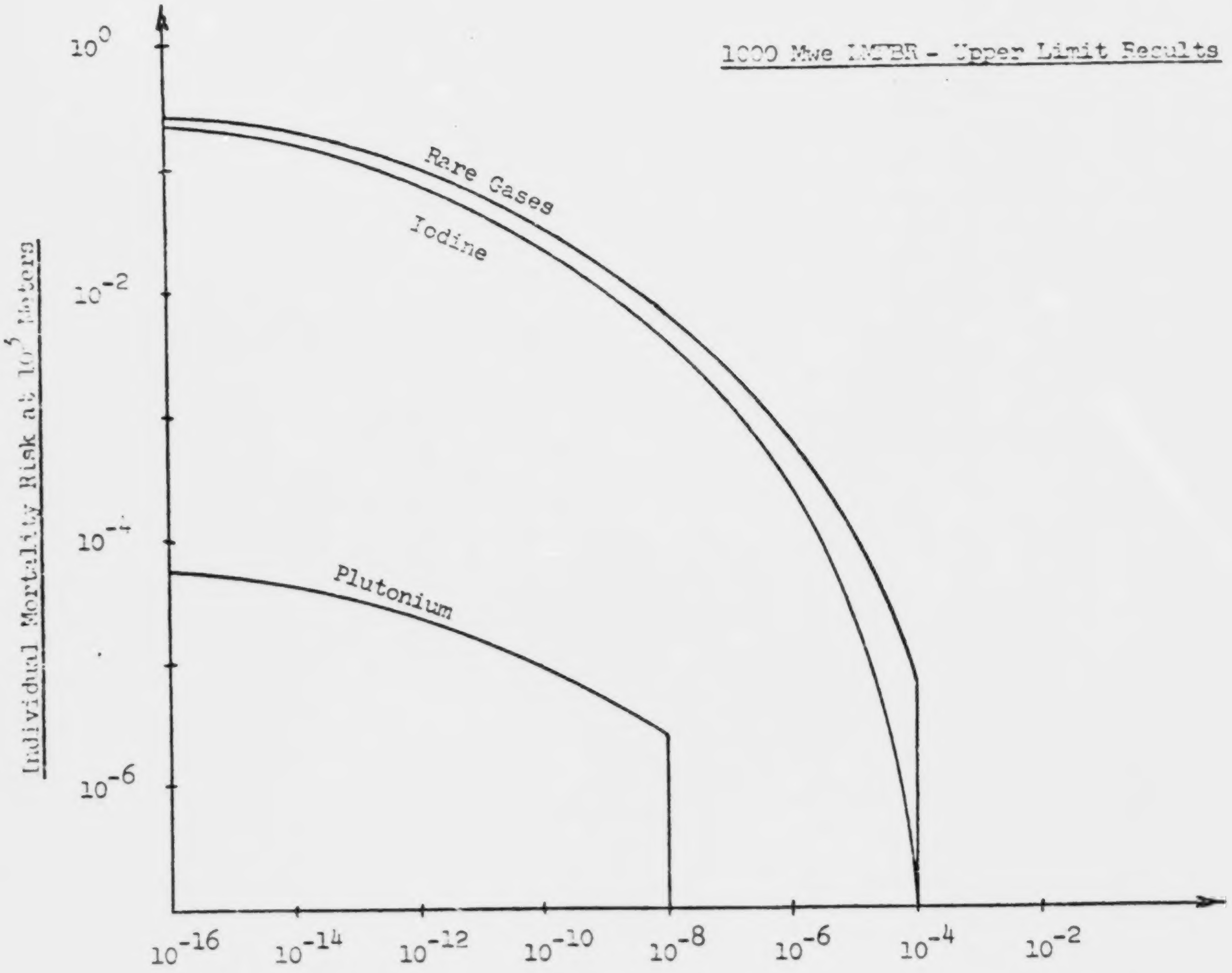

Figure 1. Probability of accidental occurrence per year

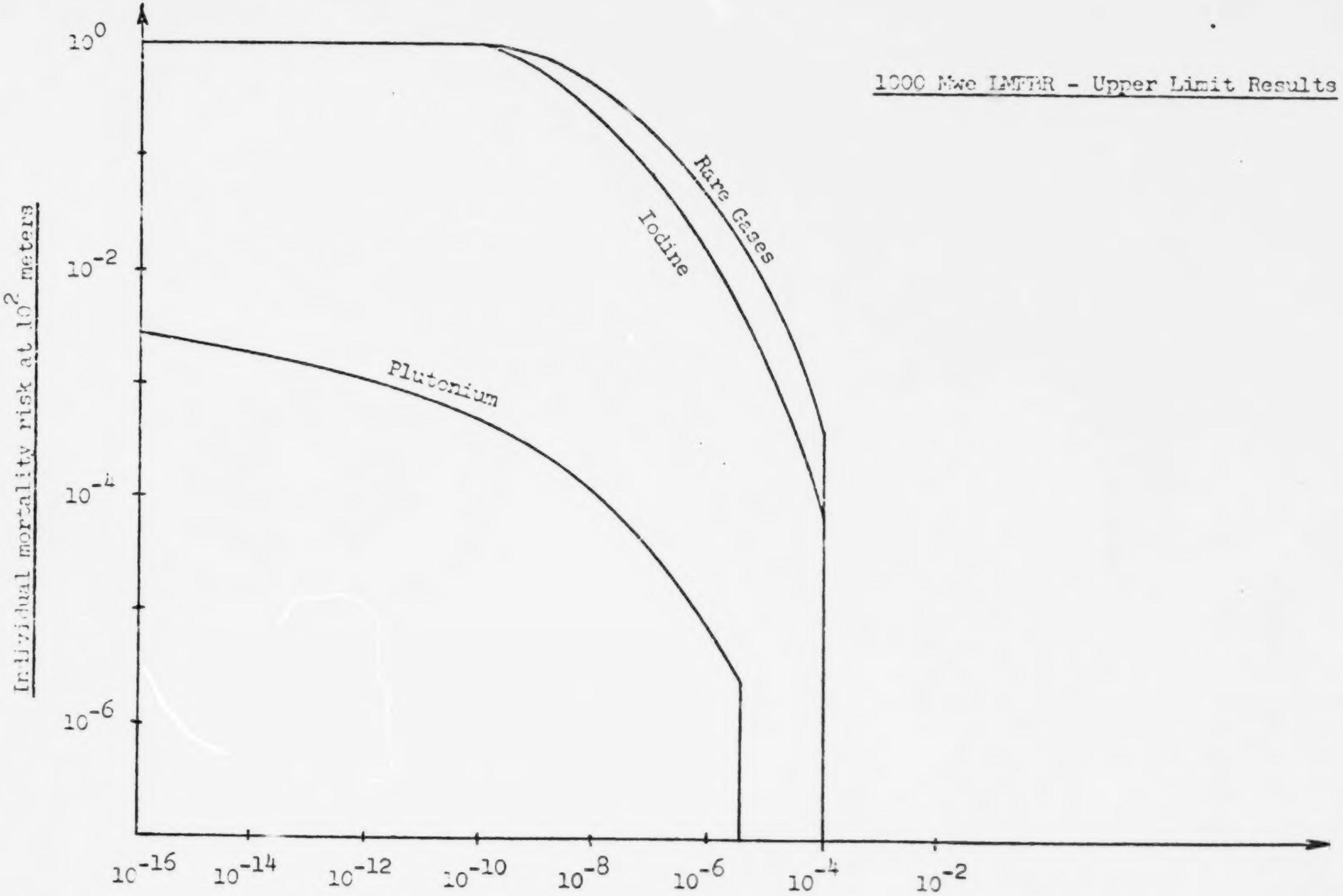

FIGURE 2

Probability of accidental occurrence per year

The French have done a detailed fault tree analysis on decay heat removal in Super Phenix (Ref. 6). They find a probability of failure of the core cooling as 1.2×10^{-10} and a probability for emergency cooling failure as 2×10^{-8} and 5.5×10^{-2} for pumping failure all for 100 day outage but allowing repair. Figure 3 presents the probability of heat removal system failure as a function of time following the accident for repair and no repair. They conclude that the probability of failure of the decay heat removal system is pessimistically, 3×10^{-8}/year.

2.4.4 Comparisons with LWR Likelihood Analyses

Recently, an extensive investigation of LWR safety has been completed (Ref. 7) which is useful for estimating the failure rates of those systems that are similar between LWR's and LMFBR's. Appendix III of WASH-1400 contains a compilation of component failure rates and assessments extracted from recent commercial LWR plant experience. WASH-1400 finds 10^{-5} as the probability of failure of on-site power given a LOCA. Most of the other system failures analyzed in WASH-1400 are not applicable to the LMFBR, with the possible exception of the containment analysis. Even this one must be examined carefully to decide if LWR/LMFBR differences are significant. The WASH-1400 compiled probabilities for natural disasters

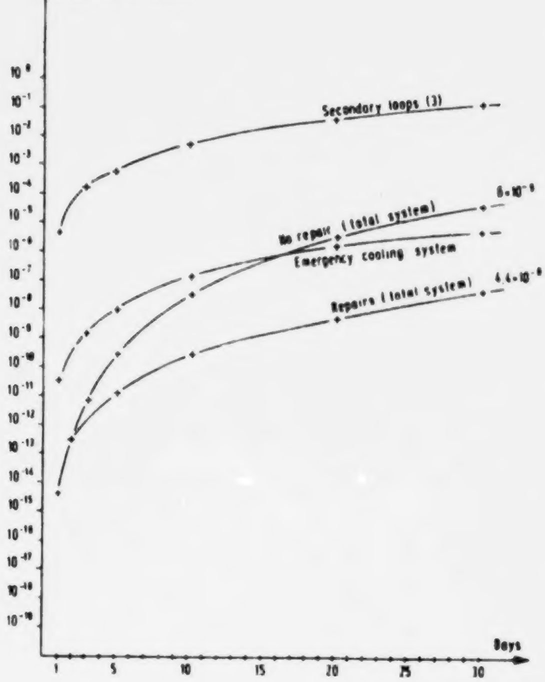

FIGURE 3 Probability of Failure Versus Time of the Cooling System Comparison of the Results no Repair-With Repairs

Estimated frequency of main primary faults in: (i) A typical GCFR design embodying features such as a PCRV with double closures, or hold-downs, steam or electrically driven circulators & a power cut back system to avoid unnecessary trips; (ii) A typical LMFBR.

Serial No.	Type of Fault	Frequency of event per r.y.		Remarks
		GCFR	LMFBR	
1	Innocuous or spurious reactor trips	3	10	
2	Main turbine trip	3	3	These faults need not terminate in a reactor trip
3	Other faults requiring power cut back	3	3	
4a	GCFR. Depressurization accident, leak area near design value (25 to 100 sq.in., say)	10^{-3}	N/A	Larger depressurization accident requires failure of secondary closure or secondary 'hold-down' device, or vessel failure
4	LMFBR. Loss of coolant loops: (i) Loop (ii) Pool	N/A N/A	10^{-3} 10^{-3}	Failure of internal or external ducts (loop type only)
5	GCFR depressurization accident more severe than design	$<10^{-7}$	N/A	
6	LMFBR total loss of coolant accident	N/A	$<10^{-7}$	Requires simultaneous failure of primary tank and leak jacket
7	Sudden severe tube failure in steam generator	10^{-3}*	10^{-3}	Frequency of leaks is higher but usually high moisture in coolant provides warning
8	Multiple tube failure in steam generator	see remarks -------		Implies either sequential failure of tubes or partial collapse of structure, likely order of magnitude 10^{-5} per r.y.
9	Reactivity faults:			
	(i) rod withdrawal of power	10^{-2}-10^{-3}	10^{-2}-10^{-3}	
	(ii) Rod withdrawal during startup	10^{-3}-10^{-4}	10^{-3}-10^{-4}	
	(iii) Reactivity withdrawal due to operator error whilst shut down	10^{-4}-10^{-5}	10^{-4}-10^{-5}	
	(iv) Subassembly faults requiring trip action	see remarks	1	Trip action not required in GCFR
10	Other severe faults requiring reactor trip	10^{-1}	10^{-1}	e.g., boiler feed faults, flow control faults
11	Loss of off-site power	0.3*	0.3*	
12	Failure of secondary containment to provide leak-tightness, on demand, within factor 100 of design value	10^{-3}	10^{-3}	Failure due to faults of containment system alone - not sequential effects

TABLE 1

---

*Not necessarily a trip condition

(earthquakes, tornadoes, floods) and external causes (aircraft impacts, turbine missiles and misc.) can be used if treated appropriately.

WASH-1400 uses the fuel-coolant interaction as being one of the most consequential accidents, but less is known about uranium-water interactions then uranium-sodium In fact WASH-1400 references LMFBR studies for the fuel-coolant explosion.

The consequence models for LWR's are not applicable to the LMFBR because of the high retention of fission products in sodium and because of differences in plant details.

2.4.5 LMFBR Reliability Design Goals

Recently a paper (Ref. 8) was presented discussing the availability goal of the Clinch River Breeder Reactor Project. Since availability and safety are directly related, this goal of 90% availability is worth discussing. Plant availability for a typical facility is given in Fig. 4 and compared with LWR and fossile plant. Figure 5 shows the NSSS Goals for the Clinch River Breeder Reactor project in order for the 90% availability goal to be achieved and Figure 6 are the goals for the balance of plant.

Type of Facility	Plant Availability (%)
LWR - 1973 Only	73
Fossil - 1972 Only	77
Fossil - 1960-1972	80
CRBRP Goal	90

FIGURE 4 Availability Comparison of 400 to 600 MWE Power Plants

SDD † No.	System	Allocation of Availability
	NSSS	(.9669)
22	Compressed Gas	.9976
23	Auxiliary Coolant	.9989
27	Reactor Containment (Seal)	.9995
28	Gas Cooling	.9985
31	Reactor	.9987
32	Reactor Enclosure	.9995
41	Refueling	.9998
44	Maintenance - NSSS	.99995
51*	Heat Transport	.9985
52	Auxiliary Steam Generator	.9961
53*	Steam Generator	.9981
54	Gas Cooling Instrumentation	.9995
55	Containment Instrumentation	.9995
56*	I&C, Na, and Steam	.9995
57	Auxiliary Cooling Instrumentation	.9995
63	System 81 Instrumentation	.9995
66	Leak Detection	.99995
67	Annunciator	.9995
68	Trace Heating	.9981
81	Auxiliary Liquid Metals	.9971
82	Inert Gas	.9957
90	Plant Control	.9995
92	Reactor Instrumentation	.9995
94	Fuel Failure	.9947
95	Flux Monitoring	.9995
99	Plant Protection	.99995

*Based on at least 2 out of 3 loops available.
†System Design Description

FIGURE 5

AVAILABILITY ESTIMATES AND ALLOCATIONS (NSSS)

SDD No.	System	Allocation of Availability
	BOP [x]	(.9774)
11	Electrical Power Transmission	.9993
12	In-Plant Electrical Distribution	.9993
13	Electrical Grounding	.9995
45	Maintenance - BOP	.99995
69	I&C BOP [xx]	.99995
71	Feedwater and Condensate	.9955
72	Maintenance and Auxiliary Steam	.9850
73	Heat Rejection	.9993
74	River Water Service	.9995
75	Treated Water	.99995
ALL	CRBRP	.945

[x] Balance of Plant

[xx] Instrument and Control Balance of Plant

FIGURE 6 Availability Estimates and Allocations (BOP)

These numbers are probably unrealistic and will not be achieved in practice. However, it is important to know that availability goals are being defined for the demonstration LMFBR and these goals are being broken down to the system level and will probably be incorporated in system availability may lead to more reliable systems and hence to a safer machine.

2.4 Summary

The event likelihoods are not known for large LMFBRs. There have been some scoping modeling and some fairly detailed modeling of subsystems. Likelihood analysis for LWR's is more detailed and better supported by nuclear plant experience component failure rate data than is the LMFBR. Little reliability data is available for liquid metal components.

REFERENCES

1. P. Godbout, "Probabilistic Safety Analysis of a Hypothetical 1000 MWe Liquid Metal Fast Breeder Reactor," UCLA Eng.-7242, May 1972.

2. Liquid Metal Engineering Center, "Failure Data Handbook for Nuclear Power Facilities," LMEC-Mans-69-7, August 15, 1969.

3. M.A. McLaughlin, "Preliminary Fault Tree Analysis for the FFTF," BNWL-874, May 1969.

4. R.R. Fullwood and R.C. Erdmann, "On the Use of Leak Path Analysis in Fault Tree Construction for Fast Reactor Safety," Proc. of the Fast Reactor Safety Meeting, Beverly Hills, Ca., April 2-4, 1974. CONF-740401-P3, p. 1493-1507.

5. L. Cave, "A Comparative Study of the Safety of Liquid Metal Cooled and Gas Cooled Fast Reactors," Proc. of the Fast Reactor Safety Meeting, Beverly Hills, Ca., April 2-4, 1974. CONF-740401-P2, p. 1452-1480.

6. C.P. Zaleski et al., "Decay Heat Removal in an LMFBR," Proc. of the Fast Reactor Safety Meeting, Beverly Hills, Ca., April 2-4, 1974. CONF-740401-P2, p. 785-801.

7. US AEC, "An Assessment of Accident Risks in U.S. Commercial Nuclear Power Plants, WASH-1400, August 1974.

8. B.J. Garrick, "Nuclear Power Plant Availability-Its Costs and Benefits." A paper presented at the AIF Workshop on Reactor Licensing and Safety, San Diego, Ca., Dec. 10-13, 1974.

3.0 EXPERIMENTAL RESEARCH

3.1 TREAT Data and Pertinent Experiments

3.1.1 Description of TREAT Facilities

TREAT (Ref. 1) is a graphite-moderated thermal pulsed reactor operated by Argonne National Laboratory, capable of producing a high integrated neutron flux. Within the operating limit of 600°C maximum core temperature, the reactor can supply an uperturbed integrated thermal-neutron flux up to about 9×10^{15} neutron/cm^2. Pulse duration can be varied from 0.05 seconds to tens of seconds. Because of the high flux capability, it is possible to perform meltdown experiments on highly enriched LMFBR fuel samples using the high-energy neutrons passed by thermal-neutron filters.

During 1971, the reactor capabilities were extended by the addition of an advanced control system utilizing two hydraulic control rods under computer control. With this system a variety of transient shapes can be obtained with a high degree of precision and reproducibility (Ref. 2). This system can be used to shape a constant-pulse transient so as to obtain steady-state-like temperatures much more quickly and with less expenditure of reactor integrated power than for a true flattop pulse. Fig. 1 illustrates this method of operation, showing the effect of an initial overpower excursion, followed by constant power, on the outlet coolant temperature for a TREAT loop test (Ref. 3). Similarly, this control system can be used to increase the degree of simulation of a tran-

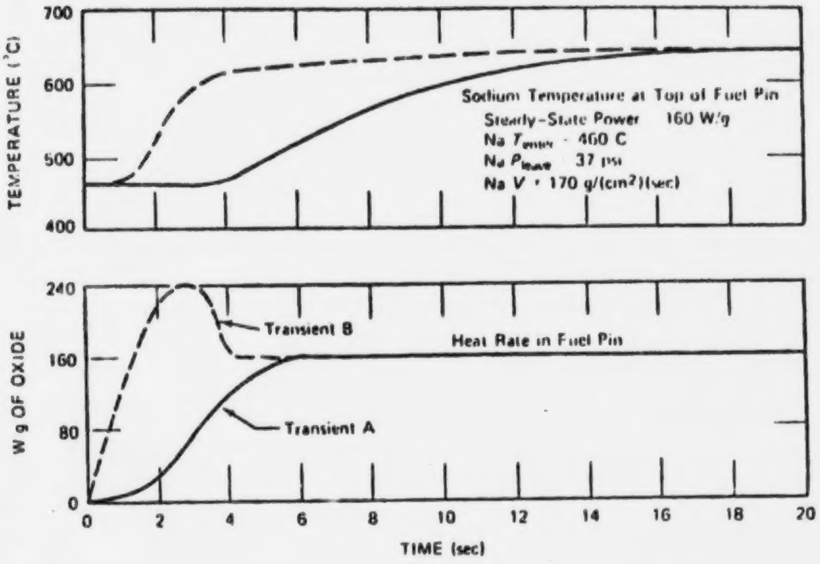

Fig. 1. Effect of the Shape of the TREAT Power Transient Upon Attainment of Steady-State Outlet Coolant Temperature.

sient overpower accident by making it possible for a TREAT transient to begin with a short "preheat" regime of a few seconds duration to establish radial and oxial temperature distributions typical of steady state prior to the actual power excursion (Ref. 4).

Before and after radiographs of the test samples are taken at TREAT using a beam of neutrons from the core. These neutron radiographs can show fuel displacements, dispersal, and even internal shrinkage voids from an unfailed pin in which fuel melting occurred (Ref. 5). Fuel motion during a transient experiment is monitored by the TREAT neutron hodoscope, which is built around a 334-channel steel collimator. Neutron detectors view the central test region in the reactor core through the collimator. An automated data-reduction system is used to process counting data and to plot the normalized neutron counting rates as a function of time and space during a transient, or to produce computer-drawn pictures showing the distribution of sample fissionable material.

Within the reactor core, space was provided for the placement of a self-contained capsule within which meltdown experiments could be performed. The most recent of such vessels is the Mark-II (Ref. 6, 7) integral sodium-test loop. This capsule was developed as a high-temperature, high-pressure hydraulic loop, which provides a flowing-sodium test environment. As shown in Fig. 2, this loop is a self-contained package employing a U-tube geometry. The test leg is instrumented at the inlet and outlet for flow, pressure and temperature. The opposite leg consists of an in-line annular induction pump for coolant circulation. The loop is enclosed within a hermetically sealed stainless steel container, equal in size to two TREAT subassemblies (4 x 8 in.). The loop was designed to withstand a static pressure rating of 340 atm at a temperature of 538°C (Ref. 7). Mockup of sodium flow conditions is achieved by adjusting the pump power, while energy simulation is obtained by altering the reactor neutronics.

3.1.1.2 Transient Overpower Experiments (Ref. 8)

3.1.1.2.1 General

During the past five years there have been a number of Fuel Dynamics TREAT experiments conducted in support of analysis of the hypothetical transient overpower accident. Most of the significant tests were conducted with oxide fuel elements in a flowing sodium environment provided by the Mark-II loop.

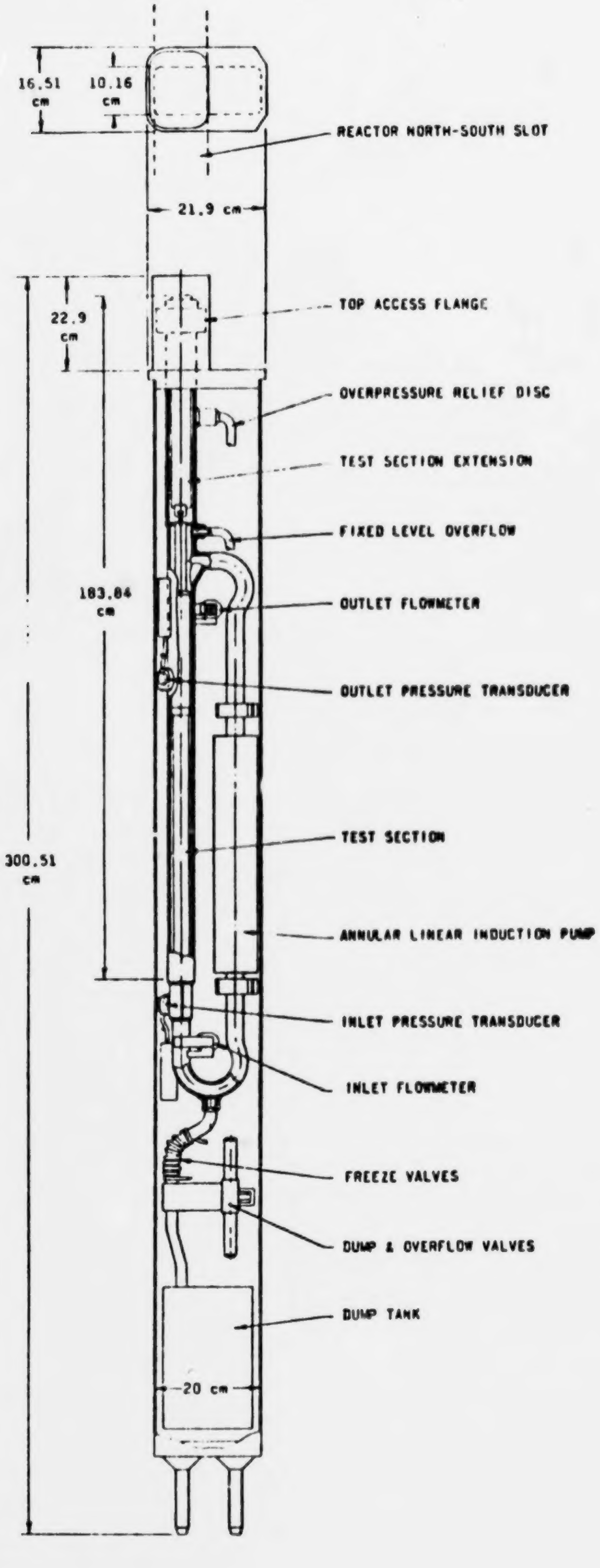
16.51 cm
10.16 cm
REACTOR NORTH-SOUTH SLOT
21.9 cm
22.9 cm
TOP ACCESS FLANGE
OVERPRESSURE RELIEF DISC
TEST SECTION EXTENSION
FIXED LEVEL OVERFLOW
183.84 cm
OUTLET FLOWMETER
OUTLET PRESSURE TRANSDUCER
TEST SECTION
300.51 cm
ANNULAR LINEAR INDUCTION PUMP
INLET PRESSURE TRANSDUCER
INLET FLOWMETER
FREEZE VALVES
DUMP & OVERFLOW VALVES
DUMP TANK
20 cm

Fig. 2. Layout of the Mark-II Integral-Sodium Test Loop (Ref. 6).

Early in the test program, the tests were primarily of a scoping nature and were intended to examine the failure threshold and consequences of oxide fuel elements, without reference to a specific fuel-element design or set of reactor conditions. In particular, Tests E1, E2, and E3 were of this nature. The initial tests on Fast Test Reactor-like elements, H2 and E4, were also generally of the scoping variety. Test H2 was intended to produce just enough energy in the fuel pin to cause failure so that the information obtained on the failure threshold and mechanism of failure would be maximized. Test E4, identical in geometry to H2, was intended to produce an energy release in the fuel considerably in excess of that necessary to cause failure, so that the transient would extend into the regime of postfailure fuel-motion events.

As the needs of the Fast Test Reactor safety analysis became focused and the new TREAT control system provided the option of shaped transients, the test program became more oriented toward integral tests aimed at obtaining information on the whole spectrum of events accompanying a hypothetical transient overpower accident. Basic variables addressed in the program have been the transient heating rate (related to the ramp reactivity addition rate) and the microstructure of the fuel. Experiment design incorporated neutron filtering and transient pulse shaping in order to achieve fuel radial temperature profiles more representative of in-reactor conditions prior to initiation of the overpower burst. Tests H3 and H5 examined the behavior of intermediate-power irradiated fuel in transients corresponding to the ramp reactivity insertions of ~50¢ to 1$/sec, while Tests E6 and E7 examined the behavior of high-power irradiated fuel in simulated 3$/sec transients. Test H4, performed recently, subjected high-power irradiated fuel to a 50¢/sec transient. Other tests are planned to complete the matrix as indicated in Table I .

Analysis of the tests has focused on extracting information useful in guidance of code development and in testing predictions of existing models used in accident analysis. Also, loop modeling studies have been initiated, in order to support extrapolation of the data to LMFBR systems. The phenomena of greatest interest include prefailure fuel movement, cladding failure, coolant dynamics and fuel-coolant interactions, and postfailure fuel motion. Since these are integral tests, the extent to which fundamental phenomenological information can be extracted is limited, but the results do serve to identify the important features of fuel behavior during accident transients so that modeling and phenomological testing can be directed at the areas of greatest concern. Likewise, the tests provide data against which the success of integrated accident-analysis codes can be measured.

Table I. Fuel Dynamics TOP Test Program through June 1974.

Fresh pins

	Prototypic fuel	Non-prototypic fuel
Low heating rate	H2	
High heating rate	E4	E1, E2

Preirradiated pins

	Intermediate-power fuel	High-power fuel	Non-prototypic fuel
50¢ - $1/sec	H3, H5	H4+	
$3 - $5/sec	E8*,+	E6 E7*	E3++

* Seven-irradiated pins, other tests have preirradiated central pin with six fresh peripheral pins.

+ H4 performed 12/19/73, E8 scheduled for June, 1974 performance.

++ Three irradiated pins.

Certain key conclusions have been drawn from the test data and analysis conducted thus far. It appears that prefailure fuel motion was an important feature for pin geometries which particularly favored such motion, but the data do not support assumption of prefailure motion under the conditions expected in a Fast Test Reactor fuel pin. Failure of fresh fuel pins in Tests H2 and E4 appears to follow a 40 to 50 msec period of localized boiling, possibly along the spacer wire where it contacts the cladding. The mechanism of failure appears to be meltthrough.

Thus, it seems that any model of fresh pin failure should consider this phenomenon. The nature of failure of irradiated fuel is less clear, although release of fission gas through small leaks seems to be an important feature of failure of high-power irradiated fuel. In general, the failure threshold data support the thesis that fresh fuel has the highest failure threshold, high-power irradiated fuel the next highest, followed by intermediate-power irradiated fuel. Melting appears to have advanced well into the unrestructured fuel at failure of high-power fuel in E6 and E7, but only to the inner boundary of high-gas-content fuel at failure in H5. No evidence of large-scale molten fuel-coolant interactions has been observed, although the tests have not been designed in such a way as to promote such interactions. A consistent feature of the results has been at least a partial flow blockage following the test. In the tests of prototypic fuel, there is a tendency for fuel to plug the flowchannels either near the failure site or in the region immediately above the fuel column rather than undergo a benign "sweepout" beyond the pin bundle (refer to section 2.1.2). Release of fission gas into the coolant channel appears to be of importance in tests of irradiated fuel pins.

3.1.1.2.2 Test Descriptions

All tests described in this paper were conducted in a Mark-II loop. The loop provides containment of the experiment and sufficient heat capacity to absorb the energy generated without experiencing excessive temperatures. For the early scoping Tests E1, E2, and E3, which used low-enrichment oxide fuel, no thermal neutron filtering was used. With the beginning of tests on mixed-oxide fuel, it was necessary to adopt thermal-neutron filtering to overcome severe self-shielding in the fuel pins. A large filter lining the containment can was used for single-pin Tests H2 and E4. For later tests on 7-pin clusters, a filter was applied directly to the exterior of the loop body, and flux-shaping collars were provided at the ends of the fuel column (Ref. 9, 10).

A variety of fuel pins has been tested in the Fuel Dynamics program. Fig. 3 depicts the various designs. All

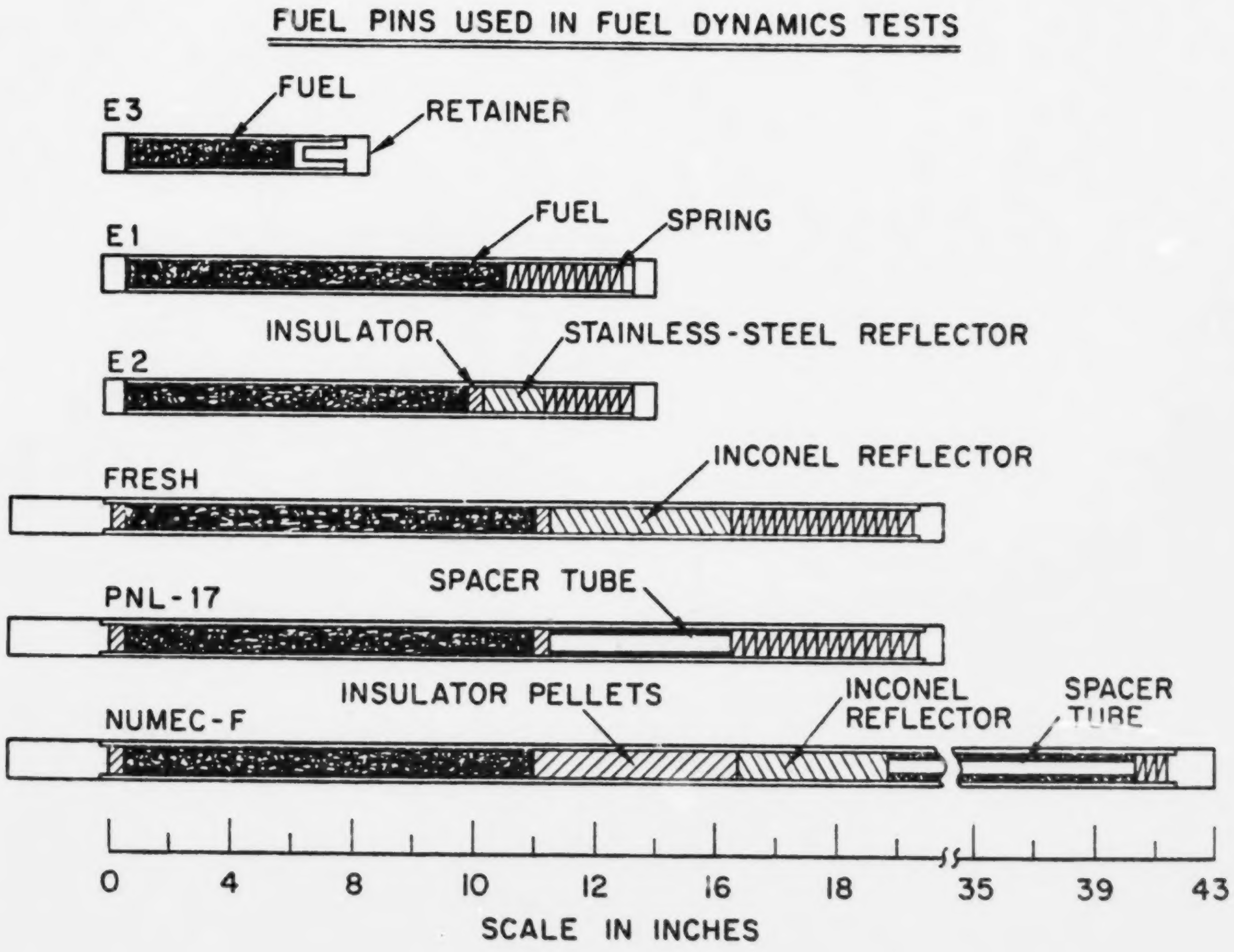
FUEL PINS USED IN FUEL DYNAMICS TESTS
E3
FUEL
RETAINER
E1
FUEL
SPRING
E2
INSULATOR
STAINLESS-STEEL REFLECTOR
FRESH
INCONEL REFLECTOR
PNL-17
SPACER TUBE
NUMEC-F
INSULATOR PELLETS
INCONEL REFLECTOR
SPACER TUBE
0
4
8
10
12
16
18
35
39
43
SCALE IN INCHES

Fig. 3. Schematics of Fuel Pins Used in Fuel Dynamics Tests (Ref. 8).

pins tested have had fuel column lengths of 13 1/2" or less. The first test, E1, used a pin having 0.290" outside diameter x 0.020" thick cladding, a 12 1/2" column of UO_2 fuel with no axial restraint as the central pin in a seven-pin cluster with six helium-filled dummy pins. This pin did not fail, apparently due to large axial movement of molten fuel, so axial restraint was added for Test E2. The same cladding was used, with an 11.3" fuel column topped by a 2"-long steel rod. Otherwise, E2 was physically the same as E1. Test E3, the first to use irradiated oxide fuel, was conducted before Fast Test Reactor-type irradiated fuel was available. The three pins used 5"-long stacks of low-enrichment oxide fuel, and 0.174" OD x 0.009"-thick cladding. Irradiation was conducted in EBR II at an initial power level of 2.5 kW/cc. The initial high-power level, which decreased markedly as the burnup increased, led to a fully-developed high-power microstructure, but a high gas retention. The estimated plenum pressure at room temperature was ~9 atm, corresponding to about 22% fission-gas release to the plenum.

All other tests have used pins having prototypic FTR cladding and fuel diameters, and mixed-oxide fuel. Single fresh PNL-17 pins were used in Tests H2 and E4, after modification involving shortening and spacer-wire replacement. Irradiated PNL-17 pins, also shortened, were used as central pins of seven-pin clusters in Tests H3 and H5. These pins are distinguished by the spacer tube above the fuel column, instead of the more prototypic reflector rod. Fresh peripheral pins were used in the seven-pin clusters of Tests H3, H5, and E6. These fresh pins were identical to the shortened PNL-17 pins, except that a reflector rod replaced the spacer tube. The central pin in test E6 was an irradiated NUMEC-F element. Test E7 employed seven irradiated NUMEC-F pins. NUMEC-F pins have a 6.7" long stack of natural-UO_2 insulator pellets over the fuel column, topped by a 5" long Inconel reflector rod. They also have a 0.040"-diameter spacer wire, compared to the 0.054"-diameter wire of the PNL-17 and fresh pins.

The PNL-17 pins were irradiated in EBR-II at two power levels, reflecting the change in reactor power from 50 MW to 62.5 MW for the last half of the irradiation. These pins have columnar, equiaxed, and unrestructured fuel zones but no central void. Their gas retention is somewhat higher than typical of pins having such structure. They have been classified as "intermediate-power" for the present discussion. The NUMEC-F pins were irradiated at high power and their structure and gas retention is clearly reflective of this history. The room-temperature gas-plenum pressures in sibling pins were ~75 psi for the PNL-17 pins and ~165 psi for NUMEC-F pins.

A fuel holder is used in each test to position the fuel pins in the loop. The designs used have varied from test to test to suit the particular needs. A cross section of each test section is shown in Fig. 4. Details of the test samples and test assemblies are given in Table II. The single-pin and seven-pin holders, except those used for H3, E1, and E2, were of the "adiabatic" type, in which a vacuum or gas-filled space separates the flow tube from the loop wall, greatly reducing radial heat losses from the heated zone. Reduction in radial heat transfer is achieved at the cost of lessened radial restraint against pressure pulse loading. The seven-pin holder used in E1 and E2 had a heavy wall without the "adiabatic" feature. The presence of the gas-filled dummy pins lends compliance to the structure, however. Test E3 is the only test in which failure occurred where the test section was relatively rigid against pressure loading.

As with variation in test-section design, there has been some variation from test to test in the details of instrumentation. Typically, each test has had pressure transducers and flowmeters at the inlet and outlet of the pin bundle. Also, coolant temperatures at inlet and outlet are measured. In some cases, other coolant or test-section-structure temperatures are measured. However, detailed fuel and cladding temperatures are not measured directly, but must be calculated, using measured reactor power, sodium inlet temperature, and flow rate. The measured reactor

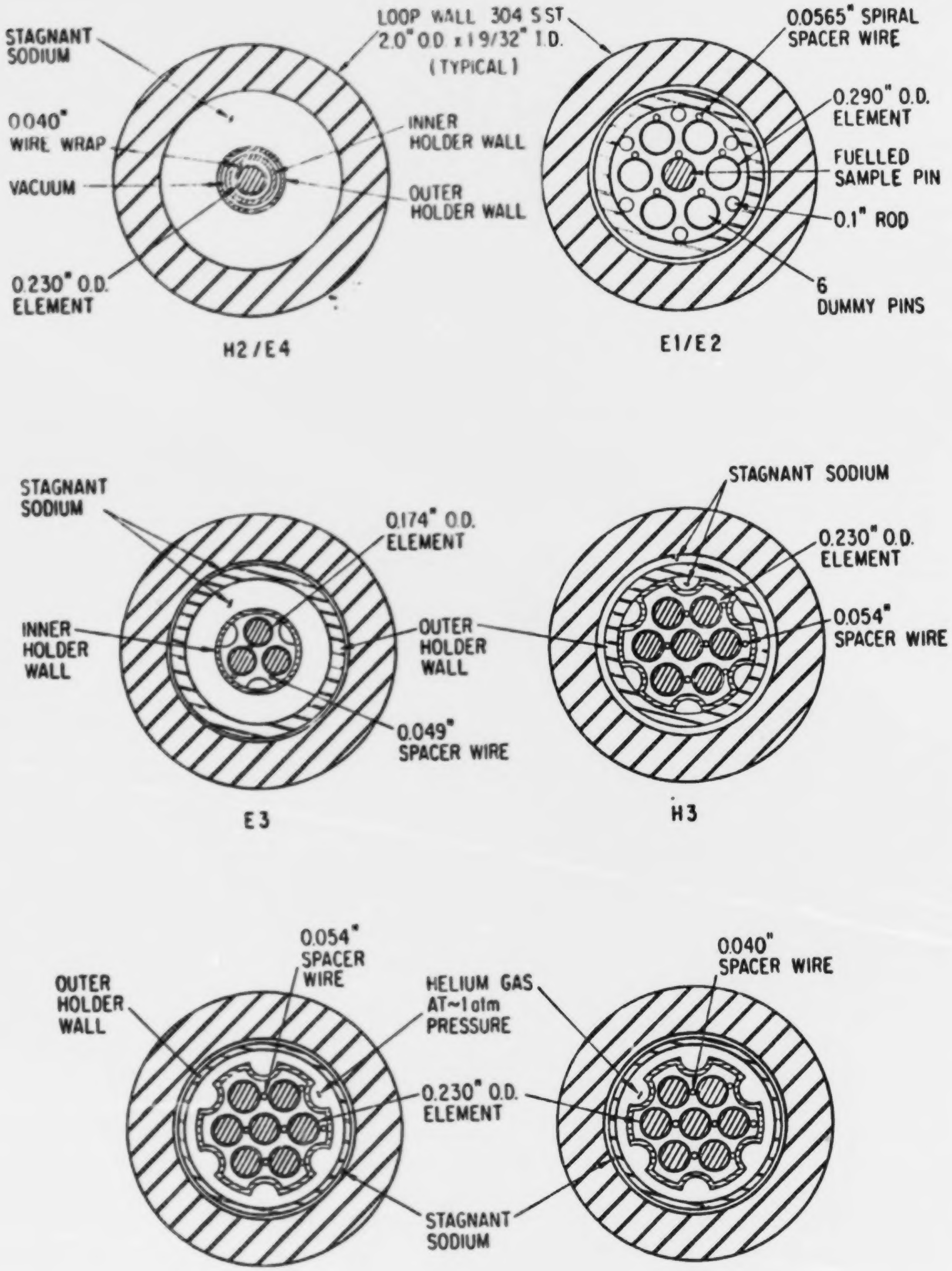
STAGNANT SODIUM
LOOP WALL 304 SST 2.0" OD x 1 9/32" I.D. (TYPICAL)
0.040" WIRE WRAP
INNER HOLDER WALL
VACUUM
OUTER HOLDER WALL
0.230" O.D. ELEMENT
H2/E4
0.0565" SPIRAL SPACER WIRE
0.290" O.D. ELEMENT
FUELLED SAMPLE PIN
0.1" ROD
6 DUMMY PINS
E1/E2
STAGNANT SODIUM
0.174" O.D. ELEMENT
INNER HOLDER WALL
OUTER HOLDER WALL
0.049" SPACER WIRE
E3
STAGNANT SODIUM
0.230" O.D. ELEMENT
0.054" SPACER WIRE
H3
0.054" SPACER WIRE
OUTER HOLDER WALL
HELIUM GAS AT~1 atm PRESSURE
0.040" SPACER WIRE
0.230" O.D. ELEMENT
STAGNANT SODIUM
H5/E6
E7

Fig. 4. Test Section Planar Views (Ref. 8).

Table II. Test Assemblies (Ref. 8).

		H2	H3	H5	E1	E2	E3	E4	E6	E7
Number and type of pins	Central	1 fresh PNL-17	1 irrad. PNL-17	1 irrad. PNL-17	Fresh UO_2, ann. 304L clad	Fresh UO_2, ann. 304L clad	3 Pins; irr. 304L clad	1 fresh PNL-17	1 NUMEC-F, 4.5% burnup	1 NUMEC-F, 4.5% burnup
	Edge		6 fresh	6 fresh	6 Hollow dummies	6 Hollow dummies			6 fresh	6 NUMEC-F, 4.5% b/u
Type of holder		Cyl. tube, adia. wall	Fluted tube, radial heat sink	Fluted tube, adia. wall	Tubular, radial heat sink	Tubular, radial heat sink	Tubular, radial heat sink	Cyl. tube, adia. wall	Fluted tube, adia. wall	Fluted tube, adia. wall
Type of thermal-neutron filter		B_6Si liner inside contain. can	B_6Si filter + shaping collars on loop	B_6Si filter+ shaping collars on loop	None	None	None	B_6Si liner inside contain. can	B_6Si filter+ shaping collars on loop	B_6Si filter+ shaping collars on loop

power is translated to power in the fuel sample using an experimentally determined power calibration factor.

Direct observation of fuel motion is achieved by use of the fast-neutron hodoscope, which determines the distribution of fission-neutron sources as a function of time during a transient with a resolution as short as a few milliseconds. In general, the hodoscope can detect depletion of fuel from a particular space element with greater sensitivity than that with which it can detect additions. Hodoscope data are most important because the hodoscope is the only source of direct detection of transient fuel movement.

The early tests (E1, E2, E3, H2, and E4) were conducted using natural, temperature-limited TREAT transients, initiated by a step reactivity insertion. Later tests, conducted after the TREAT feedback control system became operational, used shaped transients. In these transients, a preheat phase lasting 2 to 3 sec is followed by power rise on a constant period simulating the appropriate ramp-reactivity-addition accident transient. Power transient data and the initial coolant conditions for the various tests are summarized in Table III.

Table III. Test Conditions (Ref. 8).

		H2	H3	H5	E1	E2	E3	E4	E6	E7
TREAT preheat	Power level (MW)		160	115					167	142
	Duration (sec)	None	3.0	3.0	None	None	None	None	3.0	2.4
TREAT burst:	Initial period (sec)	0.08	0.9	1.2	0.064	0.050	0.035	0.066	0.188	0.180
	Maximum power (MW)	1520	425	610	1800	2870	6500	2580	2250	2470
	Final energy (MW-Sec)	490	810	1090	500	750	1250	700	1210	1450
Initial coolant velocity (ft/sec)		20.0	13.0	14.0	12.5	14.5	14.5	18.0	11.7	15.0
Corresponding volume flow (cc/sec)		165	715	770	1060	1240	365	144	640	740
Inlet temp. (°F)		795	710	670	770	760	760	850	740	765
Calibration Factor** (W/gm-MW):	Central pin	3.04	1.52	1.52	3.45	3.45	1.83*	3.14	1.63	1.63
	Hottest edge pin	——	2.05	2.05	——	——	1.87* 1.57*	——	2.05	2.19

* Three pin assembly: "Central pin" and "Hottest edge pin" designations not applicable.

** Assumes intact pin goemetries.

Test Results

Calculated conditions of fuel, cladding, and coolant at failure are tabulated in Table IV. Maximum values are included for tests in which failure did not occur. Four of the nine tests discussed here used fresh fuel pins. Of these, Test E1 did not produce failure, while E2, H2, and E4 resulted in pin failure. Prefailure axial motion of molten fuel appears to have existed to some extent in each test. Extensive axial motion of molten fuel probably led to relief of loading of the cladding during Test E1, such that failure did not occur. Apparently, the low bulk coolant temperature did not allow boiling, so the cladding could withstand contact by molten fuel. Axial restraint was added for Test E2, which impeded prefailure motion of molten fuel. It is not entirely clear what failure mechanism dominated, but cladding meltthrough under the spacer wire was found in posttest examination. This result suggests failure by this mechanism rather than by clad strain. Cladding temperatures were somewhat higher in E2 than E1. Boiling appears to have led to failure in both Tests H2 and E4, where evidence of voiding appears 40 to 50 msec prior to failure. Calculated cladding temperatures are consistent with local boiling, possibly under the spacer wire.

Table IV. Thermal Conditions in Fuel Dynamics Tests (Ref. 8).

			At elevation of max. fuel enthalpy						
Test designation	Time for which results are quoted	Pin for which results are quoted	Radial avg. fuel enthalpy (rel. to rm. temp.) cal/gm	Radial avg. fuel enthalpy (rel. to end of preheat) cal/gm	Rate of rise of rad. avg. fuel enthalpy (max. prior to time) cal/gm-sec	Clad mid-radius temperature °F	Rate of rise of clad mid-rad. temp. (max. prior to time) °F/sec	Max. coolant temp. °F	Portion of fuel cross-sectional area at or above solidus (max.) %
E1	Gross intl. Fuel motion		380	NA	1350	1600	3900	850	80
E2	Failure		430	NA	2300	1800	5600	860	92
H2	Failure		290	NA	1080	1590	3760	1470	76
E4	Failure		340	NA	1650	1930	8630	1725	100
H3	Max. cntl. Pin fuel enthalpy	Central	145	40	90	1200	350	1275	0
H3	Same	Hottest peripheral	190	55	125	1150	350	1275	33
H5	First anomaly	Central	180	95	100	1350	410	1450	25
H5	Same	Hottest peripheral	230	135	130	1350	480	1450	55
E6	First anomaly	Central	280	185	750	1510	2100	1750	80
E6	Same	Hottest peripheral	330	220	1010	1560	2300	1750	100
E7	First anomaly	Hottest peripheral	215	110	710	1150	1300	1270	63
E3	Failure	Hottest	225	NA	2340	1230	6700	1050	0

Coolant dynamic behaviors in Tests H2 and E4 are very similar, differing primarily in degree. Rapid expulsion of coolant from the channel, accompanied by pressure pulses, is characteristic of these tests. This voiding results from initial fuel release at failure, and leads to almost complete melting of the remainder of the cladding and release of molten fuel. Molten fuel appeared generally to move radially, melting through the flow tube and finally depositing on the outer wall of the fuel holder. In both cases, porous plugs of cladding and fuel were found at both ends of the fuel column with complete flow blockage in E4. Coolant voiding was not as rapid or complete in E2, so much of the cladding survived intact. Most of the fuel escaped from the pin out of the bundle into the loop. A blockage finally formed near the failure site. It seems likely that the very low bulk coolant temperature in E2, compared to those in H2 or E4, led to the extensive fuel dispersal and extensive cladding survival.

Of the five tests of irradiated fuel, only H3 did not produce failure. The central irradiated PNL-17 pin was brought to incipient fuel melting without permanent cladding deformation. Considerable release of fission gas from the equiaxed and unrestructured fuel was apparent, but little other change in the pin was noted. No prefailure fuel motion was observed, even in the fresh peripheral pins in which substantial melting occurred.

Test H5, with a pin cluster similar to that in H3, resulted in failure, as did the higher-ramp-rate Tests E6 and E7. To date, we have found no evidence of prefailure axial motion in these tests, but the hodoscope data have not yet been completely analyzed. Failure in the low-ramp-rate Test H5 appears to coincide with the beginning of melting of fuel having a high concentration of fission gas in the central pin. However, this test also included fresh peripheral pins and it is not entirely clear that the central pin failed first. Preliminary results from post-test examination reveal that the central pin is only slightly damaged 2" below the top of the fuel column. The nature and cause of failure has not yet been identified. The peripheral pins generally show clad melted off in localized areas as if due to loss of cooling. Annular shells of solid fuel were found in some areas from which clad was removed. A very small failure of the central pin from which gas was released, leading to coolant voiding and failure of the peripheral pins, appears to be the failure sequence. Alternate scenarios, not inconsistent with the data, can also be envisioned.

As was the case for H5, the nature and location of the initial failure is not entirely clear for Test E6. Failure appears to have occurred with the melting front extending well into the unrestructured fuel. Indications from pressure and flow data (especially lack of pressure pulses at the outlet and lack of pronounced inlet flow reversal) are that gas release played an important role, with failure in the central pin leading to failures of one or more peripheral pins. However, no hodoscope or posttest examination results are yet available to guide interpretation.

Evidence from posttest radiography indicates similarity of results from E6 and H5. Particularly, the peripheral pins seem substantially intact, with an indication of some loss of fuel from the central pin and fuel movement into the region opposite the fuel-pin plenum. The degree of fuel removal and motion appears greater for E6 than for H5.

Test E7 produced a result quite unlike that of any previous test. Evidence of pin failure was very benign with only a slow voiding of coolant and no measurable pressure pulses. Gas release through small cladding fissures is thought to be the cause, since no fuel removal at the time is indicated by the hodoscope. The voiding leads to a large-scale melting of all the fuel elements, followed about 300 msec later by upward fuel motion and plugging in the region immediately above the original fuel region. The posttest radiographs show extensive fuel relocation (see Fig. 5).

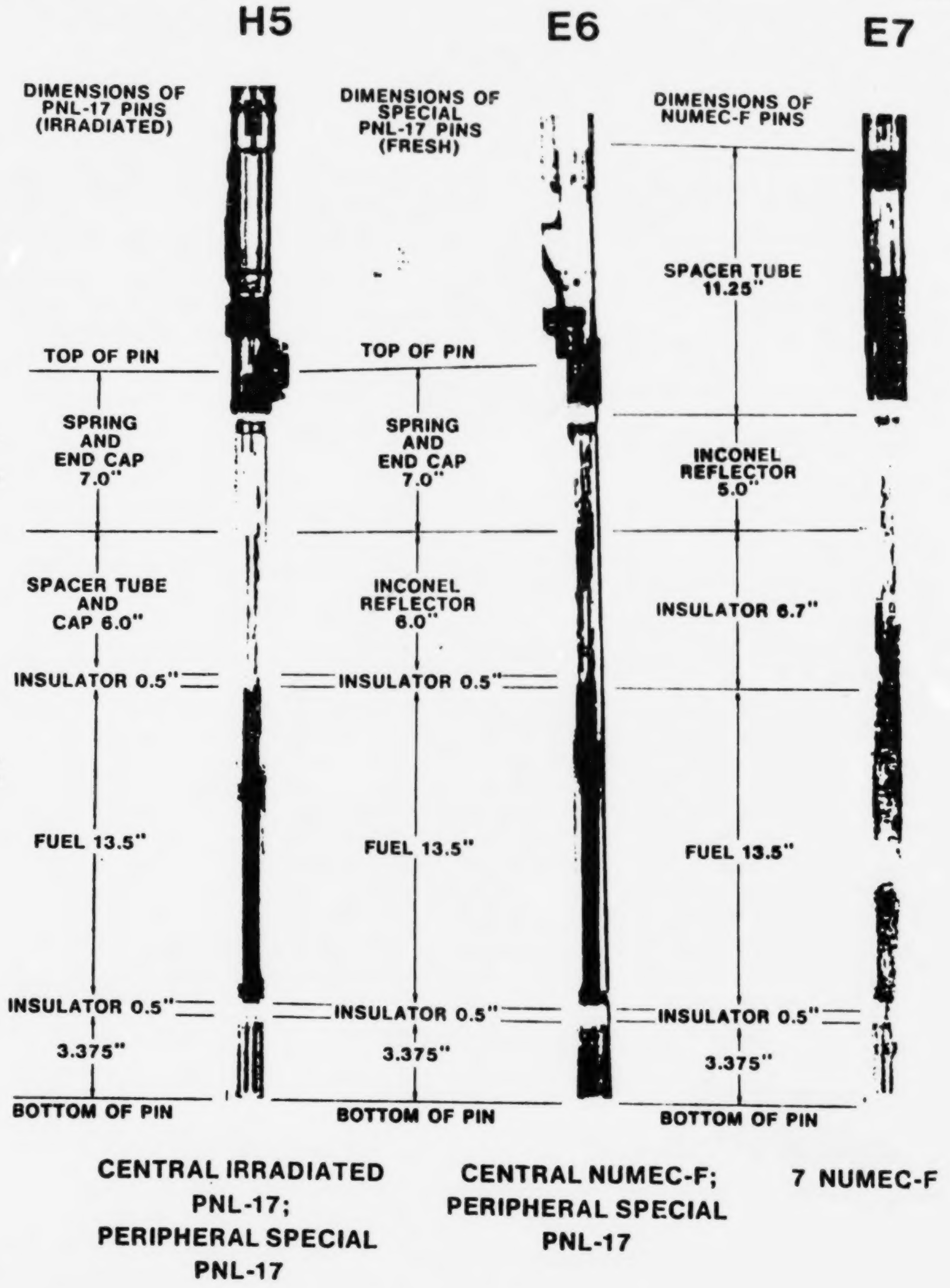
H5
E6
E7
DIMENSIONS OF PNL-17 PINS (IRRADIATED)
TOP OF PIN
SPRING AND END CAP 7.0"
SPACER TUBE AND CAP 6.0"
INSULATOR 0.5"
FUEL 13.5"
INSULATOR 0.5"
3.375"
BOTTOM OF PIN
DIMENSIONS OF SPECIAL PNL-17 PINS (FRESH)
TOP OF PIN
SPRING AND END CAP 7.0"
INCONEL REFLECTOR 6.0"
INSULATOR 0.5"
FUEL 13.5"
INSULATOR 0.5"
3.375"
BOTTOM OF PIN
DIMENSIONS OF NUMEC-F PINS
SPACER TUBE 11.25"
INCONEL REFLECTOR 5.0"
INSULATOR 6.7"
FUEL 13.5"
INSULATOR 0.5"
3.375"
BOTTOM OF PIN
CENTRAL IRRADIATED PNL-17; PERIPHERAL SPECIAL PNL-17
CENTRAL NUMEC-F; PERIPHERAL SPECIAL PNL-17
7 NUMEC-F

Fig. 5. Posttest Neutron Radiographs of H5, E6, and E7.

Test E3 also produced a unique result. Failure occurred prior to fuel melting, accompanied by the largest pressure pulses and highest flow accelerations observed in any test. Removal of fuel from the original fuel region was relatively complete, although the removal process took over 100 msec after failure, based upon results from the fast-neutron hodoscope. A flow blockage of debris eventually formed at a thermocouple rake near the pin-bundle outlet.

3.1.1.2.3 Non-Prototypic Effects

Limitations of fuel availability and facility capabilities have resulted in departures from complete prototypicality in the Fuel Dynamics experiments. Areas in which differences arise between test and reactor situations include length of fuel pins, microstructure distribution, power distribution, test-section design, and loop hydraulics.

The short fuel column height of the test pins means that the axial power distributions, both during the TREAT tests and during the prior EBR-II irradiations, are flatter than in the prototypic case. This condition results in fairly uniform oxide thermal conditions over much of the pin height and in uniform axial microstructure profiles instead of the gradations expected in FTR pins. Thus, the failure threshold in a particular test reflects that of the particular microstructure, not necessarily that of an FTR pin containing the particular microstructure. In fact, the low-power microstructure is thought to have the lowest failure threshold and low-power irradiated fuel has not yet been subjected to a loop test.

Not only does the axial power distribution in the tests differ from that of the reactor, but the radial power distribution differs as well. Since TREAT is a thermal reactor, self-shielding effects in the sample are important, and can only partially be eliminated by filtering. It is necessary to use power pulse shaping to obtain realistic radial temperature profiles. There is substantial pin-to-pin power variation, which results in a built-in non-coherence of failure and post-failure behavior. Failure-threshold data from filtered-loop tests on seven identical irradiated pins must be based on the highest power peripheral pins.

It is in the area of test-section design where boundary effects become important. Clearly, boundary effects are more important in small samples than in subassemblies. Excluding the E1/E2 and E3 test sections in which FTR-prototypicality was not a goal, the designs used in Fuel Dynamics tests have been chosen to approximate the correct hydraulic diameters. However, because of the limited number of pins, the ratio of fuel area to flow area is lower than that of the FTR. The ratios of heated perimeter to wetted perimeter and of flow area to steel cross-sectional area are also lower. It is difficult to draw quantitative conclusions from these observations, but, in general, the low fuel-to-flow area ratio would seem to operate to promote fuel motion in coolant channels, while the excessive unheated perimeter and steel cross-section would tend to cause fuel freezing on the test section wall.

The final area of non-prototypicality is that of the dynamics of loop response to events in the test section compared to that of a reactor subassembly. In general, voiding of the loop test section would occur more rapidly than would voiding of a subassembly. Reference 11 compares the hydraulic response characteristics of the TREAT loop resulting from a single mild fuel-coolant interaction with the hydraulic response of an FFTF subassumbly with the same fraction (1/7) of failed pins. The loop will tend to have more rapid coolant accelerations.

3.1.1.2.4 Conclusions

These tests have provided an experimental basis for analysis of the sequence of hypothetical transient overpower accidents.

No gross prefailure fuel movement was observed in tests H3, H5, or E7. Prefailure fuel movements were observed in single-pin tests, E2, H2 and E4, on fresh fuel with non-prototypical inertial loading. However, no prefailure fuel movements were observed in any of the fresh peripheral pins in H5 and E6, which had FTR-like axial restraint. As yet, no tests have been performed on prototypical fresh elements in the absence of irradiated fuel.

In single pin tests of fresh elements with non-prototypical axial restraint, failure is caused by meltthrough of the cladding, and in the cases of H2 and E4, is clearly preceded by surface or local boiling effects, possibly in a stagnant region under the spacer wire. The complete failure mechanism for E2 is not clear, but the pin remains are consistent with failure by meltthrough. In general, the fresh fuel had the highest failure threshold, high-power irradiated fuel the next highest, followed by intermediate-power irradiated fuel.

With irradiated fuel, the solidus boundary at failure is calculated to have progressed further into the gassy microstructure fuel at the higher fuel heating rates. This trend is in essential agreement with calculations of failure thresholds for high-power irradiated fuel, as a function of reactivity ramp rate, using the analytical model suggested by Smith and Stevenson (Ref. 12). From their analysis, the reason for this is that the rate of clad heating relative to gas release from the fuel is less for the faster ramps.

The nature of the initial gas release to the coolant has an apparent effect on secondary failure and postfailure fuel movement. The nature of this release depends on the type of clad failure. The data from E7 indicate that there was a small pinhole leak with a gas release. The data from E6 and H5 indicate fuel release associated with the initial failure.

In the tests of prototypic fuel, there is a tendency for fuel to plug the flow channels near the failure site or the region immediately above the fuel column rather than undergo a benign "sweepout" of fuel beyond the pin bundle.

Finally it should be noted that in all cases the molten fuel-coolant interactions were minimal. Even the largest conversion of fission-to-coolant mechanical energy (in E3) was much less severe than that for an energetic coherent FCI. Some of the reasons for the low energy conversion results may be the following:

1. Condensation of sodium on the intact clad and structure, as analysis by Cronenberg (Ref. 13) indicates for H2.
2. Failure into a channel voided or partially voided from boiling or the presence of fission gas, as in E7 and E6.
3. Attenuation of peak pressure by deformation of the holder wall with E4, H2, and E6.

3.1.1.3 Loss-of-Flow Experiments (Ref. 14)

3.1.1.3.1 Introduction

The tests designated L2 (Ref. 15), L3 (Ref. 16), and L4 (Ref. 17), were intended to provide experimental data against which predictions of the accident analysis codes can be compared and to guide further analysis and modeling of the initiating phases of the hypothetical accident. Before these tests, there were few data directly applicable to the loss-of-flow accident in an LMFBR and no results from integral experiments to support the analytically-derived scenario. The goal of obtaining integral data allowing comparisons of the gross features of the response of fresh and irradiated fuel elements to loss of flow has been realized.

Each of the three experiments was conducted in a Mark-II loop (Ref. 18), which was designed especially for use in tests of oxide LMFBR fuel elements in the TREAT reactor (Ref. 19). Like the reactor, the Mark-II loop is a "heat-capacity machine", as no reject heat exchanger is fitted. A particular feature of the loop system needed for the L-series tests is variation of the flow during the reactor transient, which is accomplished by servo control of the voltage to the annular-linear-induction pump.

Three different types of fuel pins were used in the present experiments. Their characteristics are summarized in Table V. The basic features of fuel type, cladding material, and cladding and fuel dimensions are common to all three cases. However, differences exist in such features of the pins as reflector pieces insulator pellets, and overall length. The pins used in Test L2 had no irradiation prior to beginning the test sequence. Those used in L3 and L4 had been irradiated in EBR-II.

The basic difference between the two types of irradiated fuel was in the fuel microstructure. Test L3 used PNL-17 pins, which had been irradiated at two different power levels due to an increase in EBR-II power level about midway in their exposure. Destructive examination of sibling pin revealed zones of columnar, equiaxed, and unrestructured fuel, but no well developed central

Table V. Fuel-Element Parameters (Ref. 14).

Test/Pin Type	L2/Fresh	L3/PNL-17	L4/NUMEC-F
Diameters (in.)			
Clad OD/Clad ID	0.230/0.200	0.230/0.200	0.230/0.200
Spacer Wire	0.054	0.054	0.040
*Fuel Pellets	0.194	0.194	0.194
Lengths (in.)			
Overall	30-7/8	30-7/8	42.984
End Plug	3-3/8	3-3/8	3-3/8
Bottom Insulator	1/2	1/2	1/2
Fuel Column	13-1/2	13-1/2	13-1/2
Upper Insulator	1/2	1/2	6.2
Reflector or Spacer	6(refl.)	6(spacer)	5(refl.)
Gas Plenum Volume (in^3)	0.15	0.32	0.34
Gas Plenum Pressure (67°F), psi	15	~75	~165
Fuel Material			
* Smear Density (% T.D.)	88	88	86
* Enrichment, w/o ^{235}U in U	65	65	77
* Enrichment, w/o ^{239}Pu + ^{241}Pu in Pu	88	89	88
Nominal Burnup (%)	0	3.5	4.3
Nominal Peak Irradiation Power (kW/ft)	-	9.2-11.2	14.0

---

* As-fabricated value

void. On the other hand, the NUMEC-F pins used in Test L4 had been irradiated at a high power level during their whole exposure. Destructive examination of a sibling pin revealed a well-developed central void, as well as zones of columnar, equiaxed, and unrestructured fuel.

Similar test sections were used in each of the tests. A cross-sectional view is shown in Fig. 6. The seven fuel pins are maintained in a hexagonal array within the fluted flow tube, which is 0.035 in. thick. The fluted tube is surrounded by a gas-filled space and a thin cover tube. In Test L2, this space was used to house an experimental void detector. The void detector was not used in Tests L3 and L4. The space was used instead for thermocouple instrumentation of the fluted tube wall. A slightly smaller tube was used for L4, than was used for L2 and L3, since the L4 pins had smaller spacer wires. Fig. 6 indicates the relationship of the pump leg of the loop and the fast-neutron hodoscope to the test cluster.

No thermal-neutron filtering was used for Tests L2, L3, and L4, which results in a nonuniformity of heating of the fuel pins. The peripheral pins in the cluster have an average heat generation about 40% greater than that of the central pin, which helps to compensate for the inherent heat losses from the edge

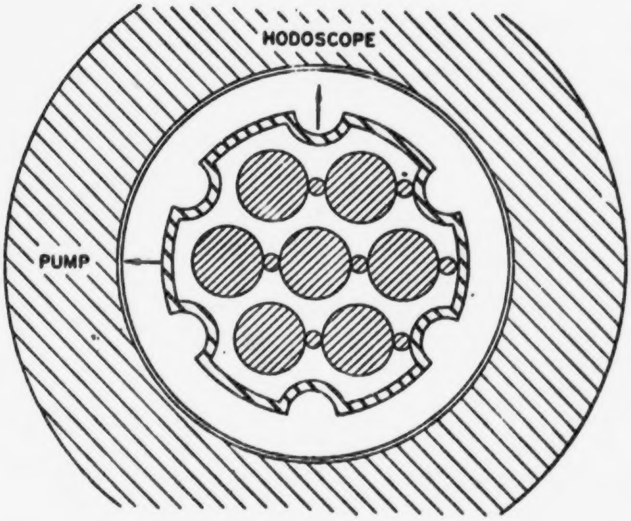
HODOSCOPE
PUMP

Fig. 6. Fuel Bundle Cross-Section for Tests L2, L3, and L4.

channels surrounding the cluster and for the radial heat transfer to the heat sink of the fluted tube and loop wall after coolant voiding. Dysprosium flux-shaping collars at the ends of the fuel column were used to produce an axial power distribution having a peak-to-average ratio of about 1.08, with an essentially flat central section.

Flow and pressure instrumentation was similar in each of the three tests, but thermocouple instrumentation differed somewhat. Coolant flow and pressure were measured at the inlet to the test section in each test. In L2 and L3, which used 31-in.-long pins, the upper flow and pressure instruments measured quantities at the outlet from the pin bundle. However, the longer NUMEC-F pins used in L4 extended past the location of the upper flow and pressure instruments. In this case, then, the measurements reflect conditions in the upper part of the pin bundle.

Thermocouples were provided to measure both inlet and outlet temperatures in each test. Due to the presence of the void detector in Test L2, the fluted tube was not instrumented, but a thermocouple was inserted in the pin bundle with its tip at the top of the fuel column. In Tests L3 and L4 thermocouples were spaced along the fluted tube between 3 in. above the bottom of the fuel column and 6 in. above the top of the fuel column. A thermocouple in the pin bundle was omitted to facilitate remote assembly. Direct observation of the fuel motion during the tests was accomplished using the fast-neutron hodoscope (Ref. 19).

Test operations followed the same pattern in each of the tests, with minor exceptions. The reactor transient consisted of two constant-power portions: a 2-sec-long preheat phase followed by the sustained-power phase. Power-level and duration data are given in Fig. 7. Test L2 consisted of three runs; the first at constant flow, the second with a decrease in flow to a nominal 60% of the initial value, and the third with a decrease in flow to a nominal 10% of the initial value. In Tests L3 and L4, only runs of the first and third type were performed. The purpose of the constant flow runs was to check the relationship between reactor power and sample power by a calorimetric measurement, and to establish the transient performance of the instruments under reactor conditions. In Test L2 and L3, the flow decrease was initiated nominally 2 sec after sustained power was achieved. For L4, the 2-sec delay was eliminated in favor of a longer time-at-power after beginning of boiling.

3.1.1.3.2 Test Results

A summary of the sequence of events during each test, based on interpretation of available data from all sources, is given

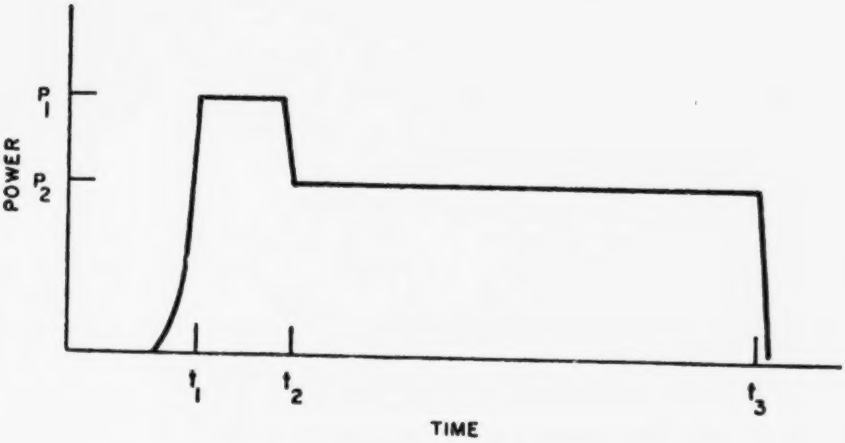

TEST DESIGNATOR	L2	L3	L4
CLUSTER AVERAGE LINEAR POWER			
P_1, kW/ft	18.0	16.1	17.0
P_2, kW/ft	10.9	9.3	10.0
TIME			
t_1, sec	5.2	5.2	5.0
t_2, sec	7.5	7.2	7.2
t_3, sec	31.1	34.0	30.2

Fig. 7. Power Transient (Ref. 14).

in Tables VI, VII and VIII. A plot of the flowmeter signals for each test, with certain events in the scenario indicated, is given in Fig. 8.

3.1.1.3.3 Boiling and Voiding

Beginning of boiling is indicated in all three tests by an irregularity in the flowmeter signals, correlated closely in time with a break in the slope of temperature-time curves for locations close to the top of the fuel column. The inlet flow drops rapidly to zero, but does not reverse, suggesting that boiling inception in various subchannels is incoherent in time. In L2 the flowmeter signals remain rather irregular for about 2.5 sec. until the thermocouple at the top of the fuel column indicates a rapid temperature rise suggesting dryout. At this time the flowmeter oscillations become very regular and grow in amplitude for slightly more than 2 sec. During this period void growth is indicated, while no void growth is indicated earlier. In the immediately following interval of about 0.2 sec, flow ceases following a prominent "spike" in the outlet flow. The cause of the "spike" is not known definitely, but rupture of the fluted tube and release of gas pressure is a possibility, as is a limited steel-sodium thermal interaction. No pressure pulses were observed at this time.

Table VI. Scenario of Events for Test L2 (Ref. 14).

Time (sec)	Event
0	Beginning of test; temp. ≃ 885°F; flow ≈ 915 cc/sec.
9.2	Flow reduction starts.
16.4	Sodium boiling begins; temp. at top of fuel column (TC4) at plateau of 1740°F; flowmeter, outlet temperature oscillations start.
17.3	Effective flow cessation; zero net flow.
19.0	Dryout suggested; TC4 completes slow rise to 1800°F; outlet temperatures increase.
20.5	Stainless steel melting indicated; TC4 reaches 2550°F.
21.1 to 21.3	Flow blockage indicated; marked ejection of sodium from test-section outlet followed by cessation of flow oscillations; peak outlet temperatures observed.
21.5	TC4 fails; presence of molten steel indicated at top of fuel column.
22.2 to 22.5	Inlet thermocouples fail; fluted-tube melting indicated.
22.3	Fuel slumping from hodoscope.
23.7	Start of quiet period from hodoscope.
27.7 (27.679-27.706)	First eructation of fuel upwards from hodoscope; flowmeter signals and coherent outlet thermocouple rises observed.
28.7	Slumping of ejected fuel almost complete from hodoscope.
29.5	Second major eructation from hodoscope.
30.9	Slumping nearly complete from hodoscope.
31.1	Reactor scram.

Table VII. Scenario of Events for Test L3 (Ref. 14).

Time (sec)	Event
0	Beginning of test; temp. ≈ 883°F; flow ≈ 910 cc/sec.
9.4	Flow reduction starts.
14.6	Flow rate down to ∿ 125 cc/sec.
15.6	Sodium boiling begins; flowmeter deviations observed; fluted-tube temperatures near top of fuel column level off at ∿ 1800°F.
15.8-16.2	Effective flow cessation; fluted-tube temperatures above fuel column level off.
17.5	Dryout on heat source suggested; gradual temperature rise of fluted tube observed.
19.0	Dryout of fluted tube; end of gradual temperature rise at about 1845°F.
22.0-24.6	Melting of fluted tube indicated.
29.8-30.5	Fuel motion in axial direction evident from hodoscope, flow perturbations, inlet pressure transducer excursions; temperatures above fuel column show a spike.
34.0	Reactor scram.

Table VIII. Scenario of Events for Test L4 (Ref. 14).

Time (sec)	Event
0	Beginning of test; temp. ≈ 860°F; flow ≈ 745 cc/sec.
7.0	Flow reduction begins.
7.5	Bowing of pins in progress.
10.0	Bowing becomes increasingly non-coherent until ∿ 14 sec.
12.0	Flow rate down to ∿ 100 cc/sec.
13.4	Sodium boiling begins; Initiation of oscillations in flowmeter. Beginning of temperature plateau at 1750°F on fluted tube near top of fuel column.
14.0	Radial fuel expansion begins and continues until ∿ 20 sec.
15.3	Sodium film dryout on fluted tube. End of temperature plateau at 1750°F on fluted-tube thermocouples. Beginning of pin motion away from pump, which continues to 17.5 sec, and even longer in the top portion of the pins.
17.0	Cladding either melted or very soft.
18.9	Upper portion of the fuel pushes through the fluted tube up to test-section wall. Fluted tube melting indicated.
20.4	Upper 2/3 of fuel indicates some disarray of pellets.
21.7	Beginning of slumping in central pin; slumping accelerates until the eructation; top 1/3 of fuel does not slump.
26.9	First major fuel motion event. Flowmeters and pressure transducers show dramatic increase in oscillation amplitude. Hodoscope shows axial movement of fuel, originating simultaneously 1/3 of the distance from the top and from the bottom of the fuel column.
30.2	Scram.
31.3	Second major fuel motion event. Flowmeters and pressure transducers show dramatic increase in oscillation amplitude.

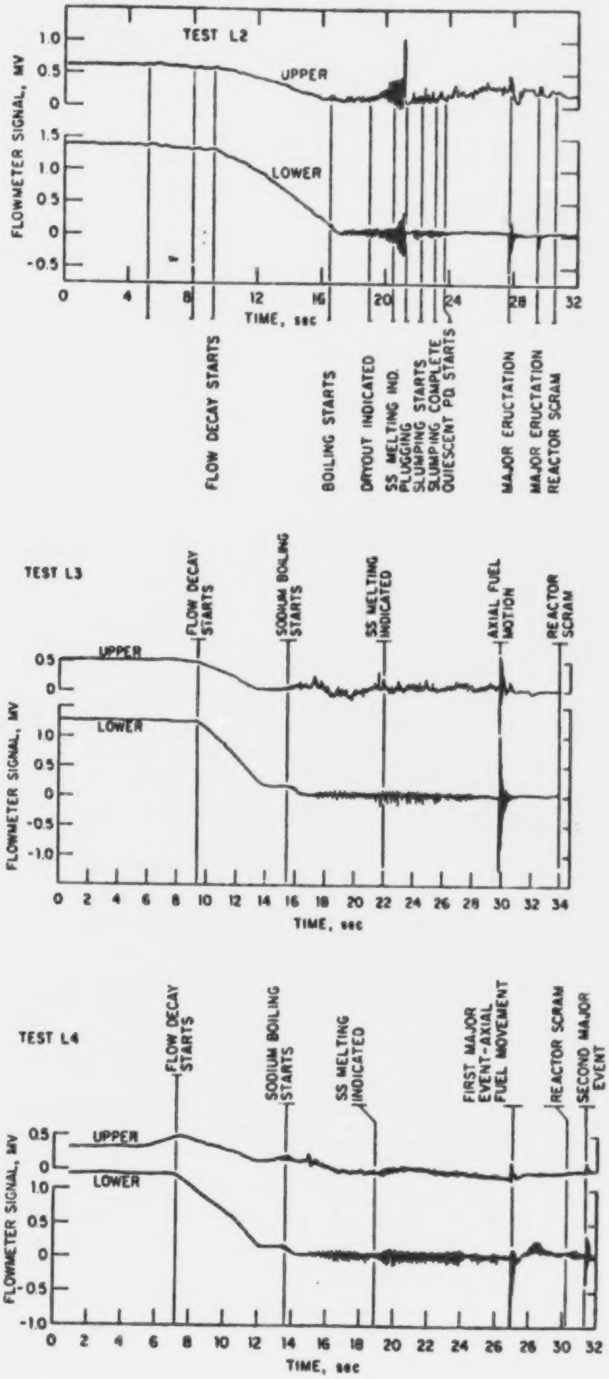

Fig. 8. Flowmeter Data and Major Events
for Tests L2, L3, and L4 (Ref. 14).

No buildup in amplitude of flow oscillations was observed in either Test L3 of L4. Both tests produced fairly regular low-amplitude oscillations which persisted through most of the transient. The outlet flow, especially in L3, was much more irregular than the inlet flow. "Beats" are evident in the lower flowmeter traces in each case. The reason for failure of chugging oscillations to appear in L3 and L4 is thought to be connected with the presence of fission gases in the irradiated-fuel tests. Presence of significant quantities of noncondensible gas will impede the boiling-condensation cycle necessary to produce the chugging. There is no clear evidence of a rapid release of fission gas into the coolant stream even well after cladding should have melted. A slow release into the boiling coolant is suggested.

Due to the very low mean level of the flowmeter signals and the resulting uncertainty in the readings, construction of a voiding curve from flowmeter data has turned out to be very speculative. In the cases of L3 and L4, a determination of the progression of boiling in the coolant can be made for the fluted tube thermocouple data. These results show that boiling progresses both ways from the top of the fuel column with interface velocities of the order of 15-20 cm/sec. If voiding were one dimensional, a clearly measurable flow should be produced, but such a flow is not seen by the flowmeters. Existence of a refluxing action of boiling and condensing is implied.

Within about 1-2 sec following beginning of boiling, the fluted tube thermocouples show a distinct rise in temperature, typically of 100°F or so, to a new level. Within another second or so, the temperatures at locations adjacent to the fuel column again begin a steady rise toward the melting point of stainless steel. The temperatures at points above the fuel column remain fairly constant. This behavior suggest dryout of the sodium film on the fuel pins resulting in increased heat input to the film on the fluted tube. This film is then evaporated, and the temperature rise towards melting begins. However, condensation of vapor maintains the fluted tube above the fuel column at a constant temperature approximately equal to the saturation temperature of the sodium. Condensation persists until gross fuel motion occurs late in the transient.

3.1.2.3.4 Clad Melting and Relocation

The progression of cladding melting and relocation during the L-series tests cannot be observed directly, as is the fuel motion. However, much useful information can be obtained by analysis of the temperature and flow data and from posttest physical examination. The best indication of cladding melting is obtained from the thermocouple in the cluster at the top of the fuel column in Test L2 and from those on the outside of the fluted tube in L3 and L4. However, none of these thermocouples measures cladding temperatures directly.

In Test L2, a temperature corresponding to melting of stainless steel is indicated at the top of the fuel column about 1.5 sec after dryout was indicated, and about 0.6-0.8 sec prior to interruption of flow oscillations. Thus, the presence of molten steel well in advance of the indicated flow blockage is verified. Melting of the fluted tube is not directly observed, but failure of the two inlet thermocouples, probably by melting of their leads opposite the fuel column, is observed within 0.1-0.2 sec of the beginning of fuel motion. Thus, extensive melting of the fluted tube prior to fuel motion seems unlikely.

Tests L3 and L4 present a somewhat different picture. In L3, melting of the fluted tube is indicated directly by its temperature about 3 sec after dryout. Cladding melting is earlier. However, there is little or no manifestation of melting in the other observations. There is little or no flow perturbation, and the hodoscope indicates little extraordinary fuel motion prior to abrupt dispersal. During the interval between melting of the fluted tube and gross fuel motion, the flowmeters indicate essentially zero net flow (with some oscillation), but this cannot be interpreted necessarily as flow blockage. In fact, the distinct responses at the flowmeters and the inlet pressure transducer at the time of axial fuel motion suggest lack of extensive blockages. Melting of the fluted tube in L4 is associated with evidence of fuel motion, in which the fuel contacts the tube and melts through. However, the timing of this motion and the resultant melting is consistent with the time difference between dryout and melting observations are absent. There appears to be little change in the flowmeter signals until the later response accompanying a major axial fuel motion. A distinct response is noted in the inlet pressure, as in L3, so a complete inlet blockage is not indicated.

Posttest examination reveals the presence of partial or complete stainless steel plugs at the ends of the fuel column in each test. The nature and extent of blockage is variable. In test L2, a complete solid blockage of stainless steel was found at the inlet to the bundle, extending from about opposite the bottom fuel pellet well downwards into the region of the end plugs. A much less massive accumulation of cladding in the channels appears in the unheated region near the top boundary of the fuel column. It is not clear that the flow area is completely obstructed at this elevation. Destruction of the fluted tube adjacent to the fuel column is complete, and most of the molten steel appears to have run downwards. It could not be determined whether the bottom plug was entirely cladding material.

A similar, although less massive, steel plug was found in L3, where a greater quantity of steel was spread along the loop wall opposite the fuel region. The impression is one of more radial motion of the fluted tube steel in L3 than in L2, a result consistent with the existence of gas pressure to promote such motion. The extent and nature of the top plug in L3 is similar to that in L2. The L3 examination also shows evidence of some fuel having moved past the top plug, probably before the plug was formed.

Posttest cladding disposition in Test L4 differs in one respect from that found in the two previous tests. No massive plug formed at the bottom of the bundle. Only a thin plug formed adjacent to the insulation pellets, with little penetration of cladding beyond the fuel column into the region of the lower end plugs. It appears that the dominant motion of molten steel in L4 was radial, as in L3, but that there was little tendency for cladding steel to move downward. No cause for this difference is obvious, except for the higher fission-gas pressure in the L4 pins compared to that in the L3 pins. The extent of steel plugging at the top of fuel column was about the same as observed in Tests L2 and L3. Penetration of some fuel beyond the level of the plug is also indicated.

3.1.1.3.5 Fuel Melting and Relocation

Extensive motion of fuel was observed in each of the tests but there were significant differences in the character of the motion.

The posttest disposition of the fuel is shown in Fig. 8, which is a composite of posttest radiographs from each test. In these radiographs, the fuel appears as a dark image, generally within the region denoted "fuel". Pretest locations of the various pin components are indicated in Fig. 9, and it is seen that there has been little or no displacement of the structural parts of the pins from their original locations.

In Test L2, the hodoscope revealed that the dominant initial motion was slumping or collapse of the fuel column, beginning about 5.9 sec after commencement of boiling and about 1.8 sec after indication of molten steel temperatures at the top of the fuel column. The collapse began with apparent loss of fuel from the central pin about 2 to 3-1/2 in. above the midplane. Fuel removal appeared to progress toward one side of the cluster, with the fuel moving downwards. Fuel from above the region of loss then dropped down, until essentially all the fuel in the top third of the cluster had collapsed. This collapse process took about 1.4 sec, with a maximum rate of fall of about 10 cm/sec. Fuel does not appear to have penetrated the fluted tube at this time.

A quiescent period of about 4 sec followed the initial slumping. Reactor power remained constant throughout this time and

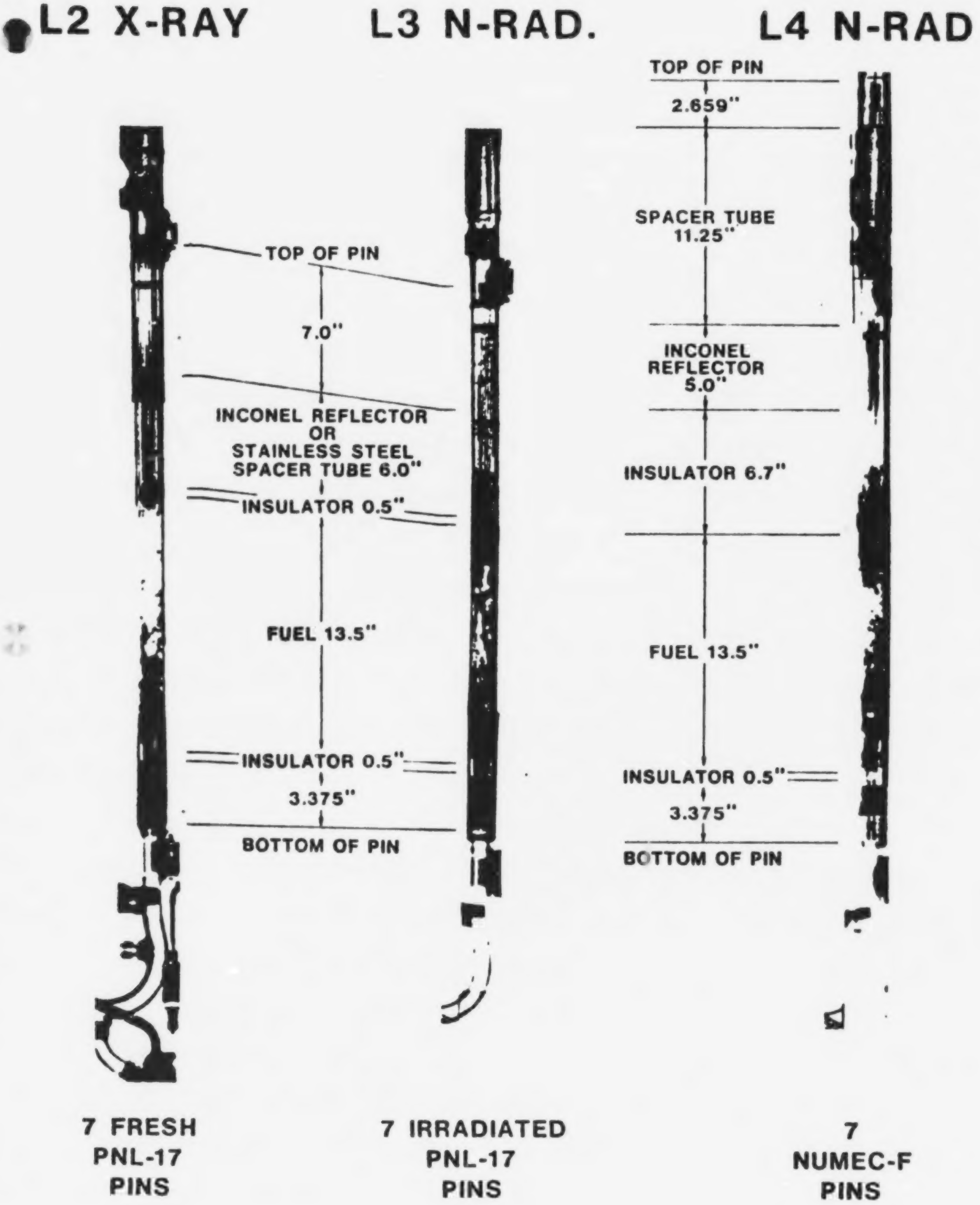
L2 X-RAY
L3 N-RAD.
L4 N-RAD
TOP OF PIN
7.0"
INCONEL REFLECTOR OR STAINLESS STEEL SPACER TUBE 6.0"
INSULATOR 0.5"
FUEL 13.5"
INSULATOR 0.5"
3.375"
BOTTOM OF PIN
TOP OF PIN
2.659"
SPACER TUBE 11.25"
INCONEL REFLECTOR 5.0"
INSULATOR 6.7"
FUEL 13.5"
INSULATOR 0.5"
3.375"
BOTTOM OF PIN
7 FRESH PNL-17 PINS
7 IRRADIATED PNL-17 PINS
7 NUMEC-F PINS

Fig. 9. Post-Test Radiographs (Ref. 14).

it is likely that considerable fuel melting took place, along with melting of the steel bordering the fuel mass. The quiescent period terminated abruptly with an ejection of fuel centered around the middle 4 in. of the original fuel column. Fuel moved outward in all directions, with the most extensive motion upward into the voided region. The ejected fuel fell back within a second of ejection, at an average speed of about 25 cm/sec. A small fraction of the ejecta adhered to the remaining pin structure at the top boundary of the fuel column. A second, similar, event occurred about 1.8 sec after the first. As a result of the second event, the remaining portions of the fluted tube gave way and fuel moved radially into its final position. Reactor scram terminated the transient before another eructation, but there is no evidence that the events would not have continued had power been maintained.

The radiograph of L2, Fig. 9, shows most of the fuel concentrated in a region about 5-in. high, extending upward from the bottom of the original fuel column. A small amount of fuel is also found at the top boundary of the fuel column. Posttest examination reveals the fuel to be a very porous mass with large voids suggestive of the earlier presence of gas or vapor bubbles. Steel was found intermixed with fuel in several locations. Non-molten pellets surrounded by once-molten fuel were found at the bottom of the fuel column. Molten steel was found to have penetrated into the interior of an unmelted pellet through cracks in the pellet. The once-molten fuel contained steel droplets nonuniformily distributed, with evidence that "streamers" of molten steel had risen through the molten fuel. It is probable that vaporization of steel was the driving force for the fuel eructation.

Contrary to Test L2, there was no early gross fuel motion in Test L3. In fact, there was little detectable fuel motion at all until an abrupt dispersal of fuel occurred, beginning about 14.2 sec after the start of boiling. The dispersal took place over a period of 0.5 to 0.7 sec, and resulted in extensive removal of fuel from a portion of the fuel column centered about 1 in. above the midplane. Most of the displaced fuel moved upwards, but some downwards motion is also indicated. Motion was confined to the one event; there was no slumping or reentry of fuel following dispersal.

The posttest radiograph in Fig. 9 shows the final fuel disposition in Test L3. Posttest examination corroborates the features of the radiograph. The bulk of the fuel is found in two separate masses: one extending downward from the original top of the fuel column and the other extending upward from the bottom. Only a small portion of the fuel penetrated beyond the top of the fuel column. Some of this fuel moved within the cladding and some apparently moved in the channels. In general, the character of the once-molten fuel is similar to that found in L2, although the number and size of the voids is much smaller. Near the bottom of the fuel column is a region of unmelted fuel, much of which is broken up and appears somewhat loose. Molten fuel did not penetrate into the very bottom of the fuel column to the same extent that it did in L2.

Test L4 resulted in gross fuel motion similar to that in L3, but more motion was observed by the hodoscope prior to the abrupt dispersal. Some bowing of the pins was observed even prior to sodium boiling. About 5.5 sec after the beginning of boiling, a rapid motion of fuel through the fluted tube to the loop wall at the top of the fuel column was observed. Evidently, the top portion of the pins fell sideways against the fluted tube, and promptly melted through. Slightly over 3 sec later, a gradual spreading of fuel in the lower portion of the column began indicating some slumping of fuel in at least one pin. Another 3 sec later, there was a rapid loss of fuel from the center of the bundle, probably as the result of melting away of the center portion of the central pin, leaving a "stalactite-stalagmite" configuration.

About 2 sec after loss of fuel from the center of the cluster, abrupt fuel motion occurred. Motion appears to have originated at two sites, essentially simultaneously, about 1/3 of the way from each end of the fuel column. The dominant motion was dispersal of fuel upward with some motion beyond the upper fuel column boundary.

Some replenishment of fuel in the central portion of the cluster is indicated. About 4.4 sec after the first abrupt fuel motion, signals consistent with a second such motion are seen on the pressure and flow instruments. Since this event occurred after scram, the hodoscope data have poor statistics, but some fuel motion is indicated.

The posttest radiograph for Test L4, Fig. 9 shows the final fuel disposition. The bulk of the fuel is between the boundaries of the original fuel column, with some penetration beyond the top. The general character of the fuel remains resembles that found in Tests L2 and L3, i.e., a porous mass of fuel with fairly large voids and with considerable entrainment of globules of steel. A sizable portion at the bottom of the fuel column is unmelted, and penetration of once-molten fuel into this region is limited.

Our present interpretation of the fuel motion data from Test L2 is that the fuel column simply fell apart once the cladding melted and gave no further mechanical support. Falling of separate, partially-melted pellets or pellet fragments could account for the apparent slow slumping of the cluster. On the other hand, the fuel pellets in Tests L3 and L4 are probably sintered together, with a strong, dense column formed by the equiaxed region. Thus, the L3 and L4 fuel would tend to retain its identity as columns and bow rather than crumble as individual pellets. Dispersal or slumping would only occur when melting proceeded through the restructured fuel, at a later time than the collapse in L2. Such behavior was observed in a dry capsule experiment (Ref. 20), in which the fuel column of an irradiated pin heated to its solidus held together after the cladding melted, and remained essentially intact even after considerable bowing and buckling.

It is likely that the mechanism causing the eructations (abrupt fuel movements) was the same in all three tests. The energy generation in the fuel at eructation relative to that at the time of flow cessation (zero net flow) is very nearly the same for each test. Intermixing of stainless steel globules with once-molten fuel as found in the posttest examinations suggests that flashing of superheated stainless steel may be the cause, although fuel vapor or a local sodium-steel-fuel interaction cannot be ruled out. At the melting temperature of UO_2, the estimated stainless-steel vapor pressure is about 1 atm, and at 4000°K it is about 20 atm.

3.1.1.3.6 Nonprototypic Effects

The short fuel column length, and limitations on initial temperature and running time dictate a low flow rate to achieve boiling early in the test. Therefore, the pump pressure is very low at the inception of boiling, and little pressure is available to impede flow reversal and drive sodium vapor flow through the voided region. Also, the axial temperature gradient is greater than would be the case for full length pins. Non-coherence of boiling due to radial temperature gradients appears to be important in governing flow reversal, as well. Higher, more prototypic vapor velocity would promote more upward cladding movement than observed in the tests. However, plugging at the top would cut off the vapor flow, so that subsequent cladding motion should be the same as in the tests.

Radial heat transfer to the fluted tube leads to overcooling of the edge channels of the cluster comparable to that in a subassembly. In the tests, it is compensated for in part by the higher heating rate in the edge pins. This effect contributes to the noncoherence of boiling noted above. After coolant voiding and melting of the fluted tube, heat loss by radiation to the loop wall becomes important. This may be a significant fraction of the heat generated in the peripheral pins, so that the temperature rise rate in the cluster after voiding may be slower than would be realized in a reactor situation where an equivalent heat sink would not be present. Thus, more time is available in these experiments for release of fission gases from the fuel at sub-melting temperature than would be available in the corresponding reactor case.

Due to limitations on running time, the slow flow coastdown of the FTR could not be simulated. The more rapid flow coastdown of the tests leads to a nonprototypic temperature decrease above the fuel column at the inception of boiling. However, the boiling and condensing action leads to heating of the fluted tube and pin structure to the sodium boiling point well in advance of axial fuel motion. Therefore, it is expected that the rapid flow decay has little effect.

The fluted tube does not incorporate spacer wires, but does provide geometric restraint partially simulating adjacent pins. When the fluted tube melts away, restraint is removed. Thus, space is available for radial motion of molten cladding and fuel. In fact, within the fuel-column height, axial motion of fuel would seem to be somewhat eased by availability of extra flow area. However, there seems to be little tendency for fuel to move preferentially in this area. In Tests L3 and L4, much once-molten steel is found here, in space which would not be available in a reactor.

Finally, reactivity feedback from fuel and cladding motion is not simulated. Such feedback would lead to power changes accompanying fuel motion. Particularly, a power burst would probably result from whole cluster slumping as indicated in L2. Additional tests are necessary to assess the effect of reactivity feedback on the behavior of the fuel.

3.1.1.3.7 Conclusions

Several conclusions can be drawn from our present understanding and interpretation of the experimental data. With respect to boiling and voiding, the distinct difference between the fresh-fuel test and those using irradiated fuel is ascribed to the fission gases released from the fuel pins acting to impede condensation and chugging. Fission-gas pressure also appears to influence motion of molten cladding, with a general increase in the tendency toward radial motion rather than purely axial motion. There is no evidence of fission gases in the pin plena acting to compact melting fuel.

Fresh fuel columns collapse shortly after the cladding melts, while the irradiated fuel pins seem to remain as a column or parts of columns capable of bending for some time after the cladding melts. When fuel melting does occur, the observed motion is downward. Fission gases do not appear to cause foaming or frothing in these tests.

Abrupt dispersal of fuel takes place for both fresh and irradiated fuel. Fission-gas effects are not required to explain the dispersal, and vaporization of superheated stainless steel previously intermixed with molten fuel appears to be the most probable cause. Although dispersal is generally away from the mid-plane, replenishment of fuel in a central portion of the cluster was observed in L4. Little fuel appears to penetrate beyond the original fuel-column boundaries.

In conclusion, the objective of providing a body of integral data on the whole core loss-of-flow against which the predictions of accident analysis codes can be compared has been achieved. Tests in which long fuel pins are used and in which reactivity effects are simulated are planned.

3.1.1.4 Fuel Coolant Experiments

3.1.1.4.1 Introduction

The objective of the S series of tests conducted in an autoclave in TREAT was to investigate the nature of possible molten fuel-coolant interactions resulting from a pin rupture in LMFBR's. The S-series experiments were planned to fit within a matrix of other experimental and analytic fuel-coolant interaction programs. Out-of-pile tasks are designed to provide information on the basic interaction parameters, e.g., modes of physical contact, fragmentation mechanisms, and necessary and sufficient conditions to obtain vapor explosions (Ref. 21-23).

The S-series experiments employ the TREAT reactor to rapidly bring fresh fuel rods (~6 inches long) from an isothermal low temperature condition (200 to 500 C) to gross fuel melting and rod failure in the presence of sodium. The test vehicle is a stagnant sodium capsule equipped to measure or infer the primary variables of interest; pressure and thermal-to-mechanical energy conversion.

The measured data available from each experiment consist of:

a. TREAT power and energy (integrated power) versus time,

b. calibration factor for test vehicle (test power versus reactor power),

c. pressure versus time,

d. piston displacement versus time,

e. sodium temperature (several locations) versus time,

f. neutron hodoscope (commencing with S6),

g. residue particle size distribution (destructive examination).

Three fundamentally different test section geometrical configurations have been employed for the eight experiments which involve FCI data. Table IX identifies the eight experiments of interest and their characterizing test parameters, while Table X presents details on the test vehicle configurations.

Results for S-3 through S-6 were presented in Ref. 24 (except for hodoscope data) along with thermal-mechanical (up to

Table IX. Experiments Involving FCI and Characterizing Parameters (Ref. 24, 27-30, 31).

Parameter	Test No.							
	3	4	5	6	7	8	11	12
Initial Temperature (°C)	165	165	165	210	500	510	~150	~150
Initial Temperature (°F)	329	329	329	410	932	950	302	302
Reactor Peak Power (MW)	2,664	6,650	3,575	5,374	4,644	10,860	18,000	18,000
Reactor Period (msec)	53	34	46	38	40	27	23	23
Reactor Integrated Power (MWsec)	669	1,050	740	975	908	1,457	~2,000	~2,000
Test Vehicle Type[a]	1	1	1	2a	2b	2b	3	3
Average Fuel Energy (Total)[b]								
cal/gm·UO_2	460	720	509	493	514	784	~1,770	~1,770
joule/gm·UO_2	1,927	3,015	2,130	2,065	2,150	3,280	~7,409	~7,409

---

[a] See Table X for Description of Test Vehicle.

[b] Based on integration of TREAT power and assuming adiabatic fuel.

Table X. Test Vehicle Configuration (Refs, 24, 27-30).

	Type 1 (S3-5)	Type 2a (S6)	Type 2b (S7-8)	Type 3 (S11-12)
Array Type	Rectangular	Triangular	Triangular	—
No. of Fuel Rods	9	7	7	1
(Dummies)	4	0	0	0
Fuel				
Pellet o.d. (in.)	0.252	0.252	0.19	0.19
Overall Length (in.)	4.875	4.875	~5	~5
Smear Density (% TD)	84 to 90	84 to 90	85	85
Cladding				
Stainless Type	304	304	316	316
Outside Diameter (in.)	0.288	0.288	0.23	0.23, 0.25
Inside Diameter (in.)	0.26	0.26	0.20	0.20
Coolant				
Ratio of Sodium to Fuel Rod Areas[a]	2.25	0.94	0.97, 1.02	2.5, 1.96
Ratio of Sodium to Total Rod Areas (including dummies)	1.25	0.94	0.97, 1.02	2.5, 1.96

---

[a] Minor variations were made in Test Vehicles 2b and 3 which affected this ratio

time of failure) analyses employing the SASIA-ASH computer model (Ref. 25) on individual fuel rods. The ARGUS heat transfer code (Ref. 26) was also employed for experiment S-6 and preferentially reported in Ref. 24.

Only very limited information on Experiments S-7 and S-8 have been reported in the ANL Monthly Progress Reports (Ref. 27,28). Of time-dependent data normally available, only pressure was provided for S-7 while pressure and piston displacement were given for S-8. Thermal analyses of these experiments have not been reported. The last of the identified experiments, S-11 and S-12, were recently performed (October-November 1972). Preliminary data, discussion, and analyses have been reported as ANL progress reports (Ref. 29, 30). The handling of the S-11 and S-12 data represent the most comprehensive analytical and experimental treatment seen throughout the entire S-series program.

A summary of reported data is presented in Table XI on the pressure, calculated conversion efficiencies, and conditions at initial fuel rod failure (defined by ANL as the first pressure pulse). Figure 10 compares the reported information on residue particle size distribution (through S6) with results of some out-of-pile dropping mode tests. In addition, a mean mass diameter of 320μ has been determined for the residue of S-7 (Ref. 31).

Table XI. S-Series Reported Data (Ref. 24, 27-30).

Quantity	Experiment							
	3	4	5	6	7	8	11	12
Energy Addition at Failure[a] (J/gm)	1842	2010	1600	1592	1508	1470	2220	2260
Ratio of Failure to Total Energy Addition (%)	95.6	66.7	84.6	77.1	70.1	44.8	31.2	31.8
Average Specimen Power[b]								
At Failure (kW/gm)	0.6	17	5	8	9	~20	57	57
At Peak (kW/gm)	6.5	18	10	11	11	24	64	61
Amplitude of Initial Pressure Pulse (psi)	460	870	69	330	160	664	2000	NA
Amplitude of Largest Pressure Pulse (psi)	540	1800	2940	2050	430	744	2000	NA
Mass Mean Residue Diameter (μm)	2700	1240	220	400	320	~400	NA	NA
Conversion Efficiency (η) x 10^5	2.1	25	190	150	0.6	2	100	NA

---

[a] Defined as first pressure pulse

[b] Inferred from reported data

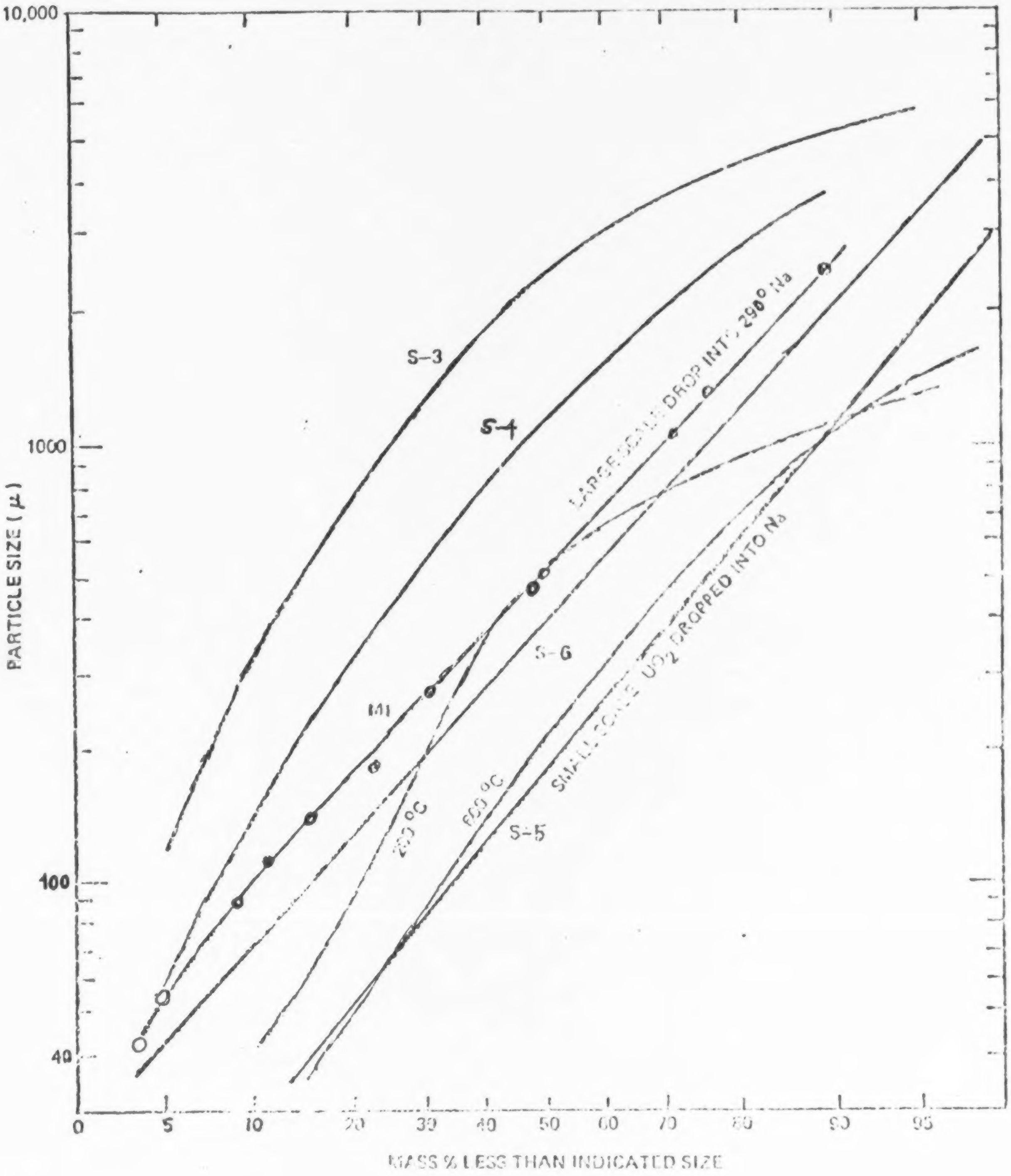

Fig. 10. UO_2 Particle Sizes from Interactions with Na (Ref. 31).

Commencing with S-6, the fast-neutron hodoscope has been employed but results have yet to be published. However, the hodoscope data was referenced as indicating that fuel motion initiated the delayed, energetic interaction seen in S-6 (Ref. 27, pg. 8.20).

3.1.1.4.2 Interpretability of the Reported Data

The primary experimental objectives are to place limits on the pressures and conversion efficiencies which can occur and to determine whether violent (explosive) interactions can occur. Peak pressures and calculated conversion efficiencies have been reported by ANL in fulfillment of these objectives. However, since the experimental results are required to cover a wide range of potential LMFBR occurrences and are, in fact, non-prototypic in several respects, the question of interpretability must be addressed. To properly utilize the reported data and calculations, an assessment of the conditions existing within the experiment during the time of the FCI must be performed and related to readily interpretable out-of-pile data. It is in this area that the S-series experiments are fundamentally weak. In support of this statement, the following comments are offered:

> The piston device often becomes locked (negating information on a prime objective variable) prior to significant FCI events (Ref. 24).
>
> The source of observed pressure oscillations ("ringing") in several tests remains unresolved (Ref. 24).

Lack of pressure transducer response to the initial interaction in S-12 is unresolved and has implications on present technique of inferring conversion efficiencies for a locked piston.

Inference of conversion efficiency from pressure response measurements and assumptions on work-producing components (e.g., sodium mass accelerated and neglect of quasi-static capsule pressurization by sodium: (Ref. 27, pg C.20) lacks verification.

Post-test thermal analyses and thermocouple data are too inconclusive to define the initial conditions which existed for the FCI (e.g., did sodium boiling occur prior to rod failure?) (Ref. 24, 29).

Use of integrated capsule power (energy addition) to characterize fuel conditions does not recognize the large energy redistributions within the capsule, and at the same time negates performing detailed comparisons with other pertinent transient overpower (TOP) data such as the ANL E-series which employ different experimental capsules and reactor periods.

In addition to the above observations on interpretability of the basic experimental data, several items of interest were identified during an independent, two-dimensional (THTE) thermal analysis of S-6 by General Electric (Ref. 31). This analysis employed an analytical calculation of the calibration factor which accounted for the two-dimensional distribution of thermal energy within the autoclave and indicated that γ heating of capsule components could be $\geq$ 10% of the total energy generation. (A similar analysis of experiment H3 is reported in Ref. 32.) Fig. 11 presents the failure equations when the ANL determined calibration factor (0.506 cal/gm-MW-sec) was utilized in conjunction with the

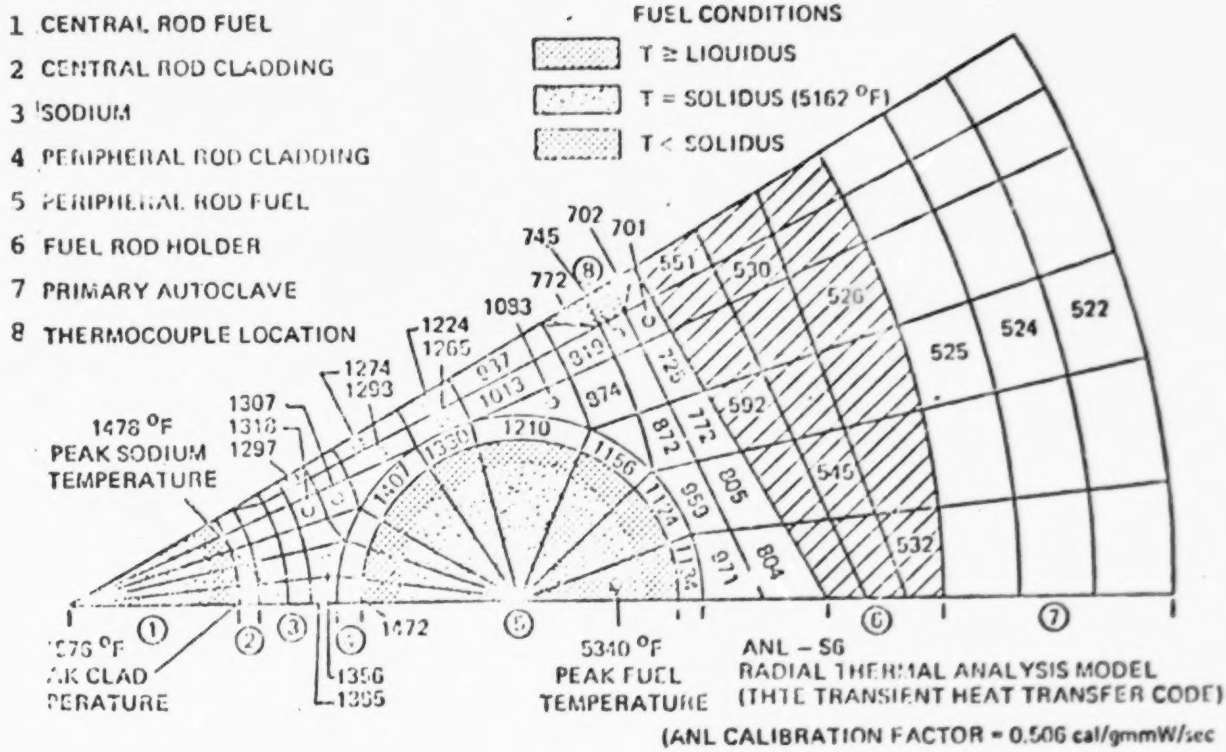
1 CENTRAL ROD FUEL
2 CENTRAL ROD CLADDING
3 SODIUM
4 PERIPHERAL ROD CLADDING
5 PERIPHERAL ROD FUEL
6 FUEL ROD HOLDER
7 PRIMARY AUTOCLAVE
8 THERMOCOUPLE LOCATION
FUEL CONDITIONS
T ≥ LIQUIDUS
T = SOLIDUS (5162 °F)
T < SOLIDUS
702
701
745
772
⑧
1093
551
530
526
1224
1265
1274
1293
937
1013
319
874
725
592
525
524
522
1307
1318
1297
1478 °F
PEAK SODIUM
TEMPERATURE
1330
1210
1156
872
772
805
545
1407
1124
959
1136
971
804
532
576 °F
AK CLAD
PERATURE
①
②
③
④
1472
1356
1355
⑤
5340 °F
PEAK FUEL
TEMPERATURE
⑥
⑦
ANL – S6
RADIAL THERMAL ANALYSIS MODEL
(THTE TRANSIENT HEAT TRANSFER CODE)
(ANL CALIBRATION FACTOR = 0.506 cal/gmmW/sec

Fig. 11. Temperature Distribution (°F) at Failure.

GE calculated spatial distribution. This GE data was considerably different from the ARGUS derived failure profile. More recent ANL information based on THTB computations was not compared since ANL felt that much better results were presently available (but unreported). Based on a review of the above analyses, the following items are noted:

It was determined that approximately 12% of the total energy was deposited externally to the fuel, mostly in the steel autoclave.

A best analytical match to thermocouple data (T.C. 8) was obtained via large, time-dependent variations in h

Two-dimensional (r,θ) effects are important when specifying temperature distributions in S-series multi-rod experiments.

The use of adiabatic fuel energy additions to characterize results within the S-series is inappropriate for interpretation of energy conversion efficiencies.

More precise time and spatial resolution of the thermocouple data is required; a difference in temperature rise (at failure) of 75°F (17% of total rise) correspond to a TC displacement of 0.02 inch or a time shift of only 10 msec in the analysis.

Thus, the thermal analyses appear subject to uncertainties of a magnitude which is currently unacceptable for an assessment of the experiment impact on LMFBR safety.

3.1.1.4.3 Applicability of the Data

The applicability of the range of energy addition rates was considered relative to HCDA analytical predictions for the FFTF (Ref. 33, 34, 35) and a Demonstration Plant study (Ref. 36). Fig. 12 depicts this along with available information from several related TREAT TOP experiments (E-series data were unavailable in this format). The plotted data are approximate and employ average values but do indicate the range of applicability for transient overpower induced FCI. It can be seen from this figure that the S-series experiments are within an envelope of interest to HCDA studies, such as the FFTF PSAR and those of Ref. 36. The more recent HEDL assessments of fuel behavior during TOP incidents (Ref. 33) result in FCI events well below the S-series data, and assessed conditions for the FCI should reflect information from such data ranges, i.e., GE C-series and ANL E-series. The S-series experiments could then be utilized to provide upper bounding values for the potential severity of FCI events and support licensing discussions.

Applicability of specific test data is unclear at this time due to the large unknowns indicated in the previous section, particularly the question of sodium conditions at FCI initiation. The experiments as a group share several nonprototypic conditions with respect to an LMFBR which affect their applicability. Particularly the low (200 to 500°C) isothermal initial condition coupled with a long (23 to 53 msec) TREAT period result in failure conditions which are atypical in several respects to a TOP HCDA initiated from opera-

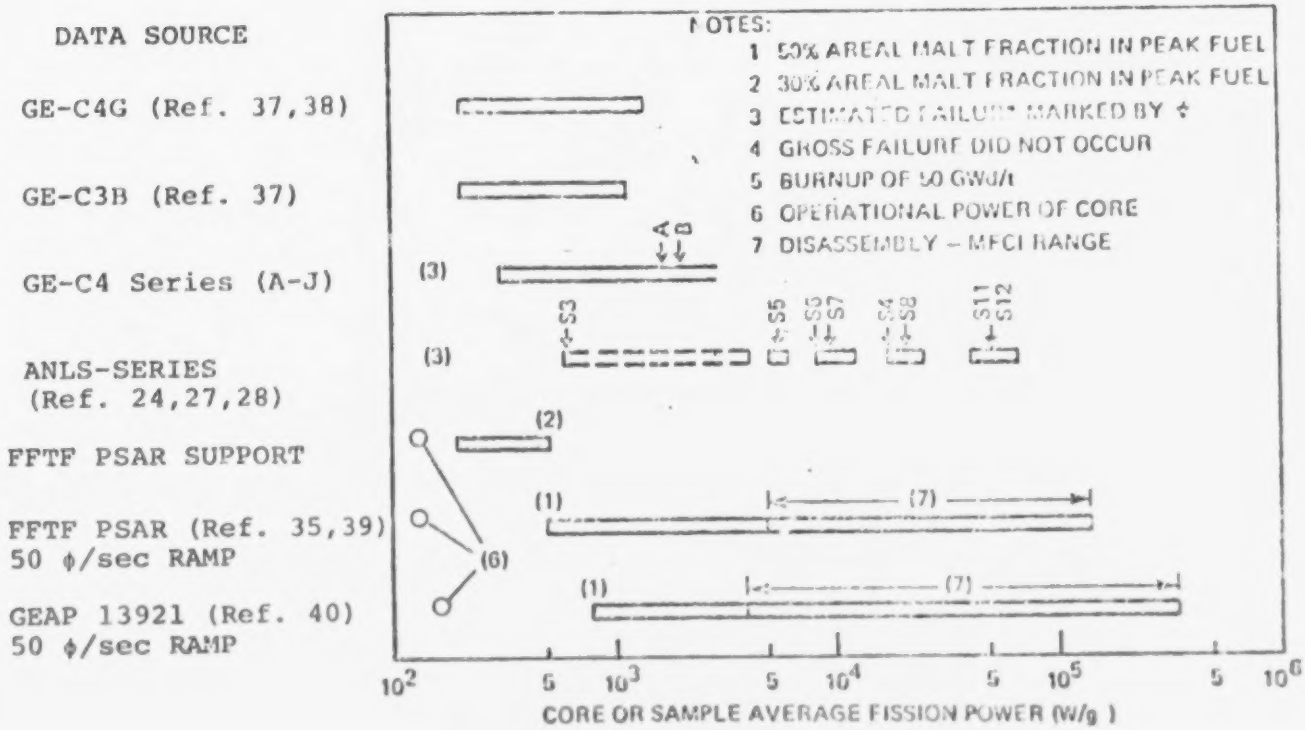

Fig. 12. Specific Power During Significant Fuel Melting and/or Failure

tional conditions in an LMFBR. The first condition relates to the fractional amount of fuel which can become superheated with respect to the channel environment. The TREAT experiment conditions result in substantially larger fractions of fuel attaining a given superheat condition while at the same time, the substantial fraction of fuel existing below the solidus (at rod failure) in an LMFBR is not reproduced in the test specimen. Secondly, sodium temperatures (and radial gradients in multi-rod experiments) are greatly enhanced, due in part to the long TREAT period, as compared with the limiting LMFBR case. The possible presence of sodium two-phase conditions at the inception of the FCI would have a pronounced negative effect on the applicability of the S-series multi-rod data to establish bounding conditions for the FCI. Another important nonprototypic aspect of the experimental vehicles is the large relative area available as heat sinks. While the initial interaction may not be too strongly perturbed, long time scale effects on the calculated energy conversion efficiency are affected (such as the delayed interaction in S-6).

To properly account for the nonprototypic effects when applying the experimental data to an LMFBR safety concern, detailed physics and thermal-mechanical comparison analyses are required of both the test vehicle and the LMFBR environment.

3.1.1.4.4 Conclusions and Recommendations

In summary, useful in-pile data on the behavior of unirradiated fuel during severe transient overpower (pre- and post-failure), fuel-coolant interaction, molten fuel properties and post-accident heat removal, are considered to be available within the accumulated data from the S-series experiments. However, the data require a concerted analytical assessment before they can be generally utilized in support of LMFBR safety evaluations.

The general applicability of the S-series data cannot be supported at this time. This premise is based upon the inadequate definition of the FCI initial conditions, a low level of thermal-mechanical and energy conversion analyses, and an absence of out-of-pile data to support the primary experimental measurements and techniques employed.

A substantial amount of information has been generated in the TREAT experiments. However, the nature of the experiments with their high degree of complexity make analysis of the results difficult. When the nonprototypical characteristics of the experiments are superimposed upon these difficulties, extension of the results to typical small LMFBR's implies large qualitative uncertainties.

Some of the questions which need to be answered in the case of transient overpower accidents include: the margins to failure; the existence of possible prefailure movements of fuel and coolant; the failure and postfailure motion of fuel and coolant; the coolability of the fuel in its final location; and the margin beyond the initial failure threshold for which damage remains localized. The loss-of-flow tests are conducted to determine fuel and clad motion resulting from a loss of coolant flow. Some of the tests must include power increases and bursts after initial voiding, and also, in order to study postburst fuel motion, a low power phase simulating the approach to decay heat levels. Also required are tests to determine the coolability of a fuel assembly after a flow transient resulting from a pipe rupture. Failure threshold tests of the type discussed above are also needed but would be conducted under off-normal flow conditions. Several key phenomena important in the postdisruptive phase of accident analysis that can be addressed with in-pile testing. These include: in-core fuel-coolant interactions; fission-gas effects; extended fuel motion; and molten core behavior.

There will also be the requirement for experimental support of advanced fuel pins. Changes in fuel, fuel-bond and coolant materials, core geometry, and operating conditions will, change the sequence of events in many accident situations, as well as the phenomenological modeling. The higher operating steady-state specific power densities required for advanced fuels and the possibility of larger fuel pin bundles or subassembly dimensions in larger LMFBR's will have to be addressed.

With the numerous nonprototypic characteristics of TREAT including: lack of preconditioning; loop hydraulics; length of pins; microstructure distribution; radial and oxial power distributions; test-section design; limitations on initial temperature and running time; and the inability to simulate reactivity feedbacks, results are uncertain when extended to LMFBR's. There appears to be a need for a large amount of experimental information which the TREAT facility can not provide.

References

1. C.E. Dickeman, "U.S. Studies on LMFBR Fuel Behavior under Accident Conditions", Nucl. Safety 14 5 p. 452-460, Sept.-Oct. 1973.

2. G.R. Larsen and J.F. Boland, System for Computer Control of Prompt-Critical Transients in TREAT, Trans. Amer. Nucl. Soc., 13(1): 238-239 (1970).

3. J.C. Carter et.al., Fuel Dynamics TREAT simulation Tests on LMFBR Loss of Flow, Trans. Amer. Nucl. Soc. 14(2): 745-746 (1971).

4. A.B. Rothman et. al., First TREAT Loop Failure Threshold Experiment on Irradiated FFTF Type Fuel Under Simulated Overpower Conditions (to be published).

5. J.F. Boland, Operating Experience with TREAT, Trans. Amer. Nucl. Soc. 12(Suppl.): 15 (1969).

6. L.E. Robinson, "Design of the Mark-II Integral Transient Reactor Test (TREAT) Facility Sodium Loop," Reactor Physics Division Annual Report, ANL-7210, 245-250 (1966).

7. L.E. Robinson, R. Purviance, and K. Schmidt, The Mark-II Integral Sodium TREAT Loop, Trans. Am. Nucl. Soc. 13(1) 354-355 (1970).

8. A.B. Rothman, L.W. Deitrich, R.C. Doerner, A.E. Wright and C.E. Dickerman, "Review of TREAT Experiments in Support of Transient Overpower (TOP) Analysis for Fast Reactor Safety", Proceedings of the Fast Reactor Safety Meeting Conf. 740401, 1974.

9. A.B. Roghman, C.E. Dickerman, G.G. Dewey and E.W. Barts, "Neutron Filter for TREAT Safety Studies on Fast Reactor Fuel", Trans. Am. Nucl. Soc., 13(1) 356 (June-July, 1970).

10. A.B. Rothman, A.E. Wright, D. Stahl, and L.J. Harrison, "First TREAT Mark II Loop Experiment with Preirradiated FFTF-Type Fuel (H3)", Trans. Am. Nucl. Socl, 16, 181 (June 1973).

11. W.L. Partain, J.C. Sonnichsen, R.J. Shields, and A.E. Waltar, "Analytical Modeling of the Mark-IIA TREAT Loop for Fuel Motion and Sodium Expulsion Studies", Proceedings of ANS Topical Meeting on Fast Reactor Safety (April 1974), To be published.

12. L.L. Smith and M.G. Stevenson, "Effect of Reactivity Insertion Rate on Fuel Pin Failure Threshold", Trans. Am. Nucl. Socl, 17, 284 (November 1973).

13. A.W. Cronenberg, H.K. Fauske, and D.T. Eggen, "Analysis of the Coolant Behavior Following Fuel Failure and Molten Fuel-Sodium Interaction in a Fast Nuclear Reactor", Nucl. Sci. and Eng. 50, 53-62 (January 1973).

14. L.W. Reitrich, E.W. Barts, A. DeVolpi, C.E. Dickerman, J.G. Eberhart, J.C. Carter, A.K. Fischer, W.F. Murphy, and G.S. Stanford, "Fuel Dynamics Experiments Supporting FTR Loss-of-Flow Analysis", Proceedings of the Fast Reactor Safety Meeting CONF 740401, 1974

15. L.W. Deitrich, A. DeVolpi. B.A. Feay, W.F. Murphy, and L. J. Harrison, "A Loss-of-Flow Simulation with Fresh FFTF-Type Pins", Trans. Am. Nucl. Socl, 16, 182 (1973).

16. E.W. Barts, L.W. Deitrich, A. DeVolpi, J.G. Eberhart, A.K. Fischer, P.H. Froehle, W.F. Murphy, D. Stahl, R.R. Steward, J.P. Tylka, and L.J. Harrison, "Loss-of-Flow Simulations with Pre-Irradiated FFTF-Type Fuel Pins (Tests L3 and L4)," Trans. Am. Nucl. Socl, 17, 363 (1973).

17. A. DeVolpi. R.R. Stewart, and L.W. Deitrich, "Fast-Neutron Hodoscope Visualization of Fuel Movement in a 7-Pin Loss-of-Flow Simulation," Trans. Am. Nucl. Soc., 16, 182 (1973).

18. L.E. Robinson, R.T. Purviance, and K.J. Schmidt, "The Mark-II Integral Sodium TREAT Loop," ANL-7692, Argonne National Laboratory (1971).

19. G.A. Freund, P. Elias, D.R. MacFarlane, J.D. Geier, and J.F. Boland, "Design Summary Report on the Transient Reactor Test Facility (TREAT), ANL-6034, Argonne National Laboratory (1960).

20. R.R. Steward, C.E. Dickerman, L.E. Robinson, and W.B. Doe, "Studies of Fast Reactor Fuel Element Behavior Under Transient Heating to Failure", ANL-7552, Argonne National Laboratory (1969).

21. D.R. Armstrong, et.al., Interaction of Sodium with Molten UO_2 and Stainless Steel Using a Dropping Mode of Contact, December 1971, (ANL-7890).

22. D.R. Armstrong, Laboratory Experiments on Mechanisms of Fragmentation and Pressure Generation, June 1972, ANL-RDP-6, p. 8.33.

23. H.K. Fauske, "Nucleation of Liquid Sodium in Fast Reactors", Reactor Technology, .5, 4, Winter 1972-73.

24. Argonne National Laboratory (ANL), Reactor Development Progress Reports, in particular, the following:

    a. ANL-7553, February 1969
    b. ANL-7632, October 1969
    c. ANL-7737, August 1970
    d. ANL-7776, January 1971
    e. ANL-7833, June 1971

25. A.K. Agrawal, et. al. Analysis of Fuel Failure Experiments with Treat, Proc. of Conf. on New Developments in Reactor Math. and Applications, USAEC Report Conf.-710302, 97-101 (1971).

26. D.F. Schoeberle, et.al., A Method of Calculating Transient Temperatures in a Multiregion, Axisymmetric, Cylindrical Configuration - The ARGUS Program, 1089/RE248, November 1963 (ANL-6654).

27. Argonne National Laboratory, Reactor Development Program Progress Report for August 1971, ANL-7854, 8.19, 1971.

28. Argonne National Laboratory, Reactor Development Program Progress Report for October 1972, ANL RDP-10, 8.34, October 1972.

29. ANL, Reactor Development Progress Report, ANL-RDP-10 October 1972.

30. ANL, Reactor Development Progress Report, ANL-RDP-13, January 1973.

31. General Electric, GEAP-13923-4, July 1973.

32. Sodium-Cooled Reactors, Fast Ceramic Reactor Development Program, Forty-Third Quarterly Report, May-July 1972, GEAP-10023-43, pp. 3-22 to 3-24, August 1972.

33. W.L. Partain, A.E. Waltar, et.al., Effects of Molten Fuel Movement During a Fast Reactor Overpower Transient, HEDL-TIME 72-109, August 1972.

34. Fast Flux Test Facility, Preliminary Safety Analysis Report, Section 15 and Appendix C, WADCO Corporation, September 1970.

35. A. Waltar, A. Padilla, and D. Simpson, Assessment of Magnitude and Uncertainties of HCDA for the FFTF, HEDL-TIME 71-34, March 1971.

36. D.M. Switick, et.al., Analysis of Hypothetical Core Disruptive Accident (HCDA), December 1972, (GEAP-13921).

37. R.T. Fernandez, B.U.B. Sarma, and J.O. Sane, R4 Round-Robin Pretest Analyses, General Electric Co., July 1973, (NEDM-13972-3).

38. G.Hoppner, et.al., R-Series R-4 Experiment, Round-Robin Pretest Analysis, prepared by Accident Analysis and Cooland Dynamics Working Group, Argonne National Laboratory, July 1973.

39. Fast Flux Test Facility, Preliminary Safety Analysis Report, Section 15 and Appendix C, WADCO Corporation, September 1970.

40. L.W. Deitrich, TREAT Test Analysis, Argonne National Laboratory, Reactor Development Program Progress Report, July 1971, (ANL-7845) p. 8.14.

3.2 ANL Critical Facilities

3.2.1 Introduction

The uncertainties in the basic cross-section data and design techniques are such that integral experiments are essentail to help ensure workable, safe and economic LMFBR designs. The program of integral measurements includes the entire LMFBR critical-assembly-experiments programs as well as shielding experiments, measurements in operating power reactors (e.g., EBR-II and FFTF) and measurements in special facilities directed at specific design areas (e.g., plutonium critical mass studies, fission product effects studies, and driven subcritical assemblies). Integral data are used for checking basic cross sections and analytical techniques for reactor design, to test and complement design methods in the prediction of reactor performance with engineering-mockup-critical (EMC) experiments and to support the planning and performance of all phases of LMFBR startup and operation. The basic objective of the critical experiments program has been discussed in Ref. 1.

Recently the critical assembly facilities have concentrated upon two major programs: the Demonstration Reactor Benchmark Critical Experiments Program and the FFTF Mockup Assembly Program.

The Demonstration Reactor Benchmark Program, which resulted from consultations with industrial firms, is aimed at providing the integral data needed for the initial Demonstration Plant design work. This coordinated program of experiments has included Zero Power Plutonium Reactor (ZPPR) Assemblies 2 and 3, both large two-zone mixed PuO_2-UO_2 assemblies, and Zero Power Reactor 6 (ZPR-6)Assembly 7, a large single-zone PuO_2-UO_2 assembly. The Assembly 4 program is nearly completed. To date the program has addressed critical mass, basic neutron balance, sodium void, and control rod worth effects.

In critical assembly experiments, actual reactors are assembled and operated at low power to allow measurements to be made. Critical experiments for the U.S. LMFBR program are perfromed in three major facilities: ZPPR at Argonne National Laboratory in Idaho, and ZPR-6 and ZPR-9 at Argonne National Laboratory in Illinois. Current staffing levels are sufficient to operate ZPPR and either ZPR-6 or ZPR-9.

This section contains a discussion of the integral experiments program including facilities and measurements in interest, and implications of integral experiments on the safety of future LMFBR designs.

3.2.2 Integral Experiments and Their Analyses

3.2.2.1 General

The U.S. fast integral experiment program is designed to meet the immediate needs of the FFTF and Demonstration reactor design programs and the long range commercial LMFBR development by meeting the following three major objectives (Ref. 2):

a. To provide integral experimental data to verify and establish calculational methods and a reliable differential data base;

b. To verify specific reactor designs by measuring design parameters on a critical assembly constructed as close as possible to the geometry and composition of the reactor in question;

c. To identify and help resolve by experiment unusual or unforeseen problems associated with reactor design.

An elaboration on these objectives is provided in Tables 1 and 2 (Ref. 3).

It is nearly obvious that approximations in calculational methods can be best evaluated using clear or benchmark type experiments to determine the sophistication required of the methods to achieve acceptable precision. On the other hand, for the direct correction, or normalization of calculated core and shielding design quantities to parameters measured in mockup experiments, the measurement environment must provide a closer simulation of the reactor environment. With a greater confidence

Table 1. Current Uses of Integral Data.

1. Testing and Evaluation of Nuclear Data and Analysis Methods
    - Adjustment of Fuel Data for ENDF/B-III
    - Testing of Shielding Data for Na and Fe
    - Evaluation of Approximations for Data Processing and Flux Solutions
2. Correction of Core & Shielding Designs to Mockup Data
    - Normalization of k_{eff}, Control Worth, Safety Parameters
    - Reduction in Design Margins to Account for Uncertainties
3. Detector Response to Complex Source-Detector Geometries
    - Effects of Control Positions and Movement

Table 2. Integral Data Uses for Operation and Safety.

1. Prediction and Optimization of Reactor Operation
    - Effects of Control Rod Positions and Fuel Burnup
    - Power Distributions, Control Rod Worths, Fuel Reaction Rate Measurements in ZPPR-3
    - Optimization of Control and Fuel Management
    - Design of Automatic Loading Following and Computer Data Acquisition Systems
2. Verification of Safety Parameters to Support Licensing
    - Measurements of Safety Coefficients, Sodium Loss Reactivity, Fuel and Control Worths, Core Redistribution Reactivity
    - Static and Transient Experiments; Startup Tests

in predicted parameters for a specific design, reduced design margins (and reduced plant and operation costs) can be achieved while still meeting established safety criteria and operating performance targets.

3.2.2.2 Estimated Precision of Design Parameters

An extremely important application of integral data is the verification of safety parameters needed to support licensing applications and to demonstrate conformance to technical specifications. Included are measurements of the Doppler coefficient, material worths, sodium voiding reactivity, fuel and control assembly worths, and reactivity effects of core redistribution. These data are obtained from critical assembly mockup experiments, reactor start-up tests, and both static and transient reactor experiments such as the SEFOR program.

The left-hand column of Table 3 lists several important nuclear design parameters. Estimated precisions in current predictions of these parameters are shown in the second column (Ref. 3). The two right-hand columns indicate precision goals for the prediction of these parameters for design of the LMFBR Demonstration Plant and for an early target commercial plant. The estimated current precision is that attainable without any additional mockup experiments or other nuclear development work.

Table 3. Precision of Design Parameters(a)
(Ref. 3).

Parameter	Estimate Current(b)	Goals(c)	
		Demo	Target
Pu Enrichment	±5%	±2%	±1%
Peak/Avg Power Density	±12%	±3%	±2%
Control Rod Worth	±15%	±3%	±2%
Doppler Coefficient	±15%	±10%	±7%
Sodium Void Reactivity	±1.5$	±0.5$	±0.3$
Flux at Reactor Vessel(d)	$\overset{\times}{\div}5$	$\overset{\times}{\div}2$	$\overset{\times}{\div}1.3$
Flux Above Reactor Head(d)	$\overset{\times}{\div}15$	$\overset{\times}{\div}5$	$\overset{\times}{\div}2$

(a). Estimated one-sigma confidence levels.

(b). Without any additional mockup experiments or related nuclear development.

(c). Precision goals for the Demonstration Plant are those required at time of design freeze for the relevant component. For the target plant, the precision goals are required for the early-to-mid-1980 period.

(d). Uncertainties expressed as multiplicative rather than additive factors. For these cases the "two-sigma" confidence level value is estimated to be the square of the "one-sigma" value.

The precision goals for the Demonstration Plant are those required at the time of the design freeze for the relevant component (Ref. 3).

The uncertainty values listed on Table 3 represent an estimated one-sigma confidence level. To provide adequate margins in the reactor design, consideration would be focused on a two-sigma confidence level, rather than one-sigma for most of the indicated parameters. For the shielding-related parameters listed at the bottom of the slide, the uncertainties have been expressed as multiplicative rather than additive factors. For those cases the two-sigma uncertainty is estimated as the square of the one-sigma value.

Most of the expected improved precision expected for the core parameters result from mockup critical experiments run in the ZPPR facility - mainly the planned engineering mockup critical and also the benchmark experiments currently underway. The most significant of these expected precision improvements, in terms of their impact on costs for design margins, are the peak-to-average power density, the control system and rod worths, and the plutonium enrichment.

As a result of the SEFOR program, and also small sample experiments, the current precision of the Doppler coefficient is acceptable (Ref. 3). For example, it is probably no longer necessary to incorporate BeO in the core design to assure an adequate Doppler coefficient. The Doppler critical experiments for the Demonstration Plant are expected, nevertheless, to provide a better estimate of the effect of a high control rod poison insertion on the Doppler coefficient. On the other hand, the indicated difference between the current precision of the sodium void reactivity and the expected after doing mockup critical experiments can have a very significant impact on the calculated energy release for the hypothetical core disassembly accident and, hence, could involve licensing delays.

3.2.2.3 Cost Benefits of Additional Integral Data

Of course, to obtain the improved precision of design parameters, there is a substantial cost in performing the measurements. Table 4 provides a crude estimate of the cost saving that might be realized (Ref. 3). To the extent that the cost benefits indicated in Table 4 may be in the right ballpark, there appears to be a strong economic incentive for conducting the physics developmental programs that will provide the integral data for the required improvements in physics design predictions. From the point of view of safety of LMFBRs, however, the present occurrence of the Doppler coefficient appears satisfactory.

Table 4. Cost Benefits of Additional Integral Data (Ref. 3).

	($1000)
Less Fuel (2 Cores) & Control Elements	1000-2000
Reduced Plant Design Margins	1000-2000
Lower Engineering Cost (Design & Licensing)	750-1500
Reduced Chance of Licensing Delay*	1000-2000
Less Time for Low Power Startup Tests*	3000-6000
Less Time for Power Ascension Startup Tests*	750-1500

*Estimated for power replacement cost of $\$1.5\times10^6$/month.

3.2.2.4 Impact on LMFBR Safety with Improved Precision of Design Parameters

The penalty for an ~15% uncertainty in rod worths is the extra fissile inventory required to compensate for the additional unnecessary control . This larger inventory could have a first-order effect in the event of an accident.

The techniques for measuring large subcriticalities, needed for control-rod worth measurements, have been greatly improved in the past few years. The rod-drop inverse-kinetics technique is the primary method, with both noise and source multiplication measurements used for verification and backup. These backup techniques are for verification and backup. These backup techniques are the primary reactivity monitoring techniques during refueling operations, and hence improvements in technology have the potential of making direct, first-order contributions to the prevention of LMFBR accidents.

Core component reactivity worth data is required for operational purposes, and the accuracy has some effects upon safety operations. Particularly, vexing has been the discrepancy between measured and calculated control-reactivity worth values, although with recent changes in cross section sets the problem is less severe than it once was.

The interaction of Doppler effects and control rods and the combined interaction of control rods, sodium voiding, and Doppler effects is important, and has been studied on the ZPPR Assembly 3.

Careful sodium-void spatial propping has been done in the most recent mock-up and benchmark critical assemblies in order that an appropriate initiation phase of an accident can be analyzed.

Power distributions are made up of a combination of the isotopic fission-rate distributions and the distribution of absorbed gamma dose. The static power distribution is important to many of the detailed thermal, hydraulic, and mechanical design considerations in the core and blanket. The impact of first-order uncertainties in power level are not of major importance in the analysis of any large-scale accident, however, where the power level could change rapidly in a short period of time.

3.2.3 Critical Facilities

3.2.3.1 General

The three ANL critical facilities are all large split table type critical facilities. They consist of a bed and two table assemblies, one moveable and one stationary. On each of the tables are horizontally stacked two inch square stainless steel matrix tubes forming an 8' x 8' or 10' x 10' cross section. Stainless steel drawers containing uranium, plutonium, sodium, and other reactor simulation materials in appropriate mixtures and dimensions are placed into the stainless steel matrix to form the reactor to be investigated. Reactor cores with blankets and reflectors up to about 3500 liters core volume may be studied on ZPR-6 and -9 and 6000 liters on ZPPR. A brief summary of the ZPPR, ZPR-6 and ZPR-9 facilities is available in the Appendix A to this section and has been obtained from Ref. 1.

As a part of the ZPR-6 facility, the Variable Temperature Rodded Zone (VTRZ) was installed in ZPR-6 in 1972 for making critical-assembly integral physics measurements in a hot, rodded environment typical of an operating LMFBR. With the VTRZ, a zone in the center of ZPR-6 can be heated to any temperature from room temperature to 550°C. The program of measurements for the VTRZ is directed at determining the effect of the hot, rodded environment on the important LMFBR physics parameters.

For the benchmark and engineering design studies of 1000-2000-MWe or larger commercial LMFBR plants, different new facilities may be needed. In addition, special facilities operable at low power may be needed as auxiliary facilities to the FFTF and DEMO programs for detailed power distribution and reactivity studies related to engineering requirements (Ref. 1).

At the time that the LMFBR Program Plan (Ref. 1) was developed in 1972, it was also expected that other critical experiment facilities would be required; there are itemized in Appendix B.

3.2.3.2 Basic Objectives of the Critical Experiment Programs

The integral measurements may be generally categorized into one of three types: benchmark experiments, EMC experiments, and special-purpose experiments as needed. For benchmark experiments the assembly design is kept relatively simple to facilitate analysis. The composition, size, and configuration are chosen to be representative of a general class of reactors with some single reactor design feature being emphasized. Benchmark experiments are aimed at the outstanding LMFBR design problem areas and have as their purpose the evaluation and confirmation of design techniques and basic data. For EMC experiments, the critical assembly closely simulates a particular LMFBR design in composition, size, and configuration so as to minimize extrapolation to confirm reactor design or performance characteristics.

The Demonstration Reactor Benchmark Experiments Program consisted of a series of clean critical assembly experiments correlated in composition, configuration, and experimental program. The primary Benchmark cores consisted of ZPR-6 Assemblies 6, and 7 and ZPPR Assemblies 2 and 3. For example, for the ZPPR-2 assembly, the dimensions and compositions were representative of an LMFBR demonstration plant core and blanket, but without control rod simulation. The ZPPR-3 assembly, on which the Demonstration Plant Benchmark Critical Experiments were conducted, was to study the influence of a strong control rod system on important nuclear parameters of a core representative of the core in the Clinch River Breeder Reactor Plant (Ref. 4). The ZPPR-4 program, which is also a cooperative effort of Argonne National Laboratory and the General Electric Company, has the dual objectives of (1) providing experimental information directly useful in the Clinch River Breeder Reactor Plant (CRBRP) design and PSAR and (2) providing an LMFBR benchmark study of breeding, blanket performance and the effects of blanket fissile buildup on core and blanket performance.

A more detailed outline of the emphasis of each of the programs is summarized in Appendix C (Ref. 2).

3.2.3.3 Typical Critical Experiments

Typical integral experiments performed on the ZPR facilities are listed below:

- Determination of critical size or critical enrichment for power-reactor compositions. Integral studies are performed on large uranium- and plutonium-fueled systems in order to obtain the basic static characteristics of such systems. Diagnostic sequences of experiments are made to provide integral data for cross-section data testing. Zoned studies are performed to obtain some of the characteristics of large systems with much reduced material inventories.

- Measurements of flux and power distribution.

- Measurement of reactivity effects such as temperature coefficients, control-rod effectiveness, and blanket effectiveness.

- Investigation of heterogeniety effects to ensure that such effects in the critical facilities, or in the associated reactors, are understood and that any necessary corrections are made.

- Measurements related to the determination of the neutron spectrum and the adjoint function (importance).

- Determination of parameters that are relevant to the prediction and understanding of the long-term behavior of the operating reactor. An example of such a quantity is the capture-to-fission ratio of the fissile isotopes. Studies related to the effects of the higher plutonium isotopes are made experimentally by the use of the zones containing such material.

- Studies of neutron and gamma transport in blanket compositions and in shielding materials in close proximity to the reactor core, including source energy spectra studies.

3.2.3.4 Results of the ZPPR-3 Critical Experiments

Only the results of the ZPPR-3 are summarized here because they are from the assembly most closely representing the Demo which has been extensively reported upon. The most significant result of the ZPPR-3 program was the finding that the control rod system has a very strong influence on the power distribution and on individual control rod reactivity worths of an LMFBR (Ref. 4).

The measured strong control rod interaction effect with changes up to 15% for both the power distribution and for individual control rod worths, was accurately predicted by calculations. Thus, the results were somewhat surprising only because control rod effects on the spatial flux distribution had not previously been regarded as a major problem area for fast reactors (Ref. 4).

Control rod system influence on the flux shape was found to increase significantly with increasing core size, which indicates that the large commercial size LMFBR cores of the future may be more sensitive to control system effects than the present generation of demonstration and prototype plants. This could have a second-order effect on the safety at large LMFBRs.

A much more important effect on safety is that sodium voiding measurements in ZPPR-3 have confirmed that a large positive central sodium voiding reactivity exists in demonstration and prototype plant core sizes (≤ 3\$ extrapolated to an equilibrium cycle core having appreciable ^{240}Pu and fission products). This plays a significant role in the analysis of the hypothetical core distuption accident (HCDA), especially for accident initiation by loss of coolant flow. Only preliminary calculations of the ZPPR-3 sodium voiding experiments have been completed to date and, although some of the calculated values are in good agreement with the measured ones, the computed results appear very sensitive to details of the calculational model (Ref. 4). This is especially the case for the method of obtaining perpendicular bucklings.

The sensitivity of the power distribution to the control withdrawal sequence during operation, coupled with a small design margin for power peaking uncertainties desirable for economic considerations, may require instantaneous on-site monitoring of the power distribution. Since in-core neutron monitors probably will not be developed for the early prototype reactors, it appears necessary to develop algorithms which will permit rapid and reasonably accurate on-line calculation of three dimensional power distributions for all reasonable control and insertion patterns during an operating interval (Ref. 4).

For monitoring system sensitivity during power operation, it is desirable to compare predicted and actual system reactivities to enable detection of anomalous reactivity on the order of three events (Ref. 4). This imposes a severe requirement on accuracies for prediction of the control system worth and of the reactivity feedbacks due to temperature coefficients, including complex core distortions and corrections for burnup.

3.2.3.4 Planned Future Critical Experiments Related to LMFBR Safety

As a part of the LMFBR Program Plan (Ref. 1) it was suggested that configuration benchmark assemblies were scheduled for principle stages and configurations of gross core meltdown and disassembly. This would be beneficial in that it would provide flux checkpoints for codes analyzing disassembly accidents.

Another plan is to perform measurements which follow the progressive stages of plutonium buildup in the blanket of an LMFBR, which would have some effect on reactivity coefficients.

Another long-term assembly plan is to develop a special assembly for Doppler measurements which would support a systematic program to evaluate the complicating effects arising in off-center Doppler measurements and fissile Doppler measurements (Ref. 1).

References

1. "LMFBR Program Plan - Physics", U.S. Atomic Energy Commission Report WASH-1109 (2nd ed.), Dec. 1972.

2. P.I. Amundson, E.F. Bennett, S.G. Carpenter, W.Y. Kato, L.G. LeSagre, R.A. Lewis, R.G. Palmar, C.E. Till, A. Travelli, B.A. Zolotar, C.E. Clifford, M.J. Driscoll, and Y.D. Harker, "U.S. Fast Integral Experiments Program", Proc. Int. Symp. on Physics of Fast Reactors Vol. I., p. 431 (1974).

3. P. Greebler and B.A. Hutchins, "Significance of Integral Parameters in the Design and Performance of Fast Breeder Reactors", Proc. Conf.New Developments in Reactor Physics (Klamesha Lake, New York), Supt. 1972.

4. P. Greebler, H.S. Bailey, S.L. Stewart, P.I. Amundson and S.G. Carpenter, "Contributions of ZPPR-3 Demonstration Plant Pre-Engineering Critical Experiments and SEFOR to Resolution of LMFBR Physics Problems", Proc Int. Symp. Physics of Fast Reactors (Tokoyo, Japan, Oct. 16-23, 1973), Vol. III, p. 1462 (1974).

Appendix A: The ZPPR, ZPR-6, and ZPR-9 Critical Facilities (Ref.1)

ZERO POWER REACTOR-6 (ZPR-6)

Location ANL, Argonne, Illinois

Status Operational

Principal Uses. The facility is used to obtain fast reactor physics integral parameters from benchmark, engineering mockup, or special purpose experiments.

Facility Description. ZPR-6 is a split-table design critical facility, consisting of matrix assemblies positioned on two large tables; one table is movable and the other is stationary. On each table are mounted approximately 2000 two by two inch square stainless steel matrix tubes which form an 8 X 8 X 4 foot matrix assembly. Figure 1 shows a photograph of ZPR-6 with the tables separated for loading. Stainless steel drawers loaded with core materials (fuel, structural, and coolant) as shown in Figure 2 are loaded into the matrix assembly. The two tables each form one half of a reactor assembly. Criticality is attained by bringing the two tables together and insertion of fuel containing control rods and removal of boron absorber rods.

Experimental Capability. Fast reactors of the Demonstration Plant reactor size (cores up to about 3000 liter volume) may be built on ZPR-6. Integral parameters such as critical mass, coolant-void and Doppler coefficients, power distributions, control rod worths, reaction rates and ratios, and reactivity coefficients, are measured in the critical experiments.

Auxiliary Equipment. Sufficient quantity of plutonium, coolant and structural materials to construct metal, oxide or carbide cores in excess of 6000 liters is available.

Radial and axial remote-positioning equipment for measuring material worths or reaction rates as a function of core position is available.

A mechanism for oscillating heated uranium and plutonium samples to permit investigation of the Doppler coefficients of these large cores is available.

An automated, high-volume, foil-counting facility, employing primarily high-resolution gamma-ray spectroscopy, where activated foils are counted to determine fission and capture distributions throughout the reactor is available.

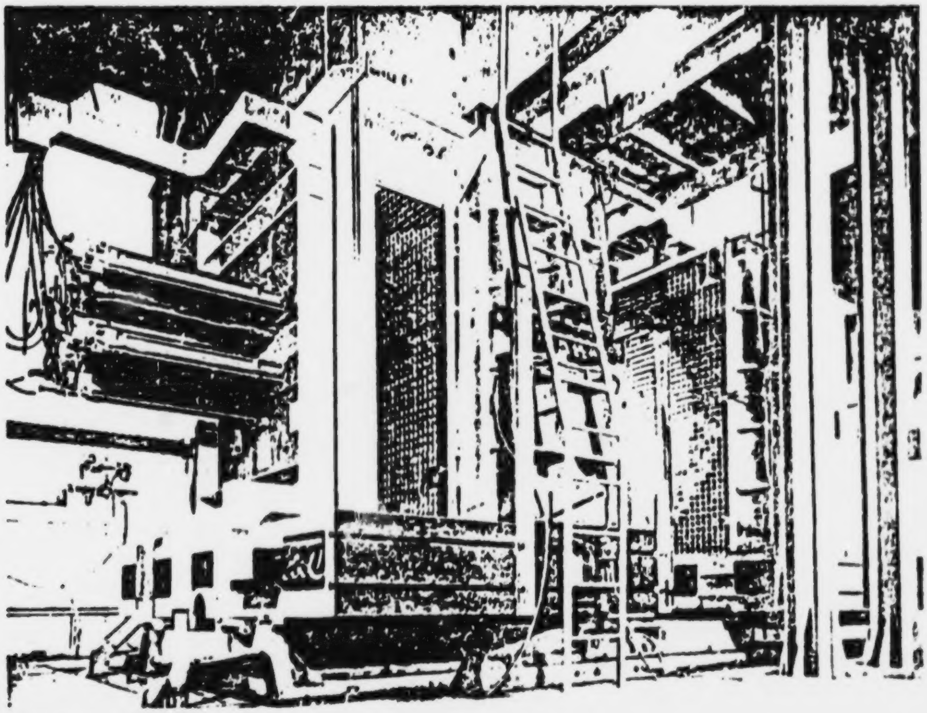

Figure 1 ZPR-6.

Reproduced from best available copy.

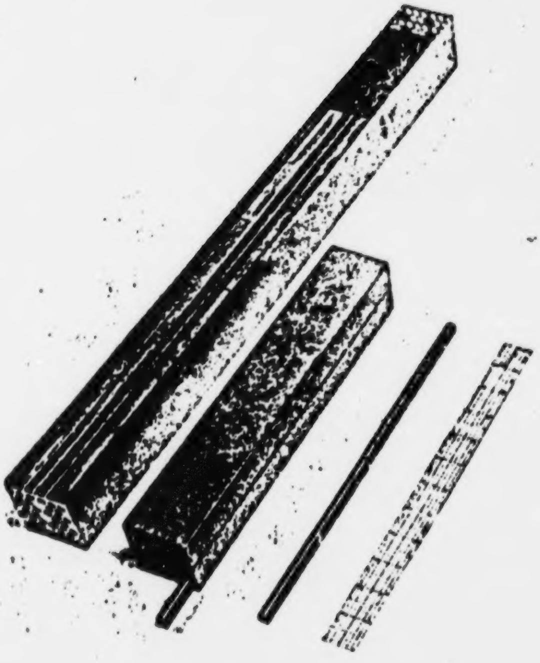

Figure 2. ZPR Loaded Drawers and Calandria.

An on-line, SEL 840-MP computer provides capability for data acquisition and immediate analysis.

Modifications Authorized. ZPR-6 is currently being modified to include the Variable Temperature Rodded Zone (VTRZ) as shown schematically in Figure 3 which will be used to study temperature and plate-rod heterogeneity effects. The VTRZ will be capable of attaining temperatures of about 500°C. A detailed schematic of the VTRZ is shown in Figure 4 and the VTRZ prototype is shown in Figure 5.

ZPR-6 will also have a 100 m path time-of-flight capability to measure the neutron spectrum in the low energy range.

The present matrix size permits studies of the Demonstration plants (~3000 liters). The reactor tables have sufficient dimensional and weight capabilities to each accommodate a 12 X 12 foot matrix. This "stretch capability" will permit the study of most LMFBR assemblies likely to be of interest in the next decade.

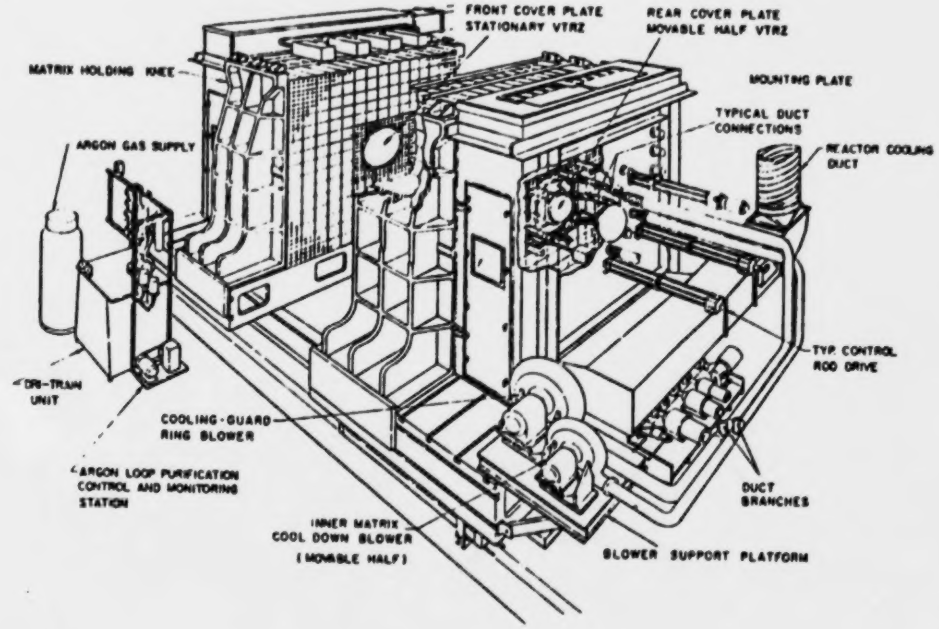
FRONT COVER PLATE
STATIONARY VTRZ
REAR COVER PLATE
MOVABLE HALF VTRZ
MATRIX HOLDING KNEE
MOUNTING PLATE
TYPICAL DUCT CONNECTIONS
ARGON GAS SUPPLY
REACTOR COOLING DUCT
TYP. CONTROL ROD DRIVE
DRI-TRAN UNIT
COOLING-GUARD RING BLOWER
ARGON LOOP PURIFICATION CONTROL AND MONITORING STATION
DUCT BRANCHES
INNER MATRIX COOL DOWN BLOWER (MOVABLE HALF)
BLOWER SUPPORT PLATFORM

Figure 3. Schematic of ZPR-6 with VTRZ.

ZERO POWER REACTOR-9 (ZPR-9)

Location ANL, Argonne, Illinois

Status Operational

Principal Uses. The facility is used to obtain fast reactor physics integral parameters from critical assemblies such as benchmark, engineering mockup, and special purpose experiments.

Facility Description. ZPR-9 is a split table critical assembly similar to ZPPR and ZPR-6. It consists of two matrix assemblies of approximately 2000 2 inch square stainless steel matrix tubes mounted on two large steel tables. One table is moveable and the other is stationary. A photograph of ZPR-9 is shown in Figure 1. Each matrix assembly is 8 X 8 X 4 feet in dimensions forming an 8 foot cube when the tables are brought together.

Experimental Capability. Large fast reactor assemblies having core volumes up to about 3000 liters may be built on ZPR-9. The physics of power reactors such as FFTF and the Demonstration Plant may be studied on ZPR-9.

The experimental program on the ZPR-9 facility includes coolant void coefficients, Doppler effects, control rods worth, power distribution, reaction rates and ratios, reactivity coefficients, and critical size and/or composition determination.

Auxiliary Equipment. Sufficient quantity of plutonium, coolant and structural materials to construct metal, oxide or carbide cores in excess of 6000 liters is available.

Radial and axial oscillators for measuring material worths or reaction rates as a function of core position. Oscillators for measuring the Doppler effects in uranium and plutonium samples.

An automated, foil counting facility, employing gamma-ray spectroscopy, where activated foils are counted to determine fission and capture distributions throughout the reactor.

An on-line SEL-840 MP computer provides capability for data acquisition and immediate analysis.

Bibliography. W. Y. Kato et al., "Final Safety Analysis Report on the Use of Plutonium in ZPR-6 and -9," ANL-7442 (1970).

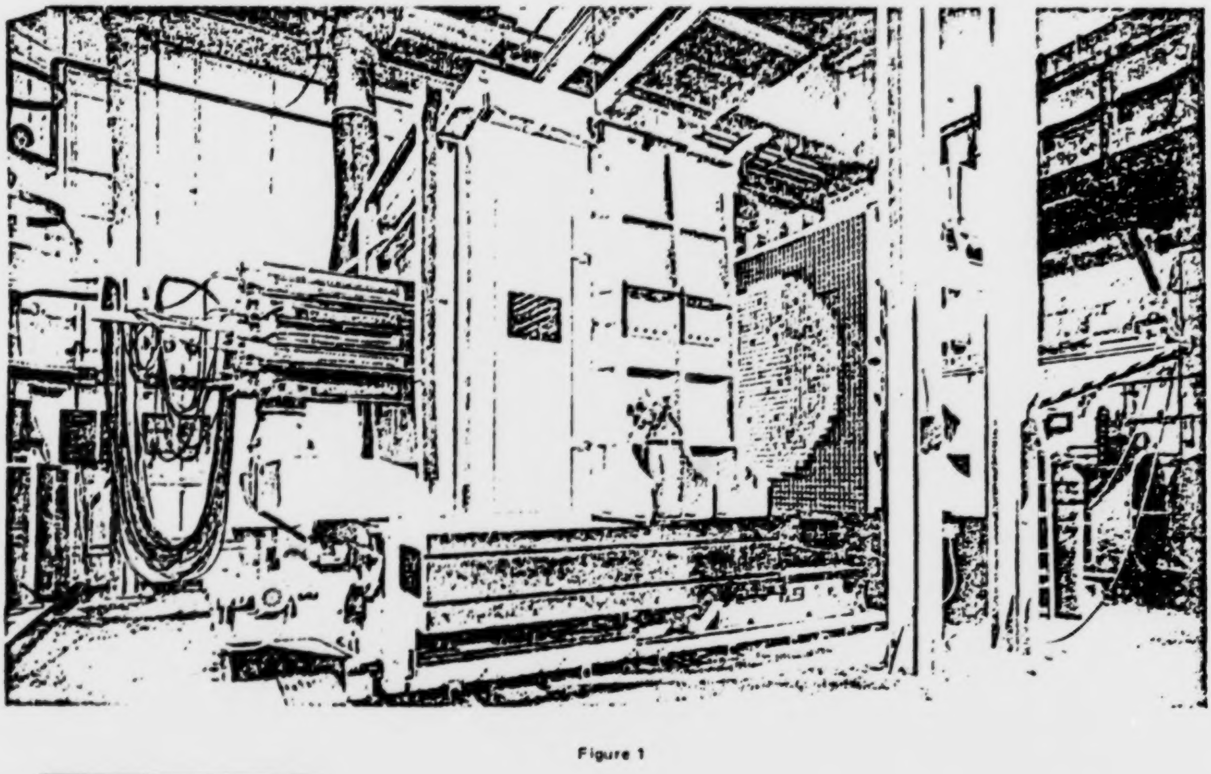

Figure 1

Reproduced from best available copy.

ZERO POWER PLUTONIUM REACTOR (ZPPR)

Location ANL, NRTS, Idaho

Status Operational

Principal Uses. The facility is used to obtain integral reactor physics parameters from fast spectrum critical assemblies such as benchmark or engineering mockup experiments.

Facility Description. ZPPR is a split-table-type critical facility designed for the study of the physics of power breeder systems. The ZPPR matrix is made up of two 10 X 10 X 4 ft assemblies of matrix tubes mounted on separate steel tables. The tables are separated while the matrix is loaded with drawers containing reactor simulated materials in the form of small plates and then brought together for operation. Figure 1 shows ZPPR loaded with Assembly 3.

Experimental Capability. ZPPR is capable of simulating fast reactor compositions characteristic of the proposed 300-500 MWe Demonstration plants and 1000 MWe commercial plants. ZPPR can be used to simulate many reactor designs to cores ranging up to about 3000 liters. Experiments include studies of the power-producing, control and safety characteristics of large plutonium-breeder power-reactor compositions.

Auxiliary Equipment. Sufficient quantity of plutonium, coolant and structural materials to construct metal, oxide or carbide cores.

Radial and axial, remote-positioning equipment for measuring material worths or reaction rates as a function of core position.

A mechanism for oscillating heated uranium and plutonium samples to permit investigation of the Doppler coefficients of these large cores.

An automated, high-volume, foil-counting facility, employing primarily high-resolution gamma-ray spectroscopy, where activated foils are counted to determine fission and capture distributions throughout the reactor.

An on-line, SEL 840 MP computer provides capability for data acquisition and immediate analysis.

Modifications Authorized. The present matrix size permits studies of the demonstration plants (~3000 liters). The reactor tables have sufficient dimensional and weight capabilities to each accommodate a 14 X 14 ft matrix. This "stretch capability" will permit the study of cores exceeding 6000 liters in volume.

Bibliography. H. Lawroski et al., "Final Safety Analysis Report, Zero Power Plutonium Reactor Facility," ANL-7471 (June 1971).

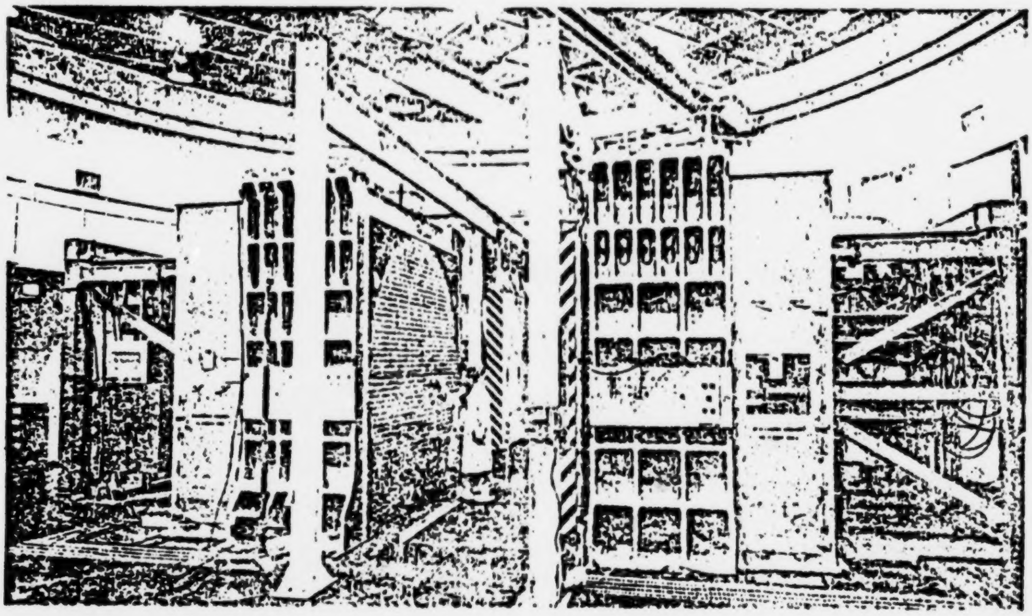

Figure 1. ZPPR.

Reproduced from best available copy.

Appendix B: Future Requirements for Experimental Facilities (Ref.1)

- The ZPPR matrix will be expanded from the current 10 × 10 × 8 ft size to a 14 × 14 × 10 ft size to allow assembly of very large cores (1000 MWe) and expand the capability in later stages of the Demonstration Reactor Program to accurately mockup shield configurations to allow (a) measurements of neutron spectra and fluences at instrument locations, (b) neutron and gamma-ray penetrations in realistic shields, and (c) neutron and gamma-ray streaming effects. Expansion of the ZPR-6 and/or ZPR-9 matrix from the current 8 × 8 × 8-ft size to a 10 × 10 × 8-ft size or a 12 × 12 × 8-ft size is a possibility for later consideration.
- Matrix-loading machines for ZPPR, ZPR-6, and ZPR-9 will be designed and built to reduce fast-neutron and gamma-ray doses to personnel and to increase the general safety and efficiency of critical facility operations.
- Expansion, redesign and reequiping of the current drawer loading workrooms will be carried out to increase the efficiency of loading operations to meet current program projections, to meet new AEC plutonium storage facility design criteria, and to have the capability of handling fuel containing high percentages of ^{240}Pu and ^{241}Pu.
- The storage facilities at ZPPR and at ZPR-6 and -9 for non-fissile materials will also be expanded. The volume of these materials exceeds current storage and handling facilities.
- Expansion and redesign of plutonium storage vault facilities at ZPPR and at ZPR-6 and -9 may become necessary to meet new AEC plutonium storage facility criteria and for possible storage of fuel containing a high percentage of ^{240}Pu and ^{241}Pu.
- Accurate low-energy neutron-spectrum measurements may be needed as a function of position in the Demonstration Reactor mockup and/or in large cores studied on ZPPR. This would require implementation of time-of-flight capability on the ZPPR system. The decision to implement this capability will strongly depend on the need and on feasibility questions that will be answered by time-of-flight measurements done on ZPR-6 in FY 1974-1975.

Appendix C: Purpose of Benchmark Programs (Ref. 2)

(a) ZPR-6-6:

- Establish basic neutronic properties of large UO_2 systems
- Investigate effects of sodium voiding by comparing measurements on reference core and in the large sodium-void zone
- Spatial mapping of the sodium-void reactivity coefficient
- Study plate heterogeneity reactivity effects.

(b) ZPR-6-7:

- Establish basic neutronic properties of large UO_2/PuO_2 system
- Investigate the effects of reactor environment changes on the basic physics and safety parameters of the core. The comparisons include:
  (1) reference plate core versus matching rodded core
  (2) reference 11% ^{240}Pu fuel versus 27% ^{240}Pu fuel
  (3) unvoided versus sodium-voided composition
  (4) unpoisoned versus B_4C-poisoned composition.
- Central control rod studies including the rod worths and the effects of the control rods on Doppler, sodium-void, reaction rates and small sample reactivity worths.

  Investigate the Doppler coefficient in a UO_2/PuO_2 spectrum for several different materials including UO_2/PuO_2 mixtures.

(c) ZPPR-2:

- Establish basic neutronic properties of a two-zone UO_2/PuO_2 Demo Benchmark core with emphasis on spatial mapping of important parameters
- Investigate B_4C and tantalum control rods including worths as a function of rod size, rod interactions and effects of rods on surrounding core
- Investigate the physics properties of both central and off-center rodded zones including the reactivity worth of the rodded zones
- Investigate the physics properties of both central and off-center sodium-voided zones.

(d) ZPPR-3:

- Establish basic neutronic properties of two-zone Demo Benchmark core with simulated control rods.
- Detailed control rod and power distribution studies including:
  (1) worths of individual and groups of control rods
  (2) effects of control rod patterns on power distributions
  (3) effects of control rod patterns on individual control rod worths.
- Study of the changes in core properties from the BOL to the MOL to the EOL configurations
- Establish the region of maximum positive sodium-void and measure the properties of the zone.

(e) ZPPR-4:

- Provision of pre-EMC data for the Demonstration plant designs
- Studies of power distribution and breeding in the blanket
- Studies of the effect of blanket fissile buildup on core parameters
- Studies of the effects of plutonium composition changes.

3.3 Scaled Vessel Accident Rupture Experiments

3.3.1 Introduction

The possibility of rapid conversion of heat energy to kinetic energy in sodium-uranium systems has given rise to many experiments analyzing pressure vessel and piping response under explosive conditions. Some early work in this direction was aimed at studying the response of the Enrico Fermi Reactor (Refs. 1,2). More recently scaled FFTF model tests have been performed at SRI (Refs. 3,4,5) and SRN model tests have been performed at AWRE (Refs. 6,7) and BELGONUCLEAIRE (Ref. 8).

3.3.2 Scaling Methods

It is desirable to avoid full-scale simulation experiments because of cost and a need to perform many experiments. The safety hazard from releasing sodium vapor and sodium liquid in an uncontrolled manner as well as the complexity of heating it to a molten state is avoided by using water to simulate the coolant. Some form of similitude modeling is often necessary to match the rate of pressure rise from explosives to that predicted for the HCDA.

The classic text on scaling is that of Bridgman (Ref. 10) and consists of listing all the physical variables necessary to describe the phenomena, and forming them into dimensionless groups. A change in one variable must be accompanied by changes in the other variable to keep the dimensionless groups constant. This is conveniently represented in terms of the "Buckingham Pi Theorem" (Ref. 11) which states that any complete physical relationship can be expressed in terms of a set of independent dimensionless products composed of the physical parameters which describe the scaled process. Reference 12 described the method by which the parameters characterizing the experiment are manipulated into the dimensionless π terms summarized in Table 3.3.2.1. The pi terms may be written in functional form as:

$$F(\pi_1, \pi_2, . . . \pi_{11}) = 0 \qquad (1)$$

$$\text{or } \pi_1 = G(\pi_2, \pi_3, . . . \pi_{11}) \qquad (2)$$

For equivalent systems, similarity dictates that the pi terms must be invariant. This can be accomplished as follows (see Table I): π_1 indicates that the deflections will scale according to model size, so that strains will be equal at homologous times. π_2 and π_3 are satisfied by constructing the same geometry as the prototype. π_4 and π_5 indicate that the model material compressibility and strength should be in the

TABLE I

Dimensionless Pi Variables for Describing Simulated HCDA - where L-Length, a-Angle, K-Bulk Modules, σ-Stress, ρ-Density, r-Gas Expansion Coefficient, W-Work, t-Time, P-Pressure, Subscript i- denotes a material or component, Subscript o-denotes a reference base.

Pi Terms		Description
π_1	$[\Delta L_i/L_o]$	Response Similarity
π_2	$[L_iL_o]$	Geometric Similarity
π_3	$[\alpha_i]$	
π_4	$[K_i/K_o]$	Constitutive Similarity
π_5	$[\sigma_i/\sigma_y$	
π_6	$[\rho_i/\rho_o]$	Density Ratios
π_7	$[\gamma_i]$	Source Expansion Similarity
π_8	K_o/P	
π_9	σ_y/P	
π_{10}	$\dfrac{\rho_o L_o^2}{Pt^2}$	
π_{11}	$P\ L^3/W$	

same ratio throughout the model. π_6 shows that the density ratios should also remain constant. π_7 requires that gas expansion characteristics be simulated. π_8 and π_9 show that the reference bulk modulus and yield strength should be maintained in a constant ratio with the peak pressure. π_{10} and π_{11} determine the scaling factors for homologous times. For example, using π_{11} and defining a scale factor λ as prototype parameter divided by model parameter produces:

$$\frac{P\ L^3}{W}\ \text{prototype} = \frac{P\ L^3}{W}\ \text{model} \tag{3}$$

$$\frac{\lambda_P\ \lambda_L^{\ 3}}{\lambda_W} = 1 \tag{4}$$

Assuming that the charge energy, W, is proportional to the cube of the characteristic model dimension produces:

$$\lambda_W = \beta\ \lambda_L^3 \quad \text{where } \beta \text{ is a constant} \tag{5}$$

Substituting into Equation 4 produces:

$$\lambda_P = \beta \tag{6}$$

Likewise, from π_8 and π_9:

$$\lambda_K = \lambda_\sigma = \lambda_p = \beta \qquad (7)$$

From term π_{10} we have

$$\frac{\lambda_\rho \lambda_L^2}{\lambda_\rho \lambda_t^2} = 1 \qquad (8)$$

$$\lambda_t = \lambda_L \frac{\lambda_\rho}{\beta} \qquad (9)$$

Thus Equation 9 provides the relationship defining the time for corresponding events. These results may be extended to determine the energy scale factor, $\lambda_E = \beta \lambda_L^3$.

3.3.3 SRI Scaled Experiments

The Stanford Research Institute has carried out many experiments to simulate a HCDA in FFTF (Refs. 3,4,5). The objective of the program was to determine whether the structural envelope comprised of the reactor vessel and primary piping will remain intact so that the post accident coolant flow and decay heat removal through the heat transport system will not be precluded.

The two main parts of the program were: (1) development of an explosive energy source for simulating the HCDA and (2) investigation of hydrodynamic and structural effects of the HCDA. In the source development, instrumented simple 1/30- and 1/10-scale models of the FFTF were employed without the vessel head. In the investigation of the hydrodynamic and structural effects of the HCDA, instrumented 1/30- and 1/10-scale complex models of the FFTF and one instrumented 1/10-scale complex model of the FTR with three primary loops.

Simulation is based on matching the pressure-volume change relationship for the expanding detonation products with the relationship obtained from the SOCOOL computer code. The source energy level calibration is based on equating gas work done during expansion to a pressure of 20 bars. This pressure was chosen because it can be contained by the reactor structure under static conditions without plastic deformation. Source calibration was concentrated on providing scaled HCDA energies of 150 and 350 MWsec, and application of the source to investigate hydrodynamic and structural effects was concentrated on a scaled HCDA energy of 150 MWsec.

Figure 1 shows the experimental setup for the simple geometry SRI HCDA experiments. The program SOCOOL was run to determine the pressuretime relationships for the 1/30 and 1/10-scale models.

An explosive source of pressure was selected because the reaction rate is independent of the response of the container. Solid explosives however generate destructively high local pressure (100 kbar) and have a pressure-time curve that is faster than the SOCOOL generated curve. A solid explosive was selected (PETN) but mixed with 35% glass balloons thus giving a peak pressure of 5 kbar. To obtain the 0.5 kbar (7350 psi) required for the simulation as predicted by SOCOOL. The detonation products were allowed to expand into the air space (figure 3.3.3.1) This source design closely matched that required by SOCOOL for the simulation.

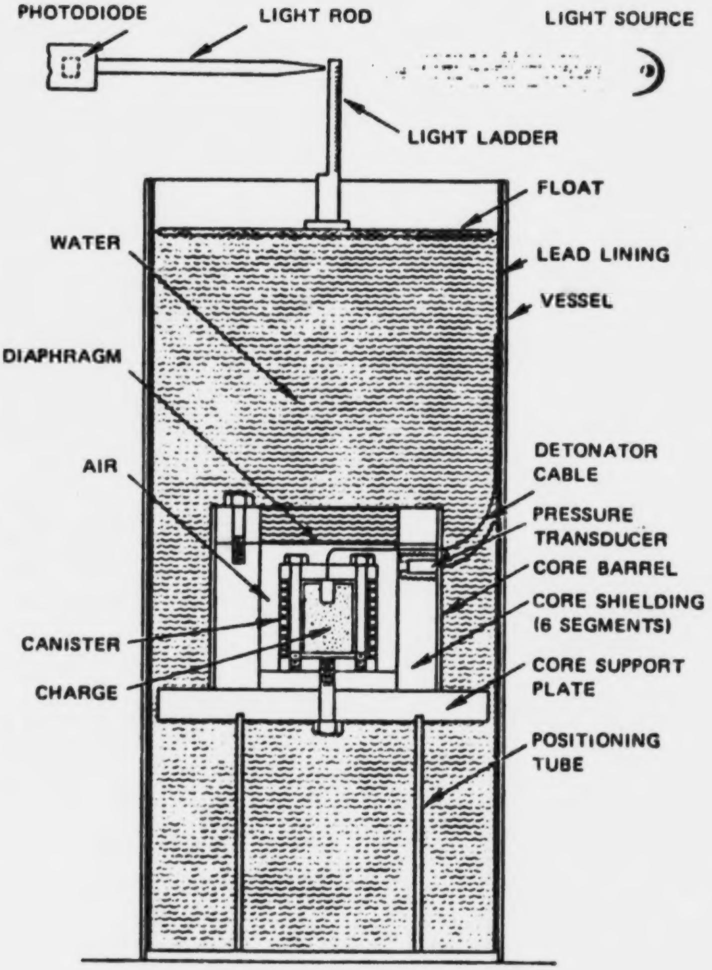
PHOTODIODE
LIGHT ROD
LIGHT SOURCE
LIGHT LADDER
FLOAT
WATER
LEAD LINING
VESSEL
DIAPHRAGM
DETONATOR CABLE
AIR
PRESSURE TRANSDUCER
CORE BARREL
CORE SHIELDING (6 SEGMENTS)
CANISTER
CHARGE
CORE SUPPORT PLATE
POSITIONING TUBE

Figure 1. Setup for SRI HCDA Experiments

The postulated HCDA would occur at normal operating temperature (1000°F) and the HCDA pressure vessel will be of Ni-200. To match these stress-strain curves to that of 304 stainless steel at room temperature, the core barrel wall thickness was reduced to 60% of that predicted by scaling and lead was added to get the correct wall mass.

The source was calibrated by determining that weight of explosives that produces the same amount of work as the portion of the scaled SOCOOL HCDA energy when both have expanded to a volume corresponding to the SOCOOL volume at 20 kbars. This is the maximum pressure that does not produce plastic deformation. The water surface was determined by the light ladder and by flash x-rays of floats containing lead pellets. These latter observations showed relative uniform water velocities over the surface (slug motion).

Experiments were performed to study a scaled HCDA pressure pulse on piping. A pulse gun using the 65/35 PETN/glass microballoons was detonated in a 1 1/2 in. dia. 2.125 in. long chamber. The pressure pulse expanded through a perforated plate (8 - 1/4 in. dia. holes) into an air chamber which was coupled by a conical section to a 3 in. I.D. pipe. (The gun for 1 1/2 in. dia. pipes was similar except the conical section was omitted). Tests were performed on single and double elbow sections of these Ni-200 pipe sizes and two experiments contained pumps.

Three complex model experiments were carried out: 2 experiments on a 1/30 scale model of FFTF and a 1/10 scale model of FFTF with three primary piping loops.

Design features include support arms from which the vessel is suspended, a cellular core support structure that is attached to the vessel wall, thermal liners and baffles, a complex head, head-core mouted instrument trees (IT), and in-vessel handling machines (IVHM). Annealed nickel 200 was chosen for the vessel, support arms, core support structure, instrument trees, and piping because of the similarity of the stress-strain relationship at room temperature to that of stainless steel 304 at 800°F in FFTF. Because nickel is denser than steel (8.9 g/cm^3 compared with 7.8 g/cm^3), the mass scaling is inaccurate, but REXCO computer code calculations indicate that the effect on the dynamic response of the FTR models is small.

For the 1/10 scale experiment with the three primary piping loops, each loop was attached to a sturdy steel framework by means of snubbers simulating the prototype loop supports. Components in each loop consisted of hydraulically modeled pump, intermediate heat exchanger (IHX), outlet isolation valve, inlet isolation valve, and check valve, all made of steel. To provide the scaled lineal mass of the prototype piping system (steel pipe, liquid sodium coolant, and insulation) while maintaining the scaled strength, the piping was wrapped with lead sheet of the appropriate thickness. Lead sheet was also added to the isolation valves to provide the scaled masses.

General conclusions from these experiments are:

In the 1/30 scale simple FFTF model experiments with a scaled 150-MWsec HCDA the following strains were not exceeded: vessel 5.8%, core barrel 1.6%, and hold-down bolts 5.2%. A typical distribution of plastic work among vessel, core barrel, and hold-down bolts is 82%, 7%, and 11%.

Results from three complex models tested for a scaled HCDA of 150 MWsec show that:

- Structural integrity of primary boundary was maintained.
- Strains did not exceed the following values: vessel 2.4%, support arms 3.8%, core barrel 5.5%, hold-down bolts 4.3%, and outlet elbows 1%.
- The head and core suport structure sustained little or no plastic deformation.

- Distribution of plastic work in the 1/10-scale model was: vessel 20%, thermal liner 6%, support arms 7%, core barrel 43%, hold-down bolts 9%, head shielding tubing 8%, and instrument trees 7%.
- Scaling of deformations from 1/30 to 1/10 scale occurred within 15%.
- Displacements in the 1/10-scale model did not exceed the following values: head lift 0.38 in., vessel drop 0.25 in., upper vessel bulge 0.25 in., middle vessel bulge 0.15 in., and outlet nozzle outward motion 0.13 in. (In the 1/30-scale models the bounding values were: 0.085, 0.065, 0.106, 0.053, and 0.040 in.)

The maximum strains are well below the ductility limits for annealed nickel 200 of the models and stainless steel 304 at 800°F of the prototype, which are well in excess of 20%.

3.3.4 Experimental Analysis

In analyzing the SRI HCDA experiments, it is necessary to correct for the deviations from similitude ($\beta = 1$). The ratio of sodium to type 304 stainless steel at 800°F. is 9.66; the density of water to nickel is 8.9 hence π_6 needs correcting for this effect. The bulk modulus of water is about 46% less than that of sodium; water is also about 24% more dense than sodium. In the analysis of Stepnewski et al., (Ref.13) corrections for deviations from similitude for the complex experiments were made by two codes. A HEDL-developed code called MOTION was used to compensate for deviations in component weights, material strength, and support ledge spring constants. REXCO-HEP results were used to correct for the substitution of water for sodium, and deviations in the Ni-200 stress-strain properties relative to those of type 304 stainless steel. With these corrections, figures 2, 3, and 4 present comparisons between scaled experiments and the simulated sodium cooled fast reactor.

Some conclusions in terms of full size equipment are that the center of head displacement (4 in.) is as predicted. Earlier calculations had predicted head doming but these experiments show the coolant to move as a slug. The head reseated after lift but because sodium head seals were not provided for the

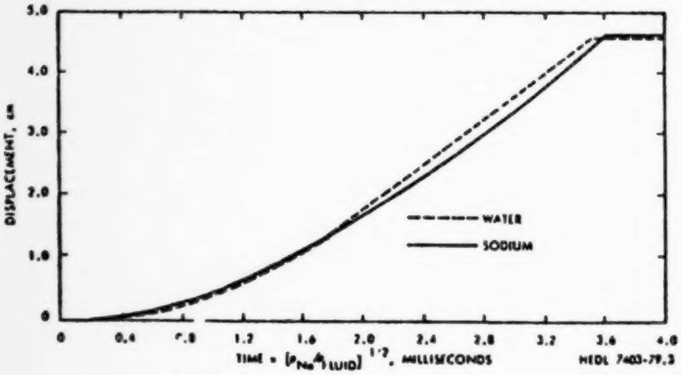

Figure 2. Comparison of Scaled Experimental Coolant Slug Displacements and Corrections for FFTF model.

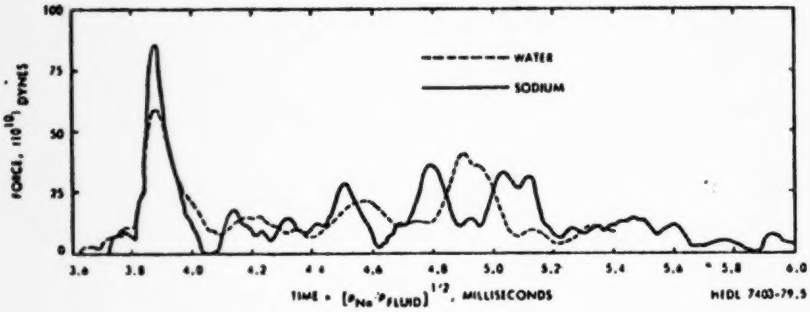

Figure 3. Comparison of Scaled Experimental Force on Vessel Head and Corrections for FFTF model.

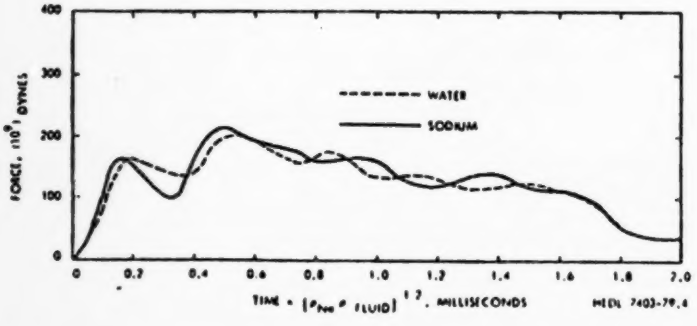

Figure 4. Comparison of Scaled Experimental Force on Core Support Plate and Correction for FFTF model.

experiments, the scaled coolant loss was 110,000 lbs. as compared to a predicted 10-20,000 lbs. of sodium release. The vessel wall strains occurring opposite core center were 1% and 3% for the upper and lower vessel areas. The support arms were strained 2.5 in. The vessel thermal liner showed some permanent deformation. The core support structure sustained a 90° weld failure in the first 1/30 scale test, 225° in the second test and none in the 1/10 scale test. Such failures if they were to occur in FFTF were judged to not interfere with post accident heat removal. The 5 to 6% core barrel strain would not produce rupture (radial displacement 3 in.). The instrument trees columns loaded the vessel head on impact sufficiently to deform the Group I head bolts. The piping modeled in the 1/10 th scale experiment was only slightly deformed (1% diametrical changes).

From these results, it was concluded that under a 150 MWsec HCDA, the FFTF vessel would remain supported and the vessel and primary cooling would maintain integrity. No effect prohibiting post accident heat removal was observed.

3.3.5 SNR Experiments

BELGO NUCLEAIRE (Brussels) and J.R.C. EURATOM (Ispra) are carrying out a theoretical and experimental program to investigate a hypothetical HCDA in SNR (Ref. 14, 15). These experiments were performed on 1/12 and 1/6 scale models and used as the explosive $KClO_4$. $Ba(NO_3)_2$, Mg and a small amount of dynamite as the booster. The experiments were carried out using water in the place of molten sodium. The explosive p-V curve was measured in a flooded quarry using charges of 1.65, 7.35 and 18.61 kg. The expansion of the gas bubble was measured and compared with predictions of the DEBUL code.

Tests were performed in a rigid water-filled 1/12 scale vessel without internals to evaluate the possible effects of confinement on the explosive charge. These experiments were analyzed using the Lagrangian REXCO, ASTARTE, ARES (Ref. 16) and the Eulerian code SURBOUM (Ref. 14). The results from the SURBOUM calculation of the p-V relationship and a REXCO calculation are compared with experimental results in Table II.

Table II

Times required for the water to hit the vessel upper lid

	TIME (10^{-6} s) D = 0	TIME (10^{-6} s) D = 0.150 m	TIME (10^{-6} s) D = 0.200 m
Experimental measurements	2545 ± 30	2590 ± 60	2645 ± 30
REXCO	2555	2670	2750
SURBOUM	2265	2413	2552

D = distance from the plug center.

Tests have also been performed on a 1/12 vessel model with a perforated plate and calculated using a modified form of SURBOUM to treat the flow through the perforations. These results show the efficiency of the perforated plate to reduce the coolant hammer effect on the upper lid.

The final test of this series has not been reported but consisted of a test on 1/6 scale SNR vessel with some internals. An 8 kg explosive charge was used to simulate a 370 MWsec accident.

KWZ (Karlsruhe) and AWRE (Foulness) are performing full scale fuel coolant interaction (FCI) experiments (Ref. 17). A series of tests are being performed with a full-sized SNR vessel in a flooded quarry to determine the maximum pressure capabilities of the vessel. The pressure generator uses a cordite charge in a perforated cylinder to generate the proper pressure-time profile. Upon completion of the full-scale water tests, experiments will be performed with about 5 kg of molten UO_2 interacting with sodium in an overstrong vessel.

3.3.6 Summary

The HCDA simulation experiments are valuable to provide a qualitative understanding of the consequences of FCI accidents and provide benchmarks for calibration and test of the accident prediction codes. Referring to the discussion and comparison of these experimental results with structural codes, good agreement is found in the mid-vessel region and in the extremes the disagreement is about 1% in hoop stress. The largest remaining uncertainty is the strength of the FCI explosion. The large scale FCI tests in the SNR vessel should be a valuable step in resolving the accident source strength.

REFERENCES

1. J.F. Proctor, W.R. Wise and L.P. Walker, "Response of Enrico Fermi Reactor to TNT Simulated Nuclear Accidents," NOLTR 62-207, 1964.

2. N.J.M. Reese, "A Model Investigation of Explosion in Simple Tank Fast Reactors," Proc. of the Conf. on Safety Fuels, and Core Design in Large Fast Power Reactors," October 11-14, 1965, ANL-7120, pp. 692-719.

3. Florence, A.L., Abrahamson, G.R., "Simulation of a Hypothetical Core Disruptive Accident in a Fast Flux Test Facility," Stanford Research Institute, Second Interim Report, November 22, 1971.

4. Florence, A.L., Abrahamson, G.R., "Simulation of a Hypothetical Core Disruptive Accident in a Fast Flux Test Facility," Final Report, HEDL-SRI-1, May 1973.

5. Ibid., Supplementary Volume, HEDL-SRI-2, May 1973.

6. G.R. Warren, Production of a Gaseous Explosion to Simulate the Thermal Interaction between Fuel and Sodium Coolant in Subassemblies of a Fast Reactor, Second Int. Conf. on Structural Mechanics in Reactor Technology, Berlin, 10-14 Sept. 1973, Paper E 1/6.

7. H. Beutel, K. Gast, "Large Scale FCI Experiments in Subassembly Geometry-Test Facility and Model Experiments," Second Specialist Meeting on Sodium Fuel Interaction in Fast Reactors," Ispra, Italy 21-23 Nov. 1973.

8. M. Eglemen- M. Namias (BELGONUCLEAIRE-Brussels, Belgium) H. Holtbecker (J.R.C.-EURATOM-Ispra, Italy), "Study of Nuclear Accidents by Chemical Explosion," Paper 39 of the Int. Conf. on Engineering of Fast Reactors for Safe and Reliable Operation. 9-13 October 1972, Karlsruhe, Germany.

9. Padilla, A., "Transient Analysis of Fuel-Sodium Interactions," Trans. Am. Nucl. Soc. 13, 375, 1970.

10. P.W. Bridgman, "Dimensional Analysis," Yale University Press, New Haven, Conn., 1949.

11. Baker, W.E., Westine, P.S., Similarity Methods in Engineering Dynamics, Hayden Book Company, Rochelle Park, N.J., 1973.

12. Fox, G.L., Stepnewski, D.D., Polentz, L.M., "Scale-up of Test Results from Simulation Experiments of a Hypothetical Core Disruptive Accidetn in the Fast Flux Test Facility," to be published.

13. D.D. Stepnewski, G.L. Fox, Jr., D.E. Simpson, R.D. Peak, "FFTF Scale Model Structural Tests," Proc. of the Fast Reactor Safety Meeting, April 2-4, 1974, Beverly Hills, Ca. CONF-740401-P2.

14. M. Eglemen - M. Namias (BELGONUCLEAIRE-Brussels, Belgium) H. Holtbecker (J.R.C.-EURATOM - Ispra, Italy), "Study of Nuclear Accidents by Chemical Explosion Experiments," Paper 39 of the Int. Conf. on Engineering of Fast Reactors for Safe and Reliable Operation. 9-13 October 1972, Karlsruhe, Germany.

15. M. Eglemen, M. Stievenart, H. Holtbecker, "Study of Nuclear Accidents by Chemical Simulation Experiments," Proc. of the Fast Reactor Safety Meeting, April 2-4, 1974, Beverly Hills, Ca., CONF-740401-P2.

16. K. Doerbecker (INTERATOM, Germany), ARES: Ein zweidimensionales Rechenprogramm zur Beschreibung der kurzzeitigen Auswirkungen einer hypothetischen unkontrollierten nuklearen Exkursions auf Reaktortank, Drehdeckel und Tankeinbauten gezeigh am Beispiel dis SNR-300," Paper A11-135 of the Reaktortagung 1972 (Deustches Atomforum) - 11-14 April, 1972.

17. K. Gast, R. Liebe, H. Will, H. Zehlein, N.J.M. Rees and G.R. Warren, "Simulated Vapor Explosion Experiments and Dynamic Elastoplastic Response of SNR Core," Proc. of the Fast Reactor Safety Meeting, April 2-4, 1974, Beverly Hills, Ca., CONF-740401-P2.

3.4 EBR Operational History

3.4.1 Introduction

The EBR-II reactor presently is the only operating LMFBR in the United States. Consequently, mere operation of the reactor gives some information regarding the durability of reactor components in an environment comprised of predominantly fast neutrons and liquid sodium. The EBR-II was designed in 1955 as a follow-up of the EBR-I reactor which underwent a melt-down incident in 1955.

In this section a brief history of the EBR-I reactor is covered, along with safety design principles learned from the reactor. The EBR-II reactor is covered in somewhat more detail, and finally some discussion is included of the impact of the EBR fuel irradiation program upon the LMFBR safety program.

3.4.2 EBR-I

The EBR-I reactor was a 1MWt reactor designed in 1948 to demonstrate fast reactor breeding and liquid metal cooling systems (Ref. 1). The first two core loadings, the Mark I and Mark II, consisted of enriched uranium slugs, NaK bonded to stainless steel tubes 0.448 in. outer diameter, spaced 0.494 in. on centers. The tubes were positioned at the bottom by the tube-plate, and above the core by a lower shield plate. The Mark-I fuel loading had spacer ribs on each steel jacket, but these were omitted for the Mark-II loading.

When operating the reactor, it was observed that a prompt positive temperature coefficient of reactivity existed, along with a slower-acting negative coefficient. It was during an attempt to observe this with the Mark-II core, by increasing the reactor power on a fairly fast period from a low power level, that the scram order was misinterpreted and a portion of fuel was melted.

The positive reactivity coefficient was later demonstrated to be due to fuel bowing. This was proved using a "rigid" Mark-III core, which consisted of uranium fuel coextruded with its zirconium jacket. Ribs on each jacket were fitted to provide very direct contact with neighboring fuel elements, and the entire assembly was clamped. The ribs contributed to stability by providing a large radial contribution to the power coefficient of reactivity and by eliminating the inward bowing of fuel rods during power increases. The following is a summary of information obtained in this respect from the operation of the EBR-I with Mark III fuel (Ref. 2).

> "The results of removing the stabilizing ribs from fuel elements demonstrated the existence of a strong positive reactivity effect which was associated with the inward bowing of fuel rods. The extrapolation of kinetic data obtained by removing the stabilizing ribs from one-third of the fuel elements gave $+2.06\times10^{-6}(\Delta k/k)$/kw for the full core with ribs removed. Since the prompt negative component of reactivity associated with fuel, coolant, and blanket expansion was -2.21×10^{-6} $(\Delta k/k)$/kw, the response of the "non-ribbed" reactor would have still been governed by a very small, but negative, prompt power coefficient.

> "Removal of the stabilizing ribs also produced an increase in the magnitude of the delayed structural component of the power coefficient. An empirical model describing the dynamic and static behaviors of the partially-ribbed core gave -2.21×10^{-6}, $+0.543\times10^{-6}$, and $-0.873\times10^{-6}(\Delta k/k)/kw$ for the respective prompt negative, rod-bowing, and delayed structural components of the power coefficient. These values may be correlated with those deduced empirically for the prompt negative and delayed structural power coefficient components for the fully-ribbed core, namely, -2.21×10^{-6} and $0.330\times10^{-6}(\Delta k/k)/kw$, respectively.

Not only does rib removal introduce rod-bowing, which gives rise to a prompt and positive feedback process, but it is the cause of a negative and extremely delayed structural component to feedback. This apparently was the result of delayed expansions in the structure of the lower shield plate. Experiments with a dummy shield plate established the existence of radial movements of the shield plate ligaments which, because of their contiguity with the fuel rod extension, effectively modified the core size following power changes. This effect was clearly negative and operated with a time dependence consistent with that analytically deduced from the Mark II test data. Because structural features such as the Mark II shield plate were eliminated in Mark III, no significant, long-delayed reactivity coefficient was observed in Mark III.

In summary, the EBR-I operating experience was a valuable contribution to the LMFBR safety program since it demonstrated the importance of providing the proper control system to prevent a catastrophic operator error, and the need for a rigid core design to help provide a negative feedback coefficient.

3.4.3 EBR-II Reactor

The EBR-II is a pool-type LMFBR with a present power rating of 62.5MWt. The reactor was originally designed as an engineering facility to demonstrate the engineering and operating feasibility of an LMFBR for central station power plant application (Ref. 3). By the time the plant became operational in 1964, however, the primary mandate for operation had shifted to that of an irradiation facility for the LMFBR program. Nonetheless the reactor and power system has been operated as a base-load station with a gross power of 20MWe which is in parallel with the utility power system at the National Reactor Testing Station (NRTS).

EBR-II represents the beginning of the "engineering phase" of the LMFBR development program since it was designed to demonstrate technical feasibility, with an emphasis upon design features that could be extrapolated to large central station applications. As such, it would appear to demonstrate an unqualified success of the state of technology in the early 1960's.

Many of the "power-station" attributes of EBR-II have been subordinated by its fuel-testing attributes, and thus the frequency of refueling shutdowns has been increased with a corresponding reduction of plant availability. However, these additional requirements have demonstrated the versatility of the reactor and power system and the reliability of the system for fuel handling, which is all performed remotely without the aid of direct visual observation. An important point to note about the refueling operations is that the EBR-II can be shut down from full power, a partial refueling of the core can be made, and the system restored to full power in less than 24 hours; this is in marked contrast to the major operations involved in refueling a light-water power reactor (Ref. 4).

Another important "spin-off" of the operation of EBR-II are such auxiliary programs as that for the identification of failed subassemblies in fast reactors. This program has been conceived and implemented at the EBR-II facility, and the experience gained is being applied to the Fast Flux Test Facility project and to the Clinch River Breeder Reactor Plant (Ref. 5).

Of course the change in the major objective of the reactor has meant that the EBR-II was not designed as well for irradiation testing as it might have been. For example, only after a few years of reactor operation was an instrumented subassembly used for providing actual measurements of sodium flow, oxide-fuel and cladding temperatures, and localized neutron flux, with which to check calculations.

As a summary of the EBR-II operations and its impact on the LMFBR program, the Appendix entitled "EBR-II Operations and the LMFBR Program Plan" provides a condensation of the material in WASH-1109, "The LMFBR Program Plan; Element 9 Physics," 1972.

3.4.4 EBR-II as an Irradiation Facility

A review of the use of EBR-II facility for fuel irradiation has been given by Kirn (Ref. 6). As pointed out, there were three early stages of operation in which the physical and neutronic characteristics of the reactor have changed. Through a gradual evolution, the irradiation tests have changed from those on the initial metallic fuel in a core with 70 to 80 subassemblies, to a larger core of 90 to 91 subassemblies with significant numbers of uranium-plutonium-oxide experiments.

The difficulty with doing irradiation experiments in the relatively small EBR-II reactor and attempting to extrapolate to conditions in a prototypic LMFBR environment is that the spectrum is generally harder, and different gamma heating rates and inlet and outlet coolant temperatures are encountered. In an LMFBR the three neutronic-related parameters that are of most interest to the large breeder reactor are fuel burnup, neutron fluence, and heat ratings (temperature). It is not possible to satisfy all three parameters in a single experiment in EBR-II; compromises and accomodations must be made.

For example, at a power level of 50-60MWt, the neutron flux in EBR-II is less than that generally envisioned in a large LMFBR. Therefore to obtain the heat production and temperature conditions expected, it is necessary to increase the fissile enrichment in the oxide fuels relative to the enrichment in a large LMFBR. Then EBR-II experiments have been able to meet the temperature and heat requirements of most of the presently proposed fuels, but the flux to produce these conditions is still that of EBR-II. Consequently the ratio of neutron fluence to burnup does not match the conditions in the large systems, so other complementary material irradiators must be performed in the reactor to assess independently the neutron damage effects.

A large portion of the irradiation program is devoted to separate irradiations of fuel cladding and reactor structural materials. On the other hand, there are experiments in the reactor whose fuel enrichment is typical of a large LMFBR, in which comparable fluence-to-burnup ratios are achieved but which have correspondingly lower heat ratings.

The success of the calculated burnup of various metallic fuel pins with those measured by post-irradiation radiochemical and mass spectroscopy can be assessed by the fact that for the first 70 some pins measured for burnup, the ratio of the average values of the measured to calculated burnup was 0.95 ± 0.05 (Ref. 6). These results were obtained over the range of heat ratings shown in the following table.

Fuel Element Material Type	Heat Rating, kW/ft Max.	Min.
(U,Pu)C	29	13
(U,Pu)O_2	22	2
U metal (5% fission alloy)		
50MWt	9	4
62.5MWt	11	5

For irradiation purposes it is common practice to characterize damage according to the fluence of neutrons with energies greater than 0.1MeV. Unfortunately, direct measurements of the flux or spectrum are not possible in EBR-II, but can be calculated with standard reactor codes and can be inferred from various activation measurements obtained inside the reactor. Typical values (as from Run 31 (Ref. 6) for the central portion of the core) are that 24% of the neutrons are above 1.0MeV, 88% are above 0.1MeV, and practically none are below 10keV.

An ever-present problem with irradiation experiments, of course, is the fact that the neutron spectra depends upon the axial spatial position. Although this effect is minor in the central rows of the core, near the depleted-uranium blanket in rows 7 and 8, a significant fall-off occurs.

Many of the neutron damage effects in materials are sensitive to the temperature of the environment. Except for occasional measurements in a particular configuration, the gamma heating is inferred from calculations which relate the gamma spectrum to the fast neutron scattering and capture. Thus the conversion factors for this are important and have been measured in the ZPR-3 critical facility.

3.4.5 The Hot Fuels Examination Facility of the EBR-II

During the conception and design of the EBR-II facility, a Fuel Cycle Facility was constructed adjacent to the EBR-II reactor to provide a pilot-scale plant for reprocessing, by pyromettalurgical methods, the fuel discharged from the EBR-II reactor. The reprocessing was accomplished remotely in hot-cells and included: Disassembly of reactor core assemblies; melt refining spent fuel pins to release fission produced gases from the fuel; replenishing, recasting, testing, and recanning the fuel-alloy rods; and reassembling components into fuel assemblies for return to the reactor.

Now that EBR-II is the prime facility for irradiating candidate fuels and structural materials in the LMFBR Program in the United States, the (renamed) Fuels and Examination Facility is devoted primarily to the examination of fuels and materials irradiated for the LMFBR program. This change in scope was accomplished by utilizing the fuel handling capabilities and conversion of the hot-cells to an examination facility. The closed cycle with the EBR-II reactor provides rapid recycling of experimental subassemblies and eliminates the need for transporting highly radioactive fuel materials.

3.4.6 EBR-II Operations: Experience Gained from Minor Incidents

As pointed out by Graham (Ref. 7), there have been at least three difficulties with EBR-II operations which can be avoided with a future LMFBR. One incident involved a pipe which had been cut during maintenance and the sodium was kept frozen with fans. A welder switched off one fan which was obstructing the welding operation, causing the release of sodium under pressure from the open end of the pipe. With improved maintenance procedures, including the depressurization of the sodium, the likelihood of recurrence of such an incident would be reduced.

A second incident involved the dropping of a fuel rod during fuel handling. This, too, was caused by an operator error, which involved an inadequate testing to insure the engagement of the top knob of the subassembly by the grapple. This could undoubtedly have been prevented with a totally automated fuel handling procedure.

A third incident involved the loss of bearings from an oscillator which was installed to do some response tests; the bearings jammed some of the control rod helical drives, although the safety rods were not affected. Not only was the design of the oscillator inadequate, but good quality control on the bearings was lacking.

3.4.7 EBR-II Operations: Fuel Irradiation Tests

EBR-II normally contains three types of fuel elements: driver fuel, encapsulated experimental fuel and unencapsulated experimental fuel. The driver fuel consists of stainless steel clad, sodium bonded, uranium-5 w/o fissile alloy rods. Since the facility was designed for this type of fuel, and its burnup is controlled to limit the failure probability to $< 10^{-4}$ at the 95% confidence level, the effects of inadvertant driver fuel failures have been minimal. In the encapsulated fuel tests, the experimental fuel element is sealed in a stainless steel tube with a stagnant sodium bond providing the heat transfer path from the fuel element to the capsule tube. Approximately 100 experimental fuel elements have been irradiated to cladding failure in capsules with no effects on reactor operation. In only two cases have the capsules containing defected fuel elements developed leaks (Ref. 8).

The majority of the experimental fuel elements in EBR-II (∿700 to 1000) are unencapsulated stainless steel clad $(U,Pu)O_2$ rods in subassemblies containing from 19 to 61 elements. The number of fuel elements in a subassembly is determined by the fuel element design and the internal subassembly hardware. In all cases the external dimensions of the subassembly are identical to a normal driver fuel subassembly. In these tests, the primary coolant is in direct contact with the cladding of the experimental fuel elements, thus a cladding leak results in the immediate release of fission products to the primary sodium and reactor cover gas systems. The potential effects of a cladding defect in this type of experiment are frequently related to the time scale involved. Thus a distinction is made between run-to-clad-failure (RTF) tests in which the test is removed as soon as the defected subassembly is located and run-beyond-clad-failure (RBF) tests where the experiment is continued for a significant burnup interval with a cladding defect. The purpose of the RBF experiments is generally to study sodium-fuel reaction and fission product release (Ref. 8).

The majority of the fuel experiments in EBR-II are performance tests in which cladding failure is not an objective. There are, however, approximately 100 $(U,Pu)O_2$ elements in the reactor that will be irradiated until cladding failure is encountered as part of the RTF program. In addition, RBF tests are in the planning stage. In the case of the fuels performance tests and the RTF tests it is very desirable from a programmatic viewpoint to detect the occurrence of a clad leak and identify the source as soon as possible. In the case of the RBF tests the problem is one of discrimination between the signals from the RBF test and a clad leak in a fuels performance experiment or an RTF test that may occur while the RBF test is in the reactor.

A summary of fuel rod failures from 1964 to the end of 1970 has been reported by Craig, et al. (Ref. 9).

PARAMETERS FOR IRRADIATED FUEL ROD FAILURES IN EBR-II

FAILED FUEL PIN	INITIAL O/M	PELLET DENSITY % T.D.	SMEARED DENSITY % T.D.	CLAD	MAX CLAD TEMP. °F	START-OF-LIFE POWER kW/ft	CALCULATED PEAK BURNUP at.%	MEASURED MAX ΔD/D % AFTER FAILURE
F2D	2.00	96.6	94.4	347	1059	16.0	12.8	34
F20	2.03	96.1	93.7	347	1066	16.3	7.2	22
F2F	2.00	96.8	93.7	I-800	1080	16.3	5.3	21
F4F*	1.975	89.1	85.8	I-800	1080	17.3	4.0	15
FOM	1.977	97.3	95.2	I-800	1247	12.0	6.4	11
E1H-33*	1.975	95.7	92.7	304	1149	15.6	9.1	24
F4D+	2.00	89.2	86.6	I-800	1080	17.2	4.0	0
X085++	2.00	89.9	85.0	316/CW	795	12.0	0.9	0.2
X106++	2.005	84.0	80.3	304	931	13.6	7.2	0

+ - F4D had gas release to capsule but no evidence of fuel-sodium interaction and very minor amounts of fuel-clad attack.

* All rods were 20 w/o PuO_2 with the exception of F4F which was 30% PuO_2 and E1H-33 was 25% PuO_2.

++ Unencapsulated fuel rods.

The results for the two unencapsulated rods were interesting in that no increase in diameter of the rods occurred, indicating that the failures were too small to allow a sufficient amount of sodium to enter the rods prior to termination of the irradiations, or possibly that the low oxygen content of the sodium in EBR-II dissolved the fuel-sodium reaction product before a sufficient quantity had formed to strain the cladding.

Based on the results of examinations of failed fuel rods and studies of the chemistry and thermodynamics of the reaction which occurs between sodium and mixed oxide fuel, an understanding of the events which occur to produce increases in diameter of failed fuel rods and ways to decrease or eliminate the diameter increases is being developed.

With no defected fuel in the reactor, the fission product activity in the primary cover gas is typically $\sim 1\text{x}10^{-3}$ μCi/ml ^{133}Xe and $\sim 2\text{x}10^{-3}$μCi/ml ^{135}Xe which results in no significant fission product activity in the reactor building. However, based on a mixture of gaseous fission products as measured in a high power $(U,Pu)O_2$ element, and a cover gas to reactor building leak rate of 1 liter per minute, the reactor building activity would reach the maximum permissible concentration of mixed fission products at a ^{133}Xe level in the cover gas corresponding to $\sim$1μCi/ml for a step release or $\sim$0.5μCi/ml for a continuous release. This means that a factor of $\sim 10^3$ increase in the ^{133}Xe activity due to the initial depressurization will result in restricted building access. A leak in a typical

EBR-II driver fuel element will normally not exceed these levels whereas a leak in a typical $(U,Pu)O_2$ element substantially exceeds these levels (Ref. 8).

In addition to limiting building access, the occurrence of a defected fuel element reduces the plant factor as a result of the operating requirement to immediately locate and remove defected fuel elements. The reactor is only operated with increased fission product activities in the cover gas for the purpose of locating defected fuel and for special tests. During these evolutions, the reactor is shut down when the fission product activities in the cover gas exceed 250 times the normal background. To minimize the time required to locate defected fuel subassemblies, all fuel experiments loaded into EBR-II for the past several years have contained a distinctive xenon tag (Ref. 8).

In conjunction with the signals observed from leaking fuel elements, it is useful to review the experience during the period March-December 1971, when cladding breaches resulted in five series of fission-product releases to the primary system of EBR-II. Four were positively identified with specific experimental subassemblies. These were, in their order of identification, X073 and X085, which contained mixed-oxide fuel; X082A, which contained high-burnup metallic driver fuel; and X106, which contained mixed-oxide fuel. The origin of the fifth release was never positively identified. Information of an inferential nature, however, indicated the involvement of low-burnup driver fuel (Ref. 10). The X073, X085 and X106 were unencapsulated mixed-oxide elements, while X082A was a standard Mark-IA driver element.

The release history for X073 indicated only a very small incremental increase in the ^{135}Xe in the primary system. The reactor shutdown was initiated by an abnormally high level of ^{133}Xe, although the fission gas monitor of the cover gas indicated no release. Since the fission gas monitor senses only short-lived xenon and krypton isotopes, it was first suspected that an encapsulated experimental assembly had failed. Only later, when xenon tag gas escaped, was the unencapsulated X073 assembly removed, and only then after an earlier assembly had been removed in an unsuccessful attempt to remove the failed assembly.

The release rate for xenon, never above 10^{-2} μCi/ml in the primary loop, never was at a sufficient level to activate any of the building alarm systems.

The X085 assembly was constructed with an intentional cladding defect such that it would fail during reactor operation after some estimated burnup (Ref. 11). The defect technique allowed a 0.005 in.-dia. hole through the cladding to "open" after an exposure in high-temperature sodium. The defect was 1/2 in. from the bottom of the fuel column, and consisted of the hole in the cladding, filled with a silver solder, which was covered with a copper patch on the outside of the cladding. The copper was covered with a nickel flashing. Dissolution of the copper by the sodium (by entrance of sodium at the ends of the patch) eventually allowed the release of the element gas pressure. The time for the release was dependent on the length of the copper dissolved and was adjusted to allow at least 100 hr of sodium exposure.

The primary objective of the test (Ref. 11) was to determine the magnitude of the fission-product inventory in the primary coolant system, as measured on the normal EBR-II reactor-monitoring system, when the cladding of a low-burnup mixed-oxide element "opened." Secondary objectives included the test of the programmed defect mechanism, an in situ test of the xenon-tag detection technique, and handling of subassemblies with exposed mixed-oxide fuel after cladding breaching. Also, this experiment represented the first in which a mixed-oxide fuel element was intentionally irradiated in EBR-II until fission products were released to the primary coolant system.

The response of the primary monitoring system was important because the magnitude of the fission-product release to the primary-system coolant and cover gas is important in formulating procedures to handle future releases. This low-burnup test, coupled with the forthcoming results of tests of a high-burnup element, can be used to modify the emergency operating procedures for releases to the primary system from oxide fuel elements. The release-to-birth ratios of various fission product isotopes might be used to determine effective holdup of fission products for an element of this heat rating.

It is important to note that when the X085 assembly failed the germanium-lithium detection system and the reactor-cover-gas monitor annunciated a substantial increase in cover-gas activity. The limits specified in the emergency operating procedures were soon exceeded, and an anticipatory shutdown was started (Ref. 9,10). Approximately 6-7 min. later, strong increases were noted in the signals from both channels on the fission gas monitor. Since no significant increase was noted in building radiation levels, as indicated by recorders in the control room, EBR-II Radiation Safety personnel entered the reactor building to obtain a cover-gas sample and to start a continuous gas sampler. A rough survey of the cover-gas sample indicated an increase from a normal level of 0.5 to about 45mR/hr.

With ten minutes or so, all readings from the reactor cover gas monitor and fission gas monitor were off scale. The reactor building was again entered, and changes were made in range settings to bring the readings back on scale. Shortly thereafter, the reactor-building radiation levels as indicated by control-room recorders began to increase. An EBR-II Radiation Safety technician equipped with supplied air reentered the building about an hour later to obtain another cover-gas sample and to retrieve an air sample.

Soon thereafter, a continuous air monitor located on the operating floor indicated an increase to approximately 10,000 counts/min from a normal level of 1500. At this time, partial building-isolation actions were initiated. No increase was noted in the activity level of the exhaust air. During the following hour, two building radiation alarms also were actuated, one located on the operating floor and another in the subbasement.

The results of the various cover-gas monitoring activities revealed that the ^{133}Xe concentration in the cover gas increased from an ambient level of about 1.0×10^{-3} to about $0.36 \mu Ci/ml$ (see Fig. 1). The release of ^{135}Xe was smaller. The concentration of this activity increased from 0.002 to $0.25 \mu Ci/ml$.

The xenon-tag technique was used in an effort to identify the leaker. Approximately 5 ft^3 of cover gas were cold-trapped on activated charcoal. The xenon fraction was then collected and analyzed with a mass spectrometer. The results of these analyses demonstrated conclusively that a xenon-tag mixture had been released and that the mixture corresponded, with a high degree of certainty, to that incorporated in subassembly X085, the first run-to-failure experiment. This is particularly impressive since the actual fission gas released was less than 1% of the inventory in the pin; this was attributed to the lack of pressure equalization between the element and the coolant or to fission-product holdup in the fuel pellets.

In summary, the failure of the X085 experiment was sufficient to increase the ^{133}Xe activity level by a factor of nearly 400, and to activate building alarm annunciators. Of even more interest, from the point of view of LMFBR safety, is the knowledge of what fraction of the activity was located in the sodium, what fraction was in the cover gas, and what fraction of gas escaped to the building itself.

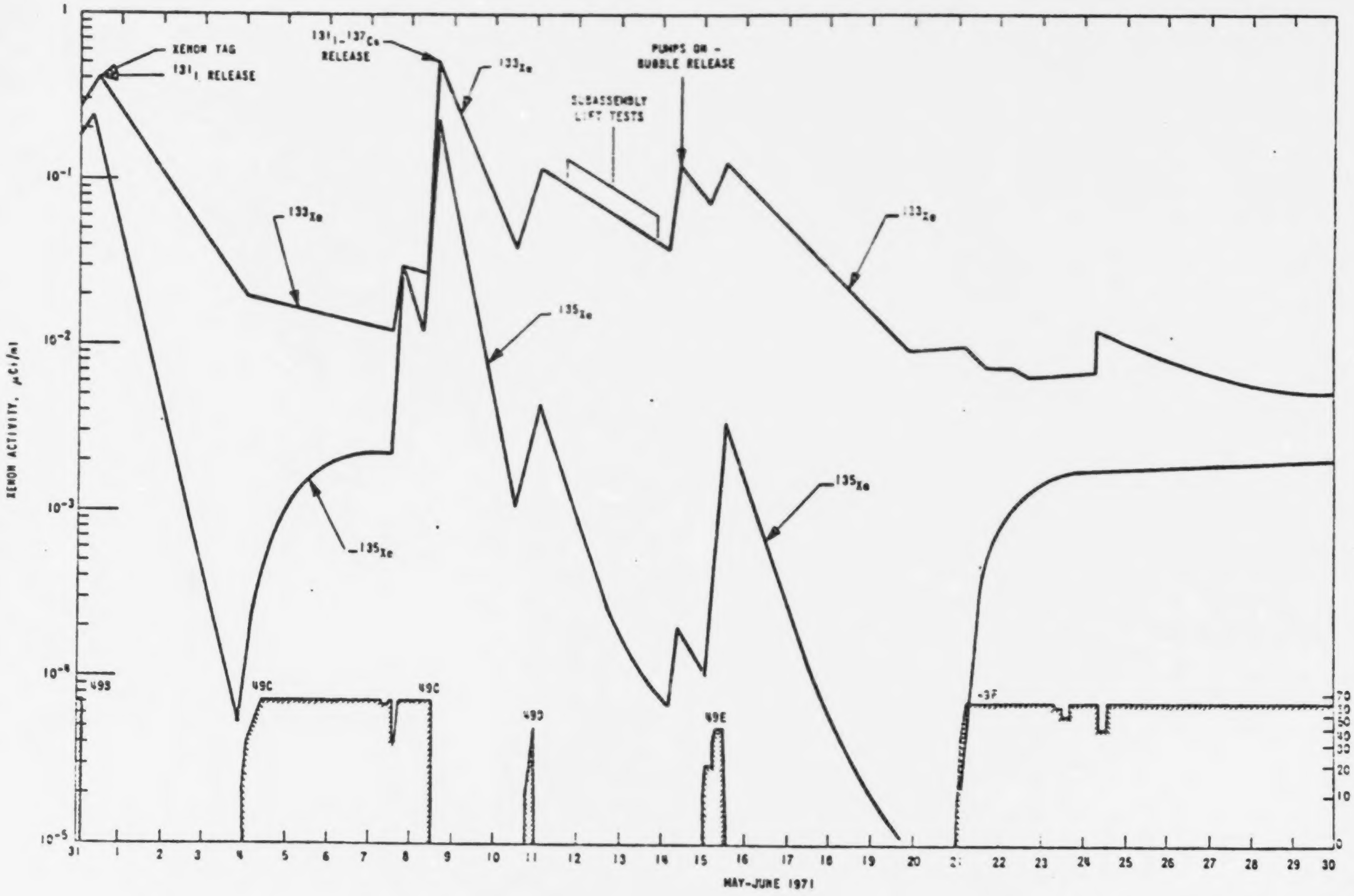

Fig. 1 ^{133}Xe and ^{135}Xe Activities in the Cover Gas, May-June 1971

It must be recognized, however, that even with such information available for the release of fission gas in EBR-II, the results could not be extrapolated to other LMFBR systems. This is because the entrainment of fission gas in the sodium is a function of the engineering design of the reactor, and the release to the cover gas is also specific to the EBR-II reactor. Furthermore, the release to the building is a function of the reactor design; in this respect it is important to note that EBR-II was never designed as a reactor for the testing of failed fuel, and that the design of the seals was probably inferior to that for such fast reactors as Dounreay in England, where such tests were planned as a part of the program under which the reactor was built.

The release from the X082A was a case in which extensive testing on and off for over a month was necessary for detecting the failed fuel assembly, and in which extensive release to the cover gas occurred. In this instance, however, there is no report of release of fission gas to the building sufficient to activate the building alarm mechanisms (Ref. 10).

Results for other fuel irradiation tests, besides X073 and X085, are summarized in Table I (Ref. 8). The ^{133}Xe and ^{135}Xe signals reported are based on the laboratory analysis of cover gas samples normalized to 62.5MW equilibrium conditions. While the operational fission gas and reactor cover gas monitors gave clear indications of a clad leak, the laboratory analysis of cover gas samples has been used to provide a quantitative basis for comparison. The signals are also described in terms of the time to reach the peak activity observed in the cover gas and the maximum release rate of ^{133}Xe to the cover gas. While these parameters provide a basis for comparison, the actual release history is frequently quite complex and hence is not well characterized by a few parameters.

One fact that is immediately apparent from Table I is that the annunciation of a clad leak in a mixed-oxide element in EBR-II is not a problem with the present background levels in the cover gas. The conduct of RBF tests in EBR-II, however, will raise these background levels making the annunciation of a clad leak somewhat more difficult. To control the activity in the cover gas during RBF tests, a recirculating cover gas purification system is very effective in reducing the ^{133}Xe level from the RBF tests while at the same time ^{133}Xe, because of its long half life (5.27 days), is effectively stored in non-defected elements. Thus, when a leak occurs in a non-RBF test, there will be a pulse of ^{133}Xe. This isotope is normally monitored by the RCGM, the GLASS and the laboratory samples. The same principle is even more effective when applied to the stable fission gases and xenon tags.

TABLE I. Fission Product Activity Signals in EBR-II Cover Gas

ubassembly Number	Type of Fuel	Burnup (at. %)	Peak Fission Product Activity in Reactor Cover Gas (μCi/ml)		Release Rate Characteristics from Defected Element	Remarks
			^{133}Xe**	^{135}Xe***		
X011	Encapsulated $(U, Pu)O_2$	3.5	5.3 (28 min)†	2.5 (28 min)	Step release; peak activity observed 28 minutes after start of release	Capsule leaked; essentially all the bond sodium was lost. Molten fuel and cladding were observed inside the capsule.
X073	Unencapsulated $(U, Pu)O_2$	2.9	1.4×10^{-2} (10 hrs)	3.4×10^{-3} (7 hrs)	Small ramp release (10^{-2} μCi/ml hr ^{133}Xe maximum release rate)	Source identified by a weak xenon tag signal(7), leaking element not yet verified.
X082A*	U-5 Fissium Mark 1A EBR-II Driver Fuel	3.3	0.70 (6 hrs)	0.22 (5 hrs)	Ramp release (0.2 μCi/ml hr ^{133}Xe maximum release rate)	Two leaking elements based on loss of sodium bond. One element has a crack over fuel, the other leak was not located.
X083A*	U-5 Fissium Mark 1A EBR-II Driver Fuel	3.4	0.52 (15 hrs)	0.17 (12 hrs)	Ramp release (0.2 μCi/ml hr ^{133}Xe maximum release rate)	Crack over fuel region. Some sodium remained in plenum. Plenum gas may not have escaped while in the reactor.
X084*	Unencapsulated $(U, Pu)O_2$	16.5	20 (17 hrs)	10 (9 hrs)	Ramp release (2 μCi/ml hr ^{133}Xe maximum release rate)	Small pin hole over the fuel region, maximum in reactor leak rate ~10 ml/hr (STP) total gas.
X085*	Unencapsulated $(U, Pu)O_2$	0.9	0.53 (4.7 hrs)	0.26 (1.4 hrs)	Ramp release (0.67 μCi/ml hr ^{133}Xe maximum release rate)	Contrived defect(9) near the bottom of the fuel column.
X106*	Unencapsulated $(U, Pu)O_2$	7.9	0.26(††)	3.5×10^{-2}(††)	Ramp release (3×10^{-2} μCi/ml hr ^{133}Xe maximum release rate)	Small pin hole at the top of the UO_2 insulator pellet, maximum in reactor leak rate ~0.014 ml/hr (STP) total gas.

*Intentional run to clad failure (RTF) experiment

**Normal full power background signal $\approx 1 \times 10^{-3}$ (μCi/ml)

***Normal full power background signal $\approx 2 \times 10^{-3}$ (μCi/ml)

†Time between first indication of release and peak signal for the major activity peak

††This release was a steadily increasing signal over a period of one week

3.4.8 Summary and Conclusions

In summary, the EBR-I and -II reactors have played an important role in the development of LMFBR technology in the United States, even though the reactors are not prototypic of future LMFBR designs. The EBR-I operating experience was a valuable contribution to the LMFBR safety program since it demonstrated the importance of providing the proper control system to prevent a catastrophic operator error, and the need for a rigid core design to help provide a negative feedback coefficient. The EBR-II likewise has played an indispensable role in the LMFBR program in that it has served as a fuel irradiation facility while functioning as the only operating LMFBR in the United States, for the several years, from which operating experience could be obtained.

Intentional run-to-clad-failure (RTF) tests have been conducted in EBR-II with both the uranium metallic driver fuel and stainless steel clad $(U,Pu)O_2$ experimental oxide fuel. Additional RTF tests are in progress and run-beyond-clad-failure (RBF) tests are being planned. All of the RTF tests completed to date have resulted in a rather slow depressurization of the fuel element gas plenum. The primary effect of these cladding defects on the operation of EBR-II has been a temporary increase in the reactor cover gas activity requiring a reactor shutdown.

The preparation of the reactor for the conduct of RTF testing of $(U,Pu)O_2$ fuel has required modifications to the experimental subassembly design and the fuel handling procedures/equipment to provide for the possibility of a severe clad failure.

To date these contingencies have not been required. The conduct of RBF testing in EBR-II will require further modification to the facility and operating procedures. The principal modifications are the installation of a cover gas purification system and a reduction of the cover gas to reactor building leak rate.

Based on the analyses completed to date it appears that the detection and location of an inadvertant defect during the course of an RBF test is practical. Depending on the sensitivity required, an on-line gas mass spectrometer may be desirable.

Because of the small size of defects which have occurred in the stainless steel clad $(U,Pu)O_2$ elements, special techniques were required to identify the defected fuel element and locate the leak site. The most sensitive technique for identification of the defected element has been γ scanning the gas plenum for ^{133}Xe. The leak sites were located by internal pressurization with helium while the element is immersed in ethyl alcohol.

In the way of recommendations for future work, it should be acknowledged that the basic objectives of the program are well-founded. In the future, however, it is hoped that irradiation tests with failed fuel can be used to provide more information about leakage from the cover gas to the reactor containment. At present, this information may have been obtained in the failure of the X085 subassembly, although it does not appear to have been published. It should be cautioned, though, that the information gained would be difficult to extrapolate to other fast reactors.

REFERENCES FOR EBR OPERATIONAL HISTORY

1. T.J. Thompson and J.G. Beckerley, *The Technology of Nuclear Reactor Safety, Vol. I., Reactor Physics and Control*, M.I.T. Press, Cambridge (1964).

2. R.R. Smith, et al., "Stability Studies with EBR-I, Mark III," Argonne National Laboratory Report ANL-6266, 1962.

3. L.J. Koch, et al., "Hazards Summary Report Experimental Breeder Reactor II," Argonne National Laboratory Report ANL-5719, May 1957, and ANL-5719 Addendum, Jan. 1964.

4. L.J. Koch, "EBR-II Plus 10: Is the U.S. Formula Right for Effective LMFBR Development?," *Nucl. News*, August 1974, p. 55.

5. P.B. Henault, G.J. Bernstein, L.F. Coleman, E.R. Ebersole, W.J. Larson, and R.R. Smith, "Identification of Failed Fuel Elements by Xenon Tag," *Trans. Am.Nucl. Soc. 12*, 102 (1969).

6. F.S. Kirn, "EBR-2 as a Fast Reactor Irradiation Facility," *Nucl. News*, March 1970, p. 62.

7. J. Graham, *Fast Reactor Safety*, Academic Press, New York, 1971.

8. J.R. Honekamp, J.F. Koenig, and T.D. Claar, "The Effects of Defected Fuel Elements on the Operation of EBR-II," *Proc. Amer. Nucl. Soc. Meeting on Irradiation Experimentation in Fast Reactors*, Jackson Lake Lodge, Wyoming, 435 (1973).

9. C.N. Craig, J.J. Regimbal, P.E. Novak, E.A. Aitken, W.E. Baily, and L.S. Rubenstein, "Behavior of Failed Fuel," *Int. Conf. on Engineering of Fast Reactors for Safe and Reliable Operation* (Karlsruhe, 9 Oct. 1972), CONF-721006, p. 605 (1972).

10. R.R. Smith, G.S. Brunson, E.R. Ebersole, R.M. Fryer, P.B. Henault, and J.F. Koenig, "Fission-Product Releases to the Primary System of EBR-II During 1971," Argonne National Lab. ANL-7956, 1972.

11. J.F. Koenig, E.R. Ebersole, C.C. Ford, R.M. Fryer, R.R. Smith, and R.V. Strain, "Performance in the EBR-II of a Mixed-Oxide Fuel Element with an Intentional Cladding Defect," Argonne National Laboratory Report ANL-7912, 1972.

APPENDIX

EBR-II Operations and the LMFBR Program Plan

Objective

The objectives of the EBR-II Project Physics task (Task 9-E-1) are to acquire and apply the analytical and experimental methods and techniques needed for the operation, safety, modification, tests, and characterization of the detailed irradiation environment of EBR-II as an irradiation facility for obtaining data needed by the LMFBR Program.

Scope

This task encompasses the adaptation and utilization of analytical and experimental techniques developed under the base program and the development of special methods where necessary for the reactor-physics-related requirements for the EBR-II project. These include the information needed for the operation, maintenance, modification, and characterization of the irradiation environment of the various EBR-II configurations.

Problems Addressed

Characterize the irradiation environment of the various EBR-II configurations, including the environment at the irradiation test locations.

Provide the analytical and experimental support needed to fulfill the reactor-physics-related EBR-II project needs.

Background Information

Because of the hererogeneous complexity of the EBR-II system, the frequent loading changes, and the need for detailed environmental characterization, physics analyses of EBR-II loadings, operations, modifications, tests, and environmental characteristics of each subassembly require extensive use of current methods of analyses as well as development and innovation of techniques. The tests and analyses of EBR-II therefore serve as indicators of the capabilities of current knowledge and methods of fast-reactor physics in satisfying the LMFBR needs. In addition, they point out areas requiring further development and data.

Following are some examples of experimental tasks performed on the EBR-II project:

-Levels of gamma heating relative to levels of direct fission heating deduced by transport analyses as checked and adjusted by the basic nuclear data of gamma and fission energy per fission.

-Space and energy distributions of neutrons and gamma flux, made by comparing calculated and measured values of critical masses, counter responses, thermoluminescent detectors, proton recoil, and foil dosimetry, in blanket, and in nickel- and steel-reflected cores.

-Capture-to-fission ratios of plutonium and uranium isotopes, calculated and compared with tests of foil activations, with consideration to core-loading details and axial-composition variations.

-Physics aspects of using a higher-burnup fuel pin (Mark-II) with a larger axial gas space.

-Tritium production in the EBR-II reactor, caused by the B_4C contained in high-worth control rods and experimental subassemblies of poisons.

Characterization of Irradiation Environment

This subtask covers the comprehensive characterization of the reactor and gamma environment required for the planning, execution, and subsequent interpretation of high-flux, high-temperature tests in EBR-II. The scope includes (1) calculation and maintenance of the burnup and fluence history of EBR-II, (2) correlation and coordination of the calculated burnup and fluence history with measured data from driver-fuel and experimental-irradiation samples, (3) planning and analysis toward an environmental instrumented subassembly, and (4) correlation of neutron- and gamma-dosimetry data for and from EBR-II.

Included are analyses of EBR-II neutron-dosimetry tests and EBR-II gamma-dosimetry tests. Results include correlation of the data in the context of most recent nuclear and thermal-hydraulic data to design and subsequent interpretation of in-core tests and irradiations in EBR-II.

Detailed test data pertaining to the local operating conditions in irradiation tests, such as neutron and gamma flux, flow, temperature, fluence, and power density, will be determined with one or more special instrumented subassemblies. The ultimate objective is to verify or to alter what are now believed to be rather conservative uncertainty factors for reactor and irradiation analysis. Data from these tests, coupled with data obtained from oxide-fueled and gamma-heated instrumented subassemblies, will be used to reduce analytical uncertainties. These data will be compared with results of neutronics, gamma, burnup, thermal, and hydraulic calculations to improve analytical correlations and confidence and to gain a firmer experimental basis for judging the potential capabilities of the irradiation environment.

Environmental neutron- and gamma-dosimetry results from the EBR-II tests will be analyzed and correlated with the results from the ZPR-III EBR-II mockup criticals. Data will be obtained from the Environmental Instrumented Subassembly (EISA). Data from the instrumented subassemblies will be analyzed.

Evaluation of self-powered neutron-gamma detectors for in-core use in EBR-II will be continued. The evaluations include experimental irradiation of detectors having rhodium, cobalt, and platinum as the emitter materials.

Work on noise or signature analysis for systems surveillance in EBR-II will be continued. Neutronic detectors, accelerometers, thermocouples, pressure transducers, and flowmeters may be used as signature detectors.

The first detailed burnup history for EBR-II will be generated and appraised. An extensive dosimetry test will be conducted with the new reflector and results correlated with dosimetry tests from the zero-power steel-reflected critical assembly. Multidimensional-neutronics-transport analyses, coupled with adaptation of nonequilibrium fuel-burnup codes, will be used to calculate the burnup history of the individual subassemblies during the EBR-II lifetime.

Methodology for a subassembly-delineated gamma history of EBR-II will be developed and a gamma history carried out. It will use thermoluminescent data from the critical-assembly mockups and gamma-heating data from EBR-II subassembly tests for correlation.

The differentiation between prompt and delayed gamma heating in an in-core subassembly will be analyzed. This will provide a basis for the performance of decay-heat tests. Similar attention will be given to heat production and cooling during postirradiation handling.

Capability for relative detailed tailoring of irradiation conditions will be further developed. Special tailoring for specific irradiations will be initiated, perhaps in the radial steel reflector, to provide an FFTF or LMFBR neutron spectrum for specific small-sample irradiations (e.g., fission-yield data).

3.5 HEDL FUEL STUDIES

3.5.1 Introduction

The primary objectives of the transient irradiation testing program at Hanford Engineering Development Laboratory (HEDL) have been to observe the performance characteristics of prototypic FFTF fuel pins during transient conditions and relate the results into transient performance models applicable to FFTF. The major areas of concern have been the failure thresholds and the fuel pin damage mechanisms while the pin is intact; those events and phenomena that occur after pin failure, such as molten fuel-coolant interactions and pin-to-pin failure propagation, are the subject of safety development programs conducted by ANL, GE, and others (Ref.1).

The HEDL fuel tests can be divided into two principal categories:

1. in-reactor power transients using the TREAT facility, and
2. resistive heating experiments with continuous gamma radiography of the sample, in addition to temperature and pressure measurements.

The objective of the first has been to correlate failure thresholds to fuel microstructures and local cladding conditions, and of the second to obtain input parameters for fuel motion models describing the response to rapid heating of unirradiated UO_2 and mixed oxide fuel irradiated in EBR-II.

3.5.2 Characterization of Microstructures (Ref. 1)

During steady state operation the mixed oxide fuel restructures, that is, the initial uniform distribution of density, porosity and fuel grain size changes as a function of time and temperature. The greatest changes take place very early in life and are a strong function of linear heat rate or local pin powers.

In general, the restructured fuel can be characterized and related to heat rate by the spatial distribution of microstructural features: 1) formation of a center void, 2) formation of columnar grains, 3) equiaxed grains, 4) unrestructured fuel, and 5) closure of the fuel-cladding gap.

If the steady state operation has been at a power greater than 9 kW/ft, columnar grain and central void formation will occur. The columnar grain region is produced by porosity migration along the temperature gradient and consists of high density ($\sim$ 96.5% theoretical density) fuel with radially-oriented grains. Densification of this fuel and gap closure leads to the formation of a central void region. The columnar grains and surrounding equiaxed grains retain very little of the generated fission gas within the fuel matrix. Unrestructured regions of the fuel are typified by relatively large fractions of retained fission gases. Thus, the spatial distribution of retained fission gas within the fuel pin is related to the spatial distribution of fuel temperatures as reflected by fuel microstructures.

3.5.3 Cladding Strain Mechanisms

An early test performed by HEDL was a transient overpower test in TREAT conducted on a mixed-oxide fuel pin that had been pre-irradiated in EBR-II to 8270 MWd/MTM (Ref.2,3). The pin consisted of 25% PuO_2 mixed-oxide sintered pellets clad in 0.250 in. diameter 304 stainless-steel tubing, and initially at about 300°F. After an irradiation with a peak pin power of 75 kW/ft with a pulse duration measured at half power of 0.97 sec, an analysis indicated that the instantaneous radial peak fuel temperature began at about 78% of the pellet radius and progressed toward the center. The peak temperature reached 4600°F at 2.65 sec after the peak transient power, and about 50 areal percent of the fuel was exposed to within approximately 500°F of the assumed 5000°F fuel melting temperature. A maximum cladding temperature of 1250°F was calculated to have occurred 1.85 sec after the power peak.

The test showed an increase in cladding diameter over the fueled length of the pin, with a maximum change of 0.55%. This was believed due to the differential thermal expansion between fuel and cladding because an insignificant amount of fission gas was released since there was no fuel melting. Hence such differential thermal expansion effects are now also considered even when analyzing the response of fuel pins in which melting has occurred.

Other results of the test were:

1. a marked change in the cracking pattern of the fuel.
2. a factor of 3 increase in gas release when compared to sibling nontransient tested pins.
3. the formation of 0.1 μm diameter bubbles with the fuel matrix.
4. grain growth and pellet interface fusion occurred during the test.

Under more severe transients, two other mechanisms causing cladding deformation may be more important than differential fuel-cladding thermal expansion:

1. volumetric expansion of fuel due to intragranular precipitation and growth of fission gas bubbles, and
2. internal gas pressure increase due to the increase in temperature of the existing gas and release of additional fission gas from the fuel during the transient.

As described by Scott et al., (Ref.1), rapid heating of equiaxed and unrestructured fuel leads to expansion of gases located at the grain boundaries and enhanced migration of matrix gas to the boundaries. The grain boundaries are separated by the rapid buildup and expansion of fission gases and localized release of fission gas results. Up to 4 volume percent expansion has been observed in fuel subjected to such an overpower transient. This behavior does not require melting of fuel to accomplish the release and has been experimentally observed in HEDL out-of-pile fuel heating tests (Ref.4) as well as in TREAT transient tests. Mechanisms for loading of the cladding by grain boundary gas release are not known at present (Ref.1).

The high temperature and high diffusion rates associated with temperatures approaching the melting point of the fuel can produce release of fission gas. Transient-induced fission gas release may occur by two mechanisms: 1) release of matrix gas due to fuel melting, and 2) release of gas precipitated at grain boundaries at temperatures somewhat below melting. Release of matrix gas by melting acts to increase pressure in the molten volume; transmission of this pressure to the cladding is dependent to a large degree upon the relative volumes of molten and solid fuel (Ref.1).

3.5.4 Models of Fuel Cladding Mechanical Interaction

The three main mechanisms for fuel cladding mechanical interaction control whether cladding ductility or cladding stress is the better basis for cladding failure criteria. A schematic of the hypothesized loading characteristics of the proposed failure mechanisms is presented in Fig. 1. (Ref.1). Figure 1a purports to show the difference between "primary" and "secondary" type loading.

Primary type loading is gas loading in which straining of the cladding does not significantly reduce the applied stress; then minor differences in the cladding ductility will not prevent failure when the applied stress exceeds the load-bearing capability. For such loading mechanisms, stress is the

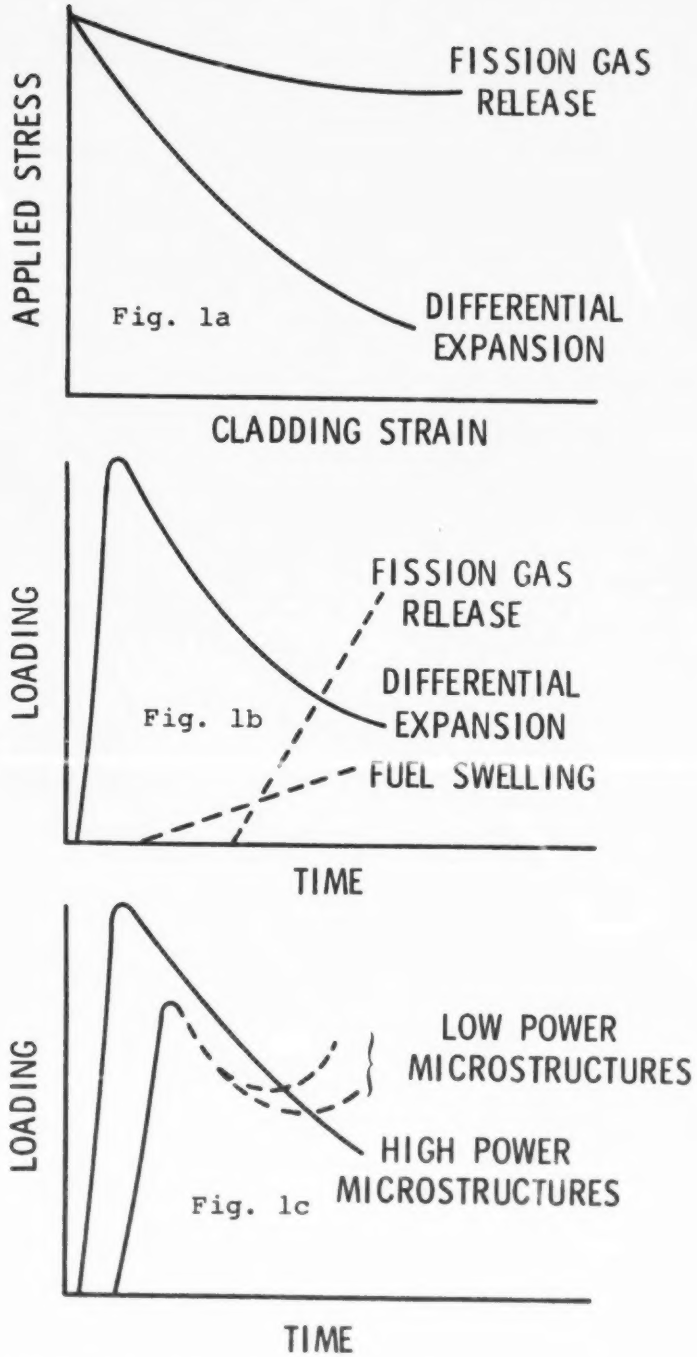

FIGURE 1. Loading Mechanisms (Ref. 1)

better criteria to correlate with failure. For example, transient-induced fission gas release will tend to be a primary type loading mechanism. For secondary-type loading such as thermal expansion, stress is relieved by cladding strain and cladding ductility would be the better failure criteria. For example, in high-power regions of the fuel pin with differential thermal expansion as the principal loading mechanism, minor differences in cladding ductility will affect failure position.

As shown in Figure 1b, and described by Scott et al., (Ref.1), fuel swelling due to intragranular precipitation and growth of fission gas bubbles will probably tend to be analogous to a primary loading mechanism (although stress may eventually diminish as the cladding strains) and a high rate dependence probably exists due to the kinetics of bubble precipitation and growth. Figure 1c illustrates how steady state fuel power level and microstructure may affect the loading characteristics. The time of initial cladding loading from differential thermal expansion is delayed for low-power microstructure because of a larger fuel-cladding radial gap. However, the low-power microstructures produce high loadings from fission gas release and fuel swelling relatively soon.

While modeling of differential thermal expansion processes is well in hand, attempts to mechanistically model and analyze the other phenomena have not been accomplished to date. Understanding of fuel pin response to thermal upset of the fission gas retention equilibrium is believed to be a key to satisfactory analytical representation of transient performance (Ref.1).

3.5.5 Implications of Cladding Properties From an Overpower Transient Simulation

As described by Scott et al., (Ref.1) during an overpower transient the temperature of the fuel pin cladding is rapidly elevated above its steady state service temperature. Simultaneously, the expanding fuel internally loads the cladding. To properly model the fuel pin transient behavior and to predict failure, the mechanical properties (specifically failure strength and ductility) of the cladding must be known under thermal and stress conditions encountered in transients. The temperature transient alters the strength, ductility and deformation behavior by allowing recover, recrystallization and annealing of the microstructure of the cold worked and irradiated cladding. Since the extent of the property alteration is dependent upon time as well as temperature, it is imperative that the mechanical properties be determined under appropriate temperature conditions induced by rapid heating. To accomplish this a specific testing program is underway at HEDL, utilizing a recently developed Fuel Cladding Transient Tester (FCTT) to generate the requisite mechanical property information on irradiated and unirradiated fast reactor fuel cladding under temperature ramp conditions.

As might be expected, the irradiated fuel pin cladding results may be characterized as exhibiting reduced ductility and lower-temperature failure during the transient than the unirradiated cladding. For example, some tests on prototypic Fast Test Reactor Type 316 stainless steel have shown a decrease in the failure temperature for an irradiated specimen relative to an unirradiated one from 1600 to 1000°F; this occurs in the region in which the irradiated cladding is most susceptible to low-ductility intergranular fracture due to helium embrittlement (Ref.5).

Under tensile stresses with conditions of low-ductility intergranular fracture, a grain boundary opening or microcrack can initiate and propagate from a highly stressed local region, without the remaining material across the section being significantly stressed. Consequently the tensile stress load-bearing capability of the material is reduced, even though the inherent hardness of the material is still high. At sufficiently high temperatures, however, above the 1000 to 1600°F range, the inherent strength of the cladding is sufficiently reduced that intergranular fracture does not proceed without appreciable prior deformation, so the failure temperature and load-bearing capability are not decreased.

It is apparent that steady state irradiation conditions and temperature transients can affect the loading of the cladding and its mechanical properties during a transient. To formulate a fuel pin failure criterion from the loading functions and cladding mechanical properties unfortunately would require detailed quantitative information which is currently unavailable, so integral failure criteria are being developed instead.

3.5.6 Failure Thresholds

Since all three strain mechanisms--differential expansion, gas release, and gas precipitation--are activated by, and are in some way proportional to, departure from the thermal equilibrium at steady state, a correlation parameter which expressed the degree of thermal upset of the system had to be chosen. That parameter was retained energy density, that is, the net energy density accumulated in the fuel due to the transient (Ref.1). To incorporate cladding properties, the calculated cladding temperature at the time and location of failure was selected.

In Figure 2, the most probable failure threshold for the three different microstructures is shown, as calculated from data recorded during TREAT tests (Ref.1). The indicated failure threshold for the high power microstructures is based on data obtained by transient testing X097 fuel pins at ANL and General Electric Series III transient irradiations. The threshold for intermediate power microstructures was derived from tests conducted on PNL-17 fuel pins by HEDL and ANL. The low-power failure threshold is based upon PNL-1 and -2 fuel pins tested by HEDL.

As described by Scott et al., (Ref.1) the limitations of this correlation are those common to most empirical correlations. The data are statistically small and the range of variables limited. In this case, the correlation applies to fuel pins between 2.5 and 5.0 a/o burnup with steady state cladding temperatures of ~925°F. Departure from these conditions requires extrapolation using out-of-reactor data.

In order to apply these criteria to FTR or LMFBR fuel pins with a complete range of microstructures it is necessary to consider the axial variation of cladding temperatures. The

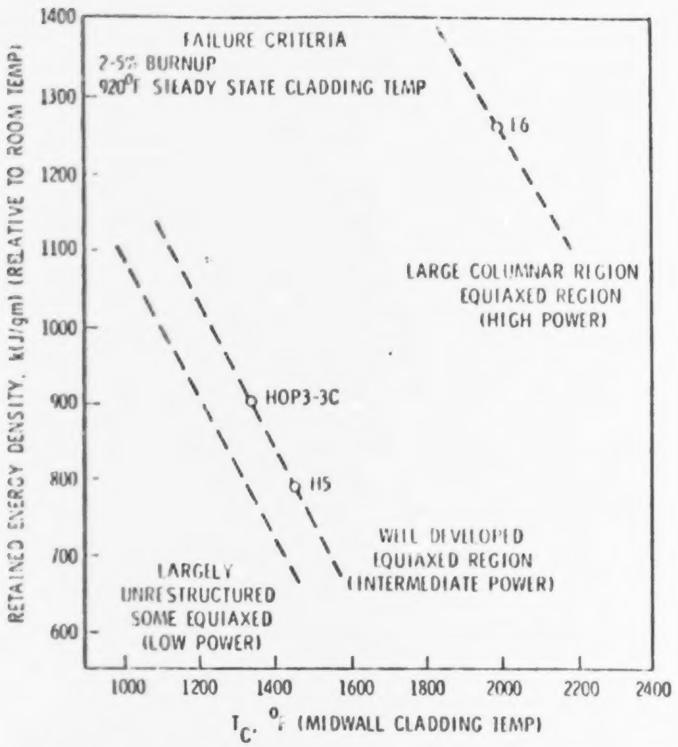

FIGURE 2. Empirical Failure Correlation and Application to FTR Pin (Ref. 5)

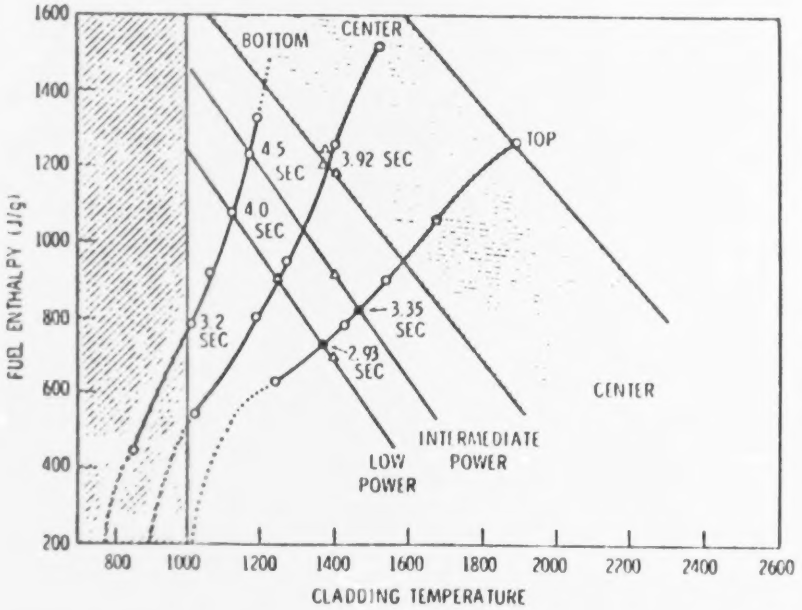

FIGURE 3. Failure Criteria for 11 kW/ft Pin (Ref. 5)

time dependence of cladding temperatures and fuel enthalpies for three axial elevations on an FTR fuel pin subjected to a 50 ¢/sec overpower transient is shown in Figure 3. The regions of low power microstructures lie between 0 and 5 inches at the bottom of the pin and between 28 and 36 inches at the top. The balance of the pin is restructured. Overlaid on Figure 3 are the empirical failure thresholds. The top of the fuel pin reaches conditions required for failure in low power microstructures at 2.93 seconds into the transient and the condition for failure of intermediate microstructures at 3.35 sec. The bottom of the pin reaches the same failure conditions at 4.0 and 4.5 seconds, respectively. Based on such considerations it is believed that fuel pin failure is biased strongly toward the region above the midplane (Ref.1).

3.5.7 Laboratory Studies on Melting and Gas Release Behavior of Irradiated Fuel (Ref. 5)

The objectives of the experiments in this area cover two important aspects of fuel material behavior: fission gas release behavior and fuel dynamics. The gas release behavior is being considered in terms of the temperature dependence for gas release and the associated mechanisms, as interpreted from fuel microstructure data. Fuel dynamics considerations are concentrated on determining temperature thresholds for fuel swelling, break-up, and ejection and the characteristics of ejected fuel.

The tests considered involve fuel element thermal transients which range in severity up to a postulated, unprotected loss-of-flow incident in which fuel surface temperatures rise at several hundred degrees per second, and a postulated unprotected overpower transient with fuel temperatures increasing by 500 - 1500°C in fractions of a second.

The major observations from these laboratory studies applicable to fuel motion considerations in safety analyses can be summarized as follows (Ref.5):

Significant gas release occurs from the solid :

1. Gas release data show significant release beginning about 2000°C.
2. Fragmentation can occur in high gas regions below 2600°C.
3. Fuel break-up and swelling results in expansion to fill available radial area.
4. Microstructures indicate extensive gas bubble precipitation in solid material at temperatures between 2000° - 2700°C.

Gas Release between 2000°C and melting can produce fuel motion :

1. Rapid heating rates and/or high gas concentrations tend to produce fuel dispersal.
2. Lower heating rates and/or gas concentrations tend to produce foam formation (fuel swelling) preceding total gas release.

REFERENCES

1. J.H. Scott, G.E. Culley, C.W. Hunter, and J.E. Hanson, "Microstructural Dependence of Failure in Mixed-Oxide LMFBR Fuel Pins," Proc. Fast Reactor Safety Meeting, CONF-740401-P2, p. 580 (1974).

2. G.E. Culley, J.E. Hanson, R.D. Leggett, and F.E. Bard, "Response of an EBR-II Irradiated, Mixed-Oxide Fuel Pin to an Overpower Transient in TREAT," Proc. Conf. on Fast Reactor Fuel Element Technology, American Nuclear Society, p. 657 (1971).

3. G.E. Culley, R.D. Leggett, and F.E. Bard, "Response of an EBR-II Irradiated, Mixed-Oxide Fuel Pin to an Overpower Transient in TREAT," Trans. Am.Nucl. Soc. 14 (Supp.1), p. 29 (1971).

4. E.T. Weber, O.D. Slagle, and C.A. Hinman, "Laboratory Studies on Melting and Gas Release Behavior of Irradiated Fuel," Proc. Fast Reactor Safety Meeting, CONF-740401-P2, p. 641 (1974).

5. D. Kramer, H.R. Brager, C.G. Rhodes, and A.G. Pard, "Helium Embrittlement in Type 304 Stainless Steel," J. Nucl. Mat. 25, p. 121 (1968).

ANL FUEL-COOLANT EXPERIMENTS

3.6 Introduction

Fuel-coolant interactions become of interest in accident sequences if a substantial amount of fuel can become molten and contact sodium. The interaction between molten fuel and coolant does not occur in a single distinct manner that can be described by one unique pressure-time history or by one unique thermal-to-mechanical energy-conversion ratio. Instead there are a number of different types of potential interactions between molten fuel and coolant (Ref.1).

Fuel-coolant interactions are of importance in two ways in whole-core accidents. First, they are of importance in characterizing fuel and coolant motion in an initiating accident where fuel pins fail before the reactor reaches prompt critical. This is the case where the TREAT experiments give directly applicable information. Secondly, they are of major importance in characterizing the damage potential from whole-core accidents if disassembly results. Two different cases are of importance here, depending on whether sodium is in the core or whether the core is largely voided at the time of disassembly (Ref.1).

In the hypothetical whole-core accident with sodium in, fuel-vapor-driven fragmentation and mixing of the molten fuel and coolant can be produced by the prompt burst. The cladding appears to be a real physical barrier to large-scale, nearly instantaneous, intimate mixing of the fuel and coolant.

In the hypothetical whole-core accident in small fast reactor like FFTF, with sodium out, fuel vaporization from the disassembly prompt burst can expel molten fuel from the voided core into the sodium above and also below the previously voided core. In this accident, molten fuel can also fall by gravity into sodium.

In full and partial flow-blockage accidents in single subassemblies, the possibility of a reentry upon molten fuel cannot yet be ruled out, although this appears to be very unlikely (Ref.1). More probable types of interaction are local coolant entrapment in molten fuel, local contact between small amounts of molten fuel coolant, and molten fuel falling into sodium.

The objectives of the Argonne National Laboratory (ANL) program on fuel-coolant interactions has been to perform in-reactor and laboratory experiments to establish the nature of pressure transients and mechanical work from the interaction of molten fuel and coolant under LMFBR accident conditions, and to develop mathematical models of these interactions. A significant portion of the work, that involving the S-E-, and H- series of tests conducted in TREAT, is discussed in the section on "TREAT Data and Pertinent Experiments." Therefore only a brief summary of these tests is provided here, with an emphasis upon the conclusions concerning fuel-coolant interactions. The primary emphasis will be focused on the laboratory experiments, which can best be understood only after consideration of some of the aspects of vapor explosive boiling and the models developed to describe it.

3.7 Summary of TREAT-Tests

The S- series tests were performed to investigate the transient pressures generated and mechanical work done by the meltdown of clad fuel pins in sodium under conditions of very energetic, overpower transients and of prompt-burst disassembly of a nearly unvoided LMFBR core. The most important result of these tests has been the demonstration that there were no energetic coherent interactions of the molten fuel and coolant of the sort calculated with some large-scale limiting-type accident-analysis models. Furthermore, even after generation of high fuel-vapor pressures before cladding failure in the S-11, test fuel-vapor-driven fragmentation and mixing did not occur as a mechanism for achieving an energetic fuel coolant interaction. Rather, the vaporized fuel was the only fluid capable of performing expansion work, while the liquid sodium acted as an energy dissipative fluid rather than a working fluid (Ref.2). Apparently in the S-11 test the molten UO_2 flashed upon entry into the liquid sodium and the fuel vapor prevented mixing of molten fuel and coolant. This is correlated well with laborabory experiments, to be discussed next.

In summary, in prompt burst or mechanical disassembly situations involving two-phase (liquid and vapor) fuel, the mechanical work appears to be bounded by the fuel vapor expansion work alone, and can be considerably reduced in analytical calculations by accounting for condensation and heat losses to the sodium and cold structures.

In the overpower transient tests in the E-series and H-series, and the L-series tests for the loss-of-flow, there has been no indication of the type of interactions commonly referred to as a vapor explosion. For the loss-of-flow incident, this conclusion had been expected since the molten fuel is produced at a time when the fuel zone is void of sodium and reentry of sodium is unlikely because of a combination of clad plugging and sodium vaporization from hot steel at the axial extremes of the test section.

Eventually, however, local contact would occur in a loss-of-flow incident, leading to nucleate and/or film boiling which will provide sufficient vaporization to prevent coherent mixing between fuel and the liquid sodium. The molten fuel is slowly quenched, which results in heat transfer rates sufficiently slow that heat losses and condensation effects will prevent any significant pressurization.

3.8 Some Aspects of Explosive Boiling for a UO_2-Na System

An important distinction between UO_2-Na and other systems potentially capable of explosive boiling is that the initial contact temperature is substantially below the homogeneous nucleation limit (see Fig.1). Furthermore, because of the apparent excellent wetting-characteristics at elevated temperatures, it is reasonable to assume that the initial interface temperature is well below the characteristic spontaneous nucleation temperature corresponding to initial liquid-liquid contact; this suggests that the UO_2-Na system provides for considerable time to allow the homogeneous nucleation limit to be approached (Ref.3).

It is important to note that the steel-Na system appears potentially much more explosive than the UO_2-Na system (Ref.3). This is because the steel-Na may achieve explosive boiling conditions immediately upon contact, prior to reaching the boiling point for steel (see Fig.1). Because of excellent wetting at elevated temperatures, the spontaneous nucleation threshold is very close to the homogeneous nucleation limit. In spite of these preliminary findings, however, a much better understanding of what constitutes the necessary constraint associated with an energetic vapor explosion will be required to determine whether steel-Na vapor explosions are possible in the LMFBR environment (Ref.3).

3.9 Models Developed to Describe Vapor Boiling

Early work on the phenomenon of sodium-fuel interaction for fast reactor safety analysis indicated an upper bound of 30% for the conversion of fuel thermal energy into mechanical (Ref.4). An energetic interaction of this magnitude could produce sizable structural damage, and hence this study formed a key role in the formulation of the experiments to study fuel-coolant interactions. All S-, E-, and H- series tests in TREAT, however, have produced energy conversion ratios at least two orders of magnitude below this thermodynamic limit, and hence there has been an effort to develop other models to better describe the data.

One of the more successful of these models is that associated with the first attempt to interpret the voiding rates obtained from an in-pile, fuel-failure experiment in the TREAT reactor in terms of a molten fuel-coolant interaction (Ref.5). Admittedly the analysis was developed for, and compared to, results for a single prototypical pin, but was successful in reproducing the first series of events for the experimental voiding history.

For the H2 experiment it was verified that two different energy processes occurred during the interaction. Initially fuel, cladding, and inert gases entered the coolant channel, resulting in slow vapor growth. This was followed by partial vapor collapse. The single-bubble thermodynamic model developed to analyze the experiment included (Ref.5):

1. The effect of the formation of condensate at cold boundaries.
2. A mixing period from the time when voiding first started to the time when rapid expulsion commenced, in order to better approximate the amount of vapor generated during fuel ejection.

It was assumed that the heat transfer from the fuel particles is controlled by the transient heat conduction in the particle. Also, the surface resistance at the fuel-coolant interface was neglected, and the boundary condition at the fuel outer edge was taken as the equilibrium temperature of the expanding sodium bubble. In the simplifying approach taken in this analysis, the fraction of fuel which interacts with the sodium was defined to represent the net heating rate and an interaction zone was specified which approximates the conditions existing during the transition region from slow to rapid vapor growth.

The most important conclusion from the comparison of the analytical model and experimental results is that the formation of condensate at the cold boundaries significantly reduces the amount of energy imparted to the expanding vapor bubble, which in turn limits the extent of the thermal-to-mechanical energy conversion process to values very much lower than the upper bound of 30%.

Overpower transient tests run with irradiated pins, such as the E3, E6, E7, and H5 tests, necessitate further modifications in modeling, because failure occurs prior to fuel melting. In the case of the transient which was not shaped, as in the E3 test, larger pressure pulses and energy conversion ratios were obtained than with fresh fuel pins. These are largely explained by the internal pressures from fission gases trapped in the oxide and subsequent expansion upon failure of the fuel pin. The fission gases appear to blanket the fuel fragments rather than providing a mechanism for rapid fuel dispersal and mixing with the coolant.

For the E6, E7, and H5 tests involving shaped transients and irradiated fuel, the coolant flow perturbations were so mild that the work done on the coolant in these tests cannot at present be assigned to even a mild sodium vapor event. The coolant expulsion observed in these tests can be readily explained by release of gas from the test pins (Ref.6). Work is currently underway at ANL to better characterize the fission gas release rate, thereby providing for better interpretation of any possible interactions between fuel and liquid sodium, and its effect upon transport of fuel.

One other ANL modeling effort should be mentioned because it resolves the dilemma of explaining the explosive vapor growth observed when liquid sodium was injected into sodium in small-scale, out-of-pile laboratory tests conducted at ANL (Refs.7-9). It was suggested that liquid sodium globules can be entrained and wet the liquid UO_2 surfaces when small amounts of liquid sodium are injected into a crucible containing molten UO_2; the lack of nucleation sites in the liquid-liquid-like system results in the overheating of the sodium until homogeneous nucleation occurs (Ref.10).

Such a phenomenon would appear impossible in a reactor environment, where fission gases and fragments, as well as solid materials and gas bubbles entrained in the liquid sodium, would promote boiling prior to reaching the threshold for homogeneous nucleation in sodium. As a consequence, only mild interactions of the type observed in the TREAT in-pile experiments would be expected.

3.10 Laboratory Experiments

The ANL out-of-pile experiments recently have been concentrated in two areas. The first is an investigation of large-scale thermal interaction studies to experimentally verify the vapor explosion model of Ref. 10. The second is a large-scale investigation of the energetics and the fragmentation resulting from molten-UO_2-sodium contact.

Earlier experimentation has demonstrated that one necessary condition for vapor explosions is the intimate contact between two different liquids at widely different temperatures. Comparison of other experiments (Refs.8,9) with results form the TREAT series suggests that a sharp thermal threshold exists for the onset of thermally explosive events; this threshold can be extracted from the model of Ref.10. This model proposes that the interface temperature upon contact of the two liquids must be greater than the spontaneous nucleation temperature of a cold working fluid for a large-scale coherent vapor explosion to occur.

In order to test the proposed mechanism, proper simulant fluids and reactor materials were required which would enable the temperature of the hot fluid to be varied over a broad range.

Freon-water and Freon-mineral oil systems were selected (Ref.11) because they offer this flexibility and have been demonstrated to be explosive systems under the proper thermal conditions. The four configuration modes tested were (Ref.11):

a. Freon(-12 or -22) dumped into a hot liquid (water or mineral oil).

b. Water dumped into Freon-22

c. A subsurface injection of water into Freon-22

d. An above surface injection of water onto Freon-22

The Freon-22-water, Freon-22-oil, and Freon-12-oil tests all demonstrated good agreement with the interface temperature, homogeneous nucleation model in that a strong thermal threshold behavior was observed within the uncertainties surrounding the theoretical result. When water was dumped into Freon-22, the basic trend of agreement remained, although the results were less distinct (Ref.11).

The subsurface injection of water into Freon-22, including tests under critical flow conditions, was done in support of basic modeling activities for the in-pile S-series tests and for the study of fuel injection into the upper plenum. The basic experimental information desired from these tests was the interaction behavior of a system, which has been clearly shown to be explosive, when the mode of contact is for injection of the hot fluid into the cold working fluid under two-phase critical flow conditions.

For the same temperature ranges, the explosive interactions for this contact mode do not produce pressures as large as those resulting from the dumping studies. One reason is that when the initial water temperature is equal to or greater than 130°C, the water is being injected under two-phase compressible flow conditions and as such is expanding radially as it leaves the mouth of the injector. As a result of this radial expansion, the higher density liquid phase responds less to the radial pressure gradients than the lighter vapor phase which generates a preferential distribution with the lighter vapor phase on the outside of the exhausting jet with the liquid concentrated in the middle. Such a flow configuration means that the large scale intimate liquid-liquid contact, that is required for vapor explosions, is impeded by the vapor layer that separates the two liquids. Therefore, although the basic thermal requirements for large scale vapor explosions are satisfied, the liquid-liquid contact requirement is not (Ref.11). Under such conditions, the pressurization was slow compared to those rise times for the two dumping modes.

This result regarding the maximum interaction pressure and the injector pressure is in excellent agreement with the in-pile S-series tests where fuel was driven into sodium under its own vapor pressure. In the S-series tests, fuel pin failure occurred at various fuel energy levels but the maximum measured interaction pressure was essentially the fuel vapor pressure at pin failure. Therefore, these subsurface water-Freon tests give an excellent verification of the in-pile results. They also demonstrate the sensitivity of explosive energy yield to the system contacting mode (Ref.11).

The basic difference between the results of the above-surface and below-surface tests lies in the results for the critical flow injections; under such conditions, the above surface injections failed to record any interaction pressure at all, whereas the subsurface injections did record the vapor pressure of the water. It is theorized that this is due to the fragmentation of the hot liquid as it expands under critical flow conditions and the one-dimensional constraint provided by these above surface injections. This particular result is of basic importance because it appears that major interactions can be avoided under explosive conditions, if the hot fluid has been finally fragmented before it comes into contact with the working fluid (Ref.11).

In summary, these simulant fluid tests have clearly demonstrated the viability of the interface temperature homogeneous nucleation model as far as describing the on-set of large scale vapor explosions. They have also shown that this criterion gives necessary but not sufficient conditions for large scale events, and in addition, they have shown that the violence of such events is heavily dependent upon the contacting mode bringing the two fluids together.

Other out-of-pile experimental tests have been conducted by a subsurface injection of molten fuel, which was generated by a "thermite-type" reaction, into a sodium pool. The thermite type reaction begins with uranium and molybdenum trioxide powders and ends with uranium dioxide and metallic molybdenum. In addition, enough energy is released to increase the temperature of the reaction from room temperature to approximately 3200°C, and this is accomplished in about 1 sec (Ref.11).

The singly most important observation of these tests is that when the injector pressure is compared to the measured interaction pressures within the vessel over the same time span, the interaction pressures are always less than the injector pressure driving the two liquids together (Ref.11). This aspect is in excellent agreement with the Freon-22-water subsurface injection studies discussed earlier and also the in-pile S-series tests. A second observation is that for a subsurface injection of fuel into sodium, extensive fuel fragmentation is observed but no explosive events are detected (Ref.11).

More extensive fragmentation experiments, involving kilogram-scale, molten-UO_2-sodium interactions in an unrestrained geometry have been performed (Ref.12). The large-scale experiments were necessitated by the combined need to study both the energetics and the fragmentation. Since it has been demonstrated that there is a marked tendency of a wide range of molten metals to fragment upon quenching in sodium (Ref.13), it is conceivable that molten fuel produced in hypothetical accidents will form particulate debris which will settle on horizontal surfaces within the primary system. Such debris beds would have significant capability to transfer fission-product decay heat to the overlying sodium pool, and hence would have to be considered in the analysis of post-accident heat removal studies.

In the experiments, the entry of molten materials into the sodium was marked first by a rapid, nonlinear increase in the vessel pressure and then, after several hundredths of a second, by a rapidly increasing sodium pressure. The rate of sodium vaporization immediately following entry of the UO_2 into the sodium was estimated from the rate of pressure increase. Short-rise-time pressure pulses in the liquid phase were observed in the tests, and these sharp pressure pulses were in the same range as those reported in Ref. 7 with a single drop of UO_2 weighing at most a few grams; thus, the pulses observed in the large-scale tests were probably caused by local events involving only a few grams of UO_2 (Ref.13). The pulses may have been caused by the collapse of sodium vapor bubbles in the subcooled liquid.

It is encouraging that large-scale versions of the small-scale vapor explosions described by Armstrong (Refs.7-9) were not observed in the three interaction experiments. The observed interaction events can be described qualitatively as rapid heating with some boiling of sodium and with perhaps a few isolated short-rise-term events occurring in the liquid phase. Except for the very small energy content of these sharp pressure pulses, the heat available in the molten UO_2-Mo mixture was transferred rather slowly to sodium with a significant fraction of the heat producing sodium vapor. Most of the work potential of the interaction appeared as vapor at an elevated pressure with a negligible fraction as kinetic energy of expelled liquid sodium (Ref.13).

It seems likely that the final particles were not formed directly from quenching molten drops, but resulted from breaking of larger solid or partially solidified particles, perhaps because of thermal shock (Ref.13). The fragmentation process occurred over roughly 1 sec for the ANL experiments of massive UO_2 and a large unrestrained sodium pool, which is very different from the fragmentation times of a few milliseconds used in calculations to represent the pressure pulses observed in TREAT tests simulating fuel melting in the coolant channels.

It is interesting to note the results of the experiments upon the calculational results obtained with the FCI Parametric Model (Ref.14). The Parametric Model was used to calculate the liquid-phase pressures and sodium-slug velocities with input conditions to simulate one of the tests. With use of the surface area of UO_2 particles recovered after the interaction experiments, the Parametric Model predicted high heat-transfer rates, large, sharp pressure pulses occurring soon after UO_2 entry, and rapid movement of the restraining sodium column. When heat-transfer rates approximating the measured lower rates were employed in the calculations, no pressure pulses were predicted as well as no significant movement of the sodium column for times up to several milliseconds (Ref.13).

Hence results from the experiment, when used in the FCI Model, tends to corroborate the conclusions that:

1. significant progress has been made in the understanding of fuel-coolant interactions, and
2. fuel-coolant interactions in hypothetical reactor accidents, much less severe than once believed, can be expected to be at worst a minor problem.

REFERENCES

1. J.F. Marchaterre, H.K. Fauske, L. Baker, C.E. Dickerman, and R.W. Wright, "Experimental Studies of Liquid-Metal Fast-Reactor Accident Conditions," Int. Conf. on Engineering of Fast Reactors For Safe and Reliable Operation, CONF-721006, p. 763 (1972).

2. M. Epstein and D.H. Cho, "Fuel Vaporization and Quenching by Cold Sodium; Interpretation of TREAT Test S-11," Proc. Fast Reactor Safety Meeting, CONF-740401-P1, p.268 (1974).

3. H.K. Fauske, "Some Aspects of Liquid-Liquid Heat Transfer and Explosive Boiling," Proc. Fast Reactor Safety Meeting, CONF-740401-P2, p.992 (1974).

4. E.P. Hicks and D.C. Menzies, "Theoretical Studies on the Fast Reactors in Maximum Accident," Proc. Conf. Safety, Fuels, and Core Design in Large Fast Power Reactors, Argonne National Laboratory Report ANL-7120, p.654 (1965).

5. A.W. Cronenberg, H.K. Fauske, and D.T. Eggen, "Analysis of the Coolant Behavior Following Fuel Failure and Molten Fuel-Sodium Interaction in a Fast Nuclear Reactor," Nucl. Sci. Eng. 50, 53 (1973).

6. A.W. Cronenberg, M.A. Grolmes, and R.C. Doerner, "A Fission-Gas-Release-Assessment of the E7 Coolant Voiding Dynamics," Trans. Am.Nucl. Soc. 19, p. 262 (1974).

7. D.R. Armstrong, F.J. Tests, and D. Raridon, "Interaction of Sodium with Molten UO_2 and Stainless Steel Using a Dropping Mode of Contact," Argonne National Laboratory Report ANL-7890 (1971).

8. D.R. Armstrong, *in* "Reactor Development Program Progress Report," Argonne National Laboratory Report ANL-RDP-2, p.8.31 (1972).

9. R.P Anderson and D.R. Armstrong, "Laboratory Tests of Molten Fuel-Coolant Interactions," Trans. Am. Nucl. Soc. 15, p.313 (1972).

10. H.K. Fauske, "On the Mechanism of Uranium Dioxide-Sodium Explosive Interactions," Nucl. Sci. Eng. 51, p.95 (1973).

11. R.E. Henry, J.D. Gabor, I.O. Winsch, E.A. Spleha, D.J . Quinn, E.G. Erickson, J.J. Heiberger, and G.T. Goldfuss, "Large Scale Vapor Explosions," Proc. Fast Reactor Safety Meeting, CONF-740401-P2, p.922 (1974).

12. T.R. Johnson, L. Baker, Jr., and J.R. Pavlik, "Large-Scale Molten Fuel-Sodium Interaction Experiments," Proc. Fast Reactor Safety Meeting, CONF-740401-P2, p. 883 (1974).

13. D.L. Swift and L. Baker, Jr., "Experimental Studies of the High-Temperature Interaction of Fuel and Cladding Materials with Liquid Sodium," Proc. Conf. Safety, Fuels, and Core Design in Large Power Reactors, Argonne National Laboratory Report ANL-7120, p. 8.39 (1965).

14. D.H. Cho, "Modeling of Molten-Fuel Coolant Interactions," Trans. Am. Nucl. Soc. 15, p.314 (1972).

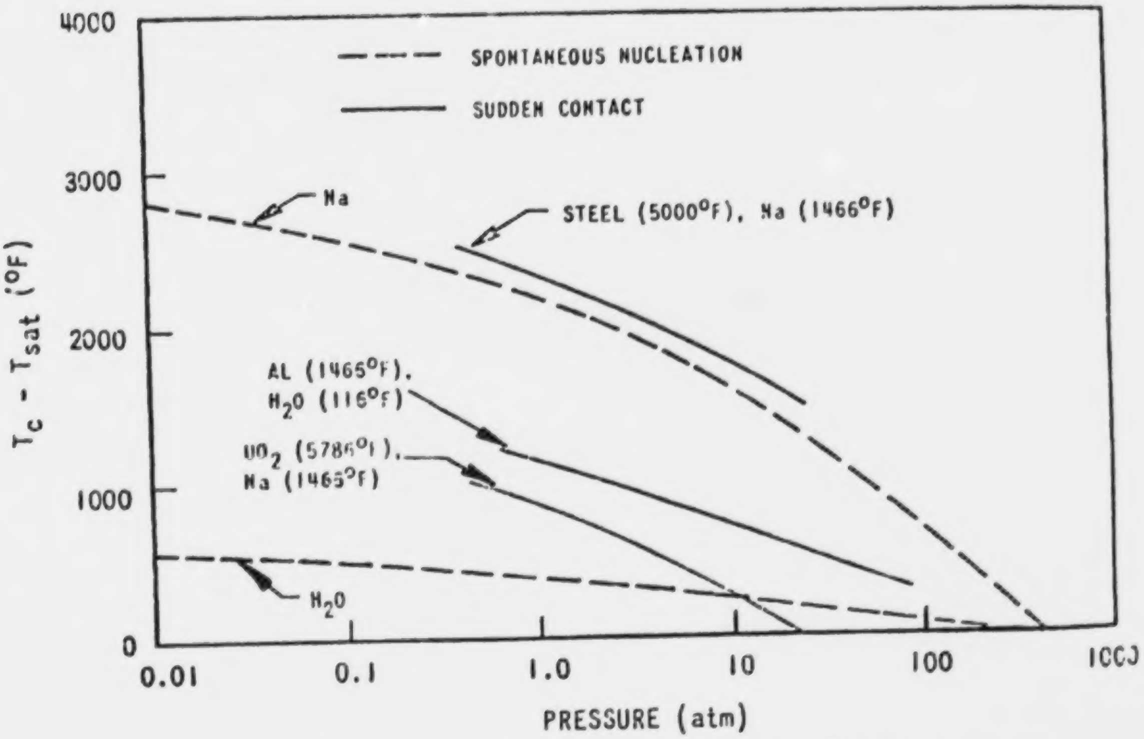

Fig. 1 Comparison between spontaneous nucleation temperatures and sudden contact temperatures for three different systems (Ref.2).

4.0 Accident Analysis Codes

Introduction

A large number of computer codes have been developed to help quantify accident behavior in LMFBR's. These codes vary greatly in their specific utility, degree of sophistication and extent of validity. Before describing the assumptions, limitations and characteristics of individual codes, a brief summary of the overall relations of these codes to safety analysis is given.

At this point in time, the mechanistic computer analysis of the two classes of accidents considered to scope LMFBR's (underflow and overpower) are divided into four phases as shown in Fig. 1. The analysis is broken into separate phases because quite different techniques are required to solve the various aspects of the overall problem. A brief description of each of these phases as related to computer programs follows using Figs. 1 and 2.

4.1 Outline

4.1.1 Initial Conditions

Initial conditions for the start of the accidents is a function of the LIFE (Ref. 1-4) series of codes of which LIFE-II (Ref. 4) is the most recent version. LIFE-II was developed to predict the steady state operational behavior of fuel pins taking into account the various phenomena that may occur. At

Argonne National Laboratory, however, separate initialization routines have been developed as a part of the accident initiation code, SAS (Ref. 5), thus reducing the necessity for information from LIFE-II. GRASS (Ref. 6), a fuel swelling and fission gas release model was developed as a subroutine to be included in LIFE-II although it has been mainly used as a stand alone code. Other LMFBR steady state fuel behavior codes in existence today include: BEHAVE-2 (Ref. 7), FMODEL (Refs. 8, 9) and GAPCON (Ref. 10). These codes have not received the emphasis that LIFE-II has in recent years.

4.1.2 Accident Initiation

This phase of mechanistic accident analysis involves a calculation of the core-neutronics and thermal behavior up to the point of loss-of-subassembly geometry as shown in Fig. 2. Since most LMFBR designs have used rigid subassembly ducts, the intact subassemblies are only coupled through inlet and outlet thermal-hydraulic conditions and reactor power. Subassemblies with similar power, flow and irradiation conditions are generally lumped together into groups for the purpose of analysis. All the subassemblies within a given group, or "channel", are assumed to behave identically. Phenomena such as transient thermal-hydraulics, sodium boiling, fuel-pin mechanics and failure, cladding and fuel motion, and fuel-coolant interactions are treated with one-dimensional models. Multichannel codes of this type which were developed under USAEC sponsorship are the FREADM (Ref. 11), MELT (Ref. 12), and SAS (Ref. 5) systems. The original purpose of these codes was simply to give a reasonable and conservative accounting of the reactivity effects in order to provide initial conditions for the core disassembly codes, although the phenomenological modeling has become more detailed in the latest versions of the MELT and SAS codes. These codes will be discussed further below as they contain the most recent and sophisticated modeling.

4.1.3 Disassembly Analysis

The disassembly phase of the calculation is entered when a prompt-critical excursion is induced and is shown in Fig. 2. The rapid heating and vaporization of the fuel produce high pressures that disassemble the core and thereby end the power burst. The disassembly process was first described by a model developed by Bethe and Tait (Ref. 13). In their approach, the core was treated as a homogeneous fluid so that the material motion during disassembly could be calculated using a hydrodynamic approach. The calculations were done in spherical geometry. The reactor power was calculated using point kinetics with first-order perturbation theory to estimate the reactivity feedback associated with the material motion.

A number of variations and improvements have subsequently been made to this basic approach (Ref. 14). Doppler feedback was included, improvements were made to the equation-of-state used to estimate the pressures, more accurate neutronics were implemented in some cases, and the capability for doing calculations in two-dimensional (r,z) geometry was added. A number of disassembly computer codes have been developed in the United States as successive improvements were made (Refs. 15-18). One of the most recent of these is the VENUS-II (Ref. 19) code developed at Argonne. Fig. 3 discusses the features of existing disassembly codes.

VENUS-II calculates the disassembly motion by a direct numerical solution of the two-dimensional (r,z geometry) hydrodynamics equations. Since the density changes associated with material motion are explicitly calculated, a more accurate density-dependent equation of state can be employed. A number of refinements have been developed to increase the applicability of the code to the calculation of mild excursions. This code will be discussed in more detail below.

4.1.4 Damage Evaluation

During or following reactor disassembly, the rate at which the thermal energy released in the transient can be converted to work must be established. This is used to evaluate the potential damage that the excursion can cause to the system. Work can either come from the expansion of the core materials themselves or the interaction of these materials with the sodium coolant and its consequent vaporization and expansion. Early studies of the damage potential of core disruptive accidents assumed that the work on the surrounding reactor structures would be done by the expanding fuel materials. As larger oxide-fueled reactors began to be considered it was recognized that the transfer of heat from the high temperature fuel to the sodium could considerably increase the potential work available to do damage. Hicks and Menzies (Ref. 20) point out the maximum work potential that could result if heat transfer to the sodium were sufficiently rapid. Since very high heat transfer rates had been observed in reactor accidents (SL-1, SPERT) attention turned to predicting these rates by assuming fragmentation of the fuel into sodium. Typically, this was done parametrically by varying the fuel particle size and mixing time and calculating the resulting heat transfer rates as a basis for assessing damage potential. Typical results of this type of calculation have been reported by Cho (Ref. 21). An excellent review of work-energy conversion has been given by Padilla (Ref. 22).

Since the heat transfer rates in these parametric models depends directly upon the particle size and mixing times, efforts have been made to establish the mechanisms by which mixing and fragmentation of fuel materials could take place (Ref. 23). It now appears that these mechanisms are sufficiently slow that they are not of concern in damage evaluation but are still of interest in assessing the course of accident behavior. Fauske (Ref. 24) discusses the current understanding of processes by which heat transfer can be made sufficiently rapid to be of concern in reactor damage evaluations. Because of its high thermal conductivity, the possibility of high temperature molten steel interacting with the sodium must be carefully evaluated.

Once the pressure source term has been established, the response of the system can be analyzed. This is usually done with a hydrodynamic calculation of the pressure propagation coupled with an analysis of the structural response of the important system components. The REXCO series of codes developed at ANL (Ref. 25) is widely used for this purpose and will be discussed further below. In addition assembly wrapper damage evaluation codes will be briefly described.

4.1.5 Postaccident Heat Removal

The final phase in the analysis is an evaluation of the postaccident heat removal (PAHR). The objective is to analyze the long-term decay heat removal from the fuel following a disruptive accident. That is, one ultimately wants to show how the fuel comes to rest in various parts of the system where it can be permanently cooled. This has mainly taken the form of predicting the spectrum of post-disruptive depositions that the fuel could have, and analyzing the subsequent coolability. The disposition of core materials and the required measures to assure cooling of the core debris are, of course, dependent on the reactor design under consideration.

4.1.6 Phase Interfaces

Although a definitive separation of the analysis has been given in Fig. 1, the computer codes in existence today overlap between phases. It was mentioned, for example, that some accident initiation codes actually have models for determining the steady state initial conditions. Presently there is no specific overlap between accident initiation codes such as SAS3A and MELT-III with disassembly codes such as VENUS-II. There is, however, concern with the problem of defining that point in the sequence in which to shift to the VENUS-II program. The

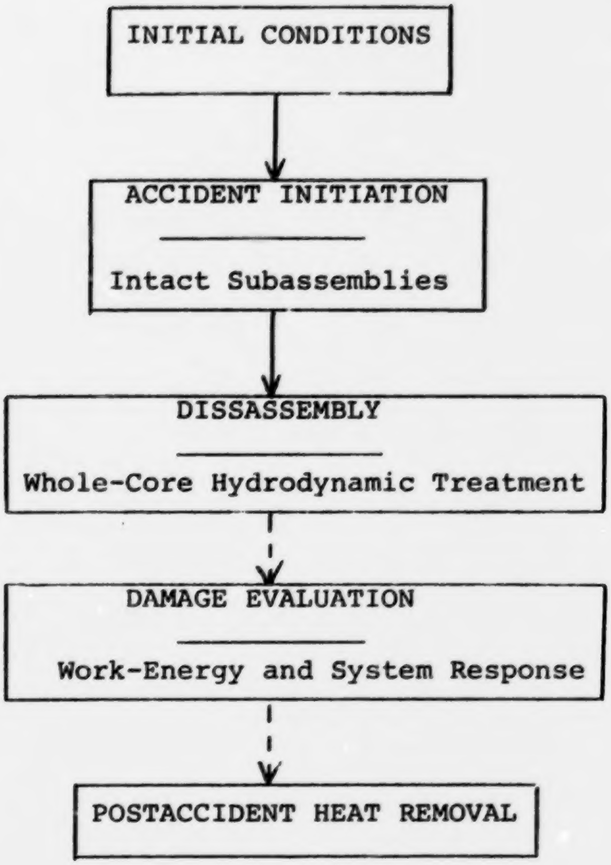
INITIAL CONDITIONS
ACCIDENT INITIATION
Intact Subassemblies
DISSASSEMBLY
Whole-Core Hydrodynamic Treatment
DAMAGE EVALUATION
Work-Energy and System Response
POSTACCIDENT HEAT REMOVAL

Fig. 1. Traditional Approach to Mechanistic Accident Analysis.

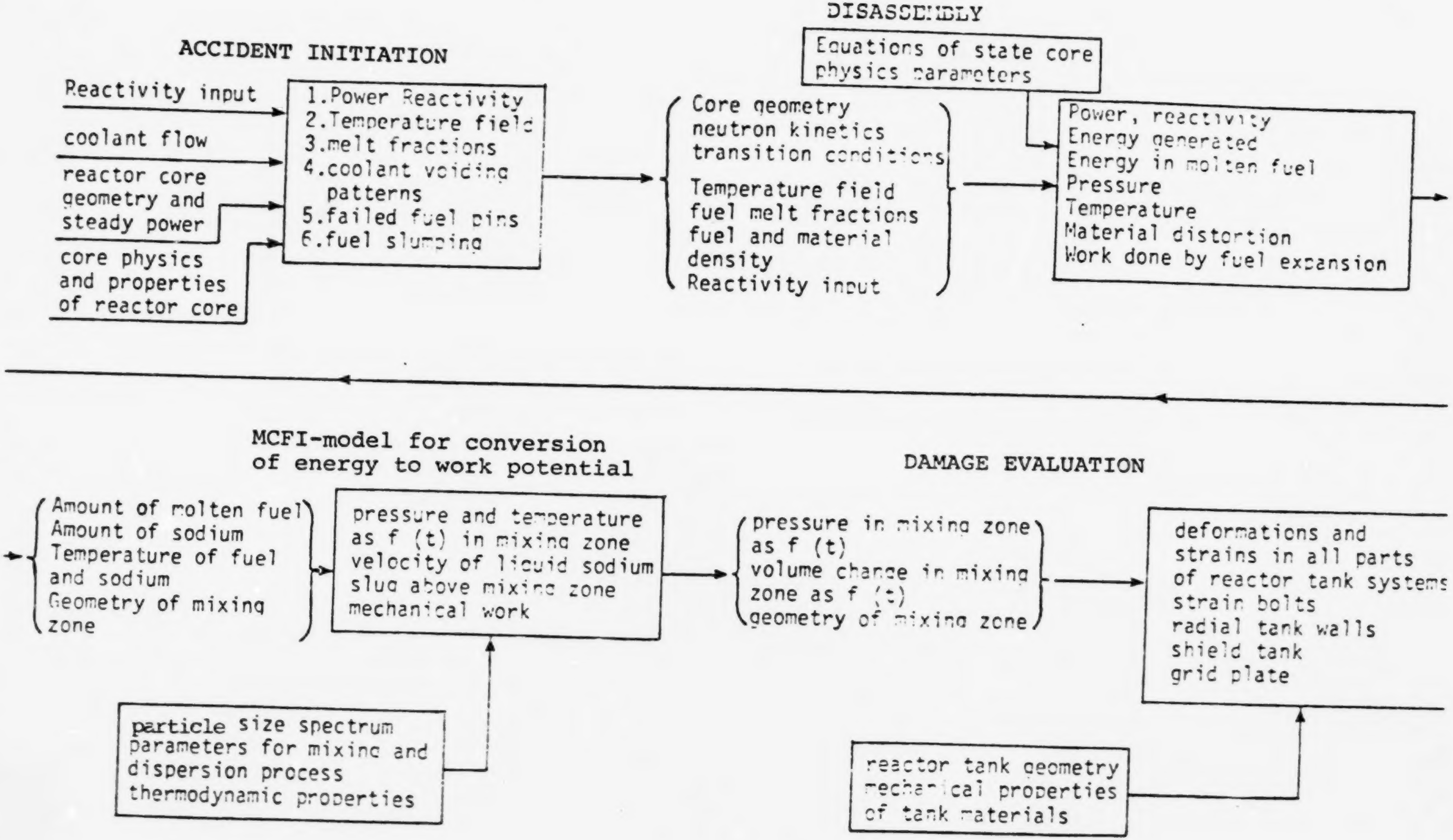
DISASSEMBLY
ACCIDENT INITIATION
Reactivity input
coolant flow
reactor core geometry and steady power
core physics and properties of reactor core
1.Power Reactivity
2.Temperature field
3.melt fractions
4.coolant voiding patterns
5.failed fuel pins
6.fuel slumping
Core geometry
neutron kinetics
transition conditions
Temperature field
fuel melt fractions
fuel and material density
Reactivity input
Equations of state core physics parameters
Power, reactivity
Energy generated
Energy in molten fuel
Pressure
Temperature
Material distortion
Work done by fuel expansion
MCFI-model for conversion of energy to work potential
DAMAGE EVALUATION
Amount of molten fuel
Amount of sodium
Temperature of fuel and sodium
Geometry of mixing zone
pressure and temperature as f (t) in mixing zone
velocity of liquid sodium slug above mixing zone
mechanical work
particle size spectrum
parameters for mixing and dispersion process
thermodynamic properties
pressure in mixing zone as f (t)
volume change in mixing zone as f (t)
geometry of mixing zone
deformations and strains in all parts of reactor tank systems
strain bolts
radial tank walls
shield tank
grid plate
reactor tank geometry
mechanical properties of tank materials

Fig. 2. Information Flow during Hypothetical Accident Calculations.

TABLE I

OUTPUTS AND FEATURES OF SELECTED DISASSEMBLY CODES OR METHODS

Code or Method	Date Operational	Features						Outputs					
		Energy or Pressure Threshold of Disassembly	No. of Dimensions	Neutronics	Equation of State	Geometry	Material Motion	Total Energy Deposition (E_0)	Energy in Molten Fuel	Kinetic Energy	PdV Work	Vapor Internal Energy	TNT Equivalent
Fuchs[26]	1946	No	1	P.K.	S.P.	Sph.	Accelerations from $1/\rho\ \nabla P$ constant pressure profile	✓					
Hansen[27]	1952	No	1	P.K.	S.P.	Sph.	"	✓					
Bethe-Tait[13]	1956	Yes	1	P.K.	S.P.	Sph.	"	✓					✓
LASL Code[28]	1957	Optional	1	Serber-Wilson or $Q.S_N$	S.P.	Sph.	"	✓		✓			
AX-1[15]	1959	Yes	1	$Q.S_N$	S.P.+V.P.	Sph.	"	✓		✓			
WEP[29]	1962	No	2	P.K.	V.P.	Cyl.	"	✓		✓			✓
RAC[30]	1963	No	1	P.K.	S.P.+V.P.	Sl.	"	✓					✓
MARS[17]	1967	Optional	2	P.K.	V.P.	Cyl.	"	✓					
FRAP[31]	1968	No	1	$Q.S_N$	S.P.+V.P.	Sph.	Lagrangian Fluid Dynamics	✓		✓			
VENUS[18]	1970	No	2	P.K.	S.P.+V.P.	Cyl.	"	✓					

TABLE I (continued)

Code or Method	Date Operational	Features						Outputs						
		Energy or Pressure Threshold of Disassembly	No. of Dimensions	Neutronics	Equation of State	Geometry	Material Motion	Total Energy Deposition (E_o)	Energy in Molten Fuel	Kinetic Energy	PdV Work	Vapor Internal Energy	TNT Equivalent
[illegible]AL[32]	1972	Optional	1	$Q.S_N$	S.P.+V.P.	Sl., Sph., Cyl.	Lagrangian Fluid Dynamics	✓	✓	✓	✓		
VENUS-II[19]	1972	Optional	2	P.K.	S.P.+V.P.	Cyl.	"	✓	✓				
S[illegible]PY[33]	1972	No	1^*	P.K.	S.P.+V.P.	Sl.+MC.	"	✓					
[illegible]-2[34]	1974	Optional	2	Q.D.T.	S.P.+V.P.	Cyl.	"	✓	✓				
[illegible]R[35]	1975	Optional	2	$T.S_N$	S.P.+V.P.	Cyl.	Implicit Multifield Eulerian Fluid Dynamics	✓	✓	✓	✓	✓	

*A multiple channel representations adds 3 dimensional character, here

P.K. = Point Kinetics

$Q.S_N$ = Quasistatic Carlson S_N method

Q.D.T. = Quasistatic Diffusion Theory

$T.S_N$ = Time dependent S_N

S.P. = Single Phase; $P = \tau + K\theta + \alpha\rho$ τ = constant θ = Temperature, ρ = density

V.P. = Vapor Pressure

Sph. = Spherical

Cyl. = Cylindrical

Sl. = Slab

Reproduced from best available copy.

consequences are sensitive to the actual shift point in many cases and several points in time are tried in many instances (Ref. 36, 37).

In addition, efforts are now underway to model disruptive modes in which a more gradual transition from energy deposition may occur (Ref. 38). Models to describe pool boiling phenomena and the gradual loss of core structural integrity are being conceived for implementation in the SAS code.

The interface between disassembly codes such as VENUS-II and damage evaluation codes such as those in the REXC0 series is more difficult to describe. In general, the REXC0 codes are used by inputting an energy source characterized by a pressure-volume relation for a given amount of work potential energy. This information comes from pressure and volume changes due to vapor expansion of either fuel or sodium. In order to obtain the necessary inputs caused by sodium expansion, MCFI models using the resultant information from the disassembly calculations are used as shown in Fig. 2. The REXC0 code system (Ref. 25) which includes such codes as REXC0-H (Refs. 39-41), REXC0-HEP (Ref. 42) and REXC0-HT (Ref. 43) (a version which includes fuel-sodium heat transfer) will be discussed below.

4.1.7 Fission Energy Conversion to Work on the Containment

Further understanding of the calculations which determine the work energy deposited in the reactor vessel and head can be gained by following the sequence in terms of energy. Fig. 3 shows the basic energy definitions as they evolve in the accidents.

The actual work done, W, (includes reactor head hold-down bolt strain energy, primary vessel strain energy, reactor vessel straps strain energy, etc) develops from the work potential and initially from the fission energy deposited, E_o. Two efficiencies are defined such that

$$W_o = E_o\eta_1, \text{ and}$$

$$W = W_o\eta_2.$$

The efficiency η_1 is associated with the work potential-fuel thermal energy ratio.

A dominant source of work energy may arise from fuel vapor expansion. Early studies emphasized fuel vapor produced during an energetic excursion as the working fluid. The work "potential", W_o, was determined by calculating $\int PdV$ during an expansion of the vapor to ambient pressure. Note that this is work potential and not an analysis of the actual work, or damage

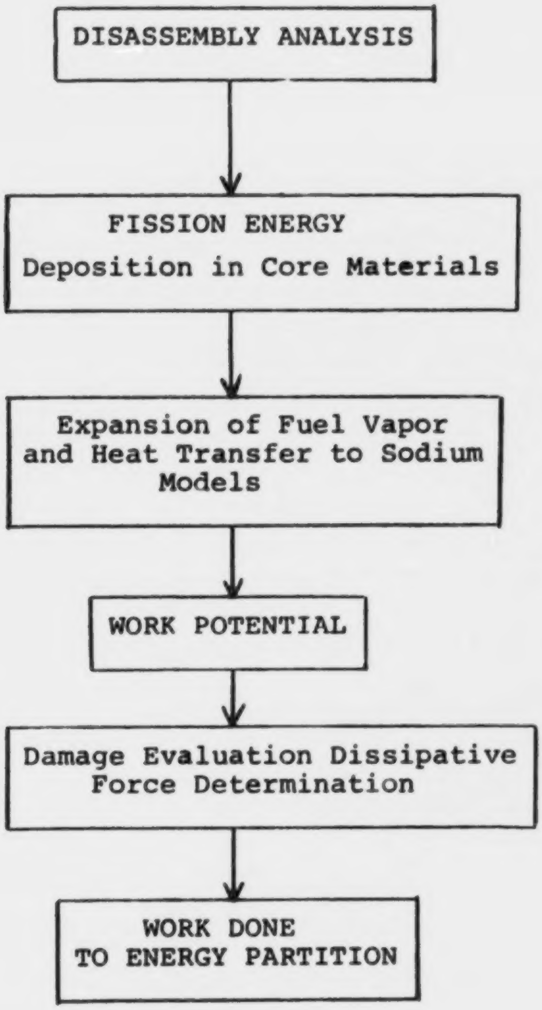
DISASSEMBLY ANALYSIS
FISSION ENERGY
Deposition in Core Materials
Expansion of Fuel Vapor and Heat Transfer to Sodium Models
WORK POTENTIAL
Damage Evaluation Dissipative Force Determination
WORK DONE TO ENERGY PARTITION

Fig. 3. Energy Terms.

that would be imparted to a given reactor design. If the power excursion is severe enough and pressures are generated rapidly enough, an analogy may be drawn between the vapors produced in the reactor and the detonation products of a high explosive. Hicks and Menzies (Ref. 44) suggest an equivalence of 1 lb. of TNT to 2 MWs of total "effective" energy (work done by isentropic vapor expansion). This analogy breaks down for mild excursions and is, again, a measure of work potential and not an explicit damage calculation. The efficiency of this process depends explicitly on the fraction of total energy deposited which becomes internal energy of the vapor. The work potential equals the change in vapor internal energy in an isentropic expansion from the state immediately following the constant volume heating of the core to a fuel temperature which corresponds to 1 atm. of vapor pressure.

The presence of sodium within the vessel complicates the analysis of energy conversion since rapid heat transfer from molten core materials can provide a mechanism to generate pressures which may load the vessel. This mechanism dominates for mild excursions in which negligible fuel vapor pressures result. Hicks and Menzies first discussed the idea that sodium is a more effective working fluid than fuel vapor and provided a conservative estimate that the upper limit of the conversion of fuel thermal energy to sodium vapor work potential is around 30%. Their model was highly idealized and is expected to provide an upper limit to the conversion efficiency.

Considerable effort has gone into more realistic work conversion assessments. Some of the tools used to this end are listed in Table II. The first three methods listed represent varying degrees of conservatism in the assessment of work potential for the fuel/coolant interaction (FCI) process. Experiments which have been performed over the years suggest that the efficiency of the fuel/coolant interaction process depends strongly on many rate-dependent processes. The ANL parametric model allows for most of these rate-dependent processes and provides results which correlate fairly well with the experimental data. In many cases, conversion efficiencies are considerably less than 1%. Both SOCOOL-II and the ANL parametric model compute a potential sodium slug kinetic energy based on a very idealized representation of the phenomena occurring above the core where the bulk mixing process is assumed to occur. Again, a conservative estimate of slug kinetic energy is gained by ignoring many of the dissipative processes which are expected to occur.

Recent hypotheses (Ref. 49) suggest that true vapor explosions (in which shock waves are observed) are not likely when liquid UO_2 mixes with Na under LMFBR conditions, but that explosions may be possible if core steel is elevated in temperatures to around the melting point of the fuel. Work efficiencies deducted from a large number of in-pile tests on Na and UO_2 were very low and no vapor explosions were observed.

TABLE II

OUTPUTS AND FEATURES OF SELECTED ENERGY-WORK CONVERSION CODES OR METHODS

Work Energy Codes or Methods in Order of Decreasing Conservatism	Features or Options	Reactor Vessel Deformation or Response	FCI Work Potential	Potential Sodium Slug Kinetic Energy	HE Equiv. of Fuel Vapor Expansion	HE Equiv. of FCI Work
Hicks-Menzies[44]	Fuel vapor work from adiabatic expansion of core to T = 3450°K, UO_2 boiling point or Instantaneous mixing of fuel and Na, infinite heat transfer rate; instantaneous thermal equilibrium. Work derived from expansion of 2 phase mixture		✓		✓	✓
SOCOOL-II[45]	Instantaneous dispersion and mixing, followed by acoustic or inertial restraint of heated region. Vaporization occurs when expansion relieves high pressures resulting from rapid heating. Heat transfer rate by conduction. H.T. cutoff from vapor blanketing optional.		✓	✓		
ANL-Parametric Model[46,47]	Finite fragmentation and mixing rate, with conduction heat transfer. Recent versions include vapor blanketing heat transfer cutoff and fuel slug reversal as pressure rises in the interaction zone.		✓	✓		
PLACO[48]	Explicit vessel and components dynamic response calculated based on an assumed p-t relation or ANL-parametric type calculation. Two-dimensional cylindrical geometry allows partition of energy in various directions.	✓		✓		

The efficiency N_2 is determined from the ratio of actual damage to the system (in terms of work) to the work potential.

One recent method (REXC0) computes the actual damage to the system, W, done by a prompt excursion. Vapor expansion causes deformation of reactor internals as well as the reactor vessel. Vapors produced cause acceleration of sodium toward the vessel head, but only about 1/3 of the energy of expansion is directed upward; the remainder is partitioned radially and downward. Modeling of various rate-dependent processes is still conservative, however, and the calculations are expected to provide upper bounds on system damage.

One final approach that is taken in disassembly analysis is to report the kinetic energy of core materials as a measure of the work potential of the excursion. This approach has its basis (Ref. 50) in successful calculations of the behavior of high density reactors (Godiva) in comparison with actual experimental data. Observations suggest that computation of core material velocities up to the point at which the expanded core occupies 8 times its original volume (double its initial radius) yields results in which the kinetic energy approximates the explosive yield. In condensed systems such as Godiva, this leads to a low-energy work conversion efficiency indeed. The system moves by thermal expansion unless ramp rates are so large (>3500 $/sec) that inertial effects become important. It is at this point that high material velocities and a small explosion can be generated in a Godiva-like system. This approach has also been successfully used on a lower density graphite moderated reactor (KIWI) which underwent experimental destruction by an intentionally induced prompt excursion in 1965 (Ref. 51, 52). The system was unreflected and had no containment surrounding it. Hence, the calculated kinetic energy of core material compared well with what would be observed from an equivalent unconfined black powder charge. An excursion in an LMFBR complicates the analogy between kinetic energy and work potential somewhat since vapors which are produced in a high void space core may also do work on the vessel. Also, the point at which vapors cease to accelerate solid and molten core material is difficult to assess.

Actual energy conversion in fast reactor excursions is dependent on system design. Mechanistic analyses are necessary to preclude the need for relying on unrealistically conservative work "potential" calculations. Several time-dependent processes compete to convert the energy deposited during the nuclear burst to work and heat. Some of these processes are effective in doing work on the vessel and other are dissipative. The efficienty of the conversion processes depends on the severity of the burst (reactivity ramp rate, mainly), on reactor core conditions at the time of burst (voided core vs. sodium-in core), on reactor design, and on the nature of the accident sequence. Also, the possibility of multiple bursts may add to the total amount of energy generated.

The total energy E_o may be divided into four components: the internal and kinetic energies of molten and solid core materials and the internal and kinetic energies of core material vapors. The partition of the total energy E_o among these components is a function of accident sequence and of time. For example, immediately following a prompt excursion in a voided core, a good deal of energy may be contained in the superheated, compressed molten fuel. As the core expands, the pressure drop, more of the core will vaporize (flash) producing more vapor. Hence, energy stored in one component may be converted to energy in another component, as a function of time and accident sequence. The most essential point is that energy-work conversion efficiency depends on the specific accident and reactor design in question. A low reactivity ramp rate may produce negligible fuel vapor pressures, leading to a vanishingly small efficiency for the isentropic vapor expansion process, but energy deposited in the molten fuel may (eventually) lead to a more efficient conversion through an FCI. On the other hand, the energy stored in molten core material may be of little mechanical damage consequence if conditions preclude a true vapor explosion.

A few examples of mechanistic analyses are cited next.

We know of no truly complete expositions of ways the fission energies, E_o, are partitioned into system damage W, nor of complete determinations of the work potential, W_o. Some examples of incomplete analyses of partitions are given below; extension of the present effort to provide a more complete breakdown of the partition is planned. An important source of the inconsistencies in the numerical values used is the lack of standard formats for presenting results.

Example 1. Super-Phenix (Ref. 53)

For a coherent core collapse ($60/sec) E_o = 46000 MWs; W_o from FCI ranges from 740 MWs to 3022 MWs, depending on the model parameters used. Hence, the ratio W_o/E_o is in the range 1.6% to 6.6%.

Example 2: FFTF Analysis (Ref. 54)

A recent study of the FFTF design margin under loss of flow without scram conditions describes the partition of the work potential from sodium vapor expansion, W_o, of 500 MW-sec, calculated to follow from an excursion characterized by a 100 $/sec insertion rate.

The reported core average temperature for this case is 4850 K. This corresponds to an E_o of about 7000 MW sec., depending on assumptions about the power distribution and rate of power input. The assumed range in W_o was from 350 MW sec to 500 MWs; hence W_o/E_o ranges from 5% to 7%.

The detailed partition of W_o into primary system damage is given in Table III. For this case the work done in damage to the system is just the first four items in Table III or 54.5 MW-sec. Hence W/W_o is in the range 10% to 15% for this case.

No other examples of the complete mechanistic analysis of energy conversion to mechanical damage has been found.

In summary, the following points are made.

1. No functional relationship exists between the fission yield, E_o, and the mechanical damage, W, independent of design and accident sequence details.
2. Nevertheless, the mechanical damage can be bounded by a work potential, W_o.
3. Thermodynamic considerations always limit the energy conversion efficiency; further limits result from details of system design and the accident sequence.

Table III. Damage Partition (MWs)

Upward kinetic energy	1.4
Shell and plate strain energy	43.3
Radial kinetic energy	0.6
Head energy	9.1

The following do not further damage the system, but yield the quasi-static equilibrium pressure in the damage system:

Coolant internal energy	7.4
Core sensible heat	67.4

> Assessments based on current technology of the consequences of specific accident sequences in systems currently being built or designed typically yield estimates showing the work potential to be less than 10% of the fission yield; and, detailed considerations for FFTF yield mechanical damage estimates less than 15% of the work potential.

These specific numerical results are the basis for the scoping estimate of an overall conversion efficiency (W/E_0) of approximately 1.5% applied to current designs.

Different accident sequences may lead to somewhat larger conversion efficiencies of the order of a few percent.

The following section begins the description of the individual codes starting with the steady state models.

4.2 Steady State Codes (GAP0N, BEHAVE, FM0DEL, LIFE)

4.2.1 Introduction

The LIFE-II, FM0DEL, GAPC0N and BEHAVE-2 computer codes represent most of the effort undertaken to model LMFBR fuel pin steady state operation in an integral fashion. The GRASS computer code will also be discussed with these models since it was conceived for inclusion as a subroutine into LIFE.

The purpose of these codes differ.

The LIFE-II code was developed to help define in-pile experiments and focus materials research efforts through parametric design studies. In addition, since it can follow actual reactor operating history and contains fuel-element failure criteria, LIFE-II can be used to monitor cumulative clad damage in operating fuel pins to predict their residual lifetime. This code has been used at Argonne National Laboratory to model LMFBR fuel pins.

The FM0DEL code was written to predict the operational performance of an LMFBR fuel pin. It was basically developed by coupling a fuel and clad mechanical model and a chemical performance model with the PR0FIL (Ref. 55) code, a thermal and heat transfer model. FM0DEL is used as a general developmental tool in the Oak Ridge National Laboratory program for the development of fast breeder reactor fuels.

The GAPC0N computer code is in the process of being developed to compute gap conductance values for fast and thermal reactor fuel.

The BEHAVE-2 code calculates the spatial position of cladding, fuel, and voidage in an operating LMFBR oxide fuel pin with unfailed cladding. In addition, stress, strain, displacement and temperature fields are calculated. BEHAVE-2 was conceived by utilizing five phenomenological views gained from data correlations and preliminary analytical work: axial fuel movement; power increases strains; fuel cracking; radial property variations; and fission product effects.

The general approach taken in these codes is to divide the fuel pin into a user-specified number of axial regions, with each axial region further divided into concentric rings. The irradiation history of interest is broken down into components or cycles, and the performance of each axial node is calculated in turn for each cycle. Changes in power as a function of time (e.g., reactor shutdown and subsequent startup) can thus be modeled in all but GAPC0N in which this capability is being developed.

Several general assumptions and simplifications are inherent in these four computer models as described below.

1. The heat transfer analysis considers heat flow in the radial direction only. The axial length is divided into a user-specified number of regions for which the calculations representing the entire region are performed for a cross section of the region.

2. Clad mechanical analysis normally assumes circumferential symmetry as well as plane strain. The effects of clad bowing due to asymmetrical distributions of neutron flux and coolant temperature are ignored in all cases. In addition, the stress effects due to the presence of wire wrap or grid spacers is ignored.

3. Time-dependent clad wastage due to the intergranular penetration of fission products at the clad inner surface is ignored.

The physical phenomena which can occur to an operating fuel rod are studied using available methods such as experiments, operating experience and analytical tools. Since these phenomena are complex, interrelated and difficult to identify and isolate, efforts to develop more complete and adequate fuel pin performance models continue. The physical phenomena which are now known to occur are here grouped under two general headings: thermal, thermodynamic and heat transfer; and mechanics and motion are shown in Tables IV and V, respectively.

Table IV. Thermal, Thermodynamic and Heat Transfer Phenomena.

thermal conductance (in solid, gas, across interface)

heat source distribution

densification

restructuring (pore migration, sintering, hot pressing)

redistribution and stoichiometry changes

fuel melting

fission production, gas release and solid migration

volatile impurities

fission product swelling

Table IV (con't). Thermal, Thermodynamic and Heat Transfer Phenomena

thermal expansion

flux induced swelling

grain growth

plenum state

Table V. Mechanics and Motion Phenomena

elastic behavior

creep

strain hardening (generation and recovery)

crack formation and healing

fuel-clad interface mechanical interaction

support forces and moments

anisotropic effects

axial fuel motion

plenum behavior

power change effect on strain

clad collapse

clad failure

4.2.1 Geometrical Assumptions

The geometrical assumptions employed in these codes is given below.

GAPCON

Axial and azimuthal symmetry of temperature and stresses is assumed. The fuel pin can be divided into 20 axial sections. Radial temperature and stress calculations are performed using 49 fuel radial nodes and inner and outer clad surface conditions. No anisotropic effects are considered.

BEHAVE-2

Axial and azimuthal symmetry of temperature and stresses is assumed. The fuel column can be axially divided into between 2 and 5 sections. The clad, structural fuel region, nontransport fuel region, and transport fuel region can be divided each into between 2 and 10 concentric rings. No anisotropic effects are considered.

FM0DEL

Axial and azimuthal symmetry of temperatures and stresses is assumed. Fuel pin performance calculations have been in many cases conducted using 9 axial nodes, 20 fuel nodes and 5 cladding nodes. No anisotropic effects are considered.

LIFE-II

Axial and azimuthal symmetry of temperatures and stresses is assumed. Radial temperature distributions are calculated using 40 fuel and 6 clad equal mass nodes. Up to 10 axial sections may be used. The mechanical analysis is performed considering 3 radial fuel regions and the clad. Integral averages for the stresses, strains and displacements are determined for these 4 radial regions using average region temperatures. No anisotropic effects are considered.

4.2.2 Thermal, Thermodynamic and Heat Transfer Phenomena

GAPC0N

The temperature in the clad and fuel is calculated using a flux depression table, temperature dependent thermal conductivities (Refs. 56-58) and standard heat transfer procedures

(Ref. 59). Fuel melting is not accounted for. The gap conductance is calculated by taking into account the effect of helium, xenon, krypton and other volatile impurities that may be released from the fuel and be present in the gap (Refs. 60-73). In addition, the gap conductance is determined as a function of the interfacial pressure (Ref. 74), roughness height of the fuel and clad (Ref. 74), gap size, temperature jump distances (from incomplete energy exchange between surface and gas) (Refs. 75, 76) and radiation heat transfer (Ref. 59). Restructuring is described by calculating a restructuring temperature (Ref. 77) and inputting an average restructured fuel density. Fuel and clad swelling and fission gas release rates are modeled by using empirical correlations. Fission product production is described using a fission yield table. Recent developments to be incorporated in GAPCØN include refinements in the fission gas release correlation, a volatile impurity release model and the gap contact conductance calculation.

BEHAVE-2

The steady state version of BEHAVE-2 uses a radial quasi-steady-state heat transfer subroutine to calculate the temperature field. A temperature and density dependent thermal conductivity expression is used in the fuel and the clad thermal conductivity expression is temperature dependent. The desired radial heat source distribution to account for self shielding can

can be incorporated through a user supplied subroutine. Heat transfer across the fuel-clad interface is modeled by using an input thermal gap conductance. Although the assumption is made that the fuel-clad gap closes upon initial application of power, the existence of a gap for heat transfer purposes is not precluded. Fuel melting is accounted for in this model.

In the BEHAVE-2 code, the fuel is divided into two phenomenological zones as shown in Fig. 4. The outer fuel zone or structural fuel zone is defined as that fuel in which the viscosity of the fuel is within a few decades in magnitude of the clad viscosity. Inward of the structural fuel zone, depending on the operating fuel temperatures, an inviscid zone is defined where the fuel viscosity is low relative to the clad viscosity. The temperature which defines the boundary between structural and inviscid zones is called the inviscidity temperature as indicated in Fig. 4. This boundary is defined as that temperature at which fuel porosity volume is reduced by 10% under a hydrostatic pressure of 400 psi in one time step. The resultant expression is a weak function of the time step.

The inviscid zone is further divided into two regions, outer nontransport region and inner transport region with the transport temperature separating them. In the outer nontransport

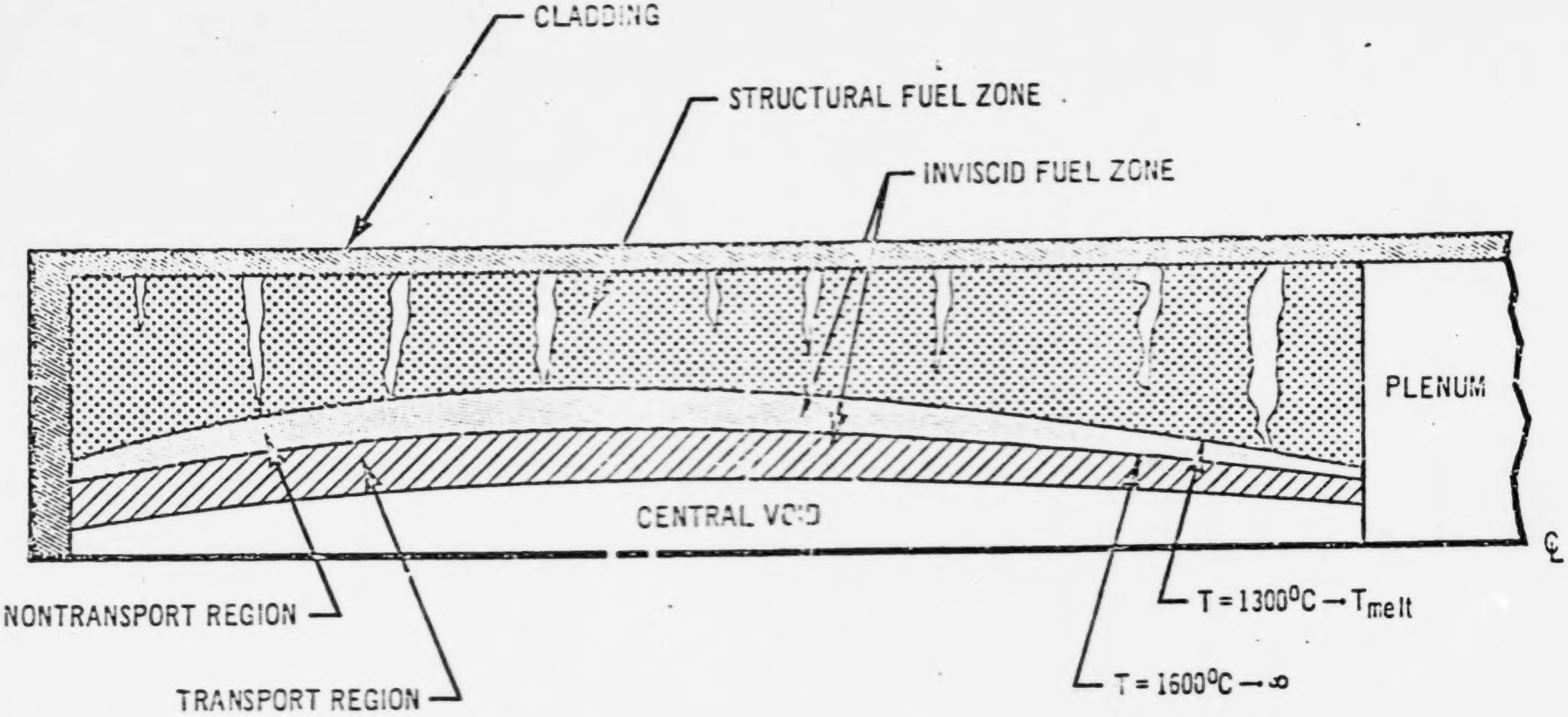
CLADDING
STRUCTURAL FUEL ZONE
INVISCID FUEL ZONE
PLENUM
CENTRAL VOID
℄
NONTRANSPORT REGION
TRANSPORT REGION
T = 1300°C → T_{melt}
T = 1600°C → ∞

Fig. 4 Division of Fuel in BEHAVE-2 (Ref. 7).

region, the fuel retains its porosity unless it is eliminated by mechanical hot pressing induced by elimination of the central void as a sink for further fuel expansion. In the transport region, on the other hand, porosity is assumed to be eliminated (except for residual porosity of 1%) by surface diffusion assuming a 1 micron typical pore radius. Fuel which is hotter than the time dependent transport temperature which is calculated considering the pore migration velocity expression by Nichols is considered to have its porosity swept instantly to the center.

Fuel swelling from fission product volume increases in BEHAVE-2 is described using an input fuel swelling rate which applies to the fuel matrix material. This model does not allow for fuel swelling by relatively large fission gas bubbles that are not dominated by surface tension forces. Fission gas production is described using input fission product yield characteristics. The gas is released and available to the plenum (a gas bottle option in which plenum communication is cut off is also included) when the fuel is above a specified gas release temperature. This temperature is set equal to the transport temperature, however, an empirical temperature and burnup dependent correlation could be easily included. Thermal expansion of the fuel and clad as well as irradiation induced clad swelling is described using empirical expressions.

FM0DEL

The temperature field in FM0DEL is calculated for each axial segment by first determining the clad outer surface temperature with knowledge of the coolant temperatures and temperature rise acriss the clad film. Using a temperature dependent clad thermal conductivity, the temperature rise across the clad is calculated. Then using a gap conductance value calculated from considerations similar to those described in GAPC0N (Ref. 78) or an input value the outer surface temperature of the fuel is determined. Once the fuel surface temperature is known, the steady state radial heat conduction equation is used to solve for the fuel temperatures (Ref. 55). A radially dependent heat source term can be specified as a function of burnup and the thermal conductivity is expressed as a function of temperature and porosity. After the fuel temperature distribution has been calculated, thermal expansion of the pellet (Refs. 79-80) is calculated so that the gap size can be recalculated. This iterative process is repeated until the present and previously calculated fuel surface temperatures agree to within 1°C. Fuel restructuring is described using Nichols' equation for pore migration due to the vaporization-condensation mechanism (Ref. 81, 82). The change in porosity in a given fuel increment is determined by the net movement of pores during the time step.

Grain growth is also calculated during irradiation as it is felt that the influence of grain size of fuel material on fission gas release, swelling and creep of mixed oxide fast reactor fuel is important. In addition, stoichiometry changes and actinide redistribution phenomenon are modeled for the mixed oxide fast reactor fuel (Ref. 83).

Fuel swelling due to fission product accumulation is calculated considering both solid and gaseous fission products (Ref. 84). A constant swelling rate due to solid fission products is used and the volume of gas bubbles is calculated. A fraction of the fission gas bubble volume is assumed to be released upon formation of the bubbles and therefore does not contribute to fuel swelling. A fraction of the fabricated porosity is assumed available to accomodate fission products. Since the magnitude of the fuel-clad contact pressure will influence the volume of fission gas bubbles, the swelling is included in the iteration to determine the fuel-clad contact pressure.

Release of fission gas is calculated from an input temperature-release fraction table. The fission gas pressure is calculated using the ideal gas law and knowledge of the gas plenum, center void, gap and fuel porosity volumes and the volume-average void temperature. No option is provided to cut off plenum communication.

Clad flux induced swelling as well as fuel and clad thermal expansion are described using empirical correlations.

LIFE-II

The radial temperature distribution in each axial section of the fuel pin model is calculated in a quasi-static manner at the beginning of each time step based on the average power level and inlet coolant temperature expected during the step, the dimensions of the fuel zones, the size of the fuel-clad gap, the cladding dimensions, and the fuel density at the end of the previous time step. Provisions are available for treatment of encapsulated elements at the user's option. A number of fuel thermal conductivity (Ref. 85, 86) options are available which are a function of the fuel temperature and porosity. A radial distribution of the heat generation rate is accounted for. The gap conductance is both pressure and temperature dependent but does not include the radiation mode. An input gas conductivity and gap closure parameter are used to fit measured gap conductance values.

Fuel restructuring is based on the theory of pore migration driven by the vapor-condensation mechanism described by Nichols (Ref. 87). An expression for the pore migration velocity is used with different constants for the columnar and equiaxed zones. These constants require calibration with experimental fuel pins to determine their magnitude. Fuel swelling due to solid fission products is treated by specifying the net solid volume created per fission and multiplying by the number of fissions occurring in each fuel region. Gaseous fission-product swelling is treated with an ideal gas law approach in the restructured regions. Gaseous fission products in the undisturbed region are assumed to be essentially incompressible, and, therefore, they contribute in that region in a manner similar to solid fission products. The predicted fuel swelling is then modified to account for hot-pressing-of the fuel.

A detailed fuel swelling model developed by Poeppel (Ref. 6) describes the production, migration, coalescence, and eventual release of gas-bubble distributions. In addition, interaction of the bubbles with structural defects and fission-gas resolution as a function of irradiation is included. This model called GRASS was designed to be incorporated as a subroutine in LIFE.

Fission gas release is described using a temperature dependent release rate correlation (Ref. 88). The plenum pressure is determined by using the ideal gas law, central void and plenum volume and the volume average temperature. Clad flux induced swelling as well as fuel and clad thermal expansion are modeled using empirical correlations (Ref. 89).

4.2.3 Mechanics and Motion Phenomena

GAPØN

The mechanical analysis included in GAPCØN is simplified by the fact that only thermal expansion of the fuel is considered and clad deflection is mechanistically modeled only in the elastic case. To find the amount of fuel thermal expansion, the fuel pellet is divided into 50 annular rings, each assumed to be a free body at its average temperature. The increase in radius of each ring in the circumferential direction is then calculated using a linear thermal expansion relation. The code then finds that node in which the maximum increase in radius occurs, and it assumes that all the thermal expansion that occurs inside that increment is accounted for by the radius increase of that increment. The total circumferential thermal expansion is then the sum of the expansion in the maximum node plus the expansion of those nodes outside the maximum node.

The clad elastic deflection uses the Lame (Ref. 90) equations for a thick-walled vessel and input elastic properties (Ref. 91). Cladding creep is a user option in that a table of cladding diameters as a function of time may be supplied.

BEHAVE-2

The mechanical analysis is performed using the finite element method. Stress and strain rate fields are calculated in the clad and structural fuel zones by dividing them radially and axially into a number of rings. Each ring has three degrees of freedom as uniform radial expansion of the inner and outer radii and uniform axial expansion is described. Shear forces are accounted for only between the fuel and clad. A special shear element at this interface permits relative slippage or produces friction-induced fuel pellet locking. The interior inviscid zone interacts with the outer structural fuel zone as a constant pressure boundary condition. The elastic-plastic solid is described using Hooke's law for the elastic case the Prandtl-Reuss flow rules in the plastic regime. By assuming the stresses are proportional to stress rates and the elastic and plastic Poisson's ratios are equal, an expression is found of the same form as Hooke's law for an elastic solid except that strains are replaced by strain rates, Young's modulus is replaced by a newly defined creep modulus and stresses are replaced by a newly defined reduced stress.

The exact Lame solution (Ref. 92) for the radial and axial displacements of an elastic thick walled cylinder under internal and external pressure is used to develop the matrix equation for a clad or unbroken fuel ring. The resultant matrix equation relates radial forces to the displacement rates at the inside and outside of the ring and axial forces to the displacement rates of the axial boundaries of the ring. This equation has displacement and dilation replaced with displacement and dilation rates, Young's modulus with the creep modulus and stresses with reduced stresses. Matrix equations are also derived to account for the altered fuel ring strength in the case of radial cracks, transverse cracks or both types of cracks. Fig. 5 shows the effect of the power upon assumed crack behavior in BEHAVE-2.

Selection of a consistent Poisson's ratio is important in this method. The assumption of clad incompressibility is equivalent to using a Poisson's ratio of 0.5, however, this makes the matrix equation singular. A value of 0.4 is used instead giving the clad a small amount of compressibility in this highly deformation resistant regime is negligible. In the plastic regime, the compressibility may have considerable effect on the calculated stresses. In this case, a value dependent upon porosity is used (Ref. 93).

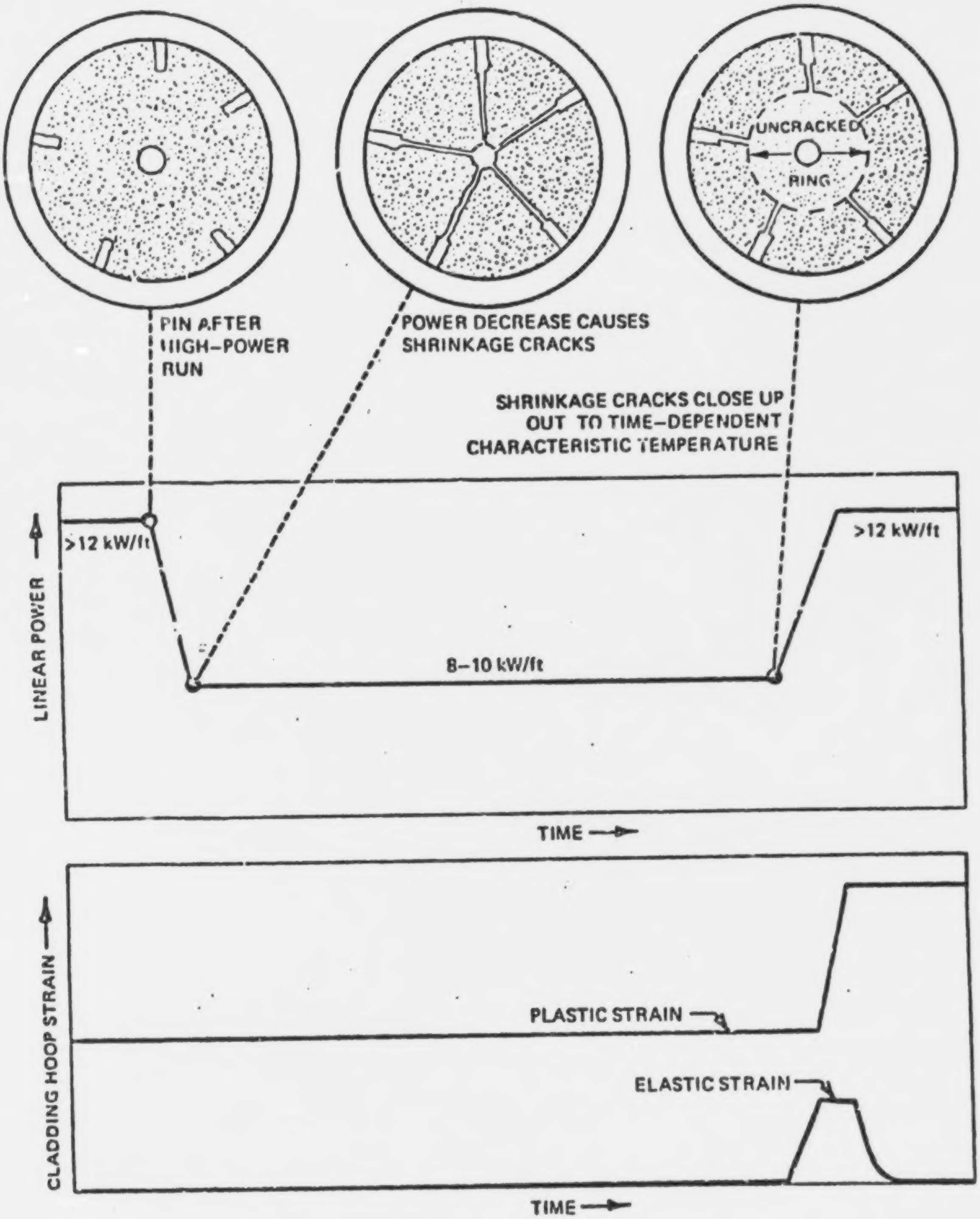
UNCRACKED
RING
PIN AFTER
HIGH-POWER
RUN
POWER DECREASE CAUSES
SHRINKAGE CRACKS
SHRINKAGE CRACKS CLOSE UP
OUT TO TIME-DEPENDENT
CHARACTERISTIC TEMPERATURE
LINEAR POWER
>12 kW/ft
8–10 kW/ft
>12 kW/ft
TIME
CLADDING HOOP STRAIN
PLASTIC STRAIN
ELASTIC STRAIN
TIME

Fig. 5. Nature of Cracking in BEHAVE-2 (Schematic) (Ref. 7).

Fig. 6 shows how deformations of the overall fuel pin structure are calculated. The matrix equations describing each fuel ring for a given axial section are coupled together resulting in 3 force-displacement rate nodal equations representing the inner, outer and axial boundaries of the fuel section. The same procedure is conducted for the clad rings. The entire axial section is then constructed by coupling a shear element to the outside of the fuel section and the inside of the clad section.

The shear element simulates the fuel-clad friction by placing an opposing shear stress on the fuel which is proportional to the difference between the mean velocity of the fuel section and velocity of the shear element's outer face.

The final step connects all of the fuel and cladding sections together, maintaining force equilibrium and displacement compatibility in the radial and axial directions. The resultant matrix equation represents the overall structure. Frictionless shearing between adjacent fuel and cladding sections in the (r,θ) plane is permitted and compatibility is not maintained between radial displacements of points in adjacent fuel or cladding sections. This is considered to be a negligible error considering the large length/diameter ratio in most problems. The complete set of structural equations are first solved for the pin by

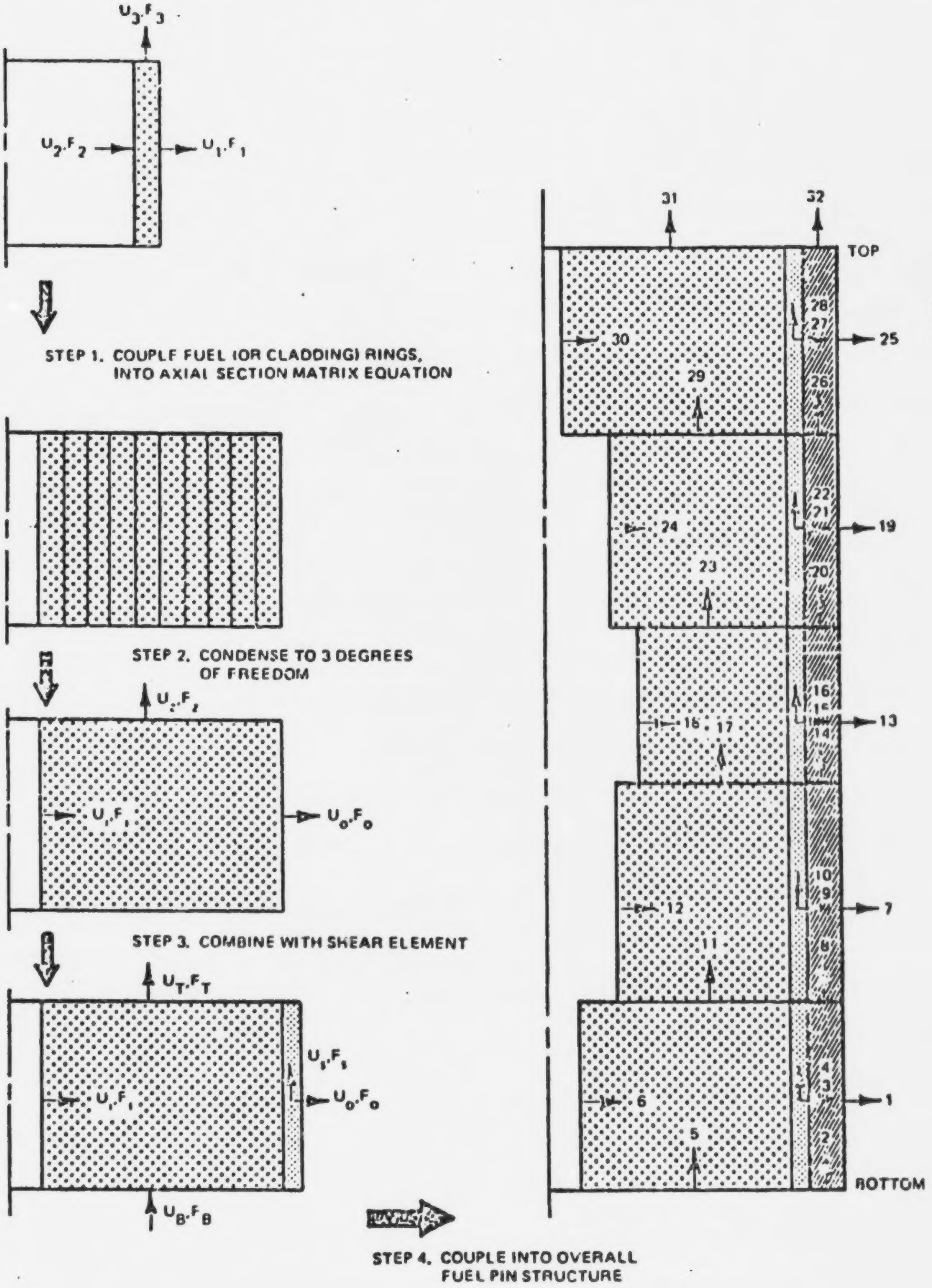
U3,F3
U2,F2
U1,F1
STEP 1. COUPLE FUEL (OR CLADDING) RINGS, INTO AXIAL SECTION MATRIX EQUATION
STEP 2. CONDENSE TO 3 DEGREES OF FREEDOM
Uz,Fz
U1,F1
Uo,Fo
STEP 3. COMBINE WITH SHEAR ELEMENT
UT,FT
Us,Fs
U1,F1
Uo,Fo
UB,FB
STEP 4. COUPLE INTO OVERALL FUEL PIN STRUCTURE
31
32
TOP
28
27
25
30
29
26
22
21
19
24
23
20
16
15
13
18
17
14
10
9
7
12
11
8
4
3
1
6
5
2
BOTTOM

Fig. 6. Assembly of Individual Ring Elements and Shear Elements into Overall Fuel Pin Structure in BEHAVE-2 (Ref. 7).

determining the creep moduli from the clad or fuel constitutive equations assuming a value of the effective strain rates. The solution gives a new estimate of the strain rates and of the creep modulus for each ring. From four to six iterations are required to converge the creep modulus to acceptable accuracy.

BEHAVE-2 allows for axial fuel mass transfer between adjacent fuel sections in certain circumstances. When all center void is exhausted in the pin, expansion of fuel matrix material in excess of the space available causes hot pressing of the non-transport region fuel. The porosity in a given ring is reduced down to a residual 1% in approximately inverse order of temperature without regard to axial location. Fuel motion allows for the distribution mass in innermost rings to occupy all the center void space and maintain a constant interior pressure.

FMØDEL

Mechanical deformation of the clad is calculated using the triaxial stress analysis similar to that developed by Johnson (Ref. 44) and Puthoff (Ref. 95). For calculational purposes, the clad is divided into a number of concentric rings, and a set of differential equations developed from the compatibility, equilibrium and triaxial stress-strain relationships.

The differential equations are solved using finite difference methods and standard matrix techniques. This solution yields radial and tangential stresses at each ring boundary. The plain strain assumption is then used to calculate the axial stress. The triaxial stress state defines an equivalent stress which is used in a cladding creep law to determine the time-dependent deformation. Because of the low thermal conductivity of oxide fuels, temperature gradients across the fuel pellet are high, leading to very high thermal stresses. At moderate heat rates the thermal stresses near the pellet surface will exceed the rupture strength of the fuel material, and radial cracks will develop to relieve the stresses. To determine the location of the radial cracks, the stress distribution is calculated across the fuel pellet, assuming that the material is elastic. The tangential stresses at each radial node are compared with the rupture modulus vs. temperature data of Roberts (Ref. 96), and the root of the radial crack is assumed to exist at the point where the tangential stress exceeds the rupture modulus. The crack extends from this point to the pellet surface. The formation of the crack provides two benefits to the calculation. It permits the assumption that the pellet is stress free (the formation of the cracks having relieved the thermal stresses), so that thermal expansion of each radial increment can be determined by the product of the average temperature and the thermal expansion coefficient. In addition, the crack allows a simple evaluation of the response of the fuel to the pressure building at the fuel-cladding interface. It is assumed that the fuel will creep in response to the pressure, and the rate of movement of the fuel surface will be described by the creep characteristics of the fuel at the roots of the radial cracks. That is, the pressure is transmitted from the fuel-cladding interface to the root of the crack by cracked chunks of cool fuel. This pressure causes the hot plastic core to deform into the central void, or be extruded axially if there is no void.

Cumulative deformation over the operating lifetime of the fuel pin is calculated by assuming discrete time intervals having constant pressure, expansion, and temperature conditions. The amount of deformation is calculated over each of these time intervals and summed over the entire operating lifetime.

In calculating mechanical deformation, the mechanical property data found in Ref. 97, yield strength data found in Ref. 98, and the creep law found in Ref. 99 are used.

Interaction between fuel and clad is considered from two causes: differential thermal expansion between fuel and clad during power increase, and fuel swelling during periods of steady-state operation. The fuel cracking model is an important factor in this interaction phenomenon. At low heat rates, where the rupture modulus of the fuel is not exceeded, the change in geometry of the fuel pellet is calculated in the same manner as for the clad. At moderate and high heat rates the fuel is assumed to crack. The formation of the cracks relieves the thermal stresses in the fuel pellet, and each radial increment of fuel expands thermally in accordance with its average temperature and thermal expansion coefficient.

During power changes the time rate of change of linear heat rate is assumed constant. The duration of a power ramp is divided into a number of time steps. The length of the time steps is under the control of the user. During each Δt the heat rate of the pin will change by ΔQ. Thermal expansion will cause changes in the outer fuel diameter (ΔD_f) and the cladding inner diameter (ΔD_c). The size of the new fuel-cladding diametral gap is given by

$$\Delta = G_0 + \Delta D_c - \Delta D_f,$$

where G_0 is the size of the gap at the beginning of the time step. If the calculated gap size (Δ) after a power change is negative, the fuel-cladding gap has closed because of differential thermal expansion, and mechanical contact exists between the fuel and cladding. The heat rate at which the gap size becomes zero is determined by linear interpolation between the existing value of Δ and the value calculated after the previous power change. The positions of the radial nodes in the fuel are "frozen" at this point so that the effect of further increases in power on the geometry of the pellet can be determined. It is assumed that the hot plastic fuel interior to the cracked region cannot expand thermally in the radial direction after the gap has closed. The contact pressure at the fuel-cladding interface, which is tranferred to the outer boundary of the hot plastic fuel core by the cracked fuel region, forces all thermal expansion in this hot core into the axial direction. The value of ΔD_f due to further power increases after gap closure is due only to the thermal expansion calculated for the fuel in the cool cracked region.

To calculate the magnitude of the contact pressure between fuel and cladding during a time period Δt after gap closure, an iterative scheme is used whereby the existing contact pressure at the beginning of the time step (this will be fission gas pressure if the gap was open at the beginning of the time step) is repeatedly doubled until the correct contact pressure range is bracketed. Then the bracket is repeatedly halved until the contact pressure is within 1% of the previously calculated value. The basis of the iteration is the amount of change in the cladding inner diameter and fuel outer diameter due to creep in response to the contact pressure. During a period of time Δt the cladding inner diameter will increase by an amount Δ_c in response to the pressure. During the same period of time the fuel outer diameter will decrease by an amount Δ_f due to the pressure transmitted from the fuel-cladding interface to the surface of the hot plastic core by the cracked outer region of fuel. Thus when the relation

$$\Delta_c + \Delta_f = -\Delta$$

is satisfied, the contact pressure used to calculate Δ_c and Δ_f represents the average contact pressure during the time step. Calculation of the contact pressure due to fuel swelling is similar to what has already been described for differential thermal expansion.

Fuel-clad mechanical interaction when a power change takes place "instantaneously" so that there is not time for fuel or clad creep to relax the interaction is also described. The calculation is accomplished by determining the differential thermal expansion that would occur if there was no interaction and then forcing the clad to instantaneously accommodate the difference through plastic deformation as well.

Potential failure criteria, neglecting chemical reactions, include a critical stress or strain, critical strain energy, and correlation with stress-rupture data. In the absence of definitive in-reactor data, the calculated internal pressure buildup is compared with biaxial stress-rupture data to predict when fuel pin failure will occur. Since internal pressure is increasing with time in a fuel pin and stress-rupture tests are conducted at constant pressure, the "life fraction" concept is used to compare calculated pressures with the constant pressure stress-rupture lifetimes. The fuel pin operating lifetime is divided into a number of discrete time intervals, and the average pressure during each interval calculated. Then this time interval divided by the stress rupture lifetime at that pressure and temperature is the life fraction expended. The life fraction values are summed over all time intervals, and when the sum reaches unity for any axial region, the pin is assumed to have failed. This method of estimating clad damage is probably valid for the gas plenum region but of limited usefulness in the fueled region of the pin, where fuel-clad mechanical interaction does not cause damage analogous to the stress-rupture data from pressurized tubes that are utilized.

LIFE-II

For the gross mechanical analysis in LIFE-II, the fuel is always divided into three radial zones, corresponding physically to the columnar grain region, the equiaxed grain region, and the unrestructured or "undisturbed" region. The cladding then forms a fourth radial zone. For each of these zones, the integral averages for the stresses, strains (including swelling), and displacements are determined using a generalized plant-strain analysis with materials properties evaluated at the average temperature of each region. This is combined with an iteration procedure that allows the code to follow changing boundary conditions resulting from reactor power fluctuations. The gross mechanical analysis is limited to four regions because the resultant equations may be readily solved algebraically, which requires less computer time.

At the start of the deformation analysis, an initial approximation is made for the change in total strains expected to occur in each region during the time step, based on the length of the time step and the changes that occurred in the previous step. From this assumption, first approximations of the average deviatoric and hydrostatic stresses in each concentric cylinder are determined using empirical creep laws and the swelling and hot-pressing relationships. These first approximations are incorporated into the complete constitutive equations, which are then combined with the equations of equilibrium, compatibility, and the kinematical relations and solved subject to the boundary conditions appropriate for the time step. This solution yields a second approximation of the change in total strains in each region, which is then compared with the initial approximation. If convergence criteria on the stress and strain are not met, iteration continues.

If the maximum changes in stress, strain, or restructuring exceed specified values, the code cuts the time step internally, and the power and coolant-temperature changes for the step are adjusted accordingly. The time step may also be cut if the convergence is too slow. If the power has changed from the previous step, the local thermal stresses in each fuel region are computed and superimposed on the global stresses to determine whether fuel fracture occurs. If the power has not changed, the amount of cracking or crack healing is determined from the average condition in each region prevailing for the time step. The mechanical properties of the fuel are adjusted accordingly, and finally the cumulative damage to the cladding is computed.

At the end of each time step, LIFE-II computes whether fuel cracking would occur in any of the three principal directions. If the power has changed, the local thermal stresses are computed as previously described and superimposed on the average stresses for each fuel region. The cracking criterion is based on the fracture strength data of Canon et. al. (Ref. 100). When any of the principal stresses in a fuel region reach the ultimate tensile strength, the fuel cracks in that region.

The stress component perpendicular to a crack vanishes in the region, and the elastic strain existing prior to cracking is then redistributed. For instance, when a crack occurs perpendicular to the axial direction, the axial stress σ_f vanishes and the other stresses are assumed to remain momentarily constant. The axial elastic strain then decreases by σ_f/E, and the strains in the other principal directions increase by $\nu\sigma_f/E$ each where E is the Young's modulus and ν is the Poisson's ratio. It is assumed that these changes in elastic strain are compensated by equal changes in plastic strain and volumetric expansion. The mechanical properties of the cracked fuel are then modified in an attempt to represent the cracked material as an isotropic material. LIFE-II allows for repeated cracking in all fuel sections and also for the cracked fuel to creep faster than the uncracked fuel by modifying the creep rate.

When the fuel element operates without a power change during a time step, crack healing is allowed. Presently, cracks are assumed to heal whenever a) the stresses in the region become compressive, b) the temperature exceeds 1400°C and (c) the time at steady state exceeds 1 hr. When the cracks heal, the mechanical properties of the fuel are again restored to their usual (temperature dependent) values.

The failure criterion currently used in LIFE-II is a linear cumulative damage law of the form

$$\sum_{i=1}^{n} \frac{t_i}{T_{Fi}} = 1,$$

where t_i is the time that the cladding is at the ith hoop-stress level, T_{Fi} is the time required for cladding rupture when at the ith level of hoop stress, and n is the total number of stress levels the cladding is subjected to in its linearized stress history.

The denominator T_{Fi} is the most critical part of this failure criterion. Stress rupture data correlations are used to determine T_{Fi}.

The cumulative damage to each axial section of the cladding, leading to eventual failure is then computed. Radiation damage, fatigue damage, and corrosion due to fission products and sodium interactions will be factored into this criterion as more data become available.

Combining the data of Taggee and Li (Ref. 101) with LIFE-II calculations, it is also possible to infer the mode of cladding failure, i.e., whether the failure will be relatively passive pinhole formation, or a more explosive type of rupture.

4.2.4 Material Properties

Analytical expressions for material behavior develop from two general approaches: first principles and empirical data correlations. Because of the many complications in a first-principles approach to modeling properties such as fuel swelling, cladding swelling, fuel-cladding gap conductance, and fuel restructuring, the development of a set of empirical options to describe these properties is necessary. These correlations complement the theoretically grounded models, particularly in analyses based on interpolation within the available data.

Properties used in LWR and LMFBR fuel rod performance models in many instances are developed to describe behavior in limited operational regimes and do not account for nonhomogeneous or nonisotropic conditions. In addition, they often indicate the need for further development in many areas such as spatially variable stoichiometry and fission product distributions. For example, many fuel properties such as fuel thermal conductivity are often expressed as a function of the fuel's temperature and/or porosity. Fuel property expressions which include these additional fission product distribution and stoichiometry effects should also be developed in the future. The as-fabricated oxygen to metal ratio should be used in these correlations until the applicable models to describe oxygen and fission product redistribution, mainly in the radial direction, are developed. In addition, correlations are needed to describe clad constituent depletion and fuel-clad chemical reactions as well as short-term plastic strain.

A list of material properties that are included in these codes is given in Table VI.

Table VI. Material Properties

1. Fuel-Cladding Heat Transfer Coefficient
2. Coolant-Cladding Heat Transfer Coefficient
3. Cladding Thermal Conductivity
4. Cladding Thermal Expansion
5. Fuel Thermal Conductivity
6. Fuel Restructuring
7. Fuel Thermal Expansion
8. Redistribution
9. Fission Gas Release
10. Gas Atoms Produced Per Fission
11. Fuel Young's Modulus
12. Fuel Poisson's Ratio
13. Cladding Shear Modulus
14. Cladding Poisson's Ratio
15. Solid Fission Product Volume Per Fission
16. Gaseous Fission Product Swelling
17. Fuel Hot Pressing
18. Cladding Swelling
19. Cladding Density
20. Cladding Thermal Creep
21. Cladding Irradiation Creep
22. Fuel Creep
23. Fuel Fracture Strength
24. Fuel Crack Healing Temperature
25. Fuel Brittle-to-Ductile Transition Temperature
26. Fuel-Cladding Friction Coefficient
27. Cladding Time-to-Rupture

4.2.5 Limitations

The major assumption for these four steady state models have been previously discussed. The descriptions of each of these codes has shown that they incorporate a large number of differing phenomena and properties. These codes must be considered in a developmental stage in which they lack experimental validation. Many of the phenomena are handled in a parametric or macroscopic manner. The extent by which fission gas behavior is modeled is an example in that very few mechanistic details are included. The LIFE-II code uses only three fuel nodes for stress-strain calculations. Since the radial temperature and stress gradients are very steep, this approximation seems quite crude. The GAPCØN code lacks mechanical analysis and thus can not accurately predict radial gap sizes.

There has been to our knowledge no program for comparing or validating these four programs against one another or against experiments. The use of these codes for initial conditions to accident analysis codes is therefore not realistic or worth the large amount of required effort at this time. Since initial conditions are so important in determining transient fuel and clad behavior, effort should be placed upon obtaining useful information from steady state codes for initialization of the transient codes.

GRASS computes the evolution of the bubble-size distribution as a function of position in the fuel for three different types of bubbles: (a) bubbles not pinned to structural defects: (b) bubbles pinned to dislocations; and (c) bubbles pinned to grain boundaries. The criteria derived by Weeks et. al. (Ref. 102) are used to determine when a bubble is large enough to be pulled free from the defect. Bubble mobility and velocity are computed on the basis of three separate mechanisms for bubble motion: (a) surface diffusion; (b) volume diffusion; and (c) evaporation condensation. In each fuel region and for each bubble size, the mechanism that gives the largest mobility and/or the highest velocity is used. Bubble-coalescence probability is computed following Gruber (Ref. 103), but in each case the mechanisms that gave the greatest probability was used. Where two or more mechanisms dominate, the calculation of the coalescence probability is based on the sum of the probabilities calculated separately from the various mechanisms.

The procedure for calculating the bubble-size distribution consists of dividing the bubbles into equal size ranges on a logarithmic scale and averaging properties over the ranges. The entire distribution can then be described by a relatively small number of equations. The bubble sizes are defined according to the number of gas atoms. The gas is assumed to obey

4.2.6 GRASS

A model (Ref. 6) to calculate in detail the in-pile behavior of fission gas in a mixed-oxide fuel has been incorporated into a computer code GRASS (Gas Release and Swelling Subroutine) that has been written for inclusion in the LIFE (Ref. 4) code. LIFE supplies the following operating conditions to GRASS: temperature, temperature gradient, fission rate, and hydrostatic stress state. Grain size and dislocation density may also be specified by LIFE, but at present they are determined within the GRASS code. GRASS may operate independently of LIFE, if the operating conditions are given. GRASS also may be used in parametric studies.

The basic model assumes gas atoms nucleate to form bubbles that move both by random motion and under the influence of a temperature gradient. The bubbles may coalesce to form larger bubbles. The gas pressure in the bubbles is balanced by capillary and hydrostatic stress in the fuel material. The gas in the larger bubbles is less dense than in the smaller bubbles. The bubbles are attracted to and pinned by structural defects, especially dislocations and grain boundaries. Bubbles can move along the defects where they continue to grow by coalescence until they are pulled off by the temperature-gradient force and then migrate to the central void. Included in the calculation of growth is a negative term that describes the rate of radiation-induced resolution.

the extrapolated equation-of-state of Harrison. This is essentailly a Van der Waal's equation, where the Van der Waal's constant is temperature and pressure dependent. When a hydrostatic stress is present, the bubble radius is a root of a quartic equation.

Based on these models for the behavior of individual gas bubbles, differential equations can be written that describe the rate of change of the number of bubbles in every size range. The equations are written in the form

$$\frac{df_i}{dt_i} = -a_i f^2{}_i - b_i f_i + c_i, \qquad (1)$$

where

f_i = number of bubbles in the ith size range

a_i = rate at which bubbles are lost from the ith range through coalescence with bubbles of the same size

b_i = rate at which bubbles are lost from the ith range through coalescence with bubbles of different sizes and by re-solution, migration, and diffusion

c_i = rate at which bubbles are formed in the ith range

and

$$f_i, a_i, b_i, c_i \geq 0.$$

The parameters b_i and c_i are functions of f_i, $j \neq i$; i.e.,

$$b_i = b_i\ (f_1, \ldots, f_{i-1}, f_{i+1}, \ldots, f_{i\ max})$$

and

$$c_i = c_i\ (f_1, \ldots, f_{i-1}, f_{i+1}, \ldots, f_{i\ max})$$

The evolution of the bubble-size distribution is found as the solution to ordinary differential equations shown in Eq. 1. In general, the solution must be found numerically, but in GRASS an efficient approximate analytical solution is based in the analysis.

Fuel swelling is calculated from the distribution in a straightforward manner using

$$\Delta V = \sum_{\text{bubble types}} \ \sum_{\text{size ranges}} f_i(t) \times \frac{4}{3} \pi r_i^{\ 3} \qquad (2)$$

where the double summation is over all bubble types and sizes, ΔV is the total bubble volume, and r_i is the average radius of bubbles in the ith size range. The swelling calculation is done separately for each fuel zone. Bubbles do migrate through the fuel and the rate of leaving any zone is included in the term b_i in Equation 1; of particular interest is the rate gas leaves the columnar zone. This, the gas release rate, is given by

$$GR = A \times \sum_{\text{bubble type}} \sum_{\text{size range}} f_i \times v_i \times s_i$$

where the bubbles pinned to dislocations are not included in the sum, GR is the rate gas atoms are released, A is the area of the inner boundary of the columnar grain region, v_i is the average velocity of bubbles in the ith size range, and s_i is the average number of atoms per bubble for bubbles in the ith range.

4.2.6.1 Limitations

The GRASS code was written to be incorporated into LIFE-II which would supply temperature, temperature gradient, fission rate, and hydrostatic stress state information. GRASS presently, however, is used as a stand alone code with the necessary information being input. This disallows a realistic determination of the hydrostatic stress since the amount of swelling and gas release is dependent on and determined to some extent by its magnitude.

Although GRASS as it presently operates has little impact on accident analysis quantification, its conception is a very important step toward future fission gas behavior models. This is true since much of the thinking employed to develop GRASS is necessary to build similar and more refined models for inclusion in deformation and fuel slumping analysis models. Since GRASS is applicable to fission gas behavior in solid fuel only, further efforts to model gas behavior in fuel as it melts is necessary for transient analysis.

4.3 Accident Initiation Codes

The most recent models employed in the SAS and MELT codes are described. Most of the models are present in the latest versions of these codes, SAS3A and MELT-III. The DEFØRM-II code is not used in SAS3A. Instead a version of DEFØRM-I modified to describe irradiated fuel is used since DEFØRM-II development is not complete.

In order to determine the stresses and strains on the clad mainly during overpower transients, the DEFØRM-I (Ref. 104) module is used in SAS3A.

4.3.1 DEFØRM-I

This module in the SAS code system calculates the thermoelastic deformation of the fuel and the elastic-plastic deformation of the cladding, using the fuel and cladding temperature profiles from the Heat Transfer Module. A quasi-static deformation analysis is employed which implies that there is no explosive loading on the fuel elements to produce shock effects. On the other hand, it is assumed that the time scale of the loading is short enough that such long-term effects as radiation growth and viscoelastic creep can be neglected. Fuel and cladding stresses and deformations are calculated by assuming a stress-free configuration at normal operating conditions. This assumption is justified if the stresses produced by the change from room temperature to operating conditions are annealed out. Therefore, in the following description the temperature at a point is the difference between the actual temperature and the temperature corresponding to the steady-state operating conditions. The following assumptions then are used in DEFØRM-I.

1. The mechanical equations are quasi-static, i.e., the whole system is assumed to be in mechanical equilibrium all the time.
2. The plane strain approximation is used, with axi-symmetry, and shear stresses are neglected except for an approximate treatment of friction between fuel and clad.
3. All materials are assumed to be isotropic and zone-wise homogeneous.

4. Local effects such as bambooing are neglected.

5. Microscopic phenomena such as transient swelling due to the fission product bubbles in fuel matrix must be described in macroscopic, parametric terms.

6. No bulk motion of molten fuel is assumed.

7. No fuel cracking is described.

8. The clad is treated as a thin membrane elastic-perfect plastic material.

9. The fuel is treated as an elastic material only.

10. A stress free condition is assumed at the start of the transient.

11. The ideal gas law is used for fission gas state calculations.

In this module, as in the Heat Transfer Module, the fuel element is divided into axial segments. Since the radial temperature variations for a reactor fuel rod are much more severe than the axial, the field equations of elasticity with the appropriate boundary conditions are solved exactly in closed form with respect to radial variations, but only approximately by iteration with respect to axial variations of stress and deformation. Depending upon the conditions of the fuel and the clad, any one of nine cases may pertain to each of these axial segments. Deformation cases 1, 2, and 3 refer to the solid fuel: 4, 5 and 6 refer to a central cavity in the fuel with either no melting or not enough to fill the central hole; and 7, 8, and 9 correspond to the case when fuel melting has occurred and the resultant liquid is exerting expansion-derived pressures on the remaining solid fuel. The three options in each set of above cases correspond, respectively, to the existence of a radial gap (Cases 1, 4, 7), the elastic deformation of the clad due to closing of the gap (Cases 2, 5, 8), and the plastic deformation of the clad due to excessive loading (Cases 3, 6, 9).

A burst criteria method of computing clad failure time and height is also incorporated. This method employs a model in which the pressure in the interior molten portion of a fuel pin is transmitted to the clad through the solid fuel. The pressure buildup is caused by the volumetric changes in the fuel as it heats up and release and expansion of fission gas. The pressure in the inner molten zone of fuel is transmitted to the clad assuming the solid fuel has no hoop strength. Thus the clad loading is approximated by

$$Pr = P_{cav} \, (r_m / r_{in}),$$

where P_r denotes the pressure loading at the inner cladding radius, P_{cav} denotes the fuel pin cavity pressure, r_m denotes the fuel melt radius, and r_{in} denotes the cladding inner radius (fuel outer radius). Clad failure is then assumed to occur when the hoop stress given by the thin-wall approximation exceeds the clad ultimate tensile strength

$$P_r \geq U(Tc)\ (\Delta r_c/\bar{r}_c),$$

where U(Tc) denotes the clad temperature dependent ultimate tensile strength, Δr_c denotes the clad thickness and $\bar{r}_c$ denotes the mean clad radius.

Because of the inability of the DEFØRM-I module to handle inelastic behavior in general with an arbitrary yield surface in both the fuel and clad and because of the one node clad representation, the development of DEFØRM-II commenced. DEFØRM-II was, in addition, needed to more fully characterize irradiated fuel.

4.3.2 DEFØRM-II

The assumptions and limitations present in DEFØRM-II are the same as those listed for DEFØRM-I except that numbers 8 and 9 have been eliminated. The objective of the DEFØRM-II model is to calculate the transient deformation of irradiated oxide fuel pins up to the point of clad failure. The mechanical analysis is based upon the quasi-static, axisymmetric, generalized plane strain approximation both for the fuel and the clad cylinders. Up to 20 mesh points can be employed radially for the numerical solution. The axial length of the fuel pin is divided into an arbitrary number of segments or nodes (up to 20) and no interactions are assumed between one segment and its axial neighbors. The rheological model adopted herein is the elasto-plastic behavior with temperature and work-hardening yield surfaces. To account for effects from the steady-state irradiation, the model allows:

(1) 3 distinct metallurgical regions in the fuel,
(2) a central cavity containing fission gas,
(3) fission gas in the fuel matrix, and
(4) a release of fission gas to the cavity at the fuel solidus.

Some consequences of the above mentioned assumptions made in DEFØRM-II shall be mentioned briefly: The plane strain approximation used in DEFØRM-II is an economical approach, but it neglects the end effects of each dished pellet within the fuel pins. Besides, the thermal expansion in the axial direction can only be calculated as one average value for the whole pin area. If the cracking effect were included, the fuel-clad gap is expected to close earlier in the transient, but the effect of fuel cracking can properly be treated only in a three-dimensional anisotropic model. The assumption of complete slip between the fuel and the cladding after their contact tends to underestimate the loading on the clad by permitting the fuel pellets to slide over the clad, and hence underestimating the axial strains in the cladding. The other extreme can be thought of as "no-slip" treatment, in which the clad would be axially stretched along with the fuel. This would lead to an increase in axial strain in the clad, somewhat reducing the radial displacements. The complete slip model therefore tends to underestimate, while the no-slip model would overestimate the axial strains. Its effect on the circumferential strain, however, seems to be small. The circumferential strain is affected not only from the lateral contraction, but also from the redistribution of the axially restrained fuel under thermal expansion. A comparison of a freeslip model calculation with no-slip model (PECT) (Ref. 106) had shown little difference in the circumferential strains.

The generalized plane-strain solutions are obtained both for the fuel and clad cylinders in semi-closed forms. In the absence of mechanical contact of the cylinders, the two solutions are coupled only weakly through the gap pressure. In the presence of contact, however, the two solutions are coupled with the requirement that the normal stress across the interface be continuous. The mode of contact is currently assumed to be a complete slip. The boundary condition at the inner surface (if any) of the fuel is the cavity pressure and that at the outer surface of the clad, the coolant pressure. Explicit axial motion of fuel upon melting is neglected in the present model, but the cavity pressure is assumed to be uniform within the molten boundary comprising liquified fuel, solid fuel at the solidus, fission gases in the original cavity, and fission gases in the fuel matrix.

At each time step, the equivalent stress is compared to the temperature-dependent yield stress and, if the former exceeds the latter, then the plastic flow is calculated from the Prandl-Reuss flow rule based upon the von Mises yield criterion. Fuel cracking is not modeled by DEFØRM-II. Radial iterations are repeated at each axial node, until the stress strain components attain acceptable convergence. In the presence of large cavity pressure changes, however, these radial iterations themselves are repeated along the axial nodes that encompass the cavity.

The interplay between SAS2A and DEF0RM-II is as follows: at the end of every transient time step SAS2A provides DEF0RM-II with thermal variables such as the temperatures of fuel, coolant and structure, the fuel melt fractions, the coolant and plenum pressures; the major variables transferred back to SAS2A at the end of each DEF0RM step are the gap widths, contact pressures and deformed radii. The actual fuel and clad temperature profiles are used to calculate the radial dependence of the thermal expansion and yield strengths in both fuel and clad.

Fig. 7 shows the results of a preliminary calculation (Ref. 107). The initial condition is an approximate representation of an unirradiated fuel pin with a cavity of radius 0.755 mm and a fuel-cladding gap of 0.0254 mm. Stresses and strains are assumed to be zero at room temperature. The power rises from 0 to 48 kW/m in 100 sec., and then there is a "transient" in which it rises to 72 kW/m in a further 3 sec. Fig. 7 shows the temperature, yield strength, stress, strain and permanent displacement of the outermost clad mesh, the pressure in the central cavity, the width of the fuel-cladding gap, and the pressure in it or the interfacial stress if it is closed.

As the power increases, the gap closes (A), loading the clad elastically. The equivalent stress increases rapidly and

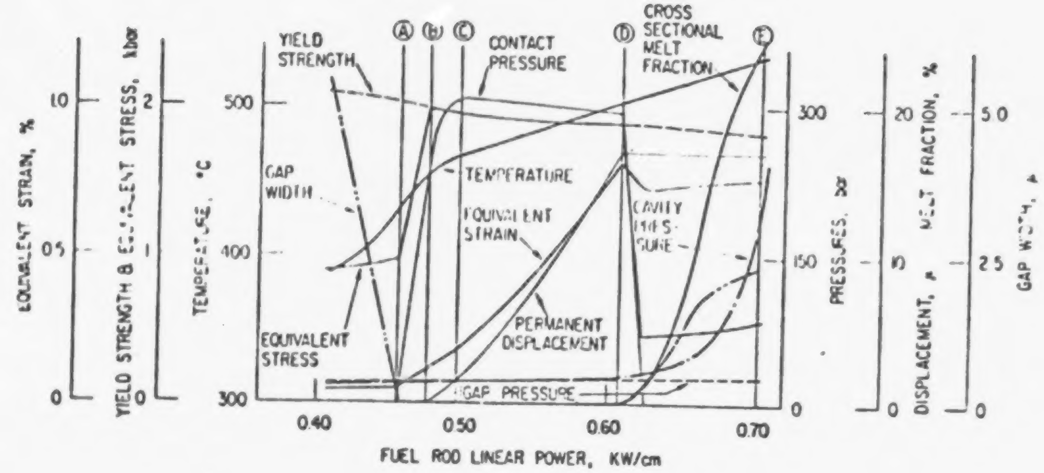

Fig. 7. Calculated Cladding Stress and Strain during a Power Transient.

the outside of the cladding begins to deform plastically (B). By (C) all the clad is plastic and the fuel-cladding contact pressure begins to decrease. At (D) the innermost fuel starts to melt. This relieves the stress on the rest of the fuel, so that it contracts, unloading the clad elastically. Gas released from melting fuel and the expansion of the molten fuel cause the pressure in the cavity to rise rapidly, until at (E) it is almost filled with molten fuel.

This illustrates the difference in clad loading for an overpower transient between an irradiated pin with a central cavity and a fresh pin. In the latter case, fuel melting subjects the cladding to a monotonically increasing load.

4.3.2.1 Limitations

The most severe limitation of the DEFØRM-II code include the lack of fuel cracking and healing models, lack of fission gas behavior models, use of the plane strain approximation and the lack of the rise of a complete, consistent set of axially dependent fuel and clad properties. In addition, as in the other ANL models, the ideal gas law is employed to describe the state of free (large bubbles with little surface tension) fission gas. A second order Van der Waals equation or similar type model is more accurate especially at higher pressures.

In summary the transient overpower accident which is very sensitive to fuel pin failure thresholds requires an integrated mechanics model to more correctly predict pin failures. The DEFØRM-II module is not capable of performing this function and most likely a new module must be completely rebuilt. Strong experimental interaction must coincide with the development of a new module so that the necessary model characteristics are conceived and developed from the start.

4.3.3 SAS3A

4.3.3.1 Introduction

The SAS integrated accident-analysis code system has been under development for some time. The initial version, SAS1A (Ref. 108) was a single-channel code which included point reactor kinetics; a combination of annular slip two-phase flow and single-bubble slug-boiling models; an elastic-plastic cladding and elastic-fuel deformation model, DEFØRM-I; a transient fuel-pin heat-transfer model; and an internal switch to the MARS disassembly module.

The sodium-boiling model was later completely rewritten as a multibubble slug boiling model for the multichannel SAS2A version (Ref. 109). A new fuel-pin deformation module, DEFØRM-II, was also included in a version of SAS2A. DEFØRM-II allows consideration of irradiated pins (restructured fuel, transient release of retained fission gas) and includes fuel plasticity in the deformation calculation. SAS2A did not include the MARS disassembly module but provided punched output as input for the VENUS-II disassembly code.

The latest version, SAS3A (Ref. 110), a preliminary version of which was reported earlier (Ref. 111), includes models which allow an integral treatment of both transient overpower and loss-of-flow unprotected accident sequences through fuel-pin disruption and up to the point of subassembly disruption. In some cases, these models can follow the sequence from initiation to neutronic shutdown by dispersive fuel motion and can be used to evaluate the possibility of establishing in-place cooling. For cases which proceed to an energetic core disassembly, the new models provide an improved definition of core conditions and reactivity insertion rate at the time of a transition to VENUS-II. The new capabilities provided by SAS3A include a steady-state fuels-initialization routine, a primary-loop hydraulics model, a fuel-coolant-interaction model for transient overpower conditions, a new moving-film treatment in the multi-bubble sodium-boiling model, and cladding and fuel motion models for voided assemblies in a loss-of-flow accident.

The phenomenological models included in SAS3A have been, in general, developed with only a partial understanding of the mechanisms involved, and thus may be modified through further comparison with experiments. The body of relevant experimental evidence has grown rapidly in the past two years, largely through experiments performed in the TREAT reactor. The recent application of the SAS3A models to in-pile tests will be summarized in addition to a discussion of the basis of the models at the time they were developed.

4.3.3.2 SAS3A Structure

The major conceptual modules in SAS3A and the relationships between these are identified in Fig. 8.

SAS3A has a multichannel capacity, and as many as ten channels (a channel is defined as an equivalent fuel pin and its associated coolant and structure) can be used to represent an LMFBR core. A typical channel is shown in Fig. 9. Different channels may be equivalent to a different number of subassemblies as well as having different fuel and clad properties to account for variable burnup effects. The main conceptual modules in SAS3A are:

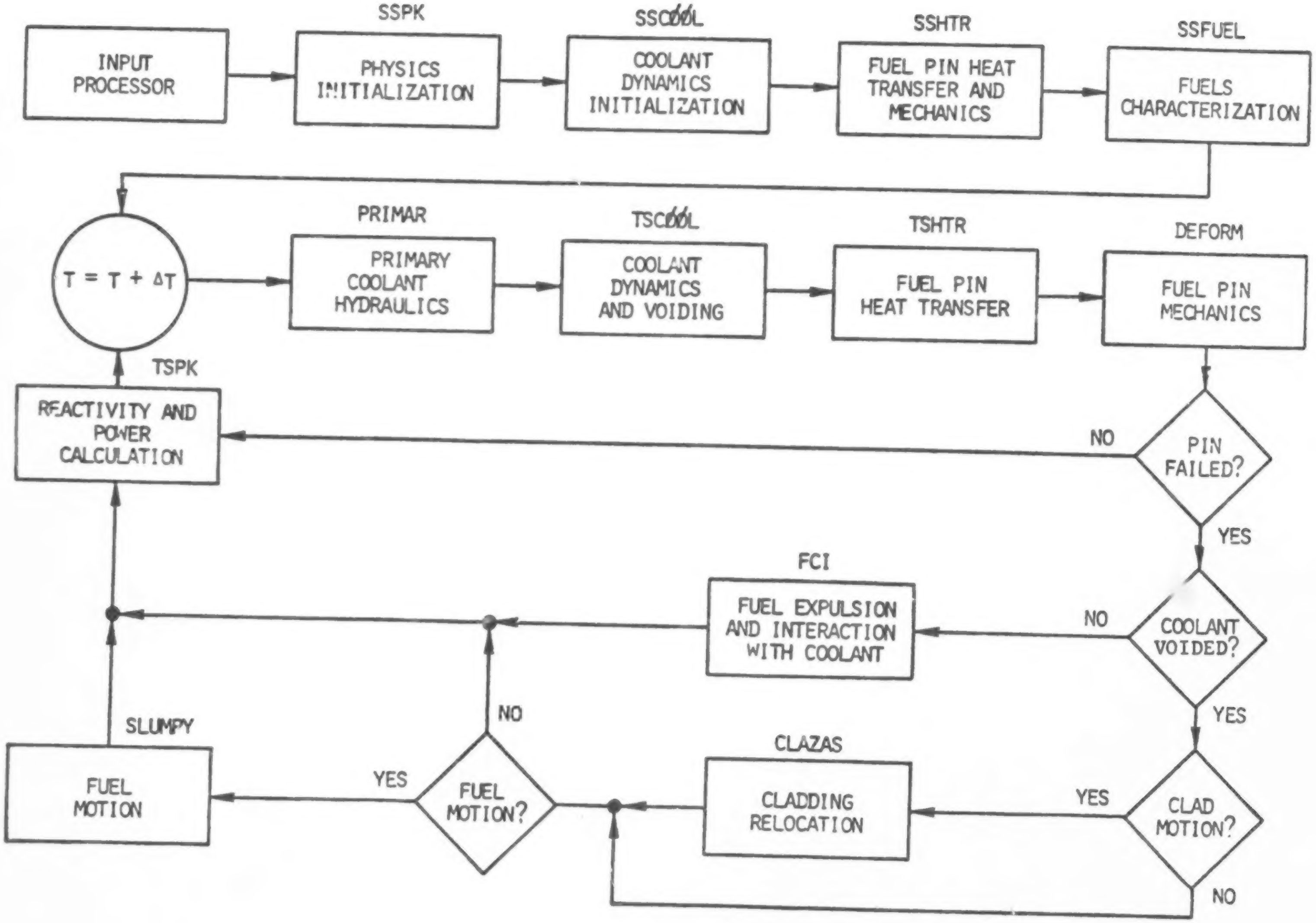
SSPK
SSCOOL
SSHTR
SSFUEL
INPUT PROCESSOR
PHYSICS INITIALIZATION
COOLANT DYNAMICS INITIALIZATION
FUEL PIN HEAT TRANSFER AND MECHANICS
FUELS CHARACTERIZATION
PRIMAR
TSCOOL
TSHTR
DEFORM
T = T + ΔT
PRIMARY COOLANT HYDRAULICS
COOLANT DYNAMICS AND VOIDING
FUEL PIN HEAT TRANSFER
FUEL PIN MECHANICS
TSPK
REACTIVITY AND POWER CALCULATION
NO
PIN FAILED?
YES
FCI
FUEL EXPULSION AND INTERACTION WITH COOLANT
NO
COOLANT VOIDED?
YES
SLUMPY
NO
CLAZAS
FUEL MOTION
YES
FUEL MOTION?
CLADDING RELOCATION
YES
CLAD MOTION?
NO

Fig. 8. SAS3A Module Relationships.

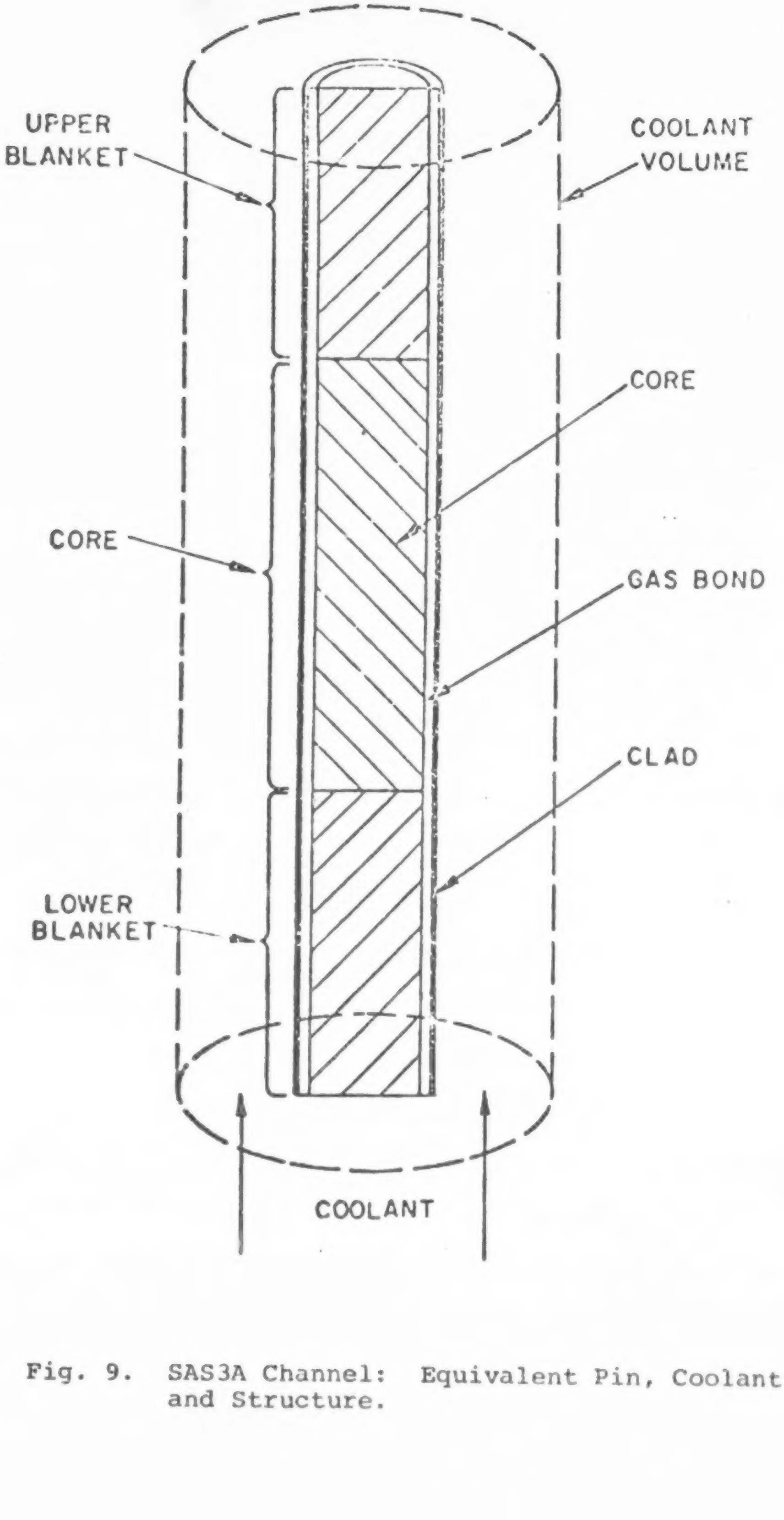
UPPER
BLANKET
COOLANT
VOLUME
CORE
CORE
GAS BOND
CLAD
LOWER
BLANKET
COOLANT

Fig. 9. SAS3A Channel: Equivalent Pin, Coolant, and Structure.

1. fuels: characterization
2. primary coolant hydraulics
3. fuel heat transfer
4. coolant dynamics and voiding
5. fuel pin mechanics (DEFØRM)
6. point kinetics and reactivity feedback
7. cladding relocation (CLAZAS)
8. fuel motion (SLUMPY)
9. fuel expulsion and interaction with coolant (SAS/FCI)

In this context a conceptual module is defined as all of the calculations pertaining to a specific model, i.e., coolant dynamics, fuel motion, etc. In actuality, the code is made up of a series of subroutines which do not have a one-to-one correspondence to the modules identified here. Typically, the calculations which fall within one module are carried out by a group of subroutines which may be entered in different ways depending on the situation. Thus, this chart represents the phenomenological structure of the code rather than the actual computational structure.

The top line of Fig. 8 consists of the modules used in the steady-state initialization process. There is an iterative loop among these modules such that the fuel pin characterization and the thermal-hydraulics are self-consistent. The second line shows the transient modules which formed SAS2A and these allow a detailed treatment up to the point at which fuel pin integrity is lost. The new modules provided in SAS3A are shown in the bottom two lines. Fig. 1 does indicate some of the restrictions on SAS3A as well as the capabilities. At the present time the cladding and fuel motion modules cannot operate simultaneously in the same channel with the FCI model, although all can operate in a partially voided channel if the location of the initial pin failure is in a nonvoided region of the channel.

The "pin failure" check following the DEFØRM box may be somewhat misleading, although loss-of-pin integrity is required before proceeding to the FCI or CLAZAS modules. In actuality there is no cladding-failure criterion based on the strains calculated by the fuel-mechanics module built into the code, and instead checks are made on thermal conditions or on a cladding strength comparison with hoop stress from either plenum fission-gas pressure (for loss-of-flow cases) or internal pressure in the fuel region due to transient release of fission gas.

Through the transient modules there are several iterative loops which are not shown in Fig. 8. For example, there is an iterative loop between TSHTR and the transient point kinetics module, TSPK, in order to converge the reactor power with the temperature-dependent reactivities prior to beginning the remaining calculations. There are several levels of time steps in the transient calculations, with the longest being the heat transfer time step. Nested inside it is the primary loop time step which in turn encompases the coolant dynamics time step. Depending on the situation, FCI or SLUMPY time steps may nest inside the coolant time step.

4.3.3.3 Fuels Characterization

In addition to geometry, hydraulics, and physics input, an important part of the initialization process in the SAS3A code is the determination of the initial conditions for irradiated fuel. Radii of the restructured fuel zones, fuel swelling, cladding swelling, and fission-gas release and retention are among the necessary information that must be input or calculated before the initiation of a transient calculation. The SAS2A code included the capability for treating restructured fuel, but providing the input without a direct link to a fuels code such as LIFE-II (Ref. 4) was a time-consuming and inefficient process. For this reason, a simple "fuels-characterization" routine, SSFUEL, was added such that restructuring calculations can be made directly and, in addition, correlations for fuel swelling, cladding swelling, and fission-gas release and retention are provided.

In these calculations, the restructuring of the fuel is based upon restructuring temperatures at each axial node for equiaxed- and columnar-grain fuel. The restructuring temperatures can be input constants (isothermal region boundaries) or can be axial- and channel-dependent as determined by a burnup dependent correlation. Fuel swelling is included simply by using an input volumetric swelling rate (linearly proportional to burnup) for each structural region. The restructuring and swelling calculations are performed in the same iteration as the steady-state heat-transfer calculations, so that the resulting fuel temperatures and structural-region boundaries are consistent. The calculational algorithm re-positions the radial temperature mesh so that the structural-region boundaries fall on a mesh boundary. Care is taken to preserve the fuel mass at each axial node. The nominal FFTF clad-swelling correlation (Ref. 112) is provided in the calculations.

The fission-gas release model is an updated version of the model of Dutt, et. al. (Ref. 113) in which the fraction of gas released is given by a linear heat rating- and burnup-dependent correlation.

The released fission gas is added to the plenum and central void when it is mixed with the amount of fill gas determined from the plenum volume and input plenum pressure at the reference temperature. In order to determine the amount of gas in each of these regions, it is assumed that the plenum gas and the central void gas are in pressure equilibrium.

4.3.3.4 Primary Loop Hydraulics

In both loss-of-flow and transient-overpower accidents, hydraulic coupling between coolant channels has a direct bearing on the development of core-voiding patterns and, in many cases, on subsequent cladding and fuel motion. For example, in the voiding phase of a loss-of-flow accident, flow diversion from voiding subassemblies delays boiling initiation in cooler subassemblies. To account for these effects the PRIMAR module was developed and included in SAS3A. Although the main objective was to provide hydraulic coupling between coolant channels, compression of cover-gas volumes and a treatment of primary-loop hydraulics was also included. The PRIMAR module is directly coupled with the coolant dynamics module (TSCOOL). However, the coupling is numerically explicit at the inlet and exit to each channel rather than implicit or iterative; thus, solution techniques in each module remain independent of each other. PRIMAR includes inlet and outlet coolant plenums which are connected to coolant channels and a bypass channel (control-rod and radial-reflector subassemblies, for example). The primary-loop module provides inlet and outlet pressures to the coolant-dynamics module, which returns detailed channel mass flow rates as input for the primary-loop calculation.

The outer primary loop contains a pump, intermediate heat exchanger, and piping. The pump pressure history is presently supplied by input. The present version also does not allow for unbalanced-loop effects or single loop pipe rupture calculations. A new version will be developed to remove these limitations in the near future.

4.3.3.5 Fuel Heat Transfer

A one-dimensional (radial) heat flow model is employed in SAS3A, thus assuming that axial and angular heat conduction are relatively unimportant for the class of accidents which are treated. In most cases, this assumption appears to be valid since the fuel pins are relatively long and thus, time constants for appreciable axial conduction in comparison to total accident times are long as well. However, it could appear that lack of angular conduction in LMFBRs which exhibit strong angular asymmetrics in the pins and the subassemblies may not be appropriate. It would seem that further studies of angular conduction effects would be warranted in order to determine whether the SAS heat transfer calculations are, indeed, properly modeled.

SAS3A assumes that a transient begins at some specified steady state. Given the dimensions, material compositions, material properties, heat generation rates, flow rates, and hydraulic conditions of each channel, the steady state portion of the heat transfer module computes the radial and axial temperature profiles and average temperatures and volume fractions in the different axial regions and channels. Initially, a heat balance is applied to the various radial increments. The resulting set of nonlinear algebraic equations for the fuel are solved simultaneously using a Gauss-Seidel iterative scheme. The gasbond gap is treated by using an effective bond conductance. Since axial conduction is neglected, the axial increments are thermally coupled via the cooled temperature and temperature calculations are made for each of the axial segments in succession, following the direction of coolant flow. The Storrer effect of heat transfer from downstream coolant to the fuel in the axial blanket is included.

The time-dependent radial temperature profile in each pin is obtained by solving the diffusion equation in cylindrical geometry, that is

$$\frac{1}{r} \frac{\partial}{\partial r} \left[K_f(T_f)\, r \frac{\partial T_f}{\partial r} \right] + Q(r) = C_f \rho_f(T_f) \frac{\partial T_f}{\partial t} \qquad (4)$$

where

T_f = fuel temperature

C_f = fuel heat capacity

ρ_f = fuel density

K_f = fuel thermal conductivity

$\dot{Q}(r)$ = volumetric heat generation rate

Note, that the material properties of the fuel are temperature dependent. This temperature dependence can either be input as tables of values versus temperature, or in the case of FPTF fuel pins, they are code generated. These calculations are very sensitive to the value of the material properties used in the calculations. If one does not have accurate values, based on experimental measurements of materials properties, the calculations could have serious errors. This is especially the case where advance fueled (carbides and nitrates) LMFBR's are being studied since their properties are not well known.

Each axial node is divided into a number of radial nodes to perform the numerical solution of the heat conduction equation by an extrapolated Crank-Nicholson difference scheme. The cladding is divided into nodes and equations which are similar to those in the fuel are solved.

When the bond consists of a gas (He), there is usually a large temperature drop through the bond and such a steep gradient may involve numerical instabilities. To alleviate this problem the heat flux through the gap is assumed to consist of a conductive and a radiative component. The conductive component is usually larger than the radiative component. When the fuel deformation module (DEFORM) predicts that the fuel and clad have come into contact, the gap thermal conductance is set to a maximum value which is pressure dependent.

In addition to calculating heat transfer in the fuel gap and clad, the code is also capable of approximating the temperature of the structural material which may be in the core (subassembly can, supporting structure, etc.). This calculation is based on a simple relation which considers the transport of heat from the coolant at the various axial modes.

The coolant temperatures and the heat transfer coefficients between the clad and coolant are always calculated before the fuel and clad temperatures. The steady-state coolant temperatures are determined by the coolant flow rate and the total heat generation rate for each axial node from which the steady-state clad and fuel temperatures are calculated. During the transient, the fuel heat transfer and cooled dynamics modules are coupled via an extrapolation of the clad temperature.

The coolant temperature calculation for a time step uses an implicitly calculated heat flux based on an extrapolated value of the clad mid-point temperature. The clad temperature extrapolation is based on the clad temperatures calculated in the previous time step. As before, the clad and fuel temperature changes for a time step are determined after the coolant temperature has been calculated.

4.3.3.6 Coolant Dynamics and Voiding

The coolant dynamics module in SAS3A has two main functions: to provide steady state and transient coolant flow rates, temperatures and heat transfer coefficients for coupling with the heat transfer module; and to provide a voiding profile for reactivity feedback calculations and for the influence of voiding on the removal of heat from the fuel pins. Temporal and spatial void distributions, along with input void reactivity coefficients, are used to obtain the coolant voiding component of the reactivity feedback which is coupled to the point kinetics module. The coupling of the coolant dynamics and fuel heat transfer modules arises naturally via the heat flux at the cladding surface.

The sodium voiding model is a multiple-bubble, slug ejection model. Voiding is assumed to result from the formation of bubbles that fill the entire cross section of the coolant channel. Up to nine bubbles, separated by liquid slugs, are allowed in one channel at any time. Each bubble may contain either sodium vapor, fission product gas, if clad rupture occurs, a combination of the two, or in the SAS3A version, a fuel-coolant interaction zone.

In SAS2A, liquid film left on the clad and structure after boiling occurs is assumed to be a static film whose thickness varies only due to vaporization and condensation. Film dry-out is predicted on this basis. The SAS3A version of the code includes a film motion treatment that also accounts for thinning or thickening of the film due to film motion under the influence of gravity and the shear forces due to streaming vapor. The addition of this model in SAS3A allows for a better prediction of the time of clad melting and rupture since the liquid film, which acts as a heat sink, may be "ripped" from the cladding surface due to high sodium vapor velocities and thus removing the heat sink.

The basic conservation equations used for a liquid slug, or for the whole channel before boiling starts, are the same as those used in SAS1A, except that a volume heat source has been included in the energy equation, corresponding to neutron and gamma ray heating of the coolant.

The basic equation used for conservation of energy in a liquid slug is :

$$\frac{\partial}{\partial t}\,(\rho H) + \frac{\partial}{\partial z}\,(GH) = \gamma\phi(z,t) + Q\,(z,t) \qquad (5)$$

where

H enthalpy,
G = mass flux,
γ = surface area of clad/volume of coolant ,
ϕ = heat flux from clad and structure , and
Q = volume source due to direct heating by neutrons and gamma rays.

At the end of each time step before voiding starts in a channel, the coolant temperature at each axial node is compared with the corresponding saturation temperature. If a user specified amount of superheat is exceeded at a node, then the time step size is reduced, and the coolant calculations for the channel are repeated for the time step, so as to satisfy the superheat criterion exactly (within a small tolerance) at the end of the time step. A vapor bubble is then formed at the node.

After voiding has started in a channel, a similar test is made at the end of each coolant time step for the formation of new bubbles within the liquid slugs. The formation of new bubbles after voiding has started is subject to the following limitations and modifications.

(a) If the maximum number of bubbles (nine bubbles) already exist in the channel, then new bubbles will not be formed.

(b) No new bubbles will be formed within a minimum distance, S_{Lmin} (minimum slug length) of a bubble-liquid interface, so nodes within S_{Lmin} of an interface are not checked for bubble formation. Interpolated coolant temperatures and saturation temperatures a distance S_{Lmin} from each interface are checked, and a bubble is formed at this position if the superheat criterion is exceeded.

(c) No more than one new bubble will be formed in a channel in any time step.

(d) After the first bubble is formed, time steps are not repeated so as to exactly match the superheat criterion for later bubbles: when the superheat criterion is exceeded, a new bubble is formed with whatever superheat happens to exist. At the end of each time step, linear extrapolation of coolant and saturation temperatures is used to predict when the next bubble will form. This prediction is used to limit the size of future time steps, so that normally the saturation criterion is exceeded only slightly when a new bubble is formed.

Bubbles are assumed to fill the whole cross section of the coolant channel, except for a liquid film left on the clad and structure. A bubble starts with zero thickness and with an initial temperature equal to the coolant liquid temperature at the time of bubble formation.

The vapor bubble pressure is assumed to be always equal to the saturation pressure corresponding to its temperature. Thus, the formation of a vapor bubble with a nonzero amount of superheat leads to an immediate jump in pressure at the bubble location.

The initial bubble growth is due mainly to two effects: (1) the initial jump in pressure, corresponding to the superheat, drives the liquid slugs apart, forming a larger bubble, and (2) heat flow through the liquid-vapor interface produces vapor to fill the bubble and sustain the pressure. When the bubble gets larger, vaporization of the liquid film on the clad becomes the main source of vapor. The vapor pressure and temperature are assumed to be spatially uniform during the initial bubble growth.

After the bubble length exceeds a user specified minimum length (usually five to ten centimeters) the vapor bubble calculation is switched to a different model. Heat flow through the liquid-vapor interfaces is ignored, but axial variations in vapor pressure within the bubble are accounted for. Vaporization of the liquid films in the hot part of the core, and condensation in cooler regions, can lead to high vapor velocities and corresponding appreciable pressure gradients within a vapor bubble. The numerical scheme that is used to calculate the time and space variations in the vapor pressure is an implicit scheme that can handle moderately large (a few milliseconds) time steps. Wave effects tend to be suppressed by the numerical scheme.

Condensation in cooler regions can cause a vapor bubble to shrink. If the bubble size decreases to below the minimum length for the pressure variation model, then the initial uniform pressure model is used again. If the bubble size decreased to less than a minimum bubble size, and if at the same time the rate of decrease of the bubble size exceeds a minimum value, then the bubble is assumed to collapse; and the bubble is eliminated from the calculation. When a bubble collapses, the liquid slugs above and below the bubble are combined into one slug; and the flow rate of the combined slug is determined by conserving the combined momentum of the two slugs.

Although this sodium-boiling model was based on previous models which were in turn based on an understanding of boiling phenomena obtained from out-of-pile experiments, the first direct experimental check of the model was provided by a calculation (Ref. 114) of an out-of-pile flow-blockage experiment reported by Peppler (Ref. 115) of Karlsruhe. In this case, the calculations and experiment were in reasonably good qualitative agreement with respect to flow rate oscillations and initial voiding behavior. However, the dryout of the film was based only on vaporization, and the experimentally observed dryout time was much shorter than the calculated time. For this reason it became necessary to consider an additional dryout mechanism, i.e., stripping of the film by streaming vapor as described by Grolmes and Fauske (Ref. 116).

To account for vapor stripping and film draining, a one-dimensional annular film-flow model (Ref. 117) has been developed as an integral part of the SAS2A boiling model for inclusion in SAS3A. The motion of the liquid film is calculated explicitly under the influence of vapor drag, wall friction, gravity, and the axial pressure gradient. Droplet entrainment is not considered.

The film-dryout time predicted by this model for the single-pin type of sodium boiling experiment of Peppler agrees well with the experimentally observed dryout time. The new model predicts film dryout at 0.47 sec after the start of boiling, whereas Peppler observed film dryout at 0.48 sec after the start of boiling.

Results of the film-motion model for a loss-of-flow transient are shown in Fig. 10. This figure shows the extent of the voided region and the film thicknesses calculated at five points in time after boiling inception. At boiling times of 0.24, 0.34, and 0.44 sec, there are a number of separate vapor bubbles and liquid slugs in the coolant channel, whereas at 0.49 sec a single void was established. The film-thickness histograms at boiling times of 0.54 and 0.64 sec make it apparent that the liquid film has been carried upward from the upper part of the core by the upward vapor flow. The lower part of the relatively cold fission-gas plenum region of the pin is also being stripped of film.

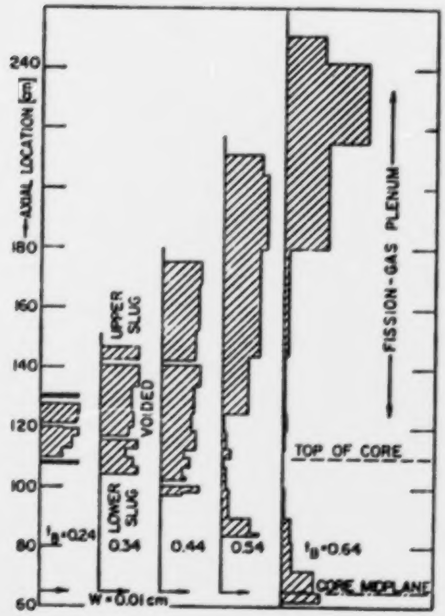

Fig. 10. Upward Film Motion and Dryout (0.64 seconds after Boiling Initiation) from SAS3A/TSCOOL Calculation.

In the SAS2A analyses of the Peppler experiment, it was observed that assuming dryout at two-thirds the original film thickness agreed with the experimental observations. Thus, most recent SAS2A calculations with the static-film model have used a minimum film thickness equal to two-thirds of the initial film thickness. A comparison of LOF calculations indicates that the two-thirds approximation agrees fairly well with the film-motion model as to film dryout times and cladding temperatures soon after dryout. However, results of the two models diverge after film dryout and, by the time the cladding melts, the differences are significant in terms of downward dryout development.

To verify further the boiling model, a pretest analysis was made of the TREAT R5 seven-pin LOF experiment (Ref. 118) and was used as part of the experiment design. The calculation of R5 was repeated following the experiment, with the only change being the use of the actual power and flow transients measured in the experiment. A comparison of the calculated and experimental results are shown in Ref. 118. Initial flow reversal and the oscillating behavior of upper and lower liquid slugs are well represented by SAS. In addition, experimental and calculated coolant temperatures at the top and bottom of the active fuel agree well into boiling, thus indicating that the overall void-growth behavior is predicted well.

While flow reversal and initial test-section voiding are predicted well by the SAS calculation, the inception of voiding is predicted to occur about 0.5 sec after that indicated in the experiment. This relatively slight variation could possibly be explained by small uncertainties in the measured power and flow transients. However, it is perhaps more reasonable to assume that this is due to local variations in radial coolant temperatures and that these variations become averaged out once sustained voiding occurs.

Although the agreement between averaged quantities is fairly good, there is no evidence that the early voiding actually exhibits a multi-bubble regime in which the vapor bubbles fill the channel area. While the multi-bubble approach is perhaps phenomenologically correct for a single subchannel at uniform temperature, it may not be correct for situations involving local variations in temperature since initial bubbles may not fill the channel. Nevertheless, for the seven-pin test section in the R5 experiment, it adequately predicted overall voiding behavior.

For much larger test sections or for full-subassembly reactor situations, a larger degree of radial temperature variation and noncoherence of boiling initiation might be expected. With wire-wrapped fuel pins, significant noncoherence of boiling initiation would be expected even in a uniform power assembly since the outer rings of pins are considerably overcooled (Ref. 119). Also, large radial power gradients exist in many subassemblies in any system, and this will also cause noncoherence of boiling initiation. The effect of noncoherent initiation on gross voiding behavior is not yet known; however, the voiding induced power increase in a large LMFBR should result in increased voiding coherence. Noncoherent voiding is under intensive investigation, and new voiding models to treat these effects must be and are being developed.

In addition to sodium boiling, SAS3A contains the model for voiding by plenum fission-gas release used in SAS2A. This model calculates the expulsion of the gas into the coolant channel and the resulting voiding for situations involving release into a nonvoided channel. The model is very similar to that of Chawla (Ref. 120).

Early analyses (Ref. 121) of a loss-of-flow accident without scram in the FFTF reactor used very conservative estimates of plenum-fission-gas pressures and irradiated-cladding strength. As a result, pin failure and plenum-gas release were calculated to occur prior to voiding. Later calculations with nominal plenum pressures and updated cladding strengths consistent with those obtained in tube-burst tests (Ref. 123) at HEDL have indicated that the pins will not fail until after sodium boiling. Since the cladding stays near the sodium saturation condition as long as the film remains on the cladding, the pins will not fail until after cladding dryout. At the present time, release of plenum gas into a fully voided channel is expected to have only a slight effect on the overall voiding behavior. It is important to note that there were no direct observations of gas release in the TREAT L3 and L4 irradiated-pin LOF tests. However, there was a noticeable difference in flow rate oscillations (chugging) as compared to the similar L2 fresh-pin test, and this has been suggested to be due to the presence of the non-condensible fission gases.

4.3.3.7 Fuel Deformation

The fuel deformation module of SAS3A (DEFORM) calculates the thermoelastic deformation of the fuel and the elastic-plastic deformation of the cladding, using the fuel and cladding temperature profiles generated by the heat transfer module. A quasi-static deformation analysis is employed which implies that there is no explosive loading on the fuel elements to produce shock effects. This module is not included in a closed loop, i.e., there is no reactivity feedback or other effect on the calculation of the transient. Since the DEFORM series of computer codes is discussed elsewhere in this report, nothing further will be mentioned about the DEFORM module in the SAS codes.

4.3.3.8 Point Kinetics and Reactivity Feedback

The standard point kinetics equations are used to solve for the reactor power level:

$$\frac{dn}{dt} = \frac{\rho - \beta}{\Lambda} n + \sum_{i=1}^{6} \lambda_i C_i, \qquad (6)$$

and

$$\frac{dC_i}{dt} = \frac{\beta_i}{\Lambda} - \lambda_i C_i; \; i = 1,6, \qquad (7)$$

where

n = neutron density,

C_i = concentration of ith delayed neutron precursor,

β_i = delayed neutron fraction from the ith group,

$\beta = \sum_{i=1}^{6} \beta_i$ = delayed neutron fraction,

λ_i = decay constant for the ith precursor,

Λ = prompt neutron generation time = ℓ/k_{eff},

ℓ = prompt neutron lifetime,

k_{eff} = effective multiplication factor,

ρ = reactivity = $(k_{eff} - 1)/k_{eff}$

These equations are solved using a standard numerical scheme (Ref. 123).

The net reactivity, ρ, in Eq.6 is the sum of seven contributions

$$\rho = \rho_P + \rho_D + \rho_c + \rho_e + \rho_d + \rho_s + \rho_{cd} \qquad (8)$$

where

ρ_P = programmed reactivity input (initial ramp and scram),

ρ_D = Doppler feedback reactivity,

ρ_c = sodium void feedback reactivity,

ρ_e = structural (radial) expansion feedback reactivity,

ρ_d = fuel density feedback reactivity,

ρ_s = slumping reactivity,

ρ_{cd} = clad relocation rectivity.

4.3.3.9 Cladding Relocation

In analyzing the loss-of-flow accident (Ref. 121) for FFTF it was recognized that, under the expected relatively constant power conditions, cladding would melt some 2-3 sec prior to fuel melting in the first voided subassemblies. Thus, although there was no direct experimental evidence of such an effect, it was reasonable to assume that the molten cladding would relocate, possibly moving out of the heated region, freezing, and plugging. The first supposition was that the cladding would drain downward and plug below the fuel region. However, it was recognized that upward sodium velocities could be high enough to cause flooding (wave formation), and the resulting high friction drag would lead to upward cladding motion, similar to the sodium-film stripping effect. This could then cause initial cladding plug formation above the fuel region, followed by draining of later cladding to melt and plugging below the fuel region.

In addition to the mechanical effect on sodium voiding and fuel dispersal, cladding relocation has an important reactivity effect and a significant thermal effect since removal of the cladding heat sink allows fuel temperatures to rise rapidly. Thus, in order to analyze cladding relocation, the CLAZAS module (Ref. 124) was developed for inclusion in SAS3A.

This model uses an explicit calculation of the motion of molten clad consistent with the sodium-vapor-pressure-gradient model. The physical picture is one of discrete clad segments which can combine by moving over other clad segments. Each segment moves under the influence of gravity, the channel pressure gradient, the frictional drag due to streaming sodium vapor, and friction between moving clad and the fuel pin. Feedback effects are included to modify the coolant-channel sodium-vapor friction, the coolant channel hydraulic diameter, and the sodium-vapor flow area. Heat-transfer effects are calculated by including a relationship describing heat transfer from moving clad to stationary clad, a relationship describing heat transfer from stationary fuel to moving clad, and a variable viscosity for molten clad as a function of internal energy. Since the viscosity is assumed to become very high as the cladding internal energy decreases through the heat of fusion, the cladding stops as it freezes.

Fig. 11 shows results from a typical calculation by the CLAZAS model. The particular example is an analysis of the cladding motion in the L2 TREAT experiment (Ref. 125), in which the fueled region extends from 10 to 45 cm. The initial cladding to melt rises under the influence of the streaming sodium vapor. These cladding nodes begin to impede the vapor flow, and the next nodes to melt drain down since the force of gravity now dominates. Downward motion appears to be primarily limited by the rate of cladding melting in the lower part of the pin. The final cladding configuration is predicted to be a fairly massive blockage below the fueled region and a lesser blockage above the fueled region.

Since the model uses relatively large segments, the detailed predictions of the model should not be expected to agree precisely with the experiment. However, these blockages are generally in qualitative agreement with the cladding plugs evident in the post-mortems of the test sections. More recent out-of-pile experiments also indicate through direct observation that, in the sodium vapor flow regime of interest in FFTF, the film motion model of cladding flow is qualitatively correct.

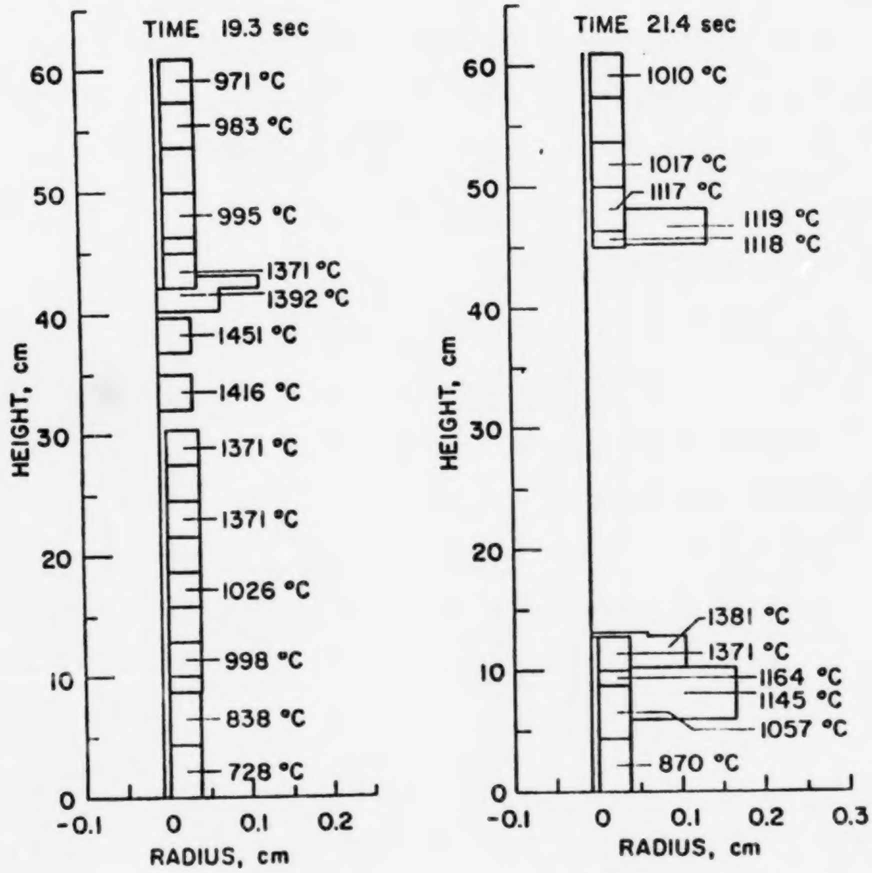

Fig. 11. CLAZAS Calculation of L2 TREAT Experiment Showing Cladding Blockage Formation at Top and Bottom of Fuel Column.

Results from the R5 TREAT experiment will provide a test of the cladding motion model validity under more prototypic conditions (fuel pins in the R-series were full-length FTR prototypic pins, whereas the L2 pins were 13 in. long to correspond to the EBR-II irradiated pins used in L3 and L4). The R5 test was oriented specifically to the cladding-relocation problem and was a LOF test in which the TREAT power transient was terminated following full test section voiding and extensive cladding melting, but prior to significant fuel melting. Posttest radiographs indicate a substantial cladding blockage near the bottom of the fuel column. Later posttest examinations will be necessary to indicate the extent of any upper cladding blockage since the radiographs do not clearly show any. For both R4 and R5 there appears to be excellent consistency between the calculations and data on overall voiding behavior and on initiation of cladding or fuel motion.

4.3.3.10 Fuel Motion

A common and quite reasonable assumption in many fast reactor accident analyses has been that fuel, driven only by gravity, slumps as it melts. This was demonstrated at HEDL by Weber et al. (Ref. 126),in fresh fuel melting experiments perfromed in a laboratory apparatus with an externally heated fuel column. Attempts have been made to include an effective viscosity to slow the free-fall process and to calibrate the effective viscosity with experimental information (Ref. 127). Following this, the first fuel slumping model used in conjunction with the SAS codes assumed that the first fuel to melt flowed as a viscous film over intact pin stubs. However, the viscosity did not seem to have an appreciable effect, since completely molten fuel is almost inviscid.

On the other hand, some overpower type experiments have indicated (Ref. 128) that release of retained fission gas could have a significant effect on fuel motion and possibly lead to a dispersal of fuel by fission gas. In addition, the first irradiated-pin experiment in the out-of-pile fuel melting tests performed by Weber et al. (Ref. 126) indicated that, under slow heating conditions, low-power gassy irradiated fuel could be dispersed rapidly by release of retained fission gas.

Since this kind of effect could be a significant factor in an unprotected loss-of-flow accident and since there appeared to be a need for an explicit model for fuel motion in a voided channel, the SLUMPY module (Ref. 129) was developed for SAS3A.

SLUMPY provides a compressible-hydrodynamics calculation of fuel motion under the influence of gravity, sodium vapor, fission gas, friction, steel vapor and fuel-vapor driving forces. It can be used either to supply detailed initial conditions to a VENUS-II two-dimensional disassembly calculation, or it can be used directly as a disassembly code within the limitation of one-dimensional motion (implying intact subassembly geometry). In most SLUMPY calculations, fuel motion is assumed to be initiated when melting begins in unrestructured fuel. This assumption is based on two fuel characteristics. First, the equiaxed region is expected to be structurally strong, and initiation of motion may require that this region be near melting. Second, the unrestructured fuel should have fission gas on grain boundaries providing a fragmentation mechanism when this fuel melts. Early irradiated UO_2 fuel pin meltdown experiments (Ref. 130) in a transparent dry capsule indicated that pins would stay intact at least until incipient melting, and the more recent R- and L-series experiments also seem to verify this latter assumption.

As the fuel melts, individual axial fuel segments join the "slumped" region treated in the SLUMPY calculation. Unmelted fuel above the slumped region can fall into or be pushed out of this slumped region. The unmelted pin below the slumped region is assumed to be stationary. Both the upper and lower solid fuel segments restrict the area available for the slumped region. Axially limiting boundaries for the slumped region are dependent on user input; or if CLAZAS is used, the boundaries may be determined by the time-dependent positions of calculated clad blockages.

The equation of state is composed of six parts. First, there is an ambient background pressure assumed to be fission gas released from the pin prior to initiation of slumping. Second, any additional fission gas released from the fuel either at slumping initiation or during fuel motion adds to this background pressure. Slip is included between gas and fuel particles. Third, the sum of the fuel vapor pressure and stainless-steel vapor pressure (if present) replaces the background fission-gas pressure if such vapor pressures are large enough. Fourth, if a transition to a single-phase liquid occurs, single-phase pressures will replace the vapor or fission-gas pressures. Fifth, the local ambient background pressure can be increased to the sodium vapor pressure predicted by the boiling model if the channel is not plugged. In this case a high friction factor is fed back to the boiling model to simulate the effect of fuel. Sixth, a psuedo-viscous pressure (Ref. 19) is added to any calculated pressure to help provide more numerical stability.

A detailed study of gas release and swelling has been carried out for inclusion in SLUMPY calculations, using a bubble coalescence model to represent the fission-gas behavior. The calculations were carried out using a relatively small computer code that has evolved from studies begun nearly ten years ago (Ref. 131). The code is currently called FRAS (Fission-gas Release And Swelling) and is similar to the GRASS code (Ref. 132).

Since the FRAS model is approximate and the major parameters are not well-known, the gas-release calculations have been calibrated (Ref. 133) with two experiments which had quite different heating conditions. The first of these is the TREAT H3 failure-threshold experiment (Ref. 134) and the second is the HEDL out-of-pile fuel-melting experiment FGR-15 (Ref. 126). The calculations with FRAS give only the release of gas to the grain boundaries. Additional assumptions must be made to describe the effect of the gas on initial fuel motion, since models do not presently exist to describe either the gas release from grain boundaries to the coolant channel or the fragmentation of the fuel due to grain-boundary gas. At the present time, the particular assumptions used lead to the formulation of a fuel-particle suspension in melting irradiated fuel. If reactor power is high, melting fuel will tend to disperse since fission gas is being released from fuel faster than it is being lost via slip. If the power is low, fission-gas slip will dominate and the fuel will tend to collapse. At steady-state power a dispersion will tend to be maintained until either steel or fuel vapor pressures build up. This latter possibility is consistent with L3 and L4 fuel motion results where little axial fuel motion was observed until the possible generation of steel or fuel vapor pressures, although the gas-particle suspension possibility is only one of several plausible scenarios.

There are several experiments, most of which have been alluded to earlier, which have a significant bearing on the SLUMPY modeling of fuel motion. First, some of the out-of-pile experiments performed by Weber et al (Ref. 126) indicated that fresh fuel columns heated from the outside would slump or fall rapidly as they melted. The fresh-fuel L2 loss-of-flow experiment in TREAT also showed fuel slumping, but mush more slowly than expected from free fall (Ref. 125). This can be duplicated in SLUMPY by varying the viscosity as the fuel goes through the heat of fusion. However, it may be more likely that the fuel motion in L2 was a complex process involving crumbling of pellet stacks (once cladding was removed) and asymmetric power distributions in the test section. A relatively simple single-pin model like SLUMPY cannot adequately analyze this situation. Although the model can be forced to fit the experiment, the mechanisms are not presently identified clearly enough to allow extrapolating to another system.

As mentioned earlier, the first melting experiments with irradiated fuel at HEDL indicated a rapid dispersal of fuel by release of retained fission gas. These experiments were with low-power irradiated gassy fuel. Later experiments with higher-power fuel did not indicate such a dramatic dispersal, although turbulent fuel motion was evident. The later experiments, particularly FGR-15, were extremely valuable in providing transient data on gas release. Also, in a SLUMPY analysis of FGR-15, the fission-gas-fuel-particle slip assumption used in SLUMPY led to a good estimate of the length of time fuel was in motion in the experiment.

The L3 and L4 EBR-II irradiated-pin loss-of-flow experiments (Ref. 125) in TREAT have also provided some important experimental information. Both of these experiments exhibited the "eructations" of fuel seen after slumping in L2.

However, in L3 and L4 there was little previous slumping as compared to that observed in L2. At the present time, there is no definitive explanation of the reason for the difference in the fresh- and irradiated-pin tests although it should be noted that the L2 pins were completely fresh with no restructuring while the L3 and L4 pins had fully developed equiaxed fuel zones. The SLUMPY calculations can be made to match the general behavior in L3 and L4 by using the appropriate fuel particle size, viscosity, and fission gas release to form a fuel-gas suspension after initiation of motion. However, this mechanism is somewhat sensitive, and slight variations in the assumptions can cause the fuel to either rise, fall, or move in both directions.

The eructations seen in all three experiments also raise questions regarding steel vapor and fuel vapor, since either or both of these, perhaps adding to fission-gas pressures are plausible driving forces. Steel vapor is the more pleasing explanation since considerable steel mixing with molten fuel occurred in the experiments as evidenced by posttest examinations and since significant steel vapor pressures are expected at the temperatures thought to exist. Again, SLUMPY calculations can be made to fit the observed eructations by making the proper assumptions and mixing in steel with the fuel.

Fig. 12 shows some results from a SLUMPY calculation of the L4 experiment. The plots show the "slumped" region between and overlapping the remaining pin stubs. Here the shaded line density is directly proportional to the fuel density. In these calculations the cladding was assumed to remain on the fuel (a thin film of remaining cladding may be physically reasonable or the spacer wires could remain after cladding melting) and was mixed in with the fuel after motion initiation. The heat transfer assumptions were such that steel vapor pressures begin moving fuel at about the time of the observed eructation. In this case the final configuration of the fuel is qualitatively similar to that observed in posttest neutron radiographs (Ref. 125).

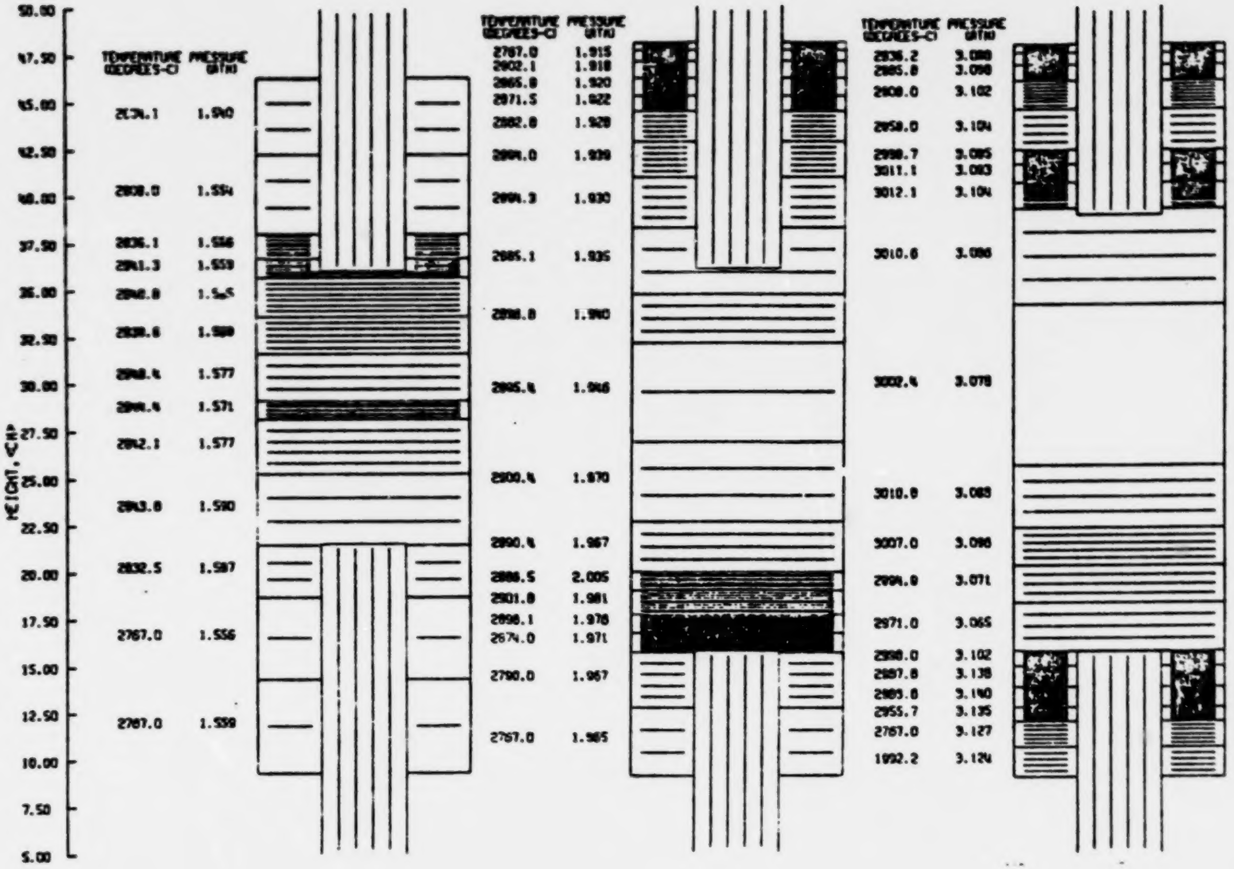
HEIGHT, CM
50.00
47.50
45.00
42.50
40.00
37.50
35.00
32.50
30.00
27.50
25.00
22.50
20.00
17.50
15.00
12.50
10.00
7.50
5.00
TEMPERATURE (DEGREES-C)
PRESSURE (ATM)
2834.1 1.540
2808.0 1.554
2836.1 1.566
2841.3 1.553
2840.8 1.565
2838.6 1.580
2848.4 1.577
2844.4 1.571
2842.1 1.577
2843.8 1.590
2832.5 1.587
2767.0 1.556
2767.0 1.559
TEMPERATURE (DEGREES-C)
PRESSURE (ATM)
2767.0 1.915
2802.1 1.918
2865.8 1.920
2871.5 1.922
2882.8 1.928
2884.0 1.939
2884.3 1.930
2885.1 1.935
2888.8 1.940
2895.4 1.946
2900.4 1.970
2890.4 1.967
2888.5 2.005
2801.8 1.981
2898.1 1.978
2674.0 1.971
2790.0 1.967
2767.0 1.985
TEMPERATURE (DEGREES-C)
PRESSURE (ATM)
2936.2 3.080
2985.8 3.090
2800.0 3.102
2858.0 3.104
2998.7 3.085
3011.1 3.083
3012.1 3.104
3010.6 3.086
3002.4 3.078
3010.8 3.083
3007.0 3.098
2994.8 3.071
2971.0 3.065
2980.0 3.102
2987.8 3.138
2985.8 3.140
2955.7 3.135
2767.0 3.127
1992.2 3.124

Fig. 12. SLUMPY Calculation of L4 TREAT Experiment Showing Eructation Induced by Steel-vapor Pressure.

The F-series experiments should provide clearer data on fuel motion mechanisms when the data is available. These tests have been designed specifically as single-pin dry-capsule tests with a heated wall in order to provide a clean separation of effects. In addition, direct electrical-heating experiments are being performed by Roberts at ANL, which will allow a better definition of fuel-motion initiation under various heating conditions for both fresh and irradiated fuel.

An important phenomenon is that of freezing and plugging as fuel is dispersed into colder regions. It is quite evident from the in-pile experiments that this should be expected in mild dispersals. Explicit modeling of plugging dynamics is being developed as part of the transition phase (Ref. 38) effort and will be included in later versions of SLUMPY.

4.3.3.11 Fuel-Coolant Interactions

Early analyses of a mild overpower transient HCDA in FFTF assumed that fuel pins failed at the midplane, and plenum fission gas could cause rapid voiding, leading to a prompt-critical transient and core disassembly (Ref. 135). Since it was recognized that this mechanism was unrealistic, later modeling concentrated on developing a more consistent scenario for the phenomena following fuel-pin failure. The FISFAX model (Ref. 136) was used in an evaluation of a sodium-in prompt critical transient in FFTF and was the first to include the effect of sodium-induced (FCI) dispersive fuel motion in terminating rapid transients. This concept, along with more realistic estimates of fuel-failure locations, went into the models used in later FFTF analyses (Ref. 137). These models indicated that a fuel-sweepout mechanism could terminate mild reactivity transients well before reaching prompt criticality. The SAS/FCI module (Ref. 138) in SAS3A includes this concept; however, both it and the improved modeling in the MELT codes were originally developed with the idea of providing a more realistic, but still conservative, estimate of the reactivity insertion rates as initial conditions for core-disassembly calculations. In this case, the early accident termination possibility came into place after model development was already partially completed.

Previous FCI models have included phenomena such as fuel ejection, sodium condensation, fuel motion reactivity, and sodium slug expulsion, in addition to the thermal interaction between molten fuel and sodium. SAS/FCI combines treatments of each of these phenomena into an integrated model. In addition, improvements over previous models include: (a) calculation of internal pin pressures from transient fission-gas release within the fuel; (b) continuous calculation of the generation of molten fuel and fission gas within the fuel pin as the fuel temperature increases;

(c) an option allowing instantaneous sweepout of solid fuel and fission gas immediately behind the clad failure point; (d) a calculation of time-dependent fuel and sodium masses within the interaction zone; and (e) a calculation of continuous acceleration and deceleration of the constraining sodium slugs. Moreover, a model for the incoherence of fuel-pin failure within fuel subassemblies is also included.

Clad failure time and location presently are set in SAS/FCI by a thermal criterion such as fuel melt fraction or fuel temperature. These criteria can be determined from correlations with the predictions of fuel-and-cladding deformation models such as DEFORM-II or with the results of analysis of TREAT experiments. An internal-pin-pressure failure criterion is also provided as an option.

At the failure time, a fuel-pin cavity whose walls are defined by the fuel solidus is established as a container for a homogeneous mixture of molten fuel, solid fuel, and fission gas which might be ejected from the pin. Increasing fuel temperatures can lead to increases in the cavity volume and the molten fuel, solid fuel, and fission-gas masses. A finite heat-transfer rate between the central void walls and the central void gas is allowed, but fission gas released during the transient is assumed to be in thermal equilibrium with the molten fuel.

Ejection from the cavity to the sodium is determined by an orifice equation for unsteady flow. Molten fuel, solid fuel, and fission gas may be ejected according to specified volume fractions or the existing volume fractions within the cavity may be used.

Fission gas ejected into the interaction zone is treated adiabatically, and molten fuel and solid fuel are assumed incompressible. Fuel-to-sodium heat transfer is similar to that of the Cho-Wright model (Ref. 139). For the sodium, the enthalpy equation of the Cho-Wright model is modified to permit a time-dependent sodium mass and to account for heat transfer between the sodium and cladding and structure. The usual single- and two-phase relationships between pressure, temperature, and enthalpy lead to a set of linear difference equations which can be solved explicitly for the sodium pressure change in a given time step. Sodium properties for subcooled and two-phase sodium are based upon properties along the liquid saturation line so that thermodynamic consistency is maintained when changing phases. Expansion of the interaction zone is controlled by the inertia of the upper and lower liquid slugs; no acoustic constraint is modeled.

As of yet, there is little direct experimental evidence which positively confirms the modeling in the SAS/FCI module. The H5 TREAT experiment (Ref. 134) appears to represent the same general kind of phenomenology, since a relatively sharp pressure spike with a following train of oscillations occurred at the initial pin failure, although the oscillations may not have been due directly to fuel ejection. Further, the neutron radiographs indicate a small, but significant, amount of fuel dispersal up above the fuel column. A direct comparison of analysis with experiment results has not yet been completed, but this is underway with the SAS/FCI module, the MELT-III code (Ref. 140), and the still more detailed PLUTO model (Ref. 141), which is to be included in a later version of SAS.

The overpower transient experiments (Ref. 134) E6 and E7 in TREAT have indicated that, if the transient is continued well beyond initial fuel failure, continued fuel melting and motion may lead to massive fuel plugging as the fuel moves out of its original position. This phenomenon is not modeled explicitly in the current codes and will need to be included in later versions, since it may have an important effect on permanent termination of the accident with inplace cooling of disrupted subassemblies.

4.3.3.12 Future Developments and Limitations

Several of the limitations of the present SAS3A code have been noted. In addition to upgrading, further internal checkout, and experimental verification of the existing models, the most significant needs for initiating-accident-phase modeling are:

(1) Treatments of multiple-pin (noncoherent) effects on voiding and on later cladding and fuel motion, (2) a consistent and integrated treatment of fuel pin mechanics incorporating fission-gas-induced fuel swelling and fission-gas release, and (3) an integrated treatment of sodium boiling, cladding motion, and fuel motion involving thermal and hydraulic interactions among all materials under conditions appropriate to accidents in large LMFBRs.

Obviously, each of these is a complex physical and modeling problem. Further, it is likely that an accident-analysis code incorporating models of this complexity in one integrated 20-30 channel calculation (as might be appropriate for a large system) would be impractical with present-generation computers except for benchmark problems. The next-generation of phenomenological models will probably be used primarily for performing studies from which the information will be fed into the multichannel accident analysis codes. Thus, the multichannel codes must concentrate on providing a means to use this information effectively to provide a consistent accident analysis.

This may be a somewhat simpler task in the future, since as larger LMFBRs become of greater interest and sodium-void reactivities tend more to dominate the accident sequences, the initiating accident codes may revert more to their original purpose of supplying input conditions to disassembly codes. However, extended transition-phase (Ref. 38) analyses still will be needed for many situations, and this must become an area of increased modeling attention.

In addition, another area that is now being developed rapidly is the coupling of the SAS code system with the space-dependent kinetics code FX2 (R.142). It is recognized that, as calculations are extended into situations involving gross material displacements, the present point kinetics with first-order perturbation reactivities may be inadequate. An initial automated but nonintegral coupling of the codes will allow consistent checks to be made of the current first-order perturbation calculations. This will also provide a good basis for designing an optimal integration of the two codes.

Some of the major limitations in SAS3A are:

1. Radial interaction or propagation of distrubances across the core are not treated.
2. An explicit calculation of disassembly initiation conditions is not performed and thus the switch to the VENUS-II code is difficult to determine.
3. No treatment of multiple-pin (noncoherent) effects on voiding, and clad and fuel motion are described.

4. There is a lack of a consistent and integrated treatment of fuel pin mechanism incorporating fission-gas-induced fuel swelling and fission gas release.

5. The treatments of sodium boiling, clad motion and fuel motion phenomena must all be integrated to describe the thermal and hydraulic interactions among all materials.

6. At present point kinetics is used. In the future SAS will be coupled with a space-dependent kinetics code FX2 for extended fuel motion analysis. Present efforts include a partial coupling with FX2 using the HOCUS-POCUS subroutines. Further work is necessary.

7. The fuel motion model, SLUMPY, needs an explicit treatment of plugging dynamics.

8. Multiple hydraulic loop (primary and secondary) capabilities for unbalanced loop effects or single loop pipe rupture calculations is needed.

9. The models are all developed for describing mixed oxide, relatively small LMFBRs (FFTF and DEMO).

Thus, analysis of large systems or advanced fueled systems with the SAS system is very speculative.

Finally there is lack of experimental validation and sensitivity analysis for most of the models included in SAS. Models such as SAS/FCI, SLUMPY and CLAZAS which represent major potential reactivity contributions need extensive experimental evaluation before any confidence in their ability to follow LMFBR accidents sequences can be obtained. At this point there has been some qualitative agreement between experiments and the CLAZAS, SLUMPY, and coolant voiding routines. The SAS/FCI model has not been verified to any extent.

4.3.4 MELT-III

4.3.4.1 Introduction

MELT-III (Ref. 12, 143-145) is an improved transient analysis code for analyzing the initiation phase of hypothetical core disruptive accidents. The code was formulated such that only information required for one channel is contained in the computer's active core. Simultaneous read and write capability between the core and a fast drum permits efficient handling of one channel at a time with the result that there is essentially no limit on the number of reactor channels that can be modeled other than the drum storage and the additional running time incurred. Channels do not have to be hexagonal rings in the reactor, but can be as small as one subassembly.

Channels can be grouped under three different pump heads which permits simulation of a core with two independent closed loops. Each channel can have up to ten axial zones which represent different geometrical cross-sections and a corresponding flow area and friction factor. One zone, normally used as the fueled region, can be subdivided radially into 11 nodes, 1 fuel surface node, 3 cladding nodes (2 of them surface), 1 coolant node and a structural node. The other 9 zones can be subdivided radially into 4 sink nodes, 1 coolant node, and 1 structural node.

One fuel pin operating at average power in its channel represents all the pins in the channel. In the non-pin area of a subassembly, the coolant flow area and structure is taken as 1/217 of the total subassembly value. The surface area of the structure is ratioed directly and the specific heat of the structural material is modified in order to correct for the distorted volume ratio.

4.3.4.2 Steady State

A subroutine called STEADY provides an initialization for the transient subroutine, ORBIT. Using the input power and shaping functions, a temperature profile is generated. The fuel is sintered and a central volume formed when the fuel temperature exceeds an input value. Thermal expansion of the fuel is based on a linear-weighted pin fuel temperature which closely approximates the expansion calculated with a shell model. Fuel expansion as a result of irradiation can also be specified. Thermal expansion of the cladding is calculated and the gap conductance is modeled by monitoring the gap between the fuel and the cladding and specifying a thermal conductivity of the interfacial gas as a function of irradiation. A minimum gap is input at which time the gap conductance becomes essentially constant. The heat transfer calculations are carried out through successive iterations as the expanding fuel and cladding radii converge to a solution. The thermal conductivity of the fuel is temperature and density dependent and increases as sintering occurs. The steady state temperature profiles identify the sintered, equiazed, and unrestructured regions in the fuel which are flagged and used subsequently in the transient portion of the code to predict variable fission gas retention.

4.3.4.3 Heat Transfer

The nodal structure incorporated in the heat transfer routine was described in the introduction. The radial nodes of the fuel pin can be input in an arbitrary manner, although they are commonly specified as either equal volume radii or equally spaced radii. The gap temperature can be taken as the average between the surface node of the fuel and the inner surface node of the cladding. Axial heat conduction within the fuel pin is neglected, but all axial positions are linked by means of heat convection, including coolant axial heat conduction through the coolant channel. Writing the energy balance equations for each axial node produces a set of dependent linear equations which form a tri-diagonal matrix plus an additional tri-diagonal matrix for the axial heat conduction in the coolant. These are solved implicitly by a Gaussian elimination scheme similar to the methods used in the SAS3A code.

4.3.4.4 Heat Transfer Between Fluid Slugs in the Channel

Axial heat conduction is calculated to occur between sodium liquid and molten fuel, and between sodium vapor and molten fuel. However, axial heat conduction is neglected between contacting slugs of sodium vapor and sodium liquid, sodium liquid and fission gas, sodium vapor and fission gas, molten fuel and fission gas.

4.3.4.5 Fuel-Coolant Interaction

The simulation of an FCI within the channel is presently available hydraulically where the user makes use of the fuel squirting to define an interaction volume and specifies characteristic pressures resulting from a FCI. This is very useful in simulating the reactivity feedback from sodium voiding and molten fuel expansion within the channel. The capability for heat transfer between sodium and fuel has been programmed into MELT-III so that a more accurate FCI model can be inserted easily as the fuel and coolant mixing model is developed.

4.3.4.6 Hydraulics

The hydraulic package represents a solution to the momentum equation in integral form. All channels with the exception of up to two independent hydraulic loops, are connected at the inlet plenum so that the same total pressure drop exits over all driver channels during the transient. Once fission gas or molten fuel enters the coolant channel, the appropriate terms are added to the continuity equation, which links the momentum and energy equations, such that fuel or fission gas become integral parts of the hydraulic balance. Logic is contained in the hydraulic routine to track up to 2 vapor slugs, 2 fission gas slugs, and 1 fuel slug at any one time within a channel. Hydraulic representation includes reentry and chugging.

4.3.4.7 Boiling

Boiling is initiated at a user input superheat temperature. The exception to this is occurrence of boiling when the coolant temperature reaches the boiling temperature if it is adjacent to either a fuel or fission gas slug which would serve as a nucleation site. Since a time step will, in general, overshoot the superheat temperature in the hottest coolant node, an interation process occurs which reduces the time step until the superheat temperature is just obtained. In the subsequent time steps a thermodynamic relationship is used to develop an iterative solution to the hydraulic balance between vapor and liquid flow. A surface film is included in the boiling nodes. It is depleted both by vaporization and due to the assumption that a velocity profile in the film matches that of the vapor. In the voiding calculations a constant friction factor is used in each zone.

4.3.4.8 Fuel Motion

Fuel motion can occur in three ways: (1) movement of fuel axially in the pin (Ref. 146), (2) movement of molten fuel from the ruptured pin into the channel, and (3) movement of fuel within the coolant channel. Driving pressure from within the pin represents the sum of volumetric expansion upon melting, thermal expansion, input specified pressure of the fission gas in the central void, and release of a specified concentration of fission gas from the fuel as a specified isotherm moves radially. Several triggers such as cladding temperature, internal void pressure, or fuel temperature can initiate cladding rupture and the associated fuel motion into the channel. The cladding rupture point is modeled by an orifice coefficient. The fuel that moves into the channel is taken uniformly from the molten fuel zone within the pin.

The motion of fuel within the channel presently contains the following assumptions: density is that of a fuel/fission gas mixture, fuel remains at the melting temperature, the same friction factor as sodium is used, and no slip between the expanding fission gas within the fuel occurs.

4.3.4.9 Fission Gas Release

The pressure of the fission gas in the plenum is input. Fission gas is assumed to flow from the plenum into the coolant channel through an orifice. The sodium friction factor is used for the fission gas movement in the channel.

4.3.4.10 Neutronics

The point kinetics equations are solved by a forward march technique (Ref. 12). Capability exists for initiating scram action in this model.

4.3.4.11 Latest Developments

MELT-III is currently under development to describe in greater detail, the phenomena occurring during transient overpower conditions. A number of modifications and new models are being constructed. The HOTPIM (Ref. 144) code is designed to be included as a fuel motion subroutine in MELT-III. This new model uses two-phase compressible hydrodynamics to describe the flow of the molten fuel/gas mixture within the central cavity after pin failure.

The assumptions used in HOTPIM are the following:

1. The flow is strictly one-dimensional.
2. The flowing medium is a two-phase, two-component fluid, with no mass transfer between the components.
3. The gas is ideal and doesn't condense, and the liquid is non-volatile.
4. The flow remains in the bubbly flow regime.
5. Flow through the cladding rupture is strictly transverse, with no velocity component parallel to the cladding wall.
6. The bubbles attain their terminal drift velocity instantaneously.
7. The correlations for steady-state drift in a hydrostatic pressure gradient apply for transient drift of fission/fill gas bubbles in molten fuel in a hydrodynamic pressure gradient.
8. The effects of dissipative forces, such as viscosity and wall friction, are insignificant.
9. There is no relative motion between pure liquid and the solid fuel grains existing when the bulk temperature of the fuel is between the solidus and the liquidus.

HOTPIM solves two phase, one dimensional, time dependent continuity, motion and conservation of energy equations to model the flow, composition and pressure inside the fuel pin cavity.

These equations use a sonic velocity applicable in the bubbly flow regime (Ref. 147). Relative motion between the gas and the molten fuel is treated as a perturbation to homogeneous flow. A volumetric drift flux correlation (Ref. 148) for single gas bubbles in liquids is employed.

The results from HOTPIM are the time dependent amount and composition of fuel and fission gas from the pin rupture. The axially dependent mass of fuel removed from inside the pin is calculated and is important in determining the reactivity effects caused by the fuel motion.

Studies accompanying HOTPIM and PLUTO (Ref. 141) show considerable different results (Ref. 149) although both these models were conceived to describe nearly the same phenomena. Further evaluations are being undertaken to understand the apparent differences.

Additional capabilities in MELT-III for modeling the overpower transient include parameter-type models for checking the sensitivity of the fuel/gas composition escaping from a ruptured fuel pin, the effects of various amounts and skews of fuel plate out (Ref. 150) and the effects of various axial density gradients of the fuel/gas mixture in the coolant channel (Ref. 150).

4.3.4.12 Limitations

The validation of the models in the MELT-III code is presently not very far advanced. Initial work to compare TREAT experiments H5 and E6 resulted in considerable changes in MELT-III in order to model the hydraulic features of the MARK-II loop. Results of MELT-III calculations for the H5 and E6 experiments are very inconclusive. The parametric nature of the FCI and other models plus the nonprototypical features of TREAT are cheifly responsible. Although the capacity for the development of integrated detailed models is well documented in codes such as PLUTO and HOTPIM, no integrated code exists to follow a transient overpower accident more than a few milliseconds into the power-burst phase. Significant effort will be required to account for phenomena such as fuel plate out or plugging, fuel particle internal heat generation and other effects in an integrated code that can follow the accident for hundreds of milliseconds. The long term deposition of the ejected fuel will require careful iterative analysis using integrated codes to be developed and the best experimental information obtainable.

4.4 Dissassembly Codes

4.4.1 VENUS-II

4.4.1.1 Introduction

The VENUS (Ref. 18, 19) series of computer codes are two-dimensional (r,z) disassembly analysis codes which normally employ the output of SAS calculations as input. VENUS-II (Ref. 19) is the most recent version of the series and will be discussed here.

In VENUS-II, the power level and the fission energy deposited in the core are calculated using point kinetics and conservation relations. The reactivity used to drive the point kinetics calculation is a combination of an input function and feedback effects resulting from Doppler broadening and material motion.

The energy is deposited throughout the reactor according to the power density distribution supplied as input. Fuel vapor pressures are found using an equation of state. The pressure drives a set of two-dimensional (r,z) hydrodynamics equations. The finite difference solutions of the hydrodynamics equations give the displacements of the mesh positions within the spatial grid. Densities of the reactor materials are adjusted, and reactivity changes resulting from material motion and Doppler broadening are calculated and fed back into the point kinetics equations.

The main functional parts of the model are:

1. power and energy (point kinetics);
2. energy balance;
3. pressure (equation of state);
4. material displacement;
5. reactivity feedback.

4.4.1.2 Power and Energy

The power level during an excursion is calculated by solving the familiar point kinetics equations which presupposes that the power is space and time separable.

The internal energy of the fuel, in finite difference form, is calculated using the following energy balance

$$\delta E^{n}_{i,j} = \left(\frac{\delta q^{n} H_{i,j}}{\rho^{o}_{i,j}} - P^{n}_{i,j} \delta V^{n} \times 10^{-7} \right) \rho^{n}_{i,j} \qquad (9)$$

where the subscripts are space mesh indices (r → i, z → j), and the superscript is the time step index,

$\delta E^n_{i,j}$ = change in the specific internal energy of the mesh cell that occurred during the nth time step (J/cm^3),

δq^n = total nuclear energy deposited throughout the reactor during the nth time step, calculated as the integral of the power over the nth time step (J),

$H_{i,j}$ = normalized power density distribution,

$\rho^n_{i,j}$ = current overall density of the mesh cell (g/cm^3)

$\rho^0_{i,j}$ = initial mesh cell density (g/cm^3)

$p^{n-1}_{i,j}$ = total pressure within the mesh cell at the end of the previous time step (dynes/cm^2),

δV^n = change in the overall mesh cell specific volume that occurred during the nth time step (cm^3/g).

4.4.1.3 Equation of State

VENUS allows the user to choose from a number of different equations of state. The most widely used one was developed at ANL The fuel pressure, p', at each mesh position is determined in the ANL equation of state, using the following density dependent expression:

$$p' = \text{MAX}(p'_v,\ p'_\ell), \qquad (10)$$

where

P' = fuel pressure (dynes/cm^3),

p'_v = fuel vapor pressure which is an empirical of its temperature,

p'_ℓ = fuel liquid pressure which is an empirical function of its internal energy, specifically volume and critical density.

The vapor pressure, p_v', is used when the fuel is in the two-phase (liquid-vapor) domain. The density dependent single-phase (liquid) pressure, p_ℓ', is used when there is no fuel vapor space within the given region.

Nonfuel regions and regions with low power densities (such as reflectors and blankets) only affect the pressure calculations in the sense that they occupy space that would otherwise be available for fuel expansion. The fuel density is calculated based on the total volume available as

$$\rho_f = \frac{M_f}{V_T - \frac{M_s}{\rho_s} - \frac{M_{ss}}{\rho_{ss}}} \qquad (11)$$

where

M_f, M_s, M_{ss} = the mass of fuel, sodium, and stainless steel within a given mesh cell (g),

ρ_s, ρ_{ss} = the density of sodium and stainless steel in the given cell (g/cm^3),

V_T = the overall cell volume (cm^3).

The bulk modulus of expansion is defined by the relationship

$$\beta_e = \rho \frac{dp'}{d\rho} \qquad (12)$$

If β_e is assumed to be a linear function of pressure, then equation (12) can be solved, giving

$$\rho = \rho^o \left(\frac{\beta_{e\ell}}{\beta_{eo}} p' + 1\right)^{1/\beta_{e\ell}}. \qquad (13)$$

The above equation is used for estimating the compression of sodium and steel where the factors β_{eo} and $\beta_{e\ell}$ for sodium and stainless steel are a function of the temperatures T_s and T_{ss}. The sodium and stainless steel temperatures, T_s and T_{ss}, are estimates of the average temperatures (°K) anticipated during the excursion and are supplied as input data. These above equations are iteratively solved by the computer code.

4.1.1.4 Material Displacement

The material motions are calculated assuming that the reactor materials can be regarded as a homogeneous, inviscid, compressible fluid. The equations are formulated in a Lagrangian reference frame in which the spatial grid deforms with the fluid.

The two-dimensional (r,z) momentum equations are,

$$\frac{\partial^2 r(r,z,t,)}{\partial t^2} = - \frac{1}{\rho(r,z,t)} \frac{\partial p(r,z,t)}{\partial r} \qquad (14)$$

$$\frac{\partial^2 z(r,z,t)}{\partial t^2} = - \frac{1}{\rho(r,z,t)} \frac{\partial p(r,z,t)}{\partial z} \qquad (15)$$

and conservation of mass is given by

$$\rho_o(r,z,t) = \frac{\rho(r,z,t)\ dv}{dV_o}$$

where r and z are the Eulerian coordinates of a given point in the Lagrangian grid mesh ρ_o and V_o are the deform density and volume, respectively and ρ and dV are deform density and volume, respectively. The pressure, p, is of the form

$$p = p' + q \qquad (16)$$

where

p' = pressure obtained from the equation of state,

q = viscous pressure

The viscous pressure, q, is added to include the effects of a shock wave on the calculation. Physically, densities, pressures, energies, and velocities are discontinuous across a shock front. Von Neumann and Richtmyer (Ref. 151) developed a pseudoviscous pressure term to approximate q of the form:

$$q = \begin{cases} \dfrac{1.44A\rho_o^2}{V}\left(\dfrac{\partial V}{\partial t}\right)^2, & \text{for } \dfrac{\partial V}{\partial t} < 0 \\ 0 \qquad\qquad\qquad\quad , & \text{for } \dfrac{\partial V}{\partial t} \geq 0, \end{cases}$$

where

A = the mesh cell area

$\frac{\partial V}{\partial t}$ = change in specific volume.

An explicit, first-order, finite difference formulation is used to solve the hydrodynamics equations. At the end of the nth time step the positions, densities, and pressures of each point are known. Thus, the hydrodynamics equations can be solved for the accelerations at each spatial mesh point. Then the velocities of each point can be found. The new mesh positions at time step n+1 can then be found. After the new mesh positions have been obtained, the densities within each mesh cell are adjusted.

4.4.1.5 Reactivity Feedback

The net reactivity is the sum of the input, Doppler, and material motion reactivities and is given by

$$\rho^*(t) = \frac{\delta k(t)}{1+\delta k(t)} \tag{18}$$

where

$\delta k(t) = \delta k_{input}(t) + \delta k_{Doppler}(t) + \delta k_{motion}(t)$

$\delta k(t) =$ net change in the multiplication factor

The input reactivity, $\delta k_{input}(t)$, is given by

$$\delta k_{input}(t) = \begin{cases} \delta k_o + At + Bt^2, & \text{for } t < t_s \\ \delta k_o + At_s + Bt_s^2, & \text{for } t > ts. \end{cases} \qquad (19)$$

and enters normally from the size of the reactivity ramp found in the SAS calculation.

The reactivity change due to the motion of material is based on the validity of first order perturbation theory, in which the material worth distribution, $W(r,\theta,z)$ is assumed independent of time.

4.4.1.6 Limitations

The basic assumptions employed in the VENUS-II model are:

1. the reactor materials behave like a homogeneous mixture, with the properties of an isotropic, inviscid fluid;
2. the reactivity change due to material motion can be calculated by first-order perturbation theory;
3. heat transfer from the fuel can be ignored;
4. fuel vapor pressure and the compression of materials are the only sources of internal pressure (fission gas and sodium vapor pressures are ignored);
5. point kinetics can be used to describe the time history of the power level;
6. angular effects are not included;
7. a potentially autocatalytic effect associated with neutron streaming through voids may require additionally modeling to account for this reactivity effect.

Assumptions 1, 3, and 4 are best satisfied during strong excursions when high temperatures and pressures are rapidly generated in the core. The reactor materials, under these conditions, more closely approximate an isotropic, homogeneous fluid than in mild excursions.

Fig. 13 shows relative power density vs. time for a "strong" ($100/sec) and a "weak" ($1/sec) excursion with zero feedback.

If Q(o) is the initial power density, and the oxide fuel is molten ($3070^{\circ}K$) at t=o, fuel motion from fuel vapor pressure will terminate the excursion somewhere around $Q(t)/Q(O) = 10^3$ for the $100/sec case (in 3 or 4 milliseconds). Because of the inertia of dense ($10\ gm/cm^3$) fuel material, it is difficult to imagine a thermo-physical process other than fuel vapor pressure which would play a significant role on this time scale. Even though displacements are small at 3 milliseconds, the fuel has acquired large momentum, and it is unlikely that its course would be significantly altered by anything but a major thermodynamic event in the core (such as a secondary excursion, for example). Hence, in the case of very strong initial excursions, the classical (VENUS) hydrodynamic assumptions probably lead to reasonable conclusions about the arrangement of fuel following gross disassembly.

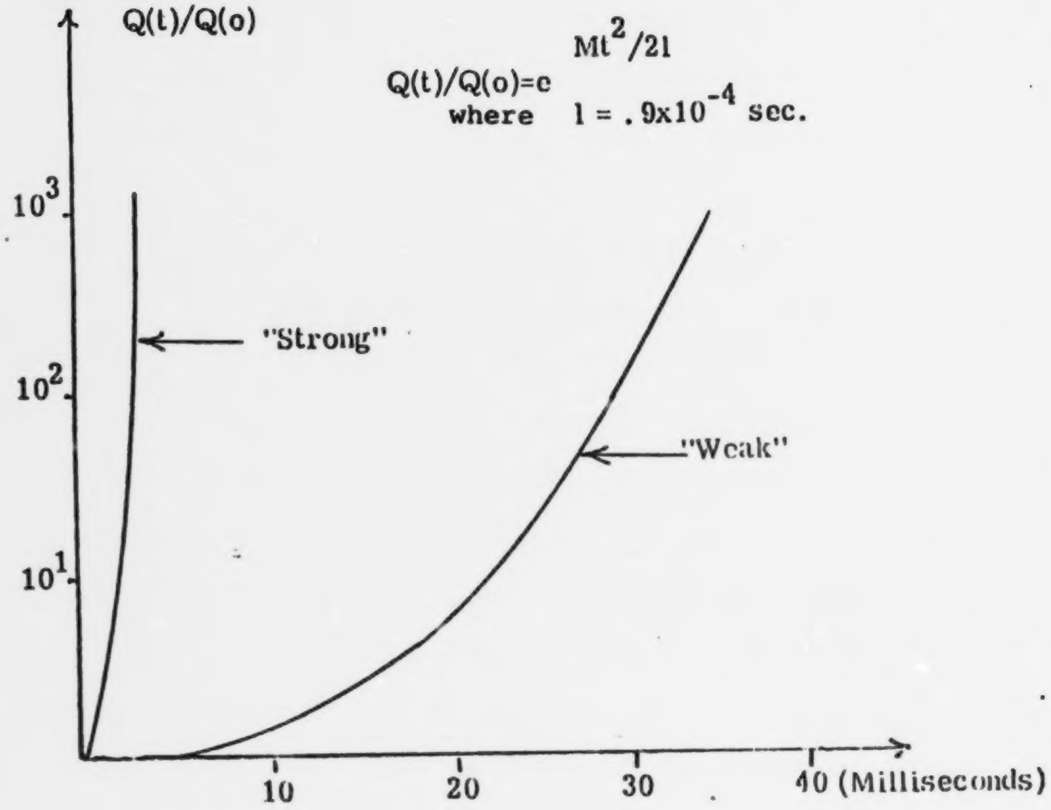

Fig 13. Relative Power Density Vs. Time for a "Strong" and a "Weak" Excursion.

In the \$1/sec case, many phenomena may lead to failure long before fuel vapor pressure becomes appreciable. For example, fission gas pressure may increase sufficiently to split the fuel pin open, blowing molten UO_2 out of the pin and, possibly, into a surrounding pool of sodium. A UO_2-Na reaction may then take place, causing a Na vapor explosion to expell the remaining (solid-liquid) fuel and core structural material. A simple dynamics calculation shows that fuel inertia prevents noticeable motion (one cm) in 0-4 milliseconds unless tremendous pressures are present (thousands of atmospheres). During the 10 to 30 millisecond time scale of the \$1/sec excursion, however, lesser pressures can yield sizeable displacements. One envisions fuel pins bursting at random in the core due to variations in their internal structure. In other words, the hottest pin may not fail first. The neutronic time constant is long enough to allow this randomness to be significant in the \$1/sec accident. Hence, the disassembly phenomena in the weak and strong excursions may be quite different. Consequently, the eventual core configuration may also vary between the strong and weak excursion.

For weak explosions having small fuel motion VENUS and VENUS II (with better numerics, a variable time step, and a better equation of state for fuel and steel) consider well the hydrodynamic nature of the core. The cylindrical geometry is appropriate to all forseeable designs. A coupled VENUS/TWOTRAN analysis for strong fuel motion problems has also been done successfully.

Cores with a large amount of sodium, in which a fuel-coolant interaction might occur, cannot be described by VENUS-II. If a fuel-coolant interaction does occur, sodium vapor pressures might develop and possibly dominate the total pressure calculation.

Fission gas pressure might also be a significant extra source of pressure during an excursion. The main difficulty in treating fission gas pressure stems from the lack of understanding of how the fission gas and molten fuel interact during a prompt-critical burst. Depending on the type of accident, this effect can be major or minor.

The use of point kinetics and perturbation theory are most valid in excursions which terminate quickly, with small material motions. Otherwise, the validity of the models is questionable during transients in which large motions occur with large density changes.

Boudreau and Erdmann (Ref. 152) have shown that the assumptions of first order perturbation theory of point kinetics might mask the real behavior of a core in which the shape of the powered material worth distributions are allowed to vary with time.

4.4.2 New Developments

4.4.2.1 Introduction

The work of Moss and Rhodes (Ref. 156) and Boudreau and Erdmann (Ref. 152) have pointed out the inadequacies of using the currently used Bethe-Tait type disassembly computer codes, such as the VENUS series for the calculation of large motion disassemblies and the calculation of determining if the mass of disassembled molten fuel-steel-sodium mixture is, indeed, subcritical. At present there are a few efforts underway to develop computer codes capable of such calculations and, in particular, capable of determining if secondary, tertiary, etc. critical configuration can be created from a mechanical disassembly.

The two most important of the "secondary criticality" codes now being developed are the SIMMER (Ref. 155) code being written by Los Alamos Scientific Laboratory and the VENUS-III (Ref. 158) code being written by Argonne National Laboratory. Since these codes are in their very early development stage detailed descriptions of the codes are not available.

Their study showed that VENUS might for very large fuel motions, tend to underestimate the possibility of secondary criticality due to a gross rearrangement of the core. In addition, the use of Lagrangian hydrodynamics does not permit large enough fuel motion to adequately calculate the possibility of secondary activity. At present, both Los Alamos Scientific Lab and Argonne National Laboratory are working on disassembly computer codes which treat the hydrodynamics with Eulerian reference frame and using spatially dependent neutronics. It would seem that for large cores, with large amounts of fuel, such codes, when developed, will be very important in answering many questions in regard to secondary criticality.

VENUS does not treat the possible effects of angular motion on disassembly calculations. Bleiweis (Ref. 153) has developed a simplified three—dimensional hydrodynamics model for VENUS applications in an attempt to determine the effects of angular motion. Again, for larger cores with angular asymetry it may be important to perform three-dimensional calculation in order to study the possibility of localized disassemblies leading to more gross core involvement.

Finally, the effect of neutron streaming through voids or gas spaces as discussed by Webb (Ref. 154) may be a potential positive feedback mechanism that is not presently accounted for. This effect in which streaming neutrons become absorbed in the fuel when the voids close can not be ignored since it appears to take effect during the peak of the excursion. This may partially compensate or perhaps even overcome the negative Doppler effect causing the total reactivity to further exceed prompt criticality. Nicholson (Ref. 155) concludes in his study that this effect could be significant and needs further investigation.

There are three chief limitations of the current disassembly codes such as VENUS which both LASL and ANL are trying to overcome: 1. The use of Lagrangian hydrodynamics which restricts motions to a few centimeters and thus prohibits material motion calculation, in which large motions create secondary critical configurations; 2. The use of point kinetics and first order perturbation theory to calculate the power and reactivity which again, limits the calculations to those having only a few centimeters of motion where spatial power (flux) shapes and material worth changes do not appreciably change with time; 3. The use of an equation of state which has a large degree of uncertainty.

4.4.2.2 SIMMER

4.4.2.2.1 Hydrodynamics

Essentially, the fluid dynamics model employed in the SIMMER code assumes that the reactor can be described as two interpenetrating substances "fuel" and "vapor" in an Eulerian frame. The fuel is assumed to be liquid globules or solid with fragments of other components such as steel. The vapor includes sodium, steel, and other materials. Initially, the model assumes the fuel to be homogeneous in which the vapor exists in proportions of materials with position and time as a result of phase transitions in the fuel and diffusion between vapors.

The most important variable in the analysis is θ, the local fraction of volume occupied by the vapor. Therefore, $1-\theta$ is the local volume fraction occupied by the fluid. Thus, the model will describe the mobility of the vapor relative to the fuel. Pressure is assumed to develop only by virtue of vapor heating and/or compression. The equation of state of the vapor will thus be partial pressures for the two components as

$$\rho = f_1 (\rho_1, I_1) + f_2 (\rho_2, I_2) \qquad (20)$$

where ρ is density and I is the specific critical energy.

The equation of state and conservation of mass, energy and momentum equation essentially represent the hydrodynamics at this present stage of development. LASL does have plans for incorporating models to account for fuel coolant interactions, flow interactions with structural elements, and sensitivity studies to detail initial conditions and possible secondary criticality.

4.4.2.2.2 Neutronics

LASL has proposed the use of two-dimensional, multi-group time-dependent neutron transport theory to calculate neutron flux and power during the excursion. They feel that transport theory is needed for conditions in which a large void space caused by a disassembly are created, thus invalidating the assumptions of diffusion theory. In addition, transport theory can more accurately calculate reactivity which is essential to the determination of a permanently subcritical configuration.

Basically, the neutron transport equation

$$\underline{V}^{-1} \frac{\partial \Psi}{\partial t} = \underline{B}\Psi + q \qquad (21)$$

will be solved by a method similar to that exployed in the one-dimensional TIMEX (Ref. 159) code. In equation (21) $\underline{V}$ contains the neutron group velocities, Ψ contains the angular fluxes and q contains inhomogeneous gases and other sources due to delayed neutrons. B is the transport operator.

The solution for the spatial and angular variables will employ standard methods such as the diamond difference scheme and discrete ordinates, respectively. The TIMEX code yields an unconditionally stable method for arbitrarily large time steps and will probably be employed for the solution of equation (21).

Cross section changes will be accounted for in the neutronics solution. The changes in cross sections due to material motion are easily incorporated since the density of materials is an output of the hydrodynamics. The changes in cross section due to temperature variation will be made by recomputing the microscopic cross sections when substantial temperature changes occur.

Other Models

Current disassembly codes assume an adiabatic system. The SIMMER code will attempt to incorporate some heat transfer into the coolant. The key heat transfer problems they will attempt to model are:

1. Freezing of steel and fuel in the lower axial shield,
2. UO_2-PuO_2 vaporization/condensation rates,
3. UO_2-PuO_2 sodium heat transfer
    a. with sodium film on structural surfaces above the core.
    b. with bulk sodium located somewhere in the upper plenum-guide tube region.

The method used to treat the first problem (plugging problem) will involve the geometrical modeling of the flow inlet region and the application of appropriate conductive and convective heat transfer equations. Freezing of material will effectively reduce the hydraulic diameter and thereby influence the flow of fuel in the downward direction.

The problem of UO_2-PuO_2 vaporization/condensation rates is important in determining the driving pressures which move the core material.

The pressure which can drive the ejected fuel slug upward is UO_2-PuO_2 vapor pressure. The vapor is produced near the surface of the molten fuel puddle at a rate which depends on the pressure acting on surface. The vapor will condense on the cold subassembly walls and on structure which remains after the ejected fuel slug passes by. The condensation rate will depend on the vapor temperature, vapor density, wall temperature, geometry, and on the presence of noncondensible gases. As a result of the tradeoff between vaporization and condensation rates within the subassembly, the ejected slug will experience a decreasing vapor pressure as it travels up the subassembly and away from the vapor source. This is an important phenomenon, since the driving pressures will influence the likelihood for the escape of the ejected slug from the subassembly.

The third problem, UO_2-PuO_2 sodium heat transfer, has had more study than the other two problems. The principal result desired in SIMMER, however, is the effect of fuel-coolant interactions on fuel dynamics. It is desired to know whether such an interaction in the upper plenum-guide tube region can drive fuel back down into the core at high velocities. It is also important to know the influence of sodium films which remain on the structural material in the upper plenum. The hot, molten fuel will interact with this sodium in some fashion, and sodium vapors which are produced will have an influence on the fuel slug motion.

4.4.2.3 VENUS-III

VENUS-III will employ Eulerian hydrodynamics based on some standard methods derived at LASL. At present, it is not clear which method will be used. In addition, VENUS-III will use FX-2 neutronic code which is a two-dimensional, multi-group, quasistatic diffusion theory code.

It would appear that both the SIMMER and VENUS-III codes are important for LMFBR safety analysis. The possibility of recriticality is an important consideration in disassembly calculation and one which needs to be accurately modelled. In particular, larger LMFBR's (1000 Mwe) will certainly require this analysis simply because they are more loosely applied than the FFTF type cores. Thus, the development of these models is essential for future LMFBR development.

4.4.3 Doppler Effect Calculations

4.4.3.1 Introduction

The reactivity effect resulting from Doppler broadening of fission and captive resonances is important in LMFBR safety calculations. It is virtually the only prompt negative reactivity effect in large LMFBR's which is responsible for reducing some of the accident consequences. For large ceramic fueled LMFBR's it is now recongized that the Doppler effect provides a negative reactivity contribution.

4.4.3.2 Calculation Methods

For a large uniform core for a uniform temperature change the Doppler effect can be estimated from a fundamental mode calculation. Assuming a fundamental mode flux and adjoint the reactivity change (for a critical system) for a given energy group corresponding to a fuel temperature change is found using perturbation theory.

This is, of course, only valid for a homogeneous, uniform core. For most LMFBR's a more exact calculation of the Doppler effect is performed by using one-, two,- or three-dimensional diffusion or transport theory calculations. For example, a computer code such as TWOTRAN (Ref. 160), which is a two-dimensional, multigroup, static transport theory code is employed to calculate the Doppler effect. Such a calculation would involve various iterations employing temperature dependent cross sections in order to obtain the reactivity change resulting from these temperature changes. These result in more accurate estimates of the Doppler effect where possible heterogenieties and spatial effects are included.

4.4.4 TWOTRAN

This code is a general purpose 2-D transport theory code based upon SN theory. It can handle both shielding type and criticality type problems as well as perform variety of other nuclear analyses. Generally in LMFBR analysis it is used in the R-Z geometry mode. It accepts a variety of multigroup cross section sets in a number of formats. It performs SN calculations with the weights being either input or generated internally. The calculation proceeds via a diamond differencing scheme having coarse mesh rebalancing. Ray effects, although not treated in this code, are being considered in a new SN code being developed at LASL at present.

A variety of boundary conditions are available for use with TWOTRAN (Ref. 160) including zero return current, vacuum, reflective, boundary sources and periodics. This code has been used in both a shielding analysis and in conjunction with VENUS for recriticality calculations. One takes the fuel motion output from VENUS and inputs this into a criticality analysis with TWOTRAN. The calculated δk between two consecutive runs then documents clearly the proper fuel worth needed as input for the disassembly analysis at the subsequent time step.

4.5 Damage Evaluation

4.5.1 REXCO

4.5.1.1 Introduction

The REXCO computer code system is under development at Argonne National Laboratory. It solves basic conservation equations and equations of state of reactor materials using numerical techniques to analyze the response of LMFBR primary, containment and components. The energy inputs in these analyses correspond to postulated nuclear excursions. A series of codes are being developed and designated REXCO-H, P, I (Reactor Excursion Code, Hydrodynamics, Particle-in-Cell, Inelastic).

Currently the analytical program at ANL has advanced to the point of being able to predict reasonably well the response of the components of the primary system. The phenomena of the HCDA can be followed up to the time of dynamic equilibrium in the system, when no further plastic work can be performed on the components. The treatment stops short of sodium spillage into the secondary containment, and provides only the pressure pulses into the primary piping, but not the response of the piping system. The analytical predictions of component response have been verified reasonably well by tests, both past and most recently.

The subject analyses and codes were applied to the safety analysis and structural response of the Fast Flux Test Facility. They are currently being applied by ANL to the Demonstration Plant safety analysis. Early versions of these ANL codes or recent variations are being applied to European LMFBR Demonstration plants.

It is the ultimate objective of the program to cover the entire LMFBR structural response to the HCDA. The extension of the present work will include among other items: (a) sodium spillage into the secondary containment, (b) response of the secondary containment to sodium fires, and (c) response of the primary piping and components to the pressure pulses originating at the core.

To verify remaining questions in existing codes and the codes yet to be written, an experimental program of component and plant response will be undertaken. It will go beyond the comparisons already performed with the FFTF model tests at Stanford Research Institute.

Finally, since these accident conditions most often constitute the basis for design, digested manuals will be prepared for the use of the LMFBR designer.

The determination of the dynamic response of the fast reactor primary containment to an HCDA is a complex problem. It involves not only the calculation of the response of containment structures, but also the calculation of the propagation of pressure waves, the interactions of fluid and structures, the flow of fluid, the loads imposed on components and structures, and the damage produced by these loads.

Because of the complexity of the problem, the early approach was to perform model experiments (Ref. 161,162) in which the HCDA was simulated by the use of high explosives and the sodium was replaced by water. However, the characteristics of a nuclear energy release are quite different than those of chemical explosions. In a nuclear excursion, most of the energy released will be mainly determined by the expanding core; for high explosives, half of the energy is immediately after detonation. Therefore, to perform a meaningful test, not only must the reactor containment structure and internals be properly represented by the scaled model, but also the rate of energy release from the core must be properly simulated by the chemical explosive.

A different approach to the problem is to use the basic conservation equations of mass, momentum, and energy, together with the equations of state of the reactor materials, and calculate the response of the surrounding structures under the postulated nuclear excursion conditions. In recent years, the development of high-speed computers has made it feasible to use computer codes to solve numerically the conservation and state equations, and to determine the loadings, strains, and the response of the primary containment during the excursion. By use of the appropriate constitutive relations for structural components, the deformation and response of these internal components can also be included in the calculations.

The latter approach has been used by Argonne National Laboratory in developing the Reactor Excursion Containment Codes (REXCO) (Ref. 25). The hydrodynamic version of the REXCO code (REXCO-H) (Ref. 39-41) has been applied to the conceptual design study of FFTF vessel head-cavity system, evaluation of coolant-impact effects on the reactor cover (Ref. 163), preliminary safety analysis of the FFTF (Ref. 164), and postaccident heat removal in LMFBR (Ref. 165). The latest version of the REXCO code (REXCO-HEP) (Ref. 42), which treats not only the hydrodynamics, but also the elastic and plastic deformations of the reactor structures and components, has been applied to the final analysis of the response of the FFTF primary system to an HCDA of 150 MW-sec (Ref. 166) and the scoping analysis of the HCDA structural response of the Demonstration Plant (Ref. 167).

Recently an Implicit Continuous Eulerian Containment Code (ICECO) is being developed at ANL, which will be applied to low-energy excursions, sodium spillage, gas bubble motion, and other containment problems. In this paper recent improvements and future developments in these codes will be described.

4.5.1.2 Recent Improvements

Inclusion of Bending Strength in the Shell Equations

In an LMFBR, the reactor vessel is normally a thin shell cylinder. If the vessel is to be treated as an elastic-plastic solid material, the thickness of the vessel wall will have to be divided into at least 3 or 4 zones. Large numbers of Lagrangian meshes will have to be used in the numerical analysis, even for a simple configuration. Therefore, as an option in the

REXCO code, vessels can be analyzed as thin shell structures.

The shell equations used in the REXCO code were those of the membrane theory which neglects all moments in the equilibrium equations. For high-energy excursions and for shells having very small bending stiffness and undergoing large deformations, neglecting the bending moments is justified. However, for low-energy excursions, the bending resistance of the shell may become important. If the end of the cylinder is not free to expand laterally, one of the recent improvements of REXCO was the inclusion of bending moments in the shell equations.

Mesh Regularization

The disadvantage of using the Lagrangian codes is the limitation imposed on the distortion of the Lagrangian meshes. In some problems, the mesh distortions are caused by the real, physical motion of the fluid. They increase with time and may become very large when there are contact discontinuities in the flow. However, in some cases, severe distortions of the Lagrangian mesh are not physically real. They are caused by the method of solution rather than the physics of the problem.

For instance, the most frequently occurring "hour-glass" distortions of a quadrilateral mesh are nonphysical, but they are mathematically the non-trivial homogeneous solutions of the three-strain equations where the strains are calculated from the motion of the four corners. Once this mode of distortion starts, it continues to grow and ultimately renders the computational results meaningless. Therefore, it is necessary to have some means to prevent this type of distortion from occurring.

LASL developed a mesh-regularizing scheme for incompressible flows. A damping force was introduced in the momentum equations that tends to keep a mesh vertex in the center of mass of its eight adjacent neighboring vertices. Hoskin (Ref. 168) has incorporated the LASL scheme into a compressible Lagrangian code, ASTARTE. A different mesh-regularizing scheme has been used in the REXCO-HEP code, which utilizes a rotational force to prevent growth of the nonphysical distortions. The magnitude of the rotational force is proportional to the rate of the relative rotation of the opposite zone sides. Since the purpose of the mesh-regularizing scheme is to damp out only the type of mesh distortions in which the successive mesh sides rotate clockwise and counter-clockwise alternately, in such a way that both the volume and strains of the mesh remain unchanged, it appears more reasonable to use a rotational force instead of a damping force. This scheme has been tested successfully in many problems. It can reduce and minimize the zone distortions in the numerical calculations, and thus extend the calculations to much longer times.

Reactor Head Cover Deformation

The reactor head cover in the REXCO code is treated as a rigid solid plate. A recent improvement has enabled the REXCO code to couple with a dynamic elastic-plastic finite-element code (Ref. 169) developed for analyzing the response of a reactor head cover under impulsive loading. A REXCO-subroutine provides the pressure variation on the reactor head cover and the bolt holddown force to the finite-element code, which in turn, furnishes the deformations of the head cover due to the dynamic pressures of the coolant slug.

Treatment of Energy Absorbing Materials

Following an HCDA, the coolant above the core is accelerated upward and eventually impacts on the head cover of the reactor. The head could lift and the upper vessel could deform radially. In order to reduce the damage potential of the moving coolant slug, energy-absorbing mechanisms have been sought. One method proposed has been the placement of a crushable material below the head cover, which, by its crushing, will reduce the peak pressures on the head and also the momentum of the coolant slug at the time of impact.

Recent improvements in the REXCO code include an option of using crushable materials underneath the reactor head to reduce the slug impact loadings on the reactor head, holddown bolts, and upper vessel wall. The mathematical model used for the reactor head consists of shield plates, crushable materials, head cover plate, and holddown bolts. Thus, the effect of the head motion as the shield plates crush the energy-absorbing material against the head cover can be included in the analysis.

Although the loading on the shield plate in a crushable model does not show any significant differences from the slug impact forces obtained in a non-crushable model, the forces transmitted to the reactor head through crushable tubes are quite different. Figure 14 shows how effectively the HCDA slug impact loads can be attenuated by the use of the crushable materials. Not only has the peak of the triangular-shaped

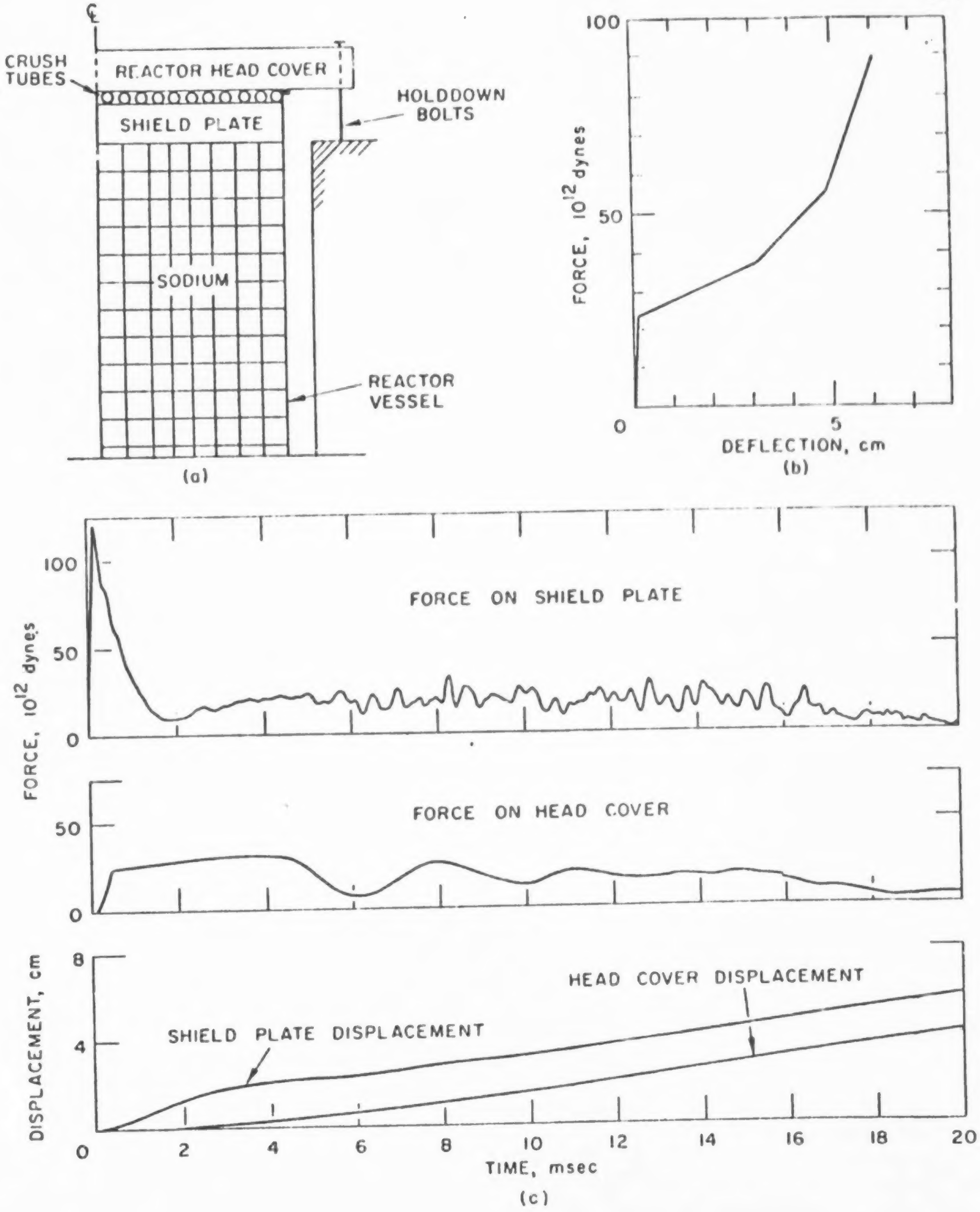

Fig. 14. Mathematical Model of the Reactor Head with Crushable Tubes and the Resulting Forces and Displacements.

impulse been reduced, but the duration of that impulse has also been extended. In the sample calculation, the peak pressure on the head was reduced by a factor of 4. This reduction should decrease considerably the severity of the head acceleration and the stresses in the head cover.

4.5.1.3 Further Developments

As mentioned earlier, one of the major concerns in the safety analysis is the coolant slug impact. When the coolant slug comes into sudden contact with the reactor cover, the head may lift and the upper vessel wall may deform radially. Even though the vessel, head cover, and holddown bolts may sustain these effects by deforming plastically, it is still quite possible that the vessel seals at the head-cover junction may rupture under the high pressures created by the slug impact. In this sequence of events the Lagrangian method is found to be inadequate for treating sodium spillage.

Another concern in the safety analysis is the final disposition of the core-gas bubble after it has produced damage to the reactor primary system. The core-gas bubble may collapse into numerous small bubbles under the intense pressure waves produced by the slug impact on the reactor head, or it may surface upward to produce a thermal loading on the reactor head cover. It is, therefore, important that the method employed in the HCDA analysis be able to analyze all stages of the bubble motion ranging from expansion, contraction, migration, recontraction to bubble collapsing or surfacing.

In Lagrangian analysis, due to the physical limitations imposed on the size and number of the Lagrangian meshes, the core-gas bubble expands, the representation of the gas bubble becomes less and less accurate, particularly when the reflected pressure waves travel back into the coolant, jet-like spikes may develop at the coolant-bubble interface. Again, the Lagrangian analysis is found to be inadequate to give detailed description of these phenomena.

To remedy these shortcomings of the Lagrangian code, an Implicit Continuous Eulerian code (ICECO) is presently being developed at ANL. It employs the full nonlinear equations of fluid dynamics to calculate the fluid motion and applies to both compressible and incompressible fluids. Preliminary results seem to indicate that this approach holds promise for both monitoring sodium spillage and studying the dynamics of an HCDA core-gas bubble in the primary containment.

When the ICECO is fully developed, it will be coupled with the REXCO-HEP code. The coupled REXCO-ICE should treat many reactor containment problems which could not be handled by present means alone.

4.5.1.4 Heat Transfer Augmentation of Containment Codes

REXCO-HT: A Containment Code with MFCI's

A difficult parameter to define when evaluating the response of an LMFBR primary containment is the pressure-energy relationship used to describe the core after the postulated off-normal event, whatever its origin has terminated. An approach used in the past depends on analysis to determine, more or less mechanistically, the sequence of events through core disassembly and nuclear burst termination. At this point the condition of the reactor is defined in terms of the amount of melted fuel including its temperature and location, the temperature of the coolant and amount of voids present, as well as a determination of the clad temperature and distribution. Using these data, the mechanical work potential of the mixture is determined if the fuel or cladding were to interact thermally with the sodium coolant, possibly resulting in severe pressure pulses. Models which describe the pressure-volume relationship of the expanding core regions range from the thermodynamic maximum (Ref. 170) to more sophisticated models which describe the time dependent heat transfer effects as well (Ref. 171,172). These models, however, are usually coupled to one-dimensional descriptions of the surroundings which do not fully evaluate the effect on pressures developed in the molten-fuel-coolant interaction (MFCI) zones.

In order to describe the molten-fuel-coolant interaction phenomenon in the REXCO containment code series, the quasi-steady-state and parametric models of Cho, et al, (Ref. 171) were adopted. Along with the addition of these heat transfer models, the heat of fusion of the fuel, noncondensible gas volumes and sodium vapor blanketing of the fuel particles are taken into account. This approach, then, results in the ability to couple the heat transfer phenomena directly with the hydrodynamic and structural response of the surroundings, thus leading to a somewhat more realistic representation of the event and its effect on the containment. Along with the ability to change the MFCI parameters from zone to zone so that temperature and material composition variations may be taken into account, all of the features of the REXCO-H (Ref. 40) containment code are available.

In REXCO-HT calculations the volumetric fractions of the fuel, coolant and non-condensible gases are specified for each MFCI zone. The remaining volume is assumed to be steel which does not take part in the heat transfer and expansion process but does act as an added mass. Input parameters also include the fuel and coolant temperatures as well as the fuel particle size. All calculations are based on one gram of sodium and the fuel and sodium within an MFCI zone are assumed to be at a uniform but different temperature. However, adjacent zones may have both fuel and sodium at different temperatures, but no heat or mass transfer is allowed across a zonal boundary.

Calculation of the pressure on a zone based on energy transfer and volume changes per time step requires an adequate treatment of the sodium equation of state for the liquid, two-phase and vapor states. The present version of the REXCO-HT code is thermodynamically consistent and includes temperature dependent sodium properties suggested by Padilla and Crawford (Ref. 173).

Heat transfer models used include the quasi-steady state, as well as the ANL parametric model (Ref. 174). Sodium vapor produced during the fuel-coolant interaction is likely to surround the fuel particles to a certain extent and thus effectively reduce the heat transfer from the fuel to the sodium. This a potentially important mechanism which reduces the heat transfer rate and results in reduced peak pressures and work produced by an FCI. There are two vapor blanketing models used in the REXCO-HT code which reflect the uncertainty of the process. Each model can be used with either heat transfer model. In the first option the thickness of the vapor film, δ_b, of the vapor blanket is calculated at each time step and the additional resistance due to the vapor blanket is included in the heat transfer coefficient

$$h^* = \frac{1}{H} + \frac{\delta_b}{k_b}^{\;-1}$$

where H is dependent upon the heat transfer model used and k_b is the thermal conductivity of the sodium vapor. The second blanketing model option assumes that a fraction of fuel particles equal to the volumetric fraction of sodium vapor (compared to the total volume of sodium) does not participate in the heat transfer process. The first option is expected to underestimate the heat transfer rate since convective heat transfer is ignored, however, one could introduce an effective thermal conductivity for the sodium vapor that would account, as a first approximation, for the convective effects.

Sample calculations (Ref. 174) using the above models have shown that the effect of vapor blanketing can be quite significant in reducing the heat transfer rate. Further, it was found that if radial motion is taken into account, vaporization can occur earlier in time and thus reduce the overall heat transferred from fuel to sodium. In subassembly configurations, slow heat transfer rates produce low initial pressures and little hoop strain in the walls with little effect contributed by the surrounding medium. However, the surroundings become important if high heat transfer rates are postulated and become important in assuring the survivability of the walls. Use of the models in whole reactor configurations in which the state of the core is specified may result in significantly changed energy partitioning that may well provide an extra margin of safety in the ability of a primary system to contain an event.

Addition to the ICECO Code

Heat transfer models added to the Implicit Continuous Eulerian Containment Code (Ref. 175) which is designed to handle lower energy excursions, consist of the molten fuel-coolant interaction models and sodium equation of state included in the REXCO-HT code (Ref. 43). One of the phenomena of importance in the calculation of an energy release is that of heat transfer from the hot sodium to the relatively cold plenum region and structure which exists in the upper part of an LMFBR subassembly. It is difficult to treat such a phenomenon with a Lagrangian code such as REXCO-HT, but relatively easy in the context of the ICECO code. Inclusion of a simple condensation model showed delays in slug arrival time, as well as reduced peak vapor pressures in the FCI zone. Also, the pressure pulse due to the reflected wave has been reduced due to the presence of condensation.

Future Improvements

Based on the development of an understanding of the molten fuel-coolant interaction in reactor environments, the heat transfer models currently used will be updated. Similarly, improvements in the sodium equation of state, especially in the pure vapor region, will be incorporated into the code.

One added possibility, especially useful in short-time calculations where heat generation may prove to have a significant effect on the molten fuel-coolant interaction, is to include a power generation time. This could describe a reactor, or subassembly for example, under operating conditions. Improvement in condensation models is contemplated in order to take advantage as much as possible of any ameliorating effects which may help reduce the severity of accidents.

Incorporation of the heat transfer models into the REXCO-HEP codes is of prime importance, since this would give a calculational capacity which would incorporate the most up-to-date containment code. This improvement would allow more realistic treatment of the core support structure, take advantage of mesh stabilization routines, as well as other improvements over the original REXCO-H code.

4.5.1.5 Application of REXCO

Mathematical Model

No computer code can include all the details of the reactor internals in the mathematical model. Therefore, to perform a manageable computer analysis, the representation of the reactor must be simplified. The important question is to what extent this can be done so that the response of the reactor under the HCDA loads can still be described accurately by the model.

The approach used for the FFTF reactor was to incorporate to the extent possible, the correct material properties and equations of state of the reactor materials, especially for critical materials such as the vessel and core barrel. Figure 15 shows the mathematical model used in the REXCO analysis. The flanges and rings on the vessel and core-barrel walls, as well as the thermal liner, are included and treated as thin shells of revolution. The inclusion of the core support in the calculation is accomplished by shaping those Lagrangian zones which represent the core support structure to conform to the actual configuration, and the structure is treated as an elastic-plastic solid material. Shields, reflectors, and fission-gas plenum in the wave-propagation properties as for the actual material, but they are considered to have no tensile strength in the axial and circumferential directions. This more closely represents the segmented nature of the shields and reflectors, which cannot resist hoop stresses. The shield plug is modeled as a rigid, solid circular plate held to the ground by holddown bolts. Since holddown bolts constitute a part of the primary boundary, it is believed that some conservatism is needed in the design to prevent rupture of the bolts during the slug impact. It is believed that the omission of the head deformation would give a somewhat greater impact force on the head cover and thus cause a greater straining of the holddown bolts.

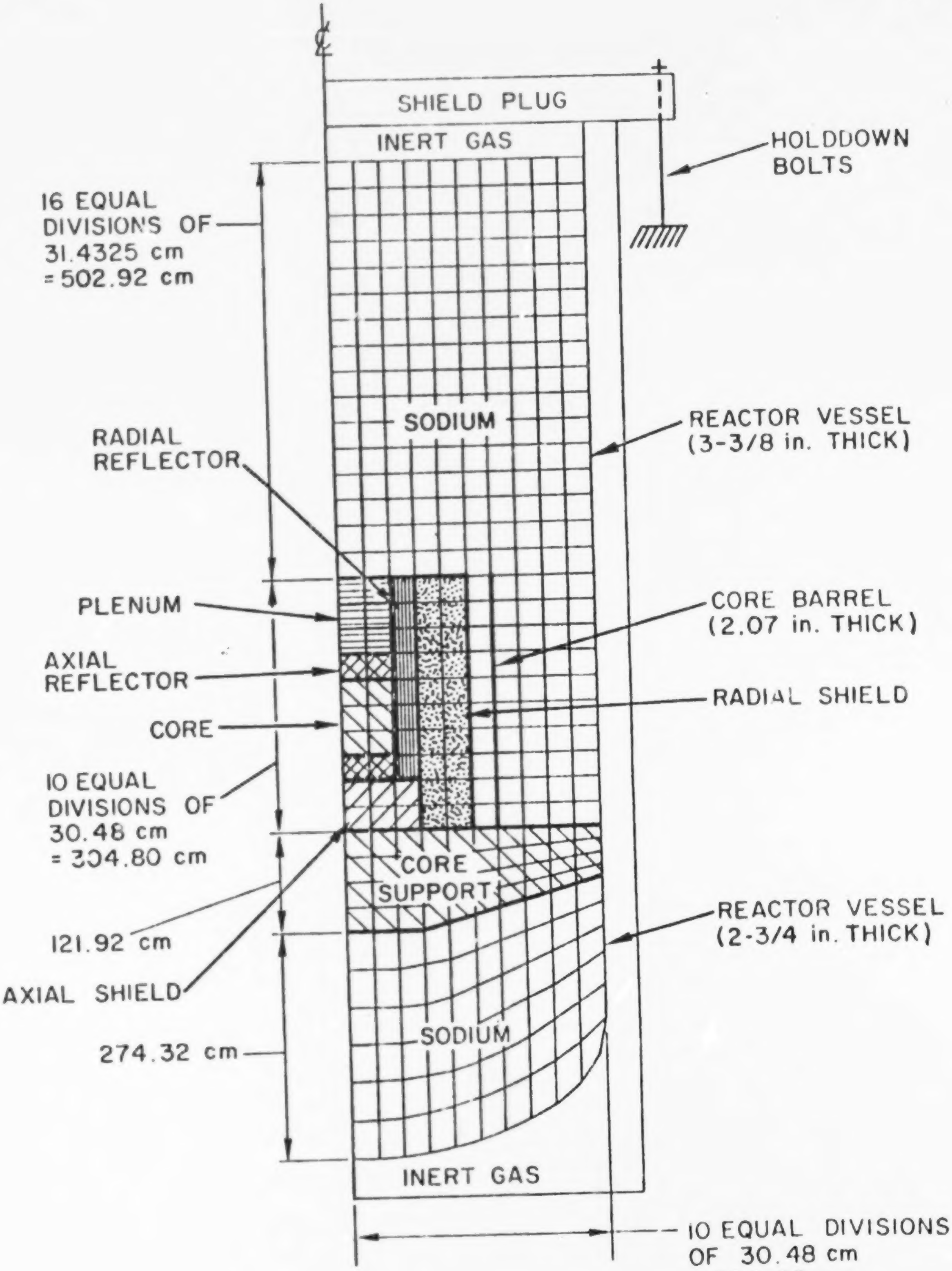

℄
SHIELD PLUG
INERT GAS
HOLDDOWN BOLTS
16 EQUAL DIVISIONS OF 31.4325 cm = 502.92 cm
SODIUM
REACTOR VESSEL (3-3/8 in. THICK)
RADIAL REFLECTOR
PLENUM
CORE BARREL (2.07 in. THICK)
AXIAL REFLECTOR
RADIAL SHIELD
CORE
10 EQUAL DIVISIONS OF 30.48 cm = 304.80 cm
CORE SUPPORT
121.92 cm
REACTOR VESSEL (2-3/4 in. THICK)
AXIAL SHIELD
SODIUM
274.32 cm
INERT GAS
10 EQUAL DIVISIONS OF 30.48 cm = 304.80 cm

Fig. 15 Mathematical Model of FFTF Reactor.

Excursion Model

It was postulated that if a small amount of coolant is still in the core during the power excursion, the molten fuel could come into contact with the coolant, causing a rapid heating of a relatively small volume of sodium and producing a sodium vapor explosion. Thus, the expansion of the high-pressure sodium vapor against the surroundings would become the mechanism of producing mechanical damage to the system. The sodium-expansion model used in the REXCO analysis is the SOCOOL model (Ref. 176). It was provided by HEDL for evaluation of the mechanical work resulting from the HCDA postulated for the FFTF reactor. The mechanical work potential of that HCDA is 150 MW-sec.

Response of the Primary System

The sequence of events occurring during the excursion is as follows. As the sodium vapor expands, it first deforms the core-surrounding structures (reflectors, shields, etc.). As it expands further, it pushes the core support structure downward, deforms the core barrel and vessel wall radially, and accelerates the liquid sodium above the core upward. When the slug of sodium, after being accelerated upward by the expanding core, comes into sudden contact with the reactor cover, a large impact force is exerted on the head cover and upper vessel wall. The holddown bolts and upper vessel wall are then deformed plastically; thus, the kinetic energy of the coolant is dissipated in strain energies of the bolts and vessel wall. Finally, the system regains dynamic equilibrium.

Figure 16 shows the partition of energy as a function of time. The work energy released from the core is first transformed into radial and axial kinetic energy of the coolant. Because of the existence of the heavy core-support structure, the downward kinetic energy of the coolant is very small. The radial kinetic energy of the coolant is later transformed into strain energy of core barrel and vessel wall(core region). The core-barrel strain energy is increasing progressively with time and leveling off after it reaches the dynamic equilibrium. The maximum deformation of the core barrel is about 6.1%, and it is completed at about t=31.9 msec. The slug impact occurs at t=40.6 msec. The strain energy of the vessel wall before the slug impact is quite small. The maximum deformation of the vessel wall adjacent to the core is about 0.57%.

After the coolant slug impinges on the reactor cover, the upward axial energy of coolant is transformed into internal

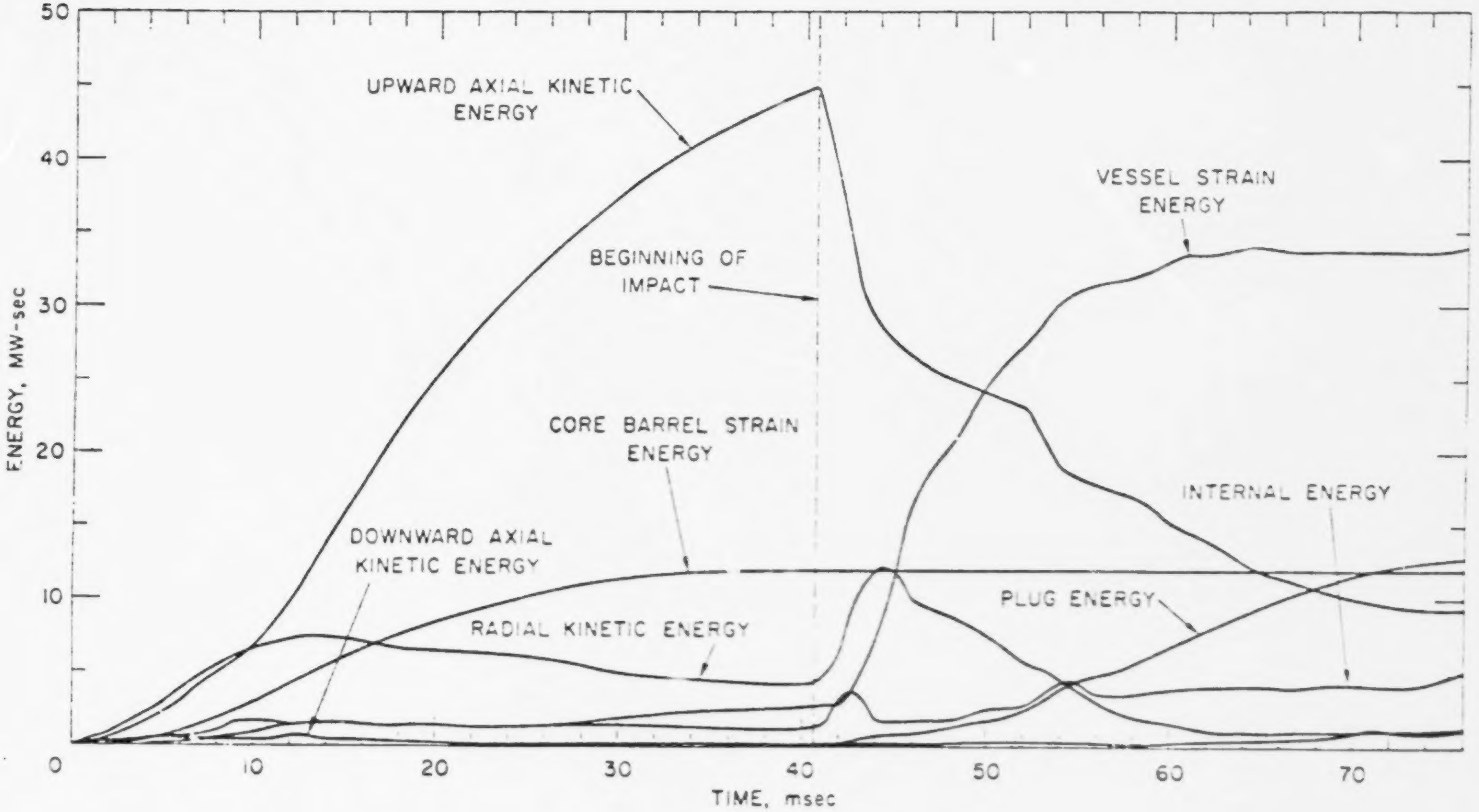

Fig. 16 Partition of Energy as a Function of Time.

energy of coolant, into radial kinetic energy of coolant, and then into strain energy of vessel wall (upper portion) and energy of plug and holddown bolts. The maximum deformation of the upper vessel wall resulting from the slug impact with the cover is about 3.5%. The strain energy of the reactor vessel reaches maximum at t = 64 msec.

At the time of slug impact, as well as at a later time when the system has reached dynamic equilibrium, the program provided partition of energy by giving

a. work energy released
b. upward kinetic energy
c. downward kinetic energy
d. radial kinetic energy
e. core barrel strain energy
f. vessel strain energy
g. coolant internal energy
h. energy imparted to reactor head and bolts.

The primary system is already in dynamic equilibrium at t = 92.774 msec. The unreleased HCDA work energy will be retained in the core for a long period of time, if the sodium is not allowed to spill out of the primary containment. This is also true for the sodium kinetic energy. The sodium vibratory motion will continue until it is finally damped out by the viscous damping force. The additional energy imparted to the reactor head and vessel wall will be very small.

Application to the LMFBR Demonstration Plant

The REXCO codes were also used to study the primary system response of the Demonstration Plant to hypothetical core disruptive accidents. The study utilized REXCO-HEP to perform a preliminary scoping analysis for the HCDA structural response, and the REXCO-HT was used to investigate the work energy release from molten fuel coolant interactions.

Structural Response to HCDA

The purpose of this study was to understand the structural response of the Demonstration Plant primary system to HCDA, to calculate HCDA loads acting on various components for the purpose of preliminary design and planning of further analysis, and to provide guidance to postaccident heat removal (PAHR) study. The response of the Demonstration Plant primary system was very similar to that of the FFTF. This was to be expected, since the Demonstration Plant design and the excursion models used in the scoping analysis are very similar to those of FFTF.

Molten Fuel-coolant Interactions

The Demonstration Plant offered an opportunity to use the REXCO-HT code to determine the response of a reactor system to a postulated whole core event. Initial conditions were determined by the use of other computer codes which resulted in the specification of fuel temperature and volume, as well as coolant temperatures, volume and quality. Several cases were studied ranging from essentially mild accidents to somewhat more energetic events which involved high temperature fuel and relatively cool liquid. One of the difficulties encountered was the inability to model the expected stiffness of the core support by removing the lower portion of the vessel and substituting a fixed plate. To avoid a rigid model, two additional horizontal zones were assumed between the bottom of the core barrel and the fixed plate.

A rather wide range of initial conditions was used in the calculations and constituted a parametric study of possible events. Results were quite similar to FFTF results described earlier in one case, while another gave a signficantly higher energy release.

4.5.1.6 Verification

To establish the validity of the REXCO codes, comparisons of analytical results with published experiments were undertaken (Refs. 177,178). Experiments performed by others, which lent themselves to comparison with code results were selected. Experiments by the British, French, and NAVORD, and the SL-1 accident compared reasonably well with code results (Refs. 177, 178). Finally, for a more systematic effort in code verification, ANL provided input to the FFTF model experiments performed at Stanford Research Institute. The SRI experiments consisted of (a) energy source development, (b) simple FFTF-model tests, and (c) complex FFTF-model tests. The work on the energy source focused on the development of a dependable, reproducible source which could simulate nuclear excursion characteristics.

Simple Model Experiments

Simple FFTF-model tests were undertaken at SRI to investigate the important test parameters prior to the initiation of the complex tests. Two scaling factors (1/30 and 1/10), and two energy levels were tested. Ni-200, instead of SS 304 was used in the tests in order to simulate the material properties of the tests at room temperature with those of the reactor at operating temperatures. The important parameters observed and compared with code predictions were:

a. partition of excursion energy
b. pressures at the reactor cover
c. pressures at the vessel walls
d. time of arrival of slug
e. core barrel deformation
f. vessel deformation at the core region and upper level
g. stretch of holddown bolts.

An extensive discussion of the comparisons of the FFTF simple tests with REXCO predictions is given in a recent report (Ref. 179).

Complex Model Comparisons

One facet of the analytical and experimental effort to predict the response of the FFTF to a hypothetical energy source was the testing of one-thirtieth-and one-tenth-scale models (Ref. 180). These models were designed to represent, as completely as possible, the main structures of the reactor, including the vessel, thermal liner, vessel head-including penetrations and crushable tubes, instrument trees, in-vessel fuel handling machine, core barrel and core support structure. The core region was designed to accommodate the gas-generator

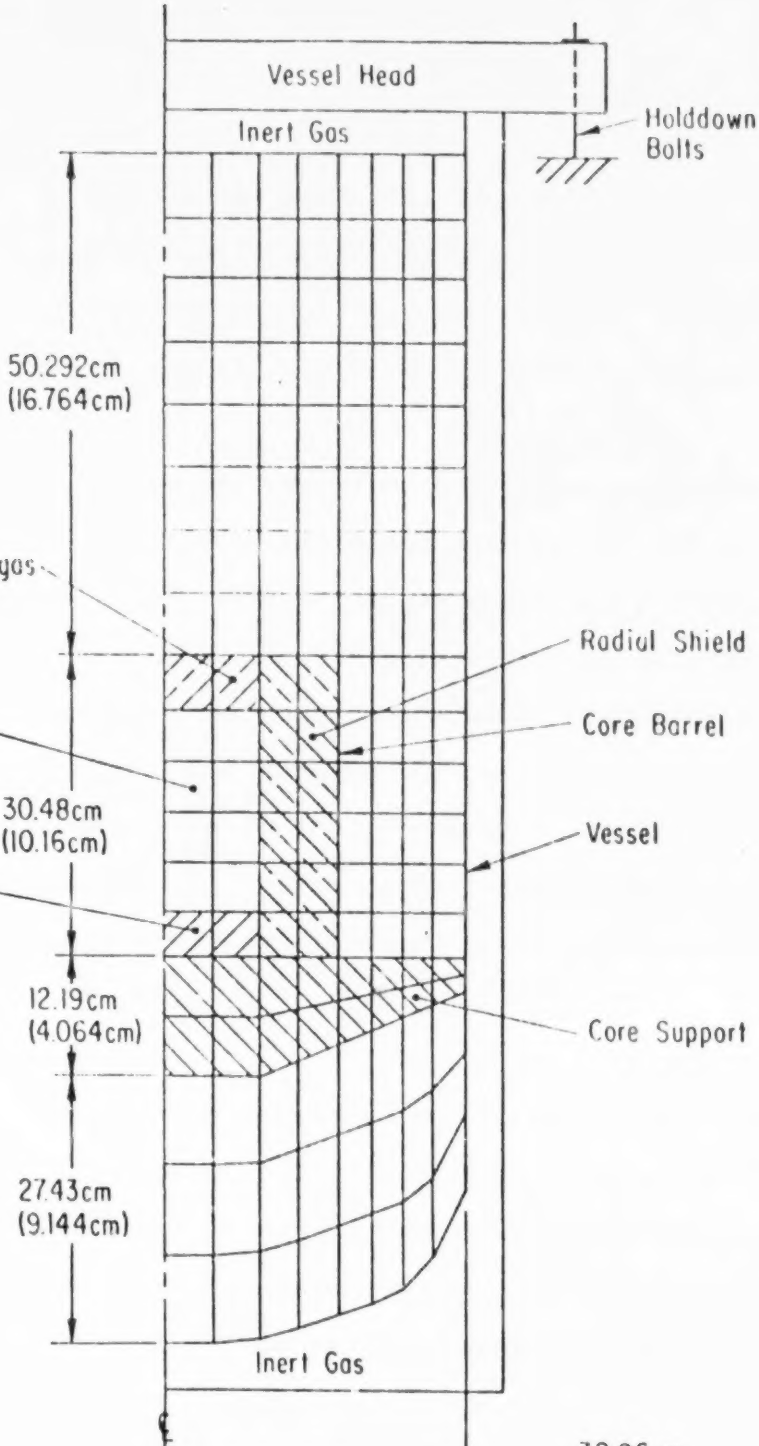
Vessel Head
Inert Gas
Holddown Bolts
50.292cm (16.764cm)
Fission-gas Plenum
Radial Shield
Core
Core Barrel
30.48cm (10.16cm)
Vessel
Axial Shield
12.19cm (4.064cm)
Core Support
27.43cm (9.144cm)
Inert Gas
℄
30.96cm (10.32cm)

Fig. 17. Computer Model of 1/10th- and 1/30th-scale FFTF Models.

device developed to duplicate the pressure-time and energy characteristics of the HCDA source, while the material used to simulate the properties of Type 304 stainless steel at operating temperatures was nickel-200 (Refs. 181, 182).

The approach taken to analyze the test results using the REXCO-HEP code was to use the same mathematical modeling techniques used to predict the response of the FFTF (Ref. 183). The task would essentially give an indication of the efficacy of the modeling technique used in the prototype calculations if reasonable agreement was obtained for several important phenomena. These comparisons included (1) the coolant slug impact time, (2) upper and mid-vessel deformations, (3) outlet-nozzle pressure-time history, and (4) vessel head movement and bolt stretch.

Mathematical representation of the one-thirtieth- and one-tenth-scale models is shown in Fig. 17. The dimensions in parentheses are those for one—thirtieth scale. Included in the vessel was the thermal liner, the heavier sections where the core support skirt and the vessel support straps join the vessel and the vessel-head flange. The pressure-volume characteristics of the model core region were determined from the simple model tests.

Of prime importance was the vessel deformation. A comparison of the one--thirtieth scale tests, CM-30-1 and CM-30-2, with the calculational results is shown in Fig.18. Good agreement was obtained in the mid-vessel region, approximately 0-17 cm above the top of the core structure. In the upper vessel region the code predicted a strain of about 3.4 percent, while the experiment showed a 2.1 percent strain. One-tenth-scale vessel profiles are shown in Fig. 19, and again show similarity in mode and magnitude of the hoop strains. Mid-vessel strain in the model was 1.2 percent, while the calculation shows a 1.0 percent strain. Upper vessel strains in the one-tenth-scale model were 1.88 percent and 3.2 percent for the test and calculation, respectively.

Slug impact times provided an interesting comparison. Experimental measurements indicate slug impact at 4.3 msec in the one-tenth-scale model, while the calculations indicate that the impact at the centerline was at 4.044 msec with complete impact several tenths of a millisecond later, with the peak force occurring at 4.3 msec. Thus, the impact times are similar.

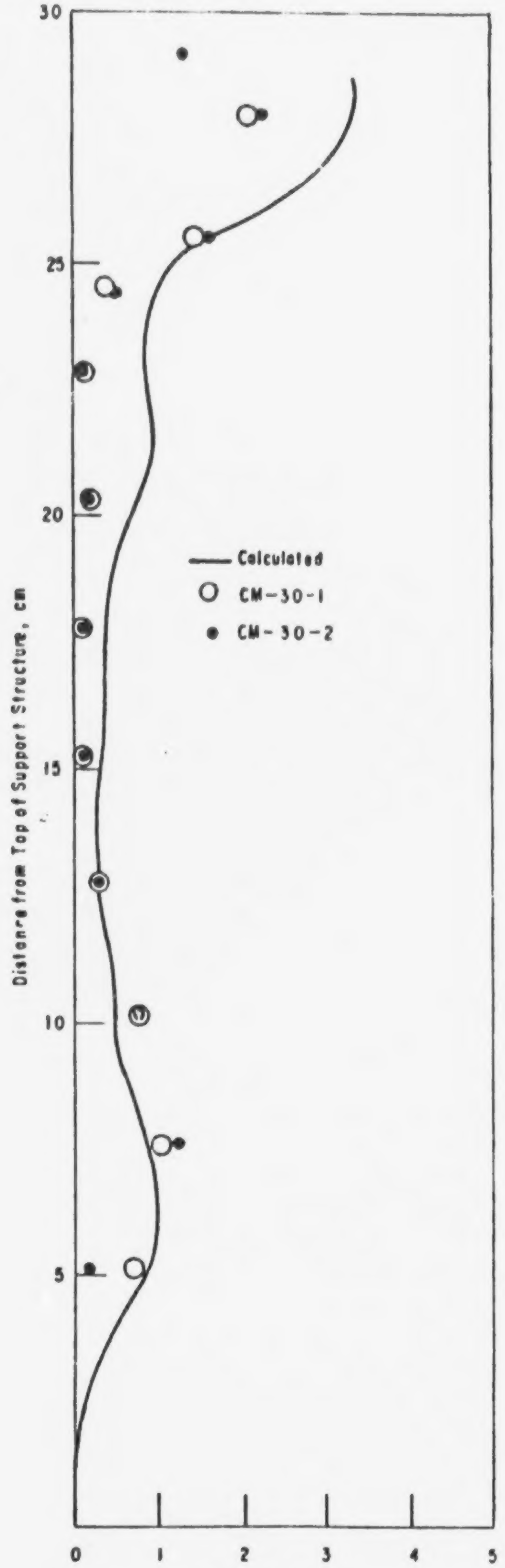

Fig. 18.
Comparison of Analytical and Experimental Vessel Deformations for 1/30th-scale FFTF Mode

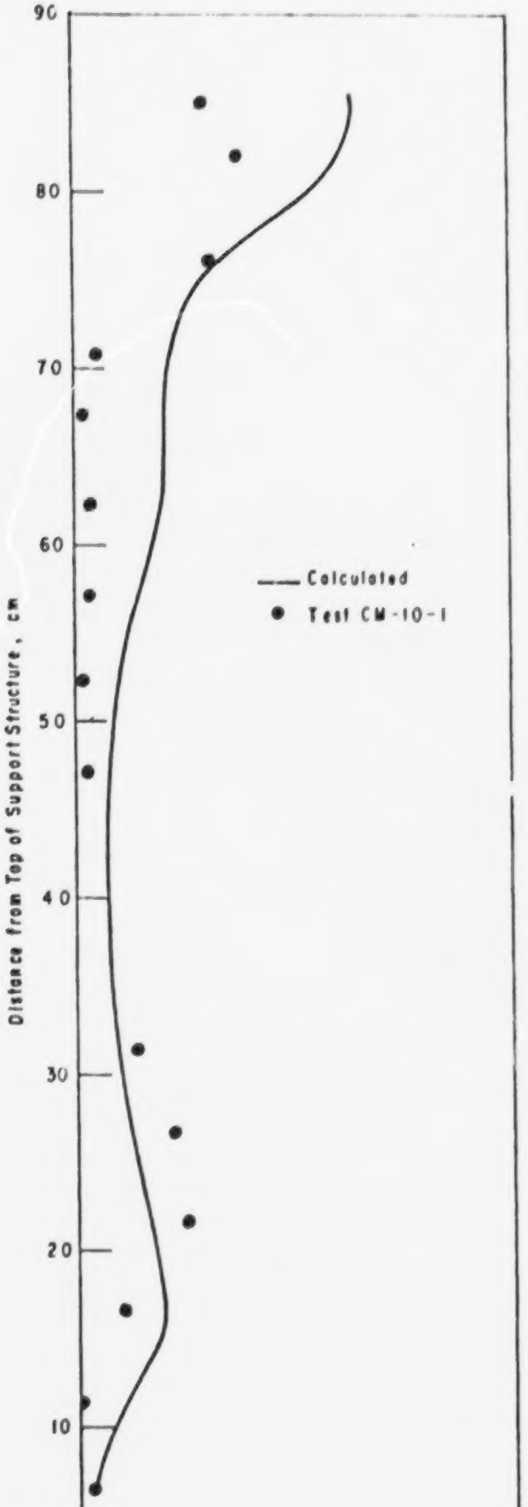

ig.19. Code Predictions Versus Experimental Results of Vessel Deformations for 1/10th-le FFTF Model.

Head movement was calculated to be 0.386 in. for the one-tenth-scale model, which corresponds to an average bolt strain of 5.6 percent, as compared to head movement of 0.38 in. and a group-one bolt strain of 4.24 percent in the experiment. The calculations are conservative in predicting head movement and bolt strain.

Figure 20 shows the outlet nozzle pressure-time history for both the one-tenth-scale experiment and calculation. The calculated pressure peak of about 45 bars is somewhat higher than the 35 bars measured in the experiment, since there is some local pressure relief due to the outlet piping. This result indicates that the REXCO code would be conservative in predicting vessel wall pressures and displacements, as indicated in the wall hoop strain curves.

Overall, the calculations of the complex model tests using the REXCO code showed very good agreement with the experimental results, indicating that the modeling techniques used to describe prototype containment response are adequate (Ref. 184).

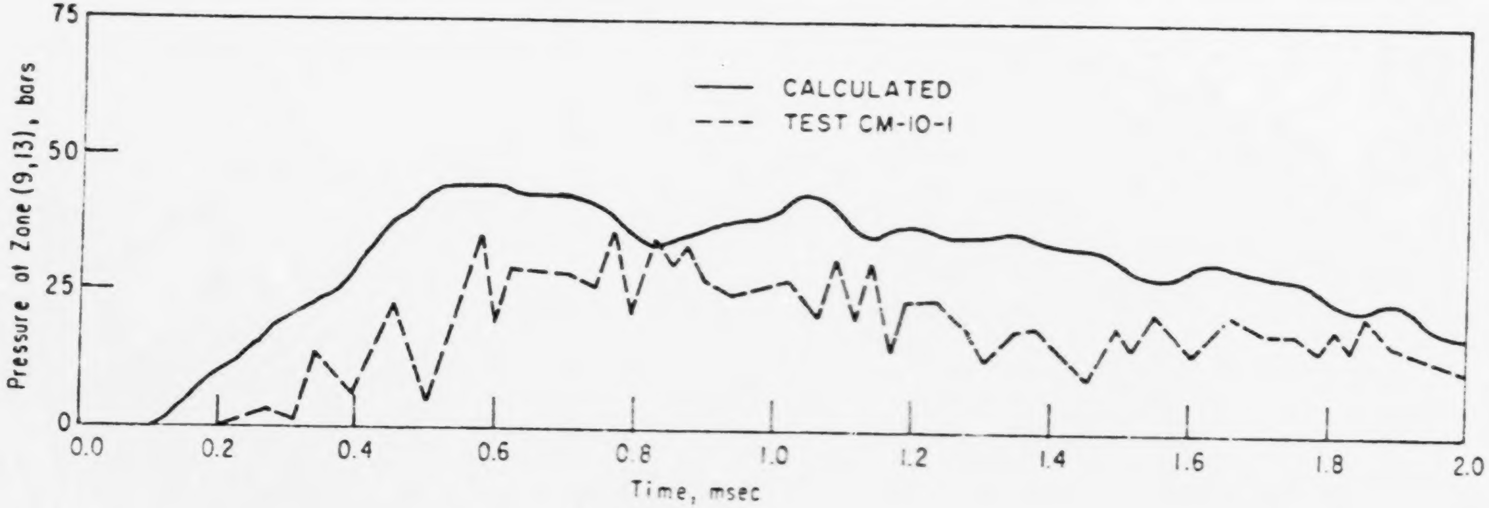

Fig. 20. Comparison of Calculated and Measured Pressures in the FFTF 1/10th-Scale Complex Model.

4.5.1.7 Limitations

There is sufficient evidence by now to indicate that the primary containment and structural response of the primary components to an HCDA can be predicted reasonably well by analyses and codes. There remain phenomena beyond those investigated by FFTF-model tests at SRI, which would still require code verification. The FFTF model tests at SRI, as successful as they were, are intended to provide information for the particular problems of the FFTF reactor. They were not designed for broad LMFBR technology development. The testing program to follow has been designed to close the code verification gaps that remain.

Further areas of needed development include more detailed considerations of fuel-sodium heat transfer. Presently this heat transfer model is included in the REXCO-HT code. More realistic MFCI conditions could be accounted for if a MFCI model was built into REXCO-HEP. This is true since REXCO-HEP models have both elastic and plastic materials.

The current limitations to the REXCO-HEP code include: treatment of the core as a homogenized body with no sliding between materials or anisotropic effects allowed; gross description of the core support structure; Lagrangian formulation cannot treat extended material motion; and it requires source input and only axisymmetric sources are able to be described.

The ICECO code, a 2-D Eulerian hydrodynamic code for calculating extended motion is being developed for coupling with REXCO-HEP to describe the reactor structures for longer times. The ICECO code is presently capable of modeling only a single fluid with rigid boundaries and structures. Further development of the REXCO-HEP and ICECO codes with their eventual coupling requires considerable effort, but provides the best hope for describing the long-term effects of LMFBR nuclear excursions.

4.5.2 STRAW and SADCAT

4.5.2.1 Description

STRAW (Structural Transient Response of Assembly Wrappers) (Refs. 185, 186) is a two dimensional (r,θ) finite element structural analysis code for evaluation of the non-linear dynamic response of reactor core subassemblies to accident pressure loadings. SADCAT (Ref. 187) is basically a three dimensional version of STRAW. These codes are presently under development at Argonne National Laboratory and will help clarify fuel failure propagation questions since they model single hexcan assembly wrappers surrounded by a prototypic environment. In addition, the codes are used to calculate the dynamic response of subassemblies adjacent to an accident subassembly to assess the damage propagation.

STRAW contains the heat transfer models and the equation-of-state of sodium from the REXCO-HT code. This provides the code with the ability to couple the heat transfer models, which describe molten-fuel-coolant interactions, to the hydrodynamic and structural response of the subassemblies, thus eliminating the need for assumptions concerning fluid characterization and structural-material behavior for interaction.

Therefore, a more realistic evaluation of the interaction of the MFCI and its surroundings is achieved.

The initial checkout of the incorporation of the MFCI models into the code was done by comparing calculations made by REXCO-HT for a similar configuration and several initial conditions. A simple cylindrical-shell configuration, consisting of four axial zones (one FCI zone and three sodium zones), was investigated for several initial conditions; good agreement was achieved between the code results.

REXCO-HT is a two-dimensional code in the r-z plane, while STRAW is a two-dimensional code in the r-θ plane. In the STRAW code, a special element represents the FCI zone in the r-θ plane, while the axial sodium zones are represented by elements termed superelements. The superelements are one-dimensional wave models which account for the axial flow of the sodium. The one-dimensional wave equation interacts with the element in the r-θ plane so the equations-of-mass conservation and state are satisfied. The pressure change in the element representing the FCI zone (or adjacent radial zones of hydrodynamic elements) provides the driving force for the axial pressure wave. The elements permit only axial flow to take place above the FCI region, but, since the axial flow area is much greater than the transverse flow area, this is a reasonable restriction.

4.5.2.2 Limitations

Both STRAW and SADCAT are under development now. SADCAT lacks heat transfer models for describing an energy source term and will require coupling with a three-dimensional fluid sodium model. Further experimental verification such as that planned for REXCO codes is necessary to assess these codes.

areas and further modeling efforts have been replaced to considerable extent by these check outs.

Future code development presently centers upon those areas in which code inadequacies have been pointed out (extended fuel motion, secondary criticality, post-accident heat removal and fuel pin failure thresholds).

The major limitations of the present day computer code capabilities in small LMFBR accident analysis are then:

1. Lack of experimental validation of most models. More experimental information about fission gas behavior, internal fuel motion, failure thresholds and incoherency effects is needed.

2. Lack of models to describe extended accident conditions including problems associated with space dependent neutronics and debris bed behavior.

3. Lack of models to describe fuel pin failure thresholds.

4. Lack of models to describe the transition from intact to disrupted geometry although these models are under development now.

5. Clarification of the importance and possible effects of neutron streaming when the void space is reduced.

4.6 Summary

The accident analysis codes (not TWOTRAN) described above are models of physical phenomena thought to occur during LMFBR accidents. These models are all mechanistic and extend from accident initiation until the occurrence of containment damage. Most of the transient codes are used for describing either the chain of events occurring in underflow or overpower accidents.

Initially, the concept of mechanistic accident analysis involved the attempt to be conservative and upper bound the possible consequences. This effort, partly because of the magnitude of the results, changed direction slightly in the early 1970's. During this period a number of previously not considered phenomena (material motion effects during underflow and over power accidents) were included in the modeling. This new phase of more detailed modeling characterized by the growth and complexity of many of the computer programs has continued until most of the known phenomena have become modeled in some manner (if even macroscopically).

Presently, the need for experimental verification of those models developed has received the highest priority in many

Larger LMFBR's (>500 MWe) and advanced fueled cores cannot presently be described with existing codes. First, a thorough assessment of their adequacy and the necessary model changes and additions must be made.

REFERENCES

1. V.Z. Jankus and R.W. Weeks, "LIFE-I, A FORTRAN-IV Computer Code for the Prediction of Fast-reactor Fuel-element Behavior," USAEC Report ANL-7736, Nov. 1970.

2. V.Z. Jankus and R.W. Weeks, "LIFE-I, A History-Dependent Analysis of Fast Reactor Fuel Element Behavior," ANS Trans. 13 (2), 830, November 1970.

3. R.W. Weeks, V.Z. Jankus, M. Katsuragawa, and J.D.B. Lambert, "Analysis of Mixed-Oxide Fuel Element Irradiations Using the LIFE-I Computer Code," Proc. ANS Topical Meeting on Fast Reactor Fuel Element Technology, New Orleans, April 1971, to be published.

4. V.Z. Jankus and R.W. Weeks, "LIFE-2, A Computer Analysis of Fast Reactor Fuel Element Behavior as a Function of Reactor Operating History," Nuclear Engineering and Design, 18, 1972.

5. M.G. Stevenson, W.R. Bohl, F.E. Dunn, T.J. Heames, G. Hoppner, and L.L. Smith, "Current Status and Experimental Basis of the SAS LMFBR Accident Analysis Code System," Proc. Conf. Fast Reactor Safety, Beverly Hills, Ca., April 1974.

6. R.B. Peopple, "An Advanced Gas Release and Swelling Subroutine," Proc. ANS Topical Meeting on Fast Reactor Fuel Element Technology, New Orleans, April 1971.

7. S. Oldberg, Jr., "BEHAVE-2: Oxide Fuel Performance Code in Two Spatial Dimensions and Time," General Electric Co., GEAP-13788, February 1972.

8. F.J. Homan, W.J. Lockey and C.M. Cox, "FMODEL-A FORTRAN IV Computer Code to Predict In-Reactor Behavior of LMFBR Fuel Pins," ORNL-4825, January 1973.

9. C.H. Cox and F.J. Homan, "Performance Analysis of a Mixed-Oxide LMFBR Fuel," Nuclear Applications and Technology, 9, 317, September 1970.

10. C. R. Hann, F.E. Panisko, "User's Guide for GAPCON: A Computer Program to Predict Fuel-to-Cladding Heat Transfer Coefficients in Oxide Fuel Pins," HEDL-TME72-128, Sept. 1972.

11. D.D. Freeman, "FREADM Code Development--A Status Report, GEAP-13936, 1973.

12. A.E. Waltar, A. Padilla, Jr., and R.J. Shield, "Melt-II, A Two-dimensional Neutronics-Heat Transfer Code for Fast Reactor Safety Analysis," HEDL-TME 72-43, 1972.

13. H.A. Bethe and J.H. Tait, "An Estimate of the Order of Magnitude of the Explosion When the Core of a Fast Reactor Collapses," UKAEA-RHM(56)/113, 1956.

14. R.B. Nicholoson, "Methods for Determining the Energy Release in Hypothetical Fast Reactor Meltdown Accidents," Nucl. Sci. Eng. *18*, pp. 207, 1964.

15. D. Okrent *et al.*, "AX-1, A Computing Program for Coupled Neutronics-Hydrodynamics Calculations on the IBM-704," ANL-5977, 1959.

16. W.R. Stratton, L.B.Engle, and D.M. Peterson, "Reactor Power Excursion Studies," *Proc. Conf. on Engineering of Fast Reactors for Safe and Reliable Operation*, Vol. 3, pp. 1331, Karlsruhe, Germany, 1972.

17. N. Hirakawa, "MARS--A Two-dimensional Excursion Code," APDA-198, 1967.

18. W.T. Sha and T.H. Hughes, "VENUS: A Two-dimensional Coupled Neutronics-Hydrodynamics Computer Program for Fast-reactor Power Excursion," ANL-7701, October 1970.

19. J.F. Jackson and R.B. Nicholson, "VENUS-II: An LMFBR Disassembly Program," ANL-7951, 1972.

20. E.P Hicks and D.C. Menzies, "Theoretical Studies on the Fast Reactor Maximum Accident," *Proc. Conf. Safety Fuels and Core Design in Large Fast Power Reactors, October 11-14, 1965*, ANL-7120, 1965.

21. D.H. Cho, "Fuel-coolant Interactions Following a Voided-core Disassembly," *Trans. Am. Nucl. Soc.* *15*, No. 2, pp. 810, 1972.

22. Andrew Padilla, Jr., "Analysis of Mechanical Work Energy for LMFBR Maximum Accidents," Nuclear Technology *12*, pp. 348, 1971.

23. L. Caldarola and G. Koutsouvelis, "Theoretical Models for the Molten Fuel-Sodium Interaction," Proc. Conf. on Engineering of Fast Reactors for Safe and Reliable Operation, Vol. 2, pp. 952, Karlsruhe, Germany, 1972.

24. H.K. Fauske, "An Assessment of Experiments on Fuel-Coolant Interactions and on Continuous Explosive Boiling," These Proceedings.

25. S.H. Fistedis, "Containment of Fast Breeder Reactors--Present Status--Remaining Problems," *First Intl. Conf. on Structural Mechanics in Reactor Technology*, Berlin, Germany, Sept. 1971.

26. K. Fuchs, "Efficiency for Very Slow Assembly," Los Alamos Scientific Laboratory report LA-596, 1946.

27. G. Hansen, "Burst Characteristics Associated with Slow Assembly of Fissionable Materials," Los Alamos Scientific Laboratory report LA-1441, July 1952.

28. W.R. Stratton, T.H. Colvin, and R.B. Lazarus, "Analysis of Prompt Excursions in Simple Systems and Idealized Fast Reactors," Proc, 2nd Intern. Conf. Peaceful Uses At. Energy, Geneva, 1958 (United Nations, New York, 1958) Paper 431, Vol. 12, pp. 196-220.

29. R.B. Nicholson and J.W. Stephense, "Reactor Explosion Program," ASTRA 417-3, 1960.

30. C.G. Chezem and W.R. Stratton, "RAC, A Computer Program for Reactor Accident Calculations," Los Alamos Scientific Laboratory report LA-2920-MS, August 1963.

31. L.I. Moss and W.A. Rhoades, "A Method for the Study of Autocatalysis and/or Pressure Histories in Fast Breeder Excursions," Mtg. Industrial Needs and Academic Research in Reactor Kinetics, Upton, NY 8-9 April 1968.

32. W.R. Stratton, L.B. Engle, D.M. Peterson, "REactor Power Transient Studies," Los Alamos Scientific Laboratory report LA-DC-72-660, June 1972.

33. W.R. Bohl and M.G. Stevenson, "A Fuel Motion Model for LMFBR Unprotected Loss-of-Flow Accident Analysis," Proc. Conf. Mathematical Models and Comp. Tech. for Analy. Nucl. Systems 1973 (Ann Arbor, Michigan, 1973), Part 1, pp. V-137 and V-158).

34. W.T. Sha, et al., "Two-Dimensional Fast Reactor Disassembly Analysis with Space-Time Kinetics," Nat'l. Topical Mtg. New Developments in Reactor Math. and Applications, Idaho Falls, Idaho, 29-31 March 1971.

35. J. Boudreau, F.H. Harlow, W.H. Reed, and J.F. Barnes, "A Proposal for Computer Investigation of LMFBR Core Meltdown Accidents," Los Alamos Scientific Laboratory report LA-UR-243, October 1973.

36. Bleiweis, P.B., Some Safety Aspects of Large Liquid Metal-Cooled Fast Breeder Reactors, Ph.D. in Engineering, University of California at Los Angeles, 1973.

37. Bleiweis, P.B., Okrent, D. and W.E. Kastenberg, "A Comparison Study and Analysis of Models for 1000 MWe and 4000 MWe LMFBR Hypothetical Accidents," Proc. Conf. Fast Reactor Safety, Beverly Hills, California, April 1974.

38. J.F. Jackson, M.G. Stevenson, J.F. Marchaterre, R.H. Sevy, R. Avery and K.O. Ott, "Trends in LMFBR Hypothetical Accident Analysis," Proc. Conf. Fast Reactor Safety, Beverly Hills, California, April 1974.

39. Y.W. Chang, J. Gvildys, and S.H. Fistedis, "Hydrodynamic Response of Primary Reactor Containment to High-energy Excursion," Nucl. Eng. Design 12, 344-360, 1970.

40. Y.W. Chang, J. Gvildys, and S.H. Fistedis, "Two dimensional Hydrodynamics Analysis for Primary Containment," ANL-7498, November 1969.

41. Y.W. Chang, and J. Gvildys, "Dynamic Response of Reactor Containment to High-energy Excursion," Proc. the First Intl. Conf. on Structural Mechanics in Reactor Technology, Berlin, Germany, 1971.

42. Y.W. Chang, and J. Gvildys, "REXCO-HEP: A Two-dimensional Computer Code for Calculating the Primary System Response in Fast Reactors," ANL report to be published.

43. C.Y. Wang, J.C. Bratis, Y.W. Chang, and S.H. Fistedis, "Analysis of Fuel-coolant Interactions by the Implicit Continuous Eulerian Containment Code," Trans. Am. Nucl. Soc., 17, 355-366, November 1973.

44. E.P. Hicks and D.C. Menzies, "Theoretical Studies on the Fast Reactor Maximum Accident," Proc. Conf. Safety, Fuels and Core Design in Large Fast Power Reactors, Argonne, Illinois, 11-14 October 1965; Argonne National Laboratory report ANL-7120, October 1965, pp. 654-670.

45. Andrew Padilla, Jr., "Analysis of Mechanical Work Energy for LMFBR Maximum Accidents," Nucl. Tech. 12, 348-355, 1971.

46. D.H. Cho and R.W. Wright, "A Rate Limited Model of Molten Fuel-Coolant Interactions," Trans. Am. Nucl. Soc. 13, 659, 1970.

47. D.H. Cho and W.L. Chen, "Improvement of Basic Parametric Model of FCI, ANL report, ANL-RDP-16, April 1973.

48. Y.W. Chang, J. Gvildys and S.H. Fistedis, "Two-Dimensional Hydrodynamics Analysis for Primary Containment," USAEC report ANL-7498, November 1969.

49. H.K. Fauske, "On the Mechanism of Uranium Dioxide-Sodium Explosive Interactions," Nucl. Sci. Eng. 51, 95, 1973.

50. W.R. Stratton, "A Review of Criticality Accidents," Los Alamos Scientific Laboratory report LA-3611, January 1967.

51. L.D.P. King, et al., "Description of the KIWI-TNT Excursion and Related Experiments," Los Alamos Scientific Laboratory report LA-3350-MS, July 1966.

52. L.D.P. King, "Safety Neutronics for Rover Reactors," Los Alamos Scientific Laboratory report LA-3358-MS, October 1965.

53. D. Antonakas, M.Fortunato, A. Meyer Heine, P. Francois, "Some Problems Concerning Fast Reactor Safety," Proc. ANS Fast Reactor Safety Meeting, April 2-4, 1974, Los Angeles, Calif.

54. D. Stepnewski and C.R. Adkins (Ed.), "Final Report of Task Force for Assessment of Additional FFTF Design Margin," WARD-317, August 1974.

55. C.M. Cox and F.J. Joman, PROFIL-A One-Dimensional FORTRAN IV Program for Computing Steady-State Temperature Distribution in Cylindrical Ceramic Fuels, ORNL-TM-2443, March 1969 and Addendum, August 1969.

56. Westinghouse Advanced Reaction Division, Oxide Fuel Element Development Quarterly Progress Report for Period Ending September 30, 1969, WARD-4135-1, November 1969.

57. M.F. Lyons, et al., *UO_2 Pellet Thermal Conductivity From Irradiation with Central Melting*, GEAP-4624, 1964.

58. S.Y. Ogawa, E.A., Lees, and M.F. Lyons, *Power Reactor High Performance UO_2 Program*, GEAP-5591, 1968.

59. C.R. Hann, C.E. Beyer and L.J. Parchen, "GAPCON-THERMAL-1: A Computer Program for Calculating the Gap Conductance in Oxide Fuel Pin," UC-78, September 1973.

60. M.J.C. Carlson, *Water and Sorbed-Gas Content of Hypostoichiometric Mixed Oxide Fuel Pellets*, WHAN-SA-77, 1972.

61. D.E. Vance, M.E. Smith, and G.R. Waterbury, *Determination of Total Amount of Volatiles in Mixed-Oxide Reactor Fuel Pellets,* LA-5108, February 1973.

62. T.B. Burley, M.D. Freshley, "Internal Gas Pressure Behavior in Mixed-Oxide Fuel Rods During Irradiation," *Nuclear Applications and Technology*, Vol. 9, August 1970.

63. M. Hurme, Observations of Fuel Pin Internal Pressure, HPR-110, June 1969.

64. D.W. Shannon Quarterly Progress Report: *Irradiation Effects on Reactor Structural Material* - Hanford Laboratories, Richland, Wash. HW-79345, November 1963.

65. V.J. Wheeler, "The Diffusion and Solubility of Hydrogen in Uranium Dioxide Single Crystals," *J. Nuclear Materials*, Vol. 40, 1971.

66. L.S. Darken, R.W. Gurry, "Physical Chemistry of Metals," McGraw-Hill Book Co., 1953.

67. H.M. Ferrari, "Nitrogen Release from UO_2 Pellets at Elevated Temperatures," Nuclear Science and Engineering, Vol. 17, 1963.

68. H.M. Ferrari, "Diffusion of Nitrogen in Uranium Dioxide," *J. Nuclear Materials*, Vol. 12, No. 2, 1964.

69. A.H. Booth, G.T. Rymeth, *Determination of the Diffusion Constant of Fission Xenon in UO_2 Crystals and Sintered Compacts*, AECL-496, 1957.

70. A.H. Booth, A Method of Calculating Fission Gas Diffusion from UO_2 Fuel and Its Application to X-2-F Loop Test, AECL-496, 1957.

71. R.B. Bird, W.E. Stewart, and E.N. Lightfoot, *Trans. Phenomena*, John Wiley and Sons, N.Y., N.Y., November 1966.

72. Hans von Ubisch, "The Thermal Conductivities of Mixtures of Rare Gases at 29°C and 320°C," *Arkiv for Fysik, Band 16, nr 7*, June 1959.

73. C.R. Hann, *Fuel Rod Gap Conductance and UO_2 Thermal Conductivity - A Study for the Reactor Systems Branch - Directorate of Licensing, USAEC*, Battelle, Pacific Northwest Laboratories Report, July 1972.

74. A.M. Ross, R.L. Stoute, *Heat Transfer Coefficients Between UO_2 and Zircaloy-2*, CRFD-1075, June 1962.

75. M. Knudsen, *The Kinetic Theory of Gases - Some Modern Aspects*, Meuthuen and Co., Ltd., 2nd Edition, 1946.

76. S. Dushman, *Scientific Foundations of Vacuum Technique*, John Wiley and Sons, New York, NY, 1958.

77. J.A. Christensen, "Columnar Grain Growth in Oxide Fuels," *Trans. Am. Nucl. Soc.*, Vol. 15, No. 1, June 1972.

78. R.S. Brokaw, "Estimating Thermal Conductivities for Non-Polar Mixtures: Simple Empirical Method," *Ind. Eng. Chem. 47:* 2398-2400, 1955.

79. J. Roth et al., "The Effects of Stoichiometry on the Thermal Expansion of 20 wt. %PuO_2-UO_2 Reactor Fuel," *Trans. Amer. Nucl. Soc.* 10(2): 457, 1967.

80. R.P. Nelson, "Thermal Expansion of Mixed UO_2-PuO_2," Quart. Progr. Report April, May, June, 1967, Reactor Fuels and Materials Development Programs for Fuels and Materials Branch of USAEC Division of Reactor Development and Technology, BNWL-473, p. 41.

81. F.A. Nichols, "Theory of Columnar Grain Growth and Central Void Formation in Oxide Fuel Rods," *J. Nucl. Material*, 22: 214, 1969.

82. F.J. Homan, "Development of a Fuel-Restructuring Model," *LMFBR Fuel Cycle Studies Progress Report for December 1970*, No. 22, ORNL-TM-3281, pp. 56-62.

83. W.J. Lackey, F.J. Homan, and A.R. Olsen, "Porosity and Actinide Redistribution During Irradiation of $(U,Pu)O_2$," *Nuclear Technology*. Also available as ORNL-TM-3762.

84. I. Goldberg, L.L. Lynn, and C.D. Sphar, FIGRO-FORTRAN IV Digital Computer Program for the Analysis of Fuel Swelling and Calculation of Temperature in Bulk Oxide Cylindrical Fuel Elements, WAPD-TM-618, December 1966.

85. W.E. Baily, F.A. Aitken, R.R. Asamoto, and C.M. Craig, "Thermal Conductivity of U-Pu Oxide Fuels," Intern. Symp. on Plutonium Fuels Tech., Scottsdale, Arizona, 1967, Nucl. Met. 13, 293-308, 1968.

86. A. Biancheria et. al., Westinghouse (USA) Report WARD-4135-1, p. 6, September 1969.

87. F.A. Nichols, "Behavior of Gaseous Fission Products in Oxide Fuel Elements," WAPD-TM-570, October 1966.

88. V.Z. Jankus and R.W. Weeks, USAEC Report ANL-7776, Reactor Development Program Progress Report, p.63, January 1971.

89. R.D. Leggett, E.O. Ballard, F.E. Bard, J.W. Weber, L.A. Pember, and R.J. Jackson, "Correlation of Predictions and Observations in Mixed Oxide Fuels," ANS Trans. 13(2), 574, November 1970.

90. Raymond J. Roark, *Formulas for Stress and Strain*, McGraw-Hill Book Company, New York City, NY, 4th ed., 1965.

91. D.B. Scott, *Physical and Mechanical Properties of Zircaloy-2 and Zircaloy-4*, WCAP-3629-41, May 1965.

92. Timoshenko and Goodier, "Theory of Elasticity," McGraw-Hill, 2nd ed., 1951.

93. Small, N.C., *An Inelastic Continuum Theory for Dilating Aggregate Materials,* Westinghouse Electric Corp., February 1965 (WAPD-TM-421).

94. Donald F. Johnson, "Analysis of Elastic-Plastic Stress Distribution in Thin-Wall Cylinders and Spheres Subjected to Internal Pressure and Nuclear Aeronautics and Space Adminstration," April 1969.

95. Richard L. Puthoff, "A Digital Computer Program for Determining the Elastic-Plastic Deformation and Creep Strains in Cylindrical Rods, Tubes, and Vessels," NASA TM-X-1723, U.S. National Aeronautics and Space Administration, January 1969.

96. J.T.A. Roberts and B.J. Wrona, "Plastic Yielding and Fracture of Mixed Oxides," Reactor Development Program Progress Report, ANL-7727, pp.129-30, August 1970.

97. U.S. Steel (National Tube Division), Bulletin NO. 26, 59th ed.

98. "Stainless Steel Cladding Development Quarterly Progress Report for Period Ending June 30, 1969," WARD-3791-41, p. 13, Westinghouse Atomic Research Div., 1969.

99. "Oxide Fuel Element Development Quarterly Progress Report for Period Ending September 30, 1969," WARD-4135-1, p.19, Westinghouse Atomic Research Div., 1969.

100. R.F. Canon, J.T.A. Roberts, and R.J. Beals, "Deformation of UO_2 at High Temperatures," J. Am. Ceramic Soc., 54, 105, 1971.

101. F.L. Yaggee and Che-Yu Li, "Failure Mechanisms for Internally Pressurized Thin-wall Tubes and their Relationship to Fuel-element Failure Criteria, USAEC Report ANL-7805.

102. Weeks, R.W., R.D. Scattergood,, and S.R. Pati, "Migration Velocities of Bubble-Defect Configurations in Nuclear Fuels," J. Nucl. Mat., 36:223-229, 1970.

103. Gruber, E.E., "Calculated Size Distributions for Gas Bubble Migration and Coalescence in Solids," J. Appl. Phys., 38:243-250, January 1967.

104. Carter, J.C., et. al., "SASIA, A Computer Code for the Analysis of Fast Reactor Power and Flow Transients," ANL-7607, October 1970.

105. Smith, L.L. and M.G. Stevenson, "Effect of Reactivity Insertion Rate on Fuel Pin Failure Threshold," Trans. Am. Nucl. Soc., 17:284-285, 1973 (paper presented at ANS Annual Meeting, San Francisco, November 1973).

106. Bard, F.E., and Dutt, D.S., "PECT-2 Analysis of the H3 Transient Test," HEDL-TME 72-28, February 1972.

107. Watanable, A. and A.M. Judd, "A Computer Code for Predicting the Behavior of Oxide Fuel in Accidents," Trans. Am. Nucl. Soc., 14, 733, 1971.

108. MacFarlane, D.R., ed. "SAS1A, A Computer Code for the Analysis of Fast Reactor Power and Flow Transients," Argonne National Laboratory, ARgonne, Illinois, ANL-7607, October 1970.

109. Dunn, F.E., T.J. Heames, P.A. Pizzica, and G. Fischer, "The SAS2A LMFBR Accident Analysis Code," Proc. of the Conf. on New Developments in Reactor Mathematics and Applications, Idaho Falls, Idaho, March 1971, American Nuclear Soc., Vol.1, pp. 120-127 [available from the National Technical Information Service, USAEC, CONF-710302].

110. Stevenson, M.G., et al., "Current Status and Experimental Basis of the SAS LMFBR Accident Analysis Code System," Proc. of the Conf. on Fast Reactor Safety, Beverly Hills, Calif., April 1974, American Nuclear Society, to be published [will be available from the U.S. National Technical Information Service, USAEC, Conf-740401].

111. W.R. Bohl, F.E. Dunn, G.J. Fischer, T.J. Heames, J.F. Jackson, R.B. Nicholson, L.L. Smith, M.G. Stevenson, J.R. Travis, and A. Watanabe, "Progress in Analysis of Severe Accidents," Proc. Intl Conf. on Engineering of Fast Reactors for Safe and Reliable Operation, Karlsruhe, Germany, October 1972.

112. LMFBR Materials Handbook, HEDL-TME 71-32, June 1971.

113. D.S. Dutt, D.C. Bullington, and R.B. Baker, A Correlated Fission Gas Release Model for Fast Reactor Fuels, Trans. Am. Nucl. Soc., 15, 198, 1972.

114. F.E. Dunn, G. Hoppner, T.J. Heames, and G.J. Fischer, "Comparison of SAS2A Sodium Boiling Analysis with Experiment," Trans. Am. Nucl. Soc., 15(1), 340, 1972.

115. F.W. Peppler, Experimentelle Untersuchungen der Siedevorganage mit Natrium in engen Kanalen und deren Arwendung auf schnelle Reaktoren, Externer Bericht GFK-IRE 817211.

116. M.A. Grolmes and H.K. Fauske, "Liquid Film Thickness and Mechanism for Dryout During LMFBR Loss-of-Flow Accidents," Trans. Am. Nucl. Soc., 14 (2) 743, 1971.

117. G. Hoppner and F.E. Dunn, "Sodium Film Model in SAS2A Voiding," Trans. Am. Nucl. Soc., 16(2), November 1973.

118. M.A. Grolmes, R.E. Holtz, B.W. Spencer, C.E. Miller, and N.A. Kramer, "R-Series Loss-of-Flow Safety Experiments in TREAT," Proc. of the Fast Reactor Safety Meeting, Beverly Hills, Calif., April 1974.

119. T.C. Chawla and H.K. Fauske, "On the Incoherency in Subassembly Voiding in FTR and its Possible Effect on the Loss-of-Flow Accident Sequence," Trans. Am. Nucl. Soc., 16,(2) 285, November 1973.

120. H.K. Fauske, T.C. Chawla, A.W. Cronenberg, J.F. Marchaterre, "Coolant Voiding and Pressure Generation Due to Boiling, Fission Gas Release, and Molten-Fuel Coolant Interaction," Trans. Am. Nucl. Soc., 13 (2), 656, 1970.

121. W. Bohl, D. Cho, F. Dunn, G. Fischer, T. Heames, J. Jackson, A Padilla, L. Smith, M. Stevenson, and A. Watanabe, "A Preliminary Study of the FFTF Hypothetical Flow Coastdown Accident," ANL/RAS 71-39, Rev.1, April 1972.

122. C.W. Hunter and R.L. Fish, "Deformation and Failure of Fast Reactor Fuel Cladding Specimens During High-Temperature Simulated Loss-of-Flow Transients," Proc. of the Fast Reactor Safety Meeting, Beverly Hills, Calif., April 1974.

123. J.J. Kaganove, "Numerical Solution of the One-group Space-independent Reactor Kinetics Equations for Neutron Density Given the Excess Reactivity," ANL-6132, February 1960.

124. W.R. Bohl and T.J. Heames, "A Clad Motion Model for LMFBR Loss-of-Flow Accident Analysis," Trans. Am. Nucl. Soc., 16, 358, 1973.

125. L.W. Deitrich, E.W. Barts, A. DeVolpi, C.E. Dickerman, J.G. Eberheart, A.K. Fischer, W.F. Murphy, and G.S. Stanford, "Fuel Dynamics Experiments Supporting FTR Loss-of-Flow Analysis," Proc. of the Fast Reactor Safety Meeting, Beverly Hills, April 1974.

126. E.T. Weber, O.D. Slagle, and C.A. Hinman, "Laboratory Studies on Melting and Gas Release Behavior of Irradiated Oxide Fuel," Proc. of the Fast Reactor Safety Meeting, Beverly Hills, April 1974.

127. P.J. Persiani, A. Watanabe, U. Wolff, S. Grifoni, and B. Warman, "Some Considerations on the Meltdown Problem for FARET," ANL-6935, Argonne National Lab., 1964.

128. T. Hikido and J.H. Field, "Molten Fuel Movement in Transient Overpower Tests of Irradiated Oxide Fuel," GEAP-13543, 1969.

129. W.R. Bohl and M.G. Stevenson, "A Fuel Motion Model for LMFBR Unprotected Loss-of-Flow Accident Analysis," CONF-730414-P2, Ann Arbor, Michigan, April 1973.

130. C.E. Dickerman, L.E. Robinson, F.L. Willis, W. Stephany, and C. August, "Status of Recent Meltdown Studies," Proc. Conf. on Safety, Fuels, and Core Design in Large Fast Power Reactors, ANL-7120, p. 534, 1971.

131. E.E. Gruber, J. Appl. Physics, 38, pp. 243-250, 1967.

132. R.B. Poeppel, " Advanced Gas Release and Swelling Subroutine, Trans. Am. Nucl. Soc., Supplement 1, 14, p. 13, April 1971.

133. E.E. Gruber, "Modeling Transient Fission-Gas Release from Oxide Fuel," to be presented at Philadelphia ANS Meeting, 1974.

134. A.B. Rothman, L.W. Deitrich, R.C. Doerner, A.E. Wright, and C.E. Dickerman, "Review of TREAT Experiments in Support of Transient Overpower (TOP) Analysis for Fast Reactor Safety," Proc. of the Fast Reactor Safety Meeting, Beverly Hills, April 1974.

135. W.T. Sha and A.E. Waltar, "An integrated Model for Analyzing Disruptive Accidents in Fast Reactors," Nucl. Sci. and Engr., 44, pp. 135-156, 1971.

136. P.G. Lorenzini and G.F. Flanagan, "An Evaluation of Fuel-Coolant Interactions During Disassembly of an LMFBR," Proc. Conf. on New Developments in Reactor Mathematics and Applications, CONF-710302, Idaho Falls, 50, March 1971.

137. G.E. Culley, J.E. Hanson, W.L. Partain, J.H. Scott, and A.E. Waltar, "Fast Reactor Safety Implications of Recent Assessments of Fuel Pin Transient Behavior," Proc. Int. Conf. on Engr. of Fast Reactors for Safe and Reliable Operation, Vol. II, p.626, Karlsruhe, Oct. 9-13 1972.

138. L.L. Smith, J.R. Travis, M.G. Stevenson, F.E. Dunn, and G.J. Fischer, "SAS/FCI, A Fuel-Coolant Interaction Model for LMFBR Whole-Core Accident Analysis," Proc. Topical Meeting on Mathematical Models and Computational Techniques for Analysis of Nuclear Systems, CONF-730414-P1, Ann Arbor, Michigan, 9-11 April 1973.

139. D.H. Cho, R.O. Ivins, and R.W. Wright, "Pressure Generation by Molten Fuel-Coolant Interactions under LMFBR Accident Conditions," Proc. Conf. on New Developments in Reactor Mathematics and Applications, Idaho Falls, Idaho, 29-31 March 1971, USAEC Report CONF-710302, pp. 25-49.

140. J.C. Sonnichsen, W.L. Partain, R.J. Shields, and A.E. Waltar, "Analytical Modeling of the Mark-IIA TREAT Loop for Fuel Motion and Sodium Expulsion Studies," Proc. of the Fast Reactor Safety Meeting, Beverly Hills, April 1974.

141. H. Wider, J.F. Jackson, L.L. Smith, and D.T. Eggen, "An Improved Analysis of Fuel Motion During an Overpower Excursion," Proc. of the Fast Reactor Safety Meeting, Beverly Hills, Calif. April 1974.

142. D.A. Meneley, G.K. Leaf, A.J. Lindeman, T.A. Daly, and W.T. Sha, "A Kinetics Model for Fast-Reactor Analysis in Two Dimensions," Dynamics of Nuclear Systems, The Univ. of Arizona Press, Tucson, 483, 1972.

143. J.C. Sonnichsen, W.L. Partain, R.J. Shields, and A.E. Waltar, "Analytical Modeling of the MARK-IIA TREAT Loop for Fuel Motion and Sodium Expulsion Studies," ANS Conf. Fast Reactor Safety, Los Angeles, April 1974.

144. H.J. Willenberg, W.L. Partain, and A.E. Waltar, "Dynamics of Molten Fuel Motion During a Fast Reactor Overpower Transient," ANS Conf. Fast Reactor Safety, Los Angeles April 1974.

145. A. Waltar, et. al., and A.E. Walter, "Melt-1 A Neutronics, Thermal-Hydraulics Computer Program for Fast Reactor Safety Analysis," Hanford Engineering Development Laboratory report HEDL-TME 72-84, June 1972.

146. H.J. Willenberg, W.L. Partain, and A.E. Waltar, "Reactivity Effects of Internal Molten Fuel Motion Models During a Fast Reactor Overpower Transient," Trans. Am. Nucl. Soc., 17, 359, November 1973.

147. G.B. Wallis, *One-Dimensional Two-Phase Flow*, McGraw-Hill Book Co., New York, 1969, p. 143.

148. Ibid., pp. 247-255.

149. A.E. Waltar, A. Padilla, Jr., H.J. Willenberg "Fuel Motion in Transient Overpower Accidents," Trans. Am. Nucl. Soc. 19, 278, October 1974.

150. W.L. Partain, A.E. Waltar, and R.J. Shields, "Effects of Fuel Density Gradients and Molten Fuel Freezing During a Fast Reactor Excursion," Trans. Am. Nucl. Soc., 17, 361, November 1973.

151. Von Neumann, J. E.R.D. Richtmyer, "A Method for the Numerical Calculation of Hydrodynamic Shocks," Journal of Applied Physics 21(3):232, 1950.

152. J.E. Boudreau and R.C. Erdmann, "On Autocatalysis During Fast Reactor Disassembly," Nucl. Sci. Engr. 51, pp. 206, 1973.

153. P. Bleiweis, W.E. Kastenberg, and D. Okrent, "A Study of Azimuthily Dependent LMFBR Disassemblies," to appear in NS&E, 1975.

154. R.E. Webb, "Some Autocatalytic Effects During Explosive Power Transients in Liquid Metal-Cooled Fast Breeder, Nuclear Power Reactors (LMFBR's)," The Ohio State Univ., 1972.

155. B. Nicholson, "Design Basis Accident Studies," AEC Report Contract No. AT(11-1)-2286, June 1974.

156. L.I. Moss and W.A. Rhoades, "A Method for the Study of Autocatalysis and/or Pressure Histories in Fast Breeder Reactor Excursion," Mtg. Industrial Needs and Academic Research in Reactor Kinetics, Upton, NY, 8-9 April 1968.

157. J.E. Boudreau, F.H. Harlow, W.H. Reed and J.F. Barnes, "A Proposal for Computer Investigation of LMFBR of LMFBR Core Meltdown Accidents," Los Alamos Scientific Laboratory report LA-UR-74-243, October 1973.

158. Personal communication with Don Ferguson, ANL, 1974.

159. Reed, Wm. H. "TIMEX: A Time-Dependent Explicit Discrete Ordinates Program for the Solution of Multigroup Transport Equations," LA-4800, 1972.

160. K.D. Lathrop and F.W. Brinkley, "Theory and Use of the General-Geometry TWOTRAN Program," Los Alamos Scientific Laboratory report LA-4432, May 1970.

161. J.F. Proctor, W.R. Wise and L.P. Walker, "Response of Enrico Fermi Reactor to TNT Simulated Nuclear Accidents," NOLTR 62-207, 1964.

162. N.J.M. Rees, "A Model Investigation of Explosion in Simple Tank Fast Reactors," Proc. of the Conf. on Safety Fuels, and Core Design in Large Fast Power Reactors," October 11-14, 1965, ANL-7120, pp. 692-719.

163. A.H. Marchertas, Y.W. Chang, and S.H. Fistedis, "Evaluation of Coolant Impact Effects on the Reactor Cover (A Parameter Study of the Plug-jump Problem for the Fast-reactor Containment Program)", ANL-7987, November 1972.

164. D.D. Stepnewski, G.C. Fox, R.D. Peak, and K.R. Merckx, "Mechanical Consequences of Hypothetical Core Disruptive Accidents," HEDL-TME 71-50, 1970.

165. J.C. Hesson, R.H. Sevy and T.J. Marciniak, "Postaccident Heat Removal in LMFBR's: In-vessel Considerations," ANL-7859, September 1971.

166. Y.W. Chang and J. Gvildys, "Analysis of the FFTF Primary-system Response to an HCDA," ANL-8066, January 1974.

167. T.D. Butler, "LINC Method Extensions," Second Intl. Conf. on Numerical Methods in Fluid Dynamics," Berkeley, Calif. Sept. 15-19, 1970.

168. N.E. Hoskin and M.R. Slough, "Stabilization of Mesh Distortion in the 2-D Lagrangian Code ASTARTE," UKAEA GRO/44/91/16.

169. D.F. Schoeberle, Y.W. Chang, J. Gvildys, and J.C. Bratis, "A Nonlinear Dynamic Study of the Reactor Head Cover Problem (Fast Reactor Containment Program)," ANL report to be published.

170. E.P. Hicks and D.C. Menzies, "Theoretical Studies on the Fast Reactor Maximum Accident," Proc. of the Conf. on Safety, Fuels and Core Design in Large, Fast Power Reactors, October 11-14, 1965, USAEC Report ANL-7120.

171. D.H. Cho, W.L. Chen, and R.W. Wright, "Pressure Pulses and Mechanical Work from Molten Fuel-coolant Interaction: A Parametric Study," Trans. Am. Nucl. Soc., 14 (1), 290, 1971.

172. L. Caldarola, "A Theoretical Model for the Molten Fuel-sodium Interaction in a Nuclear Fast Reactor," Nucl. Eng. and Design, 22, pp. 175-211, 1972.

173. A. Padilla, Jr. and R.M. Crawford, "Sodium Properties for MFCI Analyses," Trans. Am. Nucl. Soc., 15, 184, 1973.

174. J.C. Bratis and T.J. Marciniak, "Reactor Structural Response to Molten-fuel-coolant Interactions," Proc. 2nd Intl. Conf. on Structural Mechanics in Reactor Technology, Berlin, Sept. 10-14, 1973, Paper E1/4.

175. C.Y. Wang, Y.W. Chang, and S.H. Fistedis, "Application of Implicit Continuous Eulerian Containment Code to Low-energy Excursions," Trans. Am. Nucl. Soc., 16, 191, 1973.

176. A. Padilla, "Transient Analysis of Fuel-sodium Interactions," Trans. Am. Nucl. Soc., 13, 375, 1970.

177. J. Ash and R.T. Julke, "Comparison of a Two-dimensional Hydrodynamics Code (REXCO) to Excursion Experiments for Fast Reactor Containment," ANL-7911, January 1972.

178. J. Ash, Y.W. Chang, and R.T. Julke, "Comparison of a Two-dimensional Hydrodynamics Code (REXCO) to Excursion Experiments for Fast Reactor Containment," ANL-7911 Supplement, July 1972.

179. G. Nagumo and C. Fiala, "Comparison of FFTF Simple Model Tests with REXCO Predictions," ANL-8071, February 1974.

180. D.E. Simpson, "Design and Evaluation of FFTF Containment," Nuclear Safety 14 (5), Sept.-Oct. 1973.

181. A.L. Florence and G.R. Abrahamson, "Simulation of a Hypothetical Core Disruptive Accident in a Fast Flux Test Facility," HEDL-SRI-1 and 2, May 1973.

182. D.D. Stepnewski et al, "FFTF Scale Model Structural Dymanics Tests," ANS Fast Reactor Safety Meeting, April 2-4, 1974, Beverly Hills, Calif. To be published in USAEC-CONF 740401.

183. Y.W. Chang and J. Gvildys, "Analysis of the FFTF Primary System Response to an HCDA," ANL-8066, January 1974.

184. T.J. Marciniak, J. Gvildys, G. Nagumo, J.E. Ash, "Analysis of FFTF Primary Containment Complex Model Experiments," ANL-8062, January 1974.

185. J.M. Kennedy, "Nonlinear Dynamic Response of Reactor Core Subassemblies," ANL-8065, ANL Laboratory, January 1974.

186. J.M. Kennedy, T. Belytschko, "Implementation of an Energy Source in a Structural-Response Code-STRAW," Trans. Am. Nucl. Soc., 19, 160, October 1974.

187. T. Belytschko and A.H. Marchertas, "Three-Dimensional Nonlinear Finite Element Methods and Application to Dynamic Response of Reactor Fuel Subassembly, ASME Pressure Vessel and Piping Conference, Miami, Florida, June 1974.